Jacob Linder

Quantum transport and proximity effects in unconventional superconducting hybrid systems

Thesis for the degree of Philosophiae Doctor

Trondheim, March 2009

Norwegian University of Science and Technology
Faculty of Natural Sciences and Technology
Department of Physics

NTNU
Norwegian University of Science and Technology

Thesis for the degree of Philosophiae Doctor

Faculty of Natural Sciences and Technology
Department of Physics

ISBN 978-82-471-1457-5 (printed ver.)
ISBN 978-82-471-1458-2 (electronic ver.)
ISSN 1503-8181

Doctoral theses at NTNU, 2009:43

Printed by NTNU-trykk

Abstract

This thesis presents some of the main findings from twenty-five research articles. These papers may roughly be categorized into three fields: *i)* Proximity structures of superconductors and ferromagnets, *ii)* Interplay between ferromagnetism, noncentrosymmetricity, and superconductivity in bulk materials, and *iii)* Superconducting proximity-effect in graphene. In all of these cases, emphasis is placed on the thermodynamic properties and the transport properties of the systems. We address in particular how the spin-polarization of ferromagnetic elements may combine with the dissipationless flow of electric current offered by superconducting elements, and also how useful information about the superconducting state is revealed through characteristic fingerprints in the thermodynamic and transport properties of the systems under consideration.

Preface

This thesis is submitted as part of the requirements for the degree Philosophiae Doctor at the Norwegian University of Science and Technology (NTNU). The thesis represents three and a half years of work, of which teaching duties and courses equivalent to one year are included. My supervisor has been Professor Asle Sudbø, and the research has been funded by the Norwegian Research Council, Grants No. 158518/431 and No. 158547/431 (NANOMAT), and Grant No. 167498/V30 (STORFORSK).

Jacob Linder
Trondheim, November 2008

Acknowledgments

Perhaps some might argue that my section of Acknowledgments is a bit lengthy for a Ph.D.-thesis, but after three and a half years of intense studies and the pleasure of getting acquainted with scientists worldwide, what can I say, there is simply much to write. Besides, I realize that this particular section of my thesis will probably be the most interesting for my family and friends who are not experts in the field of theoretical physics, so the rest of you will have to bear with me.

Over the last years, I have had the pleasure of being part of an outstanding research community, namely the superconductivity group led by Asle Sudbø at NTNU. I was soon motivated to work hard in order to keep up with a group consisting of talented young researchers. In particular, I would like to thank Martin Grønsleth for our collaboration the first year of my study, which was very fruitful and resulted in several publications. He provided me with a patient and smooth introduction to the topic of quantum transport in the Matsubara formalism when I was completely new to the subject, and besides his scientific insight, it was also enjoyable working together with Martin due to his amiable nature. I would also like to mention Steinar Kragset whom with I shared office the first year, simply for always being helpful and for being good company. The first year also gave me the privilege to get acquainted with Egor Babaev, who was at the time post-doc in the group, and he influenced me considerably with his devotion to theoretical physics.

A great aspect of being a researcher is that one gets the opportunity to travel around the world in the context of attending various conferences. In doing so, I eventually got to know physicists in other countries, which led to healthy and productive collaborations. Although I have had the pleasure of being acquainted with several excellent scientists over the course of the last years, there are a few that deserve a special mention.

In the summer of 2007, I received an e-mail from Takehito Yokoyama related to one of my publications. I was already familiar with his work since his research interests strongly coincided with my own. It was therefore natural for me to suggest a collaboration between the two of us, and this turned out to be a big success. You have inspired me with your zealous and hard-working approach to physics, Takehito, and our continuous correspondence throughout my thesis has been an important support. I have truly enjoyed working together with you,

and I hope that our collaboration may continue to prosper in the years to come.

Not long after I was acquainted with Dr. Yokoyama, I also had the pleasure of initiating a collaboration with Professor Yukio Tanaka, which at the time was Yokoyamas Ph.D advisor, and also visiting him at Nagoya University in January 2008. I must say that not only has your scientific work been of much value and interest to me, Professor Tanaka, but your passion and hard-working mentality has been very inspiring. I am grateful for all the encouragement and support you have provided to me during my thesis, and I have greatly enjoyed collaborating with you on a number of papers.

I would also like to mention Andriy Nevidomskyy and Cyrus Turel, which I met at the 2007 APS March Meeting in Denver. Guys, I have really enjoyed working with you. Special thanks to Matthias Eschrig for his hospitality at the workshop in Karlsruhe in July 2008, and I look forward to a continued collaboration between us. Many thanks to Mario Cuoco for his generosity and our fruitful scientific exchange, and also to Annica Black-Schaffer for a great collaboration on the Josephson current in graphene. Special mention of Ph.D student Iver Sperstad as well, as I have both enjoyed working with you and been very inspired by your discipline (also, thanks for proof-reading this thesis!). Finally, I would like to direct a big thanks to a number of scientists that I have had the pleasure of collaborating and discussing with. In particular, I would like to thank: Y. Asano, M. Zareyan, A. Cottet, D. Huertas-Hernando, M. Thaule, H.-J. Skadsem, F. S. Bergeret, and J. Y. T. Wei.

My main collaborator has nevertheless been Asle Sudbø. From the very beginning, he was supportive and overbearing with my sincere, but relentless and almost foolhardy, ambitions. As I eventually got over the phase of "There's a new kid in town, and I'm gonna' show the whole world I'm here!" after about two years or so, I guess I began to mature as a scientist. A pursuit of making a big impact with my research substituted the initial yearn of a big publication list. Although I could have arrived at this conclusion earlier, as Asle certainly was in a position to discipline his over-eager rookie Ph.D.-student with a healthy dose of wisdom and common sense, he gave me time to develop as a researcher while gently guiding me in the right direction. On the purely scientific side, his contribution has truly been invaluable and very educative. However, it is not his impressive insight in theoretical physics that I would like to underline here. Rather, I would like to speculate that one of the main reasons behind his scientific achievements and the notorious hatching of successful Ph.D.-students under his supervision is a very simple one: he really enjoys what he is doing! This fact is joyfully obvious to anyone who has collaborated with Asle, and it is indeed a very valuable trait of a supervisor. So thank you for an outstanding time, Asle.

Finally, the persons I mention lastly are really the ones who has meant the most. My brother David and my parents for loving me so incredibly much and always believing in me. *Mami, deseo que tu estuviera aqui que podria agradecerte por*

todo y que podrias ver que su hijo ahora ha acabado su educación.

My wonderful wife Jenny Caroline, for everything. Over the last years, you have endured my long working hours and commitment to my work, which often has demanded sacrifices from your part. But my passion for physics cannot compare in any way to the thrill of being your husband and the fact that I can be with you every day and express my love for you. I would gladly give up all my knowledge of physics in return for a life with you, because you are the best thing in my life, *pumita*.

The last thing I want to say is a really big thank-you to God, for providing me with inspiration, health, creativity, and life itself.

I dedicate this thesis to my late mother who in a loving manner always encouraged me to prioritize my studies and work hard.

List of publications

Paper I: M. S. Grønsleth, J. Linder, J.-M. Børven, and A. Sudbø.
Interplay between ferromagnetism and superconductivity in tunneling currents.
Physical Review Letters **97**, 147002 (2006).

Paper II: J. Linder, M. S. Grønsleth, and A. Sudbø.
Tunneling currents in ferromagnetic systems with multiple broken symmetries.
Physical Review B **75**, 007702 (2006).

Paper III: J. Linder, M. S. Grønsleth, and A. Sudbø.
Conductance spectra of ferromagnetic superconductors: Quantum transport in a ferromagnetic metal/non-unitary ferromagnetic superconductor junction.
Physical Review B **75**, 054518 (2007).

Paper IV: J. Linder and A. Sudbø.
Signatures of retroreflection and induced triplet electron-hole correlations in a ferromagnet/superconductor junction. .
Physical Review B **75**, 134509 (2007).

Paper V: J. Linder and A. Sudbø.
Josephson effect in thin-film superconductor/insulator/superconductor junctions with misaligned in-plane exchange fields.
Physical Review B **76**, 064524 (2007).

Paper VI: J. Linder and A. Sudbø.
Quantum transport in noncentrosymmetric superconductors and thermodynamics of ferromagnetic superconductors.
Physical Review B **76**, 054511 (2007) [*Erratum*: PRB **77**, 069902 (2008)].

Paper VII: J. Linder and A. Sudbø.
Dirac fermions and conductance oscillations in s- and d-wave superconductor - graphene junctions.
Physical Review Letters **99**, 147001 (2007).

Paper VIII: J. Linder and A. Sudbø.
Spin-flip scattering and non-ideal interfaces in dirty ferromagnet / superconductor junctions.
Physical Review B **76**, 214508 (2007).

Paper IX: J. Linder and A. Sudbø.
Tunneling conductance in s- and d-wave superconductor-graphene junctions: Extended Blonder-Tinkham-Klapwijk formalism.
Physical Review B **77**, 064507 (2008).

Paper X: T. Yokoyama, J. Linder, and A. Sudbø.
Heat transport by Dirac fermions in normal/superconducting graphene junctions.
Physical Review B **77**, 132503 (2008).

Paper XI: J. Linder, T. Yokoyama, Y. Tanaka, Y. Asano and A. Sudbø.
Quantum transport in a normal metal/odd-frequency superconductor junction.
Physical Review B **77**, 174505 (2008).

Paper XII: J. Linder, T. Yokoyama, and A. Sudbø.
Identifying the odd-frequency superconducting state by a field-induced Josephson effect.
Physical Review B **77**, 174507 (2008).

Paper XIII: J. Linder, T. Yokoyama, D. Huertas-Hernando, and A. Sudbø.
Supercurrent switch in graphene π-junctions.
Physical Review Letters **100**, 187004 (2008).

Paper XIV: J. Linder, I. B. Sperstad, A. H. Nevidomskyy, M. Cuoco, and A. Sudbø.
Coexistence of itinerant ferromagnetism and a non-unitary superconducting state with line nodes: possible application to UGe_2.
Physical Review B **77**, 184511 (2008).

Paper XV: J. Linder, T. Yokoyama, and A. Sudbø.
The role of interface transparency and spin-dependent scattering in diffusive ferromagnet/superconductor heterostructures.
Physical Review B **77**, 174514 (2008).

Paper XVI: J. Linder, T. Yokoyama, Y. Tanaka, and A. Sudbø.
Strongly spin-polarized current generated in Zeeman-split unconventional superconductors.
Physical Review B **78**, 014516 (2008).

Paper XVII: J. Linder, T. Yokoyama, and A. Sudbø.
Density of states near a vortex core in ferromagnetic superconductors: Application to STM measurements.
Physical Review B **78**, 064520 (2008).

Paper XVIII: I. B. Sperstad, J. Linder, and A. Sudbø.
Josephson current in diffusive multilayer superconductor/ferromagnet/superconductor junctions.
Physical Review B **78**, 104509 (2008).

Paper XIX: J. Linder, A. H. Nevidomskyy, and A. Sudbø.
Nontrivial interplay of superconductivity and spin-orbit coupling in noncentrosymmetric ferromagnets.
Physical Review B **78**, 172502 (2008).

Paper XX: J. Linder and A. Sudbø.
Theory of Andreev reflection in junctions with iron-based high-T_c superconductors.
Physical Review B **79**, 020501(R) (2009).

Paper XXI: M. A. Silaev, T. Yokoyama, J. Linder, Y. Tanaka, and A. Sudbø.
Tunneling conductance and local density of states in time-reversal symmetry breaking superconductors under the influence of an external magnetic field .
Physical Review B **79**, 054508 (2009).

Paper XXII: J. Linder, M. Zareyan, and A. Sudbø.
Proximity effect in ferromagnet/superconductor hybrids: From diffusive to ballistic motion.
Physical Review B **79**, 064514 (2009).

Paper XXIII: A. Cottet and J. Linder.
Superconducting/ferromagnetic diffusive bilayer with a spin-active interface: A numerical study.
Physical Review B **79**, 054518 (2009)

Paper XXIV: J. Linder, T. Yokoyama, and A. Sudbø.
Theory of superconducting and magnetic proximity effect in S/F structures with inhomogeneous magnetization textures and spin-active interfaces.
Physical Review B **79**, 054523 (2009)

Paper XXV: J. Linder, T. Yokoyama, A. Sudbø, and M. Eschrig.
Pairing symmetry transition induced by spin-active interfaces in superconducting junctions.
Accepted for publication in Physical Review Letters.

Contents

1 Introduction **1**

2 Manifestations of the proximity effect in hybrid structures with superconductors and ferromagnets **5**
2.1 Fundamental concepts 6
2.2 Research highlights 13

3 Interplay between ferromagnetism, noncentrosymmetricity, and superconductivity in bulk materials **21**
3.1 Fundamental concepts 21
3.2 Research highlights 24

4 Superconducting proximity-effect in graphene **37**
4.1 Fundamental concepts 37
4.2 Research highlights 40

5 Conclusion and outlook **51**

Bibliography **52**

Chapter 1

Introduction

This thesis is mainly devoted to a study of superconducting and ferromagnetic order, both individually and with respect to how they influence each other. Traditionally, superconductivity and ferromagnetism have been considered as antagonists. In the conventional Bardeen-Cooper-Schrieffer (BCS) paradigm, the main constituent of the superconducting condensate is a pair of electrons bound together by an attractive potential, known as a Cooper pair. In the original BCS-theory [1], the electrons comprising the Cooper pair have opposite spin and momenta, thus residing in a spinless singlet state[1]. In a ferromagnet, on the other hand, the Coulumb repulsion and the Pauli principle conspire to yield an effective interaction between the spins of electrons, which under appropriate circumstances leads to a ferromagnetic state. In this ordered state, the majority of electrons have spins pointing in one direction of space while the minority of electrons have spins pointing in the opposite direction, resulting in a net magnetization of the sample. So when considering the spinless structure of the Cooper pair in BCS theory and the fact that superconductors tend to expel all magnetic fields inside of them[2], it is little wonder that superconducting and ferromagnetic order have been considered as incompatible orders over the years.

However, the simple picture sketched above is by no means complete and should be supplemented with important ingredients. For instance, there is no fundamental symmetry restriction which demands that the Cooper pair should exist in a spinless singlet state. In fact, so-called spin-triplet pairing is fully consistent with fermion statistics, since it is the total wavefunction of the Cooper pair which must be antisymmetric under an exchange of particle coordinates. Once we allow the Cooper pair to consist of two electrons with spins pointing in the same direction, the idea of combining superconductivity and ferromagnetism immediately becomes more plausible. Spin-triplet superconductors are, however, still considered as rarities. In fact, there exists only a handful of materials where the experimental data point strongly towards a spin-triplet state. Among

[1]The spin-singlet symmetry prescribes that the spin-part of a two-electron wavefunction should be antisymmetric under an exchange of the spin-coordinates for the electrons, while a spin-triplet wavefunction should be symmetric under the same exchange.

[2]There are exceptions to this, *e.g.* in the vortex state of a superconductor or in a thin-film geometry where the Meissner effect is suppressed.

these materials, one finds a series of Uranium-based heavy-fermion compounds (UGe_2 [2], URhGe [3], UCoGe [4], and UIr [5]). These all have in common a highly exotic property, namely that they seem to undergo a phase transition into a state which is both superconducting and ferromagnetic at very low temperatures of order 1 K. The exact nature of this coexistent state is still under intense investigation. Questions that remain to be answered are whether the two orders coexist in a spatially homogeneous manner, if they entwine each other in a helical pattern, or if they coexist in a spontaneous vortex phase, just to mention a few. In any case, it is clear that the experimental unveiling of materials where superconductivity and ferromagnetism coexist challenges our very understanding of how superconductivity is formed and in particular its interplay with ferromagnetic order.

A popular approach in the study of the interplay between superconducting and ferromagnetic order have in recent years been the fabrication of artificially created superconductor/ferromagnet (S/F) multilayers. In this scenario, the two orders influence each other through electron tunneling via an interface separating the two layers. By applying voltage differences and passing currents through such heterostructures, one may systematically probe the influence of the two orders on physically interesting properties such as the spin-polarization of the current and the resistance of the junction. In fact, the properties of spin-polarization and electrical resistance are of paramount importance in terms of achieving actual technological applications. This is perfectly exemplified through the giant magnetoresistance effect (GMR) [6, 7]. In short, this effect causes the electrical resistance of a ferromagnet/normal/ferromagnet junction to be altered considerably simply by switching the magnetization direction of one ferromagnetic layer. The discoverers of this effect earned the 2007 Nobel Prize, and the GMR technology is today used extensively in the read heads in modern hard drives and magnetic sensors.

So what can the interplay between superconductivity and ferromagnetism offer in terms of functional devices? One example is the F/S/F spin-valve, which constitutes the superconducting analogue of the conventional spin-valve setup. In this system, the critical temperature at which superconductivity is established depends on the relative orientation of the magnetizations in the ferromagnetic layers. As a practical consequence, it is thus possible to alternate between the non-superconducting and the superconducting state by controlling the magnetization direction of one of the ferromagnetic layers: the whole system acts as a spin-switch which turns on and off superconductivity. Another example is the S/F/S junction, through which a dissipationless current may flow up to a critical magnitude of the current. By tailoring the parameters of the junction (such as width, temperature, etc.), it is possible to obtain quantum ground states which are degenerate. This is of interest because it effectively renders the junction a qubit. The distinction between a qubit and a classical bit, is that while the classical bit is always exclusively in one of two possible states, the qubit may be in both simultaneously in the sense that it has a finite probability to be in either one of them at any time. The implementation of qubits in a quantum

computer would speed up certain computational tasks greatly in comparison with the classical bit [8], a fact suggesting that such S/F/S junctions could be useful in this context.

Clearly, the aspect of a spin-polarization offered by ferromagnets combined with the dissipationless flow of a current offered by superconductors, could offer opportunities in terms of obtaining functional devices in low-temperature nanotechnology. The situation becomes even more exciting when considering the fact that these two properties may as of recently actually be combined with electrons that behave relativistically in a condensed-matter system, namely graphene [9, 10]. In undoped graphene, the low-energy electrons to a very good approximation behave like massless Dirac fermions, which is distinct from the behavior of electrons in conventional metallic systems. The fact that experimentalists recently have succeeded in inducing superconducting correlations in graphene opens up a vista of new physics.

The motivation for the topic of this thesis is thus twofold. From the fundamental physics point of view, the study of how superconductivity and ferromagnetism interact with each other under various circumstances simply offers a very rich arena to explore. In terms of practical applications, the combination of spin-polarization and a dissipationless flow of a current suggests exciting prospects in low-temperature nanotechnology.

The publications included in this thesis fall into categories that may be divided roughly into three main groups. In what follows, we will treat each of these subcategories separately for clarity. In each case, some introductory concepts of the relevant field are presented, followed by some of the main research results obtained in the publications included in this thesis. The publications themselves contain the full calculations and details, and are included at the end of the thesis. In what follows, we will use units such that $\hbar = c = k_B = 1$.

Chapter 2

Manifestations of the proximity effect in hybrid structures with superconductors and ferromagnets

In this chapter, we investigate various effects that may arise in F/S heterostructures and discuss the concept of odd-frequency pairing. Papers IV, V, VIII, XI, XII, XV, XVI, XVIII, XX, XXII, XXIII, and XXIV fall into this subcategory.

Ferromagnetism and superconductivity appear to be two antagonistic long-range orders at first glance, at least in the conventional picture. The usual argument for this is that the Zeeman-energy associated with ferromagnetism is unfavorable to a spin-singlet symmetry of the Cooper pairs. Putting aside the scenario of triplet superconductors for the moment, this argumentation holds well when considering uniform and homogeneous coexistence of ferromagnetism and superconductivity. Thus, spatially homogeneous coexistence of ferromagnetism and usual BCS-superconductivity is strictly prohibited in a bulk material [11].

However, it is still possible to probe how these long-range orders affect each other by setting up a proximity structure consisting of a ferromagnetic and superconducting layer in close contact. Experimentally, these are usually separated by a thin insulating layer. A plethora of interesting phenomena occur in such a proximity F/S layer, of which some may even hold potential for future technological applications. Below, we consider the basic physics in a F/S layer and give a brief review of the most important of the effects that arise in such heterostructures. Thereafter, we briefly touch upon some of the main research results presented in the publications contained in this thesis. As section 2.1 will introduce several concepts which are also of relevance for chapters 3 and 4, it will be more comprehensive than the corresponding sections 3.1 and 4.1.

2.1 Fundamental concepts

2.1.1 Proximity effect and Andreev reflection

In the context of superconducting heterostructures, the *proximity effect* denotes physical phenomena arising when a nonsuperconducting material, such as a paramagnetic metal or a ferromagnet, is placed in contact with a superconductor. In this scenario, Cooper pairs enter the normal metal while electronic excitations leak into the superconducting region. As a result, one may observe both a decrease of the critical temperature T_c for superconductivity in the superconducting region and an induction of superconducting correlations in the normal region. For instance, it is the proximity effect which renders possible the flow of a Josephson current between two superconductors separated by a normal metal of finite width. Also, the superconducting correlations in the normal part are manifested in the density of states, where a so-called minigap is induced in the diffusive regime. The minigap amounts to a substantial suppression of the density of states over an energy interval dictated by the Thouless energy $\varepsilon_{\mathrm{Th}}$, which is the governing energy scale for the proximity effect in normal/superconductor (N/S) junctions. The Thouless energy is defined as $\varepsilon_{\mathrm{Th}} = D/d^2$, where D is the diffusion constant of the non-superconducting region while d is its width.

A key aspect in understanding low-energy quantum transport at the interface of a non-superconducting and superconducting material, *e.g.* a N/S interface, is the process of Andreev reflection. Although the existence of a gap in the energy spectrum of a superconductor implies that no quasiparticle states may persist inside the superconductor for energies below that gap, physical transport of charge and spin is still possible at a N/S interface in this energy-regime if the incoming electron is reflected as a hole with opposite charge. The remaining charge is then transferred to the superconductor in the form of a Cooper pair at Fermi level.

2.1.2 Non-monotonous decay of superconductivity

While in an N/S junction the order parameter decays monotonously upon penetrating the normal region, the presence of an exchange splitting h between the majority and minority spin energy bands in a ferromagnet gives rise to a damped oscillatory decay of the superconducting order parameter in an F/S junction (see Fig. 2.1). This may be understood physically by realizing that the Cooper pair entering the ferromagnetic region obtains a finite center-of-mass momentum due to the exchange splitting. The majority-spin electron experiences a reduction in energy by h, while the minority spin electron gains an energy h, thus leading to a center-of-mass momentum $q = 2h/v_F$. In addition to the decaying behavior of the superconducting order parameter, the scattering potential at the interface between the F and S regions may lead to a suppression of the order parameter magnitude-wise in the vicinity of the interface. For low-transparency interfaces (high barrier resistances), it is usually a good approximation to neglect this effect. As we shall see in the following

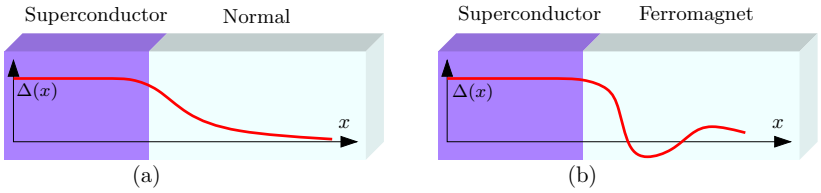

Figure 2.1: The characteristic spatial dependence of the superconducting order parameter in a (a) N/S and (b) F/S junction.

sections, the finite center-of-mass momentum acquired by the Cooper pair has a number of implications for experimentally observable quantities.

2.1.3 0-π oscillations of critical current

In a superconducting Josephson junction, two bulk superconductors are connected via a weak link to support a dissipationless flow of electrical current as long as there is a phase difference $\Delta\phi = \phi_L - \phi_R$ between the order parameters $\Delta_j = \Delta_{0,j}e^{i\phi_j}$, $j = L, R$ in each superconducting bank. The relationship between the magnitude of the current that flows through the junction and the corresponding phase difference between the superconducting banks is known as the current-phase relationship (see Ref. [12] for a detailed review). The current-phase relationship is under many circumstances given as $I = I_c \sin\Delta\phi$, where I_c is the critical (maximum) value of the current. However, it may in general include contributions from higher harmonics. In order to explain the concept of 0-π oscillations, let us nevertheless proceed with the sinusoidal form $I = I_c \sin\Delta\phi$ for the sake of clarity. The energy ground-state E of the Josephson junction is related to the phase difference as follows [13]:

$$E = \frac{I_c}{2e}(1 - \cos\Delta\phi), \tag{2.1}$$

giving the sinusoidal current-phase relationship $I = (2e)\partial E/\partial\Delta\phi = I_c \sin\Delta\phi$. From the above equation, we see that the minimum energy is obtained at $\Delta\phi = 0$ when $I_c > 0$. However, the minimum energy of the junction is obtained at $\Delta\phi = \pi$ when $I_c < 0$. The constant I_c, and in particular its sign, depends in general on the parameters of the junction, such as width, temperature, barrier transparency, etc. This means that it is possible to manipulate the preferred ground-state of the system *if* one may control the sign of I_c by altering for instance the width d of the junction. As a result, one should observe an oscillatory behavior of the critical current when plotted against a parameter in the system that may provoke a 0-π transition. Precisely such behavior was observed by Ryazanov *et al.* [14], and later by several other groups. It should also be mentioned that the current-phase relationship acquires a substantial contribution from higher harmonics than $\sin\Delta\phi$ when the interface transparency is high [15, 16], which has some interesting effects for the ground-state properties of the system [17].

2.1.4 Spin-dependent interfacial phase-shifts

An intrinsic property of F/S interfaces is that the particles partaking in the scattering processes should undergo spin-dependent interfacial phase-shifts (spin-DIPS) upon transmission and reflection at the interface. This is a result of the energy-split majority and minority spin bands in the F region. Nevertheless, these phase-shifts have not received much attention in the literature, and non-magnetic boundary conditions [18, 19] have in the vast majority of works been used to characterize F/S interfaces [20, 13]. However, the presence of spin-DIPS may have a strong influence on the system, even qualitatively. The easiest way to capture the effect of spin-DIPS is to start with a Blonder-Tinkham-Klapwijk (BTK) [21] theory for an N/S junction and incorporate a barrier potential at the interface which depends on the spin of the incident electrons, i.e. a potential $V_\sigma = V_0 + \sigma V_M$, where V_M is the magnetic part of the barrier potential. In this scenario, two effects come into play. First, the transmission amplitudes for spin-$\uparrow$ and spin-$\downarrow$ particles are no longer degenerate, but one of the spin species are favored tunneling-wise. Secondly, the scattered particles pick up phase-shifts at the interface due to the exchange splitting near the interface. These phase-shifts may actually induce triplet correlations [22]. To see this, consider a singlet correlation function in the superconductor:

$$|\psi\rangle = |\uparrow\rangle_k|\downarrow\rangle_{-k} - |\downarrow\rangle_k|\uparrow\rangle_{-k}. \tag{2.2}$$

Upon scattering at the interface, the spins acquire different phase shifts according to:

$$|\uparrow\rangle_{-k} = \mathrm{e}^{\mathrm{i}\theta_\uparrow}|\uparrow\rangle_k,\ |\downarrow\rangle_{-k} = \mathrm{e}^{\mathrm{i}\theta_\downarrow}|\downarrow\rangle_k, \tag{2.3}$$

which transforms Eq. (2.2) into

$$|\psi\rangle = -\cos(\Delta\theta)\Big(|\uparrow\rangle_k|\downarrow\rangle_{-k} - |\downarrow\rangle_k|\uparrow\rangle_{-k}\Big) - \mathrm{i}\sin(\Delta\theta)\Big(|\uparrow\rangle_k|\downarrow\rangle_{-k} + |\downarrow\rangle_k|\uparrow\rangle_{-k}\Big), \tag{2.4}$$

where $\Delta\theta = \theta_\uparrow - \theta_\downarrow$. As seen, the spin-dependent phase-shifts at the interface induce the $S_z = 0$ triplet component which contributes to the total wavefunction $|\psi\rangle$ as long as $\Delta\theta \neq 0$. If there are also spin-flip scattering processes at the interface of the type $|\uparrow\rangle_k \rightarrow |\downarrow\rangle_k$ and $|\downarrow\rangle_k \rightarrow |\uparrow\rangle_k$, equal-spin pairing $S_z = \pm 1$ components may be generated. Here, we have sketched the situation for a normal/superconductor junction with an explicitly magnetic interface. For a ferromagnet/superconductor junction, however, the barrier potential at the interface should still be modelled as spin-dependent even if the material constituting the barrier is non-magnetic, due to the close proximity of the F region.

2.1.5 Odd-frequency pairing

The presence of superconducting correlations are in general represented by a non-zero expectation value for the anomalous Green's function

$$\mathcal{F}_{\alpha_1\alpha_2}(x_1, x_2) = -\mathrm{i}T\{\langle\psi_{\alpha_1}(x_1)\psi_{\alpha_2}(x_2)\rangle\}, \tag{2.5}$$

with T as the time-ordering operator while $x_j = (\boldsymbol{r}_j, t_j)$ are the space- and time-coordinates for particle j while α_j is the spin-coordinate. This correlator must satisfy the Pauli principle at equal times $t_1 = t_2$, meaning that a sign change is due for $\boldsymbol{r}_1 \leftrightarrow \boldsymbol{r}_2, \alpha_1 \leftrightarrow \alpha_2$. This leads to a finite number of possibilities for the allowed symmetries of the space-, time- and spin-part of the Green's function. In the conventional BCS-case, the correlator is odd with respect to spin such that $\mathcal{F}_{\alpha_1\alpha_2}(\boldsymbol{r}_1, \boldsymbol{r}_2, t) = -\mathcal{F}_{\alpha_2\alpha_1}(\boldsymbol{r}_1, \boldsymbol{r}_2, t)$. This is known as an even-frequency, spin-singlet, even-parity symmetry. The wording stems from the Fourier-transformed and mixed representation [23, 24], where frequency (or energy) is the Fourier-transform of the relative time-coordinate and the momentum is the Fourier-transform of the relative space-coordinate. In fact, in this Fourier-transformed and mixed representation, the condition $\mathcal{F}_{\alpha_1\alpha_2}(\varepsilon, \boldsymbol{k}) = -\mathcal{F}_{\alpha_2\alpha_1}(-\varepsilon, -\boldsymbol{k})$ must be satisfied in general. As seen, this opens up the possibility that the anomalous Green's function, and hence the superconducting order parameter, is *odd* in frequency while even in spin and momentum.

Such an odd-frequency pairing state was proposed by Berezinskii in 1974 [25], who argued that it could be formed due to retarded paramagnon exchange in the context of ^{3}He, although it was later experimentally established that this was not the case. However, it was realized in 2001 by Bergeret *et al.* [26, 27] that the odd-frequency pairing state could be obtained by means of the proximity effect between a ferromagnet and a superconductor. Very recently, it was argued by Tanaka *et al.* [28] that odd-frequency pairing is actually generated whenever time-reversal symmetry or translational symmetry in space is broken in a superconductor. As a consequence, odd-frequency pairing should be generated under very general conditions even in N/S junctions in the absence of any exchange field.

2.1.6 Quasiclassical theory

The quasiclassical theory of superconductivity has proven to be a highly useful tool to study the proximity effect and transport properties of F/S hybrid structures. The central quantity in the quasiclassical theory of superconductivity is the quasiclassical Green's functions $\check{g}(\boldsymbol{p}_\mathrm{F}, \boldsymbol{r}; \varepsilon, t)$, which depends on the momentum at Fermi level $\boldsymbol{p}_\mathrm{F}$, the spatial coordinate $\boldsymbol{r}$, the energy measured from the chemical potential ε, and time t. For a detailed introduction to this theory, see *e.g.* Refs. [23, 24]. The quasiclassical Green's functions $\check{g}(\boldsymbol{p}_\mathrm{F}, \boldsymbol{r}; \varepsilon, t)$ is obtained from the Gor'kov Green's functions $\check{G}(\boldsymbol{p}, \boldsymbol{r}; \varepsilon, t)$ by integrating out the dependence on kinetic energy, assuming that $\check{G}$ is strongly peaked at Fermi level,

$$\check{g}(\boldsymbol{p}_\mathrm{F}, \boldsymbol{r}; \varepsilon, t) = \frac{\mathrm{i}}{\pi} \int \mathrm{d}\xi_{\boldsymbol{p}} \check{G}(\boldsymbol{p}, \boldsymbol{r}; \varepsilon, t). \tag{2.6}$$

This is typically applicable to superconducting systems where the characteristic length scale of the perturbations present, such as mean-free path and magnetic coherence length, is much larger than the Fermi wavelength. Also, the corresponding characteristic energies of such phenomena must be much smaller than the Fermi energy ε_F. The quasiclassical Green's functions may be divided into

an advanced (A), retarded (R), and Keldysh (K) component, each of which has a 4×4 matrix structure in the combined particle-hole and spin space. One has that

$$\check{g} = \begin{pmatrix} \hat{g}^{\mathrm{R}} & \hat{g}^{\mathrm{K}} \\ 0 & \hat{g}^{\mathrm{A}} \end{pmatrix}, \tag{2.7}$$

where the elements of $\check{g}(\boldsymbol{p}_{\mathrm{F}}, \boldsymbol{r}; \varepsilon, t)$ read

$$\hat{g}^{\mathrm{R,A}} = \begin{pmatrix} \underline{g}^{\mathrm{R,A}} & \underline{f}^{\mathrm{R,A}} \\ -\underline{\tilde{f}}^{\mathrm{R,A}} & -\underline{\tilde{g}}^{\mathrm{R,A}} \end{pmatrix}, \; \hat{g}^{\mathrm{K}} = \begin{pmatrix} \underline{g}^{\mathrm{K}} & \underline{f}^{\mathrm{K}} \\ \underline{\tilde{f}}^{\mathrm{K}} & \underline{\tilde{g}}^{\mathrm{K}} \end{pmatrix}. \tag{2.8}$$

The quantities $\underline{g}$ and $\underline{f}$ are 2×2 spin matrices, with the structure

$$\underline{g} = \begin{pmatrix} g_{\uparrow\uparrow} & g_{\uparrow\downarrow} \\ g_{\downarrow\uparrow} & g_{\downarrow\downarrow} \end{pmatrix}. \tag{2.9}$$

Due to internal symmetry relations between these Green's functions, all of these quantities are not independent. In particular, the tilde-operation is defined as

$$\tilde{f}(\boldsymbol{p}_{\mathrm{F}}, \boldsymbol{r}; \varepsilon, t) = [f(-\boldsymbol{p}_{\mathrm{F}}, \boldsymbol{r}; -\varepsilon, t)]^*. \tag{2.10}$$

The quasiclassical Green's functions $\check{g}(\boldsymbol{p}_{\mathrm{F}}, \boldsymbol{r}; \varepsilon, t)$ may be determined by solving the Eilenberger [29] equation, which is derived from the Gor'kov equation at the price of losing information about the physics at length scales comparable to the Fermi wavelength. It reads:

$$[\varepsilon \hat{\rho}_3 - \hat{\Sigma}, \check{g}] + \mathrm{i}\mathbf{v}_{\mathrm{F}} \boldsymbol{\nabla} \check{g} = 0, \tag{2.11}$$

where $\hat{\Sigma}$ contains the self-energies in the system such as impurity scattering, superconducting order parameter, and exchange fields. Above, we have assumed that there is no explicit time-dependence in the problem. The operation $\hat{\rho}_3 \check{g}$ inside the commutator should be understood $\hat{\rho}_3 \check{g} \equiv \mathrm{diag}\{\hat{\rho}_3, \hat{\rho}_3\}\check{g}$. Pauli-matrices in particle-hole×spin (Nambu) space are denoted as $\hat{\rho}_i$, while Pauli-matrices in spin-space are written as $\underline{\tau}_i$. The Green's functions also satisfy the normalization condition

$$\check{g} \otimes \check{g} = \check{1}. \tag{2.12}$$

The self-energies entering Eq. (2.11) should be solved in a self-consistent manner. For instance, a weak-coupling s-wave superconducting order parameter is obtained by

$$\Delta(\boldsymbol{r}; t) = -\frac{\lambda}{4} \int_{-\omega_{\mathrm{c}}}^{\omega_{\mathrm{c}}} \mathrm{d}\varepsilon \langle f^{\mathrm{K}}_{\uparrow\downarrow}(\boldsymbol{p}_{\mathrm{F}}, \boldsymbol{r}; \varepsilon, t) \rangle_{\hat{\mathbf{p}}_{\mathrm{F}}}, \tag{2.13}$$

where λ is the coupling constant and ω_{c} is the cut-off energy, which may be eliminated in favor of the transition temperature. The notation $\langle \ldots \rangle$ is to be understood as an angular averaging over the Fermi surface. In the special case of an equilibrium situation, one may express the Keldysh component in terms of the retarded and advanced Green's function by means of the relation

$$\hat{g}^{\mathrm{K}} = (\hat{g}^{\mathrm{R}} - \hat{g}^{\mathrm{A}}) \tanh(\beta\varepsilon/2), \tag{2.14}$$

where $\beta = T^{-1}$ is inverse temperature. In nonequilibrium situations, one must derive kinetic equations for nonequilbrium distribution functions in order to specify the Keldysh part.

In the dirty limit, the scattering time due to impurities satisfies $\zeta\tau \ll 1$, where τ is the impurity scattering time while ζ is the energy scale of any other self-energy in the problem. The Eilenberger equation is then reduced to the Usadel equation [30], which may be derived by expanding the Green's function in spherical harmonics and averaging the Eilenberger equation over the Fermi surface. The Usadel equation reads

$$D\nabla(\check{g}_s\nabla\check{g}_s) + \mathrm{i}[\varepsilon\hat{\rho}_3 - \Sigma_s, \check{g}_s] = 0, \tag{2.15}$$

where the 's' subscript indicates that the Green's function and self-energy has been averaged over the Fermi surface, thus rendering them independent of the direction of the momentum $\boldsymbol{p}_\mathrm{F}$. The diffusion constant is given by $D = v_\mathrm{F}^2\tau/3$. Although the Usadel equation in general requires a numerical solution, an analytical approach is permissable under certain conditions. In the case of a weak proximity effect, one may effectively linearize Eq. (2.15). This is a valid treatment for low transparency interfaces or close to T_c. In this case, Eq. (2.15) is expanded around the bulk solution. Also, it should be noted that the Green's function $\check{g}_s$ (hereafter dropping the subscript 's') may be conveniently parametrized to facilitate both analytical and numerical calculations. For instance, the Green's function in a S/F bilayer with a homogeneous magnetization may be parametrized as

$$\hat{g}_j = \begin{pmatrix} c_{\uparrow,j} & 0 & 0 & s_{\uparrow,j} \\ 0 & c_{\downarrow,j} & s_{\downarrow,j} & 0 \\ 0 & -s_{\downarrow,j} & -c_{\downarrow,j} & 0 \\ -s_{\uparrow,j} & 0 & 0 & -c_{\uparrow,j} \end{pmatrix}, \; j = \{S, F\} \tag{2.16}$$

where we have introduced $s_{\sigma,j} = \sinh(\theta_{\sigma,j})$ and $c_{\sigma,j} = \cosh(\theta_{\sigma,j})$. Note that $(\hat{g}_j)^2 = \hat{1}$ is satisfied. The parameter $\theta_{\sigma,j}$ is a measure of the proximity effect, and vanishes in the ferromagnetic region in the absence of a proximity effect. In the superconducting region, the bulk solution for a conventional s-wave BCS superconductor reads $c_\sigma = \cosh(\theta_\mathrm{BCS})$, $s_\sigma = \sigma\sinh(\theta_\mathrm{BCS})$, where $\theta_\mathrm{BCS} = \mathrm{atanh}(\Delta/\varepsilon)$.

The above equations suffice to completely describe for instance a bulk superconducting structure, but must be supplemented with boundary conditions when treating heterostructures such as F/S junctions. These boundary conditions take different forms depending on the physical properties of the interface, and we proceed to describe possible scenarios in this respect. Transport across interfaces in heterostructures may in general be characterized according to three particular properties: *i)* the transmission of the interface, *ii)* the resistivity of the compounds separated by the interface, and *iii)* whether the interface is spin-active or not. Let us clarify the distinction between the two first properties. The transmission of the barrier determines the likelihood of electron

transport to occur across the interface. On the other hand, the resistivities of the compounds separated by the interface are in principle unrelated to the transmissivity of the interface, and one may have for instance a tunneling contact with electrodes attached to it that have either a large or small resistance.

Zaitsev [31] derived boundary conditions for a clean N/S interface, while Kuprianov and Lukichev (KL) [18] worked out simplified boundary conditions in the dirty limit, valid for atomically sharp interfaces in the tunneling regime with a low barrier transparency. In a heterostructure with a region 1 located in the half-space $x < 0$ and a region 2 located in the half-space $x > 0$, the KL boundary conditions may be expressed as follows for the retarded part of the Green's function:

$$\begin{aligned} 2d_1\gamma_1(\hat{g}_1\partial_x\hat{g}_1)\Big|_{x=0} &= [\hat{g}_1,\hat{g}_2]\Big|_{x=0}, \\ 2d_2\gamma_2(\hat{g}_2\partial_x\hat{g}_2)\Big|_{x=0} &= -[\hat{g}_2,\hat{g}_1]\Big|_{x=0}. \end{aligned} \tag{2.17}$$

The parameter γ_j models the interfacial transmission properties, and is given by $\gamma_j = R_\mathrm{I}/R_j$ where R_I is the interface resistance while R_j is the resistance in region j. Also, d_j is the width of region j. In the case of an arbitrary interface transparency, the most compact way of writing the boundary conditions for the Green's functions for non-magnetic interface was introduced by Nazarov [19]:

$$\frac{\gamma_1 d_1}{2}\hat{g}_1\partial_x\hat{g}_1\Big|_{x=0} = \frac{[\hat{g}_1,\hat{g}_2]}{4+T(\{\hat{g}_1,\hat{g}_2\}-2)}\Big|_{x=0}, \tag{2.18}$$

and similarly for $\hat{g}_2$. We have here assumed that all N transmission channels at the interface are characterized by the same transmission probability, i.e. $T_N = T$. As seen, this reduces to the KL boundary condition in the tunneling limit $T \to 0$.

The third property determines to what degree the interface discriminates between incoming quasiparticles with different spins. In all the preceding references, a non-magnetic (spin-inactive) interface was assumed. The generalized boundary conditions for magnetically active interfaces have also been derived [32] and further studied in [33]. As a discussion of these boundary conditions requires an introduction of much extra notation, we refrain from this here and instead refer the reader to a detailed discussion in [33]. In Sec. 2.2.2, we will focus in particular on the spin-dependent phase shifts (see Sec. 2.1.4) that come into play when a magnetic barrier is present, which will be shown to have an appreciable effect on the physics when the term describing these phase-shifts in the boundary conditions is comparable in magnitude to the tunneling conductance $1/R_I$. In Sec. 2.2.1, we will use Nazarov's non-magnetic boundary conditions, thus implicitly assuming that the contribution from the spin-dependent phase shifts is much smaller than the tunneling conductance, as may be appropriate for a relatively weak ferromagnet.

Let us make a final remark concerning the treatment of interfaces in the quasiclassical theory of superconductivity. We previously stated that the present theory is valid as long as characteristic energies of various self-energies and perturbations in the system are much smaller than the Fermi energy. At first glance, this might seem to be irreconcilable with the presence of interfaces, which represent strong perturbations varying on atomic length scales. However, this problem may be overcome by including the interfaces as boundary conditions for the Green's functions rather than directly in the Eilenberger equation.

2.2 Research highlights

2.2.1 Numerical study of odd-frequency pairing in F/S bilayers

Upon establishing that odd-frequency pairing is ubiquitous in superconducting heterostructures, the natural question becomes: how may the odd-frequency pairing state be detected? To address this question thoroughly, we employ a numerical study using quasiclassical theory of the proximity effect in a F/S bilayer. In our study, we take into account realistic effects which are often neglected in the literature, namely a non-ideal interface region (finite interface transparency), magnetic impurities in the samples, and the effect of spin-orbit coupling. Also, we do not restrict ourselves to the weak proximity effect regime.

Let us consider here a situation where the F region is located in the space $x \in [0, d]$, while the S region occupies the space $x > d$. The main ingredients in the calculation are the Usadel equation and the boundary conditions for it. For majority and minority spin ($\sigma = \uparrow, \downarrow = \pm 1$) in the ferromagnet, the Usadel equation reads:

$$D\partial_x^2\theta_\sigma + 2\mathrm{i}(\varepsilon + \sigma h)\sinh\theta_\sigma - \frac{\sigma S_{xy}}{2\tau_{\mathrm{sf}}}\sinh(\theta_\uparrow - \theta_\downarrow) - \frac{S_z}{4\tau_{\mathrm{sf}}}\sinh 2\theta_\sigma - \frac{1}{2\tau_{\mathrm{so}}}\sinh(\theta_\uparrow + \theta_\downarrow) = 0, \tag{2.19}$$

where we have made use of Eqs. (2.15) and (2.16). Here, D is the diffusion constant, ε is the quasiparticle energy measured from Fermi level, h is the exchange field, τ_{sf} denotes the spin-flip scattering time, τ_{so} denotes the spin-orbit scattering time, while the coefficients S_{xy} and S_z determine the anisotropy of the magnetic scattering. The parameters θ_σ are related to the Green's function $\hat{g}_F$ in the ferromagnet as measures of the proximity effect ($\theta_\sigma = 0$ in the absence of a proximity effect) [16].

To model the interface regions, we employ Nazarov's boundary condition which is valid in the diffusive regime for an interface region of arbitrary conductance (transparency). At $x = \{0, d\}$, it reads

$$\frac{\gamma_{L,R}d}{2}\hat{g}_F\partial_x\hat{g}_F\bigg|_{x=\{0,d\}} = \mp\frac{[\hat{g}_F, \hat{g}_{L,R}]}{4 + T(\{\hat{g}_F, \hat{g}_{L,R}\} - 2)}\bigg|_{x=\{0,d\}}, \tag{2.20}$$

where $[\ldots]$ and $\{\ldots\}$ denote the commutator and anticommutator, respectively, and $\hat{g}_{L,R}$ denotes the Green's function on the left and right side of the ferromagnet. The parameter $\gamma_{L,R} = R_B^{L,R}/R_F$ denotes the ratio between the resistance in the left/right barrier region $R_B^{L,R}$ and the resistance in the F region R_F. We have conventionally introduced the parameter T, which is the transmissivity of the interface [19]. Giving an expression for T in terms of microscopic parameters of the interface is not very practical, and we will therefore use T as a phenomenological parameter to characterize the transparency of the interface. Here, $T = 0$ corresponds to zero transmission of quasiparticles incident on the superconducting interface, and $T = 1$ corresponds to perfect transmission. Note that we here do not consider the influence of spin-DIPS on the spectra, assuming that the phase-shifts are neglible compared to the conductance of the interface.

For later use, we define the superconducting coherence length $\xi = \sqrt{D/\Delta}$. As a measure of the strength of the spin-flip and spin-orbit scattering, which increases with decreasing spin relaxation time, we introduce $g_{\rm sf} = \tau_{\rm sf}^{-1}$ and $g_{\rm so} = \tau_{\rm so}^{-1}$. Also note that $S_z = S_{xy} = 1$ for isotropic spin-flip scattering, while $S_z = 3$ and $S_{xy} = 0$ for uniaxial spin-flip scattering along the **z**-direction. For each case, the dimensionless coefficient g represents the scattering strength divided on the Thouless energy, i.e. when studying the effect of spin-orbit coupling we have $g = g_{\rm so}/\varepsilon_T$. The spin-resolved and normalized DOS is finally obtained as

$$N_\uparrow = \mathrm{Re}\{\cosh\theta_\uparrow\},\ N_\downarrow = \mathrm{Re}\{\cosh\theta_\downarrow\}. \tag{2.21}$$

Furthermore, we define the total DOS as $N = \sum_\sigma N_\sigma/2$. We have then obtained two coupled nonlinear second order differential equations supplemented with boundary conditions which may be solved numerically.

As an example of the results attainable in our formalism, consider Fig. 2.2, where the local density of states (LDOS) is plotted for the case $h \gg \Delta$, but still considering a relatively weak ferromagnet. For $h/\Delta = 50$ (lower row), the proximity is quite weak such that neither magnetic impurity nor spin-orbit scattering influence the LDOS much at all. For $h/\Delta = 15$, the distinction between their influences can be seen more clearly. Setting $g = 0$, the LDOS is suppressed at subgap energies as might be expected due to the induced minigap from the superconducting correlations. Increasing the scattering rate g, the LDOS evolves qualitatively different upon comparing the magnetic impurity scattering with the spin-orbit scattering. In the former case, it enhances the subgap energy LDOS while in the latter case it completely suppresses it. As we shall see below, this effect pertains to the symmetry of the singlet and triplet components of the proximity-induced superconducting anomalous Green's functions, defined as:

$$\begin{aligned} f_s(\varepsilon,x) &= [\sinh\theta_\uparrow(\varepsilon,x) - \sinh\theta_\downarrow(\varepsilon,x)]/2, \\ f_t(\varepsilon,x) &= [\sinh\theta_\uparrow(\varepsilon,x) + \sinh\theta_\downarrow(\varepsilon,x)]/2. \end{aligned} \tag{2.22}$$

Since we are considering the diffusive limit, the Green's functions must have even parity symmetry, since the frequent impurity scattering would destroy any

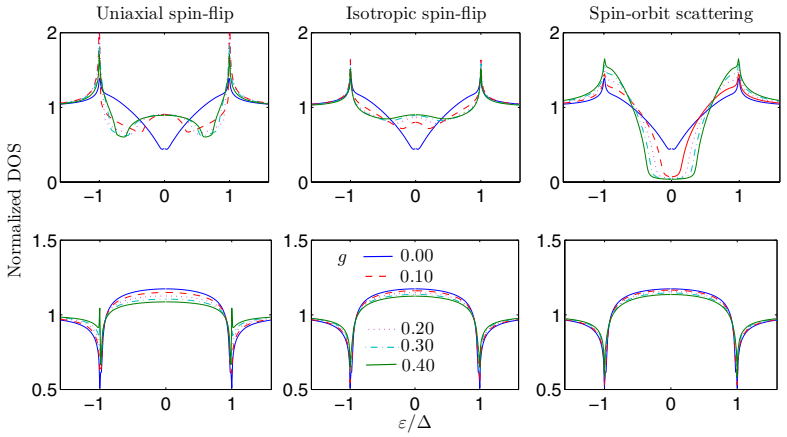

Figure 2.2: Local density of states at $x = 0$ for $h/\Delta = 15$ (upper row) and $h/\Delta = 50$ (lower row). Here, we have fixed $d/\xi = 0.1$ and $T = 0.5$ and study the role of different types of spin-dependent scattering.

odd parity component due to the isotropization. The Pauli principle then dictates that the spin-singlet component must have an even-frequency symmetry, just as for conventional BCS superconductors. In this case, it is known that the superconducting correlations tend to suppress the LDOS by inducing an energy gap. In contrast, the triplet component has an odd-frequency symmetry in the diffusive limit, and its tendency is opposite: it enhances the LDOS at low energies, since it is gapless there. Bearing this in mind, it is instructive to consider the Usadel equations in the ferromagnetic region in limiting cases. From Eq. (2.19), we obtain several important properties:

- In the presence of uniaxial spin-flip scattering ($S_z = 3, S_{xy} = 0$), by taking the limit of $\tau_{\rm sf} \to 0$ we get $\theta_\uparrow = \theta_\downarrow = 0$. Then both singlet and triplet components are suppressed. This is also the case for isotropic spin-flip scattering ($S_z = S_{xy} = 1$).

- With in-plane spin-flip scattering ($S_z = 0$), we get $\theta_\uparrow = \theta_\downarrow$ when taking the limit $\tau_{\rm sf} \to 0$. Then, the singlet component should vanish as seen from definition in Eq. (2.22).

- In the presence of pure spin-orbit scattering ($S_z = S_{xy} = 0$), by taking limit of $\tau_{\rm so} \to 0$ we get $\theta_\uparrow = -\theta_\downarrow$. Then, the triplet component should vanish as seen from Eq. (2.22).

Therefore, we find that uniaxial and isotropic spin-flip scattering is harmful to both singlet and triplet components while in-plane spin-flip scattering and spin-orbit scattering are detrimental to the singlet and triplet components, respectively. The physical manifestation of this is in the form of either a gap structure in the LDOS (induced by the singlet component) or a peak structure

(induced by the triplet component).

The above analysis emphasizes the importance of distinguishing between different types of spin-dependent scattering in terms of understanding the behavior of the DOS in a ferromagnet/superconductor bilayer. In particular, we have shown that the effect of spin-orbit scattering may differ fundamentally from spin-flip scattering (originating *e.g.* from magnetic impurities), and that this is manifested in the interplay between the singlet and triplet anomalous Green's function in the ferromagnetic layer. If the former dominates, the LDOS is suppressed, while if the latter dominates the LDOS is enhanced. The optimal conditions for generation of a strong odd-frequency proximity-amplitude in a F/S bilayer would then be to have an in-plane anisotropy for the magnetic impurity scattering and weak spin-orbit coupling.

2.2.2 Pairing symmetry transition induced by a spin-active interface in superconducting junctions

As shown in the previous sections, odd-frequency pairing is an exotic type of pairing state which should be generated whenever time-reversal symmetry or translational symmetry in space is broken. There are, however, two main difficulties associated with the detection of the odd-frequency state. One is that the odd-frequency state induced in S/F bilayers has a short penetration depth into the ferromagnetic region. It is limited by the magnetic coherence length ξ_F, which is much smaller than the superconducting coherence length ξ_S [20]. Another problem is that these odd-frequency correlations are often masked by the simultaneous presence of even-frequency correlations in the same material. Clear-cut signatures of the odd-frequency correlations are therefore only accessible in a limited parameter regime, as seen in the previous section.

In the majority of works on superconducting proximity-structures, the diffusive limit and spin-inactive interfaces have been considered [18]. For a non-magnetic bilayer, a minigap appears in the density of states of the normal metal. It scales with the Thouless energy of the normal layer and with the transmission probability of the interface. For a spin-active interface, the transmission properties of spin-$\uparrow$ and spin-$\downarrow$ electrons into a ferromagnetic metal are different, and this gives rise to both spin-dependent conductivities and spin-dependent phase shifts at the interface [32, 33, 34, 35, 36]. Here, we show that a spin-active interface in an S|N bilayer produces clear signatures of purely odd-frequency triplet pairing amplitudes that can be tested experimentally.

Let us consider the system shown in Fig. 2.3. The superconductor is conventional (even-frequency s-wave) while the interface is magnetic. We find that there is a dramatic change in the nature of proximity correlations when the spin-dependent phase shifts exceed the tunneling probability of the interface. The spin-active interface in a superconductor/normal metal (S|N) bilayer causes the even-frequency correlations to vanish at zero excitation energy (Fermi level), while odd-frequency correlations appear. At the same time, the minigap, one of

the hallmarks of the conventional proximity effect, is replaced by a low-energy band with enhanced density of states. We focus on the density of states (DOS) in the normal region, which can be probed by tunneling experiments. Since the exchange field is absent in the normal metal, our findings suggest that it should be possible to detect the odd-frequency amplitude without any interfering effects of even-frequency correlations. This resolves the two main difficulties associated with the experimental detection of odd-frequency correlations mentioned above.

We adopt the quasiclassical theory of superconductivity [23, 24], where information about the physical properties of the system is embedded in the Green's function. For an equilibrium situation, it suffices to consider the retarded part of the Green's function, here denoted $\hat{g}$. Due to the symmetry properties of $\hat{g}$, one may parametrize it conveniently in the normal (N) region by a parameter θ_σ, which allows for both singlet and triplet correlations [16]. In the superconducting (S) region, we employ the bulk solution $\hat{g}_S = c \cdot \underline{\tau_3} \otimes \underline{\sigma_0} + s \cdot \underline{\tau_1} \otimes (\mathrm{i}\underline{\sigma_2})$, $c = \cosh(\theta)$, $s = \sinh(\theta)$, $\theta = \operatorname{atanh}(\Delta/\varepsilon)$, $\underline{\tau_i}$ and $\underline{\sigma_i}$ being Pauli matrices in particle-hole and spin space, respectively.

We use the formalism described in Ref. [16], and consider the diffusive limit. Then, the orbital symmetry for all proximity amplitudes is reduced to s-wave and hence the singlet component always has an even-frequency symmetry while the triplet component has an odd-frequency symmetry. The Green's functions are subject to boundary conditions, which assume at the S|N interface in the tunneling limit the form [33, 36]: $2\gamma d\hat{g}_N \partial_x \hat{g}_N = [\hat{g}_S, \hat{g}_N] + \mathrm{i}(G_\phi/G_T)[\underline{\tau_0} \otimes \underline{\sigma_3}, \hat{g}_N]$, and at the outer interface read $\partial_x \hat{g}_N = \hat{0}$. Here, $\gamma = R_B/R_N$ where R_B (R_N) is the resistance of the barrier (normal region), and d is the width of the normal region, while G_T is the junction conductance in the normal-state. The boundary condition above contains an additional term G_ϕ compared to the usual non-magnetic boundary conditions in Ref. [18]. This term is due to spin-dependent phase shifts of quasiparticles being reflected at the interface. G_ϕ may be non-zero even if the transmission $G_T \to 0$, corresponding to a ferromagnetic insulator [33]. We define the superconducting coherence length $\xi_S = \sqrt{D/\Delta}$ and Thouless energy $\varepsilon_{\mathrm{Th}} = D/d^2$, where D is the diffusion constant, and assume that the inelastic scattering length, l_{in}, is sufficiently large, such that $d \ll l_{\mathrm{in}}$.

The Usadel [30] equation reads $D\partial_x^2\theta_\sigma + 2\mathrm{i}\varepsilon \sinh\theta_\sigma = 0$, with boundary condition $\gamma d \partial_x \theta_\sigma = (cs_\sigma - \sigma s c_\sigma) + \mathrm{i}\sigma(G_\phi/G_T)s_\sigma$ at $x = 0$ and $\partial_x\theta_\sigma = 0$ at $x = d$. Here,

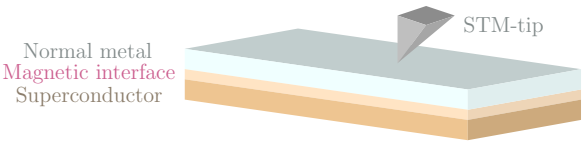

Figure 2.3: Proposed experimental setup for observation of the odd-frequency component in a diffusive normal metal layer|superconductor junction.

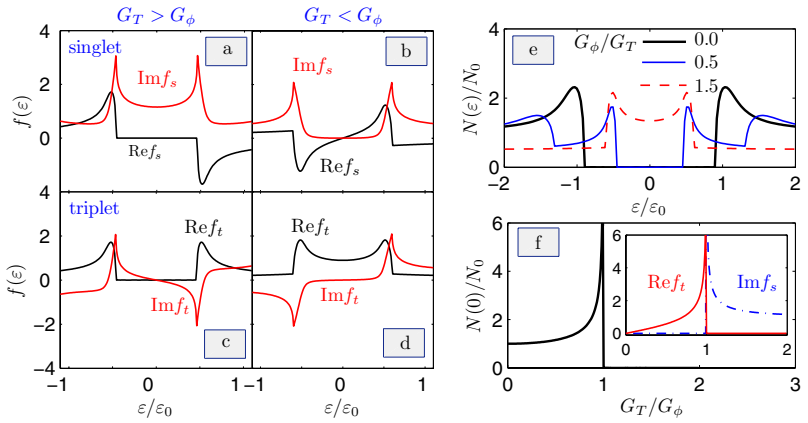

Figure 2.4: The singlet and triplet proximity amplitudes induced in the normal metal are shown for $G_\phi/G_T < 1$ [in a) and c)] and $G_\phi/G_T > 1$ [in b) and d)]. In e), we plot the energy-resolved DOS for several values of G_ϕ/G_T. Finally, f) shows the zero-energy DOS as a function of G_T/G_ϕ, with the proximity amplitudes shown in the inset.

$c_\sigma = \cosh(\theta_\sigma)$ and $s_\sigma = \sinh(\theta_\sigma)$. At zero energy, we find that the pairing amplitudes are either purely (odd-frequency) triplet,

$$f_s(0) = 0,\ f_t(0) = \frac{G_T \cdot \mathrm{sgn}(G_\phi)}{\sqrt{G_\phi^2 - G_T^2}} \quad \text{for } |G_\phi|/G_T > 1, \tag{2.23}$$

or purely (even-frequency) singlet

$$f_s(0) = \frac{\mathrm{i} \cdot G_T}{\sqrt{G_T^2 - G_\phi^2}},\ f_t(0) = 0 \quad \text{for } |G_\phi|/G_T < 1. \tag{2.24}$$

Thus, the presence of G_ϕ induces an odd-frequency component in the normal layer. The remarkable aspect of Eqs. (2.23) and (2.24) is that they are valid for any value of the width d below the inelastic scattering length, and for any interface parameter γ. Thus, the vanishing of the singlet component is a robust feature in S|N structures with spin-active interfaces, as long as $|G_\phi|/G_T > 1$. Without loss of generality, we focus on positive values of G_ϕ from now on.

The DOS is given as $N(\varepsilon)/N_0 = \sum_\sigma \mathrm{Re}\{c_\sigma\}/2$, yielding

$$N(0)/N_0 = \mathrm{Re}\{G_\phi/\sqrt{G_\phi^2 - G_T^2}\}. \tag{2.25}$$

At zero-energy, the DOS thus vanishes as long as $G_\phi/G_T < 1$, which means that the usual minigap in S|N structures survives in this regime. However, the zero-energy DOS is enhanced for $G_\phi/G_T > 1$ since the singlet component vanishes there.

The full energy-dependence of the DOS may only be obtained numerically. To model a realistic experimental setup, we fix $\gamma = 10$ and $d/\xi_S = 1.0$, although our qualitative results are independent of these particular choices. As a measure of the relevant energy scale, we define $\varepsilon_0 = \varepsilon_{\rm Th}/(2\gamma)$. The results are shown in Fig. 2.4 to investigate the effect of the spin-dependent phase shifts. The low-energy DOS is strongly enhanced due to the odd-frequency amplitude when $G_\phi/G_T > 1$ ($G_\phi/G_T = 1.5$ in the figure). Conversely, the DOS develops a minigap around $\varepsilon = 0$ when $G_\phi/G_T < 1$ ($G_\phi/G_T = 0.5$ in the figure). The ratio G_ϕ/G_T depends on the microscopic barrier properties [36]. In the tunneling limit, one finds that G_ϕ can be considerably larger than G_T. Although not included here, we underline that performing the same analysis in the ballistic limit gives the same result: namely, a complete separation between the even- and odd-frequency proximity amplitudes above a critical value of the interface resistance. This suggests that the effect predicted here should be quite robust, as it is occurs both in the clean and dirty limit and is independent of the specific system size and/or junction conductance.

We suggest the following qualitative explanation for the mechanism behind the separation between even- and odd-frequency correlations. The superconductor induces a minigap proportional to G_T in the normal metal, while the spin-active barrier induces an effective exchange field proportional to G_ϕ. The situation in the normal metal then resembles that of a thin-film conventional superconductor in the presence of an in-plane external magnetic field [37], with the role of the gap and field played by G_T and G_ϕ, respectively. In that case, it is known that superconductivity is destroyed above the Clogston-Chandrasekhar limit [38], due to pair-breaking of a spin-singlet Cooper-pair. In the present case, we observe coexistence of the exchange field and spin-singlet even-frequency superconductivity as long as G_ϕ is below the critical value of $G_\phi = G_T$. However, for $G_\phi > G_T$ spin-singlet pairing is no longer possible at the chemical potential. It is then replaced by spin-triplet pairing, which must be odd in frequency due to the isotropization of the gap in the diffusive limit. Thus, there is a natural separation between even-frequency and odd-frequency pairing in the normal metal at a critical value of the effective exchange field G_ϕ.

The simplest experimental manifestation of the odd-frequency component is probably a zero-energy peak in the DOS [39, 40, 41]. In S|F layers, where this phenomenon has been discussed previously, a clear zero-energy peak is unfortunately often masked by the simultaneous presence of singlet correlations f_s, which tend to suppress the DOS at low energies. This is not so in the system we consider, provided only that $G_T < |G_\phi|$. This is ideal for a direct observation of the odd-frequency component, manifested as a zero-energy peak in the DOS. The even-frequency correlations vanish completely when the interface transmission is sufficiently low, and the parameter G_ϕ can be increased by increasing the magnetic polarization of the barrier separating the superconducting and normal layers. By fabricating several samples with progressively increasing strength of magnetic moment of the barrier, one should be able to observe an abrupt crossover at the zero-energy DOS above a certain strength of

the magnetic moment. Alternatively, one could alter the interface transmission by varying the thickness of the insulating region.

Chapter 3

Interplay between ferromagnetism, noncentrosymmetricity, and superconductivity in bulk materials

In this chapter, we investigate the intrinsic coexistence of ferromagnetism, noncentrosymmetricity, and superconductivity in bulk materials. The noncentrosymmetricity of the crystal structure gives rise to spin-orbit coupling effects, which have strong impact on the nature of the superconducting state, while ferromagnetism also places strict restrictions on the possible realizations of superconductivity. Papers I, II, III, VI, XIV, XVII, and XIX are devoted to a study of these issues.

3.1 Fundamental concepts

3.1.1 Ferromagnetic superconductors

The very idea of a ferromagnetic superconductor may at first sight seem to be a contradiction in terms. Almost all known superconductors have a spinless singlet Cooper pair symmetry, and the superconducting state is often completely antagonistic towards any interior magnetic field. Having stated this, however, one should hasten to add that there are actually circumstances which allow superconductivity and magnetism to coexist in a stable manner. One of these circumstances is the mixed state of a type II superconductor [42], where an applied magnetic field is able to penetrate the superconductor in quantized vortices upon exceeding a lower critical field H_{c1}. The vortex consists of a normal core of size ξ where the superconducting order parameter rapidly falls towards zero in the center of the core. The magnetic flux, however, is distributed roughly over a circle centered at the normal core with a radius λ, which may differ greatly

in magnitude from ξ. In this scenario, superconductivity and magnetism may coexist in a non-uniform manner in between the vortex cores. Another way of avoiding the problem with the hostile environment for magnetism in a superconductor is to use a geometry which suppresses the Meissner effect originating from the broken gauge symmetry. For instance, it has been shown that in a thin-film geometry where the thickness t of the superconducting film satisfies $t \ll \xi, \lambda$, the Meissner effect is so strongly suppressed that the paramagnetic limitation is the decisive factor in terms of when superconductivity is destroyed [37]. In this way, one obtains effectively coexistence of spinless singlet superconductivity and a Zeeman-splitting in the superconductor induced by the external field.

However, the coexistence of magnetism and spin-triplet superconductivity appears to be a more promising scenario, since the Cooper pairs may use their spin degree of freedom to align themselves with a magnetic field. Spin-triplet superconductors are characterized by a multicomponent order parameter, which for the simplest case of a p-wave symmetry[1] may be expressed in terms of three independent components of a $\boldsymbol{d_k}$-vector [43]:

$$\boldsymbol{d_k} = \Big[\frac{\Delta_{\boldsymbol{k}\downarrow\downarrow} - \Delta_{\boldsymbol{k}\uparrow\uparrow}}{2}, \frac{-\mathrm{i}(\Delta_{\boldsymbol{k}\downarrow\downarrow} + \Delta_{\boldsymbol{k}\uparrow\uparrow})}{2}, \Delta_{\boldsymbol{k}\uparrow\downarrow}\Big]. \tag{3.1}$$

Note that $\boldsymbol{d_k}$ transforms like a vector under spin rotations, and that it has an odd parity with respect to inversion of momentum, $\boldsymbol{k} \to (-\boldsymbol{k})$. In terms of the components of $\boldsymbol{d_k}$, the order parameter itself is a 2x2 matrix that reads

$$\hat{\Delta}_{\alpha\beta}(\boldsymbol{k}) \equiv \langle c_{\boldsymbol{k},\alpha} c_{\boldsymbol{k},\beta} \rangle = [\mathrm{i}(\boldsymbol{d_k} \cdot \hat{\boldsymbol{\sigma}})\hat{\sigma}_y]_{\alpha\beta}, \tag{3.2}$$

where $\hat{\boldsymbol{\sigma}}$ is the vector of Pauli matrices, and $\{c^\dagger_{\boldsymbol{k},\alpha}, c_{\boldsymbol{k},\alpha}\}$ are the usual electron creation-annihilation operators for momentum $\boldsymbol{k}$ and spin α. The superconducting order parameter is characterized as *unitary* if the modulus of the gap is proportional to the unity matrix: $(\hat{\Delta} \cdot \hat{\Delta}^\dagger) \propto \check{1}$. Written in terms of the vector $\boldsymbol{d_k}$, this condition is equivalent to the requirement that $\langle \mathbf{S_k} \rangle = 0$, where we have introduced the net magnetic moment (or spin) of the Cooper pair

$$\langle \mathbf{S_k} \rangle \equiv \mathrm{i}(\boldsymbol{d_k} \times \boldsymbol{d_k^*}). \tag{3.3}$$

The *unitary* triplet state thus has Cooper pairs with zero magnetic moment, whereas the *non-unitary* state is characterized by non-zero value of $\langle \mathbf{S_k} \rangle \neq 0$. The latter effectively means that time-reversal symmetry is spontaneously broken in the spin part of the Cooper pairs. It is thus intuitively clear that having the spin of the Cooper pair aligned with the internal magnetic field of the ferromagnet can lower the energy of the resulting coexistence state. Distinguishing between unitary and non-unitary states in ferromagnetic superconductors is clearly one of the primary objectives in terms of identifying the correct SC order parameter.

[1] A p-wave Cooper pair has a total angular momentum of $L = 1$.

There are still many unresolved issues regarding the nature of the superconducting state in ferromagnetic superconductors, such as whether the two orders coexist uniformly or in a non-uniform way. There does, however, seem to be a general consensus regarding the pairing symmetry of the Cooper pair: only an equal spin-pairing triplet state could possibly survive the considerable Zeeman splitting in these materials, such that the order parameter realized in the ferromagnetic superconductors most likely is p-wave. Also, the Ginzburg-Landau free energy expansion strongly suggests precisely such a non-unitary spin-triplet state due to the lowest order coupling term $\gamma(\boldsymbol{d_k} \times \boldsymbol{d_k}^*) \cdot \boldsymbol{M}$, which favors a Cooper pair spin parallel or antiparallel to the bulk magnetization, depending on the sign of γ. Here $\boldsymbol{d_k}$ is a vector describing triplet superconducting pairing [43], while $\boldsymbol{M}$ is the bulk magnetization.

3.1.2 Noncentrosymmetric superconductors

The orbital symmetry of the superconducting order parameter ultimately reflects the environment it resides in, i.e. the crystal lattice of the superconducting compound. In general, the superconducting order parameter may be expanded in basis functions for irreducible representations of the crystal point group. In the case of a crystal with a center of inversion, this categorization leads to a superconducting order parameter with a definite parity in the quasiparticle basis that yields a diagonal kinetic energy. If the crystal of the compound lacks a center of inversion, i.e. it is noncentrosymmetric, this leads to an interesting singlet-triplet mixing of the superconducting order parameter, such that it lacks a definite parity in a spin basis. To label the bands split by spin-orbit coupling (SOC) and ferromagnetism (FM), it is possible to introduce a *pseudospin* basis in which the normal-state Hamiltonian is diagonalized. In the original spin basis, the SC matrix order parameter is characterized, in analogy to the p-wave state [43], by a vector $\boldsymbol{d_k}$ and scalar Δ_s so that $\hat{\Delta}_{\alpha\beta}(\boldsymbol{k}) = \mathrm{i}\Delta_s\hat{\sigma}_y + [\mathrm{i}(\boldsymbol{d_k}\cdot\hat{\boldsymbol{\sigma}})\hat{\sigma}_y]_{\alpha\beta}$. Note that, unlike the usual p-wave SC, a singlet component Δ_s of the gap will also be present since antisymmetric SOC in general mixes the parity of the order parameter.

$CePt_3Si$ was found to be the first superconducting heavy-fermion compound without a center of inversion in its crystal structure in 2004 [44]. Since then, the list of noncentrosymmetric superconductors has grown considerably. Due to the peculiarity with the intrinsic singlet-triplet mixing in noncentrosymmetric superconductors, they have attracted a lot of interest in recent years in order to unveil important fingerprints of their unusual pairing symmetry. In this context, transport measurements such as point-contact spectroscopy and Josephson tunneling have traditionally proven themselves as useful tools in order to probe essential features of the superconducting pairing symmetry. An interesting feature about noncentrosymmetric superconductors is that it has been predicted that the conductance spectra of a normal metal/noncentrosymmetric superconductor junction, *e.g.* a STM-tip tunneling experiment, should exhibit striking features at voltages equal to the sum and difference between the singlet and triplet gaps [45, 46]. Other studies have focused on strong spin-currents

[47] and fractional flux quanta [48] near the interfaces of noncentrosymmetric superconductors.

3.2 Research highlights

3.2.1 Thermodynamics of ferromagnetic superconductors

Basic model

We write down a mean-field theory Hamiltonian with equal-spin pairing Cooper pairs and a finite magnetization along the easy-axis similar to the model studied in Refs. [49, 50], namely

$$\begin{aligned}\hat{H} = &\sum_{\boldsymbol{k}} \xi_{\boldsymbol{k}} + \frac{INM^2}{2} - \frac{1}{2}\sum_{\boldsymbol{k}\sigma} \Delta^{\dagger}_{\boldsymbol{k}\sigma\sigma} b_{\boldsymbol{k}\sigma\sigma} \\ &+ \frac{1}{2}\sum_{\boldsymbol{k}\sigma} \left(\hat{c}^{\dagger}_{\boldsymbol{k}\sigma} \hat{c}_{-\boldsymbol{k}\sigma}\right) \begin{pmatrix} \xi_{\boldsymbol{k}\sigma} & \Delta_{\boldsymbol{k}\sigma\sigma} \\ \Delta^{\dagger}_{\boldsymbol{k}\sigma\sigma} & -\xi_{\boldsymbol{k}\sigma} \end{pmatrix} \begin{pmatrix} c_{\boldsymbol{k}\sigma} \\ c^{\dagger}_{-\boldsymbol{k}\sigma} \end{pmatrix}, \end{aligned} \tag{3.4}$$

where $b_{\boldsymbol{k}\sigma\sigma} = \langle c_{-\boldsymbol{k}\sigma} c_{\boldsymbol{k}\sigma} \rangle$ is the non-zero expectation value of the pair of Bloch states, I is the exchange coupling, N is the number of lattice sites, M is the magnetic order parameter, and $\Delta_{\boldsymbol{k}\sigma}$ is the superconducting gap for spin species σ. It is implicit in our notation that $\xi_{\boldsymbol{k}\sigma} = \varepsilon_{\boldsymbol{k}} - \sigma h - E_F$ is measured from Fermi level, where $\varepsilon_{\boldsymbol{k}}$ is the band dispersion. For further details, it is also instructive to consider the Ginzburg-Landau theory for a ferromagnetic superconductor treated in Ref. [51]. Also, the Bogoliubov-de Gennes eqations for a number of possible pairing symmetries in a ferromagnetic superconductor were comprehensively studied in Ref. [52]. After diagonalizing the Hamiltonian Eq. (3.4), we arrive at

$$\hat{H} = \frac{1}{2}\sum_{\boldsymbol{k}\sigma} (\xi_{\boldsymbol{k}\sigma} - E_{\boldsymbol{k}\sigma} - \Delta^{\dagger}_{\boldsymbol{k}\sigma\sigma} b_{\boldsymbol{k}\sigma\sigma}) + \frac{INM^2}{2} + \sum_{\boldsymbol{k}\sigma} E_{\boldsymbol{k}\sigma} \hat{\gamma}^{\dagger}_{\boldsymbol{k}\sigma} \hat{\gamma}_{\boldsymbol{k}\sigma}, \tag{3.5}$$

where $\{\hat{\gamma}_{\boldsymbol{k}\sigma}, \hat{\gamma}^{\dagger}_{\boldsymbol{k}\sigma}\}$ are new fermion operators and $E_{\boldsymbol{k}\sigma} = \sqrt{\xi^2_{\boldsymbol{k}\sigma} + |\Delta_{\boldsymbol{k}\sigma\sigma}|^2}$. From this, one finds that the mean-field equations for the magnetic and superconducting order parameters become [49]

$$\begin{aligned} M &= -\frac{1}{N}\sum_{\boldsymbol{k}\sigma} \frac{\sigma \xi_{\boldsymbol{k}\sigma}}{2E_{\boldsymbol{k}\sigma}} \tanh(\beta E_{\boldsymbol{k}\sigma}/2), \\ \Delta_{\boldsymbol{k}\sigma\sigma} &= -\frac{1}{N}\sum_{\boldsymbol{k}'} V_{\boldsymbol{k}\boldsymbol{k}'\sigma\sigma} \frac{\Delta_{\boldsymbol{k}'\sigma\sigma}}{2E_{\boldsymbol{k}'\sigma}} \tanh(\beta E_{\boldsymbol{k}'\sigma}/2). \end{aligned} \tag{3.6}$$

For concreteness, we now consider a specific form of the gaps, assuming that they have a p-wave symmetry and that they are fixed on the Fermi surface in the weak-coupling limit. We choose:

$$\Delta_{\boldsymbol{k}\sigma\sigma} = \Delta_{\bar{\boldsymbol{k}}_F\sigma\sigma} = \frac{\Delta_{\sigma,0}}{\sqrt{3/8\pi}} Y^{\sigma}_{l=1}(\theta, \phi), \tag{3.7}$$

where $\bar{\boldsymbol{k}}_F$ is the normalized Fermi wave-vector, such that the gap only depends on the direction of the latter. We have introduced the spherical harmonics

$$Y^{\sigma}_{l=1}(\theta,\phi) = -\sigma\sqrt{3/8\pi}\mathrm{e}^{\mathrm{i}\sigma\theta}\sin\phi, \tag{3.8}$$

such that the gaps in Eq. (3.7) experience a change in sign under inversion of momentum, i.e. $\theta \to \theta + \pi$. We shall consider the case $\sin\phi = 1$ which renders the magnitude of the gaps to be constant, similar to the A2-phase in liquid ^{3}He. The motivation for this is that it seems plausible that a spatially uniform coexistence of ferromagnetic and superconducting order may only be realized in thin-film structures where the Meissner (diamagnetic) response of the superconductor is suppressed for in-plane magnetic fields. This enables us to set $\sin\phi = 1$, since the electrons are restricted from moving in the $\hat{\mathbf{z}}$-direction in a thin-film structure. In a bulk structure, we expect that a spontaneous vortex lattice should be the favored thermodynamical state [53]. We remind the reader that the A1- and A2-phases of liquid ^{3}He are defined as $\{\Delta_{\boldsymbol{k}\uparrow\uparrow} \neq 0, \Delta_{\boldsymbol{k}\downarrow\downarrow} = 0\}$ and $\{\Delta_{\boldsymbol{k}\uparrow\uparrow} \neq \Delta_{\boldsymbol{k}\downarrow\downarrow} \neq 0\}$, respectively.

The pairing potential may now be written as

$$V_{\sigma\sigma}(\theta,\theta') = -\frac{8\pi g}{3}Y^{\sigma}(\theta)[Y^{\sigma}(\theta')]^*, \tag{3.9}$$

and in their integral form, the gap equations read

$$\begin{aligned} M &= -\frac{1}{2}\sum_{\sigma}\sigma\int_{-E_F-\sigma IM}^{\infty}\mathrm{d}\varepsilon\frac{\varepsilon N^{\sigma}(\varepsilon)}{\sqrt{\varepsilon^2+\Delta^2_{\sigma,0}}}\tanh[\beta E_{\sigma}(\varepsilon)/2], \\ 1 &= \frac{g}{2}\int_{-\omega_0}^{\omega_0}\mathrm{d}\varepsilon\frac{N^{\sigma}(\varepsilon)}{E_{\sigma}(\varepsilon)}\tanh[\beta E_{\sigma}(\varepsilon)/2], \end{aligned} \tag{3.10}$$

where ω_0 is the cut-off frequency for the bosons responsible for the attractive pairing and g is the strength of the pairing.

Zero temperature case

Consider now $T = 0$, where we are able to obtain analytical expressions for the superconductivity order parameters in the problem. Since the superconductivity gap equation reduces to

$$1 = \frac{g}{2}\int_{-\omega_0}^{\omega_0}\mathrm{d}\varepsilon\frac{N^{\sigma}(\varepsilon)}{E_{\sigma}(\varepsilon)}, \tag{3.11}$$

one readily finds

$$\Delta_{\sigma,0} = 2\omega_0\mathrm{e}^{-1/c\sqrt{1+\sigma\tilde{M}}},\ \sigma = \uparrow,\downarrow \tag{3.12}$$

where we have defined $\tilde{M} = IM/E_F$, i.e. the exchange energy scaled on the Fermi energy. Moreover, the weak coupling constant $c = gN(0)/2$ will be set to 0.2, unless specifically stated otherwise. Moreover, we set $\tilde{\omega}_0 = \omega_0/E_F = 0.01$ as the typical spectral width of the bosons responsible for the attractive pairing

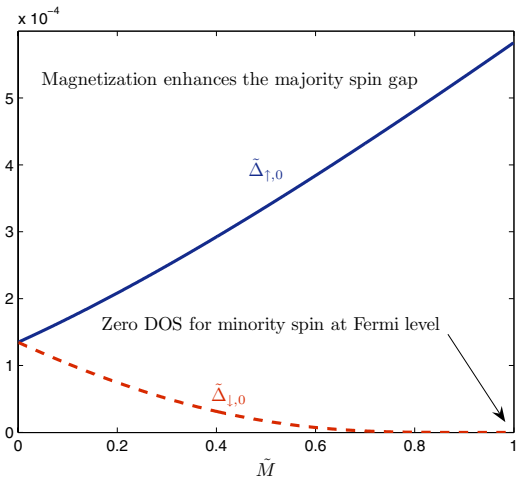

Figure 3.1: Superconducting gaps normalized to the Fermi energy (full drawn line: majority spin, dashed line: minority spin) as a function of the magnetization with $\tilde{\omega}_0 = 0.01$. When the exchange splitting equals the Fermi energy, the DOS of minority spin fermions is zero at Fermi level, resulting in a complete suppression of $\tilde{\Delta}_{\downarrow,0}$.

potential. From Eq. (3.12), we see that the effect of increasing the magnetization is an increase in the gap for majority spin. The important influence of the magnetization is that it modifies the density of states, which affects the superconductivity gaps. For $\tilde{M} = 1$, i.e. an exchange splitting equal to the Fermi energy, the minority spin gap is completely suppressed, as shown in Fig. 3.1. Thus, the presence of magnetization reduces the available phase space for the minority spin Cooper pairs, suppressing the gap and the critical temperature compared to the pure BCS case.

Finite temperature case

The critical temperature for the superconductivity order parameter is found by solving the equation

$$1 = \frac{g}{2}\int_{-\omega_0}^{\omega_0} \mathrm{d}\varepsilon \frac{N^\sigma(\varepsilon)}{\varepsilon}\tanh(\varepsilon/2T_{c,\sigma}), \tag{3.13}$$

which yields the BCS-like solution

$$T_{c,\sigma} = 1.13\omega_0 \mathrm{e}^{-1/c\sqrt{1+\sigma M(\tilde{T}_{c,\sigma})}}. \tag{3.14}$$

Since the temperature at which the transition from paramagnetism to ferromagnetism sets in is, in general, much larger than the superconducting phase

transition, one may to good approximation set $M(T_{c,\sigma}) = M(0)$. It is then evident that the critical temperature depends on the magnetization in the same manner as the gap itself, and the cutoff-dependence in Eq. (3.12) may be removed in favor of the critical temperature by substituting Eq. (3.14). In order to solve the coupled gap equations self-consistently at arbitrary temperature, we considered Eq. (3.10) with the result given in Fig. 3.2 for $\tilde{I} = IN(0) = 1.01$. It is seen that the minority-spin gap is clearly suppressed compared to the majority-spin gap in the presence of a net magnetization. Also, the graph shows that the BCS-temperature dependence constitutes an excellent approximation for the decrease of the OPs with temperature. In what follows, we shall therefore use self-consistently obtained solutions at $T = 0$ for the OPs and make use of the BCS temperature-dependence unless specifically stated otherwise. In general, the critical temperature for the ferromagnetic order parameter, $T_{c,M}$ exceeds the superconducting phase transition temperatures $T_{c,\sigma}$ by several orders of magnitude. However, for $\tilde{I}$ very close to one, we are able to make these transition temperatures comparable in magnitude. In the experimentally discovered ferromagnetic superconductors UGe_2 [2] and URhGe [3], one finds that $T_{c,M}$ is approximately fifty times higher than the temperature at which superconductivity arises.

Comparison of free energies

Although a non-trivial solution of M exists, care must be exercised before concluding that this is the energetically preferred configuration of the system. Specifically, it may in theory be possible that the systems prefers the $M = 0$ solution regardless of the value of $\tilde{I}$, corresponding to a unitary superconducting state with $\Delta_{\uparrow,0} = \Delta_{\downarrow,0}$. It is therefore necessary to compare the free energies of the $M = 0$ and $M \neq 0$ cases at values of $\tilde{I}$ where the latter is a possible solution, and also study their temperature dependence. In the general case, the analytical expression for the free energy in the coexistent non-unitary superconducting phase reads

$$F/N = \frac{IM^2}{2} + \sum_\sigma \frac{\Delta_{\sigma,0}^2}{2g} - \sum_\sigma \int_{-E_F-\sigma IM}^{\infty} \mathrm{d}\varepsilon N^\sigma(\varepsilon) \times \left[\frac{\sqrt{\varepsilon^2+\Delta_{\sigma,0}^2}}{2} + \frac{1}{\beta}\ln(1+\mathrm{e}^{-\beta\sqrt{\varepsilon^2+\Delta_{\sigma,0}^2}}) \right]. \tag{3.15}$$

We obtain a dimensionless measure of the free energy by multiplying with I/E_F^2, and denote $F_{\mathrm{NU}} = FI/(NE_F^2)$. Note that the free energies of the unitary state, pure ferromagnetic state, and paramagnetic state are obtained as follows:

$$F_{\mathrm{U}} = \lim_{M\to 0} F_{\mathrm{NU}}, \quad F_{\mathrm{PM}} = \lim_{M\to 0,\Delta_{\sigma,0}\to 0} F_{\mathrm{NU}}, \quad F_{\mathrm{FM}} = \lim_{\Delta_{\sigma,0}\to 0} F_{\mathrm{NU}}. \tag{3.16}$$

In Fig. 3.3, we plot the difference between the unitary and non-unitary solution at zero temperature, $\Delta F = F_{\mathrm{U}} - F_{\mathrm{NU}}$, which clearly shows how the system favors the non-unitary solution with spontaneous magnetization as $\tilde{I}$

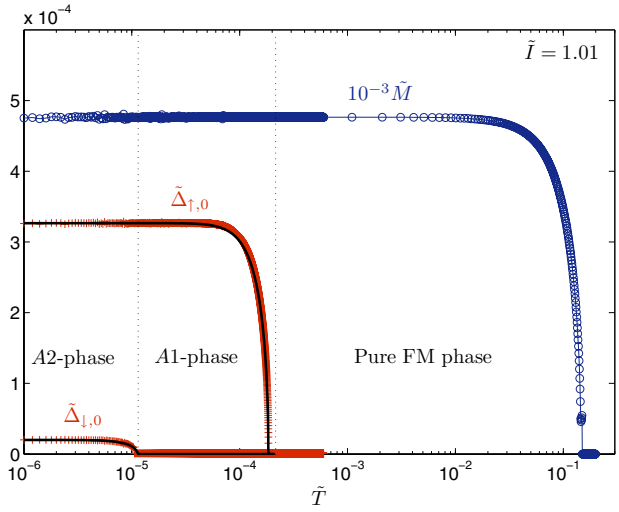

Figure 3.2: Self-consistently solved order parameters as a function of temperature for $\tilde{I} = 1.01$. Note that the temperature axis is logarithmic, such that the transition between the paramagnetic and ferromagnetic phase is much higher than the superconducting phase transitions. However, we are able to tune $\tilde{I}$ such that $T_{c,M}$ and $T_{c,\sigma}$ become comparable. We have also plotted the gaps with self-consistently solved values at $T = 0$ and then applying a BCS-temperature dependence (solid black lines), which yield excellent consistency with the solution that does not assume a BCS-temperature dependence.

increases. As a result, we suggest that the coexistent phase of ferromagnetism and superconductivity should be realized at sufficiently low temperatures whenever a magnetic exchange energy is present. For consistency, we also verified that $F_{\mathrm{NU}} < F_{\mathrm{FM}}$ at $T = 0$ since the system otherwise would prefer to leave superconductivity out of the picture and stay purely ferromagnetic.

Specific heat

We next consider some experimental signatures that could be expected in the different possible phases of a FMSC. To illustrate how the superconductivity pairing symmetry leaves important fingerprints in the heat capacity, we solved self-consistently for the specific heat capacity using two values of $\tilde{I}$ corresponding to a strong ($\tilde{M} \simeq 0.5$) and weak ($\tilde{M} \simeq 0.1$) exchange splitting. Recall that in general, a higher value of the exchange coupling $\tilde{I}$ favors a stronger magnetization. At $\tilde{I} = 1.01$, the discontinuity is clearly pronounced for $T = T_{c,\uparrow}$, but

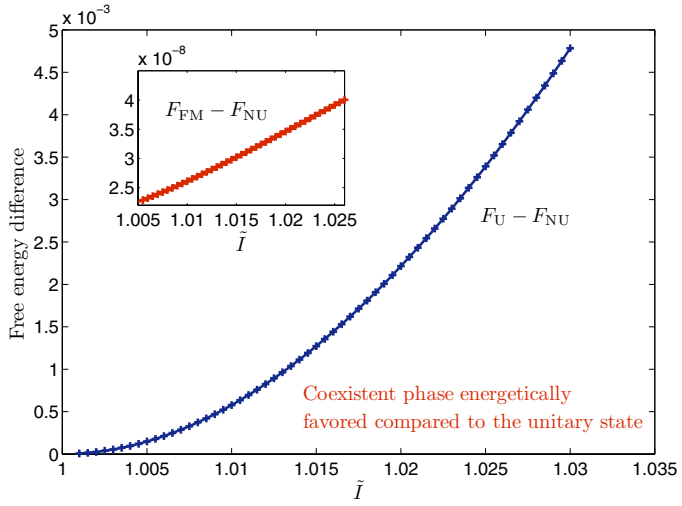

Figure 3.3: Comparison between the free energy for the non-unitary and unitary superconducting state at zero temperature. It is seen that these values are equal for $\tilde{I} = 1$ (and for $\tilde{I} < 1$), while the non-unitary state is energetically favored for increasing ferromagnetic exchange energy. Thus, the coexistent phase should be realized at sufficiently low temperatures in the presence of a ferromagnetic exchange energy.

it is hardly discernable at $T = T_{c,\downarrow}$. However, for $\tilde{I} = 1.0005$ where the superconductivity transition temperatures for majority and minority spins become comparable, a clear double-peak signature is revealed in the heat capacity. We thus propose that this particular feature should serve as unambigous evidence of a superconducting pairing corresponding to the $A2$-phase of liquid ^{3}He in ferromagnetic superconductors, where both spin species are paired.

A classic feature of the BCS-theory of superconductivity was the prediction that the jump in the heat capacity at T_c normalized on the normal-state value was a universal number, namely

$$\left(\frac{\Delta C_V}{C_V}\right)\Big|_{T=T_c} \simeq 1.43. \tag{3.17}$$

In the presence of a net magnetization, one would expect that the universality of this ratio would break down and depend on the strength of the exchange energy. This is due to the fact that the discontinuity in the specific heat at the superconducting transition is dominated by the majority-spin carriers, while

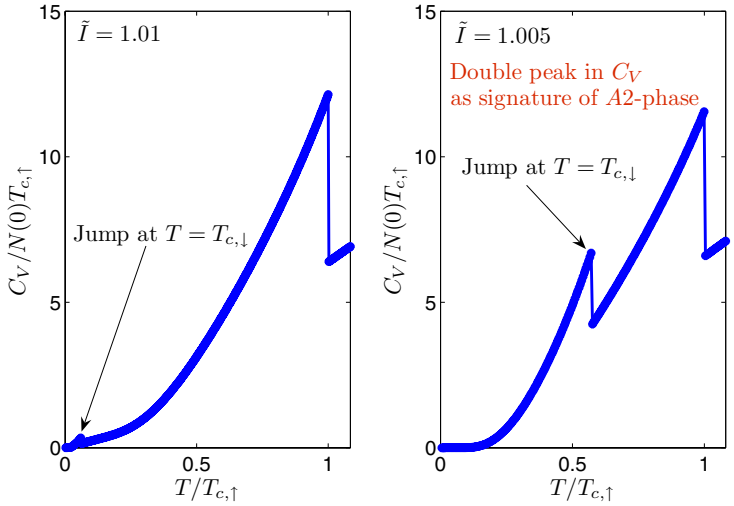

Figure 3.4: Specific heat capacity as a function of temperature for two values of $\tilde{I}$, corresponding to a strong exchange splitting ($\tilde{M} \simeq 0.5$) and a weak exchange splitting ($\tilde{M} \simeq 0.1$). A double-peak signature is clearly visible when the transition temperatures for the majority and minority spin bands are comparable.

the total specific heat to a larger extent has contributions from both minority-spin and majority spin carriers. To investigate this statement quantitatively, we consider the jump in C_V at $T = T_{c,\uparrow}$ since no analytical approach is possible at $T = T_{c,\downarrow}$. We find that the normal (ferromagnetic) state heat capacity reads

$$C_V^{\mathrm{FM}} = \frac{\pi^2 T_{c,\uparrow}}{3} \sum_\sigma N^\sigma(0), \tag{3.18}$$

where $N^\sigma(0)$ is the spin-resolved DOS at Fermi level, while the difference between the heat capacity in the coexistent state and the ferromagnetic state at $T = T_{c,\uparrow}$ reads

$$\Delta C_V = \frac{1.74^2 \Delta_{\uparrow,0}^2(0) N^\uparrow(0)}{2T_{c,\uparrow}}. \tag{3.19}$$

Since the zero-temperature value for the gap is $\Delta_{\uparrow,0}(0) = 1.76 T_{c,\uparrow}$, one arrives at

$$\left(\frac{\Delta C_V}{C_V}\right)\Big|_{T=T_{c,\uparrow}} = 1.43 \frac{1}{1 + \sqrt{\frac{1-\tilde{M}}{1+\tilde{M}}}}. \tag{3.20}$$

The above equation reduces to the BCS-limit for complete spin-polarization $\tilde{M} = 1$ (zero DOS for spin-$\downarrow$ fermions at Fermi level). As anticipated, the jump

in C_V depends on the exchange energy, as illustrated in Fig. 3.5. Of course, in the unitary state $\tilde{M} = 0$ the jump also reduces to the BCS value although this is not seen from Eq. (3.20). The reason for this is that we have implicitly assumed that $\tilde{M} \neq 0$ in the derivation of Eq. (3.20), taking $T_{c,\uparrow} > T_{c,\downarrow}$. In the case where these transition temperatures are equal, the contribution from both is additive and equal [1.43/2, to be specific, as seen from Eq. (3.20)] and gives the correct BCS result.

3.2.2 Interplay between spin-orbit coupling, ferromagnetism, and superconductivity

The heavy-fermion compound UIr stands out even among unconventional superconductors, as it may exhibit no less than three broken symmetries under high pressure: simultaneous ferromagnetism, superconductivity, and noncentrosymmetricity in its crystal structure. This raises an intriguing question: what happens when time-reversal symmetry is broken in a crystal that lacks a centre

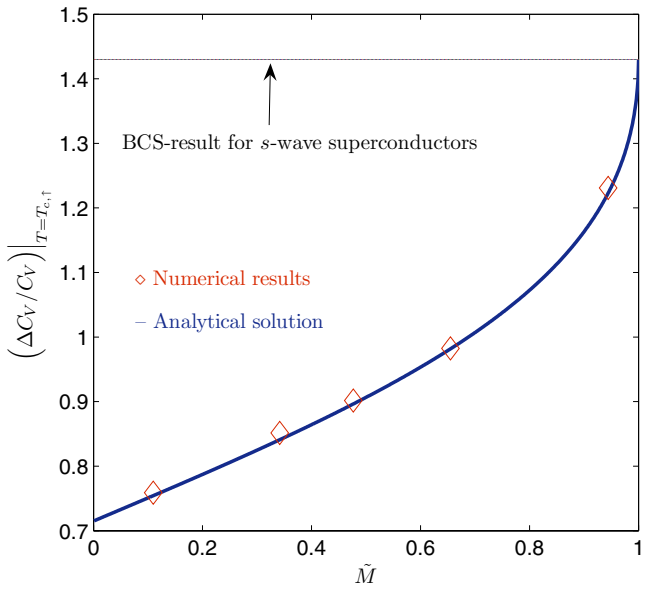

Figure 3.5: The discontinuity of the heat capacity at $T = T_{c,\uparrow}$ as a function of exchange splitting [Eq. (3.20)]. It is seen that the BCS value is recovered at $\tilde{M} = 1$. Note that it would also be recovered at $\tilde{M} = 0$, although this is not shown explicitely in the figure. The reason for this is that we have assumed that $T_{c,\downarrow} \neq T_{c,\uparrow}$. We have also plotted the numerical results ($\diamond$) for the jump with self-consistently solved OPs, i.e. without assuming BCS temperature dependence, for $\tilde{I} = \{1.001, 1.005, 1.01, 1.02, 1.05\}$, which yield good agreement with the analytical solution Eq. (3.20).

of inversion which at the same time superconducts? Spontaneous symmetry breaking in condensed matter systems is conceptually of immense importance, as it may provide clues for what could be expected in systems belonging to vastly different areas of physics. The study of a condensed-matter system such as UIr with multiple broken symmetries is likely to have impact on a number of disciplines of physics, including such disparate phenomena as mass differences between elementary particles and extremely dilute ultra-cold atomic gases.

We now study a model system of a non-centrosymmetric superconductor with substantial spin-orbit coupling, which at the same time exhibits itinerant ferromagnetism. The origin of the SOC may be either that the crystal structure lacks a center of inversion, such as in UIr, or due to a thin-film geometry where the breakdown of inversion symmetry near the surface induces transverse electrical fields, leading to the well-known Rashba SOC [54]. Our model should therefore be relevant both to the non-centrosymmetric and centrosymmetric heavy fermion compounds, since the SOC is considerable in any case due to the high atomic number. Specifically, materials that exhibit coexistence of SC and FM order and where SOC is large include UGe_2 [2], URhGe [3], UCoGe [4], and UIr [5]. For this model, we construct a mean-field theory, solve the saddle point equations for the order parameters and study the effect of spin-orbit coupling on the superconducting order parameters.

We now proceed to write down the effective Hamiltonian $H = H_{\mathrm{N}} + H_{\mathrm{SC}}$ for our system. In the normal state, the Hamiltonian in momentum-space reads [45]

$$H_{\mathrm{N}} = H_0 + \sum_{\boldsymbol{k}\alpha\beta} [c^\dagger_{\boldsymbol{k}\alpha}(\varepsilon_{\boldsymbol{k}}\hat{1} - h\hat{\sigma}_z + \hat{\boldsymbol{\sigma}} \cdot \mathbf{g}_{\boldsymbol{k}})_{\alpha\beta} c_{\boldsymbol{k}\beta}], \tag{3.21}$$

where $H_0 = INM^2/2$. Above, the dispersion relation $\varepsilon_{\boldsymbol{k}}$ is measured from chemical potential μ, and the magnetization $M = |\mathbf{M}|$ is taken along the easy-axis, while $h = IM$ is the exchange splitting of the bands and $\mathbf{g}_{\mathbf{k}}$ is the SOC vector. When superconductivity coexists with FM, the SC pairing is generally believed to be non-unitary [55], characterized by $\boldsymbol{d}_{\boldsymbol{k}} \times \boldsymbol{d}^*_{\boldsymbol{k}} \neq 0$. In such a scenario, the SC order parameter couples to the spontaneous magnetization $\mathbf{M}$ through a term $\gamma \boldsymbol{M} \cdot \boldsymbol{d}_{\boldsymbol{k}} \times \boldsymbol{d}^*_{\boldsymbol{k}}$ in the free energy, where the sign of γ is determined by the gradient of the DOS at Fermi level [56] and $\langle \boldsymbol{S}_{\boldsymbol{k}} \rangle = \mathrm{i}\boldsymbol{d}_{\boldsymbol{k}} \times \boldsymbol{d}^*_{\boldsymbol{k}}$ is the spin associated with the Cooper pair. Thus, for $\gamma < 0$ it is expected that a SC pairing state obeying $\mathrm{i}\mathbf{d}_{\boldsymbol{k}} \times \boldsymbol{d}^*_{\boldsymbol{k}} \parallel \mathbf{M}$ is energetically favored, implying that $\boldsymbol{d}_{\boldsymbol{k}}$ must be complex-valued. Our model captures broken time-reversal symmetry in addition to antisymmetric SOC. As shown by Anderson [57], the presence of the latter is detrimental to spin-triplet SC pairing state, unless $\boldsymbol{d}_{\boldsymbol{k}} \parallel \boldsymbol{g}_{\boldsymbol{k}}$. In our case, it is obvious that a non-unitary SC pairing state cannot satisfy this condition since $\boldsymbol{d}_{\boldsymbol{k}}$ is complex, whereas $\boldsymbol{g}_{\boldsymbol{k}}$ must be real for the Hamiltonian to be hermitian.

The SOC vector reads $\boldsymbol{g}_{\boldsymbol{k}} = -\boldsymbol{g}_{-\boldsymbol{k}}$, and we introduce $g_{\boldsymbol{k}} = \boldsymbol{g}_{\boldsymbol{k},x} - \mathrm{i}\boldsymbol{g}_{\boldsymbol{k},y}$ for later use. We consider the SOC in the Rashba form, namely $\boldsymbol{g}_{\boldsymbol{k}} = \lambda(k_y, -k_x, 0)$.

This corresponds to a situation where an asymmetric potential gradient is present along the **z**-axis, and is also the scenario realized in noncentrosymmetric $CePt_3Si$ [58]. We have introduced fermion operators $\{c_{\boldsymbol{k}\sigma}\}$ in a basis $\varphi_{\boldsymbol{k}} = [c_{\boldsymbol{k}\uparrow}, c_{\boldsymbol{k}\downarrow}]^{\mathrm{T}}$.

Diagonalizing the normal-state Hamiltonian yields the quasiparticle excitations $\tilde{E}_{\boldsymbol{k}\sigma} = \varepsilon_{\boldsymbol{k}} - \sigma\sqrt{h^2+\lambda^2k^2}$, which due to the SOC are characterized by the pseudospin $\sigma = \pm 1$. For later use, we define $\mathcal{N}_{\boldsymbol{k}} = [1+\lambda^2k^2/(h+\sqrt{h^2+\lambda^2k^2})^2]^{-1/2}$. The superconducting pairing is now assumed to occur between the excitations described by $\tilde{\varphi}_{\boldsymbol{k}}$. Due to the presence of antisymmetric spin-orbit coupling, this automatically leads to a mixed-parity SC state in the original spin basis. To see this, we introduce

$$H_{\mathrm{SC}} = \frac{1}{2N}\sum_{\boldsymbol{k}\boldsymbol{k}'\sigma} V_{\boldsymbol{k}\boldsymbol{k}'\sigma}\tilde{c}^{\dagger}_{\boldsymbol{k}\sigma}\tilde{c}^{\dagger}_{-\boldsymbol{k}\sigma}\tilde{c}_{-\boldsymbol{k}'\sigma}\tilde{c}_{\boldsymbol{k}'\sigma}, \tag{3.22}$$

and perform a standard mean-field decoupling, which after an additional diagonalization yields the total Hamiltonian in the superconducting state: $H = H_0 + \Sigma_{\boldsymbol{k}\sigma}(\tilde{E}_{\boldsymbol{k}\sigma} - E_{\boldsymbol{k}\sigma} - \tilde{\Delta}_{\boldsymbol{k}\sigma}\tilde{b}^{\dagger}_{\boldsymbol{k}\sigma} + 2\eta^{\dagger}_{\boldsymbol{k}\sigma}\eta_{\boldsymbol{k}\sigma})/2$, where $E_{\boldsymbol{k}\sigma} = (\tilde{E}^2_{\boldsymbol{k}\sigma} + |\tilde{\Delta}_{\boldsymbol{k}\sigma}|^2)^{1/2}$ and $\{\eta^{\dagger}_{\boldsymbol{k}\sigma}, \eta_{\boldsymbol{k}\sigma}\}$ are new fermion operators. The merit of this procedure is that we can now obtain simple self-consistency equations for the gaps $\tilde{\Delta}_{\boldsymbol{k}\sigma}$, which may then be transformed back to the gaps in the original spin-basis $\varphi_{\boldsymbol{k}}$ by means of the unitary transformation $P_{\boldsymbol{k}}$. We assume a chiral p-wave symmetry for the gaps with a corresponding pairing potential $V_{\boldsymbol{k}\boldsymbol{k}'\sigma} = -g_{sc}\mathrm{e}^{\mathrm{i}\sigma(\phi-\phi')}$, where $\tan\phi = k_x/k_y$. The motivation for this is that this choice ensures that the condition $\mathbf{d}_{\boldsymbol{k}} \parallel \mathbf{g}_{\boldsymbol{k}}$ is satisfied exactly for $h \to 0$. The condensation energy also favors a fully gapped Fermi surface, which is the case here. The gaps obtain the form $\tilde{\Delta}_{\boldsymbol{k}\sigma} = -\sigma\tilde{\Delta}_{\sigma,0}\mathrm{e}^{\mathrm{i}\sigma\phi}$ and we find a self-consistency equation of the standard BCS form with a cutoff ω on the pairing-fluctuation spectrum which we do not specify further. Moreover, $N^{\sigma}(\varepsilon)$ is the pseudospin-resolved density of states (DOS) for the $\tilde{E}_{\boldsymbol{k}\sigma}$ (σ=$\pm$) bands of the quasiparticle excitations, where

$$\begin{aligned} N^{\sigma}(\varepsilon) &= mVk_{\sigma}(\varepsilon)(2\pi^2)^{-1}/[1-\sigma m\lambda^2/\sqrt{h^2+\lambda^2k^2_{\sigma}(\varepsilon)}], \\ k_{\sigma}(\varepsilon) &= [2(\varepsilon+\mu)m + 2\lambda^2m^2 + 2\sigma\sqrt{\lambda^4m^4 + 2\lambda^2m^3(\varepsilon+\mu) + h^2m^2}]^{1/2}. \end{aligned} \tag{3.23}$$

Introducing the DOS at the Fermi level for a normal metal $N_0 = mV\sqrt{2m\mu}/\pi^2$ and defining $c = g_{\mathrm{sc}}N_0/2$, the analytical solution for the gaps reads

$$\tilde{\Delta}_{\sigma,0} = 2\omega\mathrm{e}^{-1/[cR_{\sigma}(0)]},\ R_{\sigma}(\varepsilon) = 2N^{\sigma}(\varepsilon)/N_0. \tag{3.24}$$

With the analytical solution for $\tilde{\Delta}_{\sigma,0}$ in hand, we may exploit the unitary transformation $P_{\boldsymbol{k}}$ to express the superconducting gaps in the original spin basis as follows:

$$\begin{aligned} \Delta_{\boldsymbol{k}\uparrow} &= -\mathrm{e}^{\mathrm{i}\phi}[\tilde{\Delta}_{\uparrow,0}(\mathcal{N}^{\uparrow}_{\boldsymbol{k}})^2 + \tilde{\Delta}_{\downarrow,0}(\mathcal{N}^{\downarrow}_{\boldsymbol{k}})^2\lambda^2k^2_{\downarrow}(0)\Lambda^2_{\boldsymbol{k}\downarrow}], \\ \Delta_{\boldsymbol{k}\downarrow} &= \mathrm{e}^{-\mathrm{i}\phi}[\tilde{\Delta}_{\downarrow,0}(\mathcal{N}^{\downarrow}_{\boldsymbol{k}})^2 + \tilde{\Delta}_{\uparrow,0}(\mathcal{N}^{\uparrow}_{\boldsymbol{k}})^2\lambda^2k^2_{\uparrow}(0)\Lambda^2_{\boldsymbol{k}\uparrow}], \\ \Delta_{\boldsymbol{k}\uparrow\downarrow} &= -\sum_{\sigma}\tilde{\Delta}_{\sigma,0}(\mathcal{N}^{\sigma}_{\boldsymbol{k}})^2\lambda|k_{\sigma}(0)|\Lambda_{\boldsymbol{k}\sigma},\ \sigma = \pm 1, \end{aligned} \tag{3.25}$$

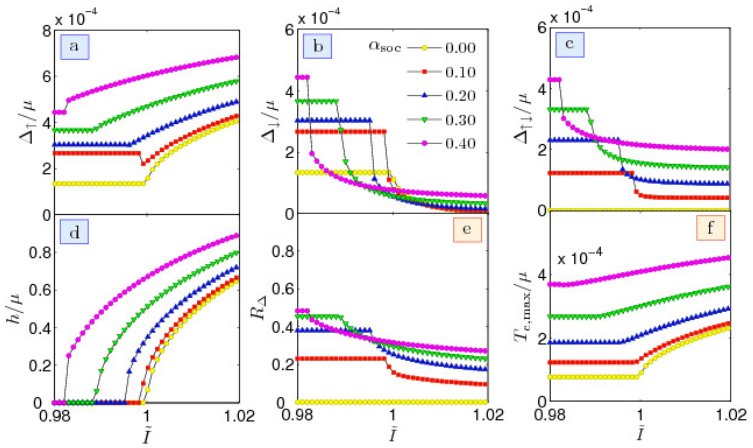

Figure 3.6: Self-consistent solution of the order parameters (a-d) as a function of the FM exchange parameter $\tilde{I}$, the ratio between the singlet and triplet gaps (e) $R_\Delta = \Delta_{\uparrow\downarrow}/(\Delta_\uparrow + \Delta_\downarrow)$ and the maximal critical temperature (f) $T_{c,\max}$ as a function of the FM exchange parameter $\tilde{I}$.

where we have defined $\mathcal{N}^\sigma_{\boldsymbol{k}} = \mathcal{N}_{\boldsymbol{k}=\boldsymbol{k}^\sigma(0)}$ and $\Lambda_{\boldsymbol{k}\sigma} = [h + \sqrt{h^2 + \lambda^2 k^2_\sigma(0)}]^{-1}$. Note that in the original spin basis, the superconducting order parameter is in general a mixture of triplet ($\Delta_{\boldsymbol{k}\sigma}$) and singlet ($\Delta_{\boldsymbol{k}\uparrow\downarrow}$) components. The self-consistency equation for the magnetization is:

$$h + \frac{\tilde{I}}{4}\sum_\sigma \int \frac{\sigma \mathrm{d}\varepsilon R^\sigma(\varepsilon) h\varepsilon}{\sqrt{[h^2 + \lambda^2 k^2_\sigma(\varepsilon)](\varepsilon^2 + \tilde{\Delta}^2_{\sigma,0})}} = 0, \tag{3.26}$$

where the integration is over the bandwidth and $\tilde{I} = IN_0$. Equations (3.25, 3.26) are the main analytical results of this work.

Let us briefly investigate some important limiting cases of Eq. (3.25). In the absence of spin-orbit coupling ($\lambda \to 0$), one finds $\mathcal{N}^\sigma_{\boldsymbol{k}} \to 1$ and $\Delta_{\boldsymbol{k}\sigma} = \tilde{\Delta}_{\boldsymbol{k}\sigma}$ while $\Delta_{\boldsymbol{k}\uparrow\downarrow} = 0$, such that we reproduce the results of Refs. [49, 45]. In the absence of an exchange energy ($h \to 0$), one finds that $\mathcal{N}^\sigma_{\boldsymbol{k}} \to 1/\sqrt{2}$ and $\Delta_{\boldsymbol{k}\uparrow} = -\mathrm{e}^{\mathrm{i}\phi}(\tilde{\Delta}_{\uparrow,0} + \tilde{\Delta}_{\downarrow,0})/2$, $\Delta_{\boldsymbol{k}\downarrow} = \mathrm{e}^{-\mathrm{i}\phi}(\tilde{\Delta}_{\uparrow,0} + \tilde{\Delta}_{\downarrow,0})/2$, and $\Delta_{\boldsymbol{k}\uparrow\downarrow} = (\tilde{\Delta}_{\downarrow,0} - \tilde{\Delta}_{\uparrow,0})/2$. As demanded by consistency, the triplet gaps are equal in magnitude since there is no exchange field and the singlet component is nonzero since $\tilde{\Delta}_{\uparrow,0} \neq \tilde{\Delta}_{\downarrow,0}$ in general. Finally, Eq. (3.26) reproduces the well-known Stoner criterion $\tilde{I} \geq 1$ for the onset of FM in the absence of SOC and superconductivity ($\lambda \to 0, g_{\mathrm{sc}} \to 0$).

We now focus on the general case in which $h \neq 0$ and $\lambda \neq 0$. First of all, we must specify the range of the parameters in the problem that corresponds to a physically realistic scenario. We allow h to range, in principle, from 0 to μ, the latter denoting a fully polarized ferromagnet. As a convenient measure of the

strength of SOC, we introduce the dimensionless quantity $\alpha_{\rm soc} \equiv \sqrt{2\lambda^2 m/\mu}$ which has a direct physical interpretation: namely, it is the ratio of the SOC (at E_F) to the Fermi energy μ. The parameter $\alpha_{\rm soc}$ is allowed to vary from 0 to δ, where δ denotes a fraction of the Fermi energy. We take $\delta = 0.5$ as a sensible upper limit. Note that generically, the SOC strength at the Fermi level is different for the two quasiparticle bands, and moreover depends on h. For a given value of h, one may derive that $\lambda \leq \delta\mu/[2\mu m + \sqrt{2m^2(h^2+\delta^2\mu^2)}]^{1/2}$ ensures that the spin-orbit energy is less than $\delta \times \mu$ for both quasiparticle bands.

In Fig. 3.6a-d, we present the self-consistent solutions for the order parameters in Eqs. (3.25) and (3.26) as a function of the FM exchange parameter $\tilde{I}$ for several values of $\alpha_{\rm soc}$. We have defined $\Delta_\sigma = |\Delta_{\boldsymbol{k}\sigma}|$ and $\Delta_{\uparrow\downarrow} = |\Delta_{\boldsymbol{k}\uparrow\downarrow}|$, and fixed $\omega/\mu = 0.01$ and $m/\mu = 5 \times 10^4$ with $c = 0.2$, which are standard choices. For $\alpha_{\rm soc} = 0$, the onset of FM occurs at $\tilde{I} = 1.0$ which lifts the degeneracy of $\Delta_\uparrow$ and $\Delta_\downarrow$, while $\Delta_{\uparrow\downarrow}$ is always zero. Upon increasing $\alpha_{\rm soc}$, it is interesting to note that the PM-FM transition occurs at lower values of $\tilde{I}$, indicating that spin-orbit coupling favors ferromagnetic ordering. For $\alpha_{\rm soc} \neq 0$, it is seen that $\Delta_{\uparrow\downarrow}$ is also non-zero, although it becomes suppressed at the onset of ferromagnetism. A common feature for all gaps is that they increase with $\alpha_{\rm soc}$ in the absence of ferromagnetism *and* deep inside the ferromagnetic phase $\tilde{I} \geq 1.02$. In the intermediate regime, there are crossovers between the gaps for different values of $\alpha_{\rm soc}$ due to the different onsets of ferromagnetic order. By comparing the behaviour between the gaps for increasing $\tilde{I}$ with $\alpha_{\rm soc} \neq 0$, one infers that $\Delta_\downarrow$ and $\Delta_{\uparrow\downarrow}$ eventually saturate at a constant non-zero value, while $\Delta_\uparrow$ continues to increase steadily. This is quite different from the case when $\alpha_{\rm soc} = 0$, where the minority spin-gap goes to zero rapidly with increasing $\tilde{I}$. This seems to suggest that the presence of spin-orbit coupling in the system ensures the survival of the minority-spin gap $\Delta_\downarrow$ and the singlet gap $\Delta_{\uparrow\downarrow}$ even though the FM exchange energy becomes strong.

In Fig. 3.6e and 3.6f, we plot the ratio of the singlet and triplet gaps, defined as $R_\Delta = \Delta_{\uparrow\downarrow}/(\Delta_\uparrow + \Delta_\downarrow)$, and the maximal critical temperature $T_{c,\rm max}$ for the onset of superconductivity. It is seen from the left panel that R_Δ increases with $\alpha_{\rm soc}$ in the PM regime, suggesting that the singlet component becomes more prominent in the system as compared to the triplet gaps. However, at the onset of FM order, R_Δ decreases since the singlet component becomes suppressed by the Zeeman-splitting. In the right panel, one observes that $T_{c,\rm max}$ increases both with $\alpha_{\rm soc}$ and $\tilde{I}$. Our findings suggest that the presence of antisymmetric SOC, originating from *e.g.* noncentrosymmetricity of the crystal structure, *enhances both* the tendency towards ferromagnetism and the magnitude of the SC gaps in all spin channels. In the absence of spin-orbit coupling, it was shown in the previous section that the simultaneous coexistence of FM and non-unitary triplet superconductivity is the thermodynamically favored state as compared to the pure normal, FM, or SC state. Since the presence of spin-orbit coupling is seen to enhance both the FM and SC order parameters, it is reasonable to expect that the coexistent state is still thermodynamically the most favorable one even when $\alpha_{\rm soc} \neq 0$.

Chapter 4

Superconducting proximity-effect in graphene

In recent years, a monolayer of graphite, known as *graphene*, has attracted an enormous interest from a broad range of physics communities. The interest pertains to the fact that graphene is a low-dimensional condensed matter system which displays highly unusual electronic properties. While the electronic correlations in pure graphene are in general quite weak (the Coulomb interaction may be neglected in many cases), experimentalists have succeeded in inducing superconducting correlations in graphene by means of the proximity effect to a host material. In this chapter, we explore the fascinating interplay between superconductivity, ferromagnetism, and the remarkable properties of charge carriers in graphene. Papers VII, IX, X, and XIII fall into this subcategory.

4.1 Fundamental concepts

4.1.1 Electronic properties of pure graphene

The most striking and crucial factor that determines the behavior of the electrons in graphene is the low-energy band dispersion. In undoped graphene, the Fermi surface reduces to six points in the Brillouin zone, all of which display a conical "valley" structure for the band dispersion. Only two of these six point are inequivalent, and they are conventionally referred to as Dirac points and dubbed K and K'. The band dispersion of graphene was first calculated by Wallace [59], and reads

$$E = \pm\gamma_0\Big[1 + 4\cos\Big(\frac{\sqrt{3}k_x a}{2}\Big)\cos\Big(\frac{k_y a}{2}\Big) + 4\cos^2\Big(\frac{k_y a}{2}\Big)\Big]^{1/2}, \qquad (4.1)$$

where $\gamma_0 \simeq 2.5$ eV, and the $\pm$ sign refers to the anti-bonding/bonding π-orbital. The remaining three valence electrons are in hybridized sp^2 σ-bonds. The energy dispersion in the Brillouin zone is plotted in Fig. 4.1, which reveals the conical structure of the conduction and valence bands at the six Fermi points.

The cosine-like conduction and valence bands are made up by a mixture of the energy bands from the sublattices in graphene, which are linear near the Fermi level. This gives rise to the conical energy dispersion at the Dirac points K and K'.

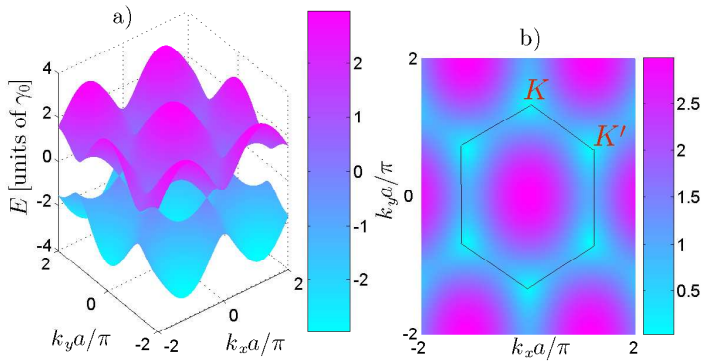

Figure 4.1: a) The energy dispersion for graphene in the Brillouin zone. The upper band is the antibonding π-orbital, while the lower band is the bonding π-orbital. It is seen that the bands touch at Fermi level ($E_F = 0$) at six discrete points, which constitutes the effective Fermi surface. b) Contour plot of the dispersion relation, clearly showing the hexagonal structure of the Fermi points. The center of each drop-like structure represents either K or K'.

The linear energy dispersion relationship near the Dirac points K and K' has paramount consequences for the charge-carriers: it renders them massless and makes the Fermi-velocity energy-independent. Due to the low density of states in undoped graphene, it is possible to alter the position of the Fermi level externally by means of a local gate voltage, which induces an electric field-effect. We underline here that by *undoped* graphene, we have in mind a Fermi level which is close the the charge neutrality point, while with *doped* graphene we mean a situation where the Fermi level is raised by either chemical doping or an electric field-effect, thus creating a finite Fermi surface. The magnitude of spin-orbit coupling in graphene is weak due to the low atomic number of carbon ($Z = 6$), and Coulomb repulsion may also be neglected compared to the kinetic energy. This might seem paradoxical in light of the low density of states, since a standard Thomas-Fermi argument would imply an extremely poor screening of the Coulomb repulsion. The resolution to this problem is found by considering the renormalization group (RG) properties of the Fermi velocity graphene [60, 61]. The importance of Coulomb interaction in graphene

is governed by the parameter [62]:

$$\lambda = \frac{Ne^2}{16\epsilon v_F}, \tag{4.2}$$

where N is the spin-degeneracy factor, ϵ is the dielectric constant in vacuum, while v_F is the Fermi velocity. Whenever $\lambda \ll 1$, the Coulomb interactions may be disregarded. In the low-energy regime, a RG analysis reveals that the Fermi velocity in graphene is renormalized in a fashion that makes it formally diverge logarithmically close to the Dirac points, thus leading to a vanishing of the interaction parameter, $\lambda \to 0$. So even if the Coulomb interaction in graphene is not screened as in conventional metallic systems, the Coulomb interaction essentially self-destructs since it adds a self-energy correction to the renormalized Fermi velocity which makes it diverge. In practice, the Fermi velocity in graphene in the low-energy regime is of course limited and given by $v_F \simeq 10^6$ m/s.

4.1.2 Proximity-induced correlations in graphene and charge inhomogeneities

The proximity effect exploits the spatial vicinity of a host material with certain desirable properties to a compound in which one wishes to induce these properties. In this way, Heersche *et al.* [63] deposited superconducting leads on top of a graphene sheet to induce superconductivity, and were able to measure a Josephson current between the leads. Prior to this experiment, Beenakker [64] had discovered some properties of Andreev reflection in graphene which were quite distinct from conventional metallic systems, while Titov and Beenakker [65] correctly had predicted a non-vanishing Josephson current in graphene even at the charge neutrality point. Recently, it was also proposed [66, 67, 68] that ferromagnetic correlations could be induced in graphene. In particular by means of depositing a magnetic insulator on top of a graphene sheet, the resulting exchange splitting in graphene was estimated to $h \simeq 5$ meV [68].

In an idealized model of graphene the chemical potential is taken to be spatially constant, which usually makes analytical considerations tractable. However, intrinsic disorder effects in graphene will alter this physical picture. By means of scanning single electron transistor techniques, it was shown in Ref. [69] that the carrier density landscape of graphene is subject to charge inhomogeneities in form of electron-hole puddles, as shown in Fig. 4.2. This observation is of importance with regard to the transport characteristics of graphene close to the Dirac point [70]. In doped graphene, where a finite Fermi surface arises, one would expect that the inhomogeneities should play a smaller role than in undoped graphene where the Fermi level lies at the charge neutrality point.

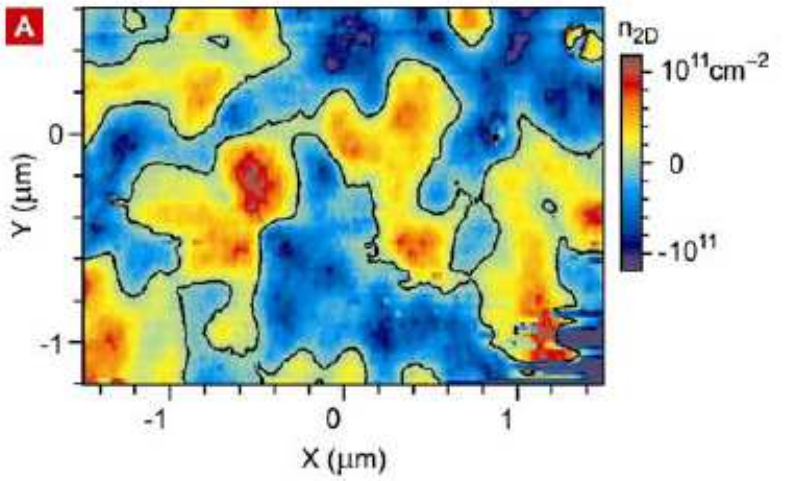

Figure 4.2: Scanning single electron transistor image of the charge inhomogeneities in a graphene sheet, manifested through the separation of charge into electron-hole puddles. Shown is a contour plot of the carrier density in the xy-plane of the graphene sheet. The image is taken from Ref. [69].

4.2 Research highlights

4.2.1 Conductance spectra of N/S graphene junctions

Graphene N/S interfaces contain a new phenomenology compared to their metallic counterpart, namely the possibility of *specular* Andreev-reflection (AR) [64]. In the process of normal AR, an incident electron from the N side is reflected as a hole which retraces the trajectory of the electron. In specular AR, the reflected hole follows the trajectory which a normally reflected electron would have. Depending on whether the graphene is doped or not, specular and normal AR will compete with each other, also depending on the position of the Fermi level with respect to the gap.

To illustrate the new physics at hand, consider a graphene sheet in which superconductivity is induced at $x > w$, while the graphene sheet is normal for $x < w$. To model the presence of a barrier region, we allow a gate voltage to alter the Fermi level in the region $0 < x < w$. In order to treat the scattering processes at the interfaces of the N/I/S junction, we make use of the full Bogoliubov-de Gennes (BdG) equation for the 2D sheet of graphene in the xy-plane, assuming that the clean limit is reached. These equations read

$$\begin{pmatrix} \check{H} - \varepsilon_{\mathrm{F}}\check{1} & \Delta_{\boldsymbol{k}}\check{1} \\ \Delta_{\boldsymbol{k}}^{\dagger}\check{1} & \varepsilon_{\mathrm{F}}\check{1} - \check{\mathcal{T}}\check{H}\check{\mathcal{T}}^{-1} \end{pmatrix} \Psi = \varepsilon\Psi, \tag{4.3}$$

where ε is the excitation energy, and Ψ is the wave-function. We use $\check{..}$ for 4×4 matrices, $\hat{..}$ for 2×2 matrices, and boldface notation for three-dimensional row vectors. Neglecting the decay of the order parameter in the vicinity of the interface, we may write for the spin-singlet order parameter $\Delta_{\boldsymbol{k}} = \Delta(\theta)\mathrm{e}^{\mathrm{i}\vartheta}\Theta(x-w)$, where $\Theta(x)$ is the Heaviside step function, while ϑ is the phase corresponding the globally broken $U(1)$ symmetry in the superconductor. We consider the weak-coupling limit with the momentum $\boldsymbol{k}$ fixed on the Fermi surface, such that $\Delta_{\boldsymbol{k}}$ only has an angular dependence $\theta = \mathrm{atan}(k_y/k_x)$. Note that in contrast to previous work, we allow for the possibility of unconventional superconductivity in the graphene layer since $\Delta_{\boldsymbol{k}}$ now may be anisotropic.

Postulating a spin-singlet even parity order parameter, the condition $\Delta(\theta) = \Delta(\pi+\theta)$ must be fulfilled. The single-particle Hamiltonian is given by $\check{H} = \mathrm{diag}(\hat{H}_+, \hat{H}_-)$, $\hat{H}_\pm = -\mathrm{i}v_\mathrm{F}(\hat{\sigma}_x\partial_x \pm \hat{\sigma}_y\partial_y)$. Here, v_F is the energy-independent Fermi velocity for graphene, while $\hat{\sigma}_i$ denotes the Pauli matrices. For later use, we also define the Pauli matrix vector $\hat{\boldsymbol{\sigma}} = (\hat{\sigma}_x, \hat{\sigma}_y, \hat{\sigma}_z)$. These Pauli matrices operate on the sublattice space of the honeycomb structure, corresponding to the A and B atoms, while the $\pm$ sign refers to the two so-called *valleys* of K and K' in the Brillouin zone. The spin indices may be suppressed since the Hamiltonian is time-reversal invariant. In addition to the spin degeneracy, there is also a valley degeneracy, which effectively allows one to consider either one of the $\hat{H}_\pm$ set. We choose $\hat{H}_+$, and consider an incident electron from the normal side of the junction ($x<0$) with energy E. For positive excitation energies $\varepsilon > 0$, the eigenvectors and corresponding momentum of the particles read $\psi_+^\mathrm{e} = [1, \mathrm{e}^{\mathrm{i}\theta}, 0, 0]^\mathrm{T}\mathrm{e}^{\mathrm{i}p^\mathrm{e}\cos\theta x}$, $p^\mathrm{e} = (\varepsilon+\varepsilon_\mathrm{F})/v_\mathrm{F}$, for a right-moving electron at angle of incidence θ, while a left-moving electron is described by the substitution $\theta \to \pi-\theta$. If Andreev-reflection takes place, a left-moving hole with energy ε and angle of reflection θ_A is generated with belonging wave-function $\psi_-^\mathrm{h} = [0,0,1,\mathrm{e}^{-\mathrm{i}\theta_\mathrm{A}}]^\mathrm{T}\mathrm{e}^{-\mathrm{i}p^\mathrm{h}\cos\theta_\mathrm{A}x}$, $p^\mathrm{h} = (\varepsilon-\varepsilon_\mathrm{F})/v_\mathrm{F}$, where the superscript e (h) denotes an electron-like (hole-like) excitation. Since translational invariance in the $\hat{\mathbf{y}}$-direction holds, the corresponding component of momentum is conserved. This condition allows for determination of the Andreev-reflection angle θ_A through $p^\mathrm{h}\sin\theta_\mathrm{A} = p^\mathrm{e}\sin\theta$. One thus infers that there is no Andreev-reflection ($\theta_\mathrm{A} = \pm\pi/2$), and consequently no subgap conductance, for angles of incidence above the critical angle $\theta_\mathrm{c} = \mathrm{asin}[|\varepsilon-\varepsilon_\mathrm{F}|/(\varepsilon+\varepsilon_\mathrm{F})]$.

On the superconducting side of the system ($x>w$), the possible wavefunctions for transmission of a right-moving quasiparticle with a given excitation energy $\varepsilon > 0$ reads

$$\begin{aligned}
\Psi_+^\mathrm{e} &= [u(\theta^+), u(\theta^+)\mathrm{e}^{\mathrm{i}\theta^+}, v(\theta^+)\mathrm{e}^{-\mathrm{i}\phi^+}, v(\theta^+)\mathrm{e}^{\mathrm{i}(\theta^+-\phi^+)}]^\mathrm{T}\mathrm{e}^{\mathrm{i}q^\mathrm{e}\cos\theta^+x},\\
q^\mathrm{e} &= (\varepsilon'_\mathrm{F} + \sqrt{\varepsilon^2-\Delta^2})/v_\mathrm{F},\\
\Psi_-^\mathrm{h} &= [v(\theta^-), v(\theta^-)\mathrm{e}^{\mathrm{i}\theta^-}, u(\theta^-)\mathrm{e}^{-\mathrm{i}\phi^-}, u(\theta^-)\mathrm{e}^{\mathrm{i}(\theta^--\phi^-)}]^\mathrm{T}\mathrm{e}^{\mathrm{i}q^\mathrm{h}\cos\theta^-x},\\
q^\mathrm{h} &= (\varepsilon'_\mathrm{F} - \sqrt{\varepsilon^2-\Delta^2})/v_\mathrm{F}.
\end{aligned} \tag{4.4}$$

The coherence factors are given by $u(\theta) = [\frac{1}{2}(1+\sqrt{\varepsilon^2-|\Delta(\theta)|^2}/\varepsilon)]^{1/2}$, $v(\theta) =$

$[\frac{1}{2}(1-\sqrt{\varepsilon^2-|\Delta(\theta)|^2}/\varepsilon)]^{1/2}$. Above, we have defined $\theta^+ = \theta_{\rm S}^{\rm e}$, $\theta^- = \pi - \theta_{\rm S}^{\rm h}$, and $\mathrm{e}^{\mathrm{i}\phi^\pm} = \mathrm{e}^{\mathrm{i}\vartheta}\Delta(\theta^\pm)/|\Delta(\theta^\pm)|$. The transmission angles $\theta_{\rm S}^{\rm (i)}$ for the electron-like (ELQ) and hole-like (HLQ) quasiparticles are given by $q^{\rm (i)}\sin\theta_{\rm S}^{\rm (i)} = p^{\rm e}\sin\theta$, i=e,h. Also, $\varepsilon'_{\rm F}$ is the Fermi level in the superconducting region, and the corresponding Fermi wavelength is $\lambda' = v_F/\varepsilon'_{\rm F}$. Note that for subgap energies $\varepsilon < \Delta$, there is a small imaginary contribution to the wavevector, which leads to exponential damping of the wavefunctions inside the superconductor. For clarity, we have omitted a common phase factor $\mathrm{e}^{\mathrm{i}k_y y}$ which corresponds to the conserved momentum in the $\hat{\mathbf{y}}$-direction. A possible Fermi vector mismatch (FVM) between the normal and superconducting region is accounted for by allowing for $\varepsilon'_{\rm F} \neq \varepsilon_{\rm F}$. The case $\varepsilon'_{\rm F} \gg \varepsilon_{\rm F}$ corresponds to a heavily doped superconducting region. Since we are using a mean-field approach to describe the superconducting part of the Hamiltonian, it is implicitly understood that phase-fluctuations of the order parameter must be small. This amounts to imposing the restriction [71] $\xi/\lambda' \gg 1$, or equivalently, $\varepsilon'_{\rm F} \gg \Delta$.

Considering here values of the Fermi level far away from the neutrality point, the conductance of the N/I/S junction is given by [21]

$$G(eV) = G_{\rm N}\int_{-\pi/2}^{\pi/2} \mathrm{d}\theta\cos\theta[1-|r(eV,\theta)|^2 + P|r_{\rm A}(-eV,\theta)|^2], \tag{4.5}$$

where r and $r_{\rm A}$ are the reflection coefficients for normal and Andreev reflection, respectively, $P = \mathrm{Re}\{\cos\theta_{\rm A}\}/\cos\theta$, while $G_{\rm N} = \int_{-\pi/2}^{\pi/2}\mathrm{d}\theta\cos\theta[4\cos^2\theta/(4\cos^2\theta + Z^2)]$ is a renormalization constant corresponding to the N/N metallic conductance [72]. In this case, we have zero intrinsic barrier such that $Z = 0$. The reflection and transmission coefficients constitute a unitary scattering matrix, a property that essentially expresses a conservation of probability. In deriving the conductance, we have ensured that the scattering coefficients have been normalized by the incoming current through the factor P. In order to obtain these coefficients, we make use of the boundary conditions $\psi|_{x=0} = \tilde{\psi}_{\rm I}|_{x=0}$, $\tilde{\psi}_{\rm I}|_{x=w} = \Psi_{\rm S}|_{x=w}$, where we have defined the wavefunction in the insulating region $\tilde{\psi}_{\rm I} = \tilde{t}_1\tilde{\psi}_+^{\rm e} + \tilde{t}_2\tilde{\psi}_-^{\rm e} + \tilde{t}_3\tilde{\psi}_+^{\rm h} + \tilde{t}_4\tilde{\psi}_-^{\rm h}$. The wavefunctions $\tilde{\psi}$ differ from ψ in that the Fermi energy is greatly shifted by means of *e.g.* an external potential, such that $\varepsilon_{\rm F} \to \varepsilon_{\rm F} - V_0$ where V_0 is the barrier (equivalent to the role of Z in Ref. [21]). The coefficients r and $r_{\rm A}$ may now be obtained by using the boundary conditions.

In the thin-barrier limit defined as $w \to 0$ and $V_0 \to \infty$ with s-wave pairing, Ref. [73] reported a π-periodicity of the conductance with respect to the parameter $\chi = V_0 d/v_{\rm F}$. In the present study, we do not restrict ourselves to isotropic pairing, nor to the thin-barrier limit, and show that new physics emerges from the presence of a finite-width barrier. We measure the width w of region I in units of $\lambda_{\rm F}$ and the potential barrier V_0 in units of $\varepsilon_{\rm F}$. The linear dispersion approximation is valid up to $\simeq 1$ eV [59], and we set $\varepsilon_{\rm F}/\Delta = 100$. In the doped case (referring here to a strong FVM between the N and S region), we set $\varepsilon'_{\rm F} = 10\varepsilon_{\rm F}$, and we also fix $V_0 = 10\varepsilon_{\rm F}$ in order to operate within the regime of

validity of the linear dispersion approximation. In the undoped case (referring here to the absence of a FVM between the N and S regions), we have $\varepsilon'_{\mathrm{F}} = \varepsilon_{\mathrm{F}}$.

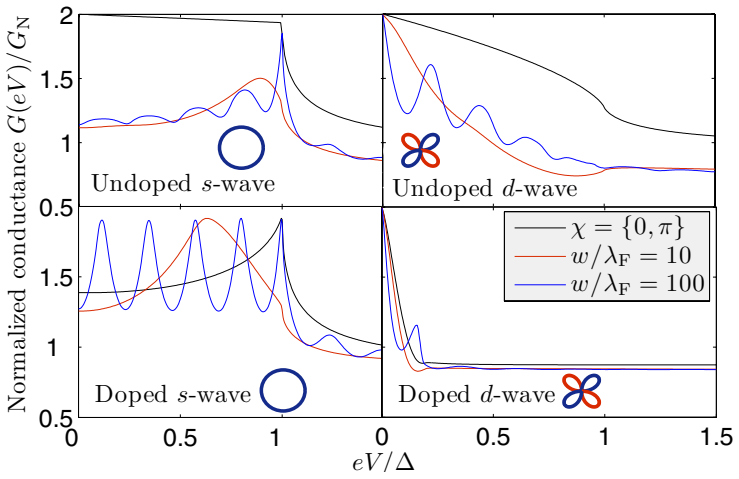

Figure 4.3: Tunneling conductance of N/I/S graphene junction for both s-wave and d-wave pairing in the undoped and doped case (see main text for parameter values). It is seen that for increasing w, a novel oscillatory behavior of the conductance as a function of voltage is present in all cases.

Consider Fig. 4.3 where we plot the normalized tunneling conductance in the two cases of s-wave and d-wave pairing, for both doped and undoped graphene. The most striking new feature compared to the thin-barrier limit is the strong oscillation of the conductance as a function of eV. We also include the thin-barrier limit with $\chi = 0$ and $\chi = \pi$ to illustrate the π-periodicity in this limit. For subgap energies, we regain the N/S conductance for undoped graphene when $\chi = 0$, with nearly perfect Andreev reflection. To model the d-wave pairing, we have used the $d_{x^2-y^2}$ model $\Delta(\theta) = \Delta\cos(2\theta - 2\alpha)$ with $\alpha = \pi/4$. The parameter α effectively models different orientations of the gap in $\boldsymbol{k}$-space with regard to the interface, and $\alpha = \pi/4$ corresponds to perfect formation of ZES in N/S metallic junctions. For $\alpha = 0$, the d-wave spectra are essentially identical to the s-wave case, since the condition for formation of zero-energy states (ZES) is not fulfilled in this case [74, 75]. It is seen that in all cases shown in Fig. 4.3 the conductance exhibits a novel oscillatory behavior as a function of applied bias voltage eV as the width w of the insulating region becomes much larger than the Fermi wavelength, i.e. $w \gg \lambda_{\mathrm{F}}$.

The oscillatory behavior of the conductance may be understood as follows. Non-relativistic free electrons with energy ε impinging upon a potential barrier V_0 are described by an exponentially decreasing non-oscillatory wavefunc-

tion e^{ikx} inside the barrier region if $\varepsilon < V_0$, since the dispersion essentially is $k \sim \sqrt{\varepsilon - V_0}$. Relativistic free electrons, on the other hand, have a dispersion $k \sim (\varepsilon - V_0)$, such that the corresponding wavefunctions do not decay inside the barrier region. Instead, the transmittance of the junction will display an oscillatory behavior as a function of the energy of incidence ε. In general, a kinetic energy given by $\sim k^\alpha$ will lead to a complex momentum $k \sim (\varepsilon - V_0)^{1/\alpha}$ inside the tunneling region, and hence damped oscillatory behavior of the wave function. Relativistic massless fermions are unique in the sense that only in this case ($\alpha = 1$) is the momentum purely real. Hence, the undamped oscillatory behavior at sub-gap energies appears as a direct manifestation of the relativistic low-energy Dirac fermions in the problem. This observation is also linked to the so-called Klein paradox which occurs for electrons with such a relativistic dispersion relation, which has been theoretically studied in normal graphene [76].

4.2.2 Josephson current in S/F/S graphene junctions

Currently, it is of considerable interest, and potentially of technological importance, to investigate how the unusual low-energy electronic properties of graphene manifest themselves in heterostructures where proximity effects are prominent. In particular, potential for future applications in devices seems plausible if such proximity-structures would combine two major functionalities in materials science, namely magnetism and superconductivity.

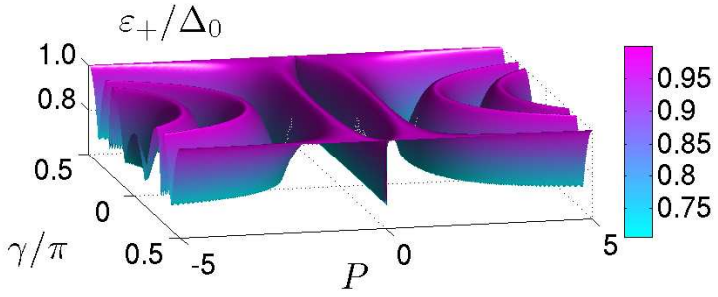

Figure 4.4: The Andreev bound state ε_+ [Eq. (2.20)] for $\Delta\phi = \pi/2$.

Here, we investigate the interplay between proximity-induced superconductivity and ferromagnetism in a graphene layer, resulting in an unusual behavior of the supercurrent through the system. Our main results are: *i)* The current-phase relationship deviates strongly from sinusoidal behavior, indicating a significant contribution from higher harmonics and *ii)* the critical current at the 0-π transition is finite and has a much larger value than the one observed in metallic systems. The latter result suggests a very efficient performance of the device as a supercurrent switch.

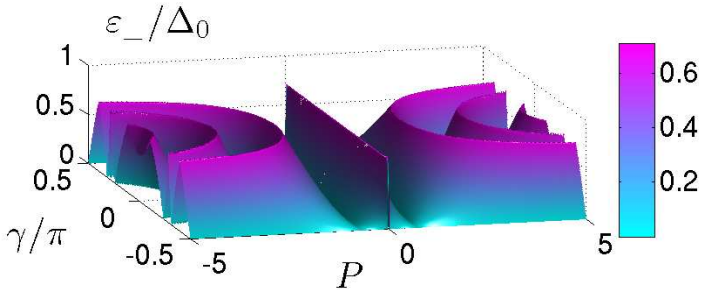

Figure 4.5: The Andreev bound state ε_- [Eq. (2.20)] for $\Delta\phi = \pi/2$.

We envisage an experimental setup where superconductivity is induced in two parts of the graphene region by means of conventional superconductors, such as Nb or Al, in close proximity. Between the superconducting regions, an exchange splitting is induced in the graphene layer by means of *e.g.* a magnetic insulating material. Instead of using a magnetic insulator such as EuO, where one in principle could tune the magnetization in the proximity layer with an external magnetic field, one also could envision using a multiferroic (*e.g.* $BiFeO_3$) or piezomagnetic material (*e.g.* $Fe_xNi_yB_z$) in close proximity to the graphene layer. Both of these classes of materials would offer the opportunity of tuning the exchange field in the material by some external control parameter – electric field due to the magnetoelectric coupling in the former case, and pressure in the latter. Upon modifying the exchange field in the proximity layer of the material, it is reasonable to assume that the proximity-induced exchange field in graphene would also be altered. Materials in which the magnetoelectric coupling is substantial are currently attracting much interest due to their potential for novel technological applications [77]. In order to control the local Fermi level in the ferromagnetic (F) region, one could possibly use a normal gate on top of the magnetic insulator to create a tunable barrier [68]. The superconducting (S) regions are assumed to be heavily doped, such that the Fermi energy satisfies $\varepsilon_F \gg \Delta$, while the F region is taken be undoped, i.e. $\varepsilon'_F \simeq 0$. Moreover, we assume sharp edges for the region separating the F and S graphene regions, and focus on the short-junction regime which is experimentally feasible.

Let us now present our results in detail. The F region separating the superconductors is taken to be undoped, such that the effective Fermi level is σh for spin-σ electrons. The regions S must be strongly doped to justify the mean-field treatment of superconductivity. We assume that this is comparable to the estimated exchange-splitting in the F region [68, 67]. Thus, we take $\varepsilon_F \simeq h$ to obtain analytically tractable results. To construct the scattering states that carry the supercurrent across the F region, we write down the Bogoliubov-de Gennes equations [64] in the presence of an exchange field h. The Bogoliubov-de Gennes equation essentially describes the eigenstates of quasiparticles in each

of the graphene regions and their belonging eigenvalues ε. It may be obtained by diagonalizing the full Hamiltonian, and constitutes the foundation for constructing the scattering states which are involved in the transport formalism we here use. For the spin-species σ, one finds that

$$\begin{pmatrix} H_0 - \sigma h(x) & \sigma\Delta(x) \\ \sigma\Delta^*(x) & -H_0 - \sigma h(x) \end{pmatrix} \begin{pmatrix} u^\sigma \\ v^{-\sigma} \end{pmatrix} = \varepsilon \begin{pmatrix} u^\sigma \\ v^{-\sigma} \end{pmatrix}. \tag{4.6}$$

Here, we have made use of the valley degeneracy and defined $H_0 = v_\mathrm{F}\mathbf{p}\cdot\boldsymbol{\sigma}$, where $\mathbf{p}$ is the momentum vector in the graphene plane and $\boldsymbol{\sigma}$ is a vector of Pauli matrices. The superconducting order parameter $\Delta(x)$ couples electron- and hole-excitations in the two valleys located at the two inequivalent corners of the hexagonal Brillouin zone. The u^σ spinor describes the electron-like part of the total wavefunction $\psi^\sigma = (u^\sigma, v^{-\sigma})^\mathrm{T}$, and in this case reads $u^\sigma = (\psi^\sigma_{A,+}, \psi^\sigma_{B,+})^\mathrm{T}$ while $v^{-\sigma} = \mathcal{T}u^\sigma$. Here, $^\mathrm{T}$ denotes the transpose while $\mathcal{T}$ is the time-reversal operator. To capture the essential physics, we write $\Delta(x) = \Delta_0 \mathrm{e}^{\mathrm{i}\phi_{\mathrm{L,R}}}$ in the left and right S region and $\Delta(x) = 0$ otherwise. Similarly, we set $h(x) = h$ in the F region and $h = 0$ otherwise. The Josephson current is computed via the usual energy-current relation summed over projections of all paths perpendicular to the tunneling barrier [78]

$$I_J(\Delta\phi) = -\frac{2e}{\hbar}\sum_i \int_{-\pi/2}^{\pi/2} \frac{\mathrm{d}\gamma\cos\gamma}{f^{-1}[\varepsilon_i(\Delta\phi)]} \frac{\mathrm{d}\varepsilon_i(\Delta\phi)}{\mathrm{d}\Delta\phi}, \tag{4.7}$$

where $\varepsilon_i(\Delta\phi)$ are the Andreev bound states carrying the current in the F region, and $\Delta\phi = \phi_\mathrm{R} - \phi_\mathrm{L}$ is the macroscopic phase difference between the superconductors. The integration over angles γ takes into account all possible trajectories and $f(x)$ is the Fermi-Dirac distribution function. We define the critical supercurrent as $I_c = |\max\{I_J(\Delta\phi)\}|$ and introduce $I_0 = 2e\Delta_0$. The procedure for obtaining $\varepsilon_i(\Delta\phi)$ is the same as in Ref. [65]. Let us introduce a parameter $P = hd/v_\mathrm{F}$ which captures the effect of both the exchange field h and the length d of the junction. To understand the nature of the Andreev bound states, consider Figs. 4.4 and 4.5 for a representative plot of $\varepsilon_\pm(\Delta\phi)$, using $\Delta\phi = \pi/2$. As is seen from both plots, the bound state energies exhibit a strong oscillatory dependence on the parameter P. This indicates that similar oscillatory behavior may be expected in the supercurrent itself. Interestingly, the oscillations seen in Figs. 4.4 and 4.5 are not damped with increasing P. This directly reflects the Dirac-cone linear dispersion of the graphene electrons and is reminiscent of the weak damping of conductance oscillations at subgap energies in graphene-superconductor junctions [79, 76].

The current-phase relationship for the S/F/S graphene junction is shown in Fig. 4.6. With increasing P, the critical current gets suppressed and finally the sign of the current is changed. Remarkably, the critical current never goes to zero. An interesting feature of the plot in Fig. 4.6a) is that the discontinuity at $\Delta\phi = \pi$ for $P = 0$ is split for increasing P. The discontinuity of the current-phase relation originates with a crossing of Andreev levels in the normal graphene (F graphene with $h = 0$) region at $\Delta\phi = \pi$. For $\Delta\phi \in [0, \pi)$, only the

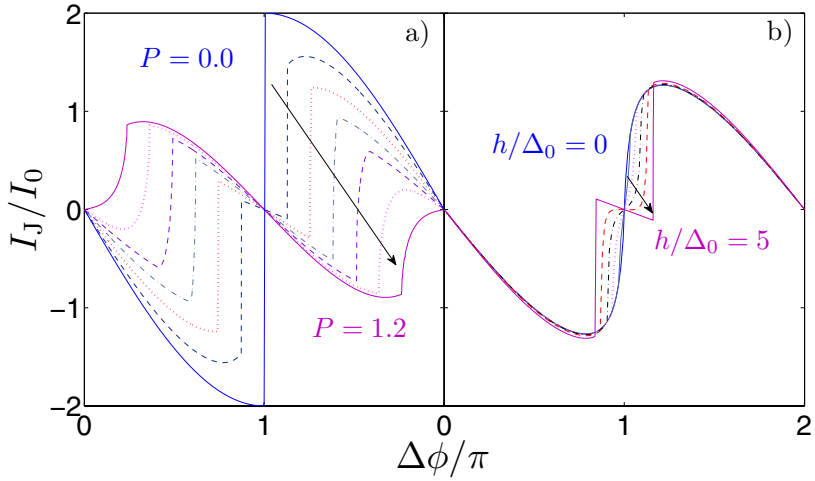

Figure 4.6: a) Current-phase relationship in the S/F/S graphene junction with undoped F region. We have fixed $\varepsilon_F = h$ and set $\varepsilon'_F = 0$. We have used values of P in the interval $[0.0, 1.2]$ in steps of 0.2. b) Current-phase relationship in the S/F/S graphene junction with doped F region. We have set $\varepsilon_F/\Delta_0 = 10$, $\varepsilon'_F/\Delta_0 = 15$, $d/\xi = 0.05$ and vary h/Δ_0 in the range $[0, 5]$ in steps of 1.

0-mode Andreev bound state carries the current. For $\Delta\phi \in (\pi, 2\pi]$, the π-mode Andreev bound state carries the current, such that there is an abrupt crossover exactly at $\Delta\phi = \pi$. The situation changes when $h \neq 0$, since the spin-splitting doubles the number of Andreev bound states. Consequently, the crossover between different modes may occur at $\Delta\phi \neq \pi$, as a result of the superharmonic current-phase relationship. We have checked explicitly that the strong deviation from a sinusoidal current-phase relationship persists for larger d that do not satisfy $d/\xi \ll 1$. However, in this case one should strictly speaking also include the contribution to the current from the continuum of supergap states [78]. This requires a separate study, and we here focus on the short-junction regime.

To show that the splitting of this discontinuity originates with the presence of an exchange field which separates the spin-$\uparrow$ and spin-$\downarrow$ bands, we have also numerically solved the current-phase relationship for a nonzero Fermi level in the ferromagnetic region. Although we have obtained analytical results in this regime, these are somewhat cumbersome and therefore omitted here. The result is shown in Fig. 4.6b) where we have chosen $\Delta_0 = 1$ meV, $\varepsilon_F = 10$ meV, and $\varepsilon'_F = 15$ meV, and varying h in the range $[0, 5]$ meV. This ensures that there are no evanescent modes, such that only the Andreev bound states carry the current. We choose a junction with $d/\xi = 0.05$, where ξ is the superconducting

coherence length, since the short junction regime $d \ll \xi$ is the experimentally most relevant one. The figures in a) and b) correspond to two quite different regimes: in a) the exchange field is much larger than the Fermi level while in b) the exchange field is much smaller than the Fermi level. The trend is nevertheless seen to be the same in both cases, namely a progressive splitting of the discontinuity located at $\Delta\phi = \pi$ in the paramagnetic case.

Assuming a heavily doped superconducting region with $\varepsilon_{\mathrm{F}} = 10$ meV and an effective gap Δ_0 of 1 meV, a mean-field treatment is justified by $\varepsilon_{\mathrm{F}} \gg \Delta_0$. Moreover, the short-junction regime requires that $d \ll \xi$. Using $v_{\mathrm{F}} \simeq 10^6$ m/s in graphene, we obtain from $\xi = v_F/\Delta$ that $d \ll 650$ nm is required.

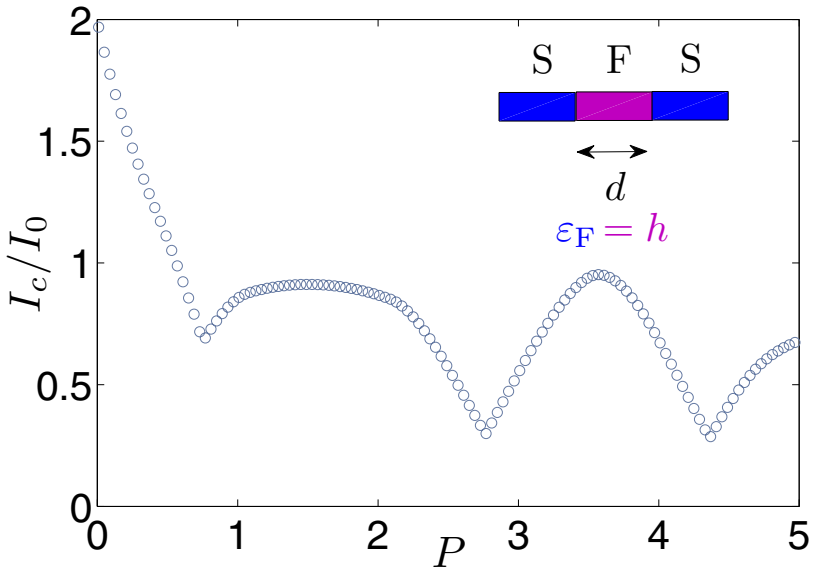

Figure 4.7: The critical supercurrent in a proximity-induced S/F/S graphene junction for $\varepsilon_{\mathrm{F}} = h$ and $\varepsilon'_{\mathrm{F}} = 0$.

This condition has been met in at least two experimental studies of proximity-induced superconductivity in graphene [63, 80]. The critical supercurrent I_c for an S/F/S graphene junction for $\varepsilon_{\mathrm{F}} = h$ and $\varepsilon'_{\mathrm{F}} = 0$ is shown in Fig. 4.7. The critical current shows oscillations with respect to P, but decays weakly compared to the metallic case and never reaches $I_c = 0$ in the relevant regime. For instance, there is a factor $\simeq 100$ in reduction of the amplitude of the current right after the second cusp in the metallic case for $h \simeq 10\Delta_0$ (see Fig. 2 in Ref. [81]) while there is only a factor $\simeq 2$ in reduction of the amplitude in the present case. Right at the cusps located at $P \simeq \{0.8, 2.8, 4.4\}$, there is a large residual value of the supercurrent which should be experimentally detectable. This is very distinct from the usual sinusoidal current-phase relationship for

the Josephson current, in which the supercurrent vanishes completely at the 0-π transition. The first switch occurs at a value $P = hd/v_F \approx 0.8$. For an exchange splitting of $h \simeq 10$ meV, this requires a junction width $d = 50$ nm. Alternatively, employing a junction width of $d = 100$ nm [63, 80] one would need an exchange splitting of $h \simeq 5$ meV [68].

In order to explain the appearance of cusps in the critical current dependent on exchange field and junction width, it is instructive to draw parallels to the metallic S/F/S junction and the behavior of the supercurrent. In most experimental situations, the effective barriers separating the F and S regions are strong, leading to a current-phase relationship which is very nearly sinusoidal, i.e. $I_c = I_0 \sin \Delta\phi$ [15]. By tuning the temperature T and width of the junction d, one is able to switch the sign of the amplitude I_0, which necessarily means that one must have $I_0 = 0$ at some point. Precisely such behavior has been observed in several experiments [14, 82]. In the present system, the current-phase relationship deviates strongly from sinusoidal behavior, and contains a significant contribution from higher harmonics. Tracking the absolute value of the current with increasing P from Fig. 4.6, it is seen that I_c never becomes zero. Instead, it has a large residual value at the points where the current changes sign. While a small, but finite value of the supercurrent at the 0-π transition also has been observed in metallic S/F/S junctions [83], the magnitude of the residual value of the supercurrent in the graphene case is huge compared to the metallic case.

Chapter 5

Conclusion and outlook

In this thesis, we have investigated how superconductivity and ferromagnetism affect each other in several contexts. We have considered artificially created proximity structures of alternating superconducting and ferromagnet layers, as well as coexistence of the two orders in a bulk material. We have mainly focused on thermodynamic and transport properties of the systems under consideration. Some of our main results are listed below.

- We find an abrupt pairing state transition from an even-to odd-frequency symmetry in a normal metal/superconductor bilayer with a magnetic interface, which occurs both in the diffusive and ballistic limit and independently of most junction parameters.
- We have studied how spin-orbit coupling arising out of a noncentrosymmetric crystal lattice structure influences ferromagnetic and superconducting order, presenting a self-consistent, analytical solution for the order parameters in the low temperature limit.
- We have studied the transport properties of graphene under the influence of a superconducting proximity effect, unveiling in particular a highly unusual behavior of the supercurrent in an S/F/S graphene heterostructure.

The interplay between ferromagnetism and superconductivity is presently a hot research field with a lot of activity. We here venture some suggestions for interesting future directions of research in this field, some of which undoubtedly will be pursued by the present author.

- In the vast majority of the literature so far, the influence of a current on the magnetization dynamics in superconducting proximity-structures has not received much attention. Nevertheless, one would expect some interesting spin-transfer torque effects to take place in inhomogeneous ferromagnetic structures. For instance, is it possible to obtain magnetization switching or current-induced domain wall motion by means of a Josephson current?
- A spontaneous vortex phase is likely to appear in ferromagnetic superconductors under general circumstances. In what way do the magnetic and superconducting order parameters coexist in this arrangement?

- The high electron mobilities in graphene and the long spin relaxation length ~ 1 μm at room temperature suggests that graphene is very suitable for spintronics applications. Is it possible to create superconducting spin-valves of graphene? How would the non-local processes of crossed Andreev-reflection and elastic co-tunneling be influenced by the Dirac-like nature of the charge carriers in graphene?

These and several other interesting venues are likely to be explored within short. Future challenges also include modelling the interface region between a ferromagnet and a superconductor in a more realistic manner, as well as taking into account complicated magnetic textures in the ferromagnetic region. For instance, inhomogeneous configurations of the magnetization texture (*e.g.* domain walls) are likely to have a non-trivial effect on the proximity-induced superconducting correlations. In the context of heavy-fermion compounds, there is also a need for a theory that may capture the essential effect of the complicated multiband structure near Fermi level which always is present for high atomic number materials.

In conclusion, while much progress has been made in the field of unusual superconducting systems that include ferromagnetic elements, this rapidly evolving field still offers many unresolved issues which need to be addressed in order to gain a fuller understanding of the physics at hand.

Bibliography

[1] J. Bardeen, L. N. Cooper, and J. R. Schrieffer, Phys. Rev. **108**, 1175 (1957).

[2] S. S. Saxena, P. Agarwal, K. Ahilan, F. M. Grosche, R. K. W. Haselwimmer, M. J. Steiner, E. Pugh, I. R. Walker, S. R. Julian, P. Monthoux, G. G. Lonzarich, A. Huxley, I. Sheikin, D. Braithwaite, and J. Flouquet, Nature **406**, 587 (2000).

[3] D. Aoki, A. Huxley, E. Ressouche, D. Braithwaite, J. Flouquet, J.-P. Brison, E. Lhotel, and C. Paulsen, Nature **413**, 613 (2001).

[4] N. T. Huy, A. Gasparini, D. E. de Nijs, Y. Huang, J. C. Klaasse, T. Gortenmulder, A. de Visser, A. Hamann, T. Görlach, and H. v. Löhneysen, Phys. Rev. Lett. **99**, 067006 (2007).

[5] T. Akazawa, H. Hidaka, H. Kotegawa, T. C. Kobayashi, T. Fujiwara, E. Yamamoto, Y. Haga, R. Settai, and Y. Onuki, J. Phys. Cond. Mat. **16**, L29 (2004); *ibid* J. Phys. Soc. Jpn. **73**, 3129 (2004).

[6] M. N. Baibich, J. M. Broto, A. Fert, F. Nguyen Van Dau, F. Petroff, P. Etienne, G. Creuzet, A. Friederich, and J. Chazelas, Phys. Rev. Lett. **61**, 2472 (1988).

[7] G. Binasch, P. Grunberg, F. Saurenbach, and W. Zinn, Phys. Rev. B **39**, 4828 (1989).

[8] J. Clarke and F. K. Wilhelm, Nature **453**, 1031 (2008).

[9] K. S. Novoselov, A.K. Geim, S.V. Morozov, D. Jiang, Y. Zhang, S.V. Dubonos, I.V. Grigorieva, and A.A. Firsov, Science **306**, 666 (2004).

[10] K.S. Novoselov, A.K. Geim, S.V. Morozov, D. Jiang, M.I. Katsnelson, I.V. Grigorieva, S.V. Dubonos, and A.A. Firsov, Nature **438**, 197 (2005).

[11] R. Shen, Z. M. Zheng, S. Liu, and D. Y. Xing, Phys. Rev. B **67**, 024514 (2003).

[12] A. A. Golubov, M. Yu. Kupriyanov, and E. IlŠichev, Rev. Mod. Phys. **76**, 411 (2004).

[13] A. I. Buzdin, Rev. Mod. Phys. **77**, 935 (2005).

[14] V.V. Ryazanov, V. A. Oboznov, A. Yu. Rusanov, A. V. Veretennikov, A. A. Golubov, and J. Aarts, Phys. Rev. Lett. **86**, 2427 (2001).

[15] G. Mohammadkhani and M. Zareyan, Phys. Rev. B **73**, 134503 (2006).

[16] J. Linder, T. Yokoyama, and A. Sudbø, Phys. Rev. B **77**, 174514 (2008).

[17] E. Goldobin, D. Koelle, R. Kleiner, and A. Buzdin, Phys. Rev. B **76**, 224523 (2007).

[18] M. Yu. Kupriyanov and V. F. Lukichev, Zh. Exp. Teor. Fiz. **94**, 139 (1988).

[19] Yu. Nazarov, Superlatt.Microstruct. **25**, 1221 (1999).

[20] F. S. Bergeret, A. Volkov, and K. B. Efetov, Rev. Mod. Phys. **77**, 1321 (2005).

[21] G. E. Blonder, M. Tinkham, and T. M. Klapwijk, Phys. Rev. B **25**, 4515 (1982).

[22] M. Eschrig, J. Kopu, J. C. Cuevas, and Gerd Schön, Phys. Rev. Lett. **90**, 137003 (2003); M. Eschrig, T. Löfwander, T. Champel, J. C. Cuevas, J. Kopu, and Gerd Schön, J. Low Temp. Phys. **147** 457 (2007).

[23] J. W. Serene and D. Rainer, Phys. Rep. **101**, 221 (1983).

[24] We will use the notation and conventions of J. P. Morten, Master Thesis, Norwegian University of Science and Technology, (2003) (unpublished), which in turn is close the notations used in Ref. [23].

[25] V. L. Berezinskii, JETP Lett. **20**, 287 (1974).

[26] F. S. Bergeret, A. F. Volkov, and K. B. Efetov, Phys. Rev. Lett. **86**, 4096 (2001).

[27] A. Volkov, F. S. Bergeret, and K. B. Efetov, Phys. Rev. Lett. **90**, 117006 (2003).

[28] Y. Tanaka, A. A. Golubov, S. Kashiwaya, and M. Ueda, Phys. Rev. Lett. **99**, 037005 (2007); Y. Tanaka and A. A. Golubov, Phys. Rev. Lett. **98**, 037003 (2007).

[29] G. Eilenberger, Sov. Phys. JETP **214**, 195 (1968).

[30] K. Usadel, Phys. Rev. Lett. **25**, 507 (1970).

[31] A. V. Zaitsev, Sov. Phys. JETP **59**, 1163 (1984).

[32] A. Millis, D. Rainer, and J. A. Sauls, Phys. Rev. B **38**, 4504 (1988).

[33] D. H. Hernando, Yu. V. Nazarov, and W. Belzig, Phys. Rev. Lett. **88**, 047003 (2002); D. H. Hernando, Yu. V. Nazarov, and W. Belzig, arXiv:cond-mat/0204116.

[34] A. Brataas, Yu. V. Nazarov, and G. E. Bauer, Phys. Rev. Lett. **11**, 2481 (2000); A. Brataas, G. E. W. Bauer, and P. J. Kelly, Phys. Rep. **427**, 157 (2006).

[35] M. Eschrig and T. Löfwander, Nature Physics **4**, 138 (2008).

[36] A. Cottet and W. Belzig, Phys. Rev. B **72**, 180503 (2005).

[37] R. Meservey and P. M. Tedrow, Phys. Rep. **238**, 173 (1994).

[38] A. M. Clogston, Phys. Rev. Lett. **9**, 266 (1962); B. S. Chandrasekhar, Appl. Phys. Lett. **1**, 7 (1962).

[39] Y. Asano, Y. Tanaka, A. A. Golubov, and S. Kashiwaya, Phys. Rev. Lett. **98**, 107002 (2007).

[40] T. Yokoyama, Y. Tanaka, and A. A. Golubov, Phys. Rev. B **75**, 134510 (2007).

[41] V. Braude and Yu. V. Nazarov, Phys. Rev. Lett. **98**, 077003 (2007).

[42] K. Fossheim and A. Sudbø, *Superconductivity: Physics and Applications* (Wiley, New York, 2004), Chap. 5.

[43] A. J. Leggett, Rev. Mod. Phys. **47**, 331 (1975).

[44] E. Bauer, G. Hilscher, H. Michor, Ch. Paul, E. W. Scheidt, A. Gribanov, Yu. Seropegin, H. Noël, M. Sigrist, and P. Rogl, Phys. Rev. Lett. **92**, 027003 (2004)

[45] J. Linder and A. Sudbø, Phys. Rev. B **76**, 054511 (2007).

[46] C. Iniotakis, N. Hayashi, Y. Sawa, T. Yokoyama, U. May, Y. Tanaka, and M. Sigrist, Phys. Rev. B **76**, 012501 (2007).

[47] A.B. Vorontsov, I. Vekhter, and M. Eschrig, Phys. Rev. Lett. **101**, 127003 (2008).

[48] C. Iniotakis, S. Fujimoto, and M. Sigrist, J. Phys. Soc. Jpn. **77**, 083701 (2008).

[49] A. H. Nevidomskyy, Phys. Rev. Lett. **94**, 097003 (2005).

[50] M. S. Grønsleth, J. Linder, J.-M. Børven, and A. Sudbø, Phys. Rev. Lett. **97**, 147002 (2006).

[51] E. K. Dahl and A. Sudbø, Phys. Rev. B **75**, 144504 (2007).

[52] B. J. Powell, James F. Annett, and B. L. Györffy, J. Phys. A **36**, 9289 (2003).

[53] S. Tewari, D. Belitz, T. R. Kirkpatrick, and J. Toner, Phys. Rev. Lett. **93**, 177002 (2004).

[54] E. I. Rashba, Sov. Phys. Solid State **2**, 1109 (1960).

[55] K. V. Samokhin and M. B. Walker, Phys. Rev. B **66**, 174501 (2002); F. Hardy and A. D. Huxley, Phys. Rev. Lett. **94**, 247006 (2005).

[56] K. Machida and T. Ohmi, Phys. Rev. Lett. **86**, 850 (2001).

[57] P. W. Anderson, J. Phys. Chem. Solids **11**, 26 (1959).

[58] P. A. Frigeri, D. F. Agterberg, A. Koga, and M. Sigrist, Phys. Rev. Lett. **92**, 097001 (2004).

[59] P. R. Wallace, Phys. Rev. **71**, 622 (1947).

[60] J. Gonzalez, F. Guinea, and M. A. Vozmediano, Phys. Rev. B **59**, R2474 (1999).

[61] J. Gonzalez, F. Guinea, and M. A. H. Vozmediano, Nucl. Phys. B **424**, 595 (1994).

[62] D. T. Son, Phys. Rev. B **75**, 235423 (2007).

[63] H. B. Heersche, P. Jarillo-Herrero, J. B. Oostinga, L. M. K. Vandersypen and A. F. Morpurgo, Nature **446**, 56 (2007).

[64] C. W. J. Beenakker, Phys. Rev. Lett. **97**, 067007 (2006).

[65] M. Titov and C. W. J. Beenakker, Phys. Rev. B **74**, 041401(R) (2006).

[66] Y.-W. Son, M. L. Cohen, and S. G. Louie, Nature **444**, 347 (2006).

[67] Y. G. Semenov, J. M. Zavada, and K. W. Kim, Phys. Rev. Lett. **101**, 147206 (2008); Phys. Rev. B **77**, 235415 (2008).

[68] H. Haugen, D. Huertas-Hernando, and A. Brataas, Phys. Rev. B **77**, 115406 (2008).

[69] J. Martin, N. Akerman, G. Ulbricht, T. Lohmann, J. H. Smet, K. von Klitzing, and A. Yacoby, Nature Physics **4**, 144 (2008).

[70] E.-A. Kim and A. H. Castro Neto, *arXiv*:0702.562.

[71] H. Kleinert, Phys. Rev. Lett. **84**, 286 (2000).

[72] S. Kashiwaya, Y. Tanaka, M. Koyanagi, and K. Kajimura, Phys. Rev. B **53**, 2667 (1996).

[73] S. Bhattacharjee and K. Sengupta, Phys. Rev. Lett. **97**, 217001 (2006).

[74] C.-R. Hu, Phys. Rev. Lett. **72**, 1526 (1994).

[75] Y. Tanaka and S. Kashiwaya, Phys. Rev. Lett. **74**, 3451 (1995).

[76] M. I. Katsnelson, K. S. Novoselov, and A. K. Geim, Nature Physics **2**, 620 (2006).

[77] R. Ramesh and N. A. Spaldin, Nature Materials **6**, 21 (2007); S.-W. Cheong and M. Mostovoy, Nature Materials **6**, 13 (2006).

[78] C. W. J. Beenakker and H. van Houten, Phys. Rev. Lett. **66**, 3056 (1991).

[79] J. Linder and A. Sudbø, Phys. Rev. Lett. **99**, 147001 (2007); Phys. Rev. B **77**, 064507 (2008).

[80] X. Du, I. Skachko, and E. Y. Andrei, *arXiv*:0710.4984.

[81] A. S. Vasenko, A. A. Golubov, M. Yu. Kupriyanov, and M. Weides, Phys. Rev. B **77**, 134507 (2008).

[82] T. Kontos, M. Aprili, J. Lesueur, F. Genet, B. Stephanidis, and R. Boursier, Phys. Rev. Lett. **89**, 137007 (2002); W. Guichard, M. Aprili, O. Bourgeois, T. Kontos, J. Lesueur, and P. Gandit, Phys. Rev. Lett. **90**, 167001 (2003).

[83] H. Sellier, C. Baraduc, F. Lefloch, and R. Calemczuk, Phys. Rev. B **68**, 054531 (2003).

Paper I

Interplay between ferromagnetism and superconductivity in tunneling currents.

Physical Review Letters **97**, 147002 (2006).

Interplay between Ferromagnetism and Superconductivity in Tunneling Currents

M. S. Grønsleth,[1] J. Linder,[1] J.-M. Børven,[1] and A. Sudbø[1]

[1]*Department of Physics, Norwegian University of Science and Technology, N-7491 Trondheim, Norway*

(Received 24 February 2006; published 3 October 2006)

We study tunneling currents in a model consisting of two nonunitary ferromagnetic spin-triplet superconductors separated by a thin insulating layer. We find a novel interplay between ferromagnetism and superconductivity, manifested in the Josephson effect. This offers the possibility of tuning dissipationless currents of charge and spin in a well-defined manner by adjusting the magnetization direction on either side of the junction.

DOI: 10.1103/PhysRevLett.97.147002 PACS numbers: 74.20.Rp, 74.50.+r

The coexistence of ferromagnetism (FM) and superconductivity (SC) has recently been experimentally confirmed [1,2]. This offers the possibility of observing new and interesting physical effects in the transport of spin and charge. The spin-singlet character of Cooper pairs in conventional superconductors suggests that FM and SC are mutually excluding properties for a material. Indeed, coexistence of magnetic order with singlet SC is not possible for uniform order parameters [3]. On the other hand, spin-triplet Cooper pairs [4,5] are, in principle, perfectly compatible with ferromagnetism. For instance, odd-in-frequency $S_z = 0$ spin-triplet superconductivity in superconductor-ferromagnet structures has been much studied in the literature [6]. The synthesis of superconductors exhibiting ferromagnetism, with simultaneously broken U(1) and O(3) symmetries, is of considerable interest from a fundamental physics point of view and, moreover, opens up a vista to a plethora of novel applications. This has been the subject of theoretical research in, e.g., Ref. [7], and has a broad range of possible applications. Also, focus on hybrid systems of ferromagnets and superconductors has arisen from the aspiration of utilizing the spin of the electron as a binary variable in device applications. This has led to spin-current-induced magnetization switching [8], and suggestions have been made for devices such as spin-torque transistors [9] and spin batteries [10]. Moreover, spin supercurrents have a long tradition in ^{3}He [11], while recent work has focused on dissipationless spin currents in unitary spin-triplet superconductors [12].

This Letter addresses the case of two p-wave superconductors arising out of a ferromagnetic metallic state, separated by a tunneling junction. Such states have been suggested to exist on experimental grounds, in compounds such as $RuSr_2GdCu_2O_8$ [13], UGe_2 [1], and URhGe [2], and have been studied theoretically in, e.g., Refs. [14–16]. Coexisting FM and spin-triplet SC have also been proposed to arise out of half-metallic ferromagnetic materials such as CrO_2 and the alloys UNiSn and NiMnSb [17]. We compute the Josephson contribution to the tunneling currents, in both the charge and spin channels, within linear response theory using the Kubo formula. Our assumption is that the superconducting order is that of spin-triplet pairing, and we consider the analog of the $A2$ phase in ^{3}He, i.e., SC order parameters that satisfy $|\Delta_{\mathbf{k}\uparrow\uparrow}| \neq |\Delta_{\mathbf{k}\downarrow\downarrow}| \neq 0$ and $\Delta_{\mathbf{k}\uparrow\downarrow} = 0$. In terms of the $\mathbf{d}_\mathbf{k}$-vector formalism [11], we then have a nonunitary state since the average spin $\langle \mathbf{S}_\mathbf{k} \rangle = i\mathbf{d}_\mathbf{k} \times \mathbf{d}_\mathbf{k}^* = \frac{1}{2}(|\Delta_{\mathbf{k}\uparrow\uparrow}|^2 - |\Delta_{\mathbf{k}\downarrow\downarrow}|^2)\hat{\mathbf{z}}$ of the Cooper pairs is nonzero. Such a scenario is compatible with uniform FM and SC, since the electrons responsible for ferromagnetism below the Curie temperature T_M condense into Cooper pairs with magnetic moments aligned with the magnetization below the critical temperature T_c. The choice of such a nonunitary state is motivated by the fact that there is strong reason to believe that the correct pairing symmetries in the ferromagnetic superconductors (FMSC) discovered so far are nonunitary [15,18,19]. The exchange field will also give rise to a Zeeman splitting between the $\uparrow$ and $\downarrow$ conduction bands, thus suppressing the SC order parameter $\Delta_{\mathbf{k}\uparrow\downarrow}$ [2], as illustrated in Fig. 1(b).

Another important issue to address is whether the SC and FM order parameters coexist uniformly, or if they are phase-separated. One possibility is that a spontaneously formed vortex lattice due to the internal magnetization $\mathbf{m}$ is realized in a spin-triplet FMSC [20]. However, there have also been reports of uniform superconducting phases in spin-triplet FMSC [21]. A key variable determining whether a vortex lattice appears or not is the strength of the internal magnetization $\mathbf{m}$ [22]. Current experimental data on URhGe apparently do not settle this issue unambiguously, while uniform coexistence of FM and SC appears to have been experimentally verified in UGe_2 [23].

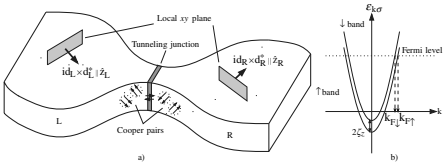

FIG. 1 (color online). (a) Tunneling of Cooper pairs between two nonunitary FMSC with noncollinear magnetization. (b) Band splitting for $\uparrow$ and $\downarrow$ electrons in the presence of a magnetization in the $\hat{\mathbf{z}}$ direction, leading to a suppression of interband pairing.

Furthermore, a bulk Meissner state in the FMSC $RuSr_2GdCu_2O_8$ has been reported in Ref. [24], indicating the existence of uniform FM and SC as a bulk effect. Consequently, we will use bulk values for the order parameters and assume that they coexist uniformly. We emphasize that one, in general, should take into account the possible suppression of the SC order parameter in the vicinity of the tunneling interface due to the formation of midgap surface states [25] which occur for certain orientations of the SC gap. The pair-breaking effect of these states in unconventional superconductors has been studied in, e.g., Ref. [26]. A sizable formation of such states would suppress the Josephson current, although it is nonvanishing in the general case. Also, we use bulk uniform magnetic order parameters, as in Refs. [27,28]. The latter is justified on the grounds that a ferromagnet with a planar order parameter is mathematically isomorphic to an s-wave superconductor, where the use of bulk values for the order parameter right up to the interface is a good approximation due to the lack of midgap surface states. Moreover, we consider thin-film FMSC such that the orbital effect does not break the Cooper pairs. Our model is illustrated in Fig. 1(a).

The main result of this Letter is that the Josephson current in the spin and charge sectors between two nonunitary FMSC can be controlled by adjusting the relative magnetization orientation on each side of the junction provided that spin-triplet Cooper pairs are present. Our system consists of two FMSC separated by an insulating layer such that the total Hamiltonian can be written as $H = H_{\mathrm{L}} + H_{\mathrm{R}} + H_T$, where L and R represent the individual FMSC on each side of the tunneling junction, and H_T describes tunneling of particles through the insulating layer separating the two pieces of bulk material. The FMSC Hamiltonian is given by [16] $H_{\mathrm{FMSC}} = H_0 + \sum_{\mathbf{k}} \psi_{\mathbf{k}}^{\dagger} \mathcal{A}_{\mathbf{k}} \psi_{\mathbf{k}}$, where $H_0 = JN\gamma(0)\mathbf{m}^2 + \frac{1}{2}\sum_{\mathbf{k}\sigma}\varepsilon_{\mathbf{k}\sigma} + \sum_{\mathbf{k}\alpha\beta}\Delta_{\mathbf{k}\alpha\beta}^{\dagger} b_{\mathbf{k}\alpha\beta}$. Here $\mathbf{k}$ is the electron momentum, $\varepsilon_{\mathbf{k}\sigma} = \varepsilon_{\mathbf{k}} - \sigma\zeta_z$, $\sigma = \uparrow, \downarrow = \pm 1$, J is a spin coupling constant, $\gamma(0)$ is the number of nearest lattice neighbors, $\mathbf{m} = \{m_x, m_y, m_z\}$ is the magnetization vector, while $\Delta_{\mathbf{k}\alpha\beta}$ is the superconducting order parameter and $b_{\mathbf{k}\alpha\beta} = \langle c_{-\mathbf{k}\beta} c_{\mathbf{k}\alpha} \rangle$ is the two-particle operator expectation value. The ferromagnetic order parameter is defined by $\zeta = 2J\gamma(0)(m_x - im_y)$ and $\zeta_z = 2J\gamma(0)m_z$. We express the Hamiltonian in the basis $\psi_{\mathbf{k}} = (c_{\mathbf{k}\uparrow} c_{\mathbf{k}\downarrow} c_{-\mathbf{k}\uparrow}^{\dagger} c_{-\mathbf{k}\downarrow}^{\dagger})^T$, where $c_{\mathbf{k}\sigma}$ ($c_{\mathbf{k}\sigma}^{\dagger}$) are annihilation (creation) fermion operators. Note that there is no spin-orbit coupling in our model; i.e., inversion symmetry is not broken. Consider now the 4×4 matrix

$$\mathcal{A}_{\mathbf{k}} = -\frac{1}{2}\begin{pmatrix} -\varepsilon_{\mathbf{k}}\mathbf{1} + \boldsymbol{\sigma}\cdot\boldsymbol{\zeta} & i\mathbf{d}_{\mathbf{k}}\cdot\boldsymbol{\sigma}\sigma_y \\ (i\mathbf{d}_{\mathbf{k}}\cdot\boldsymbol{\sigma}\sigma_y)^{\dagger} & (\varepsilon_{\mathbf{k}}\mathbf{1} - \boldsymbol{\sigma}\cdot\boldsymbol{\zeta})^T \end{pmatrix} \quad (1)$$

which is valid for a FMSC with arbitrary magnetization. As explained in the introduction, we will study in detail a nonunitary equal-spin pairing (ESP) FMSC as illustrated in Fig. 1(a), i.e., $\Delta_{\mathbf{k}\uparrow\downarrow} = \Delta_{\mathbf{k}\downarrow\uparrow} = 0$, $\zeta = 0$ in Eq. (1). Since the quantization axes of the two FMSC are not aligned, one needs to include the Wigner d function [29] denoted by $\mathcal{D}_{\sigma'\sigma}(\vartheta)$ with $j = 1/2$ to account for the fact that a $\uparrow$ spin on one side of the junction is not the same as a $\uparrow$ spin on the other side of the junction. The spin quantization axes are taken along the direction of the magnetization on each side, so that the angle ϑ is defined by $\mathbf{m}_{\mathrm{R}} \cdot \mathbf{m}_{\mathrm{L}} = m_{\mathrm{R}} m_{\mathrm{L}} \cos(\vartheta)$, where $m_i = |\mathbf{m}_i|$. The tunneling Hamiltonian then reads $H_T = \sum_{\mathbf{kp}\sigma\sigma'} \mathcal{D}_{\sigma'\sigma}(\vartheta)(T_{\mathbf{kp}} c_{\mathbf{k}\sigma}^{\dagger} d_{\mathbf{p}\sigma'} + T_{\mathbf{kp}}^{*} d_{\mathbf{p}\sigma'}^{\dagger} c_{\mathbf{k}\sigma})$, where we neglect the possibility of spin flips in the tunneling process. The validity of the tunneling Hamiltonian approach requires that the applied voltage across the junction is small. Here we will be concerned with the case of zero bias voltage, so that the tunneling Hamiltonian approach is appropriate. Note that we distinguish between fermion operators on each side of the junction corresponding to $c_{\mathbf{k}\sigma}$ and $d_{\mathbf{k}\sigma}$. Furthermore, we write the superconducting order parameters as $\Delta_{\mathbf{k}\sigma\sigma} = |\Delta_{\mathbf{k}\sigma\sigma}| e^{i(\theta_{\mathbf{k}} + \theta_{\sigma\sigma}^{\mathrm{R}})}$, where R (L) denotes the bulk superconducting phase on the right (left) side of the junction, while $\theta_{\mathbf{k}}$ is an internal phase factor originating from the specific form of the gap in $\mathbf{k}$ space that ensures odd symmetry under inversion of momentum, i.e., $\theta_{\mathbf{k}} = \theta_{-\mathbf{k}} + \pi$.

For our system, the Hamiltonian takes the form $H_{\mathrm{FMSC}} = H_0 + H_A$, $H_A = \sum_{\mathbf{k}\sigma} \phi_{\mathbf{k}\sigma}^{\dagger} A_{\mathbf{k}\sigma} \phi_{\mathbf{k}\sigma}$, where we have chosen a convenient basis $\phi_{\mathbf{k}\sigma}^{\dagger} = (c_{\mathbf{k}\sigma}^{\dagger}, c_{-\mathbf{k}\sigma})$ that block diagonalizes $\mathcal{A}_{\mathbf{k}}$ and defined $A_{\mathbf{k}\sigma} = \frac{1}{4}[2\varepsilon_{\mathbf{k}\sigma}\sigma_z + \Delta_{\mathbf{k}\sigma\sigma}(\sigma_x + i\sigma_y) + \Delta_{\mathbf{k}\sigma\sigma}^{\dagger}(\sigma_x - i\sigma_y)]$, with Pauli matrices σ_i. This Hamiltonian is diagonalized by a 2×2 spin generalized unitary matrix $U_{\mathbf{k}\sigma}$, so that the superconducting sector is expressed in the diagonal basis $\tilde{\phi}_{\mathbf{k}\sigma}^{\dagger} = \phi_{\mathbf{k}\sigma}^{\dagger} U_{\mathbf{k}\sigma} \equiv (\gamma_{\mathbf{k}\sigma}^{\dagger}, \gamma_{-\mathbf{k}\sigma})$. Thus, $H_A = \sum_{\mathbf{k}\sigma} \tilde{\phi}_{\mathbf{k}\sigma}^{\dagger} \tilde{A}_{\mathbf{k}\sigma} \tilde{\phi}_{\mathbf{k}\sigma}$, in which $\tilde{A}_{\mathbf{k}\sigma} = U_{\mathbf{k}\sigma} A_{\mathbf{k}\sigma} U_{\mathbf{k}\sigma}^{-1} = \mathrm{diag}(\tilde{E}_{\mathbf{k}\sigma}, -\tilde{E}_{\mathbf{k}\sigma})/2$, and $\tilde{E}_{\mathbf{k}\sigma} = \sqrt{\varepsilon_{\mathbf{k}\sigma}^2 + |\Delta_{\mathbf{k}\sigma\sigma}|^2}$.

In order to find the spin and charge currents over the junction, consider first the generalized number operator $N_{\alpha\beta} = \sum_{\mathbf{k}} c_{\mathbf{k}\alpha}^{\dagger} c_{\mathbf{k}\beta}$. The transport operator in the interaction picture then reads $\dot{N}_{\alpha\beta}(t) = -i\sum_{\mathbf{kp}\sigma}[\mathcal{D}_{\sigma\beta}(\vartheta) T_{\mathbf{kp}} c_{\mathbf{k}\alpha}^{\dagger}(t) d_{\mathbf{p}\sigma}(t) e^{-iteV} - \mathcal{D}_{\sigma\alpha}(\vartheta) T_{\mathbf{kp}}^{*} \times d_{\mathbf{p}\sigma}^{\dagger}(t) c_{\mathbf{k}\beta}(t) e^{iteV}]$, where $eV \equiv \mu_{\mathrm{L}} - \mu_{\mathrm{R}}$ is an externally applied potential. The general current across the junction can be written

$$\mathbf{I}(t) = \sum_{\alpha\beta} \boldsymbol{\tau}_{\alpha\beta} \langle \dot{N}_{\alpha\beta}(t) \rangle, \qquad \boldsymbol{\tau} = (-e\mathbf{1}, \boldsymbol{\sigma}) \quad (2)$$

such that the charge current is $I^C(t) = I_0(t)$ while the spin current reads $\mathbf{I}^S(t) = (I_1(t), I_2(t), I_3(t))$. Note that Eq. (2) contains both the single-particle (sp) and two-particle (tp) contributions. The concept of a spin current in this context refers to the rate at which the spin vector $\mathbf{S}$ on one side of the junction changes *as a result of tunneling across the junction*, i.e., $\dot{\mathbf{S}} = i[H_T, \mathbf{S}]$. As there is no spin-orbit coupling in our system, this definition of the spin current

serves well [30]. The spatial components of $\mathbf{I}^S$ are defined with respect to the corresponding quantization axis. We compute the currents by the Kubo formula $\langle \dot{N}_{\alpha\beta}(t)\rangle = -i\int_{-\infty}^{t} dt' \langle [\dot{N}_{\alpha\beta}(t), H_T(t')]\rangle$, where the right-hand side is the statistical expectation value in the unperturbed quantum state, i.e., when the two subsystems are not coupled. We now focus on the two-particle charge current and $\hat{\mathbf{z}}$ component of the spin current, such that only $\alpha = \beta$ contributes in Eq. (2).

Using linear response theory with the Matsubara formalism, one arrives at $\langle \dot{N}_{\alpha\alpha}(t)\rangle_{\mathrm{tp}} = 2\sum_\sigma \mathrm{Im}\{\Psi_{\alpha\sigma}(eV)e^{-2iteV}\}$, where $\Psi_{\alpha\sigma}(eV)$ is obtained by performing analytical continuation $i\omega_n \to eV + i0^+$ ($\omega_n = 2\pi n k_B T$, $n = 1, 2, 3, \ldots$) on $\tilde{\Psi}_{\alpha\sigma}(i\omega_n) = -\int_0^{1/k_BT} d\tau e^{i\omega_n\tau}\langle T_\tau M_{\alpha\sigma}(\tau) M_{\alpha\sigma}(0)\rangle$, where $M_{\alpha\sigma}(t) = \sum_{\mathbf{kp}} \mathcal{D}_{\sigma\alpha}(\vartheta) T_{\mathbf{kp}} c^\dagger_{\mathbf{k}\alpha}(t) d_{\mathbf{p}\sigma}(t)$, while T is the temperature, and T_τ denotes the time-ordering operator. Explicitly, we find

$$\Psi_{\alpha\sigma}(eV) = -\sum_{\substack{\mathbf{kp}\\ \lambda,\rho=\pm}} \mathcal{D}^2_{\sigma\alpha}(\vartheta)|T_{\mathbf{kp}}|^2 \frac{\Delta^*_{\mathbf{k}\alpha\alpha}\Delta_{\mathbf{p}\sigma\sigma}}{4E_{\mathbf{k}\alpha}E_{\mathbf{p}\sigma}} \Lambda^{\lambda\rho}_{\mathbf{kp}\alpha\sigma}(eV), \tag{3}$$

where $E_{\mathbf{k}\sigma} = \sqrt{\xi^2_{\mathbf{k}\sigma} + |\Delta_{\mathbf{k}\sigma\sigma}|^2}$, $\xi_{\mathbf{k}\sigma} = \varepsilon_{\mathbf{k}\sigma} - \mu_{\mathrm{R}}$ ($\mathrm{R} \to \mathrm{L}$ for $\mathbf{k} \to \mathbf{p}$), and $\Lambda^{\lambda\rho}_{\mathbf{kp}\alpha\sigma}(eV) = \lim_{i\omega_n \to eV + i0^+} \lambda[f(E_{\mathbf{k}\alpha}) - f(\lambda\rho E_{\mathbf{p}\sigma})]/[i\omega_\nu + \rho E_{\mathbf{k}\alpha} - \lambda E_{\mathbf{p}\sigma}]$; λ, $\rho = \pm 1$.

In Eq. (3), we have used that $T_{-\mathbf{k},-\mathbf{p}} = T^*_{\mathbf{kp}}$, which follows from time reversal symmetry, and $f(x)$ is the Fermi distribution. Note that the chemical potential has been included in the excitation energies $E_{\mathbf{k}\alpha}$. In general, Eq. (3) will give rise to a term proportional to $\cos(\theta^{\mathrm{L}}_{\sigma\sigma} - \theta^{\mathrm{R}}_{\alpha\alpha})$, the quasiparticle interference term, in addition to $\sin(\theta^{\mathrm{L}}_{\sigma\sigma} - \theta^{\mathrm{R}}_{\alpha\alpha})$, identified as the Josephson current. In the following, we shall focus on the latter, while a comprehensive treatment of all terms will be given in Ref. [31]. Consider now the case of zero externally applied voltage ($eV = 0$). From Eq. (2), we see that the Josephson charge current becomes

$$I^C_J = e\sum_{\mathbf{kp}\sigma\alpha} [1 + \sigma\alpha\cos\vartheta]\cos(\theta_{\mathbf{p}} - \theta_{\mathbf{k}})\sin(\theta^{\mathrm{L}}_{\sigma\sigma} - \theta^{\mathrm{R}}_{\alpha\alpha})|T_{\mathbf{kp}}|^2|\Delta_{\mathbf{k}\alpha\alpha}||\Delta_{\mathbf{p}\sigma\sigma}|F^{\alpha\sigma}_{\mathbf{kp}}/(E_{\mathbf{k}\alpha}E_{\mathbf{p}\sigma}), \tag{4}$$

with $F^{\alpha\sigma}_{\mathbf{kp}} = \sum_\pm [f(\pm E_{\mathbf{k}\alpha}) - f(E_{\mathbf{p}\sigma})]/(E_{\mathbf{k}\alpha} \mp E_{\mathbf{p}\sigma})$, while the expression for $I^S_{J,z}$ is equal except for a factor $(-\alpha/e)$ inside the summation. Observing that Eq. (4) may be cast into the form $I_J = I_0 + I_m\cos(\vartheta)$, we have thus found a Josephson current, for both spin and charge, that can be tuned in a well-defined manner by adjusting the relative orientation ϑ of the magnetization vectors (for corresponding results in spin-singlet superconductors with helimagnetic order, see Refs. [28,32]). Below, we discuss the detection of such an effect.

In the limit where one of the superconducting order parameters vanishes internally on both sides, i.e., the equivalent of an $A1$ phase, we see that the interplay between ϑ and $\theta_{\sigma\sigma}$ remains, as only one term contributes to the spin sum over $\{\sigma, \alpha\}$. In this case, the charge and spin currents go as $\cos^2(\vartheta/2)\sin\Delta\theta_{\sigma\sigma}$, where $\Delta\theta_{\sigma\sigma} \equiv \theta^{\mathrm{L}}_{\sigma\sigma} - \theta^{\mathrm{R}}_{\sigma\sigma}$ and $\Delta_{\mathbf{q}\sigma\sigma}$, with $\sigma = \{\uparrow, \downarrow\}$, $\mathbf{q} = \{\mathbf{k}, \mathbf{p}\}$, is the surviving order parameter. For collinear magnetization ($\vartheta = 0$), an ordinary Josephson effect driven by the superconducting phase occurs. Interestingly, one is able to tune this current to zero for $\mathbf{m}_{\mathrm{L}} \parallel -\mathbf{m}_{\mathrm{R}}$ ($\vartheta = \pi$).

Another result that can be extracted from Eq. (4) is a persistent spin-Josephson current even if the magnetizations on each side of the junction are of equal magnitude and collinear ($\vartheta = 0$). This is quite different from the Josephson-like spin current recently considered in ferromagnetic metal junctions [27,28]. There, a twist in the magnetization across the junction is required to drive the spin-Josephson effect. In this Letter, however, we have found a persistent spin current in the two-particle channel even for collinear magnetization.

In the special case of $eV = 0$ and equal SC phases on each side of the junction, i.e., $\theta^{\mathrm{L}}_{\sigma\sigma} = \theta^{\mathrm{R}}_{\sigma\sigma}$, Eq. (4) reduces to the form $I^S_{J,z} = J_0\sin^2(\vartheta/2)\sin(\theta^{\mathrm{L}}_{\downarrow\downarrow} - \theta^{\mathrm{R}}_{\uparrow\uparrow})$ while $I^C_J = 0$. This means that a two-particle spin current without any charge current can arise for noncollinear magnetizations on each side of the junction in the absence of an externally applied voltage *and* with equal SC phases $\theta^{\mathrm{L}}_{\sigma\sigma} = \theta^{\mathrm{R}}_{\sigma\sigma}$; see, however, Ref. [33].

It is well known that, for tunneling currents flowing in the presence of a magnetic field that is perpendicular to the tunneling direction, the resulting flux threading the junction leads to a Fraunhofer-like variation in the dc Josephson effect, given by a multiplicative factor $\sin(\pi\Phi/\Phi_0)/(\pi\Phi/\Phi_0)$ in the critical current. Here $\Phi_0 = \pi\hbar/e$ is the elementary flux quantum, and Φ is the total flux threading the junction due to a magnetic field. However, this is not an issue in the present case, since the magnetization is assumed to be oriented according to Fig. 1(a). Since the motion of the Cooper pairs is also restricted by the thin-film structure, there is no orbital effect from such a magnetization.

Note that the interplay between ferromagnetism and superconductivity is manifest in the charge as well as spin currents, the former being readily measurable. Since the critical Josephson currents depend on the relative magnetization orientation, one is able to tune these currents in a well-defined manner by varying ϑ. This can be done by applying an external magnetic field in the plane of the FMSC. In the presence of a rotating magnetic moment on either side of the junction, the Josephson currents will thus vary according to Eq. (4). Depending on the relative magnitudes of I_0 and I_m, the sign of the critical current may change. Note that such a variation of the magnetization vectors must take place in an adiabatic manner so that the systems can be considered to be in, or near, equilibrium at all times. Our predictions can thus be verified by measuring the critical current at $eV = 0$ for different angles ϑ and comparing the results with our theory. Recently, it has been

reported that a spin-triplet supercurrent, induced by Josephson tunneling between two s-wave superconductors across a ferromagnetic metallic contact, can be controlled by varying the magnetization of the ferromagnetic contact [34]. Moreover, detection of induced spin currents are challenging, although recent studies suggest feasible methods of measuring such quantities [35]. Observation of macroscopic spin currents in superconductors may also be possible via angle resolved photoemission experiments with circularly polarized photons [36] or in spin-resolved neutron scattering experiments [37].

We briefly mention our results in the single-particle channel, where we find that the charge current and the $\hat{\mathbf{z}}$ component of the spin current both vanish for $eV = 0$; see Ref. [31] for details. They are nonzero for $eV \neq 0$ even if the magnetization vectors are collinear. We stress that the finding of a nonpersistent $\hat{\mathbf{z}}$ component of the spin current does not conflict with the results of Refs. [27,28], as their $\hat{\mathbf{z}}$ direction corresponds to a vector in the xy plane in our system. For $\Delta_{\mathbf{k}\sigma\sigma} \to 0$, $\mathbf{I}^S_{\mathrm{sp}}(t) = 2\sum_{\mathbf{kp}} \sum_{\alpha\beta\sigma} \mathcal{D}_{\sigma\alpha}(\vartheta)\mathcal{D}_{\sigma\beta}(\vartheta)|T_{\mathbf{kp}}|^2 \ \mathrm{Im}\{\boldsymbol{\sigma}_{\beta\alpha}\Lambda^{1,1}_{\beta\sigma}(-eV)\}$, and the component of the spin current parallel to $\mathbf{m}_{\mathrm{L}} \times \mathbf{m}_{\mathrm{R}}$ is seen to vanish for $\vartheta = \{0, \pi\}$ at $eV = 0$ in agreement with Refs. [27,28].

We reemphasize that the above ideas should be experimentally realizable by, e.g., utilizing various geometries in order to vary the demagnetization fields. One may also use exchange biasing to an antiferromagnet to achieve noncollinearity [38]. We have found an interplay between FM and SC in the Josephson channel for charge and spin currents when considering nonunitary spin-triplet ESP FMSC with coexisting and uniform ferromagnetic and superconducting order.

The authors thank A. Brataas, K. Børkje, and E. K. Dahl for helpful discussions. This work was supported by the Norwegian Research Council Grants No. 157798/432 and No. 158547/431 (NANOMAT) and Grant No. 167498/V30 (STORFORSK).

[1] S. S. Saxena *et al.*, Nature (London) **406**, 587 (2000).
[2] D. Aoki, Nature (London) **413**, 613 (2001).
[3] E. I. Blount and C. M. Varma, Phys. Rev. Lett. **42**, 1079 (1979); **43**, 1843 (1979).
[4] Y. Maeno *et al.*, Nature (London) **372**, 532 (1994).
[5] K. Ishida *et al.*, Nature (London) **396**, 658 (1998).
[6] F. S. Bergeret *et al.*, Rev. Mod. Phys. **77**, 1321 (2005).
[7] A. Brataas and Y. Tserkovnyak, Phys. Rev. Lett. **93**, 087201 (2004); Y. Tanaka and S. Kashiwaya, Phys. Rev. B **70**, 012507 (2004); T. Koyama and M. Tachiki, Phys. Rev. B **30**, 6463 (1984).
[8] S. I. Kiselev *et al.*, Nature (London) **425**, 380 (2003).
[9] G. E. W. Bauer *et al.*, Appl. Phys. Lett. **82**, 3928 (2003).
[10] A. Brataas *et al.*, Phys. Rev. B **66**, 060404 (2002).
[11] A. J. Leggett, Rev. Mod. Phys. **47**, 331 (1975); Y. M. Bunkov, in *Progress in Low Temperature Physics*, edited by W. P. Halperin (Elsevier, New York, 1995), Vol. XIV, p. 69.
[12] G. Rashedi *et al.*, cond-mat/0501211; Y. Asano, Phys. Rev. B **72**, 092508 (2005).
[13] J. Tallon *et al.*, IEEE Trans. Appl. Supercond. **9**, 1696 (1999).
[14] T. R. Kirkpatrick and D. Belitz, Phys. Rev. Lett. **92**, 037001 (2004).
[15] K. Machida and T. Ohmi, Phys. Rev. Lett. **86**, 850 (2001).
[16] H. P. Dahal *et al.*, Phys. Rev. B **72**, 172506 (2005).
[17] R. E. Rudd and W. E. Pickett, J. Phys. Chem. Solids **59**, 2074 (1998).
[18] F. Hardy and A. D. Huxley, Phys. Rev. Lett. **94**, 247006 (2005).
[19] K. V. Samokhin and M. B. Walker, Phys. Rev. B **66**, 174501 (2002).
[20] S. Tewari *et al.*, Phys. Rev. Lett. **93**, 177002 (2004).
[21] D. V. Shopova and D. I. Uzunov, Phys. Rev. B **72**, 024531 (2005).
[22] V. P. Mineev and K. V. Samokhin, *Introduction to Unconventional Superconductivity* (Gordon and Breach, New York, 1999).
[23] H. Kotegawa *et al.*, J. Phys. Soc. Jpn. **74**, 705 (2005).
[24] C. Bernhard *et al.*, Phys. Rev. B **61**, R14 960 (2000).
[25] C. R. Hu, Phys. Rev. Lett. **72**, 1526 (1994).
[26] Y. Tanuma *et al.*, Phys. Rev. B **64**, 214519 (2001); see also V. Ambegaokar *et al.*, Phys. Rev. A **9**, 2676 (1974); L. J. Buchholtz and G. Zwicknagl, Phys. Rev. B **23**, 5788 (1981).
[27] F. S. Nogueira and K. H. Benneman, Europhys. Lett. **67**, 620 (2004).
[28] I. Eremin, F. S. Nogueira, and R.-J. Tarento, Phys. Rev. B **73**, 054507 (2006).
[29] E. P. Wigner, *Gruppentheorie und ihre Anwendung auf die Quantenmechanik der Atomspektren Frieder* (Vieweg, Braunschweig, 1931). $\mathcal{D}_{\uparrow\uparrow}(\vartheta) = \mathcal{D}_{\downarrow\downarrow}(\vartheta) = \cos(\vartheta/2)$, $\mathcal{D}_{\uparrow\downarrow}(\vartheta) = -\mathcal{D}_{\downarrow\uparrow}(\vartheta) = -\sin(\vartheta/2)$; a spin-rotated fermion operator reads $d_{\mathbf{p}\sigma} = \sum_{\sigma'} \mathcal{D}_{\sigma'\sigma}(\vartheta) d_{\mathbf{p}\sigma'}$.
[30] J. Shi *et al.*, Phys. Rev. Lett. **96**, 076604 (2006).
[31] J. Linder, M. Grønsleth, and A. Sudbø (to be published).
[32] M. L. Kulić, C.R. Physique **7**, 4 (2006); M. L. Kulić and I. M. Kulić, Phys. Rev. B **63**, 104503 (2001).
[33] This effect requires that $\theta^{\mathrm{L(R)}}_{\uparrow\uparrow} - \theta^{\mathrm{L(R)}}_{\downarrow\downarrow} \neq \{0, \pi\}$. If an interband Josephson coupling is present, the phases will be locked according to $\theta_{\uparrow\uparrow} - \theta_{\downarrow\downarrow} = \{0, \pi\}$. It has recently [J. Shi and Q. Niu, cond-mat/0601531] been proposed that p-wave SC could be induced by means of spin-orbit coupling in FM metals, which in turn leads to an interband Josephson coupling. However, in the general case, Eq. (4) is nonzero even if the spin-up and spin-down phases are locked to each other.
[34] R. S. Keizer *et al.*, Nature (London) **439**, 825 (2006).
[35] A. G. Mal'shukov *et al.*, Phys. Rev. Lett. **95**, 107203 (2005).
[36] M. E. Simon and C. M. Varma, Phys. Rev. Lett. **89**, 247003 (2002).
[37] J. E. Hirsch, Phys. Rev. Lett. **83**, 1834 (1999).
[38] J. Bass and W. P. Pratt, Jr., J. Magn. Magn. Mater. **200**, 274 (1999).

Paper II

Tunneling currents in ferromagnetic systems with multiple broken symmetries.

Physical Review B **75**, 007702 (2006).

PHYSICAL REVIEW B **75**, 024508 (2007)

Tunneling currents in ferromagnetic systems with multiple broken symmetries

J. Linder,[1] M. S. Grønsleth,[1] and A. Sudbø[1,2]
[1]*Department of Physics, Norwegian University of Science and Technology, N-7491 Trondheim, Norway*
[2]*Centre for Advanced Study, Norwegian Academy of Science and Letters, Drammensveien 78, N-0271 Oslo, Norway*
(Received 6 September 2006; revised manuscript received 14 November 2006; published 16 January 2007)

A system exhibiting multiple simultaneously broken symmetries offers the opportunity to influence physical phenomena such as tunneling currents by means of external control parameters. In this paper, we consider the broken SU(2) (internal spin) symmetry of ferromagnetic systems coexisting with (i) the broken U(1) symmetry of superconductors and (ii) the broken spatial inversion symmetry induced by a Rashba term in a spin-orbit coupling Hamiltonian. In order to study the effect of these broken symmetries, we consider tunneling currents that arise in two different systems; tunneling junctions consisting of nonunitary spin-triplet ferromagnetic superconductors and junctions consisting of ferromagnets with spin-orbit coupling. In the former case, we consider different pairing symmetries in a model where ferromagnetism and superconductivity coexist uniformly. An interplay between the relative magnetization orientation on each side of the junction and the superconducting phase difference is found, similarly to that found in earlier studies on spin-singlet superconductivity coexisting with spiral magnetism. This interplay gives rise to persistent spin- and charge-currents in the absence of an electrostatic voltage that can be controlled by adjusting the relative magnetization orientation on each side of the junction. In the second system, we study transport of spin in a system consisting of two ferromagnets with spin-orbit coupling separated by an insulating tunneling junction. A persistent spin-current across the junction is found, which can be controlled in a well-defined manner by external magnetic and electric fields. The behavior of this spin-current for important geometries and limits is studied.

DOI: 10.1103/PhysRevB.75.024508 PACS number(s): 74.20.Rp, 74.50.+r

I. INTRODUCTION

Due to the increasing interest in the field of spintronics in recent years,[1] the idea of utilizing the spin degree of freedom in electronic devices has triggered an extensive response in many scientific communities. The spin-Hall effect is arguably the research area which has received the most focus in this context, with substantial effort being put into theoretical considerations[2] as well as experimental observations.[3] In spintronics, a main goal is to make use of the spin degree of freedom rather than electrical charge, investigations of mechanisms that offer ways of controlling spin-currents are of great interest. The study of systems with multiple broken symmetries is highly relevant in this context, since such systems promise rich physics with the opportunity to learn if the tunneling currents can be influenced by means of external control parameters such as electric and/or magnetic fields. Here, we will focus on two specific systems: ferromagnetism coexisting with superconductivity, which we shall refer to as ferromagnetic superconductors (FMSC), and systems where ferromagnetism and spin-orbit coupling are present (FMSO). In terms of broken symmetries, we will then study the broken SU(2) (internal spin) symmetry of ferromagnetic systems coexisting with the broken U(1) symmetry of superconductors and also consider ferromagnets with broken inversion (spatial) symmetry induced by a Rashba term in a spin-orbit coupling Hamiltonian.

The coexistence of ferromagnetism (FM) and superconductivity (SC) has a short history in experimental physics,[4–6] although a theoretical proposition of this phenomenon was offered as early as 1957 by Ginzburg.[7] Spin-singlet superconductivity originating with BCS theory seems to be ruled out as a plausible pairing mechanism for a ferromagnetic superconductor,[8] at least with regard to uniform coexistence of the FM and SC order parameters ζ and Δ, respectively. It could be achieved for a superconductor taking up a so-called Fulde-Ferrell-Larkin-Ovchinnikov (FFLO) state.[9] However, it seems likely that the coexistence of FM and SC call for[10,11] *p*-wave spin-triplet Cooper pairs which have a nonzero magnetic moment. This type of pairing has been observed in superfluid ^{3}He, and is perfectly compatible with FM order. Spin-triplet superconductivity has, moreover, been experimentally verified[12,13] in Sr_2RuO_4, and the study of such a pairing in a FMSC could unveil interesting effects with respect to quantum transport. The concept of simultaneously broken U(1) and SU(2) symmetries are of great interest from a fundamental physics point of view, and could be suggestive to a range of novel applications. This topic has been the subject of theoretical research in, e.g., Refs. 14–16.

In this paper, we follow up Ref. 17 with a more comprehensive study of the tunneling currents between two *p*-wave FMSC separated by an insulating junction; $RuSr_2GdCu_2O_8$, UGe_2, and URhGe have been proposed as candidates for such unconventional superconductors.[4–6] In our model, we assume uniform coexistence of the FM and SC order parameters and that superconductivity arises from the same electrons that are responsible for the magnetism. As argued in Ref. 5, this can be understood most naturally as a spin-triplet rather than spin-singlet pairing phenomenon. Furthermore, it seems that SC in the metallic compounds mentioned above always coexists with the FM order and is enhanced by it;[18] the experiments conducted on the compounds UGe_2 and URhGe do not give any evidence for the existence of a standard normal-to-superconducting phase transition in a zero external magnetic field, but instead indicate a phase corresponding to a mixed state of FM and SC. We provide de-

tailed calculations for single-particle and Josephson (two-particle) tunneling between two nonunitary equal-spin pairing (ESP) FMSC. We examine both the charge- and spin-sector in detail within linear response theory using the Kubo formula. We find that the supercurrent of spin and charge may be controlled by adjusting the misorientation of the exchange fields on both sides of the junction. Such an effect was first discovered by Kulic and Kulic,[19] who derived an expression for the Josephson current over a junction separating two BCS superconductors with spiral magnetic order. It was found that the supercurrent could be controlled by adjusting the relative orientation of the exchange field on both sides of the junction, a finding that quite remarkably suggested a way of tuning a supercurrent in a well-defined manner from, e.g., as 0- to π-junction. Later investigations made by Eremin, Nogueira, and Tarento[20] considered a similar system as Kulic and Kulic,[19] namely two Fulde-Ferrel-Larkin-Ovchinnikov (FFLO) superconductors[9] coexisting with helimagnetic order. Recently, the same opportunity was found to exist in a FMSC/I/FMSC junction as shown by Grønsleth *et al.*[17]

In the case of a system where both ferromagnetism and spin-orbit coupling are present, it is clear that these are physical properties of a system that crucially influence the behavior of spins present in that system. For instance, the presence of spin-orbit coupling is highly important when considering ferromagnetic semiconductors.[21,22] Such materials have been proposed as devices for obtaining controllable spin injection and manipulating single electron spins by means of external electrical fields, making them a central topic of semiconductor spintronics.[23] In ferromagnetic metals, spin-orbit coupling is ordinarily significantly smaller than for semiconductors due to the band structure. However, the presence of a spin-orbit coupling in ferromagnets could lead to new effects in terms of quantum transport.

Studies of tunneling between ferromagnets have uncovered interesting physical effects.[24–26] Nogueira *et al.* predicted[24] that a dissipationless spin-current should be established across the junction of two Heisenberg ferromagnets, and that the spin-current was maximal in the special case of tunneling between planar ferromagnets. Also, there has been investigations of what kind of impact spin-orbit coupling constitutes on tunneling currents in various contexts, e.g., for noncentrosymmetric superconductors[27] and two-dimensional electron gases coupled to ferromagnets.[28] Broken time reversal- and inversion-symmetry are interesting properties of a system with regard to quantum transport of spin and charge, and the exploitment of such asymmetries has given rise to several devices in recent years. For instance, the broken $O(3)$ symmetry exhibited by ferromagnets has a broad range of possible applications. This has led to spin-current-induced magnetization switching,[29] and suggestions have been made for more exotic devices such as spin-torque transistors[30] and spin-batteries.[31] It has also led to investigations into such phenomena as spin-Hall effect in paramagnetic metals,[32] spin-pumping from ferromagnets into metals, enhanced damping of spins when spins are pumped from one ferromagnet to another through a metallic sample,[33] and the mentioned spin Josephson effects in ferromagnet/ferromagnet tunneling junctions.[24]

Here, we study the spin-current that arises over a tunneling junction separating two ferromagnetic metals with substantial spin-orbit coupling. It is found that the total current consists of three terms; one due to a twist in magnetization across the junction (in agreement with the result of Ref. 24), one term originating from the spin-orbit interactions in the system, and finally an interesting mixed term that stems from an interplay between the ferromagnetism and spin-orbit coupling. After deriving the expression for the spin-current between Heisenberg ferromagnets with substantial spin-orbit coupling, we consider important tunneling geometries and physical limits of our generally valid results. Finally, we make suggestions concerning the detection of the predicted spin-current. Our results indicate how spin transport between systems exhibiting both magnetism and spin-orbit coupling can be controlled by external fields, and should therefore be of considerable interest in terms of spintronics.

This paper is organized as follows. In Sec. II, we consider transport between spin-triplet ferromagnetic superconductors, while a study of transport between ferromagnets with spin-orbit coupling is given in Sec. III. A discussion of our results is provided in Sec. IV, with emphasis on how the effects predicted in this paper could be tested in an experimental setup. Finally, we give concluding remarks in Sec. V.

II. FERROMAGNETIC SUPERCONDUCTORS

A. Coexistence of ferromagnetism and superconductivity

An important issue to address concerning FMSC is whether the SC and FM order parameters coexist uniformly or if they are phase-separated. One possibility[34] is that a spontaneously formed vortex lattice due to the internal magnetization $\mathbf{m}$ is realized in a spin-triplet FMSC, while there also have been studies of Meissner (uniform) SC phases in spin-triplet FMSC.[18] As argued in Ref. 35, a key variable with respect to whether a vortice lattice appears or not is the strength of the internal magnetization $\mathbf{m}$. Reference 36 suggested that vortices arise if $4\pi\mathbf{m} > \mathbf{H}_{c1}$, where $\mathbf{H}_{c1}$ is the lower critical field. When considering a weak FM state coexisting with SC, a scenario which seems to be the case for URhGe, the domain structure in the absence of an external field is thus vortex-free. Current experimental data concerning URhGe are not strong enough to unambiguously settle this question, while evidence for uniform coexistence of FM and SC has been indicated[37] in UGe_2. Furthermore, a bulk Meissner state in the FMSC $RuSr_2GdCu_2O_8$ has been reported in Ref. 38, hence suggesting the existence of uniform FM and SC as a bulk effect. In our study, we shall consequently take the order parameters as coexisting homogeneously and use their bulk values, as justified by the argumentation above. However, we emphasize that one in general should take into account the possible suppression of the SC order parameter in the vicinity of the tunneling interface due to the formation of midgap surface states[39] which occur for certain orientations of the SC gap. The pair-breaking effect of these states in unconventional superconductors has been studied in, e.g., Refs. 40–42 and we discuss this in more detail in Sec. IV. A sizeable formation of such states would suppress the Josephson current, although it is nonvanishing

in the general case. Also, we use bulk uniform magnetic order parameters, as in Ref. 24. The latter is justified on the grounds that a ferromagnet with a planar order parameter is mathematically isomorphic to an *s*-wave superconductor, where the use of bulk values for the order parameter right up to the interface is a good approximation due to the lack of midgap surface states.

It is generally believed that the same electrons that are responsible for itinerant FM also participate in the formation of Cooper pairs below the SC critical temperature.[6] As a consequence, uniform coexistence of spin-singlet SC and FM can be discarded since *s*-wave Cooper pairs carry a total spin of zero, although spatially modulated order parameters could allow for magnetic *s*-wave superconductors.[19,20] However, spin-triplet Cooper pairs are in principle perfectly compatible with FM order since they can carry a net magnetic moment. To see this, consider the $\mathbf{d_k}$-vector formalism[43] which is convenient when dealing with spin-triplet superconductors, regardless of whether they are magnetic or not. For a complete and rigorous treatment of the $\mathbf{d_k}$-vector order parameter, see, e.g., Ref. 44. The spin dependence of triplet pairing can be represented by a 2×2 matrix

$$\hat{\Delta}_{\mathbf{k}} = \begin{pmatrix} \Delta_{\mathbf{k}\uparrow\uparrow} & \Delta_{\mathbf{k}\uparrow\downarrow} \\ \Delta_{\mathbf{k}\downarrow\uparrow} & \Delta_{\mathbf{k}\downarrow\downarrow} \end{pmatrix} = \begin{pmatrix} -d_x(\mathbf{k}) + id_y(\mathbf{k}) & d_z(\mathbf{k}) \\ d_z(\mathbf{k}) & d_x(\mathbf{k}) + id_y(\mathbf{k}) \end{pmatrix} = i\mathbf{d_k}\cdot\hat{\boldsymbol{\sigma}}\hat{\sigma}_y, \tag{1}$$

where $\Delta_{\mathbf{k}\alpha\beta}$ represent the SC gap parameters for different triplet pairings, $\hat{\boldsymbol{\sigma}}=(\hat{\sigma}_x,\hat{\sigma}_y,\hat{\sigma}_z)$ where $\hat{\sigma}_i$ are the Pauli matrices, and $\mathbf{d_k}=[d_x(\mathbf{k}),d_y(\mathbf{k}),d_z(\mathbf{k})]$ is given by

$$\mathbf{d_k} = \left(\frac{\Delta_{\mathbf{k}\downarrow\downarrow}-\Delta_{\mathbf{k}\uparrow\uparrow}}{2},\ -i\frac{(\Delta_{\mathbf{k}\downarrow\downarrow}+\Delta_{\mathbf{k}\uparrow\uparrow})}{2},\Delta_{\mathbf{k}\uparrow\downarrow}\right). \tag{2}$$

Note that $\mathbf{d_k}$ transforms like a vector under spin rotations and that $\Delta_{\mathbf{k}\uparrow\downarrow}=\Delta_{\mathbf{k}\downarrow\uparrow}$ for triplet pairing since it is of no significance *which* electron in the Cooper pair has spin up or down. This is because the spin-part of the two-particle wave function is symmetric under exchange of particles, as opposed to spin-singlet SC, where the gap changes sign when the spin indices are exchanged. Spin-triplet SC states are classified as unitary if $i\mathbf{d_k}\times\mathbf{d_k^*}=0$ and nonunitary if the equality sign does not hold. Since the average spin of a $\mathbf{d_k}$-state is given by[44]

$$\langle\mathbf{S_k}\rangle = i\mathbf{d_k}\times\mathbf{d_k^*}, \tag{3}$$

it is clear that we must have a nonunitary $\mathbf{d_k}$ in a model where FM and SC coexist uniformly. Indeed, there is strong reason to believe that the correct pairing symmetries in the discovered FMSC constitute nonunitary states.[11,45,46] As a consequence, one can rule out, for instance, a state where only $\Delta_{\mathbf{k}\uparrow\downarrow}\neq 0$ since it would imply $\langle\mathbf{S_k}\rangle=0$ according to Eq. (3). In the most general case where all SC gaps are included, $\Delta_{\uparrow\downarrow}$ would be suppressed in the presence of a Zeeman-splitting between the $\uparrow$, $\downarrow$ conduction bands;[6] see Fig. 1.

However, such a splitting between energy bands need not be present and one could in theory then consider a **d**-vector where

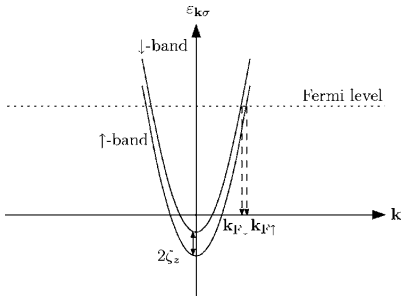

FIG. 1. Band-splitting for $\uparrow$, $\downarrow$ electrons in the presence of a magnetization in the $\hat{\mathbf{z}}$-direction. Interband pairing gives rise to a net Cooper pair momentum in the presence of a band-splitting, thus suppressing the $\Delta_{\mathbf{k}\uparrow\downarrow}$ order parameter.

$$|\Delta_{\mathbf{k}\uparrow\uparrow}| = |\Delta_{\mathbf{k}\downarrow\downarrow}| \neq 0 \quad \Delta_{\mathbf{k}\uparrow\downarrow}\neq 0, \tag{4}$$

such that $\langle\mathbf{S_k}\rangle$ lies in the local *xy*-plane. This scenario would be equivalent to an *A*2-phase as is seen when performing a spin rotation on the gap parameters into a quantization axis lying in the *xy*-plane. Denoting up- and down-spins with respect to the new quantization axis $+$ and $-$, respectively, the transformation yields

$$\begin{pmatrix} \Delta_{\mathbf{k}\uparrow\uparrow} \\ \Delta_{\mathbf{k}\uparrow\downarrow} \\ \Delta_{\mathbf{k}\downarrow\downarrow} \end{pmatrix} = \frac{1}{2}\begin{pmatrix} 1 & 2e^{i\phi} & e^{2i\phi} \\ -e^{-i\phi} & 0 & e^{i\phi} \\ e^{-2i\phi} & -2e^{-i\phi} & 1 \end{pmatrix}\begin{pmatrix} \tilde{\Delta}_{\mathbf{k}++} \\ \tilde{\Delta}_{\mathbf{k}+-} \\ \tilde{\Delta}_{\mathbf{k}--} \end{pmatrix}, \tag{5}$$

where ϕ is the azimuthal angle as shown in Fig. 2.

When introducing the conditions in Eq. (4), it is readily seen that $\tilde{\Delta}_{\mathbf{k}+-}=0$ while $|\tilde{\Delta}_{\mathbf{k}++}|\neq|\tilde{\Delta}_{\mathbf{k}--}|\neq 0$, thus corresponding to an *A*2-phase. Consequently, the entire span of physically possible pairing symmetries in a FMSC can be reduced to the equivalence of an *A*1- or *A*2-phase in ^{3}He by a change of spin-basis. The definitions of *A*-, *A*1-, and *A*2-phases in ^{3}He are as follows: an *A*-phase corresponds to a pairing symmetry such that $|\Delta_{\mathbf{k}\uparrow\uparrow}|=|\Delta_{\mathbf{k}\downarrow\downarrow}|\neq 0$, an *A*1-phase has only one gap $\Delta_{\mathbf{k}\sigma\sigma}\neq 0$ while $\Delta_{\mathbf{k},-\sigma,-\sigma}=0$, and an *A*2-phase satisfies

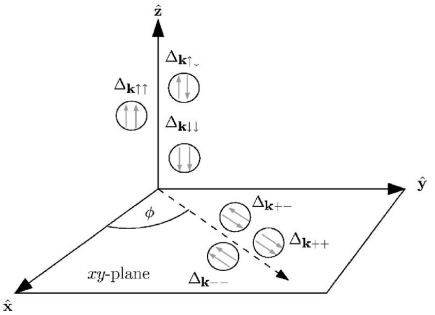

FIG. 2. Change of spin-basis for the superconducting gaps. The new quantization axis is represented by the dotted arrow.

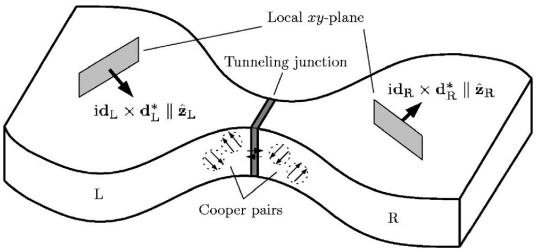

FIG. 3. Tunneling between two nonunitary ESP FMSC. The quantization axis has been taken along the direction of magnetization on each side of the junction.

$|\Delta_{\mathbf{k}\uparrow\uparrow}|\neq|\Delta_{\mathbf{k}\downarrow\downarrow}|\neq 0$. In this case, $\Delta_{\mathbf{k}\alpha\beta}$ represents the superfluid gap for the fermionic ^{3}He-atoms, and $\Delta_{\mathbf{k}\uparrow\downarrow}=0$ for all A_i-phases.

The resulting spin of the Cooper pair is then in general given by

$$\langle\mathbf{S}_\mathbf{k}\rangle=(1/2)[|\Delta_{\mathbf{k}\uparrow\uparrow}|^2-|\Delta_{\mathbf{k}\downarrow\downarrow}|^2]\hat{\mathbf{z}}. \tag{6}$$

In the following, we shall accordingly consider tunneling between nonunitary ESP FMSC in an $A1$- or $A2$-phase. Moreover, we consider thin film FMSC, ensuring that no accumulation of charge at the surface will take place due to an orbital effect. Our system can be thought to have arisen by first cooling down a sample below the Curie temperature T_M such that FM order is introduced. At further cooling below the critical temperature T_c, the same electrons that give rise to FM condense into Cooper pairs with a net magnetic moment parallel to the original direction of magnetization. Our model is shown in Fig. 3.

B. The Hamiltonian

The system consists of two FMSC separated by an insulating layer such that the total Hamiltonian can be written as[47] $H=H_\mathrm{L}+H_\mathrm{R}+H_\mathrm{T}$, where L and R represents the individual FMSC on each side of the tunneling junction, and H_T describes tunneling of particles through the insulating layer separating the two pieces of bulk material. Using mean-field theory, one finds that the individual FMSC are described by a Hamiltonian similar to the one used in Ref. 48,

$$H_\mathrm{FMSC}=H_0+\sum_\mathbf{k}\psi_\mathbf{k}^\dagger\hat{\mathcal{A}}_\mathbf{k}\psi_\mathbf{k},$$

$$H_0=JN\eta(0)\mathbf{m}^2+\frac{1}{2}\sum_{\mathbf{k}\sigma}\varepsilon_{\mathbf{k}\sigma}+\sum_{\mathbf{k}\alpha\beta}\Delta_{\mathbf{k}\alpha\beta}^\dagger b_{\mathbf{k}\alpha\beta}. \tag{7}$$

Here, $\mathbf{k}$ is the electron momentum and we have introduced

$$\varepsilon_{\mathbf{k}\sigma}=\varepsilon_\mathbf{k}-\sigma\zeta_z,\quad \sigma=\uparrow,\downarrow=\pm 1. \tag{8}$$

Furthermore, J is a spin coupling constant, $\eta(\mathbf{k})$ is a geometrical structure factor which for $\mathbf{k}=0$ reduces to the number of nearest lattice neighbors $\eta(0)$, $\mathbf{m}=\{m_x,m_y,m_z\}$ is the magnetization vector, while $\Delta_{\mathbf{k}\alpha\beta}$ is the superconducting order parameter and $b_{\mathbf{k}\alpha\beta}=\langle c_{-\mathbf{k}\beta}c_{\mathbf{k}\alpha}\rangle$ denotes the two-particle operator expectation value. The ferromagnetic order parameters are given by

$$\zeta=2J\eta(0)(m_x-im_y),\quad \zeta_z=2J\eta(0)m_z. \tag{9}$$

The interesting physics of the FMSC/FMSC junction lies in the matrix $\hat{\mathcal{A}}_\mathbf{k}$ to be given below. Above, we used a basis

$$\psi_\mathbf{k}=(c_{\mathbf{k}\uparrow}c_{\mathbf{k}\downarrow}c_{-\mathbf{k}\uparrow}^\dagger c_{-\mathbf{k}\downarrow}^\dagger)^\mathrm{T}, \tag{10}$$

where $c_{\mathbf{k}\sigma}$ ($c_{\mathbf{k}\sigma}^\dagger$) are annihilation (creation) fermion operators. Note that we have not incorporated any spin-orbit coupling of the type $(\mathbf{E}\times\mathbf{p})\cdot\hat{\boldsymbol{\sigma}}$ in the Hamiltonian described in Eq. (7) such that spatial inversion symmetry is not broken, i.e., we consider centrosymmetric FMSC.

Consider now the matrix

$$\hat{\mathcal{A}}_\mathbf{k}=-\frac{1}{2}\begin{pmatrix}-\varepsilon_{\mathbf{k}\uparrow} & \zeta & \Delta_{\mathbf{k}\uparrow\uparrow} & \Delta_{\mathbf{k}\uparrow\downarrow}\\ \zeta^\dagger & -\varepsilon_{\mathbf{k}\downarrow} & \Delta_{\mathbf{k}\downarrow\uparrow} & \Delta_{\mathbf{k}\downarrow\downarrow}\\ \Delta_{\mathbf{k}\uparrow\uparrow}^\dagger & \Delta_{\mathbf{k}\downarrow\uparrow}^\dagger & \varepsilon_{\mathbf{k}\uparrow} & -\zeta^\dagger\\ \Delta_{\mathbf{k}\uparrow\downarrow}^\dagger & \Delta_{\mathbf{k}\downarrow\downarrow}^\dagger & -\zeta & \varepsilon_{\mathbf{k}\downarrow}\end{pmatrix}, \tag{11}$$

which is valid for a FMSC with arbitrary magnetization. As explained in the previous sections, we will study in detail tunneling between nonunitary ESP FMSC, i.e., $\Delta_{\mathbf{k}\uparrow\downarrow}=\Delta_{\mathbf{k}\downarrow\uparrow}=0$, $\zeta=0$ in Eq. (11). We take the quantization axis on each side of the junction to coincide with the magnetization direction. One then needs to include the Wigner d-function[49] denoted by $\hat{\mathcal{D}}^{(j)}_{\sigma'\sigma}(\vartheta)$ with $j=1/2$ to account for the fact that a $\uparrow$ spin on one side of the junction is not the same as a $\uparrow$ spin on the other side of the junction, since the magnetization vectors point can point in different directions. The angle ϑ is consequently defined by

$$\mathbf{m}_\mathrm{R}\cdot\mathbf{m}_\mathrm{L}=m_\mathrm{R}m_\mathrm{L}\cos(\vartheta),\quad m_i=|\mathbf{m}_i|. \tag{12}$$

Specifically, we have that

$$\hat{\mathcal{D}}^{(1/2)}(\vartheta)=\begin{pmatrix}\cos(\vartheta/2) & -\sin(\vartheta/2)\\ \sin(\vartheta/2) & \cos(\vartheta/2)\end{pmatrix} \tag{13}$$

such that a spin-rotated fermion operator is given by

$$\tilde{d}_{\mathbf{p}\sigma}=\sum_{\sigma'}\hat{\mathcal{D}}^{(1/2)}_{\sigma'\sigma}(\vartheta)d_{\mathbf{p}\sigma'}. \tag{14}$$

The tunneling Hamiltonian then reads

$$H_\mathrm{T}=\sum_{\mathbf{kp}\sigma\sigma'}\hat{\mathcal{D}}^{(1/2)}_{\sigma'\sigma}(\vartheta)(T_{\mathbf{kp}}c_{\mathbf{k}\sigma}^\dagger d_{\mathbf{p}\sigma'}+T_{\mathbf{kp}}^* d_{\mathbf{p}\sigma'}^\dagger c_{\mathbf{k}\sigma}), \tag{15}$$

where we neglect the possibility of spin-flips in the tunneling process. Note that we distinguish between fermion operators on the right and left side of the junction corresponding to $c_{\mathbf{k}\sigma}$ and $d_{\mathbf{p}\sigma}$, respectively. Demanding that H_T is invariant under time reversal $\mathcal{K}$, one finds that the condition $\mathcal{K}^{-1}H_\mathrm{T}\mathcal{K}=H_\mathrm{T}$ with

$$\mathcal{K}^{-1}H_\mathrm{T}\mathcal{K}=\sum_{\mathbf{kp}\sigma\sigma'}\sigma\sigma'\hat{\mathcal{D}}^{(1/2)}_{\sigma'\sigma}(\vartheta)(T_{\mathbf{kp}}^* c_{-\mathbf{k},-\sigma}^\dagger d_{-\mathbf{p},-\sigma'}+T_{\mathbf{kp}}d_{-\mathbf{p},-\sigma'}^\dagger c_{-\mathbf{k},-\sigma}) \tag{16}$$

dictates that $T_{\mathbf{kp}}=T_{-\mathbf{k},-\mathbf{p}}^*$. Furthermore, we write the super-

conducting order parameters as $\Delta_{\mathbf{k}\sigma\sigma}=|\Delta_{\mathbf{k}\sigma\sigma}|e^{i(\theta_{\mathbf{k}}+\theta^{R}_{\sigma\sigma})}$, where R (L) denotes the bulk superconducting phase on the right (left) side of the junction while $\theta_{\mathbf{k}}$ is a general (complex) internal phase factor originating from the specific form of the gap in $\mathbf{k}$-space that ensures odd symmetry under inversion of momentum, i.e., $\theta_{\mathbf{k}}=\theta_{-\mathbf{k}}+\pi$.

For our system, Eq. (7) takes the form

$$H_{\mathrm{FMSC}}=H_0+H_A,\quad H_A=\sum_{\mathbf{k}\sigma}\phi^{\dagger}_{\mathbf{k}\sigma}\hat{A}_{\mathbf{k}\sigma}\phi_{\mathbf{k}\sigma},\tag{17}$$

where we have block-diagonalized $\hat{\mathcal{A}}_{\mathbf{k}}$ and chosen a convenient basis $\phi^{\dagger}_{\mathbf{k}\sigma}=(c^{\dagger}_{\mathbf{k}\sigma},c_{-\mathbf{k}\sigma})$, with the definition

$$\hat{A}_{\mathbf{k}\sigma}=-\frac{1}{2}\begin{pmatrix}-\varepsilon_{\mathbf{k}\sigma} & \Delta_{\mathbf{k}\sigma\sigma}\\ \Delta^{\dagger}_{\mathbf{k}\sigma\sigma} & \varepsilon_{\mathbf{k}\sigma}\end{pmatrix}.\tag{18}$$

This Hamiltonian is diagonalized by a 2×2 spin generalized unitary matrix $\hat{U}_{\mathbf{k}\sigma}$, so that the superconducting sector is expressed in the diagonal basis

$$\tilde{\phi}^{\dagger}_{\mathbf{k}\sigma}=\phi^{\dagger}_{\mathbf{k}\sigma}\hat{U}_{\mathbf{k}\sigma}\equiv(\gamma^{\dagger}_{\mathbf{k}\sigma},\gamma_{-\mathbf{k}\sigma}).\tag{19}$$

Thus $H_A=\Sigma_{\mathbf{k}\sigma}\tilde{\phi}^{\dagger}_{\mathbf{k}\sigma}\hat{\tilde{A}}_{\mathbf{k}\sigma}\tilde{\phi}_{\mathbf{k}\sigma}$, in which

$$\hat{\tilde{A}}_{\mathbf{k}\sigma}=\hat{U}_{\mathbf{k}\sigma}\hat{A}_{\mathbf{k}\sigma}\hat{U}^{-1}_{\mathbf{k}\sigma}=\mathrm{diag}(\tilde{E}_{\mathbf{k}\sigma},-\tilde{E}_{\mathbf{k}\sigma})/2,$$

$$\tilde{E}_{\mathbf{k}\sigma}=\sqrt{\varepsilon^2_{\mathbf{k}\sigma}+|\Delta_{\mathbf{k}\sigma\sigma}|^2}.\tag{20}$$

The explicit expression for $\hat{U}_{\mathbf{k}\sigma}$ is

$$\hat{U}_{\mathbf{k}\sigma}=N_{\mathbf{k}\sigma}\begin{pmatrix}1 & \dfrac{\Delta_{\mathbf{k}\sigma\sigma}}{\varepsilon_{\mathbf{k}\sigma}+\tilde{E}_{\mathbf{k}\sigma}}\\ -\dfrac{\Delta^{*}_{\mathbf{k}\sigma\sigma}}{\varepsilon_{\mathbf{k}\sigma}+\tilde{E}_{\mathbf{k}\sigma}} & 1\end{pmatrix},$$

$$N_{\mathbf{k}\sigma}=\frac{\varepsilon_{\mathbf{k}\sigma}+\tilde{E}_{\mathbf{k}\sigma}}{\sqrt{(\varepsilon_{\mathbf{k}\sigma}+\tilde{E}_{\mathbf{k}\sigma})^2+|\Delta_{\mathbf{k}\sigma\sigma}|^2}}.\tag{21}$$

We now proceed to investigate the tunneling currents that can arise across a junction of two such FMSC.

C. Tunneling formalism

Although the treatment in this section is fairly standard, it comes with a certain extension to the standard cases due to the coexistence of two simultaneously broken symmetries. Thus, for completeness, we present it here.

In order to find the spin- and charge-current over the junction, we define the generalized number operator[67] by $N_{\alpha\beta}=\Sigma_{\mathbf{k}}c^{\dagger}_{\mathbf{k}\alpha}c_{\mathbf{k}\beta}$. Consider now the transport operator

$$\dot{N}_{\alpha\beta}=i[H_{\mathrm{T}},N_{\alpha\beta}]=-i\sum_{\mathbf{kp}\sigma}[\hat{\mathcal{D}}^{(1/2)}_{\sigma\beta}(\vartheta)T_{\mathbf{kp}}c^{\dagger}_{\mathbf{k}\alpha}d_{\mathbf{p}\sigma}-\hat{\mathcal{D}}^{(1/2)}_{\sigma\alpha}(\vartheta)T^{*}_{\mathbf{kp}}d^{\dagger}_{\mathbf{p}\sigma}c_{\mathbf{k}\beta}].\tag{22}$$

We now write $H=H'+H_{\mathrm{T}}$ where $H'=H_{\mathrm{L}}+H_{\mathrm{R}}$ and $H_i=K_i+\mu_iN_i$, $i=\mathrm{L},\mathrm{R}$, where μ_i is the chemical potential on side i and N_i is the number operator. In the interaction picture, the time-dependence of $\dot{N}_{\alpha\beta}$ is then governed by

$$\dot{N}_{\alpha\beta}(t)=e^{iH't}\dot{N}_{\alpha\beta}e^{-iH't},\tag{23}$$

while the time-dependence of the fermion operators reads

$$c_{\mathbf{k}\sigma}(t)=e^{iK_{\mathrm{R}}t}c_{\mathbf{k}\sigma}e^{-iK_{\mathrm{R}}t}.\tag{24}$$

Effectively, one can write

$$K_{\mathrm{R}}=H_0+\sum_{\mathbf{k}\sigma}E_{\mathbf{k}\sigma}\gamma^{\dagger}_{\mathbf{k}\sigma}\gamma_{\mathbf{k}\sigma},\tag{25}$$

where the chemical potential is now included in the quasiparticle excitation energies $E_{\mathbf{k}\sigma}$ according to

$$E_{\mathbf{k}\sigma}=\sqrt{\xi^2_{\mathbf{k}\sigma}+|\Delta_{\mathbf{k}\sigma\sigma}|^2}\tag{26}$$

with $\xi_{\mathbf{k}\sigma}=\varepsilon_{\mathbf{k}\sigma}-\mu_{\mathrm{R}}$, and correspondingly for the left side. Consequently, we are able to write down

$$\dot{N}_{\alpha\beta}(t)=-i\sum_{\mathbf{kp}\sigma}(\hat{\mathcal{D}}^{(1/2)}_{\sigma\beta}(\vartheta)T_{\mathbf{kp}}c^{\dagger}_{\mathbf{k}\alpha}(t)d_{\mathbf{p}\sigma}(t)e^{-iteV}-\hat{\mathcal{D}}^{(1/2)}_{\sigma\alpha}(\vartheta)\times T^{*}_{\mathbf{kp}}d^{\dagger}_{\mathbf{p}\sigma}(t)c_{\mathbf{k}\beta}(t)e^{iteV}),\tag{27}$$

where $eV\equiv\mu_{\mathrm{L}}-\mu_{\mathrm{R}}$ is the externally applied potential. Within linear response theory, we can identify a general current

$$\mathbf{I}(t)=\sum_{\alpha\beta}\hat{\boldsymbol{\tau}}_{\alpha\beta}\langle\dot{N}_{\alpha\beta}(t)\rangle,\quad\hat{\boldsymbol{\tau}}=(-e\hat{1},\hat{\boldsymbol{\sigma}}),\tag{28}$$

such that the charge-current is $I^{\mathrm{C}}(t)=I_0(t)$ while the spin-current reads $\mathbf{I}^{\mathrm{S}}(t)=[I_1(t),I_2(t),I_3(t)]$. In Eq. (28), $\hat{1}$ denotes the 2×2 identity matrix. Explicitly, we have

$$I^{\mathrm{C}}(t)=I^{\mathrm{C}}_{\mathrm{sp}}(t)+I^{\mathrm{C}}_{\mathrm{tp}}(t)=-e\sum_{\alpha}\langle\dot{N}_{\alpha\alpha}(t)\rangle,$$

$$\mathbf{I}^{\mathrm{S}}(t)=\mathbf{I}^{\mathrm{S}}_{\mathrm{sp}}(t)+\mathbf{I}^{\mathrm{S}}_{\mathrm{tp}}(t)=\sum_{\alpha\beta}\hat{\boldsymbol{\sigma}}_{\alpha\beta}\langle\dot{N}_{\alpha\beta}(t)\rangle,\tag{29}$$

where the subscripts *sp* and *tp* denote the single-particle and two-particle contribution to the currents, respectively. As recently pointed out by the authors of Ref. 50, defining a spin-current is not as straightforward as defining a charge-current. Specifically, the conventional definition of a spin-current given as spin multiplied with velocity suffers from severe flaws in systems where spin is not a conserved quantity. In this paper, we define the spin-current across the junction as $\mathbf{I}^{\mathrm{S}}(t)=\langle d\mathbf{S}(t)/dt\rangle$ where $d\mathbf{S}/dt=i[H_{\mathrm{T}},\mathbf{S}]$. It is then clear that the concept of a spin-current in this context refers to the rate at which the spin-vector $\mathbf{S}$ on one side of the junction changes *as a result of tunneling across the junction*. The spatial components of $\mathbf{I}^{\mathrm{S}}$ are defined with respect to the corresponding quantization axis. In this way, we avoid nonphysical interpretations of the spin-current in terms of real spin transport as we only calculate the contribution to $d\mathbf{S}/dt$ from the tunneling Hamiltonian *instead* of the entire Hamiltonian H. Should we have chosen the latter approach, one would in general run the risk of obtaining a nonzero spin-

current due to, e.g., local spin-flip processes which are obviously not relevant in terms of real spin transport across the junction. However, in our system such spin-flip processes are absent.

The tunneling currents are calculated in the linear response regime by using the Kubo formula,

$$\langle \dot{N}_{\alpha\beta}(t)\rangle = -i\int_{-\infty}^{t} dt'\langle[\dot{N}_{\alpha\beta}(t),H_{\mathrm{T}}(t')]\rangle, \tag{30}$$

where the right-hand side is the statistical expectation value in the unperturbed quantum state, i.e., when the two subsystems are not coupled. This expression includes both single-particle and two-particle contributions to the current. Details of the calculations are found in Appendix A 1.

We now consider the cases of an $A2$- and $A1$-phase at zero external potential, giving special attention to the charge-current and $\hat{\mathbf{z}}$-component of the spin-current in the Josephson channel.

D. Two-particle currents

For an $A2$-phase in the case of zero externally applied voltage ($eV=0$), Eqs. (29) and (A13) generate a quasiparticle interference term I_{qi}, in addition to a term I_{J} identified as the Josephson current. Thus the total two-particle currents of charge and spin can be written as $I^{\mathrm{C(S)}}_{\mathrm{tp}(,z)}=I^{\mathrm{C(S)}}_{\mathrm{qi}(,z)}+I^{\mathrm{C(S)}}_{\mathrm{J}(,z)}$ where

$$I^{\mathrm{C(S)}}_{\mathrm{qi}(,z)} = \sum_{\mathbf{kp}} I^{\mathrm{C(S)}}(\theta^{\mathrm{L}}_{\sigma\sigma}-\theta^{\mathrm{R}}_{\alpha\alpha},\Delta\theta_{\mathbf{pk}}),$$

$$I^{\mathrm{C(S)}}_{\mathrm{J}(,z)} = \sum_{\mathbf{kp}} I^{\mathrm{C(S)}}(\Delta\theta_{\mathbf{pk}},\theta^{\mathrm{L}}_{\sigma\sigma}-\theta^{\mathrm{R}}_{\alpha\alpha}) \tag{31}$$

with the definitions

$$I^{\mathrm{C}}(\phi_1,\phi_2) = \frac{e}{2}\sum_{\sigma\alpha}[1+\sigma\alpha\cos(\vartheta)]|T_{\mathbf{kp}}|^2\frac{|\Delta_{\mathbf{k}\alpha\alpha}||\Delta_{\mathbf{p}\sigma\sigma}|}{E_{\mathbf{k}\alpha}E_{\mathbf{p}\sigma}} \times\cos(\phi_1)\sin(\phi_2)F_{\mathbf{kp}\alpha\sigma},$$

$$I^{\mathrm{S}}(\phi_1,\phi_2) = -\frac{1}{2}\sum_{\sigma\alpha}\alpha[1+\sigma\alpha\cos(\vartheta)]|T_{\mathbf{kp}}|^2\frac{|\Delta_{\mathbf{k}\alpha\alpha}||\Delta_{\mathbf{p}\sigma\sigma}|}{E_{\mathbf{k}\alpha}E_{\mathbf{p}\sigma}} \times\cos(\phi_1)\sin(\phi_2)F_{\mathbf{kp}\alpha\sigma}, \tag{32}$$

where we have introduced $\Delta\theta_{\mathbf{p}k}\equiv\theta_{\mathbf{p}}-\theta_{\mathbf{k}}$ and

$$F_{\mathbf{kp}\alpha\sigma} = \sum_{\pm}\frac{f(\pm E_{\mathbf{k}\alpha})-f(E_{\mathbf{p}\sigma})}{E_{\mathbf{k}\alpha}\mp E_{\mathbf{p}\sigma}}. \tag{33}$$

Above, $f(x)$ is the Fermi distribution. Thus we have found a two-particle current, for both spin and charge, that can be tuned in a well-defined manner by adjusting the relative orientation ϑ of the magnetization vectors.[68] We will discuss the detection of such an effect later in this paper. Note that the $\mathbf{k}$-dependent symmetry factor $\theta_{\mathbf{k}}$ enters the above expressions, thus giving rise to an extra contribution to the two-particle current besides the ordinary Josephson effect. This is due to the fact that we included it in the SC gaps as a factor $e^{\mathrm{i}\theta_{\mathbf{k}}}$ which in general is complex. However, this specific form may for certain models, depending on the Fermi surface in question, be reduced to a real function, i.e., $e^{\mathrm{i}\theta_{\mathbf{k}}}\rightarrow\cos\theta_{\mathbf{k}}$, in which case the quasiparticle interference term becomes zero. Hence in most of the remaining discussion we will focus on the Josephson part of the two-particle current.

The $A1$-phase with only one SC order parameter $\Delta_{\mathbf{k}\alpha\alpha}$, $\alpha\in\{\uparrow,\downarrow\}$ also corresponds to a nonunitary state $\mathbf{d}_{\mathbf{k}}$ according to Eq. (3), and is thus compatible with coexistence of FM and SC. In this case, we readily see that Eq. (32) reduces to

$$\begin{aligned} I^{\mathrm{C}}_{\mathrm{tp}} &= e\cos^2(\vartheta/2)X_\alpha \\ I^{\mathrm{S}}_{\mathrm{tp},z} &= -\alpha\cos^2(\vartheta/2)X_\alpha \end{aligned} \qquad \alpha\in\{\uparrow,\downarrow\}, \tag{34}$$

where we have defined the quantity

$$X_\alpha = \sum_{\mathbf{kp}}|T_{\mathbf{kp}}|^2\frac{|\Delta_{\mathbf{k}\alpha\alpha}\Delta_{\mathbf{p}\alpha}|}{E_{\mathbf{k}\alpha}E_{\mathbf{p}\alpha}}F_{\mathbf{kp}\alpha\alpha}[\sin\Delta\theta_{\alpha\alpha}\cos\Delta\theta_{\mathbf{pk}} + \cos\Delta\theta_{\alpha\alpha}\sin\Delta\theta_{\mathbf{pk}}], \tag{35}$$

with $\Delta\theta_{\alpha\alpha}\equiv\theta^{\mathrm{L}}_{\alpha\alpha}-\theta^{\mathrm{R}}_{\alpha\alpha}$, and $\Delta_{\mathbf{k}\alpha\alpha}$ is the surviving order parameter. As expected, the spin-current changes sign depending on whether it is the $\Delta_{\mathbf{k}\uparrow\uparrow}$ or $\Delta_{\mathbf{k}\downarrow\downarrow}$ order parameter that is present.

For collinear magnetization ($\vartheta=0$), an ordinary Josephson effect occurs with the superconducting phase difference as the driving force. Interestingly, one is able to tune both the spin- and charge-current to zero in the $A1$-phase when $\mathbf{m}_{\mathrm{L}}\|-\mathbf{m}_{\mathrm{R}}$ ($\vartheta=\pi$). It follows from Eq. (34) that the spin- and charge-current only differ by a constant prefactor

$$I^{\mathrm{C}}_{\mathrm{tp}}/I^{\mathrm{S}}_{\mathrm{tp},z} = -\alpha e, \quad \alpha=\pm 1. \tag{36}$$

It is then reasonable to draw the conclusion that we are dealing with a completely *spin-polarized current* such that both $I^{\mathrm{C}}_{\mathrm{tp}}$ and $I^{\mathrm{S}}_{\mathrm{tp},z}$ must vanish simultaneously at $\vartheta=\pi$.

Another result that can be extracted from Eqs. (32) and (34) is a persistent nonzero dc spin-Josephson current even if the magnetizations on each side of the junction are of equal magnitude and collinear ($\vartheta=0$). This is quite different from the spin-Josephson effect recently considered in ferromagnetic metal junctions.[24] In that case, a twist in the magnetization across the junction is required to drive the spin-Josephson effect.

Note that in the common approximation $T_{\mathbf{kp}}=T$, i.e., the tunneling probability is independent of the electron magnitude and direction of electron momentum, the two-particle current predicted above is identically equal to zero. Of course, such a crude approximation does not correspond to the correct physical picture (see e.g., Ref. 51), and in general one cannot neglect the directional dependence of the tunneling matrix element. This demonstrates that we are dealing with a more subtle effect than what could be unveiled when applying the approximation of a constant tunneling matrix element.

An interesting situation arises in the case of zero externally applied voltage *and* identical superconductors on each side of the junction with SC phase differences $\Delta\theta_{\sigma\sigma}=0$. In this case, we find that $I^{\mathrm{C}}_{\mathrm{J}}=0$ while

$$I^{\mathrm{S}}_{\mathrm{J},z} = -2\sum_{\mathbf{kp}} |T_{\mathbf{kp}}|^2 \sin^2(\vartheta/2)|\Delta_{\mathbf{k}\uparrow\uparrow}\Delta_{\mathbf{p}\downarrow\downarrow}|F_{\mathbf{kp}\uparrow\downarrow} \times \sin(\theta^{\mathrm{L}}_{\downarrow} - \theta^{\mathrm{R}}_{\uparrow})/(E_{\mathbf{k}\uparrow}E_{\mathbf{p}\downarrow}) \tag{37}$$

when $eV=0$, $\Delta\theta_{\sigma\sigma}=0$. Thus we have found a dissipationless spin-current in the two-particle channel without an externally applied voltage *and* without a SC phase difference. This effect is present as long as ϑ is not 0 or π, corresponding to parallel or antiparallel magnetization on each side of the junction. It is seen from Eq. (37) that the spin-current is driven by an interband phase difference on each side of the junction. A necessary condition for this effect to occur is that no interband Josephson coupling is present, i.e., electrons in the two energy-bands $E_{\mathbf{k}\uparrow}$ and $E_{\mathbf{k}\downarrow}$ do not communicate with each other. To understand why a Josephson coupling would destroy the above effect, consider the free energy density for a p-wave FMSC first proposed in Ref. 10, given by

$$\mathcal{F} = \mathcal{F}' - \lambda_{\mathrm{J}} \cos(\theta_{\uparrow\uparrow} - \theta_{\downarrow\downarrow}) \tag{38}$$

in the presence of a Josephson coupling. In Eq. (38), λ_{J} determines the strength of the interaction while $\mathcal{F}'$ contains the SC and FM contribution to the free energy density in addition to the coupling terms between the SC and FM order parameters. Consequently, the phase difference $\theta_{\uparrow\uparrow}-\theta_{\downarrow\downarrow}$ is locked to 0 or π in order to minimize $\mathcal{F}$, depending on $\mathrm{sgn}(\lambda_{\mathrm{J}})$. Considering Eq. (37), we see that $I^{\mathrm{S}}_{\mathrm{J},z}=0$ in this case, since the argument of the last sine is zero. Mechanisms that would induce a Josephson coupling include magnetic impurities causing inelastic spin-flip scattering between the energy-bands and spin-orbit coupling. Recently, the authors of Ref. 50 proposed that p-wave SC arising out of a FM metal state could be explained by the Berry curvature field that is present in ferromagnets with spin-orbit coupling. It is clear that in the case where spin-orbit coupling is included in the problem, spin-flip scattering processes occur between the energy bands such that the $\uparrow$ and $\downarrow$ spins cannot be considered as two independent species any more. The SC phases will then be locked to each other with a relative phase of 0 or π. However, note that in the general case, Eq. (32) produces a nonzero charge- and spin-current even if the spin-up and spin-down phases are locked to each other.

E. Single-particle currents

In the single-particle channel, we find that the charge and spin-currents read

$$I^{\mathrm{C}}_{\mathrm{sp}} = -e\sum_{\alpha} \langle \dot{N}_{\alpha\alpha}(t)\rangle_{\mathrm{sp}},$$

$$I^{\mathrm{S}}_{\mathrm{sp},z} = \sum_{\alpha} \alpha\langle \dot{N}_{\alpha\alpha}(t)\rangle_{\mathrm{sp}}, \tag{39}$$

as seen from Eq. (29). From Eq. (A1), we then extract the proper expectation value, which is found to be

$$\begin{aligned}\langle \dot{N}_{\alpha\alpha}(t)\rangle_{\mathrm{sp}} = 4\pi\sum_{\mathbf{kp}\sigma} [1+\sigma\alpha\cos(\vartheta)]|T_{\mathbf{kp}\alpha}|^2 N^2_{\mathbf{k}\alpha}N^2_{\mathbf{p}\sigma} \\ \times\Bigg[[f(E_{\mathbf{k}\alpha})-f(E_{\mathbf{p}\sigma})]\Bigg(\delta(-eV+E_{\mathbf{k}\alpha}-E_{\mathbf{p}\sigma}) \\ -\frac{|\Delta_{\mathbf{k}\alpha\alpha}\Delta_{\mathbf{p}\sigma\sigma}|^2}{(\xi_{\mathbf{k}\alpha}+E_{\mathbf{k}\alpha})^2(\xi_{\mathbf{p}\sigma}+E_{\mathbf{p}\sigma})^2}\delta(-eV-E_{\mathbf{p}\sigma}+E_{\mathbf{k}\alpha})\Bigg) \\ +[1-f(E_{\mathbf{k}\alpha})-f(E_{\mathbf{p}\sigma})]\Bigg(\frac{|\Delta_{\mathbf{k}\alpha\alpha}|^2}{(\xi_{\mathbf{k}\alpha}+E_{\mathbf{k}\alpha})^2}\delta(-eV \\ -E_{\mathbf{k}\alpha}-E_{\mathbf{p}\sigma})-\frac{|\Delta_{\mathbf{p}\sigma\sigma}|^2}{(\xi_{\mathbf{p}\sigma}+E_{\mathbf{p}\sigma})^2}\delta(-eV+E_{\mathbf{k}\alpha} \\ +E_{\mathbf{p}\sigma})\Bigg)\Bigg].\end{aligned} \tag{40}$$

The currents in Eq. (39) are thus seen to require an applied voltage in order to flow in the tunneling junction. Clearly, this is because the Cooper pairs need to be split up in order for a single-particle current to exist, such that both spin- and charge-currents vanish at $eV=0$.

In Ref. 24, the presence of a persistent spin-current in the single-particle channel for FM/FM junctions with a twist in magnetization across the junction was predicted. For consistency, our results must confirm this prediction for the single-particle current in the limit where SC is lost, i.e., $\Delta_{\mathbf{k}\sigma\sigma}\to 0$. Note that the $\hat{\mathbf{z}}$-direction in Ref. 24 corresponds to a vector in our local xy-plane since the present quantization axis lies parallel with the magnetization direction. Upon calculating the $\mathbf{x}$- and $\mathbf{y}$-components of the single-particle spin-current for our system in the limit where SC is lost, i.e., $\Delta_{\mathbf{k}\sigma\sigma}\to 0$, a persistent spin Josephson-like current proportional to $\sin(\vartheta)$ is identified. More precisely,

$$\mathbf{I}^{\mathrm{S}}_{\mathrm{sp}}(t) = 2\sum_{\mathbf{kp}}\sum_{\alpha\beta\sigma} \hat{\mathcal{D}}^{(1/2)}_{\sigma\alpha}(\vartheta)\hat{\mathcal{D}}^{(1/2)}_{\sigma\beta}(\vartheta)|T_{\mathbf{kp}}|^2 \times \mathrm{Im}\{\hat{\boldsymbol{\sigma}}_{\beta\alpha}\Lambda^{1,1}_{\beta\sigma}(-eV)\} \tag{41}$$

when $\Delta_{\mathbf{q}\sigma\sigma}=0$ (see Appendix for details). In agreement with Ref. 24, the component of the spin-current parallel to $\mathbf{m}_{\mathrm{L}} \times \mathbf{m}_{\mathrm{R}}$ is seen to vanish for $\vartheta=\{0,\pi\}$ at $eV=0$.

III. FERROMAGNETS WITH SPIN-ORBIT COUPLING

A. Coexistence of ferromagnetism and spin-orbit coupling

In a system where time-reversal and spatial inversion symmetry are simultaneously broken, it is clear that spins are heavily affected by these properties. There is currently much focus on ferromagnetic semiconductors where spin-orbit coupling plays a crucial role with regard to transport properties.[21,22] In fact, there has in recent years been much progress in the semiconductor research community where the spin-Hall effect in particular has received much attention.[23] With the discovery[52] of hole-mediated ferromagnetic order in (In,Mn)As, extensive research on III-V host materials was triggered. Moreover, it is clear that properties such as ferromagnetic transition temperatures in excess of 100 K[53] and

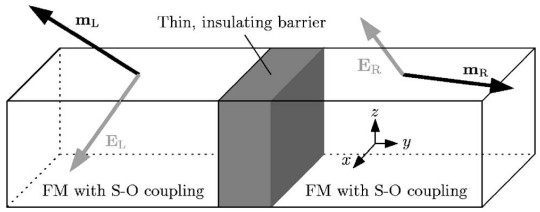

FIG. 4. Our model consisting of two ferromagnetic metals with spin-orbit coupling separated by a thin insulating barrier. The magnetization **m** and electrical field **E** are allowed to point in any direction so that our results are generally valid, while special cases such as planar magnetization, etc. are easily obtained by applying the proper limits to the general expressions.

long spin-coherence times[54] in GaAs have strongly contributed to opening up a vista plethora for information processing and storage technologies in these new magnetic mediums.[55]

Generally, spin-orbit coupling (SOC) can be roughly divided into two categories—*intrinsic* and *extrinsic*. Intrinsic SOC is found in materials with a noncentrosymmetric crystal symmetry, i.e., where inversion symmetry is broken, whereas extrinsic SOC is due to asymmetries caused by impurities, local confinements of electrons, or externally applied electrical fields.

In the present paper, we investigate the tunneling current of spin between two ferromagnetic metals with spin-orbit coupling induced by an external electric field. This way, we will have two externally controllable parameters; the magnetization **m** and the electrical field **E**. The case of tunneling between two noncentrosymmetric superconductors with significant spin-orbit coupling, but no ferromagnetism, has previously been considered in Ref. 56.

B. The Hamiltonian

Our system consists of two Heisenberg ferromagnets with substantial spin-orbit coupling, separated by a thin insulating barrier which is assumed to be spin-inactive. This is shown in Fig. 4. We now operate with only one quantization axis, such that a proper tunneling Hamiltonian for this purpose is

$$H_T = \sum_{\mathbf{kp}\sigma} (T_{\mathbf{kp}} c^\dagger_{\mathbf{k}\sigma} d_{\mathbf{p}\sigma} + \text{H.c.}), \tag{42}$$

where $\{c^\dagger_{\mathbf{k}\sigma}, c_{\mathbf{k}\sigma}\}$ and $\{d^\dagger_{\mathbf{k}\sigma}, d_{\mathbf{k}\sigma}\}$ are creation and annihilation operators for an electron with momentum $\mathbf{k}$ and spin σ on the right and left side of the junction, respectively, while $T_{\mathbf{kp}}$ is the spin-independent tunneling matrix element. In $\mathbf{k}$-space, the Hamiltonian describing the ferromagnetism reads

$$H_{FM} = \sum_{\mathbf{k}\sigma} \varepsilon_{\mathbf{k}} c^\dagger_{\mathbf{k}\sigma} c_{\mathbf{k}\sigma} - JN \sum_{\mathbf{k}} \eta(\mathbf{k}) \mathbf{S}_{\mathbf{k}} \cdot \mathbf{S}_{-\mathbf{k}} \tag{43}$$

in which $\varepsilon_{\mathbf{k}}$ is the kinetic energy of the electrons, J is the ferromagnetic coupling constant, N is the number of particles in the system, while $\mathbf{S}_{\mathbf{k}} = (1/2)\Sigma_{\alpha\beta} c^\dagger_{\mathbf{k}\alpha} \hat{\boldsymbol{\sigma}}_{\alpha\beta} c_{\mathbf{k}\beta}$ is the spin operator. As we later adopt the mean-field approximation, $\mathbf{m} = (m_x, m_y, m_z)$ will denote the magnetization of the system.

The spin-orbit interactions are accounted for by a Rashba Hamiltonian

$$H_{S\text{-}O} = -\sum_{\mathbf{k}} \varphi^\dagger_{\mathbf{k}} [\xi(\nabla V \times \mathbf{k}) \cdot \hat{\boldsymbol{\sigma}}] \varphi_{\mathbf{k}}, \tag{44}$$

where $\varphi_{\mathbf{k}} = [c_{\mathbf{k}\uparrow}, c_{\mathbf{k}\downarrow}]^T$, $\mathbf{E} = -\nabla V$ is the electrical field felt by the electrons and $\hat{\boldsymbol{\sigma}} = (\hat{\sigma}_1, \hat{\sigma}_2, \hat{\sigma}_3)$ in which $\hat{\sigma}_i$ are Pauli matrices, while the parameter ξ is material-dependent. From now on, the notation $\xi(\mathbf{E} \times \mathbf{k}) \equiv \mathbf{B}_{\mathbf{k}} = (B_{\mathbf{k},x}, B_{\mathbf{k},y}, B_{\mathbf{k},z})$ will be used. In general, the electromagnetic potential V consists of two parts V_{int} and V_{ext} (see, e.g., Ref. 23 for a detailed discussion of the spin-orbit Hamiltonian). The crystal potential of the material is represented by V_{int}, and only gives rise to a spin-orbit coupling if inversion symmetry is broken in the crystal structure. Asymmetries such as impurities and local confinements of electrons are included in V_{ext}, as well as any external electrical field. Note that any lack of crystal inversion symmetry results in a so-called Dresselhaus term in the Hamiltonian, which is present in the absence of any impurities and confinement potentials. In the following, we focus on the spin-orbit coupling resulting from V_{ext}, thus considering any symmetry-breaking electrical field that arises from charged impurities or which is applied externally. In the case where the crystal structure does not respect inversion symmetry, a Dresselhaus term[57] can be easily included in the Hamiltonian by performing the substitution

$$(\mathbf{E} \times \mathbf{k}) \cdot \hat{\boldsymbol{\sigma}} \to [(\mathbf{E} \times \mathbf{k}) + \mathcal{D}(\mathbf{k})] \cdot \hat{\boldsymbol{\sigma}}, \tag{45}$$

where $\mathcal{D}(\mathbf{k}) = -\mathcal{D}(-\mathbf{k})$.

We now proceed to calculate the spin-current that is generated across the junction as a result of tunneling. Note that in our model, the magnetization vector and electrical field are allowed to point in arbitrary directions. In this way, the obtained result for the spin-current will be generally valid and special cases, e.g., thin films, are easily obtained by taking the appropriate limits in the final result. It should be mentioned that the effective magnetic field from the spin-orbit interactions might influence the direction of the magnetization in the ferromagnet. This is, however, not the main focus of our work, and we leave this question open for study. Our emphasis in the present paper concerns the derivation of general results onto which specific restrictions may be applied as they seem appropriate.

In the mean-field approximation, the Hamiltonian for the right side of the junction can be written as $H = H_{FM} + H_{S-O}$, which in a compact form yields

$$H_R = H_0 + \sum_{\mathbf{k}} \varphi^\dagger_{\mathbf{k}} \begin{pmatrix} \varepsilon_{\mathbf{k}\uparrow} & -\zeta_R + B_{\mathbf{k},-} \\ -\zeta^\dagger_R + B_{\mathbf{k},+} & \varepsilon_{\mathbf{k}\downarrow} \end{pmatrix} \varphi_{\mathbf{k}}, \tag{46}$$

where $\varepsilon_{\mathbf{k}\sigma} \equiv \varepsilon_{\mathbf{k}} - \sigma(\zeta_{z,R} - B_{\mathbf{k},z})$ and H_0 is an irrelevant constant. The FM order parameters are $\zeta_R = 2J\eta(0)(m_{R,x} - i m_{R,y})$ and $\zeta_{z,R} = 2J\eta(0) m_{R,z}$ and $B_{\mathbf{k},\pm} \equiv B_{\mathbf{k},x} \pm i B_{\mathbf{k},y}$. For convenience, we from now on write $\zeta = |\zeta| e^{i\phi}$ and $B_{\mathbf{k},\pm} = |B_{\mathbf{k},\pm}| e^{\mp i \chi_{\mathbf{k}}}$. The Hamiltonian for the left side of the junction is obtained from Eq. (46) simply by doing the replacements $\mathbf{k} \to \mathbf{p}$ and $R \to L$.

C. Tunneling formalism

In order to obtain the expressions for the spin- and charge-tunneling currents, it is necessary to calculate the Green functions. These are given by the matrix

$$\hat{\mathcal{G}}_{\mathbf{k}}(i\omega_n) = (-i\omega_n \hat{1} + \hat{\mathcal{A}}_{\mathbf{k}})^{-1}, \tag{47}$$

where $\hat{\mathcal{A}}_{\mathbf{k}}$ is the matrix in Eq. (46). Explicitly, we have that

$$\hat{\mathcal{G}}_{\mathbf{k}}(i\omega_n) = \begin{pmatrix} G_{\mathbf{k}}^{\uparrow\uparrow}(i\omega_n) & F_{\mathbf{k}}^{\downarrow\uparrow}(i\omega_n) \\ F_{\mathbf{k}}^{\uparrow\downarrow}(i\omega_n) & G_{\mathbf{k}}^{\downarrow\downarrow}(i\omega_n) \end{pmatrix}. \tag{48}$$

Above, $\omega_n = 2(n+1)\pi/\beta, n = 0,1,2\ldots$ is the fermionic Matsubara frequency and β denotes inverse temperature. Introducing

$$X_{\mathbf{k}}(i\omega_n) = (\varepsilon_{\mathbf{k}\uparrow} - i\omega_n)(\varepsilon_{\mathbf{k}\downarrow} - i\omega_n) - |\zeta_{\mathrm{R}} - B_{\mathbf{k},-}|^2, \tag{49}$$

the normal and anomalous Green functions are

$$G_{\mathbf{k}}^{\sigma\sigma}(i\omega_n) = (\varepsilon_{\mathbf{k},-\sigma} - i\omega_n)/X_{\mathbf{k}}(i\omega_n),$$

$$F_{\mathbf{k}}^{\downarrow\uparrow}(i\omega_n) = F_{\mathbf{k}}^{\uparrow\downarrow,\dagger}(i\omega_n) = (\zeta_{\mathrm{R}} - B_{\mathbf{k},-})/X_{\mathbf{k}}(i\omega_n). \tag{50}$$

The expression for $\mathbf{I}^{\mathrm{S}}(t)$ is established by first considering the generalized number operator $N_{\alpha\beta} = \Sigma_{\mathbf{k}} c_{\mathbf{k}\alpha}^{\dagger} c_{\mathbf{k}\beta}$. This operator changes with time due to tunneling according to $\dot{N}_{\alpha\beta} = i[H_{\mathrm{T}}, N_{\alpha\beta}]$, which in the interaction picture representation becomes $\dot{N}_{\alpha\beta}(t) = -i\Sigma_{\mathbf{kp}}(T_{\mathbf{kp}} c_{\mathbf{k}\alpha}^{\dagger} d_{\mathbf{p}\beta} e^{ie\mathrm{V}} - \mathrm{H.c.})$. The voltage drop across the junction is given by the difference in chemical potential on each side, i.e., $e\mathrm{V} = \mu_{\mathrm{R}} - \mu_{\mathrm{L}}$. In the lineawr response regime, the spin-current across the junction is

$$\mathbf{I}^{\mathrm{S}}(t) = \frac{1}{2}\sum_{\alpha\beta} \hat{\boldsymbol{\sigma}}_{\alpha\beta} \langle \dot{N}_{\alpha\beta}(t) \rangle, \tag{51}$$

where the expectation value of the time derivative of the transport operator is calculated by means of the Kubo formula Eq. (30). Details will be given in Appendix A 2.

D. Single-particle currents

At $e\mathrm{V} = 0$, it is readily seen from the discussion in Appendix A 2 that the charge-current vanishes. Consider now the z-component of the spin-current in particular, which can be written as $I_z^{\mathrm{S}} = \mathrm{Im}\{\Phi(-e\mathrm{V})\}$. The Matsubara function $\Phi(-e\mathrm{V})$ is found by performing analytical continuation $i\tilde{\omega}_\nu \to -e\mathrm{V} + i0^+$ on $\tilde{\Phi}(i\tilde{\omega}_\nu)$, where

$$\tilde{\Phi}(i\tilde{\omega}_\nu) = \frac{1}{\beta}\sum_{i\omega_m, \mathbf{kp}} \sum_{\sigma} \sigma \big(G_{\mathbf{k}}^{\sigma\sigma}(i\omega_m) G_{\mathbf{p}}^{\sigma\sigma}(i\omega_m - i\tilde{\omega}_\nu) + F_{\mathbf{k}}^{-\sigma,\sigma}(i\omega_m) F_{\mathbf{p}}^{\sigma,-\sigma}(i\omega_m - i\tilde{\omega}_\nu) \big). \tag{52}$$

Here, $\tilde{\omega}_\nu = 2\nu\pi/\beta$, $\nu = 0,1,2,\ldots$ is the bosonic Matsubara frequency. Inserting the Green functions from Eq. (50) into Eq. (52), one finds that a persistent spin-current is established across the tunneling junction. For zero applied voltage, we obtain

$$I_z^{\mathrm{S}} = \sum_{\mathbf{kp}} \frac{|T_{\mathbf{kp}}|^2 J_{\mathbf{kp}}}{2\gamma_{\mathbf{k}}\gamma_{\mathbf{p}}} [|\zeta_{\mathrm{R}}\zeta_{\mathrm{L}}| \sin\Delta\phi + |B_{\mathbf{k},-}B_{\mathbf{p},-}| \sin\Delta\chi_{\mathbf{kp}} - |B_{\mathbf{k},-}\zeta_{\mathrm{L}}| \sin(\chi_{\mathbf{k}} - \phi_{\mathrm{L}}) - |B_{\mathbf{p},-}\zeta_{\mathrm{R}}| \sin(\phi_{\mathrm{R}} - \chi_{\mathbf{p}})], \tag{53a}$$

$$J_{\mathbf{kp}} = \sum_{\substack{\alpha=\pm \\ \beta=\pm}} \alpha\beta \left[\frac{n(\varepsilon_{\mathbf{k}} + \alpha\gamma_{\mathbf{k}}) - n(\varepsilon_{\mathbf{p}} + \beta\gamma_{\mathbf{p}})}{(\varepsilon_{\mathbf{k}} + \alpha\gamma_{\mathbf{k}}) - (\varepsilon_{\mathbf{p}} + \beta\gamma_{\mathbf{p}})} \right]. \tag{53b}$$

In Eqs. (53), $\Delta\chi_{\mathbf{kp}} \equiv \chi_{\mathbf{k}} - \chi_{\mathbf{p}}$, $\Delta\phi \equiv \phi_{\mathrm{R}} - \phi_{\mathrm{L}}$, while

$$\gamma_{\mathbf{k}}^2 = (\zeta_{z,\mathrm{R}} - B_{\mathbf{k},z})^2 + |\zeta_{\mathrm{R}} - B_{\mathbf{k},-}|^2 \tag{54}$$

and $n(\varepsilon)$ denotes the Fermi distribution. In the above expressions, we have implicitly associated the right side R with the momentum label $\mathbf{k}$ and L with $\mathbf{p}$ for more concise notation, such that, e.g., $B_{\mathbf{k},z} \equiv B_{\mathbf{k},z}^{\mathrm{R}}$. Defining $\zeta_i = 2J\eta(0)m_i$, we see that Eq. (54) can be written as

$$\gamma_{\mathbf{k}} = |\boldsymbol{\zeta}_{\mathrm{R}} - \mathbf{B}_{\mathbf{k}}|. \tag{55}$$

The spin-current described in Eq. (53) can be controlled by adjusting the relative orientation of the magnetization vectors on each side of the junction, i.e., $\Delta\phi$, and also responds to a change in direction of the applied electric fields. The presence of an external magnetic field $\mathbf{H}_i$ would control the orientation of the internal magnetization $\mathbf{m}_i$. Alternatively, one may also use exchange biasing to an antiferromagnet in order to lock the magnetization direction. Consequently, the spin-current can be manipulated by the external control parameters $\{\mathbf{H}_i, \mathbf{E}_i\}$ in a well-defined manner. This observation is highly suggestive in terms of novel nanotechnological devices.

We stress that Eq. (53) is *nonzero* in the general case, since $\gamma_{\mathbf{k}} \neq -\gamma_{-\mathbf{k}}$ and $\chi_{-\mathbf{k}} = \chi_{\mathbf{k}} + \pi$. Moreover, Eq. (53) is valid for any orientation of both $\mathbf{m}$ and $\mathbf{E}$ on each side of the junction, and a number of interesting special cases can now easily be considered simply by applying the appropriate limits to this general expression.

E. Special limits

Consider first the limit where ferromagnetism is absent, such that the tunneling occurs between two bulk materials with spin-orbit coupling. Applying $\mathbf{m} \to 0$ to Eq. (53), it is readily seen that the spin-current vanishes for any orientation of the electrical fields. Intuitively, one can understand this by considering the band structure of the quasiparticles with energy $E_{\mathbf{k}\sigma} = \varepsilon_{\mathbf{k}} + \sigma\gamma_{\mathbf{k}}$ and the corresponding density of states $N(E_{\mathbf{k}\sigma})$ when only spin-orbit coupling is present, as shown in Fig. 5. Since the density of states is equal for $\uparrow$ and $\downarrow$ spins,[69] one type of spin is not preferred compared to the other with regard to tunneling, resulting in a net spin-current of zero. Formally, the vanishing of the spin-current can be understood by replacing the momentum summation with integration over energy, i.e., $\Sigma_{\mathbf{kp}} \to \int\int dE_{\mathrm{R}} dE_{\mathrm{L}} N_{\mathrm{R}}(E_{\mathrm{R}}) N_{\mathrm{L}}(E_{\mathrm{L}})$. When $\mathbf{m} \to 0$, Eq. (53) dictates that

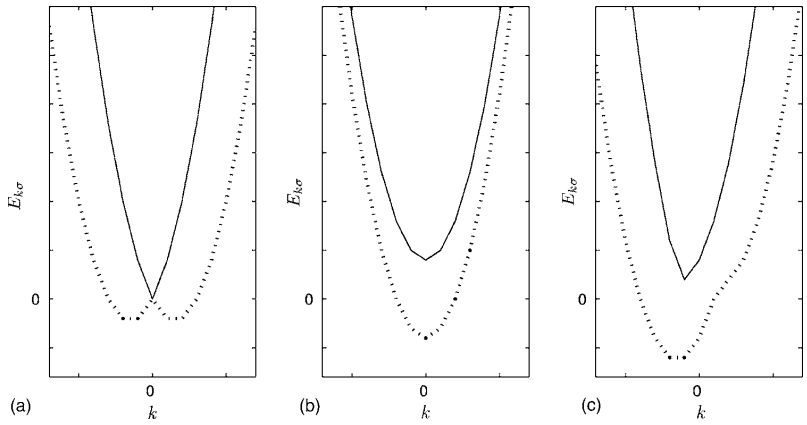

FIG. 5. Schematic illustration of the energy-bands for (a) a system with spin-orbit coupling, (b) a system with ferromagnetic ordering, and (c) a system exhibiting both of the aforementioned properties. The dotted line corresponds to quasiparticles with $\sigma=\downarrow$, while the full drawn line designates $\sigma=\uparrow$. Since the density of states $N^{\sigma}(E_{k\sigma})$ is proportional to $(\partial E_{k\sigma}/\partial k)^{-1}$, we see that a difference between $N^{\uparrow}(E_{k\sigma})$ and $N^{\downarrow}(E_{k\sigma})$ is zero at Fermi level in (a), while the density of states differ for the $\uparrow$- and $\downarrow$-populations in (b) and (c). Thus a persistent spin-current will only occur for tunneling between systems corresponding to (b) and (c).

$$I_z^S \sim \sum_{\substack{\alpha=\pm \\ \beta=\pm}} \alpha\beta \int\int dE_{\mathrm{R},\alpha} dE_{\mathrm{L},\beta} N_{\mathrm{R}}^{\alpha}(E_{\mathrm{R},\alpha}) N_{\mathrm{L}}^{\beta}(E_{\mathrm{L},\beta}) \times \left[\frac{n(E_{\mathrm{R},\alpha}) - n(E_{\mathrm{L},\beta})}{E_{\mathrm{R},\alpha} - E_{\mathrm{L},\beta}} \right]. \tag{56}$$

Since the density of states for the $\uparrow$- and $\downarrow$-populations are equal in the individual subsystems, i.e., $N^{\uparrow}(E)=N^{\downarrow}(E) \equiv N(E)$, the integrand of Eq. (56) becomes spin-independent such that the summation over α and β yields zero. Thus no spin-current will exist at eV=0 over a tunneling barrier separating two systems with spin-orbit coupling alone. In the general case where both ferromagnetism and spin-orbit coupling are present, the density of states at, say, Fermi level are different, leading to a persistent spin-current across the junction due to the difference between $N^{\uparrow}(E)$ and $N^{\downarrow}(E)$.

We now consider a special case where the bulk structures indicated in Fig. 4 are reduced to two thin-film ferromagnets in the presence of electrical fields that are perpendicular to each other, say $\mathbf{E}_{\mathrm{L}}=(E_{\mathrm{L}},0,0)$ and $\mathbf{E}_{\mathrm{R}}=(0,E_{\mathrm{R}},0)$, as shown in Figs. 6(a) and 6(b). In this case, we have chosen an in-plane magnetization for each of the thin films. Solving specifically for Fig. 6(a), it is seen that $\mathbf{m}_{\mathrm{L}}=(0,m_{\mathrm{L},y},m_{\mathrm{L},z})$ and $\mathbf{m}_{\mathrm{R}}=(m_{\mathrm{R},x},0,m_{\mathrm{R},z})$. Furthermore, assume that the electrons are restricted from moving in the "thin" dimension, i.e., $\mathbf{p}=(0,p_y,p_z)$ and $\mathbf{k}=(k_x,0,k_z)$. In this case, Eq. (53) reduces to the form

$$I_z^{\mathrm{S}} = I_0 \,\mathrm{sgn}(m_{\mathrm{L},y}) + \sum_{\mathbf{kp}} I_{1,\mathbf{kp}} \,\mathrm{sgn}(p_z), \tag{57}$$

where the constants above are

$$I_0 = \sum_{\mathbf{kp}} \frac{|T_{\mathbf{kp}}|^2 J_{\mathbf{kp}} (|\boldsymbol{\zeta}_{\mathrm{R}}\boldsymbol{\zeta}_{\mathrm{L}}| - E_{\mathrm{R}}|k_z\zeta_{\mathrm{L}}|)}{2|\boldsymbol{\zeta}_{\mathrm{R}} + \mathbf{B}_{\mathbf{k}}||\boldsymbol{\zeta}_{\mathrm{L}} + \mathbf{B}_{\mathbf{p}}|},$$

$$I_{1,\mathbf{kp}} = \frac{|T_{\mathbf{kp}}|^2 J_{\mathbf{kp}} E_{\mathrm{L}} (E_{\mathrm{R}}|k_z p_z| - |p_z\zeta_{\mathrm{R}}|)}{2|\boldsymbol{\zeta}_{\mathrm{R}} + \mathbf{B}_{\mathbf{k}}||\boldsymbol{\zeta}_{\mathrm{L}} + \mathbf{B}_{\mathbf{p}}|}, \tag{58}$$

with

$$\boldsymbol{\zeta}_{\mathrm{L}} = 2J\eta(0)(0,m_{\mathrm{L},y},m_{\mathrm{L},z}), \quad \mathbf{B}_{\mathbf{p}} = \xi_{\mathrm{L}} E_{\mathrm{L}}(0,-p_z,p_y),$$

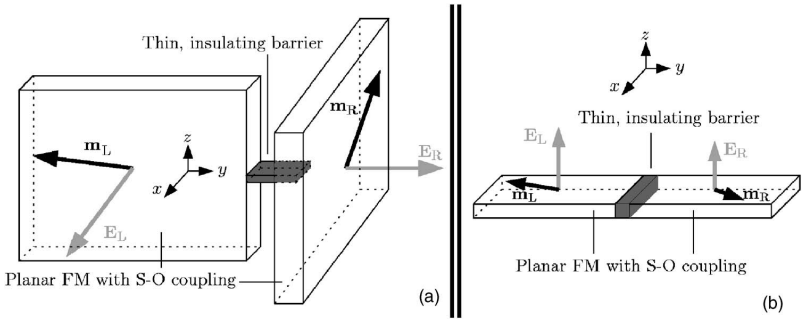

FIG. 6. Tunneling between planar ferromagnets in the presence of externally applied electrical fields $\mathbf{E}_{\mathrm{L}}$ and $\mathbf{E}_{\mathrm{R}}$ that destroy inversion symmetry and induce a spin-orbit coupling.

$$\boldsymbol{\zeta}_{\mathrm{R}} = 2J\eta(0)(m_{\mathrm{R},x},0,m_{\mathrm{R},z}), \quad \mathbf{B}_{\mathbf{k}} = \xi_{\mathrm{R}}E_{\mathrm{R}}(k_y,0,-k_x), \tag{59}$$

such that $I_{1,\mathbf{kp}} \neq I_{1,-\mathbf{k},-\mathbf{p}}$. Likewise, for the setup sketched in Fig. 6(b), one obtains

$$\begin{aligned} I_z^{\mathrm{S}} = \sum_{\mathbf{kp}} & \frac{|T_{\mathbf{kp}}|^2 J_{\mathbf{kp}}}{2|\zeta_{\mathrm{R}} + E_{\mathrm{R}}(k_y - ik_x)|^2|\zeta_{\mathrm{L}} + E_{\mathrm{L}}(p_y - ip_x)|^2} \\ & \times [|\zeta_{\mathrm{R}}\zeta_{\mathrm{L}}|\sin\Delta\phi + E_{\mathrm{R}}E_{\mathrm{L}}(k_y^2 + k_x^2)(p_y^2 + p_x^2)|\sin\Delta\chi_{\mathbf{kp}} \\ & - E_{\mathrm{R}}|\zeta_{\mathrm{L}}|(k_y^2 + k_x^2)\sin(\chi_k - \phi_{\mathrm{L}}) - E_{\mathrm{L}}|\zeta_{\mathrm{R}}|(p_y^2 + p_x^2) \\ & \times\sin(\phi_{\mathrm{R}} - \chi_{\mathbf{p}})], \end{aligned} \tag{60}$$

where $\chi_{\mathbf{q}}$ obeys

$$\tan\chi_{\mathbf{q}} = -\frac{q_x}{q_y}, \quad \mathbf{q} = \mathbf{k},\mathbf{p}. \tag{61}$$

From these observations, we can draw the following conclusions: whereas the spin-current is zero for the system in Figs. 6(a) and 6(b) if only spin-orbit coupling is considered, it is nonzero when only ferromagnetism is taken into account. However, in the general case where both ferromagnetism and spin-orbit coupling are included, an *additional term* in the spin-current is induced compared to the pure ferromagnetic case. Accordingly, there is an interplay between the magnetic order and the Rashba-interaction that produces a spin-current which is more than just the sum of the individual contributions.

IV. DISCUSSION OF RESULTS

Having presented the general results for tunneling currents between systems with multiple broken symmetries in the preceding sections, we now focus on detection and experimental issues concerning verification of our predictions.

Consider first the system consisting of two ferromagnetic superconductors separated by a thin, insulating barrier. It is well-known that for tunneling currents flowing between two *s*-wave SC in the presence of a magnetic field that is perpendicular to the tunneling direction, the resulting flux threading the junction leads to a Fraunhofer-like variation in the DC Josephson effect, given by a multiplicative factor

$$D_{\mathrm{F}}(\Phi) = \frac{\sin(\pi\Phi/\Phi_0)}{(\pi\Phi/\Phi_0)} \tag{62}$$

in the critical current. Here, $\Phi_0 = \pi\hbar/e$ is the elementary flux quantum, and Φ is the total flux threading the junction due to a magnetic field. Consequently, the presence of magnetic flux in the tunneling junction of two *s*-wave SC threatens to nullify the total Josephson current. In the present case of two *p*-wave FMSC, this is not an issue since we have assumed uniform coexistence of the SC and FM order parameters which is plausible for a weak intrinsic magnetization. The effect of an external magnetic field $\mathbf{H}$ would then simply be to rotate the internal magnetization as dictated by the term $-\mathbf{H}\cdot\mathbf{m}$ in the free energy $\mathcal{F}$ (see, e.g., Ref. 18). Thus there is no diffraction pattern present for the tunneling-currents between two nonunitary ESP FMSC, regardless of how the internal magnetization is oriented. Since the motion of the Cooper-pairs is also restricted by the thin-film structure, there is no orbital effect from such a magnetization.

Note that the interplay between ferromagnetism and superconductivity is manifest in the charge-as well as spin-currents, the former being readily measurable. Detection of the induced spin-currents would be challenging, although recent studies suggest feasible methods of measuring such quantities.[58] We comment more on this later in this section. First, we address the issue of how boundary effects affect the order parameters. Studies[40–42] have shown that interfaces/surfaces may have a pair-breaking effect on unconventional SC order parameters. This is highly relevant in tunneling junction experiments as in the present case. The suppression of the order parameter is caused by a formation of so-called midgap surface states (also known as zero-energy states)[39] which occurs for certain orientations of the $\mathbf{k}$-dependent SC gaps that satisfy a resonance condition. Note that this is not the case for conventional *s*-wave superconductors since the gap is isotropic in that case. This pair-breaking surface effect was studied specifically for *p*-wave order parameters in Refs. 40 and 41, and it was found that the component of the order parameter that experiences a sign change under the transformation $k_\perp \to -k_\perp$, where $k_\perp$ is the component of momentum perpendicular to the tunneling junction, was suppressed in the vicinity of the junction. By vicinity of the junction, we here mean a distance comparable to the coherence length, typically of order 1–10 nm. Thus depending on the explicit form of the superconducting gaps in the FMSC, these could be subject to a reduction close to the junction, which in turn would reduce the magnitude of the Josephson effect we predict. Nevertheless, the latter is nonvanishing in the general case.

Since the critical Josephson currents depend on the relative magnetization orientation, one is able to tune these currents in a well-defined manner by varying ϑ. This can be done by applying an external magnetic field in the plane of the FMSC. In the presence of a rotating magnetic moment on either side of the junction, the Josephson currents will thus vary according to Eq. (32), which may be cast into the form $I_{\mathrm{J}}^{\mathrm{C}} = I_0 + I_m\cos(\vartheta)$. Depending on the relative magnitudes of I_0 and I_m, the sign of the critical current may change. Note that such a variation of the magnetization vectors must take place in an adiabatic manner so that the systems can be considered to be in, or near, equilibrium at all times. Our predictions can thus be verified by measuring the critical current at $eV=0$ for different angles ϑ and compare the results with our theory. Recently, it has been reported that a spin-triplet supercurrent, induced by Josephson tunneling between two *s*-wave superconductors across a ferromagnetic metallic contact, can be controlled by varying the magnetization of the ferromagnetic contact.[59] Moreover, concerning the spin-Josephson current we propose, detection of induced spin-currents are challenging, although recent studies suggest feasible methods of measuring such quantities.[58] Observation of macroscopic spin-currents in superconductors may also be possible via angle resolved photoemission experiments with circularly polarized photons[60] or in spin-resolved neutron scattering experiments.[32]

We reemphasize that the above ideas should be experimentally realizable by, e.g., utilizing various geometries in

order to vary the demagnetization fields. Alternatively, one may use exchange biasing to an antiferromagnet. Such techniques of achieving noncollinearity are routinely used in ferromagnet-normal metal structures.[61]

With regard to the predicted dc spin-current in for a system consisting of two ferromagnetic metals with spin-orbit coupling, we here suggest how this effect could be probed for in an experimental setup. For instance, the authors of Ref. 62 propose a spin-mechanical device which exploits nanomechanical torque for detection and control of a spin-current. Similarly, a setup coupling the electron spin to the mechanical motion of a nanomechanical system is proposed in Ref. 58. The latter method employs the strain-induced spin-orbit interaction of electrons in a narrow gap semiconductor. In Ref. 63, it was demonstrated that a steady-state magnetic-moment current, i.e., spin-current, will induce a static electric field. This fact may be suggestive in terms of detection[64,65] and could be useful to observe the effects predicted in this paper.

V. SUMMARY

In summary, we have considered supercurrents of spin and charge that exist in FMSC/FMSC and FMSO/FMSO tunneling junctions. In the former case, we have found an interplay between the relative magnetization orientation on each side of the junction and the SC phase difference when considering tunneling between two nonunitary ESP FMSC with coexisting and uniform FM and SC order. This interplay is present in the Josephson channel, offering the opportunity to tune dissipationless currents of spin and charge in a well-defined manner by adjusting the relative magnetization orientation on each side of the junction. As a special case, we considered the case where the SC phase difference is zero, and found that a dissipationless spin-current *without* charge-current would be established across the junction. Suggestions concerning the detection of the effects we predict have been made.

Moreover, we have derived an expression for a dissipationless spin-current that arises in the junction between two Heisenberg ferromagnets with spin-orbit coupling. We have shown that the spin-current is driven by terms originating from both the ferromagnetic phase difference, in agreement with the result of Ref. 24, and the presence of spin-orbit coupling itself. In addition, it was found that the simultaneous breaking of time-reversal and inversion symmetry fosters an interplay between ferromagnetism and spin-orbit coupling in the spin-current. Availing oneself of external magnetic and electric fields, our expressions show that the spin-current can be tuned in a well-defined manner. These results are of significance in the field of spintronics in terms of quantum transport, and offer insight into how the spin-current behaves for nanostructures exhibiting both ferromagnetism and spin-orbit coupling.

ACKNOWLEDGMENTS

The authors acknowledge J.-M. Børven for his valuable contribution and thank A. Brataas, K. Børkje, and E. K. Dahl for helpful discussions. This work was supported by the Norwegian Research Council Grants No. 157798/432 and No. 158547/431 (NANOMAT), and Grant No. 167498/V30 (STORFORSK).

APPENDIX: DETAILS OF MATSUBARA FORMALISM

1. Ferromagnetic superconductors

Inserting Eq. (27) into Eq. (30), one finds that

$$\begin{aligned}\langle \dot{N}_{\alpha\beta}(t)\rangle = \langle \dot{N}_{\alpha\beta}(t)\rangle_{\mathrm{sp}} + \langle \dot{N}_{\alpha\beta}(t)\rangle_{\mathrm{tp}} = \\ -\int_{-\infty}^{t} dt'[\langle [M_{\alpha\beta}(t), M^{\dagger}(t')]\rangle e^{-ieV(t-t')} \\ -\langle [M^{\dagger}_{\beta\alpha}(t), M(t')]\rangle e^{ieV(t-t')} \\ +\langle [M_{\alpha\beta}(t), M(t')]\rangle e^{-ieV(t+t')} \\ -\langle [M^{\dagger}_{\beta\alpha}(t), M^{\dagger}(t')]\rangle e^{ieV(t+t')}],\end{aligned} \tag{A1}$$

where the two first terms in Eq. (A1) contribute to the single-particle current while the two last terms constitute the Josephson current. Above, we defined

$$M_{\alpha\beta}(t) = \sum_{\mathbf{kp}\sigma} \hat{\mathcal{D}}^{(1/2)}_{\sigma\beta}(\vartheta) T_{\mathbf{kp}} c^{\dagger}_{\mathbf{k}\alpha}(t) d_{\mathbf{p}\sigma}(t),$$

$$M(t) = \sum_{\mathbf{kp}\sigma\sigma'} \hat{\mathcal{D}}^{(1/2)}_{\sigma'\sigma}(\vartheta) T_{\mathbf{kp}} c^{\dagger}_{\mathbf{k}\sigma}(t) d_{\mathbf{p}\sigma'}(t). \tag{A2}$$

By observing that $\hat{\boldsymbol{\sigma}}_{\alpha\beta} = (\hat{\boldsymbol{\sigma}}_{\beta\alpha})^{*}$, we can combine Eqs. (30)–(42), (42)–(62), (A1), and (A2) to yield

$$\hat{\boldsymbol{\sigma}}_{\alpha\beta}\langle \dot{N}_{\alpha\beta}(t)\rangle_{\mathrm{sp}} = 2\,\mathrm{Im}\{\hat{\boldsymbol{\sigma}}_{\alpha\beta}\Phi_{\alpha\beta,\mathrm{sp}}(-eV)\},$$

$$\hat{\boldsymbol{\sigma}}_{\alpha\beta}\langle \dot{N}_{\alpha\beta}(t)\rangle_{\mathrm{tp}} = 2\,\mathrm{Im}\{\hat{\boldsymbol{\sigma}}_{\alpha\beta}\Phi_{\alpha\beta,\mathrm{J}}(eV)e^{-2ietV}\}, \tag{A3}$$

where the Matsubara functions are obtained by performing analytical continuation according to

$$\Phi_{\alpha\beta,\mathrm{sp}}(-eV) = \lim_{i\tilde{\omega}_{\nu}\to -eV+i0^{+}} \tilde{\Phi}_{\alpha\beta,\mathrm{sp}}(i\tilde{\omega}_{\nu}),$$

$$\Phi_{\alpha\beta,\mathrm{J}}(eV) = \lim_{i\tilde{\omega}_{\nu}\to eV+i0^{+}} \tilde{\Phi}_{\alpha\beta,\mathrm{tp}}(i\tilde{\omega}_{\nu}), \tag{A4}$$

In Eq. (A4), $\tilde{\omega}_{\nu} = 2\pi\nu/\beta$, $\nu = 1, 2, 3, \ldots$ is the bosonic Matsubara frequency and

$$\begin{aligned}\tilde{\Phi}_{\mathrm{sp},\alpha\beta}(i\tilde{\omega}_{\nu}) = -\int_{0}^{\beta} d\tau e^{i\tilde{\omega}_{\nu}\tau} \sum_{\substack{\mathbf{kp}\sigma \\ \mathbf{k}'\mathbf{p}'\sigma_1\sigma_2}} \hat{\mathcal{D}}^{(1/2)}_{\sigma\beta}(\vartheta)\hat{\mathcal{D}}^{(1/2)}_{\sigma_1\sigma_2}(\vartheta) \\ \times T_{\mathbf{kp}} T^{*}_{\mathbf{k}'\mathbf{p}'} \langle \tilde{T}\{c^{\dagger}_{\mathbf{k}\alpha}(\tau) d_{\mathbf{p}\sigma}(\tau) d^{\dagger}_{\mathbf{p}'\sigma_1}(0) c_{\mathbf{k}'\sigma_2}(0)\}\rangle,\end{aligned}$$

$$\tilde{\Phi}_{\mathrm{tp},\alpha\beta}(i\tilde{\omega}_\nu) = -\int_0^\beta d\tau e^{i\tilde{\omega}_\nu\tau} \sum_{\substack{\mathbf{kp}\sigma \\ \mathbf{k'p'}\sigma_1\sigma_2}} \hat{\mathcal{D}}^{(1/2)}_{\sigma\beta}(\vartheta)\hat{\mathcal{D}}^{(1/2)}_{\sigma_1\sigma_2}(\vartheta) \times T_{\mathbf{kp}}T_{\mathbf{k'p'}}\langle\tilde{T}\{c^\dagger_{\mathbf{k}\alpha}(\tau)d_{\mathbf{p}\sigma}(\tau)c^\dagger_{\mathbf{k'}\sigma_2}(0)d_{p'\sigma_1}(0)\}\rangle. \tag{A5}$$

Here, $\tilde{T}$ denotes the time-ordering operator, and $\beta = 1/k_\mathrm{B}T$ is the inverse temperature. Only $\mathbf{k'}=(-)\mathbf{k}, \mathbf{p'}=(-)\mathbf{p}$ contributes in the single-particle (two-particle) channel, while the diagonalized basis $\tilde{\varphi}_{\mathbf{k}\sigma}$ dictates that only $\sigma_2=\alpha$, $\sigma_1=\sigma$ contributes in the spin summation. Making use of the relation $\tilde{\phi}^\dagger_{\mathbf{k}\sigma}=\phi^\dagger_{\mathbf{k}\sigma}\hat{U}_{\mathbf{k}\sigma}$, Eq. (A5) becomes

$$\begin{aligned}\tilde{\Phi}_{\mathrm{sp},\alpha\beta}(i\tilde{\omega}_\nu) = \int_0^\beta d\tau e^{i\tilde{\omega}_\nu\tau}\sum_{\mathbf{kp}\sigma} \hat{\mathcal{D}}^{(1/2)}_{\sigma\beta}(\vartheta)\hat{\mathcal{D}}^{(1/2)}_{\sigma\alpha}(\vartheta)T_{\mathbf{kp}}T^*_{\mathbf{kp}} &\times\langle\tilde{T}\{[\hat{U}^*_{11\mathbf{k}\alpha}\gamma^\dagger_{\mathbf{k}\alpha}(\tau)+\hat{U}^*_{12\mathbf{k}\alpha}\gamma_{-\mathbf{k}\alpha}(\tau)] \\ &\times[\hat{U}_{11\mathbf{k}\alpha}\gamma_{\mathbf{k}\alpha}(0)+\hat{U}_{12\mathbf{k}\alpha}\gamma^\dagger_{-\mathbf{k}\alpha}(0)]\}\rangle \\ &\times\langle\tilde{T}\{[\hat{U}_{11\mathbf{p}\sigma}\gamma_{\mathbf{p}\sigma}(\tau)+\hat{U}_{12\mathbf{p}\sigma}\gamma^\dagger_{-\mathbf{p}\sigma}(\tau)] \\ &\times[\hat{U}^*_{11\mathbf{p}\sigma}\gamma^\dagger_{\mathbf{k}\sigma}(0)+\hat{U}^*_{12\mathbf{p}\sigma}\gamma_{-\mathbf{k}\sigma}(0)]\}\rangle\end{aligned} \tag{A6}$$

$$\begin{aligned}\tilde{\Phi}_{\mathrm{tp},\alpha\beta}(i\tilde{\omega}_\nu) = -\int_0^\beta d\tau e^{i\tilde{\omega}_\nu\tau}\sum_{\mathbf{kp}\sigma} \hat{\mathcal{D}}^{(1/2)}_{\sigma\beta}(\vartheta)\hat{\mathcal{D}}^{(1/2)}_{\sigma\alpha}(\vartheta)T_{\mathbf{kp}}T_{-\mathbf{k},-\mathbf{p}} &\times\langle\tilde{T}\{[\hat{U}^*_{11\mathbf{k}\alpha}\gamma^\dagger_{\mathbf{k}\sigma}(\tau)+\hat{U}^*_{12\mathbf{k}\alpha}\gamma_{-\mathbf{k}\sigma}(\tau)] \\ &\times[\hat{U}_{21\mathbf{k}\alpha}\gamma_{\mathbf{k}\sigma}(0)+\hat{U}_{22\mathbf{k}\alpha}\gamma^\dagger_{-\mathbf{k}\sigma}(0)]\}\rangle \\ &\times\langle\tilde{T}\{[\hat{U}^*_{21\mathbf{p}\sigma}\gamma^\dagger_{\mathbf{p}\sigma}(0)+\hat{U}^*_{22\mathbf{p}\sigma}\gamma_{-\mathbf{p}\sigma}(0)] \\ &\times[\hat{U}_{11\mathbf{p}\sigma}\gamma_{\mathbf{p}\sigma}(\tau)+\hat{U}_{12\mathbf{p}\sigma}\gamma^\dagger_{-\mathbf{p}\sigma}(\tau)]\}\rangle.\end{aligned} \tag{A7}$$

Since our diagonalized Hamiltonian has the form of a free-electron gas, i.e.,

$$H_{\mathrm{FMSC}} = \tilde{H}_0 + \sum_{\mathbf{k}\sigma} E_{\mathbf{k}\sigma}\gamma^\dagger_{\mathbf{k}\sigma}\gamma_{\mathbf{k}\sigma} \tag{A8}$$

with $\tilde{H}_0=H_0-(E_{\mathbf{k}\uparrow}+E_{\mathbf{k}\downarrow})$, the product of the new fermion operators $\tilde{\varphi}_{\mathbf{k}\sigma}$ in Eq. (A6) yield unperturbed Green's functions according to

$$G_\alpha(\mathbf{k},\tau-\tau') = \langle\tilde{T}\{c^\dagger_{\mathbf{p}\alpha}(\tau')c_{\mathbf{k}\alpha}(\tau)\}\rangle. \tag{A9}$$

We then Fourier-transform Eq. (A9) into

$$G_\alpha(\mathbf{k},\tau) = \frac{1}{\beta}\sum_{\omega_m} e^{-i\omega_m\tau}G_\alpha(\mathbf{p},i\omega_m), \tag{A10}$$

where $\omega_m=(2m+1)\pi/\beta$, $m=1,2,3,\ldots$ is a fermionic Matsubara frequency. The frequency summation over m is evaluated by contour integration as in, i.e., Ref. 66 to yield the result

$$\begin{aligned}\frac{1}{\beta}\sum_m G_\alpha(\mathbf{k},i\omega_m)G_\sigma(\mathbf{p},i\tilde{\omega}_\nu+i\omega_m) &= \frac{f(E_{\mathbf{k}\alpha})-f(E_{\mathbf{p}\sigma})}{i\tilde{\omega}_\nu+E_{\mathbf{k}\alpha}-E_{\mathbf{p}\sigma}}, \\ \frac{1}{\beta}\sum_m G_\alpha(\mathbf{k},i\omega_m)G_\sigma(\mathbf{p},i\tilde{\omega}_\nu-i\omega_m) &= \frac{f(E_{\mathbf{p}\sigma})-f(-E_{\mathbf{k}\alpha})}{i\tilde{\omega}_\nu-E_{\mathbf{k}\alpha}-E_{\mathbf{p}\sigma}},\end{aligned} \tag{A11}$$

where $f(E)=1-f(-E)=1/(1+e^{\beta E})$ is the Fermi distribution. It is then a matter of straightforward calculations to obtain the result

$$\begin{aligned}\Phi_{\mathrm{sp},\alpha\beta}(-eV) = \sum_{\mathbf{kp}\sigma}\hat{\mathcal{D}}^{(1/2)}_{\sigma\beta}(\vartheta)\hat{\mathcal{D}}^{(1/2)}_{\sigma\alpha}(\vartheta)T_{\mathbf{kp}}T^*_{\mathbf{kp}}N^2_{\mathbf{k}\alpha}N^2_{\mathbf{p}\sigma} &\times\left[\frac{|\Delta_{\mathbf{k}\alpha\alpha}\Delta_{\mathbf{p}\sigma\sigma}|^2\Lambda^{-1,-1}_{\mathbf{kp}\sigma\alpha}(-eV)}{(\xi_{\mathbf{k}\alpha}+E_{\mathbf{k}\alpha})(\xi_{\mathbf{p}\sigma}+E_{\mathbf{p}\sigma})}+\Lambda^{1,1}_{\mathbf{kp}\sigma\alpha}(-eV)\right. \\ &+\frac{|\Delta_{\mathbf{p}\sigma\sigma}|^2\Lambda^{-1,1}_{\mathbf{kp}\sigma\alpha}(-eV)}{\xi_{\mathbf{p}\sigma}+E_{\mathbf{p}\sigma}} \\ &\left.+\frac{|\Delta_{\mathbf{k}\alpha\alpha}|^2\Lambda^{1,-1}_{\mathbf{kp}\sigma\alpha}(-eV)}{\xi_{\mathbf{k}\alpha}+E_{\mathbf{k}\alpha}}\right],\end{aligned} \tag{A12}$$

$$\begin{aligned}\Phi_{\mathrm{tp},\alpha\beta}(eV) = -\sum_{\mathbf{kp}\sigma}\hat{\mathcal{D}}^{(1/2)}_{\sigma\beta}(\vartheta)\hat{\mathcal{D}}^{(1/2)}_{\sigma\alpha}(\vartheta)T_{\mathbf{kp}}T_{-\mathbf{k},-\mathbf{p}} &\times\frac{\Delta^*_{\mathbf{k}\alpha\alpha}\Delta_{\mathbf{p}\sigma\sigma}}{4E_{\mathbf{k}\alpha}E_{\mathbf{p}\sigma}}\sum_{\substack{\lambda=\pm1 \\ \rho=\pm1}}\Lambda^{\lambda\rho}_{\mathbf{kp}\sigma\alpha}(eV),\end{aligned} \tag{A13}$$

where $\Lambda^{\lambda\rho}_{\mathbf{kp}\sigma\alpha}(eV)$ is obtained by performing analytical continuation $i\tilde{\omega}_\nu\to eV+i0^+$ on

$$\tilde{\Lambda}^{\lambda\rho}_{\mathbf{kp}\sigma\alpha}(i\tilde{\omega}_\nu) = \frac{\lambda[f(E_{\mathbf{k}\alpha})-f(\lambda\rho E_{\mathbf{p}\sigma})]}{i\tilde{\omega}_\nu+\rho E_{\mathbf{k}\alpha}-\lambda E_{\mathbf{p}\sigma}}; \quad \lambda,\rho=\pm1. \tag{A14}$$

We also provide the details of the persistent spin-supercurrent for $\Delta_{\sigma\sigma}=0$. Writing the Josephson current Eq. (32) out explicitly, one has that $I^\mathrm{C}_\mathrm{J}=eI^+$ and $I^\mathrm{S}_\mathrm{J}=-I^-$ where

$$\begin{aligned}I^\pm = \sum_{\mathbf{kp}}|T_{\mathbf{kp}}|^2\Bigg[&\cos^2(\vartheta/2)\frac{|\Delta_{\mathbf{k}\uparrow\uparrow}\Delta_{\mathbf{p}\uparrow\uparrow}|}{E_{\mathbf{k}\uparrow}E_{\mathbf{p}\uparrow}}\sin\Delta\theta_{\uparrow\uparrow}F_{\mathbf{kp}\uparrow\uparrow} \\ &+\sin^2(\vartheta/2)\frac{|\Delta_{\mathbf{k}\uparrow\uparrow}\Delta_{\mathbf{p}\downarrow\downarrow}|}{E_{\mathbf{k}\uparrow}E_{\mathbf{p}\downarrow}}\sin(\theta^\mathrm{L}_{\downarrow\downarrow}-\theta^\mathrm{R}_{\uparrow\uparrow})F_{\mathbf{kp}\uparrow\downarrow} \\ &\pm\sin^2(\vartheta/2)\frac{|\Delta_{\mathbf{k}\downarrow\downarrow}\Delta_{\mathbf{p}\uparrow\uparrow}|}{E_{\mathbf{k}\downarrow}E_{\mathbf{p}\uparrow}}\sin(\theta^\mathrm{L}_{\uparrow\uparrow}-\theta^\mathrm{R}_{\downarrow\downarrow})F_{\mathbf{kp}\downarrow\uparrow} \\ &\pm\cos^2(\vartheta/2)\frac{|\Delta_{\mathbf{k}\downarrow\downarrow}\Delta_{\mathbf{p}\downarrow\downarrow}|}{E_{\mathbf{k}\downarrow}E_{\mathbf{p}\downarrow}}\sin\Delta\theta_{\downarrow\downarrow}F_{\mathbf{kp}\downarrow\downarrow}\Bigg].\end{aligned} \tag{A15}$$

The first and fourth term above vanish when $\Delta\theta_{\sigma\sigma}=0$. By observing that $F_{\mathbf{kp}\uparrow\downarrow}=F_{\mathbf{pk}\downarrow\uparrow}$, we are then able to rewrite Eq. (A15) as

$$I^{\pm} = \sum_{\mathbf{kp}} |T_{\mathbf{kp}}|^2 \sin^2(\vartheta/2) \frac{|\Delta_{\mathbf{k}\uparrow}\Delta_{\mathbf{p}\downarrow}|}{E_{\mathbf{k}\uparrow}E_{\mathbf{p}\downarrow}} F_{\mathbf{kp}\uparrow\downarrow} \times [\sin(\theta_{\downarrow}^{\mathrm{L}} - \theta_{\uparrow}^{\mathrm{R}}) \pm \sin(\theta_{\uparrow}^{\mathrm{L}} - \theta_{\downarrow}^{\mathrm{R}})]$$

$$= e\sum_{\mathbf{kp}} |T_{\mathbf{kp}}|^2 \sin^2(\vartheta/2) \frac{|\Delta_{\mathbf{k}\uparrow}\Delta_{\mathbf{p}\downarrow}|}{E_{\mathbf{k}\uparrow}E_{\mathbf{p}\downarrow}} F_{\mathbf{kp}\uparrow\downarrow} \times [\sin((\theta_{\downarrow}^{\mathrm{L}} \mp \theta_{\downarrow}^{\mathrm{R}} - \theta_{\uparrow}^{\mathrm{R}} \pm \theta_{\uparrow}^{\mathrm{L}})/2) \times \cos((\theta_{\downarrow}^{\mathrm{L}} \pm \theta_{\downarrow}^{\mathrm{R}} - \theta_{\uparrow}^{\mathrm{R}} \mp \theta_{\uparrow}^{\mathrm{L}})/2)]. \quad \text{(A16)}$$

It is clear that the argument of the sine gives 0 for the upper sign, such that $I_{\mathrm{J}}^{\mathrm{C}}=0$. But for the lower sign, the argument of the cosine is equal to 0, such that Eq. (37) is obtained.

2. Ferromagnets with spin-orbit coupling

The spin-current across the junction can be written as

$$\mathbf{I}^{\mathrm{S}} = \mathrm{Im}\{\mathbf{\Phi}(-eV)\},$$

$$\mathbf{\Phi}(-eV) = \lim_{i\tilde{\omega}_\nu \to -eV + i0^+} \tilde{\mathbf{\Phi}}(i\tilde{\omega}_\nu), \quad \text{(A17)}$$

where we have defined the Matsubara function

$$\tilde{\mathbf{\Phi}}(i\tilde{\omega}_\nu) = \sum_{\mathbf{kp}\alpha\beta\sigma} |T_{\mathbf{kp}}|^2 \hat{\boldsymbol{\sigma}}_{\alpha\beta} \int_0^\beta d\tau e^{i\tilde{\omega}_\nu \tau} \times \langle T\{c_{\mathbf{k}\sigma}(0) c_{\mathbf{k}\alpha}^\dagger(\tau)\}\rangle \langle T\{d_{\mathbf{p}\beta}(\tau) d_{\mathbf{p}\sigma}^\dagger(0)\}\rangle. \quad \text{(A18)}$$

In Eq. (A18), we defined the time-ordering operator T while β in the upper integration limit is inverse temperature and $\tilde{\omega}_\nu = 2n\pi/\beta$, $n=0,1,2,\ldots$ is a bosonic Matsubara frequency. From the definition of the spin-generalized Green's function

$$G_{\mathbf{k}}^{\alpha\beta}(\tau - \tau') = -\langle T\{c_{\mathbf{k}\alpha}(\tau) c_{\mathbf{k}\beta}^\dagger(\tau')\}\rangle, \quad \text{(A19)}$$

Eq. (A18) can be written out explicitly to yield

$$\tilde{\mathbf{\Phi}}(i\tilde{\omega}_\nu) = \frac{1}{\beta}\sum_{\mathbf{kp},m} |T_{\mathbf{kp}}|^2 [\hat{\boldsymbol{\sigma}}_{\uparrow\uparrow}(G_{\mathbf{k}}^{\uparrow\uparrow}(i\omega_m) G_{\mathbf{p}}^{\uparrow\uparrow}(i\omega_m - i\tilde{\omega}_\nu) + G_{\mathbf{k}}^{\downarrow\uparrow}(i\omega_m) G_{\mathbf{p}}^{\uparrow\downarrow}(i\omega_m - i\tilde{\omega}_\nu)) + \hat{\boldsymbol{\sigma}}_{\uparrow\downarrow}(G_{\mathbf{k}}^{\uparrow\uparrow}(i\omega_m) \times G_{\mathbf{p}}^{\downarrow\uparrow}(i\omega_m - i\tilde{\omega}_\nu) + G_{\mathbf{k}}^{\downarrow\uparrow}(i\omega_m) G_{\mathbf{p}}^{\downarrow\downarrow}(i\omega_m - i\tilde{\omega}_\nu)) + \hat{\boldsymbol{\sigma}}_{\downarrow\uparrow}(G_{\mathbf{k}}^{\uparrow\downarrow}(i\omega_m) G_{\mathbf{p}}^{\uparrow\uparrow}(i\omega_m - i\tilde{\omega}_\nu) + G_{\mathbf{k}}^{\downarrow\downarrow}(i\omega_m) G_{\mathbf{p}}^{\uparrow\downarrow}(i\omega_m - i\tilde{\omega}_\nu)) + \hat{\boldsymbol{\sigma}}_{\downarrow\downarrow}(G_{\mathbf{k}}^{\uparrow\downarrow}(i\omega_m) G_{\mathbf{p}}^{\downarrow\uparrow}(i\omega_m - i\tilde{\omega}_\nu) + G_{\mathbf{k}}^{\downarrow\downarrow}(i\omega_m) G_{\mathbf{p}}^{\downarrow\downarrow}(i\omega_m - i\tilde{\omega}_\nu))]. \quad \text{(A20)}$$

We made use of the Fourier-transformations

$$G_{\mathbf{k}}^{\alpha\beta}(i\omega_m) = \int_0^\beta d\tau e^{i\omega_m} G_{\mathbf{k}}^{\alpha\beta}(\tau),$$

$$G_{\mathbf{k}}^{\alpha\beta}(\tau) = \frac{1}{\beta}\sum_m e^{-i\omega_m \tau} G_{\mathbf{k}}^{\alpha\beta}(i\omega_m) \quad \text{(A21)}$$

in writing down Eq. (A20), where $\omega_m = 2(m+1)\pi/\beta$, $m=0,1,2,\ldots$ is a fermionic Matsubara frequency. Having written down the full expression for the Matsubara function in Eq. (A20), one can now easily distinguish between components of the spin-current. For instance, only $\hat{\boldsymbol{\sigma}}_{\alpha\alpha}$ will contribute to the $\hat{\mathbf{z}}$-component of $\mathbf{I}^{\mathrm{S}}$, and the corresponding terms can be read out from Eq. (A20). From the present Green functions in Eq. (50), it is obvious that three types of frequency summations must be performed, namely

$$J_{\mathbf{kp},r} = \frac{1}{\beta}\sum_m \left[\frac{\omega_m^r}{[(\varepsilon_{\mathbf{k}\uparrow} - i\omega_m)(\varepsilon_{\mathbf{k}\downarrow} - i\omega_m) - y_{\mathbf{k}}^2]} \times \frac{1}{[(\varepsilon_{\mathbf{p}\uparrow} - i\omega_m + i\tilde{\omega}_\nu)(\varepsilon_{\mathbf{p}\downarrow} - i\omega_m + i\tilde{\omega}_\nu) - y_{\mathbf{p}}^2]} \right], \quad \text{(A22)}$$

with r an integer. Performing the summation over m using residue calculus, one finds that

$$J_{\mathbf{kp},r} = \sum_{\substack{\alpha=\pm \\ \beta=\pm}} \frac{\alpha\beta}{4 y_{\mathbf{k}} y_{\mathbf{p}}} \left[\frac{\psi_{\mathbf{k}\alpha}^r n(\psi_{\mathbf{k}\alpha}) - (i\tilde{\omega}_\nu + \psi_{\mathbf{p}\beta})^r n(\psi_{\mathbf{p}\beta})}{-i\tilde{\omega}_\nu + \psi_{\mathbf{k}\alpha} - \psi_{\mathbf{p}\beta}} \right] \quad \text{(A23)}$$

with the definition $\psi_{\mathbf{k}\alpha} \equiv \varepsilon_{\mathbf{k}} + \alpha y_{\mathbf{k}}$. Separating the general expression Eq. (A20) into its spatial components $\tilde{\mathbf{\Phi}} = (\tilde{\Phi}_x, \tilde{\Phi}_y, \tilde{\Phi}_z)$, the components of the spin-current can be extracted according to $I_i^{\mathrm{S}} = \mathrm{Im}\{\Phi_i(-eV)\}$, $i=x,y,z$. Note that the charge-current in this model, which vanishes for $eV=0$, is obtained by the performing the replacement $\hat{\boldsymbol{\sigma}}_{\alpha\beta} \to \hat{1}_{\alpha\beta}$, where $\hat{1}$ is the 2×2 unit matrix. We find that

$$\tilde{\Phi}_x(i\tilde{\omega}_\nu) = \sum_{\mathbf{kp}} \frac{|T_{\mathbf{kp}}|^2}{4\gamma_{\mathbf{k}}\gamma_{\mathbf{p}}} [J_{\mathbf{kp},0}(\varepsilon_{\mathbf{k}\downarrow}(\zeta_{\mathrm{L}} - B_{\mathbf{p},-}) + (\varepsilon_{\mathbf{p}\uparrow} + i\tilde{\omega}_\nu) \times (\zeta_{\mathrm{R}} - B_{\mathbf{k},-}) + (\varepsilon_{\mathbf{p}\downarrow} + i\tilde{\omega}_\nu)(\zeta_{\mathrm{R}}^\dagger - B_{\mathbf{k},+}) + \varepsilon_{\mathbf{k}\uparrow} \times (\zeta_{\mathrm{L}}^\dagger - B_{\mathbf{p},-})) - J_{\mathbf{kp},1}((\zeta_{\mathrm{L}} - B_{\mathbf{p},-}) + (\zeta_{\mathrm{R}} - B_{\mathbf{k},-}) + (\zeta_{\mathrm{R}}^\dagger - B_{\mathbf{k},+}) + (\zeta_{\mathrm{L}}^\dagger - B_{\mathbf{p},+}))],$$

$$\tilde{\Phi}_y(i\tilde{\omega}_\nu) = \sum_{\mathbf{kp}} i\frac{|T_{\mathbf{kp}}|^2}{4\gamma_{\mathbf{k}}\gamma_{\mathbf{p}}} [J_{\mathbf{kp},0}(-\varepsilon_{\mathbf{k}\downarrow}(\zeta_{\mathrm{L}} - B_{\mathbf{p},-}) - (\varepsilon_{\mathbf{p}\uparrow} + i\tilde{\omega}_\nu) \times (\zeta_{\mathrm{R}} - B_{\mathbf{k},-}) + (\varepsilon_{\mathbf{p}\downarrow} + i\tilde{\omega}_\nu)(\zeta_{\mathrm{R}}^\dagger - B_{\mathbf{k},+}) + \varepsilon_{\mathbf{k}\uparrow} \times (\zeta_{\mathrm{L}}^\dagger - B_{\mathbf{p},-})) - J_{\mathbf{kp},1}(-(\zeta_{\mathrm{L}} - B_{\mathbf{p},-}) - (\zeta_{\mathrm{R}} - B_{\mathbf{k},-}) + (\zeta_{\mathrm{R}}^\dagger - B_{\mathbf{k},+}) + (\zeta_{\mathrm{L}}^\dagger - B_{\mathbf{p},+}))],$$

$$\tilde{\Phi}_z(i\tilde{\omega}_\nu) = \sum_{\mathbf{kp}} \frac{|T_{\mathbf{kp}}|^2}{4\gamma_{\mathbf{k}}\gamma_{\mathbf{p}}} [J_{\mathbf{kp},0}(\varepsilon_{\mathbf{k}\downarrow}(\varepsilon_{\mathbf{p}\downarrow} + i\tilde{\omega}_\nu) - \varepsilon_{\mathbf{k}\uparrow}(\varepsilon_{\mathbf{p}\uparrow} + i\tilde{\omega}_\nu) + (\zeta_{\mathrm{R}} - B_{\mathbf{k},-})(\zeta_{\mathrm{L}}^\dagger - B_{\mathbf{p},+}) - (\zeta_{\mathrm{R}}^\dagger - B_{\mathbf{k},+})(\zeta_{\mathrm{L}} - B_{\mathbf{p},-})) + J_{\mathbf{kp},1}(\varepsilon_{\mathbf{k}\uparrow} - \varepsilon_{\mathbf{k}\downarrow} + \varepsilon_{\mathbf{p}\uparrow} - \varepsilon_{\mathbf{p}\downarrow})]. \quad \text{(A24)}$$

[1] I. Zutic, J. Fabian, and S. D. Sarma, Rev. Mod. Phys. **76**, 323 (2004).
[2] M. I. D'yakonov and V. I. Perel, Phys. Lett. A **35**, 459 (1971).
[3] J. Wunderlich, B. Kaestner, J. Sinova, and T. Jungwirth, Phys. Rev. Lett. **94**, 047204 (2005).
[4] J. Tallon, C. Bernhard, M. Bowden, P. Gilberd, T. Stoto, and D. Pringle, IEEE Trans. Appl. Supercond. **9**, 1696 (1999).
[5] S. S. Saxena, P. Agarwal, K. Ahilan, F. M. Grosche, R. K. W. Haselwimmer, M. J. Steiner, E. Pugh, I. R. Walker, S. R. Julian, and P. Monthoux, Nature (London) **406**, 587 (2000).
[6] D. Aoki, A. Huxley, E. Ressouche, D. Braihwaite, J. Flouquet, J.-P. Brison, E. Lhotel, and C. Paulsen, Nature (London) **413**, 613 (2001).
[7] V. L. Ginzburg, Sov. Phys. JETP **4**, 153 (1957).
[8] R. Shen, Z. M. Zheng, S. Liu, and D. Y. Xing, Phys. Rev. B **67**, 024514 (2003).
[9] P. Fulde and R. A. Ferrel, Phys. Rev. **135**, A550 (1964); A. I. Larkin and Y. N. Ovchinnikov, Zh. Eksp. Teor. Fiz. **47**, 1136 (1964) [Sov. Phys. JETP **20**, 762 (1965)].
[10] M. B. Walker and K. V. Samokhin, Phys. Rev. Lett. **88**, 207001 (2002).
[11] K. Machida and T. Ohmi, Phys. Rev. Lett. **86**, 850 (2001).
[12] K. Ishida, H. Mukuda, Y. Kitaoka, K. Asayama, Z. Q. Mao, Y. Mori, and Y. Maeno, Nature (London) **396**, 658 (1998).
[13] K. D. Nelson, Z. Q. Mao, Y. Maeno, and Y. Liu, Science **306**, 1151 (2004).
[14] A. Brataas and Y. Tserkovnyak, Phys. Rev. Lett. **93**, 087201 (2004).
[15] Y. Tanaka and S. Kashiwaya, Phys. Rev. B **70**, 012507 (2004).
[16] T. Koyama and M. Tachiki, Phys. Rev. B **30**, 6463 (1984).
[17] M. S. Grønsleth, J. Linder, J.-M. Børven, and A. Sudbø, Phys. Rev. Lett. **97**, 147002 (2006).
[18] D. V. Shopova and D. I. Uzunov, Phys. Rev. B **72**, 024531 (2005).
[19] M. L. Kulic, C. R. Phys. **7**, 4 (2006); M. L. Kulic and I. M. Kulic, Phys. Rev. B **63**, 104503 (2001).
[20] I. Eremin, F. S. Nogueira, and R.-J. Tarento, Phys. Rev. B **73**, 054507 (2006).
[21] T. Dietl, Semicond. Sci. Technol. **17**, 377 (2002).
[22] F. Matsukura, H. Ohno, and T. Dietl, *Handbook of Magnetic Materials*, Vol. 14 (Elsevier, New York, 2002).
[23] H.-A. Engel, E. I. Rashba, and B. I. Halperin, in *Handbook of Magnetism and Advanced Magnetic Materials*, Vol. 5 (Wiley, New York, 2006).
[24] F. S. Nogueira and K.-H. Bennemann, Europhys. Lett. **67**, 620 (2004).
[25] Y.-L. Lee and Y.-W. Lee, Phys. Rev. B **68**, 184413 (2003).
[26] J. C. Slonczewski, Phys. Rev. B **39**, 6995 (1989).
[27] T. Yokoyama, Y. Tanaka, and J. Inoue, Phys. Rev. B **72**, 220504(R) (2005).
[28] J. Wang and K. S. Chan, cond-mat/0512430 (to be published).
[29] S. I. Kiselev, J. C. Sankey, I. N. Krivorotov, N. C. Emley, R. J. Schoelkopf, R. A. Buhrman, and D. C. Ralph, Nature (London) **425**, 380 (2003).
[30] G. E. W. Bauer, A. Brataas, Y. Tserkovnyak, and B. J. van Wees, Appl. Phys. Lett. **82**, 3928 (2003).
[31] A. Brataas, Y. Tserkovnyak, G. E. W. Bauer, and B. I. Halperin, Phys. Rev. B **66**, 060404(R) (2002).
[32] J. E. Hirsch, Phys. Rev. Lett. **83**, 1834 (1999).
[33] Y. Tserkovnyak, A. Brataas, and G. E. W. Bauer, Phys. Rev. Lett. **88**, 117601 (2002).
[34] S. Tewari, D. Belitz, T. R. Kirkpatrick, and J. Toner, Phys. Rev. Lett. **93**, 177002 (2004).
[35] V. P. Mineev, cond-mat/0507572 (to be published).
[36] V. P. Mineev and K. V. Samokhin, *Introduction to Unconventional Superconductivity* (Gordon and Breach, New York, 1999).
[37] H. Kotegawa, A. Harada, S. Kawasaki, Y. Kawasaki, Y. Kitaoka, Y. Haga, E. Yamamoto, Y. Onuki, K. M. Itoh, and E. E. Haller, J. Phys. Soc. Jpn. **74**, 705 (2005).
[38] C. Bernhard, J. L. Tallon, E. Brucher, and R. K. Kremer, Phys. Rev. B **61**, R14960 (2000).
[39] C.-R. Hu, Phys. Rev. Lett. **72**, 1526 (1994).
[40] V. Ambegaokar, P. G. deGennes, and D. Rainer, Phys. Rev. A **9**, 2676 (1974).
[41] L. J. Buchholtz and G. Zwicknagl, Phys. Rev. B **23**, 5788 (1981).
[42] Y. Tanuma, Y. Tanaka, and S. Kashiwaya, Phys. Rev. B **64**, 214519 (2001).
[43] S. Datta and B. Das, Appl. Phys. Lett. **56**, 665 (1990).
[44] A. J. Leggett, Rev. Mod. Phys. **47**, 331 (1975).
[45] F. Hardy and A. D. Huxley, Phys. Rev. Lett. **94**, 247006 (2005).
[46] K. V. Samokhin and M. B. Walker, Phys. Rev. B **66**, 174501 (2002).
[47] M. H. Cohen, L. M. Falicov, and J. C. Phillips, Phys. Rev. Lett. **8**, 316 (1962).
[48] H. P. Dahal, J. Jackiewicz, and K. S. Bedell, Phys. Rev. B **72**, 172506 (2005).
[49] E. P. Wigner, *Gruppentheorie und ihre Anwendung auf die Quantenmechanik der Atomspektren* (Frieder. Vieweg, Braunschweig, 1931).
[50] J. Shi and Q. Niu, cond-mat/0601531 (to be published).
[51] C. Bruder, A. van Otterlo, and G. T. Zimanyi, Phys. Rev. B **51**, 12904 (1995).
[52] H. Ohno, H. Munekata, T. Penney, S. von Molnar, and L. L. Chang, Phys. Rev. Lett. **68**, 2664 (1992).
[53] F. Matsukura, H. Ohno, A. Shen, and Y. Sugawara, Phys. Rev. B **57**, R2037 (1998).
[54] J. Kikkawa and D. Awschalom, Nature (London) **397**, 139 (1999).
[55] T. Jungwirth, Q. Niu, and A. H. MacDonald, Phys. Rev. Lett. **88**, 207208 (2002).
[56] K. Børkje and A. Sudbø, Phys. Rev. B **74**, 054506 (2006).
[57] G. Dresselhaus, Phys. Rev. **100**, 580 (1955).
[58] A. G. Mal'shukov, C. S. Tang, C. S. Chu, and K. A. Chao, Phys. Rev. Lett. **95**, 107203 (2005).
[59] R. S. Keizer, S. T. B. Goennenwein, T. M. Klapwijk, G. Miao, G. Xiao, and A. Gupta, Nature (London) **439**, 825 (2006).
[60] M. E. Simon and C. M. Varma, Phys. Rev. Lett. **89**, 247003 (2002).
[61] J. Bass and W. P. Pratt, Jr., J. Magn. Magn. Mater. **200**, 274 (1999).
[62] P. Mohanty, G. Zolfagharkhani, S. Kettemann, and P. Fulde, Phys. Rev. B **70**, 195301 (2004).
[63] Q. Feng Sun, H. Guo, and J. Wang, Phys. Rev. B **69**, 054409 (2004).
[64] F. Meier and D. Loss, Phys. Rev. Lett. **90**, 167204 (2003).
[65] F. Schutz, M. Kollar, and P. Kopietz, Phys. Rev. Lett. **91**, 017205 (2003).
[66] G. D. Mahan, *Many-Particle Physics* 3rd ed. (Kluwer Academic/Plenum Publishers, Dordrecht, 2002).

[67] Note that $N_{\alpha\beta}$ reduces to the number operator when we sum over equal spins, i.e., $N=\Sigma_\sigma N_{\sigma\sigma}$.

[68] For corresponding results in spin-singlet superconductors with helimagnetic order, see Refs. 19 and 20.

[69] Note that the index α on the quasiparticles does not denote the physical spin of electrons, but is rather to be considered as some unspecified helicity index. The usage of the word "spin" in this context then refers to this helicity.

Paper III

Conductance spectra of ferromagnetic superconductors: Quantum transport in a ferromagnetic metal/non-unitary ferromagnetic superconductor junction.

Physical Review B **75**, 054518 (2007).

PHYSICAL REVIEW B **75**, 054518 (2007)

Conductance spectra of ferromagnetic superconductors: Quantum transport in a ferromagnetic metal/non-unitary ferromagnetic superconductor junction

J. Linder and M. S. Grønsleth
Department of Physics, Norwegian University of Science and Technology, N-7491 Trondheim, Norway

A. Sudbø
Department of Physics, Norwegian University of Science and Technology, N-7491 Trondheim, Norway and Center for Advanced Study, Norwegian Academy of Science and Letters, Drammensveien 78, N-0271 Oslo, Norway

(Received 3 November 2006; revised manuscript received 3 January 2007; published 21 February 2007)

Recent findings of superconductors that simultaneously exhibit multiple spontaneously broken symmetries, such as ferromagnetic order or lack of an inversion center and even combinations of such broken symmetries, have led to much theoretical and experimental research. We consider quantum transport in a junction consisting of a ferromagnetic metal and a non-unitary ferromagnetic superconductor. It is shown that the conductance spectra provide detailed information about the superconducting gaps, and are thus helpful in determining the pairing symmetry of the Cooper pairs in ferromagnetic superconductors.

DOI: 10.1103/PhysRevB.75.054518 PACS number(s): 74.20.Rp, 74.50.+r

I. INTRODUCTION

Spontaneous symmetry breaking in condensed-matter systems ranks among the most profound emergent phenomena in many-body physics. Multiple spontaneously broken symmetries are not only of interest in terms of studying properties of specific condensed-matter systems but are also due to the fact that it may provide clues for what could be expected in other systems in vastly different areas of physics. An attempt[1] at describing the physics of magnetic spin-singlet superconductors was made long ago, and the discovery of ferromagnetic superconductors (FMSCs),[2,3] displaying coexisting superconductivity (SC) and ferromagnetism (FM) well below the Curie temperature, has produced a realization of a physically rich system that exhibits simultaneously broken SU(2) and U(1) symmetries. Spontaneous breaking of symmetry is responsible for a wide range of physical phenomena, such as the mass differences of elementary particles, phase transitions in condensed-matter systems, and even emergent phenomena in biology.[4] In many cases, the phenomena can, in fact, be described by the same equations. Thus, a study of ferromagnetic superconductors is of interest not only in terms of having an obvious potential for leading to a different set of devices in, for instance, nanotechnology and spintronics but also from a fundamental physics point of view.

A successful model describing an FMSC demands that two important issues be addressed: (i) the symmetry of the pairing state and (ii) whether the superconducting and ferromagnetic order parameters are coexistent or phase separated in space-time. Cooper pairs in conventional superconductors (*s* wave) are spin singlets. Thus, *s*-wave pairing and uniform FM are antagonists.[5,6] Spin-triplet Cooper pairs, however, can carry a net magnetic moment. Such Cooper pairs are presently the prime candidate for explaining the coexistence of FM and SC in, e.g., UGe_2 and URhGe.[2,3] In these materials, SC occurs deep within the ferromagnetic phase. It is therefore natural to view the SC pairing as originating with electrons that also contribute to FM. Thus, the electrons responsible for FM below the Curie temperature T_M condense into Cooper pairs with magnetic moments aligned along the magnetization below the critical temperature T_c. While spin-singlet superconductivity coexisting with uniform ferromagnetism appears to be unlikely, it could coexist with helically ordered magnets. Tunneling phenomena in such systems have indeed been considered theoretically.[7,8] This is, however, physically quite different from the case we will present in this paper.

Bulk FMSCs are expected to display an unusual feature, namely, the spontaneous formation of an Abrikosov vortex lattice.[9] Uniform superconducting phases have also been investigated,[10] but in a bulk system it seems reasonable to assume that this must be associated with a nonuniform magnetic state.[7,8] A key variable determining whether a vortex lattice appears or not seems to be the strength of the internal magnetization $\mathbf{m}$.[11] The current experimental data[3] available for URhGe apparently do not settle this issue unambiguously, while uniform coexistence of FM and SC appears to have been experimentally verified[12] in UGe_2. Moreover, a bulk Meissner state in the FMSC $RuSr_2GdCu_2O_8$ has been reported.[13] No consensus has so far been reached concerning the correct pairing symmetry for the FMSCs, although theoretical considerations strongly suggest that a non-unitary state is favored.[14–16] In terms of the $\mathbf{d_k}$-vector formalism (see below), this means that the relation $i(\mathbf{d_k} \times \mathbf{d_k^*}) \neq 0$ is satisfied, which is equivalent to saying that the Cooper pairs carry a net spin.[17] The study of pairing symmetries in unconventional superconductors has a long tradition[18] where tunneling currents have played a crucial role. For the case of spin-triplet nonmagnetic superconductors, theoretical studies of tunneling to a normal metal or ferromagnet have been suggestive in terms of establishing the correct pairing symmetry for the superconductor.[19,20]

In this paper, we consider quantum transport between two thin films of a non-unitary FMSC and an easy-axis ferromagnet, respectively. We demonstrate how the resulting conductance spectra can be exploited to obtain useful information about the superconducting gaps. The SC and FM order pa-

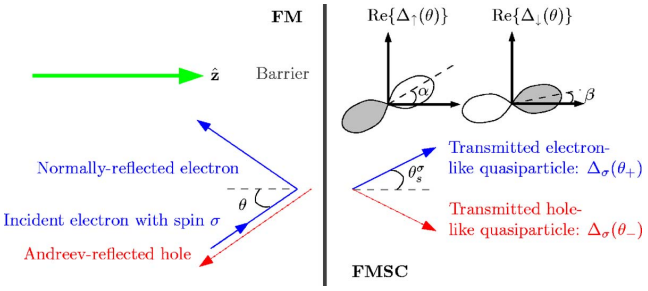

FIG. 1. (Color online) Model system of an FM-FMSC interface in a slab geometry in the clean limit. Retroreflection symmetry is not broken since the hole carries the same spin as the incident electron. We have sketched gaps corresponding to the analog (Ref. 17) of the $A2$ phase in liquid ^{3}He.

rameters are assumed not to be phase separated. Moreover, the choice of a thin-film FMSC is motivated by the fact that the pair-breaking orbital effect on Cooper pairs with an in-plane magnetization is suppressed, and that one will avoid vortices present in the compound if the thickness t of the film is smaller than the diameter of a vortex,[21] $t<\xi_0\ll\lambda_0$. Here, ξ_0 is the coherence length (typical size of Cooper pairs), while λ_0 is the penetration depth (typical radius of vortex). In the cases[2,3] of UGe_2 and URhGe, this amounts to $t\sim 10$ nm, which is well within reach of current experimental techniques.

This paper is organized as follows. In Sec. II, we establish the model and formalism which we will apply to the problem. Results are given in Sec. III, in addition to a discussion of our findings. Concluding remarks are given in Sec. IV.

II. MODEL AND FORMULATION

Our model is illustrated in Fig. 1, where the superconducting pairing symmetry is equivalent to that of an $A2$ phase in ^{3}He [see Ref. 17 and the discussion below Eq. (1)].

The Bogoliubov-de Gennes (BdG) equations for a FMSC (Ref. 22) may be written in a compact matrix form as

$$\begin{pmatrix} \hat{\mathcal{M}}_{\mathbf{k}} & \hat{\Delta}_{\mathbf{k}} \\ \hat{\Delta}_{\mathbf{k}}^* & -\hat{\mathcal{M}}_{\mathbf{k}} \end{pmatrix} \begin{pmatrix} u_{\mathbf{k}\sigma} \\ v_{\mathbf{k}\sigma} \end{pmatrix} = E_{\mathbf{k}\sigma} \begin{pmatrix} u_{\mathbf{k}\sigma} \\ v_{\mathbf{k}\sigma} \end{pmatrix}, \tag{1}$$

where we have introduced the 2×2 matrices

$$\hat{\mathcal{M}}_{\mathbf{k}} = \varepsilon_{\mathbf{k}}\hat{1} - \hat{\sigma}_z U_{R(L)},$$

$$\hat{\Delta}_{\mathbf{k}} = (\Delta_0\hat{1} + \hat{\boldsymbol{\sigma}}\cdot\mathbf{d}_{\mathbf{k}})i\hat{\sigma}_y, \tag{2}$$

in addition to the vectors

$$u_{\mathbf{k}\sigma} = [u_{\mathbf{k}\uparrow\sigma},\ u_{\mathbf{k}\downarrow\sigma}]^{\mathrm{T}},$$

$$v_{\mathbf{k}\sigma} = [v_{\mathbf{k}\uparrow\sigma},\ v_{\mathbf{k}\downarrow\sigma}]^{\mathrm{T}}. \tag{3}$$

Here, $\varepsilon_{\mathbf{k}}$ is a kinetic energy term, $\hat{\boldsymbol{\sigma}}=(\hat{\sigma}_x,\hat{\sigma}_y,\hat{\sigma}_z)$ is a vector containing the Pauli matrices, and $U_{R(L)}$ describes the magnetic exchange energy of right (left) part of the system. Moreover, the $\mathbf{d}_{\mathbf{k}}$ vectors are given by

$$\mathbf{d}_{\mathbf{k}} = \frac{1}{2}[\Delta_{\mathbf{k}\downarrow\downarrow} - \Delta_{\mathbf{k}\uparrow\uparrow}, -i(\Delta_{\mathbf{k}\downarrow\downarrow} + \Delta_{\mathbf{k}\uparrow\uparrow}), 2\Delta_{\mathbf{k}\uparrow\downarrow}], \tag{4}$$

and Δ_0 and $\Delta_{\mathbf{k}\alpha\beta}$ are the superconducting spin-singlet and spin-triplet order parameters, respectively. Finally, $u_{\mathbf{k}\sigma}$ and $v_{\mathbf{k}\sigma}$ are the wave-function solutions with eigenvalue $E_{\mathbf{k}\sigma}$. In the following, we set the $\mathbf{k}$-independent singlet amplitude Δ_0 to zero, as we do not consider the case of coexistent s-wave SC and FM.[16] Also, the opposite-spin triplet pairing giving rise to the gap $\Delta_{\mathbf{k}\uparrow\downarrow}$ is, in general, believed to be suppressed, since it requires interband pairing of Zeeman-split electrons.[3] Hence, our model is that of a non-unitary spin-triplet state with equal-spin pairing, i.e., $\Delta_{\mathbf{k}\uparrow\downarrow}=0$ and $\Delta_{\mathbf{k}\sigma\sigma}\neq 0$, equivalent to the $A2$ phase in liquid ^{3}He (see, e.g., Ref. 17) with a nonvanishing magnetic moment associated with the Cooper pairs.

As indicated in Fig. 1, the reflected and transmitted electronlike and holelike excitations feel different pairing potentials due to the orbital symmetry of the superconducting gaps. The angle into which they are scattered depends on the spin σ of the incident electron, since there is a magnetic exchange energy U_R present in the superconducting state. In the following, we will consider the momentum of the quasiparticles as fixed on the Fermi surface for spin σ so that the superconducting gaps correspondingly only depend on the direction of momentum, i.e., $\Delta_{\mathbf{k}\sigma\sigma}\to\Delta_\sigma(\theta_s^\sigma)$, where θ_s^σ is defined in Fig. 1. Throughout this paper, we shall insert the superconducting gap *a priori* instead of solving it self-consistently in order to obtain analytical formulas. This is justified by the fact that detailed calculations taking into account the modification of the pair potential near the barrier demonstrate that no new qualitative features appear in the conductance spectra compared to the case when the gap is modeled by a step function at the interface.[23] However, the proximity effect at a FM/SC interface may cause two important phenomena to occur: (i) induction of a SC order parameter (possible mixture of singlet and triplet) in the FM region[24] and (ii) the formation of midgap surface states on the interface,[25] leading to a suppression of the order parameter in the vicinity of the interface. The competition and coexistence of these two phenomena have been studied in Ref. 26. In this work, we will mainly be concerned with a SC pairing symmetry analogous to the $A2$ phase in liquid ^{3}He, for which the latter of these effects is only present for a specific trajectory of the incoming electrons. Thus, we believe that our results capture the essential qualitative features of the conductance spectra, although a self-consistent approach would be required in order to obtain the entire picture.

For the simplest model that illustrates the physics, we have chosen a two-dimensional FM-FMSC junction with a barrier modeled by the potential $V(\mathbf{r})=V_0\delta(z)$ and supercon-

ducting gaps $\Delta_\sigma(\theta_s^\sigma,\mathbf{r})=\Delta_\sigma(\theta_s^\sigma)\Theta(z)$. Here, $\delta(z)$ and $\Theta(z)$ represent the Kronecker delta and Heaviside functions, respectively. Solving the BdG equations and applying the Blonder-Tinkham-Klapwijk formalism,[27] which has proven to yield good consistency with experimental findings,[28] one finds that our system in Fig. 1 is described by the wave functions for particles and holes with spin σ in the ferromagnet (ψ^σ) and FMSC (Ψ^σ) sides of the barrier. Explicitly, the total wave function

$$\Psi^\sigma_{\mathrm{tot}}(z)=\Theta(-z)\psi^\sigma(z)+\Theta(z)\Psi^\sigma(z) \tag{5}$$

then has the components

$$\psi^\sigma(z)=e^{ik^\sigma \sin\theta y}\left[\begin{pmatrix}1\\0\end{pmatrix}e^{ik^\sigma\cos\theta z}+r_e^\sigma(E,\theta)\begin{pmatrix}1\\0\end{pmatrix}e^{-ik^\sigma\cos\theta z}+r_h^\sigma(E,\theta)\begin{pmatrix}0\\1\end{pmatrix}e^{ik^\sigma\cos\theta z}\right],$$

$$\Psi^\sigma(z)=e^{iq^\sigma\sin\theta y}\left[t_e^\sigma(E,\theta)\begin{pmatrix}u_\sigma(\theta_{s+}^\sigma)\\ v_\sigma(\theta_{s+}^\sigma)\gamma_\sigma^*(\theta_{s+}^\sigma)\end{pmatrix}e^{iq^\sigma\cos\theta_s^\sigma z}+t_h^\sigma(E,\theta)\begin{pmatrix}v_\sigma(\theta_{s-}^\sigma)\gamma_\sigma(\theta_{s-}^\sigma)\\ u_\sigma(\theta_{s-}^\sigma)\end{pmatrix}e^{-iq^\sigma\cos\theta_s^\sigma z}\right], \tag{6}$$

where $\gamma_\sigma(\theta)=\Delta_\sigma(\theta)/|\Delta_\sigma(\theta)|$ and $\theta_{s+}^\sigma=\theta_s^\sigma$, $\theta_{s-}^\sigma=\pi-\theta_s^\sigma$. The wave vectors read

$$k^\sigma=[2m(E_F+\sigma U_L)]^{1/2},$$

$$q^\sigma=[2m(E_F+\sigma U_R)]^{1/2}, \tag{7}$$

while the spin-generalized coherence factors are

$$u_\sigma(\theta_{s\pm}^\sigma)=\frac{1}{4}\{1+\sqrt{1-(|\Delta_\sigma(\theta_{s\pm}^\sigma)|/E)^2}\}^{1/2},$$

$$v_\sigma(\theta_{s\pm}^\sigma)=\frac{1}{4}\{1-\sqrt{1-(|\Delta_\sigma(\theta_{s\pm}^\sigma)|/E)^2}\}^{1/2}. \tag{8}$$

In writing down Eq. (6), we have implicitly incorporated conservation of group velocity and conservation of momentum parallel to the barrier, i.e., $k^\sigma\sin\theta=q^\sigma\sin\theta_s^\sigma$. As seen from the expressions of the wave vectors above, we have taken the effective mass m and Fermi energy E_F to be equal on both sides of the junction. For the spin-unpolarized case, i.e., normal/nonmagnetic superconductor junction, it suffices to consider the interfacial parameter Z (given below) to account for the subgap conductance, since any Fermi wave-vector mismatch corresponds to an increase in the effective Z. However, when spin polarization comes into play, it was shown in Ref. 29 that the subgap conductance could be enhanced due to the Fermi wave-vector mismatch. This effect could not be reproduced by varying Z alone, hence implying that the effect of different bandwidths due to different Fermi energies should be taken into account upon comparison between experimental results and theoretical predictions. In our model, we do not study the effect of Fermi wave-vector mismatch, leaving this for future investigations.

III. RESULTS AND DISCUSSION

The normal- and Andreev-reflection coefficients can be calculated by making use of the boundary conditions

$$\text{(i)}\ \psi^\sigma(0)=\Psi^\sigma(0),$$

$$\text{(ii)}\ 2mV_0\psi^\sigma(0)=\partial/\partial z\,[\Psi^\sigma(z)-\psi^\sigma(z)]\big|_{z=0}. \tag{9}$$

Let us introduce $Z=2mV_0/k_F$ and

$$\Upsilon_\pm^\sigma=q^\sigma\cos\theta_s^\sigma\pm k^\sigma\cos\theta\pm \mathrm{i}k_FZ, \tag{10}$$

while $P_\sigma^{L(R)}=(E_F+\sigma U_{L(R)})/2E_F$ denotes the spin polarization on the left (right) side of the junction. Our calculations then lead to the explicit expressions for the Andreev- and normal-reflection coefficients for this FM-FMSC junction, namely,

$$r_e^\sigma=-1+2k^\sigma\cos\theta[u_\sigma(\theta_{s+}^\sigma)u_\sigma(\theta_{s-}^\sigma)(\Upsilon_+^\sigma)^*+v_\sigma(\theta_{s-}^\sigma)v_\sigma(\theta_{s+}^\sigma)\gamma_\sigma(\theta_{s-}^\sigma)\gamma_\sigma^*(\theta_{s+}^\sigma)(\Upsilon_-^\sigma)^*]/D^\sigma,$$

$$r_h^\sigma=4k^\sigma\cos\theta q^\sigma\cos\theta_s^\sigma v_\sigma(\theta_{s+}^\sigma)u_\sigma(\theta_{s-}^\sigma)\gamma_\sigma^*(\theta_{s+}^\sigma)/D^\sigma, \tag{11}$$

upon defining the quantity

$$D^\sigma=u_\sigma(\theta_{s+}^\sigma)u_\sigma(\theta_{s-}^\sigma)|\Upsilon_+^\sigma|^2-v_\sigma(\theta_{s-}^\sigma)v_\sigma(\theta_{s+}^\sigma)\gamma_\sigma(\theta_{s-}^\sigma)\gamma_\sigma^*(\theta_{s+}^\sigma)\times|\Upsilon_-^\sigma|^2. \tag{12}$$

In the limit of weak FM where all quasiparticle momenta equal k_F, our results are found to be consistent with a spin-generalized augmentation of the equations in Ref. 31, where the reflection coefficients for a normal-anisotropic superconductor junction were derived. Tanaka and Kashiwaya put forth a natural explanation for the observed zero-bias conductance peaks (ZBCPs) as a result of the different phases felt by the scattered electronlike and holelike quasiparticles in the superconductor. In their general form, the coefficients in Eq. (11) are results that include the effect of magnetism on the superconducting side of the barrier. As demanded by consistency, one obtains total reflection $|r_e^\sigma|^2=1$ when $\theta>\arcsin(q^\sigma/k^\sigma)$. Having obtained the above quantities, one may calculate the conductance $G(E)$ of the setup [in units of the normal conductance, i.e., $\Delta_\sigma(\theta)\to 0$]. We find that it is given by

$$G(E)=\sum_\sigma G^\sigma(E)\Big/\sum_\sigma F^\sigma, \tag{13}$$

where we have defined the quantities

$$G^\sigma(E)=\int_{-\pi/2}^{\pi/2}d\theta\cos\theta g^\sigma(E,\theta)P_\sigma^LP_\sigma^R,$$

$$g^\sigma(E,\theta)=1+|r_h^\sigma(E,\theta)|^2-|r_e^\sigma(E,\theta)|^2,$$

$$F^\sigma=\int_{-\pi/2}^{\pi/2}d\theta\cos\theta f^\sigma(\theta)P_\sigma^LP_\sigma^R,$$

$$f^\sigma(\theta)=1-|1-2k^\sigma\cos\theta/\Upsilon_+^\sigma|^2. \tag{14}$$

We next demonstrate how the conductance spectra yield useful information about the superconducting gaps upon varying

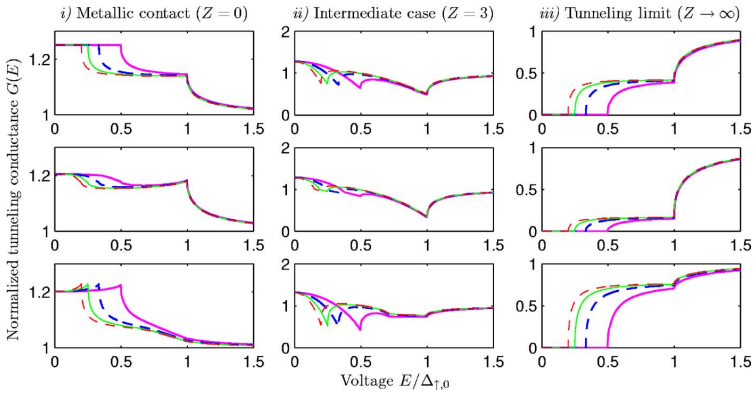

FIG. 2. (Color online) Plot of the conductance $G(E)$ for a FM/FMSC junction in the case of a metallic contact, the tunneling limit, and an intermediate case. The gaps are given by Eq. (15) in this case, for which $G(E)$ is found to be insensitive to $\{\alpha,\beta\}$. In the above, $\{\alpha,\beta\}=0$. The columns for each case provide the spectrum for $U_L=0.05E_F$, $U_L=0.5E_F$, and $U_L=-0.5E_F$, in descending order. For each figure, we have plotted several ratios between the magnitude of the superconducting gaps. These are given by $R_\Delta=\{2,3,4,5\}$, represented by the magenta (thick, full-drawn), blue (thick, dashed), green (thin, full-drawn), and red lines (thin, dashed), respectively.

the relative orientation of the gaps, their magnitude, and the strength of the magnetic exchange energy on each side of the junction. To be specific, we first consider the analog of the $A2$ phase in liquid ^{3}He, such that the gaps may be written as[30]

$$\Delta_\uparrow(\theta^\sigma_{s\pm}) = -\Delta_{\uparrow,0}e^{i(\theta^\sigma_{s\pm}-\alpha)}, \quad \Delta_\downarrow(\theta^\sigma_{s\pm}) = \Delta_{\downarrow,0}e^{i(\theta^\sigma_{s\pm}-\beta)}, \quad (15)$$

as illustrated in Fig. 1. We stress that $\theta^\sigma_{s\pm}$ is *not* the global broken U(1) superconducting phase, but rather an internal phase originating with the odd symmetry of the p-wave gaps (see Fig. 1). The exchange energy of the FMSC will be kept fixed at $U_R=0.05E_F$. In Fig. 2, we have plotted the conductance spectra for a FM/FMSC junction for three distinct cases. We have defined the ratio between magnitude of the superconducting gaps as $R_\Delta=\Delta_{\uparrow,0}/\Delta_{\downarrow,0}$. Introducing the dimensionless barrier strength $Z=2mV_0/k_F$, where k_F is the Fermi momentum, we consider (i) the metallic contact case with no barrier ($Z=0$), (ii) the intermediate case with a moderate barrier ($Z=3$), and (iii) the tunneling limit with an insulator in the junction ($Z\to\infty$). For each case, we have allowed the magnetic exchange energy U_L to vary from weak, favoring $\uparrow$-spins ($U=0.05E_F$) to strong, favoring $\uparrow$-spins in one case ($U=0.5E_F$) and $\downarrow$-spins in the other case ($U=-0.5E_F$). These are shown in descending order in each column. We have also considered the conductance $G(E)$ for several values of $\{\alpha,\beta\}$. For the gaps chosen above, we find that the $G(E)$ did not depend on different choices of these parameters. This can be understood by observing that the angular averaging over $G^\sigma(E,\theta)$ allows for factors $e^{-i\alpha(\beta)}$ to be separated on equal footing as the factor corresponding to the globally broken U(1) symmetry, whose value does not affect the conductance spectra. This will, however, not be the case for other possible triplet symmetries, as discussed below.

An important, and obvious, feature of the conductance spectra is a characteristic behavior occurring at voltages corresponding to $E=\Delta_{\sigma,0}$, $\sigma=\uparrow,\downarrow$, where peaks are displayed. This offers the opportunity to utilize the conductance spectra to reap explicit information on the size of the superconducting gaps in the FMSC. From Fig. 2, it is seen that the effect of increasing the exchange energy on the ferromagnetic side to $U_L=\pm 0.5E_F$ is a sharpening of the peaks located at $E=\Delta_{\sigma,0}$, where σ is the spin species energetically favored by U_L. Concomitantly, the peak located at $E=\Delta_{-\sigma,0}$ is suppressed. Such a response is consistent with what one would expect, since increased (decreased) spin polarization on the ferromagnetic side enhances (suppresses) the conductance of the corresponding spin component. In the tunneling limit (large Z), we see that the conductance spectra exhibit sharp transitions at $E=\Delta_{\sigma,0}$, corresponding to the sudden appearance of a tunneling current as the voltage exceeds the magnitude of the gaps. We have also considered $G(E)$ in the case of vanishing FM on the left side, i.e., a N/FMSC junction. The results we find are very similar to the case of weak FM displayed in the upper row of Fig. 2, and are therefore not displayed.

For the gaps in Eq. (15), the conductance was found to be insensitive to $\{\alpha,\beta\}$. However, in general this is different, and the orientation of the gaps relative to the barrier is essential in determining the conductance spectrum. We illustrate this with a somewhat different choice of anisotropic gaps. When the superconducting gap is oriented in a fashion that leaves it invariant under inversion of the component of momentum perpendicular to the junction, $k_z\to -k_z$ in this case (equivalently, $\theta\to\pi-\theta$), no ZBCP should be expected as there is no formation of current-carrying zero energy states.[25] However, when the gap changes sign under such an inversion of momentum, ZBCPs appear.[31] Since the momentum perpendicular to the junction of the holelike excitation in the anisotropic superconductor is reversed compared to the electronlike excitation, a gap that satisfies $\Delta_\sigma(\theta)\neq\Delta_\sigma(\pi-\theta)$ will cause the hole to feel a pairing potential different from that of the electronlike excitation. This is

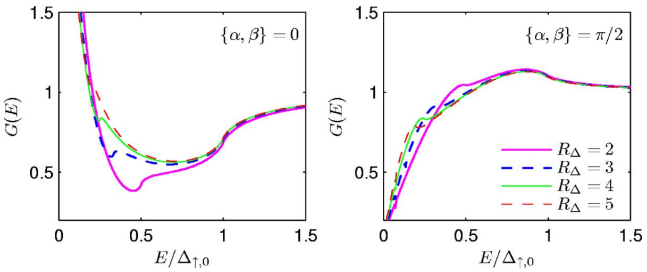

FIG. 3. (Color online) Plot of the conductance $G(E)$ for FM/FMSC junction with gaps given by Eq. (16), for which $G(E)$ is sensitive to $\{\alpha,\beta\}$. We have chosen $Z=3$, and $R_\Delta=\{2,3,4,5\}$ are represented by the magenta, blue, green, and red lines, respectively.

the fundamental reason for the appearance of a ZBCP. However, in the present case of p-wave superconducting gaps analogous to the $A2$ phase in ^{3}He, both gaps are *asymmetric* under the operation $\theta\rightarrow\pi-\theta$ regardless of the value of $\{\alpha,\beta\}$ except for the single value $\theta=0$. Therefore, a small contribution to zero energy current-carrying states, i.e., $G(0)\neq 0$, will occur, as shown in Fig. 2. However, this contribution does not lead to a ZBCP, for which all values of θ contribute to the formation of zero energy states due to the asymmetry of the gaps. In a model where the p-wave gaps are represented by the odd-symmetry analog of $d_{x^2-y^2}$-wave gaps, i.e.,

$$\Delta_\uparrow(\theta)=\Delta_{\uparrow,0}\cos(\theta-\alpha),\quad \Delta_\downarrow(\theta)=\Delta_{\downarrow,0}\cos(\theta-\beta), \tag{16}$$

the formation of ZBCP will then be predictable from the orientation of the gaps as these can now display symmetry/antisymmetry/asymmetry when $\theta\rightarrow\pi-\theta$, depending on $\{\alpha,\beta\}$ (see Fig. 1). Indeed, insertion of the above gaps into our model produces conductance spectra that display a ZBCP for, e.g., $\alpha=\beta=0$, as can be seen in Fig. 3. In this case, as in Fig. 2, the conductance spectra also allow for the magnitude of the superconducting gaps to be read out, although the features are not as clear as those seen in Fig. 2.

From the results of Figs. 2 and 3, it is clear that the conductance spectra $G(E)$ exhibit strong dependence on the exchange energy, while the relative orientation of the gaps is insignificant for the superconducting gaps [Eq. (15)]. Thus, our results will shed light on the magnitude of the various components of the superconducting gaps and their relative orientations in $\mathbf{k}$ space if the gaps display symmetry/antisymmetry under $\theta\rightarrow\pi-\theta$ for some orientation. Moreover, we are dealing with an easily observable effect, since distinguishing between the peaks occurring for various values of R_Δ requires a resolution of order $\mathcal{O}(10^{-1}\Delta_{\uparrow,0})$, which typically corresponds to 0.1–1 meV. These structures should be then readily resolved with present-day scanning tunneling microscopy technology. However, it should be pointed out that a challenge with respect to tunneling junctions is dealing with nonidealities at the interface, which may affect the conductance spectrum. Also, the importance of spin-flip processes in the vicinity of the interface (if such are indeed present) has recently been pointed out.[32,33] Finally, we stress the fact that multiple conductance measurements for several interface orientations are, in general, required to unambiguously determine the pairing symmetry of the superconducting condensate, a point underlined by recent findings that show how both chiral p-wave and d-wave pairing may account for the superconducting properties of strontium ruthenate.[34]

IV. CONCLUSION

In summary, we have studied the conductance spectra $G(E)$ for systems consisting of a ferromagnetic metal separated from a non-unitary p-wave FMSC by a thin, insulating barrier. We have considered the cases of weak, intermediate, and strong barriers and considered three different strengths of the ferromagnetic exchange energy. We have considered two classes of anisotropic spin-triplet superconducting gaps, with results given in Figs. 2 and 3. Our results show how the magnitude of the superconducting gaps Δ_σ, $\sigma=\uparrow,\downarrow$ may be inferred from the conductance spectra. Moreover, the class of superconducting gaps given in Eq. (15) renders $G(E)$ insensitive to $\{\alpha,\beta\}$; the results are shown in Fig. 2 for $\{\alpha,\beta\}=0$. Conversely, for the orientations of the p-wave gaps modeled by Eq. (16), specific values of $\{\alpha,\beta\}$ are essential to the formation of ZBCPs in $G(E)$ in Fig. 3 and the characteristic behavior at $E=\Delta_{\sigma,0}$, $\sigma=\uparrow,\downarrow$. These results should provide useful insights in determining the relative orientation between the superconducting gaps as well as their magnitude in ferromagnetic spin-triplet superconductors.

ACKNOWLEDGMENTS

This work was supported by the Norwegian Research Council Grants No. 157798/432 and No. 158547/431 (NANOMAT) and Grant No. 167498/V30 (STORFORSK).

[1] V. L. Ginzburg, Zh. Eksp. Teor. Fiz. **31**, 202 (1956).
[2] S. S. Saxena, P. Agarwal, K. Ahilan, F. M. Grosche, R. K. W. Haselwimmer, M. J. Steiner, E. Pugh, I. R. Walker, S. R. Julian, P. Monthoux, G. G. Lonzarich, A. Huxley, I. Sheikin, D. Braithwaite, and J. Flouquet, Nature (London) **406**, 587 (2000).
[3] D. Aoki, A. Huxley, E. Ressouche, D. Braithwaite, J. Flouquet, J.-P. Brison, E. Lhotel, and C. Paulsen, Nature (London) **413**, 613 (2001).

[4] P. W. Anderson, *Basic Notions of Condensed Matter Physics* (Addison-Wesley, Reading, MA, 1980).
[5] E. I. Blount and C. M. Varma, Phys. Rev. Lett. **42**, 1079 (1979); E. I. Blount and C. M. Varma, Phys. Rev. Lett. **43**, 1843 (1979).
[6] R. Shen, Z. M. Zheng, S. Liu, and D. Y. Xing, Phys. Rev. B **67**, 024514 (2003).
[7] M. L. Kulic and I. M. Kulic, Phys. Rev. B **63**, 104503 (2001); M. L. Kulic, C. R. Phys. **7**, 4 (2006); cond-mat/0508276 (to be published).
[8] I. Eremin, F. S. Nogueira, and R.-J. Tarento, Phys. Rev. B **73**, 054507 (2006).
[9] S. Tewari, D. Belitz, T. R. Kirkpatrick, and J. Toner, Phys. Rev. Lett. **93**, 177002 (2004).
[10] D. V. Shopova and D. I. Uzunov, Phys. Rev. B **72**, 024531 (2005).
[11] V. P. Mineev and K. V. Samokhin, *Introduction to Unconventional Superconductivity* (Gordon and Breach, New York, 1999).
[12] H. Kotegawa, A. Harada, S. Kawasaki, Y. Kawasaki, Y. Kitaoka, Y. Haga, E. Yamamoto, Y. Onuki, K. M. Itoh, E. E. Haller, and H. Harima, J. Phys. Soc. Jpn. **74**, 705 (2005).
[13] C. Bernhard, J. L. Tallon, E. Brücher, and R. K. Kremer, Phys. Rev. B **61**, R14960 (2000).
[14] F. Hardy and A. D. Huxley, Phys. Rev. Lett. **94**, 247006 (2005).
[15] K. V. Samokhin and M. B. Walker, Phys. Rev. B **66**, 174501 (2002).
[16] K. Machida and T. Ohmi, Phys. Rev. Lett. **86**, 850 (2001).
[17] A. J. Leggett, Rev. Mod. Phys. **47**, 331 (1975).
[18] T. Yokoyama, Y. Tanaka, and J. Inoue, Phys. Rev. B **72**, 220504(R) (2005); R. Kleiner, A. S. Katz, A. G. Sun, R. Summer, D. A. Gajewski, S. H. Han, S. I. Woods, E. Dantsker, B. Chen, K. Char, M. B. Maple, R. C. Dynes, and J. Clarke, Phys. Rev. Lett. **76**, 2161 (1996); J. H. Xu, J. L. Shen, J. H. Miller, Jr., and C. S. Ting, *ibid.* **73**, 2492 (1994).
[19] C. J. Bolech and T. Giamarchi, Phys. Rev. Lett. **92**, 127001 (2004).
[20] N. Stefanakis, Phys. Rev. B **65**, 064533 (2002); N. Stefanakis, Phys. Rev. B **64**, 224502 (2001).
[21] R. Meservey and P. M. Tedrow, Phys. Rep. **238**, 173 (1994).
[22] B. J. Powell, J. F. Annett, and B. L. Györffy, J. Phys. A **36**, 9289 (2003).
[23] Y. S. Barash, H. Burkhardt, and D. Rainer, Phys. Rev. Lett. **77**, 4070 (1996); Y. Tanaka and S. Kashiwaya, Phys. Rev. B **58**, R2948 (1998); Y. Tanaka, T. Asai, N. Yoshida, J. Inoue, and S. Kashiwaya, *ibid.* **61**, R11902 (2000).
[24] M. Eschrig, J. Kopu, J. C. Cuevas, and G. Schon, Phys. Rev. Lett. **90**, 137003 (2003).
[25] C.-R. Hu, Phys. Rev. Lett. **72**, 1526 (1994).
[26] Y. Tanaka, Y. V. Nazarov, and S. Kashiwaya, Phys. Rev. Lett. **90**, 167003 (2003).
[27] G. E. Blonder, M. Tinkham, and T. M. Klapwijk, Phys. Rev. B **25**, 4515 (1982).
[28] J. Y. T. Wei, N.-C. Yeh, D. F. Garrigus, and M. Strasik, Phys. Rev. Lett. **81**, 2542 (1998).
[29] I. Zutic and O. T. Valls, Phys. Rev. B **60**, 6320 (1999); I. Zutic and O. T. Valls, Phys. Rev. B **61**, 1555 (2000).
[30] A. P. Mackenzie and Y. Maeno, Rev. Mod. Phys. **75**, 657 (2003).
[31] Y. Tanaka and S. Kashiwaya, Phys. Rev. Lett. **74**, 3451 (1995).
[32] S. Kreuzer, J. Moser, W. Wegscheider, D. Weiss, M. Bichler, and D. Schuh, Appl. Phys. Lett. **80**, 4582 (2002).
[33] S. Garzon, I. Zutic, and R. A. Webb, Phys. Rev. Lett. **94**, 176601 (2005).
[34] I. Zutic and I. Mazin, Phys. Rev. Lett. **95**, 217004 (2005).

Paper IV

Signatures of retroreflection and induced triplet electron-hole correlations in a ferromagnet/superconductor junction.

Physical Review B **75**, 134509 (2007).

Signatures of retroreflection and induced triplet electron-hole correlations in ferromagnet–*s*-wave-superconductor structures

J. Linder[1] and A. Sudbø[1,2]
[1]*Department of Physics, Norwegian University of Science and Technology, N-7491 Trondheim, Norway*
[2]*Center for Advanced Study, The Norwegian Academy of Science and Letters, N-0271 Oslo, Norway*
(Received 22 December 2006; revised manuscript received 8 February 2007; published 12 April 2007)

We present a theoretical study of a ferromagnet–*s*-wave-superconductor junction to investigate the signatures of induced triplet correlations in the system. We apply the extended Blonder-Tinkham-Klapwijk formalism and allow for an arbitrary magnetization strength and direction of the ferromagnet, a spin-active barrier, Fermi-vector mismatch, and different effective masses in the two systems. It is found that the phase associated with the *xy* components of the magnetization in the ferromagnet couples with the superconducting phase and induces spin triplet pairing correlations in the superconductor, if the tunneling barrier acts as a spin filter. This feature leads to an induced spin-triplet pairing correlation in the ferromagnet, along with a spin-triplet electron-hole coherence due to an interplay between the ferromagnetic and superconducting phases. As our main result, we investigate the experimental signatures of retrorelection, manifested in the tunneling conductance of a ferromagnet–*s*-wave-superconductor junction with a spin-active interface.

DOI: 10.1103/PhysRevB.75.134509 PACS number(s): 74.20.Rp, 74.20.−z, 74.50.+r

I. INTRODUCTION

The proximity effect[1] in a normal/superconductor (N/S) junction refers to the induced superconducting (SC) correlations between electrons and holes in the normal part of the system. Even far away from the junction (typically distances much larger than the superconducting coherence length ξ) where the pairing potential is identically equal to zero, these correlations may persist. Consequently, the proximity effect is responsible for a plethora of interesting physical phenomena, including the Josephson effect in S/N/S junctions,[2] the spin-valve effect in ferromagnet/superconductor (F/S) layers,[3] and the realization of so-called π junctions, which in particular have received much attention both theoretically[4] and experimentally[5] during the past decades. The understanding of Andreev-reflection processes[6] is crucial when dealing with the proximity effect in N/S systems. Roughly speaking, this phenomenon may be thought of as a coherently propagating electron with energy less than the superconducting gap Δ incident from the N side of the barrier being reflected as coherently propagating hole, while in the process generating a propagating Cooper pair in the S. Such processes are highly relevant in the context of transport properties of N/S heterostructures in the low-energy regime and have proven to be an effective tool in probing the pairing symmetry of unconventional SCs (see Ref. 7 and references therein).

In recent years, the fabrication of ferromagnet-superconductor heterostructures has been subject to substantial advances due to the development of techniques in material growth and high quality interfaces.[8,9] With an increasing number of recently discovered unconventional superconductors with exotic pairing symmetries,[10–12] there exists an urgent need to refine the traditional methods, such as tunneling spectroscopy, in order to correctly identify the experimental signatures which reveal the nature of the pairing potential for such superconductors. For one thing, this amounts to taking into account effects which are known to be present in tunneling junction experiments and that may significantly influence the conductance spectra, such as local spin-flip processes and the nonideality of the interface.[13] Also, with the aim of producing theoretical tools that may serve as a guide for identifying the superconducting pairing symmetry, possible spin-filter effects of interface in ferromagnet-superconductor heterostructures warrant attention.[14]

Studies of quantum transport in F/S junctions have a long tradition for both conventional and unconventional pairing symmetries in the superconductor.[15–17,19] Currently, such systems have become the subject of much investigation, not only due to their interesting properties from a fundamental physics point of view, but also because such heterostructures may hold great potential for applications in nanotechnological devices. An important characteristic of most F/S junctions is that, unlike N/S junctions, *retroreflection* is absent for the hole in the F part of the system. This means that the reflected hole, which carries opposite spin of the original electron, does not retrace the trajectory of the incoming electron. The absence of retroreflection is due to the presence of an exchange interaction. Previous studies of such systems have primarily focused on a magnetization lying in the plane of the F/S junction, where in most cases the barrier contains a pure nonmagnetic scattering potential.[15–17] Kashiwaya *et al.*[19] included the effect of a magnetic scattering potential in this type of junction—i.e., spin-active barriers—and very recently, it was suggested by Kastening *et al.*[20] that the presence of both intrinsic and spin-active scattering potentials in the barrier of a S/S junction may lead to qualitatively new effects for the Josephson current. So far, the influence of the F phase associated with the planar magnetization perpendicular to the interface has been largely unexplored, although Ref. 20 considers the one-dimensional (1D) case of this situation.

It is therefore the purpose of this paper to investigate two interesting features that arise in a F/S junction in the presence of planar magnetization components: (i) the interplay between the planar magnetization and the presence of a spin-

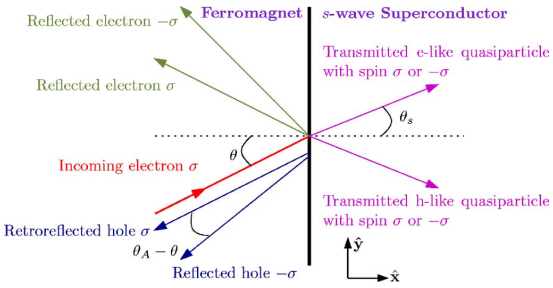

FIG. 1. (Color online) Schematic overview of the relevant scattering processes that take place at the F/S interface. We take into account the possibility of retroreflected holes with equal spin as the incoming electron. This is due to the presence of spin-flip processes manifested in the form of planar magnetization and a spin-active barrier.

active barrier may restore retroreflection for a given parameter range, and (ii) the resulting induced electron-hole pair correlations exhibit a coupling between ϕ and the S phase γ. Since our findings suggest that the traditional picture of absent retroreflection does not hold for planar magnetization with respect to the junction in the presence of a spin-active barrier, we argue that these results are of major importance in the study of F/S junctions. The presence of retroreflection in a F/S junction thus influences the spin-charge dynamics in a significant way, giving rise to new possibilites of quantum transport involving charge and spin flow in such a heterostructure. Elucidating the consequences of this is of fundamental importance. It is also of considerable importance in device fabrication, since our results imply that the spin-active properties of a tunneling barrier play a crucial role.

This paper is organized as follows. In Sec. II, we define the model we study and set up definitions of the scattering amplitudes to be considered. In Sec. III we investigate what conditions are necessary for retroreflection to occur. In Sec. IV, we give our results for the conductance. In Sec. IV A, we consider the influence of Fermi-vector mismatch on the conductance spectrum $G(E)$, in Sec. IV B we consider the effect of exchange energy on $G(E)$, in Sec. IV C we consider the effect of differing effective masses across the tunneling junction on $G(E)$, and in Sec. IV D we consider the effect on $G(E)$ of varying the relative strength of magnetic and nonmagnetic scattering potentials in the contact region between F and S. In Sec. V we provide a discussion of results, including a comparison of our results to earlier ones on similar problems. We highlight what our new findings are compared to earlier results. Finally, Sec. VI summarizes our results.

II. MODEL AND FORMULATION

We define our model as follows. Consider a 2D F/S junction as illustrated in Fig. 1. As is seen from the figure, θ is the angle of incidence for electrons with spin σ that feel a barrier strength $V_\sigma(x)=(V_0-\sigma V_s)\delta(x)$, where V_0 and V_s are the nonmagnetic and magnetic scattering potentials, respectively; i.e., the barrier is spin active.[19] Physically, this means that the barrier acts as a spin filter. Furthermore, θ_A is the angle of reflection for particles with spin $-\sigma$. The Bogoliubov–de Gennes (BdG) equations that describe the quasiparticle states $\Psi(x,y)$ with energy eigenvalues E in the two subsystems are given by

$$\begin{pmatrix} \hat{H}_0(x,y) & \hat{\Delta}(x) \\ -\hat{\Delta}^\dagger(x) & -\hat{H}_0^{\mathrm{T}}(x,y) \end{pmatrix} \Psi(x,y) = E\Psi(x,y), \tag{1}$$

where we have defined the single-particle Hamiltonian

$$\hat{H}_0(x,y) = -\boldsymbol{\nabla}_{xy}^2/[2m_{\mathrm{F}}\Theta(-x) + 2m_{\mathrm{S}}\Theta(x)] - \hat{\boldsymbol{\sigma}}\cdot\boldsymbol{M}\Theta(-x) + \mathrm{diag}(V_\uparrow(x), V_\downarrow(x)), \tag{2}$$

while $\hat{\Delta}(x)=\mathrm{i}\hat{\sigma_y}\Delta(x)$. We allow for different effective masses in the two systems, given by m_{F} and m_{S}. The magnetic exchange energy splitting is denoted

$$M = (M_{xy}^2 + M_z^2)^{1/2}, \tag{3}$$

where $M_{xy}^2=M_x^2+M_y^2$ is the planar contribution of the magnetic exchange energy, while $2M_z$ is the energy splitting between spin-$\uparrow$ and spin-$\downarrow$ bands. The quasiparticle wave vectors are then given by

$$k^\sigma = \sqrt{2m_{\mathrm{F}}(E_{\mathrm{F}} + \sigma M)},$$

$$q = \sqrt{2m_{\mathrm{S}}E_{\mathrm{S}}}, \tag{4}$$

in the F part and S part of the system, respectively, where E_i is the Fermi energy. We have made use of the standard approximation $E_i \gg \Delta$. Moreover, we take the S order parameter to be constant up to the junction such that $\Delta(\gamma,x)=\Delta e^{i\gamma}\Theta(x)$. Solving the BdG equations, the wave functions ψ on the F side and Ψ on the S side become

$$\psi(x,y) = e^{ik_y y}\left[\begin{pmatrix} s_\uparrow a \\ s_\uparrow b e^{-i\phi} \\ 0 \\ 0 \end{pmatrix} e^{ik^\uparrow \cos\theta x} + \begin{pmatrix} -s_\downarrow b e^{i\phi} \\ s_\downarrow a \\ 0 \\ 0 \end{pmatrix} e^{ik^\downarrow \cos\theta x} + r_e^\uparrow \begin{pmatrix} a \\ b e^{-i\phi} \\ 0 \\ 0 \end{pmatrix} e^{-ik^\uparrow Sx} + r_e^\downarrow \begin{pmatrix} -b e^{i\phi} \\ a \\ 0 \\ 0 \end{pmatrix} e^{-ik^\downarrow \tilde{S}x} + r_h^\uparrow \begin{pmatrix} 0 \\ 0 \\ a \\ b e^{i\phi} \end{pmatrix} e^{ik^\uparrow Sx} + r_h^\downarrow \begin{pmatrix} 0 \\ 0 \\ -b e^{i\phi} \\ a \end{pmatrix} e^{ik^\downarrow \tilde{S}x}\right],$$

$$\Psi(x,y) = e^{ik_y y}\left[t_e^{\uparrow}\begin{pmatrix} u \\ 0 \\ 0 \\ ve^{-i\gamma} \end{pmatrix} e^{iq\cos\theta_s x} + t_e^{\downarrow}\begin{pmatrix} 0 \\ u \\ -ve^{-i\gamma} \\ 0 \end{pmatrix} e^{iq\cos\theta_s x} + t_h^{\uparrow}\begin{pmatrix} 0 \\ -ve^{i\gamma} \\ u \\ 0 \end{pmatrix} e^{-iq\cos\theta_s x} + t_h^{\downarrow}\begin{pmatrix} ve^{i\gamma} \\ 0 \\ 0 \\ u \end{pmatrix} e^{-iq\cos\theta_s x} \right]. \tag{5}$$

The elements entering in the wave functions above describing the quasiparticles read

$$a = \frac{1}{\sqrt{1+[M_{xy}/(M+M_z)]^2}}, \quad b = \frac{aM_{xy}}{M+M_z}, \tag{6}$$

for the F part, while the superconducting coherence factors read

$$u = \sqrt{\frac{1}{2} + \frac{\sqrt{E^2-\Delta^2}}{2E}},$$

$$v = \sqrt{\frac{1}{2} - \frac{\sqrt{E^2-\Delta^2}}{2E}}. \tag{7}$$

We denote the F phase by ϕ and S phase by γ. Note that $\tan\phi = -M_y/M_x$, such that the physical interpretation of the F phase is directly related to the direction of the magnetization in the xy plane characterized by the azimuthal angle. An incoming electron with spin $\uparrow$ is described by $\{s_\uparrow = 1, s_\downarrow = 0\}$ while a spin-$\downarrow$ electron is given by $\{s_\uparrow = 0, s_\downarrow = 1\}$. For convenience, we also introduce $S = s_\uparrow \cos\theta + s_\downarrow \cos\theta_A$ and $\tilde{S} = s_\uparrow \cos\theta_A + s_\downarrow \cos\theta$. The boundary conditions for these wave functions read

$$\psi_F(0,y) = \Psi_S(0,y),$$

$$\frac{\Psi_S'(x,y)|_{x=0}}{2m_S} - \frac{\psi_F'(x,y)|_{x=0}}{2m_F} = V_0 - V_s\eta, \tag{8}$$

where $\eta = (1,-1,1,-1)^T$ and a prime denotes derivation with respect to x. Translational invariance along the $\hat{\mathbf{y}}$ direction implies conservation of the momentum k_y. This allows us to determine θ_s and θ_A as follows:

$$(s_\uparrow k^\uparrow + s_\downarrow k^\downarrow)\sin\theta = q\sin\theta_s,$$

$$(s_\uparrow k^\uparrow + s_\downarrow k^\downarrow)\sin\theta = (s_\uparrow k^\downarrow + s_\downarrow k^\uparrow)\sin\theta_A. \tag{9}$$

III. PRESENCE OF RETROREFLECTION

Several cases may now be studied, such as different effective masses in the F and S parts, Fermi-vector mismatch, and the presence of a spin-active barrier. Solving Eq. (8) for the wave functions in Eqs. (5), one is able to obtain explicit expressions for the reflection coefficients of the scattering problem. This amounts to solving for 16 unknown coefficients, and their derivation may be found in the Appendix . While the expressions for their amplitudes are quite cumbersome, their phase dependences are simple and illustrate the new physics. In Table I, we provide this phase dependence for the cases of incoming $\uparrow$ and $\downarrow$ electrons.[36] It is seen that a coupling between ϕ and γ is present in the phase of the hole with the same spin σ as the incident electron. Ordinarily, retroreflection is absent in the Andreev-scattering process at the F/S junction such that the reflected hole and the incident electron carry opposite spins. However, it is clear from Table I that were a hole with spin σ to be generated in the scattering process, it would carry information about both the F and S phases. We interpret this as *induced spin-triplet pairing correlations* in the S part of the system, along with an electron-hole correlation in the ferromagnet.

TABLE I. Phase dependence of reflection coefficients. Here, "1" means that the quantity is real. An interplay between γ and ϕ occurs when retroreflection is present.

Refl. coeff.	$r_h^\uparrow$	$r_h^\downarrow$	$r_e^\uparrow$	$r_e^\downarrow$
Inc. spin $\uparrow$	$e^{-i(\phi+\gamma)}$	$e^{-i\gamma}$	1	$e^{-i\phi}$
Inc. spin $\downarrow$	$e^{-i\gamma}$	$e^{i(\phi-\gamma)}$	$e^{i\phi}$	1

Although the phase dependence of the reflection coefficients displayed in Table I is intriguing, it remains to be demonstrated that the *amplitudes* of these coefficients are nonzero. To illustrate that this is so, consider Fig. 2 where we have plotted the probability coefficients [that differ from the reflection coefficients by a prefactor; see Eq. (19)] for normal incidence $\theta = 0$; their derivation may be found in the Appendix. In (a), we have no exchange energy and a purely nonmagnetic interfacial resistance, from which the result of Ref. 22 is reproduced. In (b), we have allowed for an exchange energy $M_z = 0.5E_F$, which results in a reduction of the Andreev-reflection amplitude. This is a consequence of the reduced carrier density of the spin-$\downarrow$ band due to the presence of a magnetic exchange energy. In the extreme limit of a completely spin-polarized ferromagnet, $M_z = E_F$, the subgap conductance is completely absent since there are no charge carriers in the spin-$\downarrow$ band at the Fermi level. In (c), we also incorporated the effect of a magnetic scattering potential in the interfacial resistance, which is seen to slightly reduce the probability of the Andreev reflection at $E = \Delta$. The novel features of the F/S junction are now presented in (d). When we allow for both a magnetic scattering potential *and* local spin-flip processes in the form of a planar component of the magnetization, it seen that retroreflection is established. In other words, a new transport channel is opened up for both spin and charge—namely, reflected holelike excitations with the same spin as the incoming electron. Note that the inclusion of this process is absent in most of the literature treating F/S junctions so far.[15,18,19]

To investigate how large the magnitude of the retroreflection coefficient may become, possibly even outgrowing the probability for "normal" Andreev reflection, we plotted the case of zero net polarization for several values of M_{xy} in Fig. 3. It is seen that as M_{xy} increases, the probability for retrore-

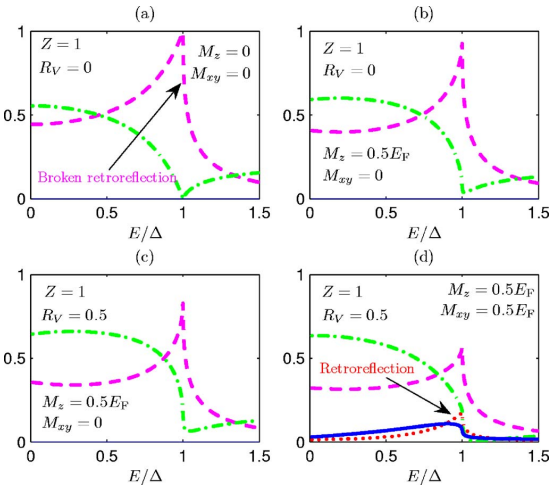

FIG. 2. (Color online) Plot of the probability coefficients associated with the scattering processes at the interface. For an electron with incoming spin σ, the green (dash-dotted) line corresponds to normal reflection with spin σ, the magenta (dashed) line corresponds to Andreev-reflection of a hole with spin $-\sigma$, and the blue (solid) line designates reflection without branch crossing with spin $-\sigma$, while the presence of retroreflection—i.e., Andreev reflection of a hole with spin σ—is indicated by the red (dotted) line. Note from (d) that in order to get retroreflection, both an in-plane magnetization *and* a spin-active barrier are required.

flection grows and eventually becomes much larger than the probability for ordinary Andreev reflection. Thus, for a tunneling junction with a barrier that discriminates significantly between spin-↑ and spin-↓ electrons, the presence of spin-flip processes may induce a substantial modification to the traditional picture of broken retroreflection.

Having established the presence of retroreflection, the next step is the consideration of how retroreflection leaves its signatures in experimentally measurable quantities. In this paper, we investigate how the presence of retroreflection may leave an experimental signature manifested in the conductance spectrum of a F/S junction. Although this shall be our focus, we note in passing that the reflection coefficients de-

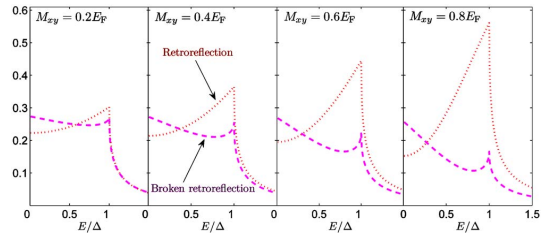

FIG. 3. (Color online) Plot of probability coefficients for $Z=1$ and $R_V=0.95$ in the absence of any net polarization for several values of M_{xy}. It is seen that for increasing M_{xy}—i.e., larger effect of spin-flip scattering—the retroreflection process dominates the "normal" Andreev reflection.

rived in the Appendix may also be used for the purpose of obtaining the current-voltage characteristics, spin-current, and spin conductance of the F/S junction. Normally, the charge and spin current may be written as

$$j_{\text{charge}} = -e\sum_{\sigma} j^{\sigma}, \quad j_{\text{spin}} = \sum_{\sigma} \sigma j^{\sigma}, \tag{10}$$

where j^{σ} is the particle current of electrons with spin σ over the interface. However, in the presence of spin-flip scattering, defining a proper spin current requires a more careful analysis.[21] One can always write down a well-defined spin current in terms of physical spin transport across the junction, but it may be very hard to experimentally distinguish whether the spin accumulation on either side of the interface should be attributed to physical spin transport or local spin-flip processes. The latter are present in, e.g., systems with significant spin-orbit coupling or an in-plane magnetic field with respect to the quantization axis, which results in scattering between the two spin bands. Accordingly, in this paper we will concern ourselves with the charge current and the resulting conductance spectrum.

IV. RESULTS

In our theory, we have included the possibility of having a spin-active barrier, Fermi-vector mismatch, arbitrary strength of the exchange energy on the F side, and different effective masses in the two systems. Thus, we believe our model should be able to capture many essential and realistic features of a F/S junction that pertain to both interfacial properties, as well as bulk effects on the F and S sides, respectively. Since the case of easy-axis magnetization has been thoroughly investigated, we shall be mainly concerned with the presence of retroreflection, *which requires both spin-flip processes and a barrier acting as a spin filter*.

The single-particle tunneling conductance may be calculated by using the Blonder-Tinkham-Klapwijk (BTK) formalism[22] and reads

$$G(E) = \sum_{\sigma} G^{\sigma}(E),$$

$$G^{\sigma}(E) = \int_{-\pi/2}^{\pi/2} \mathrm{d}\theta \cos\theta P^{\sigma} G^{\sigma}(E,\theta),$$

$$G^{\sigma}(E,\theta) = G_N^{-1}[1 + R_h^{\uparrow}(E,\theta) + R_h^{\downarrow}(E,\theta) - R_e^{\uparrow}(E,\theta) - R_e^{\downarrow}(E,\theta)],$$

$$G_N = \int_{-\pi/2}^{\pi/2} \mathrm{d}\theta \cos\theta \frac{4\cos^2\theta}{4\cos^2\theta + Z^2}, \tag{11}$$

where $Z=2m_F V/k_F$ and G_N is the tunneling conductance for a N/N junction. Note that the right-hand side (rhs) of the equation for $G^{\sigma}(E,\theta)$ appears to be independent of σ. However, it is implicitly understood in this notation that the reflection coefficients appearing on the rhs have been solved for an incoming electron with spin σ, and these differ in the cases $\sigma=\uparrow$ and $\sigma=\downarrow$ since the wave function is different [see Eq. (5)]. The different probabilities for having spin injection

σ in the presence of a net polarization is accounted for by the factor $P^\sigma=(1+\sigma M_Z/E_F)/2$. The quantities $\{R_h^\sigma, R_e^\sigma\}$ are the probability coefficients for normal and Andreev reflection and will be derived below. Note that these are *not* in general equal to the square amplitude of the scattering coefficients and, in particular, not so in this case. To see this, consider a current density of probability $\mathbf{J}_{\rm inc}$ that is incident on the barrier,

$$\mathbf{J}_{\rm inc}=\frac{1}{2m_{\rm F}\mathrm{i}}(\psi^*\boldsymbol{\nabla}\psi-\psi\boldsymbol{\nabla}\psi^*), \tag{12}$$

obeying the conservation law

$$\frac{\partial P}{\partial t}+\boldsymbol{\nabla}\cdot\mathbf{J}_{\rm inc}=0. \tag{13}$$

Here, $P=|\psi|^2$. Consulting Eq. (5) and extracting the part of ψ that corresponds to the incident wave function, one readily obtains

$$\mathbf{J}_{\rm inc}=\frac{\cos\theta}{m_{\rm F}}(s_\uparrow k^\uparrow+s_\downarrow k^\downarrow)\hat{\mathbf{x}}. \tag{14}$$

Since probability must be conserved, we have

$$\mathbf{J}_{\rm inc}=-\mathbf{J}_{\rm refl}+\mathbf{J}_{\rm trans}, \tag{15}$$

where the reflected probability current density reads

$$\mathbf{J}_{\rm refl}=\frac{1}{2m_{\rm F}\mathrm{i}}[(\psi_e^*\boldsymbol{\nabla}\psi_e-\mathrm{H.c.})-(\psi_h^*\boldsymbol{\nabla}\psi_h-\mathrm{H.c.})],$$

$$\psi_e=r_e^\uparrow\begin{pmatrix}a\\ b\mathrm{e}^{-\mathrm{i}\phi}\end{pmatrix}\mathrm{e}^{-\mathrm{i}k^\uparrow Sx}+r_e^\downarrow\begin{pmatrix}-b\mathrm{e}^{\mathrm{i}\phi}\\ a\end{pmatrix}\mathrm{e}^{-\mathrm{i}k^\downarrow\tilde{S}x},$$

$$\psi_h=r_h^\uparrow\begin{pmatrix}a\\ b\mathrm{e}^{\mathrm{i}\phi}\end{pmatrix}\mathrm{e}^{\mathrm{i}k^\uparrow Sx}+r_h^\downarrow\begin{pmatrix}-b\mathrm{e}^{-\mathrm{i}\phi}\\ a\end{pmatrix}\mathrm{e}^{\mathrm{i}k^\downarrow\tilde{S}x}. \tag{16}$$

The opposite signs of the electron and hole parts of ψ entering $\mathbf{J}_{\rm refl}$ pertain to the fact that their energy eigenvalues have opposite signs, as one may infer from the BdG equations that are used to derive the explicit expression for $\mathbf{J}_{\rm refl}$ from Eq. (15). One finds that

$$\mathbf{J}_{\rm refl}=-\frac{1}{m_{\rm F}}[k^\uparrow S|r_e^\uparrow|^2+k^\uparrow S|r_h^\uparrow|^2+k^\downarrow\tilde{S}|r_e^\downarrow|^2+k^\downarrow\tilde{S}|r_h^\downarrow|^2]\hat{\mathbf{x}}. \tag{17}$$

The same procedure may now be applied to $\mathbf{J}_{\rm trans}$, such that Eq. (15) can be written as

$$1=\sum_\sigma(R_e^\sigma+R_h^\sigma+T_e^\sigma+T_h^\sigma) \tag{18}$$

upon division with $|\mathbf{J}_{\rm inc}|$. From this, one infers that

$$R_e^\uparrow=|r_e^\uparrow|^2\frac{k^\uparrow S}{s_\uparrow k^\uparrow\cos\theta+s_\downarrow k^\downarrow\cos\theta},$$

$$R_e^\downarrow=|r_e^\downarrow|^2\frac{k^\downarrow\tilde{S}}{s_\uparrow k^\uparrow\cos\theta+s_\downarrow k^\downarrow\cos\theta},$$

$$R_h^\uparrow=|r_h^\uparrow|^2\frac{k^\uparrow S}{s_\uparrow k^\uparrow\cos\theta+s_\downarrow k^\downarrow\cos\theta},$$

$$R_h^\downarrow=|r_h^\downarrow|^2\frac{k^\downarrow\tilde{S}}{s_\uparrow k^\uparrow\cos\theta+s_\downarrow k^\downarrow\cos\theta}. \tag{19}$$

The coefficients $\{R_e^\sigma, R_h^\sigma, T_e^\sigma, T_h^\sigma\}$ have the status of probability coefficients for their respective processes and obey the conservation law, Eq. (18). Note that in the absence of exchange splitting—i.e., F→ N and $\theta_A=\theta$—one obtains $R_i^\sigma=|r_i^\sigma|^2$.

A. Effect of Fermi-vector mismatch

To account for the Fermi-vector mismatch, we introduce a parameter $R_E=E_S/E_F$. This allows the Fermi energies in the F and S regions to be different, which effectively models unequal carrier densities and bandwidths on each side of the junction. For ferromagnet/high-T_c-superconductor junctions, an appropriate choice appears to be[18] $R_E\leq 1$. In our study, however, we will consider values of R_E both less than and greater than unity. To begin with, we fix the strength of the planar contribution to the exchange energy at $M_{xy}=0.1E_F$ and set $M_z=0$, plotting the conductance spectrum for several values of R_E. We fix the ratio $R_V=V_s/V_0=0.5$, such that the conditions for retroreflection are fulfilled. For each figure, we consider zero ($Z=0$), weak ($Z=1$), and large ($Z=10$) interfacial resistance; $Z=0$ corresponds to the point contact (also called metallic contact in some of the literature) while $Z\to\infty$ is equivalent to the tunneling limit. The conductance spectrum for weak spin-flip scattering ($M_{xy}=0.1E_F$) and $M_z=0$ with $R_V=0.5$ for several values of Z is depicted in Fig. 4. From Fig. 4, we infer that the conductance behaves in a monotonic way upon variation of R_E and that the conductance is suppressed with decreasing R_E.

Next, we increase the exchange energy to $M_{xy}=0.5E_F$ and set $R_V=0.95$ such that spin-flip processes become more dominant and the barrier discriminates strongly between spin-↑ and spin-↓ electrons. The resulting $G(E)$ is illustrated in Fig. 5, where it is seen that a nonmonotonic behavior appears. Specifically, the peak at $E=\Delta$ vanishes for $R_E\simeq 1$, as is most clearly seen for the case of large interfacial resistance.

One of the results of Refs. 17 and 18 was that the effect of Fermi-vector mismatch yielded an increased subgap conductance when there was a net spin polarization. As an important consequence, this finding suggested that the interfacial barrier parameter Z was not sufficient to account for the conductance features in the presence of both spin polarization and Fermi-vector mismatch, since the increase of subgap conductance could not be reproduced by varying Z alone. In Figs. 4 and 5, no such increase in subgap conductance was found, but these correspond to an unpolarized case since $M_z=0$. In order to investigate how the spin-flip scattering and spin-active barrier affects this particular feature of the Fermi-vector mismatch, we plot the normal incidence $\theta=0$ conductance $G(E,\theta=0)$ for the same parameters as Fig. 1 in Refs. 17 and 18 for the sake of direct comparison. Note that

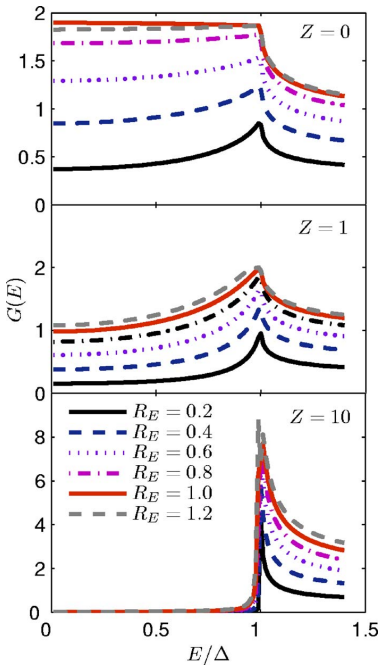

FIG. 4. (Color online) Conductance spectrum for weak spin-flip scattering (M_{xy}=0.1E_F) and M_z=0 with R_V=0.5 for several values of Z.

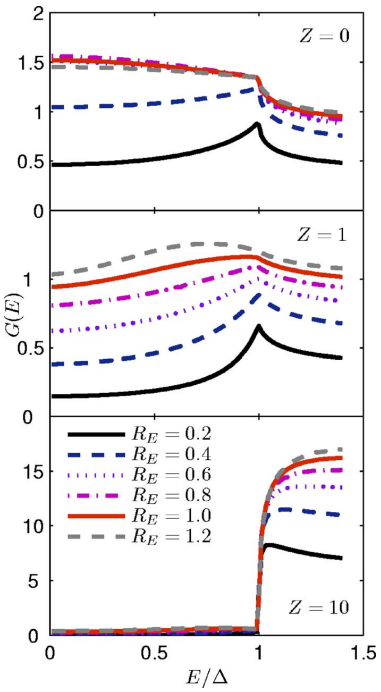

FIG. 5. (Color online) Conductance spectrum for strong spin-flip scattering (M_{xy}=0.5E_F) and M_z=0 with a strongly spin-dependent barrier (R_V=0.95) for several values of Z.

due to a different scaling of the conductance to make it dimensionless, the quantitative results for $G(E,\theta=0)$ are not the same as the result in Refs. 17 and 18, although the qualitative aspect is identical. This is because we scale the conductance on G_N given by Eq. (11). For Z=0, this merely amounts to a factor of 2. In the upper panel of Fig. 6, we reproduce Fig. 1(b) of Ref. 18 to illustrate our consistency with their results. Note that the parameter L_0^2 in Ref. 18 is equivalent to our R_E when R_m=1; i.e., the effective masses are the same. The middle panel now includes spin-flip scattering with M_{xy}=0.4E_F, while Z=0. The lower panel shows the combined effect of planar magnetization and a spin-active barrier, resulting in triplet correlations, with M_{xy} =0.4E_F and $\{Z=1, R_V=0.95\}$. It is seen that the qualitative change is most dramatic when the conditions for retroreflection are fulfilled.

B. Effect of exchange energy

We now proceed to consider how the strength of the exchange energy, both planar (M_{xy}) and easy axis (M_z), affects the conductance spectrum. We set the masses and Fermi energies to be equal in the F and S parts of the system and study how the angularly averaged $G(E)$ is affected by increasing M_Z for a given M_{xy}. Let us first set M_{xy}=0.1E_F and R_V=0.5, as shown in Fig. 7. In accordance with our previous observation that Andreev reflection is inhibited by a net polarization in the F part of the system, it is seen that the conductance is suppressed with increasing M_z. However, in the lower panel of Fig. 7 where the tunneling limit of the junction is considered, the conductance increases with M_z for $E>\Delta$.

Increasing the strength of the spin-flip scattering and also the spin dependence of the barrier, the resulting conductance spectra are shown in Fig. 8 with M_{xy}=0.5E_F and R_V=0.95. The general effect of optimizing the conditions for the presence of retroreflection processes seems to be a "smoothing out" of the conductance: the sharp features at $E=\Delta$ become blunt, an observation which is most clearly revealed in the tunneling limit. As an experimental consequence, the nature of the features at $E=\Delta$ in the case of a high-resistance interface could thus offer information concerning to what degree retroreflection is present in the system.

C. Effect of different effective masses

To investigate the effect of different effective masses in the F and S parts of the system, we consider three ratios: $R_m=m_S/m_F \in \{0.01, 0.1, 1\}$. In Fig. 9, we have plotted the case of weak spin-flip scattering and a moderate spin dependence of the barrier, while in Fig. 10 we investigate significant spin-flip scattering and a strongly spin-dependent interfacial resistance. In the first case, decreasing R_m clearly inhibits the tunneling conductance with no exotic features present except the usual peak at $E=\Delta$. In the tunneling limit,

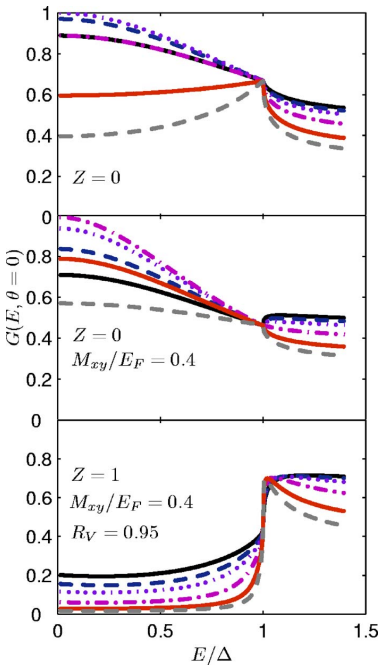

FIG. 6. (Color online) Conductance spectrum for zero spin-flip scattering and purely nonmagnetic scattering potential (upper panel), spin-flip scattering and purely nonmagnetic scattering potential (middle panel), and spin-flip scattering and mixed magnetic and nonmagnetic scattering potential (lower panel). For all panels, M_z/E_F=0.866 for comparison with Ref. 18. The lines are given at E=1.4 for the upper panel as follows (from top to bottom): R_E $=\{1,1/\sqrt{2},1/2,1/4,1/9,1/16\}$.

it is interesting to observe that only in the case R_m=1 is the maximum of the conductance located at E=Δ. Upon decreasing R_m, one sees that the characteristic peak of the spectrum is translated to lower energies and that it becomes less sharp. There is still a sudden increase of current at E=Δ, manifested as a jump in the conductance spectrum, but it is less protruding for lower ratios of R_m than unity.

When the conditions for retroreflection become more pronounced, as is the case in Fig. 10, one may again observe the general modification of the conductance to a more featureless curve in the case of no barrier and a weak barrier (Z =1), as was the case in the previous subsection. In the tunneling limit, the presence of retroreflection also modifies the spectra such that the sharp peak is lost at the gap energy, although the sudden jump due to the initiated flow of current at E=Δ is still there.

D. Effect of magnetic and nonmagnetic scattering potentials

In this section, we show that the conductance spectrum may reveal clear-cut signatures of the presence of retroreflection as a result of the interplay between V_0 and V_s when $M_{xy}\neq 0$. We keep the latter fixed at M_{xy}=0.5E_F and plot

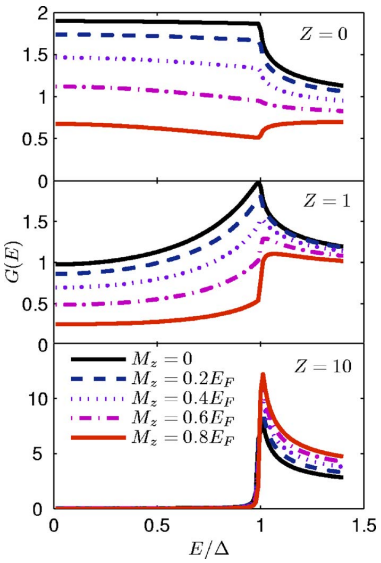

FIG. 7. (Color online) Conductance spectra for various nonmagnetic scattering potentials upon varying the polarization of the ferromagnet with M_{xy}=0.1E_F and R_V=0.5.

$G(E)$ for $Z\in\{0.1,1,5\}$ while varying the strength of the magnetic scattering potential. From Fig. 11, we see that at Z=0.1, the presence of retroreflection is very weak and the conductance spectrum remains virtually unaltered as V_s is varied. At Z=1, the effect of increasing the strength of the magnetic potential of the barrier, acting as a spin filter, cor-

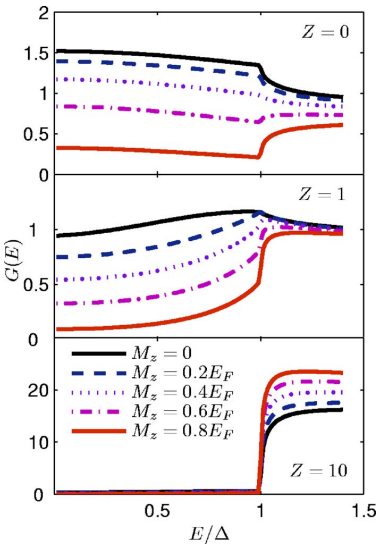

FIG. 8. (Color online) Conductance spectra for various nonmagnetic scattering potentials upon varying the polarization of the ferromagnet with M_{xy}=0.5E_F and R_V=0.95.

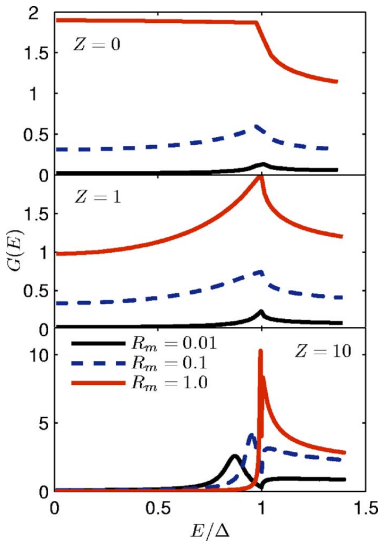

FIG. 9. (Color online) Conductance spectra for different effective masses with parameters M_{xy}=0.1E_F and R_V=0.5.

responds to a reduction of the conductance peak at E=Δ. This is in agreement with our previous observations that the presence of retroreflection appears to have a smoothing effect on the conductance spectrum, causing it to soften its characteristic features. At Z=5, the crossover from a sharp peak at E=Δ at small R_V to a "waterfall" shape for large R_V is clearly illustrated. We suggest that this signature could be used as a feature that unveils the presence of retroreflected holes in the system and thus indicates triplet correlations due

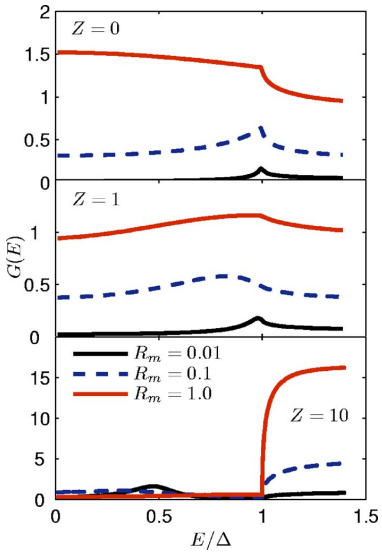

FIG. 10. (Color online) Conductance spectra for different effective masses with parameters M_{xy}=0.5E_F and R_V=0.95.

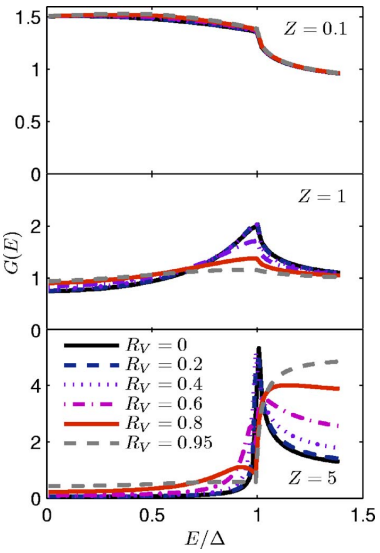

FIG. 11. (Color online) Conductance spectra in the presence of retroreflection but in the absence of any net polarization. Here, M_{xy}=0.5E_F while M_Z=0.

tothe interplay between spin-flip processes and a barrier acting as a spin filter.

To investigate how a net polarization will affect the conductance spectra in this case, consider Fig. 12 which illustrates the conductance for the same parameters as in Fig. 11 except that now M_z=0.5E_F. In agreement with previous remarks, the conductance suffers a general reduction due to the

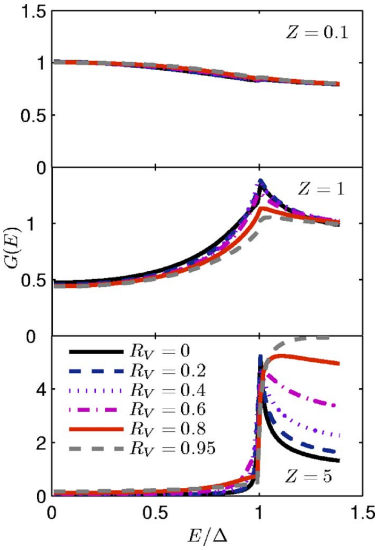

FIG. 12. (Color online) Conductance spectra in the presence of retroreflection and a net polarization. Here, M_{xy}=0.5E_F while M_Z =0.5E_F.

net polarization in the upper and lower panels. Apart from this, the same features as in Fig. 11 are present, with retroreflection leaving its fingerprint most obviously in the behavior of the conductance at $E=\Delta$ in the tunneling limit.

V. DISCUSSION

We have shown that the presence of a spin-active barrier combined with a planar component of the magnetization in the F induces new features in the proximity effect in a F/S junction. Physically, this may be understood by realizing that only an $S_z=0$ triplet component is induced for a spin-active barrier in the absence of spin-flip processes near the junction, while the equal-spin ($S_z=\pm 1$) triplet components are generated only if a spin-flip potential is also present. On the other hand, spin-flip processes alone in the absence of a spin-active barrier would inhibit singlet pairing without generating any triplet components. An interesting opportunity that arises due to the restoration of retroreflection is the fact that one may generate currents with a varying degree of spin polarization in the F part. In the conventional case, an incident electron with spin σ is reflected as either an electron with spin σ or hole with spin $-\sigma$ in these systems. In the present case, however, the reflected electrons and holes may carry *either* $\uparrow$ and $\downarrow$ spin, depending on parameters such as the magnitude of the exchange energy and the intrinsic and spin-dependent barrier strength. In principle, it could be possible to generate pure spin currents without charge currents and vice versa, as a result of the additional allowed spin state of the reflected holes and electrons. It is also intriguing to observe that due to the coupling between ϕ and γ, it may be possible to obtain a Josephson current in a S/F/S hybrid structure that is sensitive to a rotation of the magnetization in the ferromagnetic part, which has been recently discussed in Refs. 24 and 25.

It was shown in Ref. 26 that if a local inhomogeneity of the magnetization in the vicinity of a F/S interface was present, a spin-triplet component of the S order parameter will be generated and penetrate into the F much deeper than the spin-singlet component. In a S/half-metal/S junction, it has been found that S triplet correlations would be induced on both sides of the junctions in the presence of spin mixing and spin-flip scattering at the interfaces[27] (see also Ref. 28). We have found that spin-triplet pairing correlations may be induced in the presence of a spin-active barrier—i.e., intrinsic spin-mixing at the interface—and a planar magnetization relative to the quantization axis. It seems reasonable to suggest that these findings are closely related to the conditions put forward by Ref. 27, since planar magnetization components may effectively act as a spin-flip scattering potential. Our results are thus consistent with the findings of recent studies, although we have adressed several new aspects of the scattering problem in the present paper. In particular, we have found an interplay between the in-plane magnetization direction and superconducting phase. Moreover, we compute detailed conductance spectra of the F/S junction under many different conditions.

One of the important findings of Refs. 17 and 18 was that a zero-bias conductance peak (ZBCP) would develop under the right conditions in the F/S junction, and the effect was attributed to the influence of Fermi-vector mismatch. Usually, the appearance of a ZBCP is associated with unconventional superconductivity where it may appear due to the different phases felt by the transmitted electronlike and holelike quasiparticles in the superconductor.[23] However, Zutic and Valls[17,18] showed that no unconventional superconductivity was required to obtain a ZBCP and that the effect of Fermi-vector mismatch in a F/S junction thus offered a different mechanism for the formation of a ZBCP than the usual one, attributed to a **k**-dependent gap. However, it should be noted that the ZBCP obtained in Refs. 17 and 18 is not as sharp (δ-function like) as the ZBCP depicted in, e.g., Ref. 23, where unconventional superconductors (high-T_c d wave, to be specific) were considered.

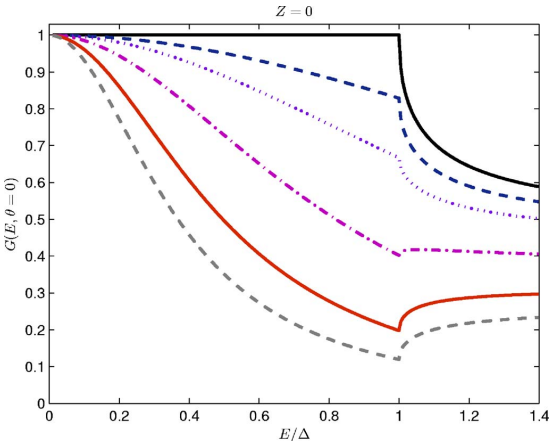

FIG. 13. (Color online) In the limit $M_{xy}\to 0$, the formation of a ZBCP is observed with decreasing R_E. This illustrates how the effect of Fermi-vector mismatch may "mimick" the usual signature of unconventional superconductivity—namely, the appearance of a ZBCP for certain crystal orientations. This was first discussed in Ref. 18, see their Fig. 3. From top to bottom, the curves correspond to the following pairs of $(R_E, M_z/E_F)$: $(1,0)$, $\left(\frac{1}{\sqrt{2}},\frac{1}{\sqrt{2}}\right)$, $\left(\frac{1}{2},0.866\right)$, $\left(\frac{1}{4},0.968\right)$, $\left(\frac{1}{9},0.994\right)$, and $\left(\frac{1}{16},0.998\right)$.

In the present paper, we consider a more general situation than Zutic and Valls, allowing for a completely arbitrary magnetization direction and a spin-active barrier. As we have shown, this changes the physical picture dramatically and opens up a new transport channel for both charge and spin—namely, retroreflected holes. For consistency, we show that we are able to completely reproduce Fig. 3 of Ref. 18, where the conductance for normal incidence $\theta=0$ is presented (our Fig. 13).

In contrast to Zutic and Valls,[18] due to the unwieldy expressions for the reflection coefficients (see the Appendix A), we are not able to give analytically the condition that yields the largest value of the conductance at zero bias [cf. their Eq. (3.4)]. It is thus not straightforward to identify the proper parameter regime that would yield the maximum value of $G(0)$. We therefore leave the question concerning how spin-flip scattering and a spin-active barrier affect the formation of a ZBCP in a F/S junction as open.

Scattering on the barrier leads to a suppression of the S order parameter close [of the order of the coherence length,

$O(\xi)$] to the junction. For a weakly polarized ferromagnet, we expect that inclusion of a spatial variation of the order parameter does not change our results qualitatively, since it is well known that the approximation of a constant order parameter up to the junction is excellent in a N/*s*-wave superconductor junction (see, e.g., Ref. 29). For a strongly polarized ferromagnet, the superconducting singlet order parameter may, however, be suppressed significantly in the vicinity of the gap.[27] For unconventional pairing symmetries (*d*-wave), it was shown in Ref. 30 that the effect of taking into account the suppression of the order parameter in the presence of Andreev bound surface states remains almost unchanged around zero bias voltage, although a broadening of the ZBCP is observed. Since no zero-energy surface states are present for a pure *s*-wave singlet component of the superconducting order parameter, we believe that our approximation of a step function Δ should be justified.

It is worth noting that a F/S junction as considered here with a spin-active barrier is in some respects similar to previously studied F/F/S junctions[31] if the magnetization directions of the two F layers are noncollinear. While Ref. 31 considers the conductance spectrum in the case of collinear magnetization directions of the F layers, a previous study[32] has developed a quite general framework for dealing with F/S junctions by introducing a phenomenological spin-mixing angle which describes a spin-active interface. In Ref. 32, the conductance is explicitly calculated for a half-metallic ferromagnet/*s*-wave superconductor junction. In the present paper, we have developed a similar framework for treating F/S junctions with a spin-active interface, but using a different formalism. Our theory allows for describing a very wide range of physical phenomena, such as arbitrary magnetization strength and direction of the ferromagnet, a spin-active barrier, Fermi-vector mismatch, and different effective masses in the two systems. We have explicitly computed the conductance spectra for the metallic case with noncollinear magnetizations between the F part and the spin-active barrier in a F/S system. Hence, our work expands on the results of Refs. 31 and 32, and we reproduce their results in the appropriate limits.

The similarity of our model with F/F/S junction with noncollinear magnetizations may be understood by realizing that using a spin basis that diagonalizes the scattering matrix of one ferromagnet will cause the magnetization in the other ferromagnet to effectively look like a spin-flip term and vice versa. Although this analogy could be of some use for comparing the present system under consideration with F/F/S junctions, it should not be taken too far since in our case we are dealing with an insulating, very thin barrier with both magnetic and nonmagnetic scattering potentials as opposed to a conducting ferromagnetic layer.

Another issue that deserves mentioning is that the magnetic field due to the magnetization of the F will penetrate into the thin-film structure of the S along the plane. An in-plane magnetic field may actually coexist uniformly[33] with *s*-wave S in a thin film (in contrast to the bulk case[34,35]), and effects such as orbital pair breaking or formation of vortices will be prohibited as long as the thickness t of the film is less than both λ and ξ_0. It is also reasonable to neglect any exchange interactions in the S since the induced field due to the magnetization is much smaller [of order $O(10^{-3})$] than the exchange field in the F and can thus be safely neglected.[1] Moreover, we stress that the clean limit has been considered in the present paper, which hopefully provides an initial idea of the physics that can be expected when the effect of disorder is included in the system, although this requires a separate analysis.

VI. SUMMARY

In this paper, we have presented a detailed investigation of the conductance spectra of a F/S junction, expanding previous work substantially by allowing for a completely arbitrary direction of magnetization, which effectively accounts for spin-flip scattering due to a planar component of the magnetization and a spin-active barrier. Our procedures amount to an extension of the BTK formalism along the lines of several other workers (e.g., Refs. 19 and 23) and have given us the advantage of obtaining analytical solutions, primarily due to the step-function approximation for the superconducting and magnetic order parameters.

From our results, one may infer that several new qualitative features arise due to the presence of spin-flip scattering and a spin-active barrier. We demonstrate the reentrance of retroreflection for the Andreev-reflected hole, which is absent for an easy-axis ferromagnet with a purely nonmagnetic interfacial scattering potential. This opens up a new transport channel for both spin and charge, and is interpreted as a signature of spin-triplet correlations in the system. In this context, a most interesting interplay between the superconducting phase γ and the planar magnetization orientation characterized by the azimuthal angle ϕ arises in the phase coherence of retroreflected holes. This particular feature may be exploited in terms of a Josephson current in a S/F/S junction that responds to a rotation of ϕ.

As our main result, we have investigated the influence on the conductance spectra due to different effective masses, Fermi-vector mismatch, strength of the exchange energy, and the influence of varying the relative strength of magnetic and nonmagnetic scattering in the F/S junction. Our findings are consistent with those of Ref. 18 with respect to the observation of an increased subgap conductance for increasing Fermi-vector mismatch for a large spin polarization. In the presence of a spin-active barrier, however, this effect vanishes. The general influence of retroreflection on the conductance spectra seems to be a softening of the sharp features such as peaks and dips at $E=\Delta$. Also, as a signature which should be clearly discernable experimentally, a crossover from peak to "waterfall" shape takes place in the tunneling limit at the gap energy.

We believe that our angle of approach for treating the F/S junction in the extended BTK formalism should suffice to shed light on the rich physics and concomitant important phenomena that are present in such systems, which is of particular relevance in the context of spin-polarized tunneling spectroscopy.

ACKNOWLEDGMENTS

J.L. acknowledges useful discussions with M. Gabureac.

This work was supported by Norwegian Research Council Grants Nos. 158518/431, 158547/431 (NANOMAT), and 167498/V30 (STORFORSK).

APPENDIX: DERIVATION OF SCATTERING COEFFICIENTS

From the boundary conditions, the condition of continuity of the wave function yields the expressions

$$s_\uparrow a - s_\downarrow b e^{-i\phi} + r_e^\uparrow - r_e^\downarrow b e^{i\phi} = t_e^\uparrow u + t_h^\downarrow v e^{i\gamma},$$

$$s_\uparrow b e^{-i\phi} + s_\downarrow a + r_e^\uparrow b e^{-i\phi} + r_e^\downarrow a = t_e^\downarrow u - t_h^\uparrow v e^{i\gamma},$$

$$r_h^\uparrow a - r_h^\downarrow b e^{-i\phi} = -t_e^\downarrow v e^{-i\gamma} + t_h^\uparrow u,$$

$$r_h^\uparrow b e^{i\phi} + r_h^\downarrow a = t_e^\uparrow v e^{-i\gamma} + t_h^\downarrow u, \tag{A1}$$

while the matching of derivatives at $x=0$ yields

$$\begin{aligned}
&(V_0 - V_s)(t_e^\uparrow u + t_h^\downarrow v e^{i\gamma}) \\
&\quad = \frac{iq\cos\theta_s}{2m_S}(u t_e^\uparrow - v e^{i\gamma} t_h^\downarrow) \\
&\qquad - \frac{i}{2m_F}[\cos\theta(k^\uparrow s_\uparrow a - k^\downarrow s_\downarrow b e^{i\phi}) - k^\uparrow S a r_e^\uparrow + k^\downarrow \tilde{S} b e^{i\phi} r_e^\downarrow], \\
&(V_0 + V_s)(t_e^\downarrow u - t_h^\uparrow v e^{i\gamma}) \\
&\quad = \frac{iq\cos\theta_s}{2m_S}(u t_e^\downarrow + v e^{i\gamma} t_h^\uparrow) - \frac{i}{2m_F} \\
&\qquad \times[\cos\theta(k^\uparrow s_\uparrow b e^{-i\phi} + k^\downarrow s_\downarrow a) - k^\uparrow S b e^{-i\phi} r_e^\uparrow - k^\downarrow \tilde{S} a r_e^\downarrow], \\
&(V_0 - V_s)(-t_e^\downarrow v e^{-i\gamma} + t_h^\uparrow u) \\
&\quad = -\frac{iq\cos\theta_s}{2m_S}(v e^{-i\gamma} t_e^\downarrow + u t_h^\uparrow) - \frac{i}{2m_F}(k^\uparrow S a r_h^\uparrow - k^\downarrow \tilde{S} b e^{-i\phi} r_h^\downarrow), \\
&(V_0 + V_s)(t_e^\uparrow v e^{-i\gamma} + t_h^\downarrow u) = \frac{iq\cos\theta_s}{2m_S}(t_e^\uparrow v e^{-i\gamma} - t_h^\downarrow u) \\
&\qquad - \frac{i}{2m_F}(k^\uparrow S b e^{i\phi} r_h^\uparrow + k^\downarrow \tilde{S} a r_h^\downarrow).
\end{aligned} \tag{A2}$$

Solving for the transmission coefficients, one is left with the reduced set of equations

$$\begin{aligned}
&t_e^\uparrow A_1 + t_e^\downarrow B_1 e^{i\phi} + t_h^\uparrow C_1 e^{i(\phi+\gamma)} + t_h^\downarrow D_1 e^{i\gamma} = X_1, \\
&t_e^\uparrow A_2 e^{-i\phi} + t_e^\downarrow B_2 + t_h^\uparrow C_2 e^{i\gamma} + t_h^\downarrow D_2 e^{i(\gamma-\phi)} = X_2, \\
&t_e^\uparrow A_3 e^{-i(\phi+\gamma)} + t_e^\downarrow B_3 e^{-i\gamma} + t_h^\uparrow C_3 + t_h^\downarrow D_3 e^{-i\phi} = 0, \\
&t_e^\uparrow A_4 e^{-i\gamma} + t_e^\downarrow B_4 e^{i(\phi-\gamma)} + t_h^\uparrow C_4 e^{i\phi} + t_h^\downarrow D_4 = 0.
\end{aligned} \tag{A3}$$

From Eqs. (A3), one finds that

$$t_h^\downarrow = X_1 F_1 e^{-i\gamma} + X_2 F_2 e^{i(\phi-\gamma)},$$

$$t_h^\uparrow = X_2 R_1 e^{-i\gamma} + R_e t_h^\downarrow e^{-i\phi},$$

$$t_e^\downarrow = P_1 t_h^\uparrow e^{i\gamma} + P_2 t_h^\downarrow e^{i(\gamma-\phi)},$$

$$t_e^\uparrow = -(B_4 t_e^\downarrow e^{i\phi} + C_4 t_h^\uparrow e^{i(\phi+\gamma)} + D_4 t_h^\downarrow e^{i\gamma})/A_4, \tag{A4}$$

such that the reflection coefficients $\{r_h^\sigma, r_e^\sigma\}$ may be obtained by back-substitution of Eqs. (A4) into Eqs. (A1). We have defined the following auxiliary quantities:

$$X_1 = \frac{1}{2m_F}(k^\uparrow \cos\theta s_\uparrow a - k^\downarrow \cos\theta s_\downarrow b e^{i\phi} + k^\uparrow S a s_\uparrow - k^\downarrow \tilde{S} s_\downarrow e^{i\phi}), \tag{A5}$$

$$X_2 = \frac{1}{2m_F}(k^\uparrow \cos\theta b e^{-i\phi} + k^\downarrow \cos\theta s_\downarrow a + k^\uparrow S s_\uparrow e^{-i\phi} + k^\downarrow \tilde{S} s_\downarrow a), \tag{A6}$$

$$F_1 = \left[D_1 + C_1 R_2 + P_1 B_1 R_2 + B_1 P_2 - \frac{A_1}{A_4}(B_4 P_2 + B_4 P_1 R_2 + R_2 C_4 + D_4) \right]^{-1}, \tag{A7}$$

$$F_2 = F_1 \left[\frac{A_1}{A_4}(B_4 P_1 R_1 + R_1 C_4) - B_1 P_1 R_1 - C_1 R_1 \right], \tag{A8}$$

$$R_1 = \left[C_2 + B_2 P_1 - \frac{A_2}{A_4}(B_4 P_1 + C_4) \right]^{-1}, \tag{A9}$$

$$P_1 = \left(\frac{C_4 A_3}{A_4} - C_3 \right) \Big/ \left(B_3 - \frac{A_3 B_4}{A_4} \right), \tag{A10}$$

$$R_2 = R_1 \left[B_2 P_2 + D_2 - \frac{A_2}{A_4}(B_4 P_2 + D_4) \right], \tag{A11}$$

$$P_2 = \left(\frac{D_4 A_3}{A_4} - D_3 \right) \Big/ \left(B_3 - \frac{A_3 B_4}{A_4} \right), \tag{A12}$$

in addition to

$$A_1 = i(V_0 - V_s)u + \frac{1}{2m_S} q\cos\theta_s u + \frac{u}{2m_F}(k^\uparrow S a^2 + k^\downarrow \tilde{S} b^2),$$

$$A_2 = \frac{1}{2m_F}(k^\uparrow S - k^\downarrow \tilde{S}) abu, \tag{A13}$$

$$A_3 = \frac{1}{2m_F}(k^\downarrow \tilde{S} - k^\uparrow S) abv,$$

$$A_4 = i(V_0 + V_s)v + \frac{1}{2m_S} q\cos\theta_s v - \frac{v}{2m_F}(k^\uparrow S b^2 + k^\downarrow \tilde{S} a^2), \tag{A14}$$

$$B_1 = \frac{1}{2m_F}(k^\uparrow S - k^\downarrow \tilde{S}) abu,$$

$$B_2 = \mathrm{i}(V_0 + V_s)u + \frac{1}{2m_\mathrm{S}} q \cos\,\theta_s u + \frac{u}{2m_\mathrm{F}}(k^\uparrow S a^2 + k^\downarrow \widetilde{S} b^2), \tag{A15}$$

$$B_3 = -\mathrm{i}(V_0 - V_s)v - \frac{1}{2m_\mathrm{S}} q \cos\,\theta_s v + \frac{v}{2m_\mathrm{F}}(k^\uparrow S a^2 + k^\downarrow \widetilde{S} b^2),$$

$$B_4 = -\frac{1}{2m_\mathrm{F}}(k^\downarrow \widetilde{S} - k^\uparrow S) abv, \tag{A16}$$

$$C_1 = \frac{1}{2m_\mathrm{F}}(k^\downarrow \widetilde{S} - k^\uparrow S) abv,$$

$$C_2 = -\mathrm{i}(V_0 + V_s)v + \frac{1}{2m_\mathrm{S}} q \cos\,\theta_s v - \frac{v}{2m_\mathrm{F}}(k^\uparrow S b^2 + k^\downarrow \widetilde{S} a^2), \tag{A17}$$

$$C_3 = \mathrm{i}(V_0 - V_s)u - \frac{1}{2m_\mathrm{S}} q \cos\,\theta_s u - \frac{u}{2m_\mathrm{F}}(k^\uparrow S a^2 + k^\downarrow \widetilde{S} b^2),$$

$$C_4 = -\frac{1}{2m_\mathrm{F}}(k^\uparrow S - k^\downarrow \widetilde{S}) abu, \tag{A18}$$

$$D_1 = \mathrm{i}(V_0 - V_s)v - \frac{1}{2m_\mathrm{S}} q \cos\,\theta_s v + \frac{v}{2m_\mathrm{F}}(k^\uparrow S a^2 + k^\downarrow \widetilde{S} b^2),$$

$$D_2 = \frac{1}{2m_\mathrm{F}}(k^\uparrow S - k^\downarrow \widetilde{S}) abu, \tag{A19}$$

$$D_3 = \frac{1}{2m_\mathrm{F}}(k^\downarrow \widetilde{S} - k^\uparrow S) abu,$$

$$D_4 = \mathrm{i}(V_0 + V_s)u - \frac{1}{2m_\mathrm{S}} q \cos\,\theta_s u - \frac{u}{2m_\mathrm{F}}(k^\uparrow S b^2 + k^\downarrow \widetilde{S} a^2). \tag{A20}$$

[1] A. I. Buzdin, Rev. Mod. Phys. **77**, 935 (2005).
[2] I. O. Kulik, Sov. Phys. JETP **30**, 944 (1970).
[3] A. I. Buzdin, A. V. Vedyayev, and N. V. Ryzhanova, Europhys. Lett. **48**, 686 (1999).
[4] L. N. Bulaevskii, V. V. Kuzii, and A. A. Sobyanin, Pis'ma Zh. Eksp. Teor. Fiz., **25**, 314 (1977) [JETP Lett. **25**, 290 (1977)]; A. V. Andreev, A. I. Buzdin, and R. M. Osgood III, Phys. Rev. B **43**, 10124 (1991); F. S. Bergeret, A. F. Volkov, and K. B. Efetov, *ibid.* **64**, 134506 (2001).
[5] V. V. Ryazanov, V. A. Oboznov, A. Y. Rusanov, A. V. Veretennikov, A. A. Golubov, and J. Aarts, Phys. Rev. Lett. **86**, 2427 (2001); A. Bauer, J. Bentner, M. Aprili, M. L. Della-Rocca, M. Reinwald, W. Wegscheider, C. Strunk, *ibid.* **92**, 217001 (2004).
[6] A. F. Andreev, Sov. Phys. JETP **19**, 1228 (1964).
[7] G. Deutscher, Rev. Mod. Phys. **77**, 109 (2005).
[8] M. Weides, M. Kemmler, H. Kohlstedt, A. Buzdin, E. Goldobin, D. Koelle, and R. Kleiner, Appl. Phys. Lett. **89**, 122511 (2006).
[9] J. Y. T. Wei, N.-C. Yeh, D. F. Garrigus, and M. Strasik, Phys. Rev. Lett. **81**, 2542 (1998).
[10] S. S. Saxena, *et al.*, Nature (London) **406**, 587 (2000).
[11] E. Bauer, G. Hilscher, H. Michor, C. Paul, E. W. Scheidt, A. Gribanov, Y. Seropegin, H. Noel, M. Sigrist, and P. Rogl, Phys. Rev. Lett. **92**, 027003 (2004).
[12] T. Akasawa *et al.*, J. Phys.: Condens. Matter **16**, L29 (2004).
[13] S. Kreuzer *et al.*, Appl. Phys. Lett. **80**, 4582 (2002).
[14] V. Garcia, M. Bibes, J.-L. Maurice, E. Jacquet, K. Bouzehouane, J.-P. Contour, and A. Barthelemy, Appl. Phys. Lett. **87**, 212501 (2005).
[15] M. J. M. de Jong and C. W. J. Beenakker, Phys. Rev. Lett. **74**, 1657–1660 (1995).
[16] J. X. Zhu, B. Friedman, and C. S. Ting, Phys. Rev. B **59**, 9558 (1999).
[17] I. Zutic and O. T. Valls, Phys. Rev. B **60**, 6320 (1999).
[18] I. Zutic and O. T. Valls, Phys. Rev. B **61**, 1555 (2000).
[19] S. Kashiwaya, Y. Tanaka, N. Yoshida, and M. R. Beasley, Phys. Rev. B **60**, 3572 (1999).
[20] B. Kastening *et al.*, cond-mat/0610283 (unpublished).
[21] J. Shi, P. Zhang, D. Xiao, and Q. Niu, Phys. Rev. Lett. **96**, 076604 (2006).
[22] G. E. Blonder, M. Tinkham, and T. M. Klapwijk, Phys. Rev. B **25**, 4515 (1982).
[23] Y. Tanaka and S. Kashiwaya, Phys. Rev. Lett. **74**, 3451 (1995).
[24] B. Crouzy, S. Tollis, and D. A. Ivanov, Phys. Rev. B **75**, 054503 (2007).
[25] Z. Pajovic, M. Bozovic, Z. Radovic, J. Cayssol, and A. Buzdin, Phys. Rev. B **74**, 184509 (2006).
[26] F. S. Bergeret, A. F. Volkov, and K. B. Efetov, Phys. Rev. Lett. **86**, 4096 (2001).
[27] M. Eschrig, J. Kopu, J. C. Cuevas, and G. Schon, Phys. Rev. Lett. **90**, 137003 (2003).
[28] T. Tokuyasu, J. A. Sauls, and D. Rainer, Phys. Rev. B **38**, 8823 (1988).
[29] C. Bruder, Phys. Rev. B **41**, 4017 (1990).
[30] Y. Tanaka, T. Asai, N. Yoshida, J. Inoue, and S. Kashiwaya, Phys. Rev. B **61**, R11902 (2000).
[31] K. Kikuchi, H. Imamura, S. Takahashi, and S. Maekawa, Phys. Rev. B **65**, 020508(R) (2001).
[32] J. Kopu, M. Eschrig, J. C. Cuevas, and M. Fogelström, Phys. Rev. B **69**, 094501 (2004).
[33] R. Meservey and P. M. Tedrow, Phys. Rep. **238**, 173 (1994).
[34] E. I. Blount and C. M. Varma, Phys. Rev. Lett. **42**, 1079 (1979); **43**, 1843 (1979).
[35] R. Shen, Z. M. Zheng, S. Liu, and D. Y. Xing, Phys. Rev. B **67**, 024514 (2003).
[36] In general, there is also a contribution $e^{-i[\arccos(E/\Delta)]}$ for $E<\Delta$, but this is irrelevant for the present discussion.

Paper V

Josephson effect in thin-film superconductor/insulator/superconductor junctions with misaligned in-plane exchange fields.

Physical Review B **76**, 064524 (2007).

Josephson effect in thin-film superconductor/insulator/superconductor junctions with misaligned in-plane magnetic fields

J. Linder[1] and A. Sudbø[1,2]
[1]*Department of Physics, Norwegian University of Science and Technology, N-7491 Trondheim, Norway*
[2]*Center for Advanced Study, The Norwegian Academy of Science and Letters, N-0271 Oslo, Norway*
(Received 11 December 2006; revised manuscript received 10 April 2007; published 20 August 2007)

We study a tunnel junction consisting of two thin-film *s*-wave superconductors separated by a thin, insulating barrier in the presence of misaligned in-plane exchange fields. We find an interesting interplay between the superconducting phase difference and the relative orientation of the exchange fields, manifested in the Josephson current across the junction. Specifically, this may be written $I_J^C=(I_0+I_m\cos\varphi)\sin\Delta\theta$, where I_0 and I_m are constants, and φ is the relative orientation of the exchange fields, while $\Delta\theta$ is the superconducting phase difference. Similar results have recently been obtained in other superconductor-insulator-superconductor junctions coexisting with helimagnetic or ferromagnetic order. We calculate the superconducting order parameter self-consistently, and investigate quantitatively the effect which the misaligned exchange fields constitute on the Josephson current, to see if I_m may have an appreciable effect on the Josephson current. It is found that I_0 and I_m become comparable in magnitude at sufficiently low temperatures and fields close to the critical value, in agreement with previous work. From our analytical results, it then follows that the Josephson current in the present system may be controlled in a well-defined manner by a rotation of the exchange fields on both sides of the junction. We discuss a possible experimental realization of this proposition.

DOI: 10.1103/PhysRevB.76.064524 PACS number(s): 74.20.Rp, 74.50.+r, 74.20.−z

I. INTRODUCTION

The study of physical effects that arise due to an interplay between superconductivity (SC) and ferromagnetism (FM) has grown considerably over the last decade (see Refs. 1 and 2 and references therein). Much effort has been devoted to obtaining a better understanding of the exotic phenomena that may appear in heterostructures of superconductors and ferromagnets. To mention a few of these, it is natural to highlight the study of π junctions, both theoretically[3] and experimentally,[4] and the proximity effects giving rise to induced SC correlations in normal metals, half-metals, and FM metals[5,6] as prime examples of the potential that lies within this field of research. Also, quite recently, the coexistence of SC and FM in the same material was discovered in[7,8] UGe_2 and URhGe, and possibly[9,10] also in $ZrZn_2$. Such ferromagnetic superconductors (FMSCs) display simultaneously multiple broken symmetries [SU(2) and U(1)], an interesting property that may be exploited in terms of dissipationless quantum transport of spin and/or charge between such materials.[11–13]

Besides the interest have a fundamental physics point of view, transport properties in SC/FM heterostructures have currently attracted much attention, since it is hoped that the new physics that emerges in this type of systems may be useful for applications in nanotechnology and spintronics.[14] The discoveries of unconventional superconductors displaying *d*-wave singlet,[15] *p*-wave triplet,[16] and even mixed singlet-triplet SC pairing symmetries[17,18] offer the theoretician a true goldmine in terms of rich physics and opportunities to explore. In the present paper, however, we will be concerned with a system of two thin-film spin-singlet *s*-wave superconductors separated by a thin, insulating barrier in the presence of a misaligned in-plane exchange field. This would be equivalent to a ferromagnet-superconductor-insulator-superconductor-ferromagnet (F/S/I/S/F) system assuming that the S/F bilayer is thin and thus may be represented by a Bardeen-Cooper-Schrieffer (BCS) superconductor[38] in the presence of a homogeneous magnetic field.[19] Indeed, for superconducting films of thickness $t<\xi\ll\lambda$, where ξ is the coherence length (average size of the Cooper pairs) and λ is the magnetic field penetration depth, a magnetic field which is applied in the plane of the film will penetrate it practically uniformly. In this case, the Meissner effect response of the superconductor is incomplete, such that the screening currents are minimal.[20] Since orbital effects are suppressed in such a geometry, the critical field is determined by the paramagnetic limitation. Such types of systems have been considered earlier.[21–24] Nevertheless, we hope to shed some light on a matter which has not been investigated extensively in such systems: manipulating a supercurrent of spin and/or charge by controlling a misalignment of magnetic fields present on both sides of the barrier. Such a proposition was made by Kulic and Kulic[11] in 2001 (albeit in a physically completely different system), who derived an expression for the Josephson current over a junction separating two spin-singlet superconductors with spiral magnetic order. It was found that the supercurrent could be controlled by adjusting the relative orientation of the exchange field on both sides of the junction, a finding that quite remarkably suggested a way of tuning a supercurrent in a well-defined manner from, e.g., a 0 to π junction. However, from an experimental point of view such states are very hard to realize. Moreover, it is extremely difficult, if not impossible, to control the magnetization misalignment across the tunneling junction for such a system. Later investigations made by Eremin, Nogueira, and Tarento[12] considered a similar system as Kulic and Kulic: namely, two Fulde-Ferrel-Larkin-Ovchinnikov (FFLO) superconductors[25] coexisting with helimagnetic order.[26] Recently, the same effect was found to exist in a FMSC/I/

FMSC junction as shown by Grønsleth *et al.*,[13] a system which presumably has a much better potential for being realized.

In the present paper, we show that a similar effect may be realized by applying misaligned in-plane exchange fields in a thin-film F/S/I/S/F junction, where S represents an *s*-wave thin-film superconductor in an external magnetic field provided by F (a ferromagnet). Such a system should be possible to realize experimentally. We derive the linear-response expression for the Josephson current within the Matsubara formalism and solve for the SC order parameter self-consistently, thereafter providing numerical results for the supercurrent that arises in the system for arbitrary misalignment of the magnetic field across the junction. We investigate under what experimental conditions the predicted modulation of the total Josepshon current is most easily observed. We also suggest an experimental setup to test these predictions.

This paper is organized as follows. In Sec. II, we establish our model and the formulation to be used throughout the paper and solve for the SC order parameter self-consistently. The Josephson current is calculated within the tunneling Hamiltonian formalism in Sec. III. Our main findings for the numerical values of the parameters that determine the modulation of the Josephson current as a function of the twist in the orientation of the exchange fields on both sides of the junction are presented in Sec. IV with a discussion given in Sec. V. In this section, we also provide a description of a possible heterostructure for realizing the physical situation we describe in this paper. Specifically, we suggest how one may be able to physically misalign an external field across the tunneling junction (by an arbitrary amount). Finally, we summarize our results in Sec. VI and reemphasize what our findings are compared to previous results.

II. MODEL AND FORMULATION

The total Hamiltonian H for a system consisting of two superconductors separated by an insulating layer in the presence of an in-plane exchange field can be written as[27] $H=H_{\mathrm{L}}+H_{\mathrm{R}}+H_{\mathrm{T}}$, where L and R represent the individual superconductors on each side of the tunneling junction and H_{T} describes tunneling of particles through the insulating layer separating the two superconductors. At the level of mean-field theory the individual superconductors are described by

$$H = H_0 + \sum_{\mathbf{k}} \varphi_{\mathbf{k}}^{\dagger} \mathcal{A}_{\mathbf{k}} \varphi_{\mathbf{k}}, \tag{1}$$

where H_0 is given by

$$H_0 = \sum_{\mathbf{k}} \xi_{\mathbf{k}} - \sum_{\mathbf{k}} \Delta^{\dagger} b_{\mathbf{k}} + \frac{|\mathbf{H}|^2}{2\mu_0},$$

$$\mathcal{A}_{\mathbf{k}} = \begin{pmatrix} \xi_{\mathbf{k}} - h & \Delta e^{i\theta} \\ \Delta e^{-i\theta} & -\xi_{\mathbf{k}} - h \end{pmatrix}. \tag{2}$$

Here, $\mathbf{k}$ is the electron momentum, $\xi_{\mathbf{k}}=\varepsilon_{\mathbf{k}}-\mu$, $\sigma=\uparrow,\downarrow=\pm 1$, μ is the chemical potential (which at $T=0$ is completely equivalent to the Fermi energy), $\mathbf{H}$ is the magnetic field, h is the exchange energy, and μ_0 is the magnetic permeability, while $\Delta e^{i\theta}$ is the superconducting order parameter and $b_{\mathbf{k}}=\langle c_{-\mathbf{k}\downarrow} c_{\mathbf{k}\uparrow}\rangle$ denotes the two-particle operator expectation value. Equation (2) is valid for an *s*-wave superconductor with an in-plane exchange field giving rise to an exchange interaction. At this point, some comments are in order. We assume that no vortices are present in the system. This puts limitations on the dimension of the thin film. Our assumption of a homogeneous exchange field in the superconductors can only be justified given that the thickness of the film is smaller than[20] both the penetration depth λ and coherence length ξ. The physical reason for this is that an externally applied in-plane magnetic field is found to penetrate the superconductor without creating vortices as long as there is no room for the vortices, which typically have a diameter of $\mathcal{O}(\xi)$. This amounts to a thickness of order 10 nm, which is well within reach of current experimental techniques.

Moreover, we will neglect phase fluctuations and amplitude fluctuations in the superconducting order parameter in this paper. Amplitude fluctuations may safely be neglected.[28,29] In a strong type-II superconductor, neglecting critical fluctuations (which are transverse phase fluctuations, or equivalently vortices) is certainly not valid close enough to the normal-metal–superconductor transition.[28,29] In type-II superconductors, neglect of critical fluctuations is expected to be reasonable provided we are outside the critical region, which is expected to be quite narrow around the critical temperature and critical field unless the superconductors are of the extreme type II.[28,29] In deep type-I superconductors, the mean-field approximation is expected to be excellent in any case, since the phase transition in such systems is of first order.[30–32]

In Eq. (1), our basis is

$$\varphi_{\mathbf{k}} = (c_{\mathbf{k}\uparrow} c_{-\mathbf{k}\downarrow}^{\dagger})^{\mathrm{T}}, \tag{3}$$

where $\{c_{\mathbf{k}\sigma}, c_{\mathbf{k}\sigma}^{\dagger}\}$ are annihilation and creation fermion operators with momentum $\mathbf{k}$ and spin σ. By diagonalizing Eq. (2) through $\mathcal{A}_{\mathbf{k}}=P_{\mathbf{k}} D_{\mathbf{k}} P_{\mathbf{k}}^{\dagger}$, Eq. (1) turns into

$$H = H_0 + \sum_{\mathbf{k}} \tilde{\varphi}_{\mathbf{k}}^{\dagger} D_{\mathbf{k}} \tilde{\varphi}_{\mathbf{k}}, \tag{4}$$

where the diagonal matrix reads $D_{\mathbf{k}}=\mathrm{diag}(E_{\mathbf{k}\uparrow}, E_{\mathbf{k}\downarrow})$ and the basis $\tilde{\varphi}_{\mathbf{k}}$ consists of new fermion operators according to

$$\tilde{\varphi}_{\mathbf{k}} = P_{\mathbf{k}}^{\dagger} \varphi_{\mathbf{k}} = (\mathcal{C}_{\mathbf{k}\uparrow} \mathcal{C}_{-\mathbf{k}\downarrow}^{\dagger})^{\mathrm{T}}. \tag{5}$$

Upon defining the auxiliary quantity

$$R_{\mathbf{k}} = \frac{\Delta}{\xi_{\mathbf{k}} + \sqrt{\xi_{\mathbf{k}}^2 + \Delta^2}}, \tag{6}$$

the diagonalization matrix may be written as

$$P_{\mathbf{k}} = N_{\mathbf{k}} \begin{pmatrix} 1 & -R_{\mathbf{k}} e^{i\theta} \\ R_{\mathbf{k}} e^{-i\theta} & 1 \end{pmatrix},$$

$$N_{\mathbf{k}} = 1/\sqrt{1+R_{\mathbf{k}}^2}. \tag{7}$$

We find that the energy eigenvalues may be written as

$$E_{\mathbf{k}\sigma} = \sigma\sqrt{\xi_{\mathbf{k}}^2 + \Delta^2} - h. \tag{8}$$

Concerning ourselves with s-wave pairing ($\mathbf{k}$-independent gap), we note that $E_{\mathbf{k}\sigma}=E_{-\mathbf{k}\sigma}$, which allows us to recast Eq. (4) into the form

$$H = H_0 - \sum_{\mathbf{k}} E_{\mathbf{k}\downarrow} + \sum_{\mathbf{k}\sigma} \sigma E_{\mathbf{k}\sigma} \mathcal{C}_{\mathbf{k}\sigma}^{\dagger} \mathcal{C}_{\mathbf{k}\sigma}. \tag{9}$$

The self-consistent gap equations are derived from the free energy given by

$$F = H_0 - \sum_{\mathbf{k}} E_{\mathbf{k}\downarrow} - \frac{1}{\beta} \sum_{\mathbf{k}\sigma} \ln(1 + \mathrm{e}^{-\beta\sigma E_{\mathbf{k}\sigma}}). \tag{10}$$

yielding the self-consistency equation

$$g(\Delta) \equiv 1 - \frac{c}{2} \int_{-\omega_0}^{\omega_0} \mathrm{d}\xi \left\{ \frac{1 - f[E_{\uparrow}(\xi)] - f[-E_{\downarrow}(\xi)]}{\sqrt{\xi^2 + \Delta^2}} \right\} = 0, \tag{11}$$

where the weak-coupling constant $c=VN(0)$ is set to 0.2 hereafter, while ω_0 is arbitrarily set to 1% of the Fermi energy, i.e., $\mu/100$, which corresponds to $\omega_0/\Delta \approx 70$, which essentially is equivalent to $\omega_0/\Delta \to \infty$. ($\omega_0/\Delta \approx 10$ suffices to achieve this limit in the quantities we consider in this paper.) In the limit of zero exchange field, $h \to 0$, the well-known result (see, e.g., Ref. 23) is obtained. The Fermi-Dirac distribution functions entering in Eq. (11) are given as $f(\xi) = 1/(1+\mathrm{e}^{\beta\xi})$ where β is inverse temperature. We have introduced the usual simplification of a pairing potential that is attractive in a small energy interval around the Fermi level,

$$V_{\mathbf{k}\mathbf{k}'\alpha\beta} = -V \quad \text{for} \quad |\xi_{\mathbf{k}(\mathbf{k}')} - \mu| < \omega_0, \tag{12}$$

with $(V>0)$ and zero otherwise. Here, ω_0 is a typical frequency cutoff defining the spectral width of the bosons responsible for the pairing. We do not further specify what these bosons are. Equation (11) will be the governing equation for the gap $\Delta=\Delta(T,h)$ at an arbitrary temperature and arbitrary in-plane exchange field. The orbital effect from the exchange field in this configuration is suppressed, since the electrons are restricted from moving in the $\hat{\mathbf{z}}$ direction due to the thin-film structure.

The order parameter may now be solved for numerically by integrating the gap equation (11). Consider first the zero-temperature case, where we have plotted the dependence of $g(\Delta)$ on h in Fig. 1, such that the possible solutions are identified by locating the intersection with the dotted line defined by $g(\Delta)=0$. In agreement with previous results,[25] we find that for $h/\Delta_0 < 0.5$ there is a unique solution of $\Delta(0,h)$ that satisfies $g[\Delta(0,h)]=0$, while another solution $\Delta(0,h) < \Delta_0$ is present for $0.5 < h/\Delta_0 < 1.0$. However, this has been found to be unstable, such that we will only consider the solution for the largest gap.[25] In this case, one may simply write

$$\Delta(0,h) = \begin{cases} \Delta_0 & \text{if } h < \Delta_0, \\ 0 & \text{if } h > \Delta_0. \end{cases} \tag{13}$$

In the inset of Fig. 1, we have plotted the field dependence of the stable solution $\Delta(0,h)$. As shown, there is a first-order phase transition at $h=\Delta_0$ whereas the gap remains independent on h for $h<\Delta_0$. Consider now the dependence of the critical temperature as a function of h, illustrated in Fig. 2. Effectively, the T_c vs h curve gives the phase diagram of a superconductor with an in-plane exchange field. Note that although a nonzero solution for Δ exists under the dotted line in Fig. 2, one must turn to free energy considerations in order to determine whether the normal state or superconducting state is favored. Such a study was undertaken in Ref. 19 (see

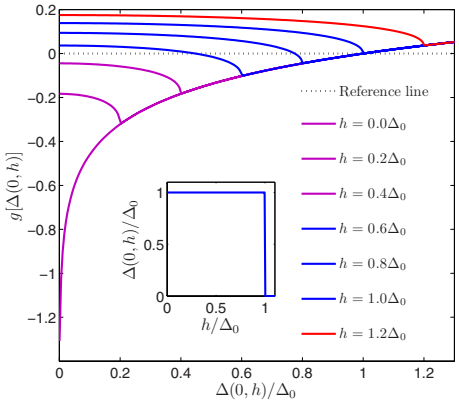

FIG. 1. (Color online) Plot of the function $g[\Delta(0,h)]$ given by Eq. (11) to illustrate the possible solutions for the gap, given by where the curves intersect the dotted line. When $h/\Delta_0 > 0.5$, there is more than one solution to the gap equation, but only one of these is stable. As shown in the inset, where we have plotted the field dependence of this stable solution, a first-order phase transition to the normal state is present at zero temperature.

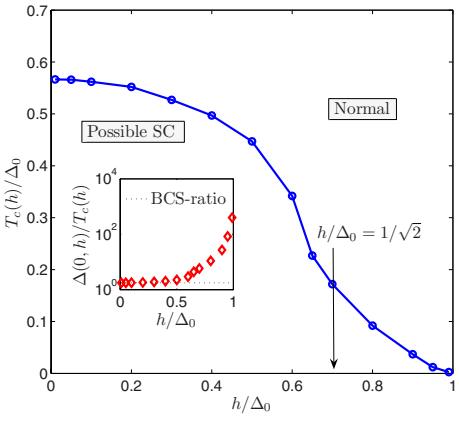

FIG. 2. (Color online) The phase diagram in the $h-T$ plane for a superconductor in the presence of an exchange field. A nonzero solution for the gap exists under the dotted line, indicating a possible SC phase. The exact regime where SC is energetically favored over the normal state was studied in Ref. 19; see their Fig. 1. Since the phase transition is first order, note that the ratio $\Delta(T,h)/T_c(h)$ is not constant as in the pure BCS case, as shown in the inset.

TABLE I. Critical field at the five representative temperatures we will study (Ref. 19).

Temperature T/Δ_0	Critical field h_c/Δ_0
0.001	0.70
0.1	0.68
0.2	0.65
0.3	0.52
0.4	0.35

their Fig. 1). The Clogston-Chandrasekhar critical field $h=\Delta_0/\sqrt{2}$ at $T=0$ is also given in the Fig. 2.[33,34] In the present paper, we will be concerned with the field dependence of the physical quantities and thus choose five representative temperatures (see Table I) at which the SC state is indeed the thermodynamical state favored, as given by Ref. 19.

Finally, we give a plot of the field dependence of Δ at finite temperatures, illustrated in Fig. 3. It is seen that the phase transition at the critical field remains discontinuous also at finite temperatures.[35–37]

III. JOSEPHSON CURRENT

In order to calculate the Josephson charge current over the junction,[38] we make use of the equilibrium Matsubara Green's-function formalism at finite temperatures (see, e.g., Ref. 39). Since we are interested in misaligned exchange fields on both sides of the junction, we will use different quantization axes on the left and right sides of the barrier. By including the Wigner d function,[40] one may then account for the fact that an $\uparrow$ spin on one side of the junction is not the same as an $\uparrow$ spin on the other side. Defining

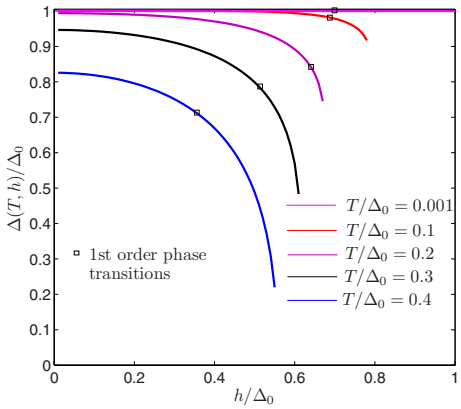

FIG. 3. (Color online) Field dependence h of the superconducting order parameter $\Delta=\Delta(T,h)$ at finite temperatures. The sudden end of the curves clearly shows the sharp drop in the gap, indicating a discontinuous nature of the normal metal-superconductor phase transition.

$$\mathcal{D}(\varphi)=\begin{pmatrix}\cos(\varphi/2) & -\sin(\varphi/2)\\ \sin(\varphi/2) & \cos(\varphi/2)\end{pmatrix}, \tag{14}$$

the tunneling Hamiltonian of the present system may be written as

$$H_T=\sum_{\mathbf{kp}\sigma\sigma'}[\mathcal{D}(\varphi)]_{\sigma\sigma'}\mathcal{T}_{\mathbf{kp}}c^\dagger_{\mathbf{k}\sigma}d_{\mathbf{p}\sigma'}+\text{H.c.} \tag{15}$$

Above, $c_{\mathbf{k}\sigma}$ designates fermion operators on the right side of the junction, while $d_{\mathbf{p}\sigma}$ represents fermion operators on the left side of the junction, and $\mathcal{T}_{\mathbf{kp}}$ is the tunneling probability amplitude. The Josephson charge current is now defined as

$$I_J(t)=-e\left\langle\frac{dN_L(t)}{dt}\right\rangle, \tag{16}$$

where the time derivative of the number operator is given by

$$\frac{dN_L(t)}{dt}=ie^{iH't}[H_t,N_L]e^{-iH't}. \tag{17}$$

We have defined $H'=H_L+H_R$ and only taken into account the contribution from the tunneling Hamiltonian to the time derivative. In this way, the calculated current will only consist of processes corresponding to physical transport across the junction and not any additional contributions originating from a lack of particle conservation number on each side of the junction, respectively. The procedure to obtain $I(t)$ is now fairly straightforward and may be reviewed in, e.g., Refs. 11–13 and 41. We find that at zero applied voltage, the Josephson current is time independent and reads

$$I_J=(I_0+I_m\cos\varphi)\sin\Delta\theta, \tag{18}$$

where φ is the relative orientation of the exchange fields and $\Delta\theta$ is the superconductivity phase difference across the junction. This establishes a Josephson current which may be controlled through an adiabatic rotation of misaligned exchange fields in a planar S/I/S system, or equivalently an F/S/I/S/F layer. While it is not clear how the exchange field could be experimentally controlled in a well-defined manner in junctions with BCS[11] and FFLO[12] superconductors coexisting with helimagnetic order, where this effect has been discussed previously,[11,12] we will proceed to show that experimental verification of this type of effect should be more feasible in the present system. The amplitudes entering in Eq. (18) read

$$I_0=2e\mathcal{T}^2\sum_{\mathbf{kp}}N^2_{\mathbf{k}}R_{\mathbf{k}}N^2_{\mathbf{p}}R_{\mathbf{p}}F^+_{\mathbf{kp}},$$

$$I_m=2e\mathcal{T}^2\sum_{\mathbf{kp}}N^2_{\mathbf{k}}R_{\mathbf{k}}N^2_{\mathbf{p}}R_{\mathbf{p}}F^-_{\mathbf{kp}}, \tag{19}$$

where $\mathcal{T}=|\mathcal{T}_{\mathbf{kp}}|$ is the tunneling amplitude (see discussion below) and

$$F^\pm_{\mathbf{kp}}=\sum_{\alpha\beta}\alpha\beta\left[\frac{f(E_{\mathbf{k}\sigma})-f(E_{\mathbf{p}\beta})}{E_{\mathbf{k}\alpha}-E_{\mathbf{p}\beta}}\pm\frac{1-f(E_{\mathbf{k}\alpha})-f(E_{\mathbf{p}\beta})}{E_{\mathbf{k}\alpha}+E_{\mathbf{p}\beta}}\right]. \tag{20}$$

Note that when the exchange field vanishes, we have that $F^-_{\mathbf{kp}}=0$, such that $I_m=0$. In general; therefore, for weak ex-

change fields we expect that $I_m \ll I_0$. Hence, an appreciable amount of modulation of the total Josephson current I_J by a twist in the magnetization across the junction will require a certain amount of fine-tuning. We will detail this below.

IV. RESULTS

We now consider the Josephson current as a function of both temperature and twist in the exchange fields upon insertion of the self-consistent solutions of $|\Delta(T,h)|$ into the expression for the Josephson current, Eq. (18). To this end, we replace summation over momenta by integration over energies by means of the formula

$$\frac{1}{N}\sum_{\mathbf{k}} \mathcal{F}_{\mathbf{k}} = \int\int \mathrm{d}\varepsilon\, \mathrm{d}\Omega\, N(\varepsilon,\Omega)\mathcal{F}(\varepsilon,\Omega), \tag{21}$$

where $\int \mathrm{d}\Omega$ corresponds to an angular integration over a constant sheet of energy ε in momentum space, $N(\varepsilon,\Omega)$ is the angularly resolved density of states, and $\mathcal{F}(\varepsilon,\Omega) = \mathcal{F}[\mathbf{k}(\varepsilon,\Omega)]$ is an arbitrary function. In general, it is necessary to specify the nature of the tunneling matrix element in some detail, since the crude approximation $|\mathcal{T}_{\mathbf{kp}}|^2 = \mathcal{T}^2$ may lead to unphysical results.[42] A plausible conjecture for the tunneling matrix element should incorporate two key elements: (i) quasiparticles moving perpendicularly towards the junction should have a higher probability of tunneling than quasiparticles moving parallel to it, and (ii) the direction of momentum should be conserved in the tunneling-process; i.e., a right-moving quasiparticle on the left side of the junction should only tunnel into a right-moving quasiparticle on the right side of the junction and vice versa. However, due to the isotropic gap in the present system, taking into account explicitly the angular dependence of the tunneling probability merely corresponds to a numerical prefactor. For anisotropic superconductors with **k**-dependent gaps, such an approximation is clearly not valid. Similarly to Ref. 43, one should then make the ansatz

$$|\mathcal{T}_{\mathbf{kp}}|^2 = \mathcal{T}^2 \sin\vartheta_{\mathrm{R}} \sin\vartheta_{\mathrm{L}} \Theta[\mathrm{sgn}(\sin\vartheta_{\mathrm{R}})\mathrm{sgn}(\sin\vartheta_{\mathrm{L}})], \tag{22}$$

where $\mathcal{T}$ is a real constant and the angles entering in Eq. (22) define the trajectories of the quasiparticles involved in tunneling; see Fig. 4.

Having stated this, we are now able to investigate quantitatively how the Josephson charge current in our system depends on the relative orientation of the exchange fields on both sides of the junction. The misalignment φ of the exchange fields enters the expression for the Josephson charge current through Eq. (18), which accounts for the qualitative behavior. Converting the summation to integration as described above, we obtain

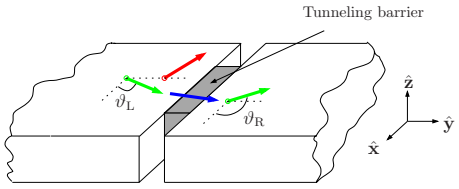

FIG. 4. (Color online) The tunneling scenario illustrated for two quasiparticles approaching the barrier separating the superconductors. For incoming momenta with a large component perpendicular to the barrier (green), tunneling occurs with greater probability than for incoming momenta with a small component perpendicular to the barrier (red). The sign of the component of momentum perpendicular to the barrier must be preserved in the process. For *s*-wave superconductors, the tunneling matrix element may be approximated by a constant, while it may not for anisotropic superconductors.

$$I_0 = 2e\mathcal{T}^2[N(0)]^2\Delta(T,h)^2 \int_{-\omega_0}^{\omega_0}\int_{-\omega_0}^{\omega_0} F^{+}(\xi_1,\xi_2) \times \prod_{i=1,2}\left[\left(1+\frac{[\Delta(T,h)]^2}{\{\xi_i+\sqrt{\xi_i^2+[\Delta(T,h)]^2}\}^2}\right)^{-1} \times \frac{\mathrm{d}\xi_i}{\xi_i+\sqrt{\xi_i^2+[\Delta(T,h)^2]}}\right], \tag{23}$$

while I_m is given by the above expression by performing the substitution $F^{+}(\xi_1,\xi_2) \to F^{-}(\xi_1,\xi_2)$. However, it is obvious that if $I_0 \gg I_m$, the effect of rotating φ will be very small. For the purpose of obtaining a Josephson current which may be controlled by rotating the exchange fields, we are interested in obtaining I_m as large as possible. To see if this is possible, we need to investigate under what circumstances varying φ will have an appreciable effect on the total Josephson current. Earlier works[19,24] have considered similar systems as the one considered in this paper, but restricted the exchange field orientations to be either parallel or antiparallel. Hence, our work represents a considerable extension of these results. Furthermore, we explicitly compute the relative magnitude between the term I_m, which provides the possibility of controlling I_J by rotating φ, and the "intrinsic" Josephson term I_0. Consider Fig. 5 for a plot of $I_0/2e[N(0)]^2\mathcal{T}^2\pi^2$ and $I_m/2e[N(0)]^2\mathcal{T}^2\pi^2$ and Fig. 6 for the total Josephson current I_J, as a function of h/Δ_0 for several values of T/Δ_0. From Fig. 5, it is seen that I_m is nonzero only when $h \to h_c$ for any temperature. This suggests that the Josephson current will only respond to a rotation of the exchange fields through the $I_m \cos\varphi$ term at very low temperatures and fields close to their critical values. Specifically, for the parallel and antiparallel configurations, this statement is consistent with the findings of Refs. 19 and 24. In general, however, we have here shown that an adiabatic rotation of φ may offer a well-defined mechanism of tuning the magnitude of the Josephson current, as shown in Fig. 7. One infers that the increase of I_J may be as large as 20%. Note that the formal logarithmic divergence of the current in Fig. 6 for $h \to \Delta_0$ when $T \to 0$

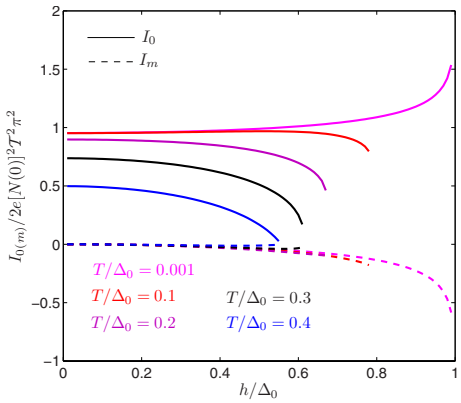

FIG. 5. (Color online) Plot of the components I_0 and I_m as a function of exchange field h for several temperatures T. It is seen that I_m becomes nonzero only as h increases towards Δ_0, such that the Josephson current is only sensitive to a rotation of the misorientation of the exchange fields in this regime.

may be removed by considering higher orders of the tunneling matrix probability.[24] Practically speaking, this divergence is clearly not of any concern since the critical field is determined by Table I, which states that $h_c/\Delta_0 \to 1/\sqrt{2}$ as $T \to 0$.

V. DISCUSSION

A possible realization of the system proposed in the present paper could be achieved by either applying external magnetic fields to a thin-film S/I/S structure or by considering two thin S/F bilayers with misaligned magnetization orientations separated by a thin, insulating barrier (see Fig. 8). In such a geometry, the influence of the FM layers is non

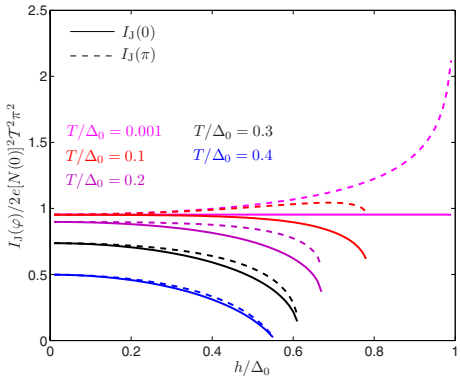

FIG. 6. (Color online) Plot of the total Josephson current in the parallel $I_J(0)$ and antiparallel $I_J(\pi)$ configurations of the exchange fields on both sides of the junction. It is seen that the Josephson current is actually enhanced with increasing field strength for the antiparallel configuration for low enough temperatures, in agreement with the result of Refs. 19 and 24.

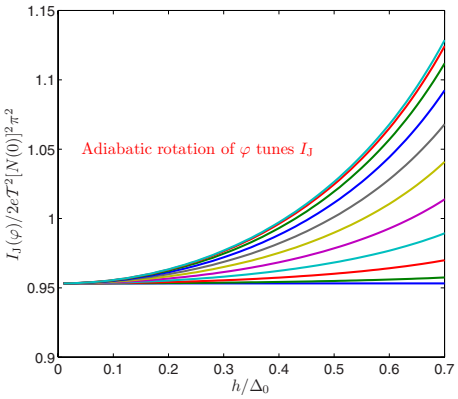

FIG. 7. (Color online) Plot of the total Josephson charge current at $T/\Delta_0=0.001$ as a function of h up to the critical field $h_c=0.7\Delta_0$ in the presence of an adiabatic rotation of φ, ranging from $\varphi=0$ to $\varphi=\pi$ in steps of 0.1π from bottom to top.

local in the superconductor, such that the exchange field may be considered homogeneous.[6] Another important point concerns the thickness of the superconducting films, which would need to fulfill $d < \xi \ll \lambda$ in order for the exchange field to penetrate the film uniformly (note that the screening currents giving rise to the Meissner effect are suppressed in this geometry),[20] although making the film too thin could give rise to problems with T_c being too small.[44] Moreover, it is likely that the Josephson current would display a Fraunhofer diffraction pattern if one cannot find a way of avoiding magnetic flux from the FM layers to penetrate the barrier. In this respect, the antiparallel alignment of the exchange fields is probably the most promising, since the flux penetration of the barrier could be expected to cancel out. Applying a field perpendicular to the stack would not give rise to a Fraunhofer diffraction pattern, but since the demagnetization factor n in such a geometry is close to 1, the critical field would be very small.[44] Recall that the relation between an applied field $\mathbf{H}_a$ and the field set up by the superconductor $\mathbf{H}_i$ may be written as[45]

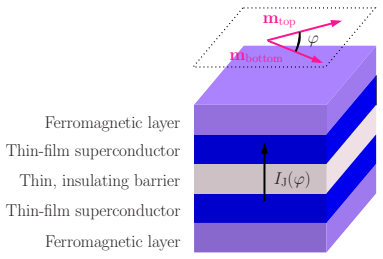

FIG. 8. (Color online) Suggested experimental setup for achieving homogeneous exchange fields in the superconductor. The antiparallel alignment of the exchange fields is probably the most viable to realize in order to avoid the Fraunhofer diffraction of the resulting Josephson current.

$$\mathbf{H}_{\mathrm{i}} = \frac{1}{1-n}\mathbf{H}_{\mathrm{a}}. \tag{24}$$

In the present paper, we have studied the tunneling limit equivalent to a low-transparency barrier. The effect of increasing the transparency of the barrier was treated within the Blonder-Tinkham-Klapwijk-formalism[46] in Ref. 19, where it was found that I_{J} was no longer enhanced by increasing h, regardless of whether the orientation of the exchange fields was parallel or antiparallel. In the high-transparency case, I_{J} actually decreased more rapidly as a function of h when $\varphi=\pi$ compared to $\varphi=0$. This shows that the Josephson current would still be sensitive to a rotation of φ, although now the $\varphi=0$ configuration would correspond to the largest critical current.

If an experimental setup as suggested here could be realized, the effect of the interplay between φ and $\Delta\theta$ in I_{J} may be observed in the following manner. For a superconductor/superconductor junction, the critical Josephson current is detected through the emission of microwave radiation with a power determined by the magnitude of the current and by the rate of change of the relative orientation between the exchange fields on both sides of the junction. This is the magnetic analogy of supplying an electrostatic potential to maintain an ac Josephson effect in the charge channel. In this way, one maintains the ac oscillations in the Josephson current by rotating the exchange fields, even in the absence of an electrostatic voltage. Hence, a feasible experimental verification of the effect we predict in this paper would be the detection of microwave radiation associated with an ac Josephson effect originating with a rotating magnetic field such that the misalignment angle varies with time. Note that rotating the fields on both sides of the junction with equal frequencies gives no ac effect.

We close by reemphasizing that the above ideas should be experimentally realizable by, e.g., utilizing various geometries in order to vary the demagnetization fields. Alternatively, one may use exchange biasing to an antiferromagnet by depositing an antiferromagnetic layer on top of the whole structure shown in Fig. 8. Techniques of achieving noncollinearity are routinely used in ferromagnet–normal-metal structures.[47]

VI. SUMMARY

In this paper, we have studied the Josephson charge current that arises over a junction separating two thin-film s-wave singlet superconductors in the presence of misaligned in-plane exchange fields. A possible realization of such a system is visualized in Fig. 8, where the idea is that a thin S/F layer may be considered as a superconductor with a homogeneous exchange field present.[20] The analytical solution within the Matsubara formalism reveals an interplay between the misorientation of the exchange fields, described by the angle φ, and the SC phase difference $\Delta\theta$ through the relation $I_{\mathrm{J}}=(I_0+I_m\cos\varphi)\sin\Delta\theta$, where I_0 and I_m are real constants. Using a self-consistently obtained solution of the SC order parameter, we obtain a numerical plot of the Josephson current for arbitrary exchange fields and temperatures. Specifically, we examine the magnitude of I_0 and I_m in order to investigate whether the I_m term may contribute significantly to I_{J} or not. While previous works have considered only the parallel ($\varphi=0$) or antiparallel ($\varphi=\pi$) configurations of the fields, our results show that the Josephson current will respond to any rotation of the orientation of the fields through the term $I_m\cos\varphi$. Consequently, we have analytically and numerically made an important distinction between the contributions to I_{J} that stem from an "intrinsic" Josephson term I_0 and the term I_m that allows for a manipulation of the Josephson current through a tuning of φ. This clarifies exactly how I_{J} depends on the field orientations in any configuration. We find that I_0 and I_m become comparable only for values of the exchange field close to the critical value. In this case, the Josephson charge current may be enhanced by the presence of the exchange fields and controlled in a well-defined manner by adiabatically rotating the field directions on each side of the junction.

ACKNOWLEDGMENTS

J.L. gratefully acknowledges G. Burnell for very helpful comments with regard to experimental considerations and E. K. Dahl for clarifying an important point concerning the superconducting-normal phase transition. This work was supported by the Norwegian Research Council Grants No. 157798/432 and No. 158547/431 (NANOMAT), and Grant No. 167498/V30 (STORFORSK). The authors acknowledge the Center for Advanced Study at the Norwegian Academy of Science and Letters for their hospitality.

[1] F. S. Bergeret, A. F. Volkov, and K. B. Efetov, Rev. Mod. Phys. **77**, 1321 (2005).

[2] A. I. Buzdin, Rev. Mod. Phys. **77**, 935 (2005).

[3] L. N. Bulaevskii, V. V. Kuzii, and A. A. Sobyanin, Pis'ma Zh. Eksp. Teor. Fiz. **25**, 314 (1977) [JETP Lett. **25**, 290 (1977)]; A. V. Andreev, A. I. Buzdin, and R. M. Osgood, Phys. Rev. B **43**, 10124 (1991); F. S. Bergeret, A. F. Volkov, and K. B. Efetov, *ibid.* **64**, 134506 (2001).

[4] V. V. Ryazanov, V. A. Oboznov, A. Y. Rusanov, A. V. Veretennikov, A. A. Golubov, and J. Aarts, Phys. Rev. Lett. **86**, 2427 (2001); A. Bauer, J. Bentner, M. Aprili, M. L. Della-Rocca, M. Reinwald, W. Wegscheider, and C. Strunk, *ibid.* **92**, 217001 (2004).

[5] M. Eschrig, J. Kopu, J. C. Cuevas, and G. Schön, Phys. Rev. Lett. **90**, 137003 (2003).

[6] F. S. Bergeret, A. F. Volkov, and K. B. Efetov, Phys. Rev. Lett. **86**, 4096 (2001).

[7] D. Aoki, Nature (London) **413**, 613 (2001).

[8] S. S. Saxena, P. Agarwal, K. Ahilan, F. M. Gorsche, R. K. W. Haselwimmer, M. J. Steiner, E. Pugh, I. R. Walker, S. R. Julian,

P. Monthoux, G. G. Lonzarich, A. Huxley, I. Sheikin, D. Braithwaite, and J. Flouquet, Nature (London) **406**, 587 (2000).
[9] C. Pfleiderer, M. Uhlarz, S. M. Hayden, R. Vollmer, H. v. Löhneysen, N. R. Bernhoeft, and G. G. Lonzarich, Nature (London) **412**, 58 (2001).
[10] E. A. Yelland, S. M. Hayden, S. J. C. Yates, C. Pfleiderer, M. Uhlarz, R. Vollmer, H. v. Löhneysen, N. R. Bernhoeft, R. P. Smith, S. S. Saxena, and N. Kimura, Phys. Rev. B **72**, 214523 (2005).
[11] M. L. Kulic, C. R. Phys. **7**, 4 (2006); M. L. Kulic and I. M. Kulic, Phys. Rev. B **63**, 104503 (2001).
[12] I. Eremin, F. S. Nogueira, and R.-J. Tarento, Phys. Rev. B **73**, 054507 (2006).
[13] M. S. Grønsleth, J. Linder, J.-M. Børven, and A. Sudbø, Phys. Rev. Lett. **97**, 147002 (2006).
[14] I. Zutic, J. Fabian, and S. Das Sarma, Rev. Mod. Phys. **76**, 323 (2004).
[15] D. J. Van Harlingen, Rev. Mod. Phys. **67**, 515 (1995).
[16] A. P. Mackenzie and Y. Maeno, Rev. Mod. Phys. **75**, 657 (2003).
[17] L. P. Gor'kov and E. I. Rashba, Phys. Rev. Lett. **87**, 037004 (2001); M. Eschrig, J. Ferrer, and M. Fogelström, Phys. Rev. B **63**, 220509(R) (2001).
[18] E. Bauer, G. Hilscher, H. Michor, Ch. Paul, E. W. Scheidt, A. Gribanov, Yu. Seropegin, H. Noel, M. Sigrist, and P. Rogl, Phys. Rev. Lett. **92**, 027003 (2004).
[19] X. Li, Z. Zheng, D. Y. Xing, G. Sun, and Z. Dong, Phys. Rev. B **65**, 134507 (2002).
[20] R. Meservey and P. M. Tedrow, Phys. Rep. **238**, 173 (1994).
[21] V. Ambegaokar and A. Baratoff, Phys. Rev. Lett. **10**, 486 (1963).
[22] M. D. Fiske, Rev. Mod. Phys. **36**, 221 (1964).
[23] K. K. Likharev, Rev. Mod. Phys. **51**, 101 (1979).
[24] F. S. Bergeret, A. F. Volkov, and K. B. Efetov, Phys. Rev. Lett. **86**, 3140 (2001).
[25] P. Fulde and R. A. Ferrel, Phys. Rev. **135**, A550 (1964); A. I. Larkin and Y. N. Ovchinnikov, Zh. Eksp. Teor. Fiz. **47**, 1136 (1964) [Sov. Phys. JETP **20**, 762 (1965)].
[26] E. I. Blount and C. M. Varma, Phys. Rev. Lett. **42**, 1079 (1979); **43**, 1843 (1979).
[27] M. H. Cohen, L. M. Falicov, and J. C. Phillips, Phys. Rev. Lett. **8**, 316 (1962).
[28] Z. Tesanovic, Phys. Rev. B **59**, 6449 (1999).
[29] A. K. Nguyen and A. Sudbø, Europhys. Lett. **46**, 780 (1999); Phys. Rev. B **60**, 15307 (1999).
[30] B. I. Halperin, T. C. Lubensky, and S. K. Ma, Phys. Rev. Lett. **32**, 292 (1974).
[31] J. Bartholomew, Phys. Rev. B **28**, 5378 (1983).
[32] S. Mo, J. Hove, and A. Sudbø, Phys. Rev. B **65**, 104501 (2002).
[33] A. M. Clogston, Phys. Rev. Lett. **9**, 266 (1962).
[34] B. S. Chandrasekhar, Appl. Phys. Lett. **1**, 7 (1962).
[35] G. Sarma, J. Phys. Chem. Solids **24**, 1029 (1963).
[36] K. Maki and T. Tsuneto, Prog. Theor. Phys. **31**, 945 (1964).
[37] K. Maki, Prog. Theor. Phys. **32**, 29 (1964).
[38] J. Bardeen, L. N. Cooper, and J. R. Schrieffer, Phys. Rev. **108**, 1175 (1957).
[39] G. D. Mahan, *Many-Particle Physics*, 3rd ed. (Kluwer Academic, Dordrecht, 2000), Chaps. 8 and 10.
[40] E. P. Wigner, *Gruppentheorie und ihre Anwendung auf die Quantenmechanik der Atomspektren* (Frieder. Vieweg, Braunschweig, 1931).
[41] J. Linder, M. S. Grønsleth, and A. Sudbø, Phys. Rev. B **75**, 024508 (2007).
[42] C. Bruder, A. van Otterlo, and G. T. Zimanyi, Phys. Rev. B **51**, 12904(R) (1995).
[43] K. Børkje and A. Sudbø, Phys. Rev. B **74**, 054506 (2006).
[44] G. Burnell (private communication).
[45] K. Fossheim and A. Sudbø, *Superconductivity: Physics and Applications* (Wiley, New York, 2004).
[46] G. E. Blonder, M. Tinkham, and T. M. Klapwijk, Phys. Rev. B **25**, 4515 (1982).
[47] J. Bass and W. P. Pratt, Jr., J. Magn. Magn. Mater. **200**, 274 (1999).

Paper VI

Quantum transport in noncentrosymmetric superconductors and thermodynamics of ferromagnetic superconductors.

Physical Review B **76**, 054511 (2007).

Quantum transport in noncentrosymmetric superconductors and thermodynamics of ferromagnetic superconductors

J. Linder[1] and A. Sudbø[1,2]
[1]*Department of Physics, Norwegian University of Science and Technology, N-7491 Trondheim, Norway*
[2]*Centre for Advanced Study, Norwegian Academy of Science and Letters, Drammensveien 78, N-0271 Oslo, Norway*
(Received 23 February 2007; revised manuscript received 21 May 2007; published 13 August 2007)

Motivated by recent findings of unconventional superconductors exhibiting multiple broken symmetries, we consider a general Hamiltonian describing coexistence of itinerant ferromagnetism, spin-orbit coupling, and mixed spin-singlet and spin-triplet superconducting pairing in the context of mean-field theory. The Hamiltonian is diagonalized and exact eigenvalues are obtained, thus allowing us to write down the coupled gap equations for the different order parameters. Our results may then be applied to any model describing coexistence of any combination of these three phenomena. As a specific application of our results, we consider tunneling between a normal metal and a noncentrosymmetric superconductor with mixed singlet and triplet gaps. The conductance spectrum reveals information about these gaps in addition to how the influence of spin-orbit coupling is manifested. Explicitly, we find well-pronounced peaks and bumps in the spectrum at voltages corresponding to the sum and the difference of the magnitude of the singlet and triplet components. Our results may thus be helpful in determining the relative sizes of the singlet and triplet gaps in noncentrosymmetric superconductors. We also consider the coexistence of itinerant ferromagnetism and triplet superconductivity as a model for recently discovered ferromagnetic superconductors. The coupled gap equations are solved self-consistently, and we study the conditions necessary to obtain the coexistent regime of ferromagnetism and superconductivity. Analytical expressions are presented for the order parameters, and we provide an analysis of the free energy to identify the preferred system state. It is found that the uniform coexistence of ferromagnetism and superconductivity is energetically favored compared to both the purely ferromagnetic state and the unitary superconducting state with zero magnetization. Moreover, we make specific predictions concerning the heat capacity for a ferromagnetic superconductor. In particular, we report a nonuniversal relative jump in the specific heat, depending on the magnetization of the system, at the uppermost superconducting phase transition. We propose that this may be exploited to obtain information about the superconducting pairing symmetry realized in ferromagnetic superconductors, in addition to the magnitude of the exchange splitting between majority- and minority-spin bands.

DOI: 10.1103/PhysRevB.76.054511 PACS number(s): 74.20.Rp

I. INTRODUCTION

Recent findings of superconductors that simultaneously exhibit multiple spontaneously broken symmetries, such as ferromagnetic order or lack of an inversion center[1–3] and even combinations of such broken symmetries,[4] have led to much theoretical and experimental research.[5–7] The symmetry of the superconducting gap in these and other unconventional superconductors is presently a matter of intense investigation.[8–12] Multiple spontaneously broken symmetries are of interest not only in terms of studying the properties of specific condensed matter systems but also due to the fact that it may provide clues for what could be expected in other systems in vastly different areas of physics. Topics such as mass differences of elementary particles and emergent phenomena in biology are caused by spontaneously broken symmetries,[13] and in many cases, the phenomena may even be described by the same type of equations. In this paper, we will address the issue of competition and coexistence between three phenomena giving rise to broken symmetries which are highly relevant in condensed-matter physics: ferromagnetism, superconductivity, and spin-orbit coupling.

The discovery of superconducting materials that lack a center of inversion,[3,4,9,14,15] such as $CePt_3Si$, UIr, Li_2Pd_3B, Li_2Pt_3B, and $Cd_2Re_2O_7$, has lately triggered extensive theoretical work on these compounds. Properties of a superconductor without an inversion center were investigated early by Edelstein,[16] while in Ref. 17, it was shown that a two-dimentional (2D) superconducting system with a significant spin-orbit coupling induced by the lack of inversion symmetry would display a mixed singlet-triplet superconducting state. This means that the superconducting order parameter would possess the exotic feature of having no definite parity. Later studies[18–20] also investigated specific noncentrosymmetric superconductors with a model Hamiltonian consisting of a superposition of spin-orbit and superconducting terms. In an attempt to determine the correct pairing symmetry of the superconducting state in such unconventional superconductors, it was found that the favored triplet pairing state[21] for the heavy-fermion material $CePt_3Si$ is $\mathbf{d}_{\mathbf{k}} \propto (k_y, -k_x, 0)$. Very recently, however, an experimental study[22] of thermal transport properties in the present compound concluded that the correct gap function ($\mathbf{d}_{\mathbf{k}}$ vector) may exhibit nodal lines in contrast to the point nodes displayed by the $\mathbf{d}_{\mathbf{k}}$ vector suggested by Ref. 21. It is therefore of considerable interest to investigate several specific models for noncentrosymmetric superconductors in order to reveal characteristic features in physical observables that might be helpful in classifying the symmetry of the superconducting order parameter.

In Ref. 23, the authors studied tunneling between a normal metal and a noncentrosymmetric superconductor considering the particular form of $\mathbf{d}_\mathbf{k}$ suggested by Ref. 21 in the limit of weak spin-orbit coupling and in the absence of spin-singlet pairing. Anderson[24] showed that the only stable triplet pairing states in the presence of a spin-orbit coupling would have to satisfy $\mathbf{d}_\mathbf{k} \| \mathbf{g}_\mathbf{k}$, where $\mathbf{g}_\mathbf{k} = -\mathbf{g}_{-\mathbf{k}}$ is the vector function describing this interaction, such that in $CePt_3Si$, one also has $\mathbf{g}_\mathbf{k} = \lambda(k_y, -k_x, 0)$. Moreover, it was demonstrated by Samokhin *et al.*[25] that the spin-orbit coupling in this particular material is significant, i.e., $\gg k_B T_c$, which indicates admixturing of singlet and triplet Cooper pairs. In the present paper, we solve the full Bogoliubov–de Gennes (BdG) equations for a system with spin-orbit coupling including both spin-singlet and spin-triplet superconducting gaps, studying a gap vector $\mathbf{d}_{\mathbf{k},\mathrm{point}} \propto (k_y, -k_x, 0)$ as suggested by Ref. 21. We then apply this gap vector to what we believe is the simplest model that captures the essential features that could be expected to appear in the conductance spectrum of a 2D normal/$CePt_3Si$ junction. Our work then significantly extends the considerations made in Ref. 23 primarily in that we present analytical and numerical results that allow for *both* triplet and singlet gap components. Also note that a similar Hamiltonian was studied very recently in Ref. 26, where it was shown that the presence of a weak external magnetic field would significantly change the nodal topology of $CePt_3Si$. With regard to noncentrosymmetricity, we underline that breaking the symmetry of spatial inversion does not, in general, give rise to a significant spin-orbit coupling. Also, it is well known that spin-orbit coupling may be induced in a centrosymmetric crystal by means of an external symmetry-breaking electrical field. In the latter case, however, the broken symmetry is strictly speaking not spontaneous as it certainly is for, e.g., a crystal lattice undergoing a structural phase transition which breaks spatial inversion.[9]

Another interesting scenario in the context of spontaneously broken symmetries is the study of superconductors that exhibit coexistence of ferromagnetic and superconducting order, i.e., systems where two continuous internal symmetries, SU(2) and U(1), are simultaneously broken. Due to the preferred orientation of the spins in a ferromagnetic system, time-reversal symmetry [or equivalently spinor SU(2) rotational symmetry] is broken such that angular momentum is no longer a conserved quantity. Similarly, in a superconducting system, the broken U(1) symmetry breaks the conservation of particle number. Note that by the terminology broken symmetry, we are referring to the fact that the wave function describing the state of the system acquires a complex phase which characterizes the ground state. In the ferromagnetic and superconducting systems we will consider in this paper, superconductivity appears at a lower temperature than the temperature at which onset of ferromagnetism is found. This may be simply due to the fact that the energy scales for the two phenomena are quite different, with the exchange energy naturally being the largest. It may, however, also be due to the fact that superconductivity is dependent on ferromagnetism for its very existence. Such a suggestion has recently been put forth.[27]

In the context of ferromagnetic superconductors (FMSCs), it is crucial to address the question of whether the superconductivity and ferromagnetism order parameters coexist uniformly or if they are phase separated. One plausible scenario[28] is that a spontaneously formed vortex lattice due to the internal magnetization $\mathbf{M}$ is realized, but studies of a uniform superconducting phase in spin-triplet FMSCs[29] has also been conducted. As argued by Mineev in Ref. 30, an important factor with respect to whether a vortex lattice appears or not should be the magnitude of the internal magnetization $\mathbf{M}$. Specifically, Ref. 31 suggested that vortices may arise if $4\pi\mathbf{M} > \mathbf{H}_{c1}$, where $\mathbf{H}_{c1}$ is the lower critical field. In the case of URhGe, a weakly ferromagnetic state coexisting with superconductivity seems to be realized, and the domain structure in the absence of an external field is thus vortex-free. Unfortunately, current experimental data concerning URhGe are not as of yet strong enough to unambiguously settle this question. On the other hand, evidence for uniform coexistence of ferromagnetism and superconductivity has been indicated[32] in UGe_2.

Although this is an unsettled issue, it seems natural to assume that in FMSCs, the electrons involved in the SU(2) symmetry breaking also participate in the U(1) symmetry breaking. As a consequence, uniform coexistence of spin-singlet superconductivity and ferromagnetism can be discarded since *s*-wave Cooper pairs carry a total spin of zero, although spatially modulated order parameters could allow for magnetic *s*-wave superconductors.[33,34] However, spin-triplet Cooper pairs are, in principle, perfectly compatible with ferromagnetic order since they can carry a net magnetic moment. There is strong reason to believe that the correct pairing symmetries in the discovered FMSCs constitute nonunitary states.[35,36] Spin-triplet superconductors have a multicomponent order parameter $\mathbf{d}_\mathbf{k}$, which for a given spin basis reads

$$\mathbf{d}_\mathbf{k} = \left[\frac{\Delta_{\mathbf{k}\downarrow\downarrow} - \Delta_{\mathbf{k}\uparrow\uparrow}}{2}, \frac{-i(\Delta_{\mathbf{k}\downarrow} + \Delta_{\mathbf{k}\uparrow\uparrow})}{2}, \Delta_{\mathbf{k}\uparrow\downarrow} \right]. \tag{1}$$

Note that $\mathbf{d}_\mathbf{k}$ transforms like a vector under spin rotations. The superconducting order parameter is characterized as nonunitary if $i(\mathbf{d}_\mathbf{k} \times \mathbf{d}_\mathbf{k}^*) \neq 0$, which effectively means that time-reversal symmetry is broken in the spin part of the Cooper pairs, since the average spin of Cooper pairs is given as $\langle \mathbf{S}_\mathbf{k} \rangle = i(\mathbf{d}_\mathbf{k} \times \mathbf{d}_\mathbf{k}^*)$. Note that time-reversal symmetry may be broken in the orbital part (angular momentum) of the Cooper pair wave function even if the state is unitary. In the general case where all superconducting (SC) gaps are included, it is generally argued that $\Delta_{\mathbf{k}\uparrow\downarrow}$ would be suppressed in the presence of a Zeeman splitting between the $\uparrow$, $\downarrow$ conduction bands. Distinguishing between unitary and nonunitary states in FMSCs is clearly one of the primary objectives in terms of identifying the correct order parameter. Studies of quantum transport in junctions involving FMSCs have explicitly shown that the conductance spectrum should be helpful in revealing the correct pairing symmetry.[37,38] Hence, an itinerant electron model of ferromagnetism augmented by a suitable pairing kernel should be a reasonable starting point for describing such systems.

Although we have mentioned two specific examples of systems exhibiting multiple broken symmetries, our aim with

this paper is to construct a solid starting point for consideration of a condensed-matter system exhibiting any combination of the broken symmetries resulting from superconductivity, ferromagnetism, and/or spin-orbit coupling. By applying the appropriate limits to our theory, one may then obtain special cases such as FMSCs or noncentrosymmetric superconductors with significant spin-orbit coupling.

This paper is organized as follows. In Sec. II, we establish the Hamiltonian accounting for general coexistence of ferromagnetism, spin-orbit coupling, and superconductivity. The diagonalization procedure and coupled gap equations are described in Sec. III. Then, we apply our findings to a model of normal/noncentrosymmetric superconductor junction, calculating the tunneling conductance spectrum, in Sec. IV, in addition to a discussion of these results. As a second application, we consider a FMSC in Sec. V, solving the coupled gap equations self-consistently and calculating the free energy and heat capacity of such a system. Our main conclusions are summarized in Sec. VI. We will use boldface notation for vectors, $\hat{}$ for operators, and $\check{}$ for 2×2 matrices.

II. MODEL FOR COEXISTENCE OF FERROMAGNETISM, SPIN-ORBIT COUPLING, AND SUPERCONDUCTIVITY

For our model, we will write down a Hamiltonian describing the kinetic energy, exchange energy, spin-orbit coupling, and attractive electron-electron interaction, respectively. The total Hamiltonian can then be written as

$$\hat{H} = \hat{H}_{\rm kin} + \hat{H}_{\rm FM} + \hat{H}_{\rm SOC} + \hat{H}_{\rm SC}, \tag{2}$$

where the respective individual terms read

$$\hat{H}_{\rm kin} = \sum_{\mathbf{k}\sigma} \xi_{\mathbf{k}} \hat{c}^{\dagger}_{\mathbf{k}\sigma} \hat{c}_{\mathbf{k}\sigma},$$

$$\hat{H}_{\rm FM} = -JN \sum_{\mathbf{k}} \gamma(\mathbf{k}) \hat{\mathbf{S}}_{\mathbf{k}} \cdot \hat{\mathbf{S}}_{-\mathbf{k}},$$

$$\hat{H}_{\rm SOC} = \sum_{\mathbf{k}\alpha\beta} \hat{c}^{\dagger}_{\mathbf{k}\alpha} (\mathbf{g}_{\mathbf{k}} \cdot \check{\boldsymbol{\sigma}})_{\alpha\beta} \hat{c}_{\mathbf{k}\beta},$$

$$\hat{H}_{\rm SC} = \frac{1}{2N} \sum_{\mathbf{k}\mathbf{k}'\alpha\beta} (V^{S}_{\mathbf{k}\mathbf{k}'\alpha\beta} + V^{\rm T}_{\mathbf{k}\mathbf{k}'\alpha\beta}) \hat{c}^{\dagger}_{\mathbf{k}\alpha} \hat{c}^{\dagger}_{-\mathbf{k}\beta} \hat{c}_{-\mathbf{k}'\beta} \hat{c}_{\mathbf{k}'\alpha}. \tag{3}$$

Above, $\xi_{\mathbf{k}} = \varepsilon_{\mathbf{k}} - \mu$, where $\varepsilon_{\mathbf{k}}$ is the dispersion relation for the free fermions and μ is the chemical potential,[39] $J>0$ is a ferromagnetic coupling parameter, $\gamma(\mathbf{k})$ is a geometrical structure factor for the lattice, $\mathbf{g}_{\mathbf{k}}$ is a vector function accounting for the antisymmetric spin-orbit coupling, and $V_{\mathbf{k}\mathbf{k}'\alpha\beta}$ is an attractive pair potential. The factor of $1/2$ in $\hat{H}_{\rm SC}$ is included to obtain more convenient expressions later on and simply corresponds to a redefinition of $V^{\rm S,T}_{\mathbf{k}\mathbf{k}'\alpha\beta} \to \frac{1}{2} V^{\rm S,T}_{\mathbf{k}\mathbf{k}'\alpha\beta}$. In Eqs. (3), the spin operators are given by

$$\hat{\mathbf{S}}_{\mathbf{k}} = \frac{1}{N} \sum_{\mathbf{k}'} \hat{c}^{\dagger}_{\mathbf{k}'\alpha} \check{\boldsymbol{\sigma}}_{\alpha\beta} \hat{c}_{(\mathbf{k}+\mathbf{k}')\beta}. \tag{4}$$

Moreover, we have explicitly split the attractive pairing potential into a singlet and a triplet part according to $V_{\mathbf{k}\mathbf{k}'\alpha\beta} = V^{S}_{\mathbf{k}\mathbf{k}'\alpha\beta} + V^{\rm T}_{\mathbf{k}\mathbf{k}'\alpha\beta}$. The symmetry properties of the antisymmetric spin-orbit coupling and superconductivity terms with respect to spatial inversion symmetry read

$$\mathbf{g}_{\mathbf{k}} = -\mathbf{g}_{-\mathbf{k}}, \quad V^{S}_{\mathbf{k}\mathbf{k}'\alpha\beta} = V^{S}_{\pm\mathbf{k}\pm'\mathbf{k}'\alpha\beta},$$

$$V^{\rm T}_{\mathbf{k}\mathbf{k}'\alpha\beta} = \pm\pm' V^{\rm T}_{\pm\mathbf{k}\pm'\mathbf{k}'\alpha\beta}. \tag{5}$$

In order to find eigenvalues and gap equations for our system, we introduce the mean-field approximation for the two-particle Hamiltonians (ferromagnetic and superconducting terms), such that the operators $\hat{\mathbf{S}}_{\mathbf{k}}$ and $\hat{c}^{\dagger}_{\mathbf{k}\alpha}\hat{c}^{\dagger}_{-\mathbf{k}\beta}$ may be written as a mean-field value plus small fluctuations. We define $\langle \hat{c}^{\dagger}_{\mathbf{k}\alpha}\hat{c}^{\dagger}_{-\mathbf{k}\beta}\rangle = b_{\mathbf{k}\alpha\beta}$ and write

$$\hat{\mathbf{S}}_{\mathbf{k}} = \langle \hat{\mathbf{S}}_{\mathbf{k}} \rangle + \delta\langle \hat{\mathbf{S}}_{\mathbf{k}} \rangle,$$

$$\hat{c}^{\dagger}_{\mathbf{k}\alpha}\hat{c}^{\dagger}_{-\mathbf{k}\beta} = b_{\mathbf{k}\alpha\beta} + \delta b_{\mathbf{k}\alpha\beta}. \tag{6}$$

Inserting Eqs. (6) into Eqs. (3) and discarding all terms of order $\mathcal{O}(\delta^2)$, one obtains in the standard fashion

$$\hat{H}_{\rm FM} = -\sum_{\mathbf{k}\alpha\beta} \hat{c}^{\dagger}_{\mathbf{k}\alpha} (\mathbf{V}_M \cdot \check{\boldsymbol{\sigma}})_{\alpha\beta} \hat{c}_{\mathbf{k}\beta} + \frac{INM^2}{2},$$

$$\hat{H}_{\rm SC} = \frac{1}{2} \sum_{\mathbf{k}\alpha\beta} \{ [(\Delta^{\rm S}_{\mathbf{k}\alpha\beta})^{\dagger} + (\Delta^{\rm T}_{\mathbf{k}\alpha\beta})^{\dagger}] \hat{c}_{-\mathbf{k}\beta} \hat{c}_{\mathbf{k}\alpha} + [\Delta^{\rm S}_{\mathbf{k}\alpha\beta} + \Delta^{\rm T}_{\mathbf{k}\alpha\beta}] \times [\hat{c}^{\dagger}_{\mathbf{k}\alpha}\hat{c}^{\dagger}_{-\mathbf{k}\beta} - b^{\dagger}_{\mathbf{k}\alpha\beta}] \}. \tag{7}$$

In Eqs. (7), $\mathbf{M} = (M_x, M_y, M_z) = \langle \hat{\mathbf{S}}_i \rangle = \langle \hat{\mathbf{S}}_{\mathbf{k}=0} \rangle$ denotes the mean value of the spin operators in real space, interpreted as the magnetization of the system. We have introduced the vector describing the magnetic exchange energy $\mathbf{V}_M = I\mathbf{M}$ and the order parameters (OPs)

$$\mathcal{V} = (\mathbf{V}_M)_x - i(\mathbf{V}_M)_y = I(M_x - iM_y), \quad \mathcal{V}_z = IM_z, \tag{8}$$

for ferromagnetism, while the OP for superconductivity is described by

$$\Delta^{\rm S,T}_{\mathbf{k}\alpha\beta} = \frac{1}{N} \sum_{\mathbf{k}'} V^{\rm S,T}_{\mathbf{k}\mathbf{k}'\alpha\beta} b_{\mathbf{k}'\alpha\beta},$$

$$\Delta^{\rm S,T}_{\mathbf{k}'\alpha\beta} = \frac{1}{N} \sum_{\mathbf{k}} V^{\rm S,T}_{\mathbf{k}\mathbf{k}'\alpha\beta} b^{\dagger}_{\mathbf{k}\alpha\beta}. \tag{9}$$

The quantity I appearing in Eq. (8) is a measure of the strength of the magnetic exchange coupling. Although we have derived the ferromagnetic part of our Hamiltonian from a lattice model [where $I = 2JN\gamma(0)$], this generic Hamiltonian describes a general mean-field model of a system with magnetic exchange energy. The Pauli principle places the following restrictions upon the superconductivity OPs:

$$\text{singlet pairing: } \Delta^{\rm S}_{\mathbf{k}\alpha\beta} = -\Delta^{\rm S}_{\mathbf{k}\beta\alpha}, \quad \Delta^{\rm S}_{\mathbf{k}\alpha\beta} = \Delta^{\rm S}_{-\mathbf{k}\alpha\beta},$$

$$\text{triplet pairing: } \Delta^{\rm T}_{\mathbf{k}\alpha\beta} = \Delta^{\rm T}_{\mathbf{k}\beta\alpha}, \quad \Delta^{\rm T}_{\mathbf{k}\alpha\beta} = -\Delta^{\rm T}_{-\mathbf{k}\alpha\beta}. \tag{10}$$

In total, we have thus obtained a Hamiltonian $\hat{H}$ describing coexistence of ferromagnetism, spin-orbit coupling, and

superconductivity in the mean-field approximation by adding all of the above terms. For more compact notation, one may introduce a basis for fermion operators $\hat{\phi}_{\mathbf{k}}=[\hat{c}_{\mathbf{k}\uparrow},\hat{c}_{\mathbf{k}\downarrow},\hat{c}^{\dagger}_{-\mathbf{k}\uparrow},\hat{c}^{\dagger}_{-\mathbf{k}\downarrow}]^{\mathrm{T}}$ and write

$$\hat{H}=\hat{H}_{\mathrm{kin}}+\hat{H}_{\mathrm{FM}}+\hat{H}_{\mathrm{SOC}}+\hat{H}_{\mathrm{SC}}=H_0+\frac{1}{2}\sum_{\mathbf{k}}\hat{\phi}^{\dagger}_{\mathbf{k}}A_{\mathbf{k}}\hat{\phi}_{\mathbf{k}}, \tag{11}$$

where we have introduced the quantities

$$H_0=\sum_{\mathbf{k}}\xi_{\mathbf{k}}+\frac{INM^2}{2}-\frac{N(\mathcal{V}+\mathcal{V}^{\dagger})}{2}-\frac{1}{2}\sum_{\mathbf{k}\alpha\beta}(\Delta^{\mathrm{S}}_{\mathbf{k}\alpha\beta}+\Delta^{\mathrm{T}}_{\mathbf{k}\alpha\beta})b^{\dagger}_{\mathbf{k}\alpha\beta},$$

$$A_{\mathbf{k}}=\begin{pmatrix}\xi_{\mathbf{k}\uparrow}+g_{\mathbf{k},z} & -\mathcal{V}+g_{\mathbf{k},-} & \Delta^{\mathrm{T}}_{\mathbf{k}\uparrow\uparrow} & \Delta^{\mathrm{S}}_{\mathbf{k}\uparrow\downarrow}+\Delta^{\mathrm{T}}_{\mathbf{k}\uparrow\downarrow}\\ -\mathcal{V}^{\dagger}+g_{\mathbf{k},+} & \xi_{\mathbf{k}\downarrow}-g_{\mathbf{k},z} & -\Delta^{\mathrm{S}}_{\mathbf{k}\uparrow\downarrow}+\Delta^{\mathrm{T}}_{\mathbf{k}\uparrow\downarrow} & \Delta^{\mathrm{T}}_{\mathbf{k}\downarrow\downarrow}\\ (\Delta^{\mathrm{T}}_{\mathbf{k}\uparrow\uparrow})^{\dagger} & (\Delta^{\mathrm{T}}_{\mathbf{k}\uparrow\downarrow})^{\dagger}-(\Delta^{\mathrm{S}}_{\mathbf{k}\uparrow\downarrow})^{\dagger} & -\xi_{\mathbf{k}\uparrow}+g_{\mathbf{k},z} & \mathcal{V}^{\dagger}+g_{\mathbf{k},+}\\ (\Delta^{\mathrm{T}}_{\mathbf{k}\uparrow\downarrow})^{\dagger}+(\Delta^{\mathrm{S}}_{\mathbf{k}\uparrow\downarrow})^{\dagger} & (\Delta^{\mathrm{T}}_{\mathbf{k}\downarrow\downarrow})^{\dagger} & \mathcal{V}+g_{\mathbf{k},-} & -\xi_{\mathbf{k}\downarrow}-g_{\mathbf{k},z}\end{pmatrix}. \tag{12}$$

Above, we have defined $\xi_{\mathbf{k}\sigma}=\xi_{\mathbf{k}}-\sigma\mathcal{V}_z$ in addition to $g_{\mathbf{k},\pm}=(\mathbf{g}_{\mathbf{k}})_x\pm i(\mathbf{g}_{\mathbf{k}})_y$. The matrix $A_{\mathbf{k}}$ will be central in this work, and we note that it may be further compactified by introducing the $\mathbf{d}_{\mathbf{k}}$-vector formalism.[40] By means of the definitions $d_{\mathbf{k},0}=\Delta^{\mathrm{S}}_{\mathbf{k}\uparrow\downarrow}$ and

$$\mathbf{d}_{\mathbf{k}}=\frac{1}{2}[\Delta^{\mathrm{T}}_{\mathbf{k}\downarrow\downarrow}-\Delta^{\mathrm{T}}_{\mathbf{k}\uparrow\uparrow},-i(\Delta^{\mathrm{T}}_{\mathbf{k}\uparrow\uparrow}+\Delta^{\mathrm{T}}_{\mathbf{k}\downarrow\downarrow}),2\Delta^{\mathrm{T}}_{\mathbf{k}\uparrow\downarrow}] \tag{13}$$

that transforms like a vector under spin rotations, one may write

$$A_{\mathbf{k}}=\begin{pmatrix}\xi_{\mathbf{k}}\check{\mathbf{1}}-\check{\boldsymbol{\sigma}}\cdot(\mathbf{V}_M-\mathbf{g}_{\mathbf{k}}) & i(d_{0,\mathbf{k}}+\mathbf{d}_{\mathbf{k}}\cdot\check{\boldsymbol{\sigma}})\check{\sigma}_y\\ [i(d_{0,\mathbf{k}}+\mathbf{d}_{\mathbf{k}}\cdot\check{\boldsymbol{\sigma}})\check{\sigma}_y]^{\dagger} & -\xi_{\mathbf{k}}\check{\mathbf{1}}+(\mathbf{V}_M+\mathbf{g}_{\mathbf{k}})\cdot\check{\boldsymbol{\sigma}}^{\mathcal{T}}\end{pmatrix}, \tag{14}$$

where $\check{\mathbf{1}}$ denotes the identity matrix and $\mathcal{T}$ designates the matrix transpose. The rest of this paper will now be devoted to obtaining the excitation energies for $\hat{H}$ by diagonalizing $A_{\mathbf{k}}$, writing down the coupled gap equations, and considering some important special cases.

III. EXCITATION ENERGIES AND GAP EQUATIONS

The characteristic polynomial for a general matrix $A_{\mathbf{k}}$ with eigenvalues $E_{\mathbf{k}}$ may be written as[41]

$$\rho(E_{\mathbf{k}})=E^4_{\mathbf{k}}-(\mathrm{Tr}\{A_{\mathbf{k}}\})E^3_{\mathbf{k}}+\left\{\frac{1}{2}[|A_{\mathbf{k}}-I|+|A_{\mathbf{k}}+I|]-1-\det A_{\mathbf{k}}\right\}E^2_{\mathbf{k}}+\frac{1}{2}[|A_{\mathbf{k}}-I|-|A_{\mathbf{k}}+I|]E_{\mathbf{k}}+\det A_{\mathbf{k}}=0, \tag{15}$$

where I denotes the 4×4 identity matrix. Since $A_{\mathbf{k}}$ in our case is Hermitian, $\mathrm{Tr}\{A_{\mathbf{k}}\}=0$, and the polynomial reduces to a depressed quartic equation. For ease of notation, we introduce the quantity

$$\eta^{\pm}_{\mathbf{k}}\equiv\frac{1}{2}[|A_{\mathbf{k}}-I|\pm|A_{\mathbf{k}}+I|], \tag{16}$$

such that Eq. (15) is rewritten as

$$E^4_{\mathbf{k}}+(\eta^{+}_{\mathbf{k}}-1-\det A_{\mathbf{k}})E^2_{\mathbf{k}}+\eta^{-}_{\mathbf{k}}E_{\mathbf{k}}+\det A_{\mathbf{k}}=0. \tag{17}$$

The solutions of $E_{\mathbf{k}}$ can be written as[42]

$$2E_{\mathbf{k}_{\alpha\beta}}=\alpha a_{\mathbf{k}}+\beta\left\{-\left[3(\eta^{+}_{\mathbf{k}}-1-\det A_{\mathbf{k}})+2y_{\mathbf{k}}+\alpha\frac{2\eta^{-}_{\mathbf{k}}}{a_{\mathbf{k}}}\right]\right\}^{1/2}. \tag{18}$$

Here, we have defined the auxiliary quantities

$$a_{\mathbf{k}}=\sqrt{(\eta^{+}_{\mathbf{k}}-1-\det A_{\mathbf{k}})+2y_{\mathbf{k}}},$$

$$y_{\mathbf{k}}=-\frac{5(\eta^{+}_{\mathbf{k}}-1-\det A_{\mathbf{k}})}{6}-b_{\mathbf{k}},$$

$$b_{\mathbf{k}}=R^{1/3}_{\mathbf{k}},\quad R_{\mathbf{k}}=\frac{Q_{\mathbf{k}}}{2}+\sqrt{\frac{Q^2_{\mathbf{k}}}{4}+\frac{P^3_{\mathbf{k}}}{27}},$$

$$Q_{\mathbf{k}}=\frac{(\eta^{+}_{\mathbf{k}}-1-\det A_{\mathbf{k}})\det A_{\mathbf{k}}}{3}-\frac{(\eta^{-}_{\mathbf{k}})^2}{8}-\frac{(\eta^{+}_{\mathbf{k}}-1-\det A_{\mathbf{k}})^3}{108}, \tag{19}$$

$$P_{\mathbf{k}}=-\frac{(\eta^{+}_{\mathbf{k}}-1-\det A_{\mathbf{k}})^2}{12}-\det A_{\mathbf{k}}.$$

In Eq. (18), $\{\alpha,\beta\}$ take the values +1 and −1 such that there exists a total of four solutions for $E_{\mathbf{k}}$. Also note that any of the roots in the expressions for $b_{\mathbf{k}}$ and $R_{\mathbf{k}}$ will do the job. A special case of the above solutions, which occurs quite frequently in various contexts, considerably simplifies the obtained eigenvalues: $\frac{1}{2}[|A_{\mathbf{k}}-I|-|A_{\mathbf{k}}+I|]=0$. In this case, the quartic equation reduces to an effective quadratic equation with the solutions

$$2E_{\mathbf{k}_{\alpha\beta}} = \alpha[-2(\eta_{\mathbf{k}}^{+} - 1 - \det A_{\mathbf{k}}) + 2\beta\sqrt{(\eta_{\mathbf{k}}^{+} - 1 - \det A_{\mathbf{k}})^2 - 4\det A_{\mathbf{k}}}]^{1/2}. \quad (20)$$

This is the situation considered in most problems dealing with superconductors. Having calculated the energy eigenvalues, Eq. (11) may now be diagonalized by writing

$$\hat{H} = H_0 + \frac{1}{2}\sum_{\mathbf{k}} \hat{\phi}_{\mathbf{k}}^{\dagger} A_{\mathbf{k}} \hat{\phi}_{\mathbf{k}} = H_0 + \frac{1}{2}\sum_{\mathbf{k}} (\hat{\phi}_{\mathbf{k}}^{\dagger} P_{\mathbf{k}})(P_{\mathbf{k}}^{\dagger} A_{\mathbf{k}} P_{\mathbf{k}})(P_{\mathbf{k}}^{\dagger}\hat{\phi}_{\mathbf{k}}) = H_0 + \sum_{\mathbf{k}} \hat{\tilde{\phi}}_{\mathbf{k}}^{\dagger} D_{\mathbf{k}} \hat{\tilde{\phi}}_{\mathbf{k}}, \quad (21)$$

where $D_{\mathbf{k}} = \mathrm{diag}(E_{\mathbf{k},1}, E_{\mathbf{k},2}, E_{\mathbf{k},3}, E_{\mathbf{k},4})$ is a diagonal matrix containing the eigenvalues of $A_{\mathbf{k}}$. Here, we have defined [see Eq. (18)]

$$E_{\mathbf{k},1} = \frac{1}{2}E_{\mathbf{k}_{++}}, \quad \frac{1}{2}E_{\mathbf{k},2} = E_{\mathbf{k}_{+-}},$$

$$E_{\mathbf{k},3} = \frac{1}{2}E_{\mathbf{k}_{-+}}, \quad \frac{1}{2}E_{\mathbf{k},4} = E_{\mathbf{k}_{--}}, \quad (22)$$

thus absorbing the factor $\frac{1}{2}$ in front of $\Sigma_{\mathbf{k}}$ into the eigenvalues. Above, $P_{\mathbf{k}}$ are the orthonormal diagonalizing matrices which, by the Hermiticity of $A_{\mathbf{k}}$, are ensured to be unitary. We write our new basis of fermion operators as

$$\hat{\tilde{\phi}}_{\mathbf{k}}^{\dagger} = [\hat{\gamma}_{\mathbf{k}\uparrow}^{\dagger}, \hat{\gamma}_{\mathbf{k}\downarrow}^{\dagger}, \hat{\gamma}_{-\mathbf{k}\uparrow}, \hat{\gamma}_{-\mathbf{k}\downarrow}]. \quad (23)$$

These operators satisfy the fermion anticommutation relations, as can be verified by direct insertion. From Eq. (21), we may now write

$$\begin{aligned}\hat{H} &= H_0 + \sum_{\mathbf{k}} [\gamma_{\mathbf{k}\uparrow}^{\dagger}\gamma_{\mathbf{k}\uparrow}E_{\mathbf{k},1} + \gamma_{\mathbf{k}\downarrow}^{\dagger}\gamma_{\mathbf{k}\downarrow}E_{\mathbf{k},2} + \gamma_{-\mathbf{k}\uparrow}\gamma_{-\mathbf{k}\uparrow}^{\dagger}E_{\mathbf{k},3} + \gamma_{-\mathbf{k}\downarrow}\gamma_{-\mathbf{k}\downarrow}^{\dagger}E_{\mathbf{k},4}] \\ &= \left[H_0 + \sum_{\mathbf{k}}(E_{\mathbf{k},3} + E_{\mathbf{k},4})\right] + \sum_{\mathbf{k}} [\gamma_{\mathbf{k}\uparrow}^{\dagger}\gamma_{\mathbf{k}\uparrow}(E_{\mathbf{k},1} - E_{-\mathbf{k},3}) + \gamma_{\mathbf{k}\downarrow}^{\dagger}\gamma_{\mathbf{k}\downarrow}(E_{\mathbf{k},2} - E_{-\mathbf{k},4})] = \tilde{H}_0 + \sum_{\mathbf{k}} [\gamma_{\mathbf{k}\uparrow}^{\dagger}\gamma_{\mathbf{k}\uparrow}\tilde{E}_{\mathbf{k},1} + \gamma_{\mathbf{k}\downarrow}^{\dagger}\gamma_{\mathbf{k}\downarrow}\tilde{E}_{\mathbf{k},2}], \end{aligned} \quad (24)$$

where we have defined $\tilde{H}_0 = H_0 + \Sigma_{\mathbf{k}}(E_{\mathbf{k},3} + E_{\mathbf{k},4})$ and $\tilde{E}_{\mathbf{k},1} = (E_{\mathbf{k},1} - E_{-\mathbf{k},3})$, $\tilde{E}_{\mathbf{k},2} = (E_{\mathbf{k},2} - E_{-\mathbf{k},4})$. Our Hamiltonian now has the form of a free-fermion theory. It is then readily seen that the free energy of the system is given by

$$F = \tilde{H}_0 - \frac{1}{\beta}\sum_{\mathbf{k}} [\ln(1 + e^{-\beta\tilde{E}_{\mathbf{k},1}}) + \ln(1 + e^{-\beta\tilde{E}_{\mathbf{k},2}})]. \quad (25)$$

From F, the gap equations for the ferromagnetic and superconducting OPs $\mathcal{V}$, $\mathcal{V}_z$, and $\Delta_{\mathbf{k}\alpha\beta}^{\mathrm{S,T}}$ may be obtained by demanding the value of these which corresponds to a minimum in F. The possible extrema of F are given by the conditions

$$\frac{\partial F}{\partial \Delta_{\mathbf{k}\alpha\beta}^{S,T}} = 0, \quad \frac{\partial F}{\partial (\Delta_{\mathbf{k}\alpha\beta}^{S,T})^{\dagger}} = 0,$$

$$\frac{\partial F}{\partial \mathcal{V}_z} = 0, \quad \frac{\partial F}{\partial \mathcal{V}} = 0, \quad \frac{\partial F}{\partial \mathcal{V}^{\dagger}} = 0. \quad (26)$$

By first defining the quantity

$$\mathcal{F}(x) = \sum_{\mathbf{k}} \left[n_F(\tilde{E}_{\mathbf{k},1}) \frac{\partial \tilde{E}_{\mathbf{k},1}}{\partial x} e^{-\beta\tilde{E}_{\mathbf{k},1}} + \frac{\partial E_{\mathbf{k},3}}{\partial x} + n_F(\tilde{E}_{\mathbf{k},2}) \frac{\partial \tilde{E}_{\mathbf{k},2}}{\partial x} e^{-\beta\tilde{E}_{\mathbf{k},2}} + \frac{\partial E_{\mathbf{k},4}}{\partial x} \right], \quad (27)$$

where $n_F(E) = 1/(1 + e^{\beta E})$ is the Fermi distribution, the conditions in Eqs. (26) may be evaluated by inserting Eq. (25). The extrema of F are thus determined by the following equations:

$$-b_{\mathbf{k}\alpha\beta}^{\dagger} + \mathcal{F}(\Delta_{\mathbf{k}\alpha\beta}^{\mathrm{S,T}}) = 0, \quad (28)$$

$$-b_{\mathbf{k}\alpha\beta} + \mathcal{F}[(\Delta_{\mathbf{k}\alpha\beta}^{\mathrm{S,T}})^{\dagger}] = 0, \quad (29)$$

$$\frac{N\mathcal{V}_z}{2J\gamma(0)} + \mathcal{F}(\mathcal{V}_z) = 0, \quad (30)$$

$$-\frac{N}{2} + \frac{N\mathcal{V}^{\dagger}}{2J\gamma(0)} + \mathcal{F}(\mathcal{V}) = 0, \quad (31)$$

$$-\frac{N}{2} + \frac{N\mathcal{V}}{2J\gamma(0)} + \mathcal{F}(\mathcal{V}^{\dagger}) = 0. \quad (32)$$

The challenge then lies in obtaining the derivatives of the energies $E_{\mathbf{k},i}$ with respect to the different order parameters. In the general case described by Eq. (12), this is a formidable task. Nevertheless, the above provides a general framework which may serve as a starting point for any model considering the coexistence of ferromagnetism, spin-orbit coupling, and superconductivity. We will apply our findings onto a specific case which currently is a topic attracting much attention: noncentrosymmetric superconductors with significant spin-orbit coupling.

IV. PROBING THE PAIRING SYMMETRY OF NONCENTROSYMMETRIC SUPERCONDUCTORS

As an application of our model, we consider tunneling between a normal metal and a noncentrosymmetric superconductor treated in the spin-generalized Blonder-Tinkham-Klapwijk formalism.[43,44]

A. Model and formulation

The Hamiltonian in the superconducting state using standard mean-field theory with a spin-orbit coupling may be written as

$$\hat{H} = H_0 + \frac{1}{2}\sum_{\mathbf{k}} \hat{\phi}_{\mathbf{k}}^{\dagger} M_{\mathbf{k}} \hat{\phi}_{\mathbf{k}}, \quad (33)$$

using a spin basis $\hat{\phi}_{\mathbf{k}} = [\hat{c}_{\mathbf{k}\uparrow}, \hat{c}_{\mathbf{k}\downarrow}, \hat{c}_{-\mathbf{k}\uparrow}^{\dagger}, \hat{c}_{-\mathbf{k}\downarrow}^{\dagger}]^{\mathrm{T}}$ and with

$$M_{\mathbf{k}} = \begin{pmatrix} \varepsilon_{\mathbf{k}} & g_{\mathbf{k},-} & \Delta_{\mathbf{k}\uparrow\uparrow} & \Delta_{\mathbf{k}} \\ g_{\mathbf{k},+} & \varepsilon_{\mathbf{k}} & -\Delta_{\mathbf{k}} & \Delta_{\mathbf{k}\downarrow\downarrow} \\ \Delta^{\dagger}_{\mathbf{k}\uparrow\uparrow} & -\Delta^{\dagger}_{\mathbf{k}} & -\varepsilon_{\mathbf{k}} & g_{\mathbf{k},+} \\ \Delta^{\dagger}_{\mathbf{k}} & \Delta^{\dagger}_{\mathbf{k}\downarrow\downarrow} & g_{\mathbf{k},-} & -\varepsilon_{\mathbf{k}} \end{pmatrix}. \tag{34}$$

In Eq. (34), all quantities have been defined in the previous section. It is usually argued that interband pairing in a noncentrosymmetric superconductors can be neglected due to a spin-split Fermi surface in the presence of spin-orbit coupling. This is motivated by realizing that the splitting could be as large as[25] 50–200 meV for the noncentrosymmetric superconductor $CePt_3Si$, thus far greater than the superconducting critical temperature $k_B T_c \simeq 0.06$ meV in that compound. Accordingly, one might be tempted to also exclude the spin-singlet gap in the presence of a strong spin-orbit coupling motivated on physical grounds by the suppression of interband pairing due to the spin-split Fermi surfaces. However, it is necessary to investigate the presence, although possibly small in magnitude, of a spin-singlet component of the gap to examine whether the conductance spectrum changes significantly in any respect compared to the scenario with exclusively triplet pairing. Another motivation for including the singlet gap is that the authors of Ref. 21 demonstrated that for small spin-orbit coupling, $\mathbf{d}_{\mathbf{k}} \| \mathbf{g}_{\mathbf{k}}$ yields the highest T_C for $CePt_3Si$. This would thus correspond to a scenario where the triplet gap $\Delta_{\mathbf{k}\uparrow\downarrow}$ is suppressed due to the above condition, although intraband pairing is not strictly forbidden as a result of weak spin-orbit coupling, thus allowing for singlet pairing.

Consider now a gap vector exhibiting point nodes. Since $\mathbf{d}_{\mathbf{k}}$, in general, is given by Eq. (1), the vector characterizing spin-orbit coupling $\mathbf{g}_{\mathbf{k}} = \lambda(k_y, -k_x, 0)$ suggested by Ref. 21 results in

$$\Delta_{\mathbf{k}\uparrow\uparrow} = -\frac{\Delta_t}{2|\mathbf{k}|}(k_y + ik_x), \quad \Delta_{\mathbf{k}\downarrow\downarrow} = \frac{\Delta_t}{2|\mathbf{k}|}(k_y - ik_x). \tag{35}$$

Diagonalization of the Hamiltonian in Eq. (33) yields eigenvalues and eigenvectors which are necessary to calculate the normal- and Andreev-reflection coefficients in a $N/CePt_3Si$ junction. Assuming the simplest form of a s-wave superconducting gap that obeys the symmetry requirements dictated by the Pauli principle, namely, an isotropic gap $\Delta_{\mathbf{k}} = \Delta_s$, we find that the eigenvalues of $M_{\mathbf{k}}$ read

$$E_{\mathbf{k}_{\alpha\beta}} = \alpha\sqrt{(\varepsilon + \beta|\mathbf{g}_{\mathbf{k}}|)^2 + |\Delta_s + \beta\Delta_t/2|^2}. \tag{36}$$

This is in complete agreement with the result of Ref. 26. We are here assuming that all gaps have the same phase associated with the broken U(1) gauge symmetry. In Eq. (36), $\alpha = +\ (-)$ refers to electronlike (holelike) excitations, while $\beta = +\ (-)$ denotes the spin-orbit helicity index. The wave vectors may then be written as

$$q_e^{\uparrow} = q_h^{\uparrow} = \sqrt{k_F^2 + m^2\lambda^2} - m\lambda,$$

$$q_e^{\downarrow} = q_h^{\downarrow} = \sqrt{k_F^2 + m^2\lambda^2} + m\lambda, \tag{37}$$

when making the approximation that the magnitude of the superconducting gaps is small compared to the Fermi energy μ and considering the low-energy transport regime. Here, k_F is the Fermi wave vector.

We now calculate the normal- and Andreev-reflection coefficients for an incident electron with spin σ, which, in turn, will allow us to derive the tunneling conductance of the junction. To do so, we first set up the Bogoliubov–de Gennes (BdG) equations for the system which read (see the Appendix for a derivation)

$$\begin{pmatrix} -\frac{\hat{\nabla}^2}{2m} - \mu + V_0\delta(x) & \lambda(\hat{p}_y + i\hat{p}_x)\Theta(x) & \Delta_{\mathbf{k}\uparrow\uparrow}\Theta(x) & \Delta_s\Theta(x) \\ \lambda(\hat{p}_y - i\hat{p}_x)\Theta(x) & -\frac{\hat{\nabla}^2}{2m} - \mu + V_0\delta(x) & -\Delta_s\Theta(x) & \Delta_{\mathbf{k}\downarrow\downarrow}\Theta(x) \\ \Delta^{\dagger}_{\mathbf{k}\uparrow\uparrow}\Theta(x) & -\Delta_s^{\dagger}\Theta(x) & \frac{\hat{\nabla}^2}{2m} + \mu - V_0\delta(x) & \lambda(\hat{p}_y - i\hat{p}_x)\Theta(x) \\ \Delta_s^{\dagger}\Theta(x) & \Delta^{\dagger}_{\mathbf{k}\downarrow\downarrow}\Theta(x) & \lambda(\hat{p}_y + i\hat{p}_x)\Theta(x) & \frac{\hat{\nabla}^2}{2m} + \mu - V_0\delta(x) \end{pmatrix} \Psi(x,y) = E\Psi(x,y), \tag{38}$$

where $\hat{p}_{x(y)} = -i\hat{\partial}_{x(y)}$ and we make use of the following boundary conditions:

$$\psi(0) = \Psi(0) \text{ (continuity of wave function)},$$

$$2mV_0\psi(0) = \hat{\partial}_x\Psi(0) - \hat{\partial}_x\psi'(0) - m\lambda\eta\Psi(0) \text{ (continuity of flux)}. \tag{39}$$

Note that we have applied the usual step-function approximation for the order parameters instead of solving for their spatial dependence self-consistently near the interface, i.e.,

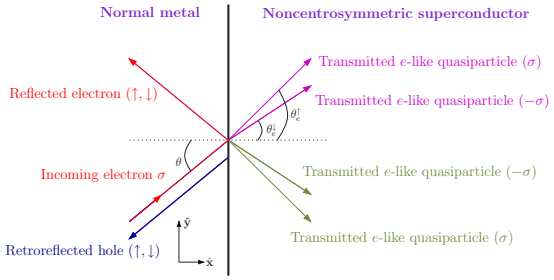

FIG. 1. (Color online) Schematic illustration of the scattering processes taking place at the interface of the 2D planar N/$CePt_3Si$ junction. The arrows indicate the direction of group velocity (which is not equal to the momentum vector for the holes). Note that the presence of spin-orbit coupling causes electronlike and holelike excitations on the superconducting side to be spread into different angles.

$\Delta_{\mathbf{k}\sigma\sigma}(\mathbf{r})=\Delta_{\mathbf{k}\sigma\sigma}\Theta(x)$ and $\Delta(\mathbf{r})=\Delta\Theta(x)$ (we comment further on this later). For convenience, we have defined the 4×4 matrix

$$\eta=\begin{pmatrix}0&1&0&0\\-1&0&0&0\\0&0&0&1\\0&0&-1&0\end{pmatrix}. \tag{40}$$

The presence of spin-orbit coupling leads to off-diagonal components in the velocity operator, such that it would be erroneous to merely match the derivatives of the wave function in this case.[45] The coupled gap equations that arise by demanding a minimum in the free energy are obtained by considering Eqs. (27) and (28). For the sake of obtaining analytical results, we continue our discussion of the conductance spectra of noncentrosymmetric superconductors by inserting values of the superconductivity gaps *a priori* instead of using the self-consistent solutions. This approach does not, then, account for the entire physical picture but has proven to yield satisfactory results for many aspects of quasiparticle tunneling in the case of, e.g., spin-singlet *d*-wave superconductors.[43,46] For the simplest model that illustrates the physics, we have thus chosen a two-dimensional N/$CePt_3Si$ junction with a barrier modeled by $V(\mathbf{r})=V_0\delta(x)$ and superconductivity gaps $\Delta_{\mathbf{k}\sigma\sigma}(\mathbf{r})=\Delta_{\mathbf{k}\sigma\sigma}\Theta(x)$ [$\delta(x)$ and $\Theta(x)$ represent the delta and Heaviside functions, respectively]. Consider Fig. 1 for an overview. Choosing a plane-wave solution $\Psi(x,y)=\Psi(x)e^{ik_yy}$, for $\sigma=\uparrow$, the wave function on the normal [$\psi(x)$] side of the junction reads

$$\psi(x)=\begin{pmatrix}e^{ik_F\cos\theta x}+r_e^{\uparrow}e^{-ik_F\cos\theta x}\\r_e^{\downarrow}e^{-ik_F\cos\theta x}\\r_h^{\uparrow}e^{ik_F\cos\theta x}\\r_h^{\downarrow}e^{ik_F\cos\theta x}\end{pmatrix}. \tag{41}$$

On the superconducting side [$\Psi(x)$], the BdG equation may be written, for our particular choice of $\mathbf{g_k}$ and gaps in Eq. (35), as

$$\begin{pmatrix}\varepsilon_{\mathbf{k}}&|g_{\mathbf{k}}|e^{i\phi}&-(\Delta_t/2)e^{i\phi}&\Delta_s\\|g_{\mathbf{k}}|e^{-i\phi}&\varepsilon_{\mathbf{k}}&-\Delta_s&(\Delta_t/2)e^{-i\phi}\\-(\Delta_t/2)e^{-i\phi}&-\Delta_s&-\varepsilon_{\mathbf{k}}&|g_{\mathbf{k}}|e^{-i\phi}\\\Delta_s&(\Delta_t/2)e^{i\phi}&|g_{\mathbf{k}}|e^{i\phi}&-\varepsilon_{\mathbf{k}}\end{pmatrix}\Psi$$
$$=E\Psi \quad \text{with } \tan\phi(\theta)=1/\tan\theta. \tag{42}$$

We are here concerned with positive excitations $E\geqslant0$, assuming an incident electron above Fermi level. In this case, there are four possible solutions for wave vectors $\mathbf{k}$ with a given energy $E\geqslant0$. Consequently, one may verify that the correct wave function for $x>0$, which is a linear combination of these allowed states, reads

$$\Psi(x)=\frac{t_e^{\uparrow}}{\sqrt{2}}\begin{pmatrix}u(\Delta_+)\\u(\Delta_+)e^{-i\phi(\theta_e^{\uparrow})}\\-v(\Delta_+)e^{-i\phi(\theta_e^{\uparrow})}\\v(\Delta_+)\end{pmatrix}e^{iq_e^{\uparrow}\cos\theta_e^{\uparrow}x}$$
$$+\frac{t_e^{\downarrow}}{\sqrt{2}}\begin{pmatrix}u(\Delta_-)\\-u(\Delta_-)e^{-i\phi(\theta_e^{\downarrow})}\\v(\Delta_-)e^{-i\phi(\theta_e^{\downarrow})}\\v(\Delta_-)\end{pmatrix}e^{iq_e^{\downarrow}\cos\theta_e^{\downarrow}x}$$
$$+\frac{t_h^{\uparrow}}{\sqrt{2}}\begin{pmatrix}v(\Delta_+)\\v(\Delta_+)e^{-i\phi(\theta_h^{\uparrow})}\\-u(\Delta_+)e^{-i\phi(\theta_h^{\uparrow})}\\u(\Delta_+)\end{pmatrix}e^{iq_h^{\uparrow}\cos\theta_h^{\uparrow}x}$$
$$+\frac{t_h^{\downarrow}}{\sqrt{2}}\begin{pmatrix}v(\Delta_-)\\-v(\Delta_-)e^{-i\phi(\theta_h^{\downarrow})}\\u(\Delta_-)e^{-i\phi(\theta_h^{\downarrow})}\\u(\Delta_-)(74)\end{pmatrix}e^{iq_h^{\downarrow}\cos\theta_h^{\downarrow}x}. \tag{43}$$

We have defined $\Delta_\pm=\Delta_s\pm(\Delta_t/2)$, and the spreading angles in Eq. (43) are given as $\sin\theta_e^{\sigma}=(k_F\sin\theta)/q^{\sigma}$, $\theta_h^{\sigma}=\pi-\theta_e^{\sigma}$. This follows from the fact that translational symmetry is conserved along the y axis. The coherence factors entering the wave functions in Eq. (43) are given as

$$u(\Delta)=\sqrt{\frac{1}{2}+\frac{\sqrt{E^2-|\Delta|^2}}{2E}},\quad v(\Delta)=\sqrt{\frac{1}{2}-\frac{\sqrt{E^2-|\Delta|^2}}{2E}}. \tag{44}$$

We also define the dimensionless parameters $Z=2mV_0/k_F$ and $\beta=2m\lambda/k_F$ as measures of the intrinsic barrier strength and magnitude of the spin-orbit coupling, respectively.

Note that we are using the same effective masses in the normal part of the system as in the superconducting part. The mass of the quasiparticles in heavy-fermion materials is, as the name itself implies, ordinarily much larger than in normal metals. It was recently shown by Yokoyama *et al.*[47] that in a two-dimensional electron gas (2DEG)/superconductor junction where spin-orbit coupling was substantial in the 2DEG, the effect of including a larger effective mass in the 2DEG was equivalent to that caused by an increase of Z.

Note that in the presence of a time-reversal breaking magnetic field, it was shown in Refs. 48 and 49 that the effect of Fermi-vector mismatch could not be reproduced simply by varying the barrier parameter Z. Since there is no time-reversal breaking field present in this case, however, we here restrict ourselves to considering equal effective masses in the two systems. With the above equations, one is able to find explicit expressions for $\{r_e^\sigma, r_h^\sigma\}$. The procedure illustrated here is identical for incoming electrons with $\sigma=\downarrow$ when using

$$\psi(x) = \begin{pmatrix} r_e^{\uparrow} e^{-ik_F \cos\theta x} \\ e^{ik_F \cos\theta x} + r_e^{\downarrow} e^{-ik_F \cos\theta x} \\ r_h^{\uparrow} e^{ik_F \cos\theta x} \\ r_h^{\downarrow} e^{ik_F \cos\theta x} \end{pmatrix} \tag{45}$$

instead of Eq. (41). This establishes the framework which serves as the basis for calculating the conductance spectrum.

B. Conductance spectra for noncentrosymmetric superconductors

We now proceed to calculate the tunneling conductance for our setup. Generalizing the theory of Blonder *et al.*[44] one obtains a conductance $G(E,\theta)$ (scaled on the conductance in a N-N junction) for an incoming electron with angle θ to the junction normal with spin σ, where

$$G(E,\theta) = 1 + \sum_\alpha (|r_h^\alpha(E,\theta)|^2 - |r_e^\alpha(E,\theta)|^2), \tag{46}$$

and $R_{N\text{-}N} = \int_{-\pi/2}^{\pi/2} [(4\cos^3\theta)/(4\cos^2\theta + Z^2)] d\theta$. The angularly averaged conductance reads

$$G(E) = (R_{N\text{-}N})^{-1} \int_{-\pi/2}^{\pi/2} G(E,\theta) P(\theta) d\theta, \tag{47}$$

where $P(\theta)$ is the probability distribution function $[P(0)=1]$ for incoming electrons at an angle θ. This is, in many cases, set to $P(\theta)=\cos\theta$, but other forms modeling, e.g., effective tunneling cones may also be applied. In obtaining the total conductance, one has to find $G(E)$ for both $\sigma=\uparrow$ and $\sigma=\downarrow$ and then add these contributions. The original derivation of this specific formula for the tunneling conductance given in Ref. 48 relies on the relation

$$|r_h^\sigma(E)|^2 = |r_h^\sigma(-E)|^2 \tag{48}$$

to hold. This is known to be valid for subgap energies, but for energies above the gap, the relationship does not hold in general, a fact which implies that the conductance formula derived in Ref. 48 is only valid for applied voltages below the gap, strictly speaking. However, since the probability for Andreev reflection rapidly diminishes for energies above the gap (especially for $Z \neq 0$), the conductance formula may still be applied for larger voltages as a reasonable approximation, even for the high-transparency case of low values for Z.

The explicit analytical expressions for the normal- and Andreev-reflection probabilities, $|r_e^\sigma|^2$ and $|r_h^\sigma|^2$, respectively, are too large and unwieldy to be of any instructive use. We shall therefore be content with plotting these expressions to reveal the physics embedded within them. In most scanning tunneling microscopy (STM) experiments, a high-transparency interface is often realized, corresponding to low Z. Also, since the band splitting $2\lambda k_F$ at the Fermi level may be of order[25] of 100 meV for $CePt_3Si$, a simple analysis relating this to our dimensionless parameter β yields that $\beta \simeq 0.05$. We therefore plot in Fig. 2 the angularly averaged (and normalized) conductance spectrum for several values of barrier strength and singlet/triplet gap ratios, fixing the spin-orbit coupling parameter at $\beta=0.05$. From Fig. 2, we see that one may infer the relative size of the singlet and triplet components of the gap by the characteristic behavior of $G(E)$ at voltages corresponding to $\Delta_s \pm \Delta_t/2$. This is in agreement with what one could expect by studying the form of the eigenvalues in Eq. (36), since it is this precise combination of the gaps that appears in the expression.

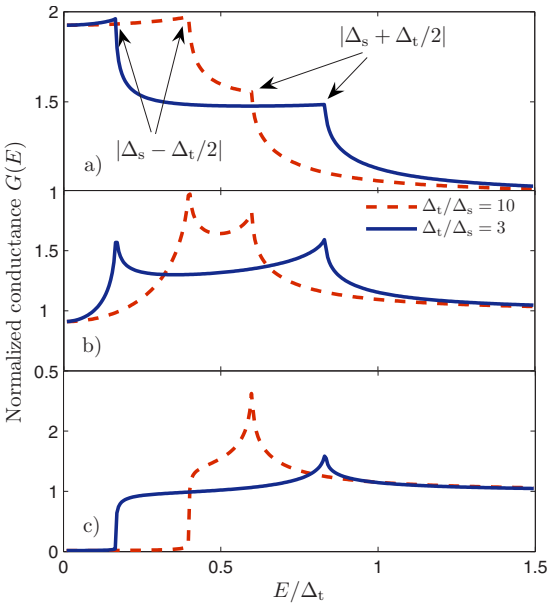

FIG. 2. (Color online) Tunneling conductance for $N/CePt_3Si$ junction with $\beta=0.05$. We study barrier strengths corresponding to (a) $Z=0.1$, (b) $Z=1$, and (c) $Z=10$. In all cases, we plot the ratios $\Delta_t/\Delta_s=\{3,10\}$ to see how the spectra are affected. It is seen that the conductance spectra reveal information about the relative size of the singlet and triplet components of the gaps by characteristic features located at bias voltages $E=|\Delta_s \pm \Delta_t/2|$.

In a recent study[50] by Iniotakis *et al.*, a normal/noncentrosymmetric superconductor junction was studied for low-transparency interfaces, where it was found that zero-bias anomalies would take place for certain STM measurement orientations if a specific form of the mixed singlet-triplet order parameter was realized. This may be attributed to the formation of zero-energy bound states,[51] which is possible when the gap contains nodes. In the present study, we are using an isotropic spin-singlet gap and also isotropic p-wave gaps ($|\Delta_{\mathbf{k}\sigma\sigma}|=$constant),[52] such one does not expect

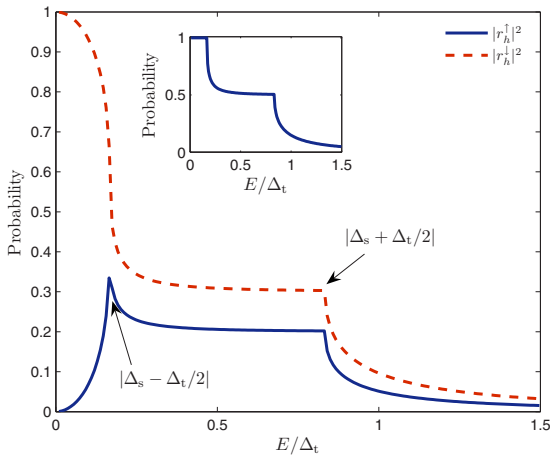

FIG. 3. (Color online) Andreev-reflection coefficients for spin-↑ and spin-↓ fermions in the case of incoming $\sigma=\uparrow$ electrons. It is seen that the degree of spin polarization of the generated quasiparticle current will vary with the bias voltage. The inset contains a plot of the sum of reflection coefficients (both normal and Andreev), showing that no transmittance of quasiparticles occurs for voltages below $E=|\Delta_s-\Delta_t/2|$.

the appearance of a zero-bias conductance peak, in contrast to Ref. 50. Moreover, we note that the spin-orbit coupling in the system gives rise to effectively spin-active boundary conditions [see Eq. (39)].[53,54]

It is also instructive to consider the Andreev-reflection probabilities explicitly to resolve the spin structure of the quasiparticle current, as shown in Fig. 3 for an incoming electron with spin $\sigma=\uparrow$. It is seen that the spin-↓ coefficient becomes larger with increasing voltage, such that the spin polarization of the current will vary with the bias voltage. The proper definition of a spin current in systems exhibiting spin-orbit coupling has, however, been shown[55] to be more subtle than applying the usual relations for charge and spin currents,

$$\mathbf{j}_{\text{charge}} = -e\sum_{\sigma}\mathbf{j}_{\sigma}, \quad \mathbf{j}_{\text{spin}} = \sum_{\sigma}\sigma\mathbf{j}_{\sigma}, \tag{49}$$

where $\mathbf{j}_{\sigma}$ is the particle current of fermions with spin σ. Therefore, it is fair to claim that it is not obvious how one might detect such a change in polarization of the quasiparticle current with a change in bias voltage. On the other hand, the charge current remains unaffected by these considerations, and our results thus indicate that the conductance spectrum of the charge current in a $N/CePt_3Si$ junction may provide valuable information about the relative size of the singlet and triplet components of the superconductivity gap.

We now comment on effects that have not been taken into account in our analysis of this problem. First, the issue of how boundary effects affect the order parameters is addressed. Studies[56–58] have shown that interfaces and/or surfaces may have a pair-breaking effect on unconventional superconductivity order parameters. This is relevant in tunneling junction experiments as in the present case. The suppression of the order parameter is caused by a formation of the so-called midgap surface states (also known as zero-energy states),[51] which occurs for certain orientations of the **k**-dependent superconducting gaps that satisfy a resonance condition. Note that this is not the case for conventional *s*-wave superconductors since the gap is isotropic in that case. This pair-breaking surface effect was studied specifically for *p*-wave order parameters in Refs. 56 and 57, and it was found that the component of the order parameter that experiences a sign change under the transformation $k_{\perp}\rightarrow -k_{\perp}$, where $k_{\perp}$ is the component of momentum perpendicular to the tunneling junction, was suppressed in the vicinity of the junction. By vicinity of the junction, we mean here a distance comparable to the coherence length, typically of order of 1–10 nm. Thus, depending on the explicit form of the superconducting gaps in the noncentrosymmetric superconductor, these could be suppressed close to the interface. Moreover, we are dealing with an easily observable effect, since distinguishing between the peaks occurring for various values of R_{Δ} requires a resolution of order $\mathcal{O}(10^{-1}\Delta_{\uparrow,0})$, which typically corresponds to 0.1–1 meV. These structures should readily be resolved with present-day STM technology. However, it should be pointed out that a challenge with respect to tunneling junctions is dealing with nonidealities at the interface, which may affect the conductance spectrum.

In order to fully consider the possible pair-breaking effect of the interface in an enhanced model, one would obviously need to solve the scattering problem self-consistently in order to obtain more precise results for the conductance, especially in terms of the quantitative aspect. To obtain analytical results, however, we have inserted the gaps *a priori*, since we believe that our model captures essential qualitative features in a $N/CePt_3Si$ junction that could be probed for. This belief is motivated by studies[59] for $d_{x^2-y^2}$ superconductors which show that the conductance shape around zero bias remains essentially unchanged even if the spatial dependence of the order parameters is taken into account. The spectra around the gap edges may be modified in the sense that since the gap, in general, will be somewhat reduced close the interface, the appearance of characteristic features in the conductance could occur at lower bias voltages than the bulk value of the gaps. However, it seems reasonable to hope that our simple model may be of use in predicting qualitative features of the conductance spectrum when considering junctions involving noncentrosymmetric superconductors such as $CePt_3Si$.

V. PROBING THE PAIRING SYMMETRY OF FERROMAGNETIC SUPERCONDUCTORS

As a second application of our model, we consider a model of a ferromagnetic superconductor described by uniformly coexisting itinerant ferromagnetism and equal-spin pairing nonunitary spin-triplet superconductivity.

A. Model and formulation

We write down a mean-field theory Hamiltonian with equal-spin pairing Cooper pairs and a finite magnetization

along the easy axis similar to the model studied in Refs. 60–62, namely,

$$\hat{H} = \sum_{\mathbf{k}} \xi_{\mathbf{k}} + \frac{INM^2}{2} - \frac{1}{2}\sum_{\mathbf{k}\sigma} \Delta^{\dagger}_{\mathbf{k}\sigma\sigma} b_{\mathbf{k}\sigma\sigma} + \frac{1}{2}\sum_{\mathbf{k}\sigma} (\hat{c}^{\dagger}_{\mathbf{k}\sigma}\hat{c}_{-\mathbf{k}\sigma}) \times \begin{pmatrix} \xi_{\mathbf{k}\sigma} & \Delta_{\mathbf{k}\sigma\sigma} \\ \Delta^{\dagger}_{\mathbf{k}\sigma\sigma} & -\xi_{\mathbf{k}\sigma} \end{pmatrix} \begin{pmatrix} \hat{c}_{\mathbf{k}\sigma} \\ \hat{c}^{\dagger}_{-\mathbf{k}\sigma} \end{pmatrix}, \tag{50}$$

Applying the diagonalization procedure described in Sec. II, we arrive at

$$\hat{H} = H_0 + \sum_{\mathbf{k}\sigma} E_{\mathbf{k}\sigma} \hat{\gamma}^{\dagger}_{\mathbf{k}\sigma} \hat{\gamma}_{\mathbf{k}\sigma},$$

$$H_0 = \frac{1}{2}\sum_{\mathbf{k}\sigma} (\xi_{\mathbf{k}\sigma} - E_{\mathbf{k}\sigma} - \Delta^{\dagger}_{\mathbf{k}\sigma\sigma} b_{\mathbf{k}\sigma\sigma}) + \frac{INM^2}{2}, \tag{51}$$

where $\{\hat{\gamma}_{\mathbf{k}\sigma}, \hat{\gamma}^{\dagger}_{\mathbf{k}\sigma}\}$ are new fermion operators and the eigenvalues read

$$E_{\mathbf{k}\sigma} = \sqrt{\xi^2_{\mathbf{k}\sigma} + |\Delta_{\mathbf{k}\sigma\sigma}|^2}. \tag{52}$$

Recall that it is implicit in our notation that $\xi_{\mathbf{k}}$ is measured from the Fermi level. The free energy is obtained by using the procedure explained in Sec. II, and one obtains

$$F = H_0 - \frac{1}{\beta}\sum_{\mathbf{k}\sigma} \ln(1 + e^{-\beta E_{\mathbf{k}\sigma}}), \tag{53}$$

such that the gap equations for the magnetic and superconducting order parameters become[60]

$$M = -\frac{1}{N}\sum_{\mathbf{k}\sigma} \frac{\sigma\xi_{\mathbf{k}\sigma}}{2E_{\mathbf{k}\sigma}} \tanh\left(\frac{\beta E_{\mathbf{k}\sigma}}{2}\right),$$

$$\Delta_{\mathbf{k}\sigma\sigma} = -\frac{1}{N}\sum_{\mathbf{k}'} V_{\mathbf{k}\mathbf{k}'\sigma\sigma} \frac{\Delta_{\mathbf{k}'\sigma\sigma}}{2E_{\mathbf{k}'\sigma}} \tanh\left(\frac{\beta E_{\mathbf{k}'\sigma}}{2}\right). \tag{54}$$

For concreteness, we now consider a specific form of the gaps, similar to those studied in Refs. 60 and 62. Assuming that the gap is fixed on the Fermi surface in the weak-coupling limit, we write

$$\Delta_{\mathbf{k}\sigma\sigma} = \Delta_{\bar{\mathbf{k}}_F\sigma\sigma} = \frac{\Delta_{\sigma,0}}{\sqrt{3/8\pi}} Y^{\sigma}_{l=1}(\theta,\phi), \tag{55}$$

where $\bar{\mathbf{k}}_F$ is the normalized Fermi wave vector, such that the gap only depends on the direction of the latter. We have introduced the spherical harmonics

$$Y^{\sigma}_{l=1}(\theta,\phi) = -\sigma\sqrt{3/8\pi} e^{i\sigma\theta} \sin\phi, \tag{56}$$

such that the gaps in Eq. (55) experience a change in sign under inversion of momentum, i.e., $\theta \to \theta + \pi$. We shall consider the case $\sin\phi = 1$ which renders the magnitude of the gaps to be constant, similar to the $A2$ phase in liquid ^{3}He. The motivation for this is that it seems plausible that uniform coexistence of ferromagnetic and superconducting orders may only be realized in thin-film structures, where the Meissner (diamagnetic) response of the superconductor is suppressed for in-plane magnetic fields. This enables us to set $\sin\phi = 1$, since the electrons are restricted from moving in the $\hat{\mathbf{z}}$ direction in a thin-film structure. In a bulk structure, as considered in Ref. 62, we expect that a spontaneous vortex lattice should be the favored thermodynamical state.[28] The pairing potential may then, in general, be written as

$$V_{\sigma\sigma}(\theta,\theta') = -\sum_m \frac{g^m_{\sigma\sigma}}{3/8\pi} Y^{\sigma}(\theta)[Y^{\sigma}(\theta')]^*, \tag{57}$$

which for the chosen gaps reduces to

$$V_{\sigma\sigma}(\theta,\theta') = -\frac{8\pi g}{3} Y^{\sigma}(\theta)[Y^{\sigma}(\theta')]^*. \tag{58}$$

Conversion to integral gap equations is accomplished by means of the identity

$$\frac{1}{N}\sum_{\mathbf{k}} f(\xi_{\mathbf{k}\sigma}) = \int d\varepsilon N^{\sigma}(\varepsilon), \tag{59}$$

where $N^{\sigma}(\varepsilon)$ is the spin-resolved density of states. In three spatial dimensions, this may be calculated from the dispersion relation by using the formula

$$N^{\sigma}(\varepsilon) = \frac{V}{(2\pi)^3} \int_{\varepsilon_{\mathbf{k}\sigma}=\text{const}} \frac{dS_{\varepsilon_{\mathbf{k}\sigma}}}{|\hat{\nabla}_{\mathbf{k}}\varepsilon_{\mathbf{k}\sigma}|}. \tag{60}$$

With the dispersion relation $\xi_{\mathbf{k}\sigma} = \varepsilon_{\mathbf{k}} - \sigma IM - E_F$ (having set the chemical potential equal to the Fermi energy, $\mu = E_F$), one obtains

$$N^{\sigma}(\varepsilon) = \frac{mV\sqrt{2m(\varepsilon + \sigma IM) + E_F}}{2\pi^2}. \tag{61}$$

In their integral form, the gap equations read

$$M = -\frac{1}{2}\sum_{\sigma} \sigma \int_{-E_F - \sigma IM}^{\infty} d\varepsilon \frac{\varepsilon N^{\sigma}(\varepsilon)}{\sqrt{\varepsilon^2 + \Delta^2_{\sigma,0}}} \tanh\left[\frac{\beta E_{\sigma}(\varepsilon)}{2}\right],$$

$$1 = \frac{g}{2}\int_{-\omega_0}^{\omega_0} d\varepsilon \frac{N^{\sigma}(\varepsilon)}{E_{\sigma}(\varepsilon)} \tanh\left[\frac{\beta E_{\sigma}(\varepsilon)}{2}\right]. \tag{62}$$

B. Zero-temperature case

Consider now $T = 0$, where we are able to obtain analytical expressions for the superconductivity order parameters in the problem. Since the superconductivity gap equation reduces to

$$1 = \frac{g}{2}\int_{-\omega_0}^{\omega_0} d\varepsilon \frac{N^{\sigma}(\varepsilon)}{E_{\sigma}(\varepsilon)}, \tag{63}$$

one readily finds

$$\Delta_{\sigma,0} = 2\omega_0 e^{-1/c\sqrt{1+\sigma\tilde{M}}}, \quad \sigma = \uparrow, \downarrow, \tag{64}$$

where we have defined $\tilde{M} = IM/E_F$, i.e., the exchange energy scaled on the Fermi energy. Moreover, the weak-coupling constant $c = gN(0)/2$ will be set to 0.2 throughout the rest of this paper, unless specifically stated otherwise. Moreover, we

set $\tilde{\omega}_0=\omega_0/E_F=0.01$ as the typical spectral width of the bosons responsible for the attractive pairing potential. From Eq. (64), we see that the effect of increasing the magnetization is an increase in the gap for majority spin. The important influence of the magnetization is that it modifies the density of states, which affects the superconductivity gaps. For $\tilde{M}=1$, i.e., an exchange splitting equal to the Fermi energy, the minority-spin gap is completely suppressed, as shown in Fig. 4. Thus, the presence of magnetization reduces the available phase space for the minority-spin Cooper pairs, suppressing the gap and the critical temperature compared to the pure Bardeen-Cooper-Schrieffer (BCS) case.

After the appropriate algebraic manipulations of Eq. (62), the self-consistency equation for the magnetization becomes

$$f(\tilde{M})=\tilde{M}+\frac{\tilde{I}}{4}\int_{-1-\tilde{M}}^{\infty}dx\sqrt{1+x+\tilde{M}}\left\{\frac{[1-2\Theta(-\sqrt{x^2+\tilde{\Delta}_{\uparrow,0}^2(\tilde{M})})]}{x^{-1}\sqrt{x^2+\tilde{\Delta}_{\uparrow,0}^2(\tilde{M})}}-\frac{[1-2\Theta(-\sqrt{(x+2\tilde{M})^2+\tilde{\Delta}_{\downarrow,0}^2(\tilde{M})})]}{(x+2\tilde{M})^{-1}\sqrt{(x+2\tilde{M})^2+\tilde{\Delta}_{\downarrow,0}^2(\tilde{M})}}\right\}=0, \quad (65)$$

where we have defined the parameter $\tilde{I}=IN(0)$, in similarity to Ref. 60, and introduced $\tilde{\Delta}_{\sigma,0}(\tilde{M})=\Delta_{\sigma,0}/E_F$. We have thus managed to decouple the gap equations completely, such that one only has to solve Eq. (65) to find the magnetization, and then plug that value into Eq. (64). Note that strictly speaking, one should divide the integral in Eq. (65) into three parts: $\{-1-\tilde{M},-\omega_0\}$, $\{\omega_0,\infty\}$, and $\{-\omega_0,\omega_0\}$, where the superconductivity gaps are only nonzero in the latter interval. However, the error associated with doing the integration numerically over the entire regime with a finite value for the gaps is completely negligible. From Eq. (65), we see that the trivial solution $\tilde{M}=0$ is always possible. Interestingly, we find that a nontrivial solution implying coexistence of ferromagnetism and superconductivity is only possible when $\tilde{I}>1$ (in agreement with Ref. 60). To illustrate this fact, consider Fig. 5 for a plot of $f(\tilde{M})$ in Eq. (65) as a function of $\tilde{M}$ for several values of $\tilde{I}$. In fact, it is seen that more than one solution is possible for any $\tilde{I}>1$: the trivial solution $\tilde{M}=0$ corresponding to a unitary superconducting state and a nontrivial solution $\tilde{M}=\tilde{M}_0$ representing a nonunitary superconducting state. Recall that in terms of the $\mathbf{d_k}$-vector formalism, these classifications are defined as

$$\text{unitary:}\mathbf{d_k}\times\mathbf{d_k}^*=0, \quad \text{nonunitary:}\mathbf{d_k}\times\mathbf{d_k}^*\neq 0. \quad (66)$$

We will later show that the free energy is minimal in the nonunitary state, which implies that the coexistence of ferromagnetism and superconductivity may indeed be realized in our model.

The order parameters depend on the parameters $(T,\tilde{I},c)$. To illustrate their dependence on $\tilde{I}$ at $T=0$, consider Fig. 6. It is clearly seen that the superconductivity gaps are equal for $\tilde{I}<1$, corresponding to a unitary spin-triplet pairing state. For $\tilde{I}>1$, a spontaneous magnetization arises and the majority- (minority-) spin gap increases (decreases). This corresponds to the coexistent phase of ferromagnetism and superconductivity. An important point concerning Eq. (65) is the inclusion of the step-function factors, which are superfluous as long as we are considering the coexistent regime of ferromagnetism and superconductivity, since their argument is always negative. However, if one, for instance, were to set one or both of the superconductivity gaps to zero, the correct gap equation for the magnetization would not be reproduced without them. This is due to the loss of generality in taking the limit $\tanh(\beta E_\sigma)\to 1$ when $\beta\to\infty$ in deriving Eq. (65), since $E_\sigma>0$ is replaced with ε when superconductivity is lost, which can be both larger and smaller than zero when $\Delta_{\sigma,0}\to 0$. The present form of Eq. (65) is generally valid for the purely magnetic and the coexistent $A1$ and $A2$ phases of the ferromagnetic superconductor.

In order to correctly characterize the pairing symmetry of FMSCs, it is of interest to find clear-cut experimental signatures that distinguish between the possible phases of such an unconventional superconductors. As we have alluded to, it seems reasonable to assume that a superconducting phase analogous to the $A1$ or $A2$ phase of ^{3}He may be realized in FMSCs. We now investigate how the magnetization at $T=0$ depends on the ferromagnetic exchange energy constant $\tilde{I}$ in these possible phases and compare them to the purely ferromagnetic case. Our results are shown in Fig. 7, where we have self-consistently solved for $\tilde{M}$ as a function of $\tilde{I}$ in three cases: (1) the purely ferromagnetic phase, (2) the $A1$ phase where only spin-$\uparrow$ fermions are paired, and (3) the $A2$ phase where all spin bands participate in the superconducting pairing. It is seen that the magnetization is practically identical in all phases regardless of the value of $\tilde{I}$. Analytically, this may be understood since the difference Δf [see Eq. (65)] between the gap equation for the magnetization in the purely ferromagnetic case and the coexistent state reads

$$\Delta f=\sum_\sigma \sigma\left[\int_{-\omega_0}^{\omega_0}d\varepsilon N^\sigma(\varepsilon)\left(1-\frac{|\varepsilon|}{\sqrt{\varepsilon^2+\Delta_{\sigma,0}^2}}\right)\right]\simeq 0. \quad (67)$$

Note that in our results, an enhancement of the magnetization below the superconductivity critical temperature is absent, contrary to the results of Ref. 62, which predicted that the magnetization should be enhanced in the coexistent phases compared to the purely ferromagnetic phase. For the weak-coupling approach applied here, it seems reasonable

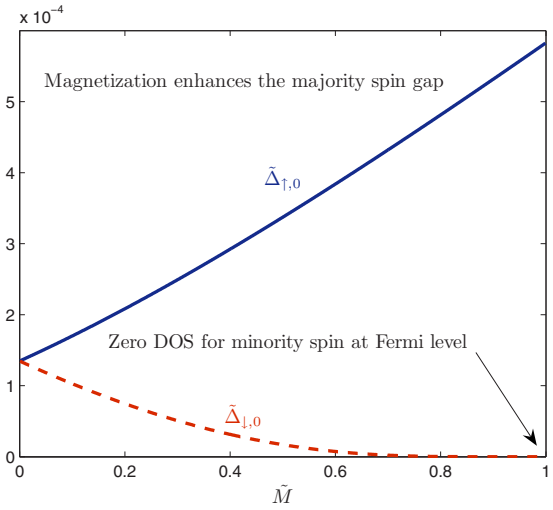

FIG. 4. (Color online) Superconducting gaps (full drawn line, majority spin; dashed line, minority spin) as a function of the magnetization with $\omega_0=0.01E_F$. When the exchange splitting equals the Fermi energy, the DOS of minority-spin fermions is zero at the Fermi level, resulting in a complete suppression of $\Delta_{\sigma,0}$.

that the presence of superconductivity should not alter the magnetization much, while superconductivity itself is drastically modified depending on the strength of the exchange energy. The result of Ref. 62 may be a consequence of the fact that they do not set $\sin\phi=1$ [Eq. (56)] and, consequently, have additional nodes compared to the gaps we are using.

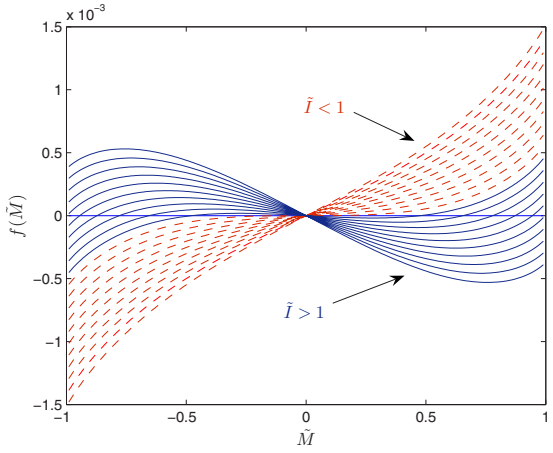

FIG. 5. (Color online) Plot of $f(\tilde{M})$ in Eq. (65) as a function of $\tilde{M}$. Only the trivial solution exists for $\tilde{I}<1$, while three possible solutions are present at $\tilde{I}>1$. We have plotted Eq. (65) for values of $\tilde{I}=[0.9,1.1]$ in steps of 0.01.

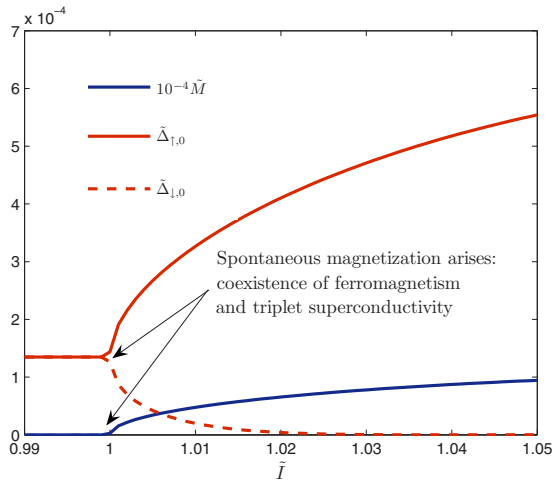

FIG. 6. (Color online) Self-consistently solved order parameters at $T=0$ as a function of $\tilde{I}$. It is seen that the coexistent regime of ferromagnetism and superconductivity is located at $\tilde{I}>1$, where a spontaneous magnetization arises.

C. Finite temperature case

The critical temperature for the superconductivity order parameter is found by solving the equation

$$1=\frac{g}{2}\int_{-\omega_0}^{\omega_0}d\varepsilon\frac{N^{\sigma}(\varepsilon)}{\varepsilon}\tanh\left(\frac{\varepsilon}{2T_{c,\sigma}}\right), \tag{68}$$

which yields the BCS-like solution

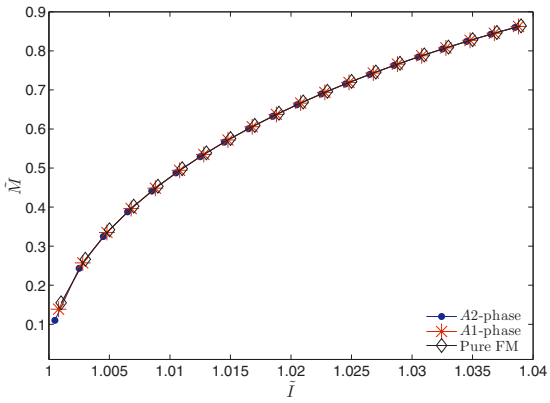

FIG. 7. (Color online) Plot of the exchange energy $\tilde{M}=IM/E_F$ at $T=0$ as a function of $\tilde{I}=IN(0)$ for two possible phases of a FMSC (the $A1$ and $A2$ phases) compared to the purely ferromagnetic case. It is seen that $\tilde{M}$ is virtually unaltered by the presence of superconductivity, at least in the weak-coupling approach we have adopted here (see also Ref. 62).

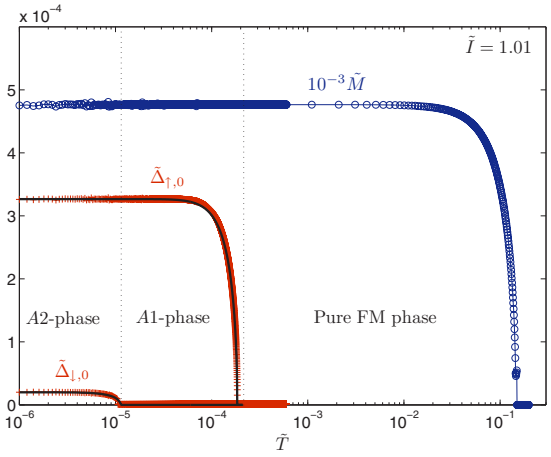

FIG. 8. (Color online) Self-consistently solved order parameters as a function of temperature for $\tilde{I}=1.01$. Note that the temperature axis is logarithmic, such that the transition between the paramagnetic and ferromagnetic phase is much higher than the superconducting phase transitions. However, we are able to tune $\tilde{I}$ such that $T_{c,M}$ and $T_{c,\sigma}$ become comparable. We have also plotted the gaps with self-consistently solved values at $T=0$ and then applying a BCS-temperature dependence (solid black lines), which yields excellent consistency with the solution that does not assume a BCS-temperature dependence.

$$T_{c,\sigma} = 1.13\omega_0 e^{-1/c\sqrt{1+\sigma M(\tilde{T}_{c,\sigma})}}. \tag{69}$$

Since the transition temperature for paramagnetism-ferromagnetism is, in general, much larger than the superconducting phase transition, one may, to good approximation, set $M(T_{c,\sigma})=M(0)$. It is then evident that the critical temperature depends on the magnetization in the same manner as the gap itself, and the cutoff dependence in Eq. (64) may be removed in favor of the critical temperature by substituting Eq. (69). In order to solve the coupled gap equations self-consistently at arbitrary temperature, we considered Eq. (62) with the result given in Fig. 8. It is seen that the minority-spin gap is clearly suppressed compared to the majority-spin gap in the presence of a net magnetization. Also, the graph clearly shows that the BCS-temperature dependence constitutes an excellent approximation for the decrease of the OPs with temperature. In what follows, we shall therefore use self-consistently obtained solutions at $T=0$ for the OPs and make use of the BCS-temperature dependence unless specifically stated otherwise. In general, the critical temperature for the ferromagnetic order parameter $T_{c,M}$ exceeds the superconducting phase transition temperatures $T_{c,\sigma}$ by several orders of magnitude. However, for $\tilde{I}$ very close to 1, we are able to make these transition temperatures comparable in magnitude. In the experimentally discovered FMSCs UGe_2 and URhGe, one finds that $T_{c,M}$ is 50–100 times higher than the temperature at which superconductivity arises.

To illustrate how the magnetic order parameter depends on $\tilde{I}$, consider Fig. 9 for a plot of the temperature dependence

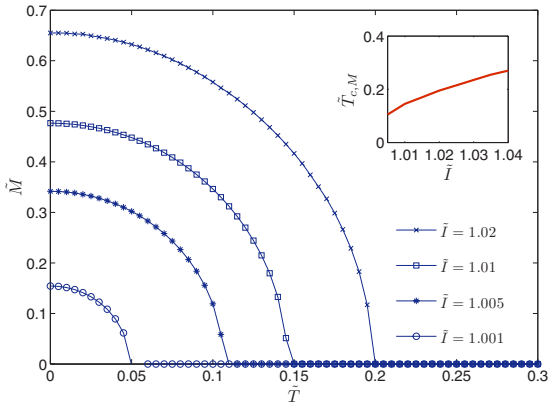

FIG. 9. (Color online) Temperature dependence of the magnetic order parameter for several values of $\tilde{I}$. The inset shows how the critical temperature depends on $\tilde{I}$.

for several values of $\tilde{I}$. The inset shows how the critical temperature depends on this parameter.

D. Comparison of free energies

Although a nontrivial solution of M exists, care must be exercised before concluding that this is the preferred energetical configuration of the system. Specifically, it may in theory be possible that the systems prefers the $M=0$ solution regardless of the value of $\tilde{I}$, corresponding to a unitary superconducting state with $\Delta_{\uparrow,0}=\Delta_{\downarrow,0}$. It is therefore necessary to compare the free energies of the $M=0$ and $M\neq 0$ cases at values of $\tilde{I}$ where the latter is a possible solution and also study their temperature dependence. In the general case, the analytical expression for the free energy in the coexistent nonunitary superconducting phase reads

$$\frac{F}{N} = \frac{IM^2}{2} + \sum_\sigma \frac{\Delta_{\sigma,0}^2}{2g} - \sum_\sigma \int_{-E_F-\sigma IM}^{\infty} d\varepsilon N^\sigma(\varepsilon)\left[\frac{\sqrt{\varepsilon^2+\Delta_{\sigma,0}^2}}{2} + \frac{1}{\beta}\ln(1+e^{-\beta\sqrt{\varepsilon^2+\Delta_{\sigma,0}^2}})\right]. \tag{70}$$

Note that the gap should be set to zero in the above equation everywhere except in the interval $\{-\omega_0,\omega_0\}$. We obtain a dimensionless measure of the free energy by multiplying with I/E_F^2 and denote $F_{\mathrm{NU}}=FI/(NE_F^2)$. Note that the free energies of the unitary state, pure ferromagnetic state, and paramagnetic state are obtained as follows:

$$F_{\mathrm{U}} = \lim_{M\to 0} F_{\mathrm{NU}},$$

$$F_{\mathrm{PM}} = \lim_{M\to 0,\Delta_{\sigma,0}\to 0} F_{\mathrm{NU}},$$

$$F_{\mathrm{FM}} = \lim_{\Delta_{\sigma,0}\to 0} F_{\mathrm{NU}}. \tag{71}$$

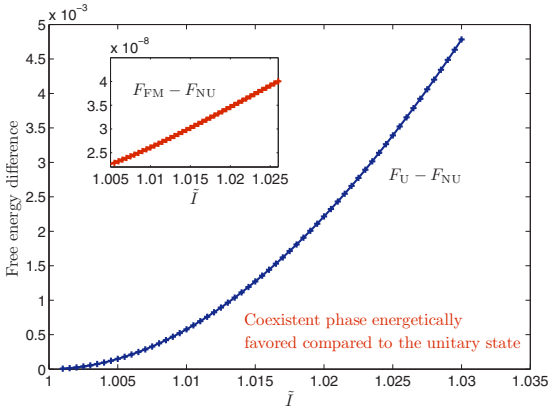

FIG. 10. (Color online) Comparison between the free energies for the nonunitary and unitary superconducting state at zero temperature. It is seen that these values are equal for $\tilde{I}=1$ (and for $\tilde{I}<1$), while the nonunitary state is energetically favored for increasing ferromagnetic exchange energy. Thus, the coexistent phase should be realized at sufficiently low temperatures in the presence of a ferromagnetic exchange energy.

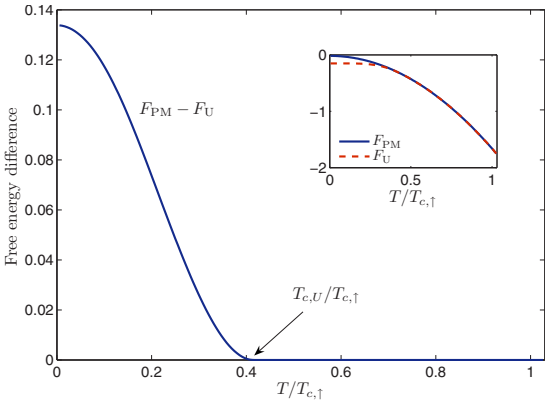

FIG. 11. (Color online) Free energy difference between the paramagnetic state (F_{PM}) and the unitary superconducting state (F_{U}). In consistency with established results (see, e.g., Ref. 68), the free energies merge continuously as the temperature gets closer to $T_{c,U}$. In the inset, we have chosen the zero-temperature value of the paramagnetic free energy as zero, serving as a reference point. We have solved all order parameters self-consistently for $\tilde{I}=1.01$.

In Fig. 10, we plot the difference between the unitary and nonunitary solutions at zero temperature, $\Delta F=F_{\mathrm{U}}-F_{\mathrm{NU}}$, which clearly shows how the system favors the nonunitary solution with spontaneous magnetization as $\tilde{I}$ increases. As a result, we suggest that the coexistent phase of ferromagnetism and superconductivity should be realized at sufficiently low temperatures whenever a magnetic exchange energy is present. For consistency, we also verified that $F_{\mathrm{NU}}<F_{\mathrm{FM}}$ at $T=0$, since the system otherwise would prefer to leave superconductivity out of the picture and stay purely ferromagnetic.

We now turn to the temperature dependence of the free energy at the fixed value of $\tilde{I}=1.01$ (the order parameters were self-consistently solved for this value and plotted in Fig. 8). The results are shown in Figs. 11–13. Note that we now use a different scaling of the free energy, namely, $F_{\mathrm{NU}}=F/[NN(0)E_F^2]$. The well-known result that the free energy of a purely superconducting state joins the free energy of the paramagnetic state continuously as the temperature increases is reproduced in Fig. 11. In Fig. 12, we see that the coexistent phase of ferromagnetism and superconductivity is energetically favored compared to the purely ferromagnetic case, which is consistent with the experimental fact that a transition to superconductivity occurs below the Curie temperature for certain materials.[1,2] Finally, in Fig. 13, we have plotted the energy difference between the unitary and nonunitary free energies in addition to the difference between the paramagnetic and ferromagnetic phases. It is seen that the nonunitary state is energetically preferred over the unitary state, a statement which, strictly speaking, has only been shown to hold for our current choice of $\tilde{I}$ ($\tilde{I}=1.01$), but it seems reasonable to assume that it holds under quite general circumstances due to the presence of an exchange energy. At $T=T_{c,\uparrow}$, when all superconductivity is lost, the two curves join each other smoothly since $F_{\mathrm{NU}}\to F_{\mathrm{FM}}$ and $F_{\mathrm{U}}\to F_{\mathrm{PM}}$ when $T>T_{c,\uparrow}$. Our results then suggest the very real possibility of a coexistent phase of spin-triplet superconducting pairing and itinerant ferromagnetism being realized in the experimentally discovered ferromagnetic superconductors, since we have shown that the coexistent phase is energetically favored over both the purely magnetic and the nonmagnetic superconducting state.

E. Specific heat

We next consider some experimental signatures that could be expected in the different possible phases of a FMSC. Consequently, we have calculated the electronic contribution to the specific heat of the system by making use of $C_V=T\frac{\partial S}{\partial T}$ with

$$S=-\sum_{\mathbf{k}\sigma}\{f(E_{\mathbf{k}\sigma})\ln[f(E_{\mathbf{k}\sigma})]+[1-f(E_{\mathbf{k}\sigma})]\ln[1-f(E_{\mathbf{k}\sigma})]\} \tag{72}$$

as the entropy, leading to

$$C_V=\frac{\beta^2}{4}\sum_{\mathbf{k}\sigma}\frac{E_{\mathbf{k}\sigma}^2-\beta^{-1}\left(\Delta_{\sigma,0}\frac{\partial\Delta_{\sigma,0}}{\partial T}-\sigma\varepsilon_{\mathbf{k}\sigma}I\frac{\partial M}{\partial T}\right)}{\cosh^2(\beta E_{\mathbf{k}\sigma}/2)}. \tag{73}$$

Note that the above equation reduces to the correct normal-state heat capacity in the limit $\{\Delta_{\sigma,0},M\}\to 0$, with the usual linear T dependence. The term $\frac{\partial\Delta_{\sigma,0}}{\partial T}$ ensures that the well-known mean-field BCS discontinuity (strictly speaking valid only for a type-I superconductor,[63] but clearly invalid at the transition temperature of a strong type II

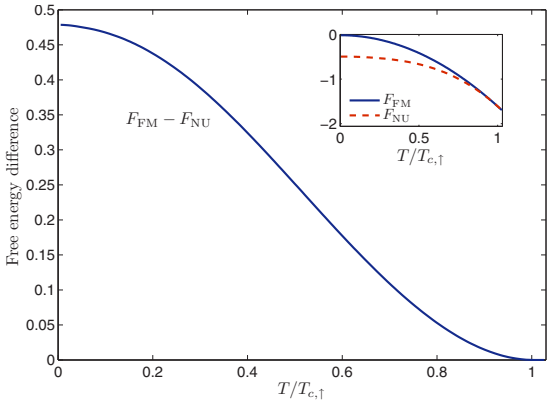

FIG. 12. (Color online) Free energy difference between the ferromagnetic state ($F_{\rm FM}$) and the nonunitary superconducting state ($F_{\rm NU}$), which displays coexistence of ferromagnetism and superconductivity. It is seen that the nonunitary phase is favored compared to the purely ferromagnetic state. In the inset, we have chosen the zero-temperature value of the ferromagnetic free energy as zero, serving as a reference point. We have solved all order parameters self-consistently for $\tilde{I}=1.01$. The curves of this figure and Fig. 13 may be made congruent by a simple scaling of the axes. This is a consequence of the weak-coupling limit, where superconductivity sets in at a temperature much smaller than the ferromagnet-paramagnet transition temperature, such the that magnetic order parameter across the superconducting transition is essentially a temperature-independent constant.

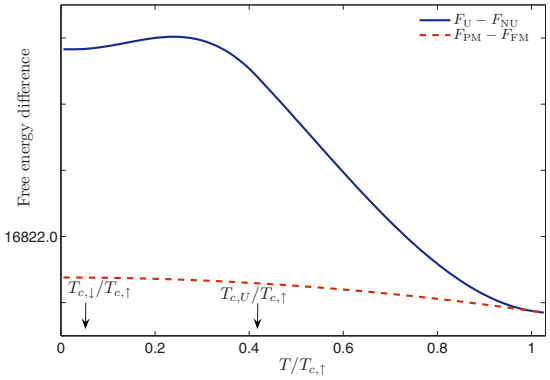

FIG. 13. (Color online) Free energy difference between the unitary and nonunitary states ($F_{\rm U}-F_{\rm NU}$) as well as the paramagnetic and ferromagnetic state ($F_{\rm PM}-F_{\rm FM}$). At $T=T_{c,\uparrow}$, the curves merge smoothly into each other since all superconductivity is lost. Each step along the ordinate corresponds to an increment of unit 0.1. We have solved all order parameters self-consistently for $\tilde{I}=1.01$.

superconductor[64–66]) at the superconducting critical temperature is present in the heat capacity, while the presence of ferromagnetism induces another term proportional to $\frac{\partial M}{\partial T}$. However, due to our previous argument that $T_{c,M} \gg T_{c,\sigma}$, this term may be neglected since the magnetization remains virtually unaltered in the temperature regime around $T_{c,\sigma}$. Going to the integral representation of the equation for the heat capacity, one thus obtains

$$C_V = \frac{\beta^2}{4}\sum_\sigma \int_{-E_F-\sigma IM}^{\infty} d\varepsilon N^\sigma(\varepsilon)\left[E_\sigma^2(\varepsilon) - \frac{\partial \Delta_{\sigma,0}}{\partial T}\Delta_{\sigma,0} T\right]\cosh^{-2}\left[\frac{\beta E_\sigma(\varepsilon)}{2}\right]. \quad (74)$$

Strictly speaking, one should again divide the above integral into the regions $\{-E_F,-\omega_0\}$, $\{\omega_0,\infty\}$, and $\{-\omega_0,\omega_0\}$, where the superconductivity gap should be set to zero in all regions except the latter. However, since the integrand is strongly peaked around $\varepsilon=0$ (Fermi level), there is little error made in using the form of Eq. (74). In order to obtain the derivatives of the gap functions with respect to temperature, an analytical approach is permissible since the gaps have the BCS-temperature dependence (see Fig. 8)

$$\Delta_{\sigma,0}(T) = \Delta_{\sigma,0}(0)\tanh(1.74\sqrt{T_{c,\sigma}/T-1}), \quad (75)$$

where the superconductivity critical temperature for spin-σ fermions is given by Eq. (69). To illustrate how the superconductivity pairing symmetry leaves important fingerprints in the heat capacity, we solved Eq. (74) self-consistently for two values of $\tilde{I}$ corresponding to strong ($\tilde{M}\simeq 0.5$) and weak ($\tilde{M}\simeq 0.1$) exchange splittings (Fig. 14). At $\tilde{I}=1.01$, the discontinuity is clearly pronounced for $T=T_{c,\uparrow}$, but it is hardly discernible at $T=T_{c,\downarrow}$. However, for $\tilde{I}=1.0005$ where the superconductivity transition temperatures for majority and minority spins become comparable, a clear double-peak signature is revealed in the heat capacity. We thus propose that this particular feature should serve as unambiguous evidence of a superconducting pairing corresponding to the $A2$ phase of liquid ^{3}He in ferromagnetic superconductors.

An classic feature of the BCS theory of superconductivity was the prediction that the jump in the heat capacity at T_c normalized on the normal-state value was a universal number, namely,

$$\left(\frac{\Delta C_V}{C_V}\right)\Big|_{T=T_c} \simeq 1.43. \quad (76)$$

In the presence of a net magnetization, one would expect that the universality of this ratio would break down and depend on the strength of the exchange energy. This is due to the fact that the discontinuity in the specific heat at the superconducting transition is dominated by the majority-spin carriers, while the total specific heat to a larger extent has contributions from both minority-spin and majority-spin carriers. To investigate this statement quantitatively, we consider the jump in C_V at $T=T_{c,\uparrow}$ since no analytical approach is possible at $T=T_{c,\downarrow}$, as seen from Eq. (74). We find that the normal (ferromagnetic) state heat capacity reads

$$C_V^{\rm FM} = \frac{\pi^2 T_{c,\uparrow}}{3}\sum_\sigma N^\sigma(0), \quad (77)$$

where $N^\sigma(0)$ is the spin-resolved density of states (DOS) at Fermi level, while the difference between the heat capacity

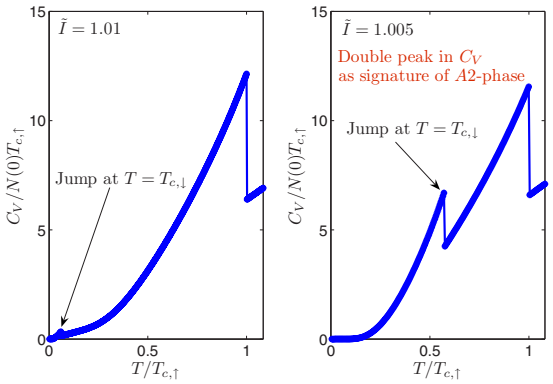

FIG. 14. (Color online) Specific heat capacity as a function of temperature for two values of $\tilde{I}$, corresponding to a strong exchange splitting ($\tilde{M} \simeq 0.5$) and a weak exchange splitting ($\tilde{M} \simeq 0.1$). A double-peak signature is clearly visible when the transition temperatures for the majority- and minority-spin bands are comparable.

in the coexistent state and in the ferromagnetic state at $T = T_{c,\uparrow}$ reads

$$\Delta C_V = \frac{1.74^2 \Delta_{\uparrow,0}^2(0) N^{\uparrow}(0)}{2T_{c,\uparrow}}. \tag{78}$$

Since the zero-temperature value for the gap is $\Delta_{\uparrow,0}(0) = 1.76 T_{c,\uparrow}$, one arrives at

$$\left(\frac{\Delta C_V}{C_V}\right)\Bigg|_{T=T_{c,\uparrow}} = 1.43 \frac{1}{1 + \sqrt{\dfrac{1-\tilde{M}}{1+\tilde{M}}}}. \tag{79}$$

The above equation reduces to the BCS limit for complete spin polarization $\tilde{M} = 1$ (zero DOS for spin-$\downarrow$ fermions at Fermi level). This is due to, as noted above, the larger extent to which majority-spin carriers dominate the *jump* in specific heat compared to the total specific heat. As anticipated, the jump in C_V depends on the exchange energy, as illustrated in Fig. 15. Of course, in the unitary state $\tilde{M} = 0$, the jump also reduces to the BCS value although this is not seen from Eq. (79). The reason for this is that we have implicitly assumed that $\tilde{M} \neq 0$ in the derivation of Eq. (79), taking $T_{c,\uparrow} > T_{c,\downarrow}$. In the case where these transition temperatures are equal, the contribution from both is additive and equal [1.43/2, to be specificc, as seen from Eq. (79)] and gives the correct BCS result.

Our study of C_V then offers two interesting opportunities: (i) the presence or absence of a double-peak signature in the heat capacity reveals information about the superconductivity pairing symmetry realized in the FMSC, and (ii) the normalized value of the discontinuous jump at $T_{c,\uparrow}$ contains information about the exchange splitting between the majority- and minority-spin carrier bands.

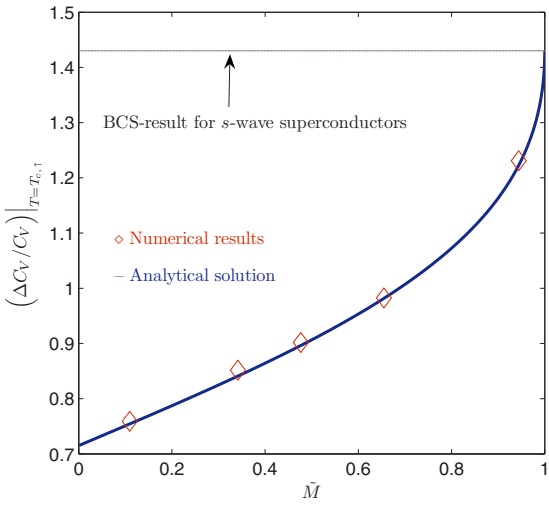

FIG. 15. (Color online) The discontinuity of the heat capacity at $T = T_{c,\uparrow}$ as a function of exchange splitting [Eq. (79)]. It is seen that the BCS value is recovered at $\tilde{M} = 1$. Note that it would also be recovered at $\tilde{M} = 0$, although this is not shown explicitly in the figure. The reason for this is that we have assumed that $T_{c,\downarrow} \neq T_{c,\uparrow}$. We have also plotted the numerical results ($\diamond$) for the jump with self-consistently solved OPs, i.e., without assuming BCS-temperature dependence, for $\tilde{I} = \{1.001, 1.005, 1.01, 1.02, 1.05\}$, which yields good agreement with the analytical solution [Eq. (79)].

VI. SUMMARY

In summary, we have derived a general Hamiltonian describing coexistence of itinerant ferromagnetism, spin-orbit coupling, and mixed spin-singlet and spin-triplet superconducting pairing using mean-field theory. Exact eigenvalues and coupled gap equations for the different order parameters have been obtained. Our results may serve as a starting point for any model describing coexistence of any combination of these three phenomena simply by applying the appropriate limit.

As a specific application of our results, we have studied quantum transport between a normal metal and a superconductor lacking an inversion center with mixed singlet and triplet gaps. We find that there are pronounced peaks and bumps in the conductance spectrum at voltages corresponding to the sum and difference of the magnitude of the singlet and triplet gaps. Consequently, our results may be helpful in obtaining information about the size of the relative contribution of different pairing symmetries.

Moreover, we considered a system where itinerant ferromagnetism uniformly coexists with spin-triplet superconductivity as a second application of our theory. We solved the coupled gap equations numerically and presented analytical expressions for the order parameters and their dependences on quantities such as exchange energy and temperature. It was found that the coexistent regime of ferromagnetism and superconductivity may indeed be realized, since it is ener-

getically favored compared to a unitary superconducting state ($M=0$) and a purely ferromagnetic state. In order to make contact with the experimental situation, we studied the heat capacity and found interesting signatures in the spectrum that may be used in order to obtain information about both the superconductivity pairing symmetry present in the system and the magnitude of the exchange energy.

ACKNOWLEDGMENTS

J.L. gratefully acknowledges A. Nevidomskyy for stimulating communications and thanks E. K. Dahl, S. Kragset, and K. Berland for providing useful comments. This work was supported by the Norwegian Research Council Grants No. 157798/432 and No. 158547/431 (NANOMAT) and Grant No. 167498/V30 (STORFORSK).

APPENDIX: BOGOLIUBOV–DE GENNES EQUATIONS FOR SYSTEMS EXHIBITING COEXISTENCE OF FERROMAGNETISM, SPIN-ORBIT COUPLING, AND SUPERCONDUCTIVITY

1. Derivation

We start out with a real-space Hamiltonian described by fermionic field operators $\psi^{(\dagger)}(\mathbf{r},t)$ with a general attractive pairing kernel $V_{\alpha\beta}(|\mathbf{r}-\mathbf{r}'|)$, namely,

$$\hat{H}=\sum_{\alpha\beta}\int d\mathbf{r}\psi_\alpha^\dagger(\mathbf{r},t)\Bigg\{-\frac{\hat{\nabla}_\mathbf{r}^2}{2m}-\mu+\{V+\alpha V_s)\delta(x)+[-\mathbf{V}_M+\mathbf{g}(\hat{\mathbf{p}})]\cdot\check{\boldsymbol{\sigma}}_{\alpha\beta}\psi_\beta^\dagger(\mathbf{r},t)+\frac{1}{2}\sum_{\alpha\beta}\int\int d\mathbf{r}d\mathbf{r}'\times V_{\alpha\beta}(|\mathbf{r}-\mathbf{r}'|)\psi_\alpha^\dagger(\mathbf{r},t)\psi_\beta^\dagger(\mathbf{r}')\psi_\beta(\mathbf{r}')\psi_\alpha(\mathbf{r},t). \tag{A1}$$

Here, V_0 accounts for a nonmagnetic scattering potential associated with a barrier located at $x=0$, while V_s is the magnetic scattering potential, i.e., the barrier is spin active. Moreover, $\mathbf{V}_M$ is the magnetic exchange energy vector, $\mathbf{g}(\hat{\mathbf{p}})=-\mathbf{g}(-\hat{\mathbf{p}})$ is a term describing an antisymmetric spin-orbit coupling energy ($\hat{\mathbf{p}}=-i\hat{\nabla}_\mathbf{r}$), and $\check{\boldsymbol{\sigma}}$ is the vector of Pauli matrices. We now introduce the mean-field approximation

$$\psi_\alpha^\dagger(\mathbf{r},t)\psi_\beta^\dagger(\mathbf{r}')=\langle\psi_\alpha^\dagger(\mathbf{r},t)\psi_\beta^\dagger(\mathbf{r}',t)\rangle+\delta\psi_{\alpha\beta}^\dagger, \tag{A2}$$

where the last term describes the fluctuations around the average field, and also define the superconducting order parameter

$$\Delta_{\alpha\beta}(\mathbf{r},\mathbf{r}')=V_{\alpha\beta}(|\mathbf{r}-\mathbf{r}'|)\langle\psi_\beta(\mathbf{r}',t)\psi_\alpha(\mathbf{r},t)\rangle. \tag{A3}$$

Above, we have explicitly made the superconductivity order parameter time independent, which effectively amounts to saying that it does not depend on energy (the weak-coupling limit). This provides us with

$$\hat{H}=\sum_{\alpha\beta}\int d\mathbf{r}\psi_\alpha^\dagger(\mathbf{r},t)\Bigg\{-\frac{\hat{\nabla}_\mathbf{r}^2}{2m}-\mu+\{V+\alpha V_s)\delta(x)+[-\mathbf{V}_M+\mathbf{g}(\hat{\mathbf{p}})]\cdot\check{\boldsymbol{\sigma}}\Bigg\}_{\alpha\beta}\psi_\beta^\dagger(\mathbf{r},t)+\frac{1}{2}\sum_{\alpha\beta}\int\int d\mathbf{r}d\mathbf{r}'[\Delta_{\alpha\beta}^\dagger(\mathbf{r},\mathbf{r}')\psi_\beta(\mathbf{r}',t)\psi_\alpha(\mathbf{r},t)+\Delta_{\alpha\beta}(\mathbf{r},\mathbf{r}')\psi_\alpha^\dagger(\mathbf{r},t)\psi_\beta^\dagger(\mathbf{r}',t)-V_{\alpha\beta}(|\mathbf{r}-\mathbf{r}'|)\times\langle\psi_\alpha^\dagger(\mathbf{r},t)\psi_\beta^\dagger(\mathbf{r}',t)\rangle\langle\psi_\beta(\mathbf{r}',t)\psi_\alpha(\mathbf{r},t)\rangle]. \tag{A4}$$

The time-dependent field operators $\psi(\mathbf{r},t)=e^{i\hat{H}t}\psi(\mathbf{r})e^{-i\hat{H}t}$ obey the Heisenberg equations of motion,

$$i\partial_t\psi_\alpha(\mathbf{r},t)=[\psi_\alpha(\mathbf{r},t),\hat{H}]=\sum_\beta\int d\mathbf{r}'\,\delta(\mathbf{r}-\mathbf{r}')\hat{H}_{\alpha\beta}^0(\mathbf{r}',\hat{\mathbf{p}})\psi_\beta(\mathbf{r}',t)+\sum_\beta\int d\mathbf{r}'\Delta_{\alpha\beta}(\mathbf{r},\mathbf{r}')\psi_\beta^\dagger(\mathbf{r}',t),$$

$$i\partial_t\psi_\alpha^\dagger(\mathbf{r},t)=[\psi_\alpha^\dagger(\mathbf{r},t),\hat{H}]=\sum_\beta\int d\mathbf{r}'\,\delta(\mathbf{r}-\mathbf{r}')[-\hat{H}^0(\mathbf{r}',-\hat{\mathbf{p}})]_{\alpha\beta}^{\mathcal{T}}\psi_\beta^\dagger(\mathbf{r}',t)+\sum_\beta\int d\mathbf{r}'\Delta_{\alpha\beta}^\dagger(\mathbf{r},\mathbf{r}')\psi_\beta(\mathbf{r}',t). \tag{A5}$$

For convenience, we have defined

$$\hat{H}_{\alpha\beta}^0(\mathbf{r},\hat{\mathbf{p}})=\Bigg\{-\frac{\hat{\nabla}_\mathbf{r}^2}{2m}-\mu+\{V+\alpha V_s)\delta(x)+[-\mathbf{V}_M+\mathbf{g}(\hat{\mathbf{p}})]\cdot\check{\boldsymbol{\sigma}}_{\alpha\beta}. \tag{A6}$$

The above equations may be comprised in compact matrix form,

$$i\partial_t\Psi(\mathbf{r},t)=\int d\mathbf{r}'\mathcal{H}(\mathbf{r},\mathbf{r}')\Psi(\mathbf{r}',t),$$

$$\Psi(\mathbf{r},t)=[\psi_\uparrow(\mathbf{r},t),\psi_\downarrow(\mathbf{r},t),\psi_\uparrow^\dagger(\mathbf{r},t),\psi_\downarrow^\dagger(\mathbf{r},t)]^{\mathrm{T}},$$

$$\mathcal{H}(\mathbf{r},\mathbf{r}')=\begin{pmatrix}\hat{H}^0(\mathbf{r}',\hat{\mathbf{p}})\delta_{\mathbf{r}\mathbf{r}'} & \hat{\boldsymbol{\Delta}}(\mathbf{r},\mathbf{r}')\\ \hat{\boldsymbol{\Delta}}^\dagger(\mathbf{r},\mathbf{r}') & [-\hat{H}^0(\mathbf{r}',-\hat{\mathbf{p}})]^{\mathcal{T}}\delta_{\mathbf{r}\mathbf{r}'}\end{pmatrix}, \tag{A7}$$

with $\delta(\mathbf{r}-\mathbf{r}')=\delta_{\mathbf{r}\mathbf{r}'}$, and where we have defined

$$\hat{\boldsymbol{\Delta}}(\mathbf{r},\mathbf{r}')=\begin{pmatrix}\Delta_{\uparrow\uparrow}(\mathbf{r},\mathbf{r}') & \Delta_{\uparrow\downarrow}(\mathbf{r},\mathbf{r}')\\ \Delta_{\downarrow\uparrow}(\mathbf{r},\mathbf{r}') & \Delta_{\downarrow\downarrow}(\mathbf{r},\mathbf{r}')\end{pmatrix}. \tag{A8}$$

Note that $\Delta_{\uparrow\downarrow}(\mathbf{r},\mathbf{r}')$ is, in general, a superposition of triplet (T) and singlet (S) components that satisfies

$$\Delta_{\uparrow\downarrow}(\mathbf{r},\mathbf{r}')=\Delta_{\uparrow\downarrow}^{\mathrm{T}}(\mathbf{r},\mathbf{r}')+\Delta_{\uparrow\downarrow}^{\mathrm{S}}(\mathbf{r},\mathbf{r}'),$$

$$\Delta^{\mathrm{T}}_{\uparrow\downarrow}(\mathbf{r},\mathbf{r}') = \Delta^{\mathrm{T}}_{\downarrow\uparrow}(\mathbf{r},\mathbf{r}'),$$

$$\Delta^{\mathrm{S}}_{\uparrow\downarrow}(\mathbf{r},\mathbf{r}') = -\Delta^{\mathrm{S}}_{\downarrow\uparrow}(\mathbf{r},\mathbf{r}'). \tag{A9}$$

Regarding $\Psi(\mathbf{r},t)$ as a c number and assuming a stationary solution $\Psi(\mathbf{r},t)=\Psi(\mathbf{r})e^{-iEt}$, with E as the wave function energy, it suffices to solve the equation

$$E\Psi(\mathbf{r}) = \int d\mathbf{r}'\mathcal{H}(\mathbf{r},\mathbf{r}')\Psi(\mathbf{r}'). \tag{A10}$$

By considering a plane-wave solution of $\Psi(\mathbf{r})$ and dividing out the fast oscillations on an atomic scale (see, e.g., Ref. 67), one is left with the most familiar form of the BdG equations appearing in the literature, namely,

$$\begin{pmatrix} \hat{H}^0(\mathbf{r},\hat{\mathbf{p}}) & \hat{\mathbf{\Delta}}(\mathbf{k},\mathbf{r}) \\ \hat{\mathbf{\Delta}}^{\dagger}(\mathbf{k},\mathbf{r}) & [-\hat{H}^0(\mathbf{r},-\hat{\mathbf{p}})]^{\mathcal{T}} \end{pmatrix}\Psi(\mathbf{r}) = E\Psi(\mathbf{r}), \tag{A11}$$

where the quasiparticle momentum $\mathbf{k}$ is the Fourier transform of the relative coordinate $\mathbf{s}=(\mathbf{r}-\mathbf{r}')/2$, i.e.,

$$\mathcal{F}\{f(\mathbf{k})\} = \int d\mathbf{s} f(\mathbf{s}) e^{-i\mathbf{k}\cdot\mathbf{s}}. \tag{A12}$$

This is usually assumed to be fixed on the Fermi surface, such that only the directional dependence of $\mathbf{k}$ enters in Eq. (A11), $\mathbf{k}\to k_F\hat{\mathbf{k}}$.

2. Boundary conditions

We proceed to provide a general approach in order to obtain the correct boundary conditions at the interface for the wave functions. Continuity of the wave function itself is assumed in this context. Consider our Eq. (38) which describes the Hamiltonian for the $\mathrm{N/CePt_3Si}$ junction. The first row of the equation explicitly reads

$$\left[-\frac{1}{2m}\left(\frac{\partial^2}{\partial x^2}+\frac{\partial^2}{\partial y^2}\right)-\mu+V_0\delta(x)\right]\psi_{\uparrow}(x,y) + \lambda\left(\frac{\partial}{\partial x}-i\frac{\partial}{\partial y}\right)\Theta(x)\psi_{\downarrow}(x,y)+\Delta_{\mathbf{k}\uparrow\uparrow}\Theta(x)\psi^{\dagger}_{\uparrow}(x,y) + \Delta\Theta(-x)\psi^{\dagger}_{\downarrow}(x,y) = E\psi_{\uparrow}(x,y). \tag{A13}$$

If we now integrate the above equation over a an interval $[\epsilon,-\epsilon]$ along the $\hat{\mathbf{x}}$ axis and apply the limit $\epsilon\to 0^+$, one obtains

$$\lim_{\epsilon\to 0^+}\left\{-\frac{1}{2m}[\psi'_{\uparrow}(\epsilon,y)-\psi'_{\uparrow}(-\epsilon,y)]+V_0\psi_{\uparrow}(0,y) + \lambda\int_{-\epsilon}^{\epsilon}dx[\Theta(x)\psi_{\downarrow}(x,y)]'\right\}=0, \tag{A14}$$

where $'$ denotes derivation with respect to x. The last term yields $\frac{1}{2}\lambda\psi_{\downarrow}(\epsilon,0)$ [since $\Theta(0)=\frac{1}{2}$], such that the boundary condition for derivative of the $\psi_{\uparrow}(x,y)$ component becomes

$$\lim_{\epsilon\to 0^+}\{[\psi'_{\uparrow}(\epsilon,y)-\psi'_{\uparrow}(-\epsilon,y)]-m\lambda\psi_{\downarrow}(\epsilon,0)\}=2mV_0\psi_{\uparrow}(0,y). \tag{A15}$$

It is seen that the presence of spin-orbit coupling and the delta-function barrier leads to a discontinuity of the derivative of the wave-function. A similar procedure may be applied to the other components of $\Psi(x,y)$, and this method can also be extended to include different effective masses on each side of the junction modeled by a simple step function $\Theta(x)$.

[1] S. S. Saxena, P. Agarwal, K. Ahilan, F. M. Grosche, R. K. W. Haselwimmer, M. J. Steiner, E. Pugh, I. R. Walker, S. R. Julian, P. Monthoux, G. G. Lonzarich, A. Huxley, I. Sheikin, D. Braithwaite, and J. Flouquet, Nature (London) **406**, 587 (2000).

[2] D. Aoki, A. Huxley, E. Ressouche, D. Braithwaite, J. Flouquet, J.-P. Brison, E. Lhotel, and C. Paulsen, Nature (London) **413**, 613 (2001).

[3] E. Bauer, G. Hilscher, H. Michor, Ch. Paul, E. W. Scheidt, A. Gribanov, Yu. Seropegin, H. Noel, M. Sigrist, and P. Rogl, Phys. Rev. Lett. **92**, 027003 (2004).

[4] T. Akazawa, H. Hidaka, T. Fujiwara, T. C. Kobayashi, E. Yamamoto, Y. Haga, R. Settai, and Y. Onuki, J. Phys.: Condens. Matter **16**, L29 (2004).

[5] F. Hardy and A. D. Huxley, Phys. Rev. Lett. **94**, 247006 (2005).

[6] K. V. Samokhin and M. B. Walker, Phys. Rev. B **66**, 174501 (2002).

[7] K. Machida and T. Ohmi, Phys. Rev. Lett. **86**, 850 (2001).

[8] K. D. Nelson, Z. Q. Mao, Y. Maeno, and Y. Liu, Science **306**, 1151 (2004).

[9] H. Q. Yuan, D. F. Agterberg, N. Hayashi, P. Badica, D. Vandervelde, K. Togano, M. Sigrist, and M. B. Salamon, Phys. Rev. Lett. **97**, 017006 (2006).

[10] N. J. Curro, T. Caldwell, E. D. Bauer, L. A. Morales, M. J. Graf, Y. Bang, A. V. Balatsky, J. D. Thompson, and J. L. Sarrao, Nature (London) **434**, 622 (2005).

[11] A. G. Lebed, Phys. Rev. Lett. **96**, 037002 (2006).

[12] I. Zutic and I. Mazin, Phys. Rev. Lett. **95**, 217004 (2005).

[13] P. W. Anderson, *Basic Notions of Condensed Matter Physics* (Addison Wesley, Reading, MA, 1980).

[14] I. A. Sergienko, V. Keppens, M. McGuire, R. Jin, J. He, S. H. Curnoe, B. C. Sales, P. Blaha, D. J. Singh, K. Schwarz, and D. Mandrus, Phys. Rev. Lett. **92**, 065501 (2004).

[15] M. Yogi, Y. Kitaoka, S. Hashimoto, T. Yasuda, R. Settai, T. D. Matsuda, Y. Haga, Y. Onuki, P. Rogl, and E. Bauer, Phys. Rev. Lett. **93**, 027003 (2004).

[16] V. M. Edelstein, Sov. Phys. JETP **68**, 1244 (1989); V. M. Edelstein, Phys. Rev. Lett. **75**, 2004 (1995).

[17] L. P. Gor'kov and E. I. Rashba, Phys. Rev. Lett. **87**, 037004 (2001).

[18] I. A. Sergienko and S. H. Curnoe, Phys. Rev. B **70**, 214510 (2004).

[19] K. Børkje and A. Sudbø, Phys. Rev. B **74**, 054506 (2006).

[20] P. A. Frigeri, D. F. Agterberg, and I. Milat, M. Sigrist, Eur. Phys. J. B **54**, 435 (2006).
[21] P. A. Frigeri, D. F. Agterberg, A. Koga, and M. Sigrist, Phys. Rev. Lett. **92**, 097001 (2004).
[22] K. Izawa, Y. Kasahara, Y. Matsuda, K. Behnia, T. Yasuda, R. Settai, and Y. Onuki, Phys. Rev. Lett. **94**, 197002 (2005).
[23] T. Yokoyama, Y. Tanaka, and J. Inoue, Phys. Rev. B **72**, 220504(R) (2005).
[24] P. W. Anderson, Phys. Rev. B **30**, 4000 (1984).
[25] K. V. Samokhin, E. S. Zijlstra, and S. K. Bose, Phys. Rev. B **69**, 094514 (2004).
[26] I. Eremin and J. F. Annett, Phys. Rev. B **74**, 184524 (2006).
[27] J. Shi and Q. Niu, arXiv:cond-mat/0601531 (unpublished).
[28] S. Tewari, D. Belitz, T. R. Kirkpatrick, and J. Toner, Phys. Rev. Lett. **93**, 177002 (2004).
[29] D. V. Shopova and D. I. Uzunov, Phys. Rev. B **72**, 024531 (2005).
[30] V. P. Mineev, C. R. Phys. **7**, 35 (2006).
[31] V. P. Mineev and K. V. Samokhin, *Introduction to Unconventional Superconductivity* (Gordon and Breach, New York, 1999).
[32] H. Kotegawa, A. Harada, S. Kawasaki, Y. Kawasaki, Y. Kitaoka, Y. Haga, E. Yamamoto, Y. Onuki, K. M. Itoh, and E. E. Haller, J. Phys. Soc. Jpn. **74**, 705 (2005).
[33] M. L. Kulic, C. R. Phys. **7**, 4 (2006); M. L. Kulic and I. M. Kulic, Phys. Rev. B **63**, 104503 (2001).
[34] I. Eremin, F. S. Nogueira, and R.-J. Tarento, Phys. Rev. B **73**, 054507 (2006).
[35] F. Hardy and A. D. Huxley, Phys. Rev. Lett. **94**, 247006 (2005).
[36] K. V. Samokhin and M. B. Walker, Phys. Rev. B **66**, 174501 (2002).
[37] J. Linder, M. S. Grønsleth, and A. Sudbø, Phys. Rev. B **75**, 054518 (2007).
[38] T. Yokoyama and Y. Tanaka, Phys. Rev. B **75**, 132503 (2007).
[39] At zero temperature, the chemical potential is identically equal to the Fermi energy. In this context, we introduce it as a reference point for energy measurements such that the single-particle kinetic energies are measured relative to μ.
[40] A. J. Leggett, Rev. Mod. Phys. **47**, 331 (1975).
[41] C. H. Edwards, Jr., and D. E. Penney, *Elementary Linear Algebra* (Prentice-Hall, Englewood Cliffs, NJ, 1988).
[42] M. Abramowitz and I. A. Stegun, *Handbook of Mathematical Functions* (Dover, New York 1972).
[43] Y. Tanaka and S. Kashiwaya, Phys. Rev. Lett. **74**, 3451 (1995).
[44] G. E. Blonder, M. Tinkham, and T. M. Klapwijk, Phys. Rev. B **25**, 4515 (1982).
[45] L. W. Molenkamp, G. Schmidt, and G. E. W. Bauer, Phys. Rev. B **64**, 121202(R) (2001).
[46] Y. Tanaka and S. Kashiwaya, Phys. Rev. B **56**, 892 (1997).
[47] T. Yokoyama, Y. Tanaka, and J. Inoue, Phys. Rev. B **74**, 035318 (2006).
[48] I. Zutic and O. T. Valls, Phys. Rev. B **60**, 6320 (1999).
[49] I. Zutic and O. T. Valls, Phys. Rev. B **61**, 1555 (2000).
[50] C. Iniotakis, N. Hayashi, Y. Sawa, T. Yokoyama, U. May, Y. Tanaka, and M. Sigrist, Phys. Rev. B **76**, 012501 (2007).
[51] C.-R. Hu, Phys. Rev. Lett. **72**, 1526 (1995).
[52] G. F. Wang and K. Maki, Europhys. Lett. **45**, 71 (1999).
[53] S. Kashiwaya, Y. Tanaka, N. Yoshida, and M. R. Beasley, Phys. Rev. B **60**, 3572 (1999).
[54] J. Linder and A. Sudbø, Phys. Rev. B **75**, 134509 (2007).
[55] J. Shi, P. Zhang, D. Xiao, and Q. Niu, Phys. Rev. Lett. **96**, 076604 (2006).
[56] V. Ambegaokar, P. G. deGennes, and D. Rainer, Phys. Rev. A **9**, 2676 (1974).
[57] L. J. Buchholtz and G. Zwicknagl, Phys. Rev. B **23**, 5788 (1981).
[58] Y. Tanuma, Y. Tanaka, and S. Kashiwaya, Phys. Rev. B **64**, 214519 (2001).
[59] Y. S. Barash, H. Burkhardt, and D. Rainer, Phys. Rev. Lett. **77**, 4070 (1996); Y. Tanaka and S. Kashiwaya, Phys. Rev. B **58**, R2948 (1998); Y. Tanaka, T. Asai, N. Yoshida, J. Inoue, and S. Kashiwaya, *ibid.* **61**, R11902 (2000).
[60] A. H. Nevidomskyy, Phys. Rev. Lett. **94**, 097003 (2005).
[61] M. S. Grønsleth, J. Linder, J.-M. Børven, and A. Sudbø, Phys. Rev. Lett. **97**, 147002 (2006); J. Linder, M. S. Grønsleth, and A. Sudbø, Phys. Rev. B **75**, 024508 (2007).
[62] H. P. Dahal, J. Jackiewicz, and K. S. Bedell, Phys. Rev. B **72**, 172506 (2005).
[63] B. I. Halperin, T. C. Lubensky, and S.-K. Ma, Phys. Rev. Lett. **32**, 292 (1974).
[64] C. Dasgupta and B. I. Halperin, Phys. Rev. Lett. **47**, 1556 (1981).
[65] Z. Tesanovic, Phys. Rev. B **59**, 6449 (1999).
[66] A. K. Nguyen and A. Sudbø, Phys. Rev. B **60**, 15307 (1999); Europhys. Lett. **46**, 780 (1999).
[67] C. Bruder, Phys. Rev. B **41**, 4017 (1990).
[68] M. Tinkham, *Introduction to Superconductivity*, 2nd ed. (MacGraw-Hill, New York, 1996).

Erratum: Quantum transport in noncentrosymmetric superconductors and thermodynamics of ferromagnetic superconductors [Phys. Rev. B 76, 054511 (2007)]

J. Linder and A. Sudbø

(Received 8 January 2008; published 20 February 2008)

DOI: 10.1103/PhysRevB.77.069902 PACS number(s): 74.20.Rp, 99.10.Cd

There are some typos in Ref. 1 that we here correct. These typos do not alter our conclusions or results in any way.

(1) In the sentence before Eq. (6) and in Eq. (6) itself, $b_{\mathbf{k}\alpha\beta}$ and $\delta b_{\mathbf{k}\alpha\beta}$ should be conjugated, i.e., replaced with $b^\dagger_{\mathbf{k}\alpha\beta}$ and $\delta b^\dagger_{\mathbf{k}\alpha\beta}$. Also, $\Delta^{\mathrm{S,T}}_{\mathbf{k}'\alpha\beta}$ in Eq. (9) should be conjugated, i.e., $(\Delta^{\mathrm{S,T}}_{\mathbf{k}'\alpha\beta})^\dagger$.

(2) In Eq. (61), a parenthesis has been misplaced. The equation should read

$$N^\sigma(\varepsilon) = \frac{mV\sqrt{2m(\varepsilon + \sigma IM + E_F)}}{2\pi^2}. \tag{1}$$

(3) In the first column of page 14, E_F^2 should be replaced with $T_{c,\uparrow}^2$, i.e., the scaling should be $F_{\mathrm{NU}}=F/[NN(0)T_{c,\uparrow}^2]$.

(4) In the last line of Eq. (A5), the + sign in front of Σ_β should be a − sign.

(5) In Eq. (27), the factors $e^{-\beta\tilde{E}_{\mathbf{k},1}}$ and $e^{-\beta\tilde{E}_{\mathbf{k},2}}$ should be removed.

(6) In Eq. (A7), $\hat{\mathbf{\Delta}}^\dagger(\mathbf{r},\mathbf{r}')$ should be replaced with $-\hat{\mathbf{\Delta}}^*(\mathbf{r},\mathbf{r}')$.

(7) In Eq. (A6) the right-hand side should read

$$\left\{ -\frac{\hat{\boldsymbol{\nabla}}_{\mathbf{r}}^2}{2m} - \mu + (V + \alpha V_s)\delta(x) + [-V_M + \mathbf{g}(\hat{\mathbf{p}})]\cdot\check{\boldsymbol{\sigma}} \right\}_{\alpha\beta}.$$

Paper VII

Dirac fermions and conductance oscillations in s- and d-wave superconductor - graphene junctions.

Physical Review Letters **99**, 147001 (2007).

Dirac Fermions and Conductance Oscillations in s- and d-Wave Superconductor-Graphene Junctions

J. Linder and A. Sudbø

Department of Physics, Norwegian University of Science and Technology, N-7491 Trondheim, Norway
(Received 1 June 2007; published 1 October 2007)

We investigate quantum transport in a normal-superconductor graphene heterostructure, including the possibility of an anisotropic pairing potential in the superconducting region. We find that under certain circumstances, the conductance displays an undamped, oscillatory behavior as a function of applied bias voltage. Also, we investigate how the conductance spectra are affected by a d-wave pairing symmetry. These results combine unusual features of the electronic structure of graphene with the unconventional pairing symmetry found for instance in high-T_c superconductors.

DOI: 10.1103/PhysRevLett.99.147001 PACS numbers: 74.45.+c, 71.10.Pm, 73.23.−b, 74.78.Na

Graphene is a monatomic layer of graphite with a honeycomb lattice structure [1]. The electronic properties of graphene display several intriguing features, such as a six-point Fermi surface and Dirac-like low-energy energy dispersion around the Fermi points. Condensed matter systems with such ''relativistic'' electronic structure properties constitute fascinating examples of low-energy emergent symmetries (in this case Lorentz invariance). Another example where precisely this occurs is in one-dimensional interacting fermion systems, where phenomena like breakdown of Fermi-liquid theory and spin-charge separation take place. Graphene features certain similarities to, but also important differences from, the nodal Dirac fermions emerging in the low-energy sector of the pseudogap phase of d-wave superconductors such as the high-T_c cuprates. When Lorentz invariance emerges in the low-energy sector of higher-dimensional condensed matter systems, it is bound to attract much interest from a fundamental physics point of view.

Various aspects of resonant tunneling phenomena in N/N and $N/I/N$ graphene structures have recently been investigated (N denotes normal metal and I denotes insulator) [2]. Although superconductivity does not appear intrinsically in graphene, it may nonetheless be induced by means of the proximity effect [3]. Motivated by this, the authors of Refs. [4,5] considered quantum transport in N/S and $N/I/S$ graphene junctions (S denotes superconductor) for the case where the pairing potential is isotropic, leading to s-wave superconductivity. However, the hexagonal symmetry of the graphene lattice also admits unconventional order parameters such as p-wave or d-wave. The possible pairing symmetries on a hexagonal lattice up to f-wave pairing ($l = 3$) was given in Ref. [6]. Interestingly, among the allowed order parameters, one finds the $d_{x^2-y^2}$ symmetry, which is believed to be the dominant pairing symmetry in high-T_c superconductors. Consequently, it should be possible to induce superconductivity with nodes in the gap in graphene by manufacturing heterostructures of graphene and unconventional superconductors. It is of interest to investigate how this would affect coherent quantum transport in junctions with normal and superconducting graphene. In particular, it is essential to study possible zero-energy states (ZES) at the interface of such a junction. Such states are known to give rise to zero-bias conductance peaks (ZBCPs) in metallic N/S junctions [7] and will influence the conductance spectra of $N/I/S$ junctions.

In this Letter, we take into account the possibility of an anisotropic pairing potential induced in graphene and study coherent quantum transport in both N/S and $N/I/S$ junctions. In addition, we show that in the latter structure, novel conductance oscillations as a function of bias voltage are present both for s-wave and d-wave symmetry of the superconducting condensate due to the presence of low-energy ''relativistic'' nodal fermions on the N side. The period of the oscillations decreases with increasing width w of the insulating region and persists even if the Fermi energy in I is strongly shifted. This contrasts sharply to metallic $N/I/S$ junctions, where the presence of a potential barrier causes the transmittance of the junction to go to zero with increasing w. The feature of conductance oscillations is thus unique to $N/I/S$ junctions with low-energy Dirac-fermion excitations. Moreover, we contrast the N/S or $N/I/S$ conductance spectra for the cases where s-wave and $d_{x^2-y^2}$-wave superconductors constitute the S side. The former has no nodes in the gap and lacks Andreev bound states. The latter has line nodes that always cross the Fermi surface in the gap, and thus also features, in addition to Andreev bound states, nodal relativistic low-energy Dirac fermions. The quantum transport properties in a heterostructure of two such widely disparate systems, both featuring a particular intriguing emergent low-energy symmetry, are of considerable importance.

The Brillouin zone of graphene is hexagonal and the energy bands touch the Fermi level at the edges of this zone, amounting to six discrete points. Out of these only two are inequivalent, denoted K and K' and referred to as Dirac points. The energy dispersion in the Brillouin zone was calculated within a tight-binding model [8], revealing

a conical structure of the conduction and valence bands close to the six Fermi points, giving rise to an essentially linear dispersion. Graphene N/S interfaces contain a new phenomenology compared to their metallic counterpart, namely, the possibility of specular Andreev reflection (AR) [4]. In the process of normal AR, an incident electron from the N side is reflected as a hole which retraces the trajectory of the electron. In specular AR, the reflected hole follows the trajectory which a normally reflected electron would have. Depending on whether the graphene is doped or not, specular and normal AR will compete with each other, also depending on the position of the Fermi level with respect to the gap.

In order to treat the scattering processes at the interfaces of the $N/I/S$ junction, we make use of the full Bogoliubov–de Gennes equation for the 2D sheet of graphene in the xy plane, assuming the clean limit. These equations read

$$\begin{pmatrix} \check{H} - E_F\check{1} & \Delta_{\mathbf{k}}\check{1} \\ \Delta_{\mathbf{k}}^{\dagger}\check{1} & E_F\check{1} - \check{\mathcal{T}}\check{H}\check{\mathcal{T}}^{-1} \end{pmatrix}\Psi = E\Psi, \qquad (1)$$

where E is the excitation energy, and Ψ is the wave function. We use $\check{..}$ for 4×4 matrices, $\hat{..}$ for 2×2 matrices, and boldface notation for three-dimensional row vectors. Assuming that the superconducting region is located at $x>0$ and neglecting the decay of the order parameter in the vicinity of the interface [9], we may write for the spin-singlet order parameter $\Delta_{\mathbf{k}} = \Delta(\theta)e^{i\vartheta}\Theta(x)$, where $\Theta(x)$ is the Heaviside step function, while ϑ is the phase corresponding to the globally broken $U(1)$ symmetry in the superconductor. We consider the weak-coupling limit with the momentum $\mathbf{k}$ fixed on the Fermi surface, such that $\Delta_{\mathbf{k}}$ only has an angular dependence $\theta = \mathrm{atan}(k_y/k_x)$. Note that in contrast to previous work, we allow for the possibility of unconventional superconductivity in the graphene layer since $\Delta_{\mathbf{k}}$ now may be anisotropic.

Postulating a spin-singlet even parity order parameter, the condition $\Delta(\theta) = \Delta(\pi+\theta)$ must be fulfilled. The single-particle Hamiltonian is given by $\check{H} = \mathrm{diag}(\hat{H}_+, \hat{H}_-)$, $\hat{H}_\pm = -iv_F(\hat{\sigma}_x\partial_x \pm \hat{\sigma}_y\partial_y)$. Here, v_F is the energy-independent Fermi velocity for graphene, while $\hat{\sigma}_i$ denotes the Pauli matrices. For later use, we also define the Pauli matrix vector $\hat{\boldsymbol{\sigma}} = (\hat{\sigma}_x, \hat{\sigma}_y, \hat{\sigma}_z)$. These Pauli matrices operate on the sublattice space of the honeycomb structure, corresponding to the A and B atoms, while the $\pm$ sign refers to the two so-called valleys of K and K' in the Brillouin zone. The spin indices may be suppressed since the Hamiltonian is time-reversal invariant. In addition to the spin degeneracy, there is also a valley degeneracy, which effectively allows one to consider either one of the $\hat{H}_\pm$ set. We choose $\hat{H}_+$, and consider an incident electron from the normal side of the junction ($x<0$) with energy E. For positive excitation energies $E>0$, the eigenvectors and corresponding momentum of the particles read $\psi_+^e = [1, e^{i\theta}, 0, 0]^T e^{ip^e\cos\theta x}$, $p^e = (E+E_F)/v_F$, for a right-moving electron at angle of incidence θ, while a left-moving electron is described by the substitution $\theta \to \pi-\theta$. If Andreev reflection takes place, a left-moving hole with energy $(-E)$ and angle of reflection θ_A is generated with belonging wave function $\psi_-^h = [0, 0, 1, e^{-i\theta_A}]^T e^{-ip^h\cos\theta_A x}$, $p^h = (E-E_F)/v_F$, where the superscript e (h) denotes an electronlike (holelike) excitation. Since translational invariance in the $\hat{\mathbf{y}}$ direction holds, the corresponding component of momentum is conserved. This condition allows for determination of the Andreev-reflection angle θ_A through $p^h\sin\theta_A = p^e\sin\theta$. One thus infers that there is no Andreev reflection ($\theta_A = \pm\pi/2$), and consequently no subgap conductance, for angles of incidence above the critical angle $\theta_c = \mathrm{asin}[|E-E_F|/(E+E_F)]$.

On the superconducting side of the system ($x>w$), the possible wave functions for transmission of a right-moving quasiparticle with a given excitation energy $E>0$ read $\Psi_+^e = [u(\theta^+), u(\theta^+)e^{i\theta^+}, v(\theta^+)e^{-i\phi^+}, v(\theta^+)e^{i(\theta^+-\phi^+)}]^T \times e^{iq^e\cos\theta^+ x}$, $q^e = (E_F' + \sqrt{E^2-\Delta^2})/v_F$, and $\Psi_-^h = [v(\theta^-), v(\theta^-)e^{i\theta^-}, u(\theta^-)e^{-i\phi^-}, u(\theta^-)e^{i(\theta^- - \phi^-)}]^T \times e^{iq^h\cos\theta^- x}$, $q^h = (E_F' - \sqrt{E^2-\Delta^2})/v_F$. The coherence factors are given by $u(\theta) = \{\frac{1}{2}[1+\sqrt{E^2-|\Delta(\theta)|^2}/E]\}^{1/2}$, $v(\theta) = \{\frac{1}{2}\times[1-\sqrt{E^2-|\Delta(\theta)|^2}/E]\}^{1/2}$. Above, we have defined $\theta^+ = \theta_S^e$, $\theta^- = \pi-\theta_S^h$, and $e^{i\phi^\pm} = e^{i\vartheta}\Delta(\theta^\pm)/|\Delta(\theta^\pm)|$. The transmission angles $\theta_S^{(i)}$ for the electronlike and holelike quasiparticles are given by $q^{(i)}\sin\theta_S^{(i)} = p^e\sin\theta$, $i = e, h$. Note that for subgap energies $E<\Delta$, there is a small imaginary contribution to the wave vector, which leads to exponential damping of the wave functions inside the superconductor. For clarity, we have omitted a common phase factor $e^{ik_y y}$, which corresponds to the conserved momentum in the $\hat{\mathbf{y}}$ direction. A possible Fermi vector mismatch (FVM) between the normal and superconducting region is accounted for by allowing for $E_F' \neq E_F$. The case $E_F' \gg E_F$ corresponds to a heavily doped superconducting region, while $E_F' = E_F$ describes undoped graphene. Since we are using a mean-field approach to describe the superconducting part of the Hamiltonian, it is implicitly understood that phase fluctuations of the order parameter must be small. This amounts to imposing the restriction [10] $\xi/\lambda_F' \gg 1$, or equivalently, $E_F' \gg \Delta$, where ξ is the superconducting coherence length.

The conductance of the $N/I/S$ junction is given by [11] $G(eV) = G_N\int_{-\theta_c}^{\theta_c} d\theta\cos\theta[1-|r(eV,\theta)|^2 + P|r_A(-eV,\theta)|^2]$, where r and r_A are the reflection coefficients for normal and Andreev reflection, respectively, $P = |p_h|\cos\theta_A/(|p_e|\cos\theta)$, while $G_N = \int_{-\pi/2}^{\pi/2} d\theta\cos\theta[4\cos^2\theta/(4\cos^2\theta+Z^2)]$ is a renormalization constant corresponding to the N/N metallic conductance [12]. In this case, we have zero intrinsic barrier such that $Z=0$. We will apply the usual approximation $|r_A(-eV,\theta)| \simeq |r_A(eV,\theta)|$, which holds for subgap ener-

gies. Although it is not valid for energies above the gap, this is of little consequence for the final result, since Andreev reflection is suppressed for $eV > \Delta$. The reflection and transmission coefficients constitute a unitary scattering matrix, a property that essentially expresses a conservation of probability. In deriving the conductance, we have ensured that the scattering coefficients have been normalized by the incoming current through the factor P. In order to obtain these coefficients, we make use of the boundary conditions $\psi|_{x=0} = \tilde{\psi}_I|_{x=0}$, $\tilde{\psi}_I|_{x=w} = \Psi_S|_{x=w}$, where we have defined the wave function in the insulating region $\tilde{\psi}_I = \tilde{t}_1\tilde{\psi}^e_+ + \tilde{t}_2\tilde{\psi}^e_- + \tilde{t}_3\tilde{\psi}^h_+ + \tilde{t}_4\tilde{\psi}^h_-$. The wave functions $\tilde{\psi}$ differ from ψ in that the Fermi energy is greatly shifted by means of, e.g., an external potential, such that $E_F \rightarrow E_F - V_0$, where V_0 is the barrier (equivalent to the role of Z in Ref. [11]). The coefficients r and r_A may now be obtained by using the boundary conditions, but we leave the explicit calculations and somewhat cumbersome analytical results for a forthcoming paper.

Consider first a $N/I/S$ graphene junction. In the thin-barrier limit defined as $w \rightarrow 0$ and $V_0 \rightarrow \infty$ with s-wave pairing, Ref. [5] reported a π periodicity of the conductance with respect to the parameter $\chi = V_0 w/v_F$. In the present study, we do not restrict ourselves to isotropic pairing, nor to the thin-barrier limit, and show that new physics emerges from the presence of a finite-width barrier. We measure the width w of region I in units of λ_F and the potential barrier V_0 in units of E_F. The linear dispersion approximation is valid up to $\simeq 1$ eV [8], and we will consider typical Fermi energies in graphene of $E_F = 100$ meV in the undoped case and a gap $\Delta = 1$ meV [1]. In the doped case, we set $E'_F = 10E_F$, and we also fix $V_0 = 10E_F$ in order to operate within the regime of validity of the linear dispersion approximation. The undoped situation originally refers to the case where the Fermi level is located at the Dirac point, although real experimental graphene samples will have free carriers, such that E_F is pushed upwards. The doped case denotes a large FVM between the N and S region which may be induced by chemical doping or by a gate voltage.

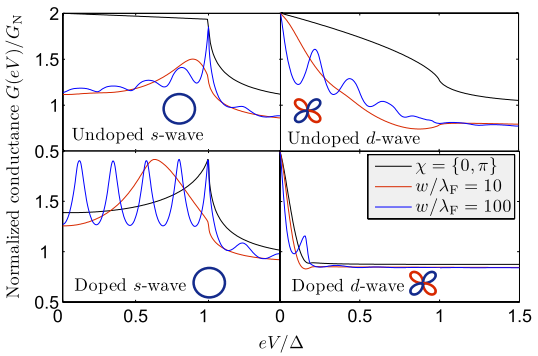

FIG. 1 (color online). Tunneling conductance of $N/I/S$ graphene junction for both s-wave and d-wave pairing in the undoped and doped case (see main text for parameter values). It is seen that for increasing w, a novel oscillatory behavior of the conductance as a function of voltage is present in all cases.

Consider Fig. 1, where we plot the normalized tunneling conductance in the two cases of s-wave and d-wave pairing, for both doped and undoped graphene. The most striking new feature compared to the thin-barrier limit is the strong oscillations in the conductance as a function of eV. We also include the thin-barrier limit with $\chi = 0$ and $\chi = \pi$ to illustrate the π periodicity in this limit. For subgap energies, we regain the N/S conductance for undoped graphene when $\chi = 0$, with nearly perfect Andreev reflection. To model the d-wave pairing, we have used the $d_{x^2-y^2}$ model $\Delta(\theta) = \Delta\cos(2\theta - 2\alpha)$, with $\alpha = \pi/4$. The parameter α effectively models different orientations of the gap in $\mathbf{k}$ space with regard to the interface, and $\alpha = \pi/4$ corresponds to perfect formation of ZES in N/S metallic junctions. For $\alpha = 0$, the d-wave spectra are essentially identical to the s-wave case, since the condition for formation of ZES is not fulfilled in this case [7]. It is seen that in all cases shown in Fig. 1 the conductance exhibits a novel oscillatory behavior as a function of applied bias voltage eV as the width w of the insulating region becomes much larger than the Fermi wavelength, i.e., $w \gg \lambda_F$.

The oscillatory behavior of the conductance may be understood as follows. Nonrelativistic free electrons with energy E impinging upon a potential barrier V_0 are described by an exponentially decreasing nonoscillatory wave function e^{ikx} inside the barrier region if $E < V_0$, since the dispersion essentially is $k \sim \sqrt{E - V_0}$. Relativistic free electrons, on the other hand, have a dispersion $k \sim (E - V_0)$, such that the corresponding wave functions do not decay inside the barrier region. Instead, the transmittance of the junction will display an oscillatory behavior as a function of the energy of incidence E. In general, a kinetic energy given by $\sim k^\alpha$ will lead to a complex momentum $k \sim (E - V_0)^{1/\alpha}$ inside the tunneling region and hence damped oscillatory behavior of the wave function. Relativistic massless fermions are unique in the sense that only in this case ($\alpha = 1$) is the momentum purely real. Hence, the undamped oscillatory behavior at subgap energies appears as a direct manifestation of the relativistic low-energy Dirac fermions in the problem. This observation is also linked to the so-called Klein paradox which occurs for electrons with such a relativistic dispersion relation, which has been theoretically studied in normal graphene [2].

We next discuss why the illustrated conductance spectra are different for s-wave and d-wave symmetry, in addition to comparing the doped and undoped case. The doping level may be considered as an effective FVM, acting as a source of normal reflection in the scattering processes. This is why the subgap conductance at thin-barrier limit is reduced in the doped case. Moving away from the thin-

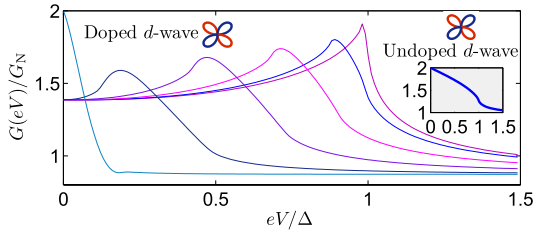

FIG. 2 (color online). Conductance spectra for a doped N/S graphene junction in the d-wave case, varying the orientation angle α. From right to left, the curves vary in the interval $\alpha \in [0, \pi/4]$ in steps of $\pi/20$. The inset shows the undoped case for $\alpha = \pi/4$.

barrier limit, it is seen that oscillations emerge in the conductance spectra. For s-wave pairing, the amplitude of the oscillations is larger in the doped case than in the undoped case, and the period of oscillations remains the same. This period depends on w, while the amplitude of the oscillations is governed by the wave vectors in the regions I and S. The maximum value of the oscillations occurs when $2w$ equals an integer number of wavelengths, corresponding to a constructive interference between the scattered waves. Physically, the amplitude dependence of the oscillations on doping originates with the fact that doping effectively acts as an increase in barrier strength. By making V_0 larger, one introduces a stronger source of normal reflection. When the resonance condition for the oscillations is not met, the barrier reflects the incoming particles more efficiently. This is also the reason why increasing V_0 directly and increasing E_F' has the same effect on the spectra.

We now turn to the difference between the s wave and d wave for the undoped case. It is seen that the conductance is reduced in the d-wave case compared to the s-wave case. One may understand the reduction in subgap conductance in the undoped case as a consequence of tunneling into the nodes of the gap, which is not present in the s-wave case. Hence, Andreev reflection which significantly contributes to the conductance is reduced in the d-wave case compared to the s-wave case. Moreover, we see that a ZBCP is formed in the doped case, equivalent to a stronger barrier, and this is interpreted as the usual formation of ZES leading to a transmission at zero bias with a sharp drop for increasing voltage.

Finally, we briefly investigate how the conductance spectra of a N/S graphene junction (without the insulating region) change when going from a s-wave to a d-wave order parameter in the superconducting part of the system. Consider Fig. 2 for the case of doped graphene, where we plot the conductance to see how it evolves upon a rotation of the gap. The behavior is quite distinct from that encountered in a N/S metallic junction. From Fig. 2, we see that the peak of the conductance shifts from $eV = \Delta$ to progressively lower values as α increases from 0 to $\pi/4$, but only for α very close to $\pi/4$ is a ZBCP present. This is different from what is observed in metallic N/S junctions, where the formation of a ZBCP starts immediately as one moves away from $\alpha = 0$ in the presence of a FVM, corresponding to the doped case here. In Fig. 2 the conductance spectra actually mimics a lower value of the gap than what is the case if one were to infer the gap magnitude from the position of the singularity in the spectra. This should be an easily observable feature in experiments and provides a direct way of testing our theory. For undoped graphene, we found very little difference in the conductance spectra upon varying α. The inset of Fig. 2 illustrates the undoped case for $\alpha = \pi/4$, where the deviation from perfect Andreev reflection for $eV < \Delta$ is due to tunneling into the nodes of the gap.

In summary, we have studied coherent quantum transport in N/S and $N/I/S$ graphene junctions, investigating also the role of d-wave pairing symmetry on the tunneling conductance. We report a new oscillatory behavior of the conductance as a function of bias voltage for insulating regions that satisfy $w \gg \lambda_F$, which is present both for s- and d-wave pairing. In the latter case, we have also studied the conductance of a N/S junction and find very distinct behavior from metallic N/S junctions: a rotation of α is accompanied by a progressive shift of the peak in the conductance. All of our predictions should be easily experimentally observable.

J. L. gratefully acknowledges D. Huertas-Hernando for very useful discussions in the initial stages of this work. This work was supported by the Norwegian Research Council Grants No. 158518/431, No. 158547/431 (NANOMAT), and No. 167498/V30 (STORFORSK).

[1] K. S. Novoselov *et al.*, Science **306**, 666 (2004); Y. Zhang *et al.*, Nature (London) **438**, 201 (2005).
[2] M. I. Katsnelson *et al.*, Nature Phys. **2**, 620 (2006); J. Milton Pereira Jr., P. Vasilopoulos, and F. M. Peeters, arXiv:cond-mat/0702596.
[3] H. B. Heersche *et al.*, Nature (London) **446**, 56 (2007); A. Yu. Kasumov *et al.*, Science **284**, 1508 (1999); A. F. Morpurgo *et al.*, Science **286**, 263 (1999); M. R. Buitelaar *et al.*, Phys. Rev. Lett. **91**, 057005 (2003); P. Jarillo-Herrero, J. A. van Dam, and L. P. Kouwenhoven, Nature (London) **439**, 953 (2006).
[4] C. W. J. Beenakker, Phys. Rev. Lett. **97**, 067007 (2006).
[5] S. Bhattacharjee and K. Sengupta, Phys. Rev. Lett. **97**, 217001 (2006).
[6] I. I. Mazin and M. D. Johannes, Nature Phys. **1**, 91 (2005).
[7] Y. Tanaka and S. Kashiwaya, Phys. Rev. Lett. **74**, 3451 (1995).
[8] P. R. Wallace, Phys. Rev. **71**, 622 (1947).
[9] C. Bruder, Phys. Rev. B **41**, 4017 (1990).
[10] H. Kleinert, Phys. Rev. Lett. **84**, 286 (2000).
[11] G. E. Blonder, M. Tinkham, and T. M. Klapwijk, Phys. Rev. B **25**, 4515 (1982).
[12] S. Kashiwaya *et al.*, Phys. Rev. B **53**, 2667 (1996).

Paper VIII

Spin-flip scattering and non-ideal interfaces in dirty ferromagnet / superconductor junctions.

Physical Review B **76**, 214508 (2007).

PHYSICAL REVIEW B **76**, 214508 (2007)

Spin-flip scattering and nonideal interfaces in dirty ferromagnet/superconductor junctions

Jacob Linder and Asle Sudbø
Department of Physics, Norwegian University of Science and Technology, N-7491 Trondheim, Norway
(Received 20 July 2007; published 18 December 2007)

We study the proximity-induced superconducting correlations as well as the local density of states of a ferromagnet, in a ferromagnet/*s*-wave superconductor heterostructure. We include the effects of spin-flip scattering, nonideal interfaces, and the presence of impurities in the sample. We employ the quasiclassical theory of superconductivity, solving the Usadel equation with emphasis on obtaining transparent analytical results. As our main result, we report that in a certain parameter regime the spatial oscillations of the anomalous (superconducting) part of the Green's function induced in the ferromagnet by the proximity effect from the *s*-wave superconductor, are damped out due to the presence of spin-flip processes. As a consequence, spin-flip scattering may under certain conditions actually enhance the local density of states due to the oscillatory behavior of the latter in ferromagnet/superconductor structures. We also conjecture that the damping could be manifested in the behavior of the critical temperature (T_c) of the *s*-wave superconductor in contact with the ferromagnet. More specifically, we argue that the nonmonotonic decrease of T_c in ferromagnet/*s*-wave superconductor junctions without magnetic impurities is altered to a monotonic, nonoscillatory decrease when the condition $1 > 16\tau_{sf}^2 h^2$ is fulfilled, where τ_{sf} is the spin-flip relaxation time and h is the exchange field.

DOI: 10.1103/PhysRevB.76.214508 PACS number(s): 74.20.Rp, 74.50.+r, 74.70.Kn

I. INTRODUCTION

Proximity structures consisting of ferromagnetic and superconducting materials offer a synthesis between two important physical phenomena that may hold the potential for future applications in nanotechnology: spin-polarization and dissipationless flow of a current. Ferromagnetism is antagonistic to conventional superconductors, since the exchange field acts as a depairing agent for spin-singlet Cooper pairs. However, the proximity effect does not merely suppress the spin-singlet superconducting order parameter, but may also induce long-ranged spin-triplet correlations under certain circumstances.[1] Much effort has been invested over the last decade to unveil various physical phenomena that occur in ferromagnet/superconductor (F/S) heterostructures.[2–6] Among the highlights of such phenomena, it is natural to mention the π state that is realized in $S/F/S$ structures, which has been studied intensively both theoretically[7–10] and experimentally.[11,12] In this state, the superconducting order parameters differ in sign in contrast to the usual 0 state in $S/N/S$ structure. The transition from a 0 to π state may be controlled by the width of the ferromagnet separating the superconductors, thus offering a way of manipulating the Josephson supercurrent that occurs in such systems. Another way of obtaining a π state makes use of misaligned exchange fields in S/F heterostructures. This opportunity arises in a variety of systems, ranging from superconductors with spiral magnetic order,[13–15] thin S/F bilayers,[16–19] and so-called ferromagnetic superconductors[20,21] where ferromagnetic and superconducting order seem to coexist uniformly. The latter is most often interpreted as evidence for triplet pairing in the superconducting sector.

Although various theoretical idealizations allow for a relatively simple approach to F/S heterostructures in the quasiclassical framework, the presence of factors such as nonideal interfaces and both magnetic and nonmagnetic impurities should be taken into account to obtain more precise agreement between theory and experiment. A particularly interesting feature in such hybrid structures is the generation of a spin-triplet superconducting component in the ferromagnet which survives even in the dirty limit due to a special symmetry property which was first suggested by Berezinskii *et al.*,[22] and later predicted to occur in F/S junctions by[23,24] Bergeret *et al.* This issue has been the subject of intense investigations during the past decade (see, for instance, Refs. 1 and 2, and references therein). In particular, the role of triplet pairing in superconductor/half-metal/superconductor structures has received much attention lately,[25–28] much due to the experimental verification of a Josephson current in such a setup.[29]

With regard to F/S junctions, two recent publications have addressed some aspects of how spin-flip processes affect the critical temperature[30] and the density of states.[31] Here, we will consider two different geometries to study the impact of spin-flip scattering and nonideal interfaces in heterostructures involving ferromagnets and superconductors. The geometry of the systems we study are given in Fig. 1. In the top figure, we consider a dirty ferromagnet of width d sandwiched between a ferromagnetic and superconducting reservoir, where the Green's functions are assumed to be in their bulk form. In the bottom figure, the ferromagnetic reservoir is replaced with vacuum, effectively leading to a F/S junction.

In this paper, we study the influence of magnetic impurities and nonideal interfaces on the spatial and energy dependence of the anomalous (superconducting) part of the quasiclassical Green's functions induced in the ferromagnet by the proximity effect from the *s*-wave superconductor. In particular, we investigate how this is manifested in the local density of states (LDOS). We present analytical results that may elucidate features obtained numerically in Ref. 31. In agreement with Ref. 30, we find that spin-flip processes alter the decay and oscillation length of the anomalous Green's function in

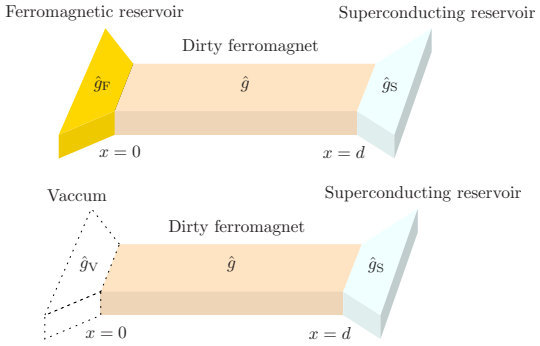

FIG. 1. (Color online) The figure shows geometries that will be considered in this paper. In the top figure, we consider a $F/F/S$ junction consisting of a dirty ferromagnet sandwiched between a ferromagnetic and superconducting reservoir where the Green's functions are described by their bulk values. In the bottom figure, we consider a F/S junction consisting of a dirty ferromagnet connected to a superconducting reservoir.

the ferromagnet. Our main result is that under certain conditions, the usual oscillations of the Green's function in F/S junctions without magnetic impurities vanish completely when the condition $1>16\tau_{sf}^2h^2$ is fulfilled, where τ_{sf} is the spin-flip relaxation time and h is the exchange field. Defining $\Gamma=1/\tau_{sf}$, an equivalent statement is to say that the oscillations vanish when the energy associated with spin-flip scattering exceeds a critical value $\Gamma_c=4h$. As a direct consequence, the spin-flip scattering may actually enhance the LDOS due to the oscillations of the anomalous Green's function in the ferromagnet. A detailed study is performed concerning how the length scales associated with the decay and the oscillations of the Green's function are affected by magnetic impurities. This is important in the context of understanding the behavior of, for instance, the Josephson current in S/F/S structures, since spin-flip scattering will always be present to some degree in real samples. Including such effects will presumably yield a more satisfactory quantitative agreement with experimental data.

We organize this paper as follows. In Sec. II, we establish the theoretical framework we will use to treat the F/S hybrid structure. Namely, we employ the Keldysh formalism in the quasiclassical approximation to study the Usadel equation with appropriate boundary conditions at the interfaces. In Sec. III, we present our results for the spatial and energy dependence of the anomalous Green's function in the dirty ferromagnet, as well as results for the local density of states, both without (for reference) and with spin-flip scattering. We also discuss how the decay length and oscillation length scales of the Green's function are affected by the spin-flip scattering, providing transparent analytical results. In Secs. IV and V, we discuss and summarize the main results of the paper. We will use boldface notation for three-vectors, $\check{\ldots}$ for 8×8 matrices, $\hat{\ldots}$ for 4×4 matrices, and $\underline{\ldots}$ for 2×2 matrices.

II. THEORETICAL FORMULATION

A. Quasiclassical theory

The central quantity in the quasiclassical theory of superconductivity is the quasiclassical Green's functions $\check{g}(\mathbf{p}_F,\mathbf{R};\varepsilon,t)$, which depends on the momentum at Fermi level $\mathbf{p}_F$, the spatial coordinate $\mathbf{R}$, energy measured from the chemical potential ε, and time t. A considerable literature covers the Keldysh formalism and nonequilibrium Green's functions.[32–36] Here we only briefly sketch the theoretical structure, for the sake of readability and for establishing notation. The quasiclassical Green's functions $\check{g}(\mathbf{p}_F,\mathbf{R};\varepsilon,t)$ is obtained from the Gor'kov Green's functions $\check{G}(\mathbf{p},\mathbf{R};\varepsilon,t)$ by integrating out the dependence on kinetic energy, assuming that $\check{G}$ is strongly peaked at the Fermi level,

$$\check{g}(\mathbf{p}_F,\mathbf{R};\varepsilon,t)=\frac{i}{\pi}\int d\xi_{\mathbf{p}}\check{G}(\mathbf{p},\mathbf{R};\varepsilon,t). \tag{1}$$

The above is typically applicable to superconducting systems where the characteristic length scale of the perturbations present, such as mean-free path and magnetic coherence length, is much smaller than the Fermi wavelength. Also, the corresponding characteristic energies of such phenomena must be much smaller than the Fermi energy ε_F. The quasiclassical Green's functions may be divided into an advanced (A), retarded (R), and Keldysh (K) component, each of which has a 4×4 matrix structure in the combined particle-hole and spin space. One has that

$$\check{g}=\begin{pmatrix}\hat{g}^R & \hat{g}^K\\ 0 & \hat{g}^A\end{pmatrix}, \tag{2}$$

where the elements of $\check{g}(\mathbf{p}_F,\mathbf{R};\varepsilon,t)$ read

$$\hat{g}^{R,A}=\begin{pmatrix}\underline{g}^{R,A} & \underline{f}^{R,A}\\ -\underline{\tilde{f}}^{R,A} & -\underline{\tilde{g}}^{R,A}\end{pmatrix},\quad \hat{g}^K=\begin{pmatrix}\underline{g}^K & \underline{f}^K\\ \underline{\tilde{f}}^K & \underline{\tilde{g}}^K\end{pmatrix}. \tag{3}$$

The quantities $\underline{g}$ and $\underline{f}$ are 2×2 spin matrices, with the structure

$$\underline{g}=\begin{pmatrix}g_{\uparrow\uparrow} & g_{\uparrow\downarrow}\\ g_{\downarrow\uparrow} & g_{\downarrow\downarrow}\end{pmatrix}. \tag{4}$$

Due to internal symmetry relations between these Green's functions, all of these quantities are not independent. In particular, the tilde operation is defined as

$$\tilde{f}(\mathbf{p}_F,\mathbf{R};\varepsilon,t)=f(-\mathbf{p}_F,\mathbf{R};-\varepsilon,t)^*. \tag{5}$$

The quasiclassical Green's functions $g(\mathbf{p}_F,\mathbf{R};\varepsilon,t)$ may be determined by solving the Eilenberger[37] equation

$$[\varepsilon\hat{\rho}_3-\hat{\Sigma},\check{g}]_\otimes+i\mathbf{v}_F\nabla\check{g}=0, \tag{6}$$

where $\hat{\Sigma}$ contains the self-energies in the system such as impurity scattering, superconducting order parameter, and exchange fields. The star product $\otimes$ is noncommutative and is defined in Appendix A. When there is no explicit time dependence in the problem, the star product reduces to normal multiplication. This is the case we will consider through-

out the paper. The operation $\hat{\rho}_3\check{g}$ inside the commutator should be understood as $\hat{\rho}_3\check{g} \equiv \mathrm{diag}\{\hat{\rho}_3, \hat{\rho}_3\}\check{g}$. Pauli matrices in particle hole $\times$ spin (Nambu) space are denoted as $\hat{\rho}_i$, while Pauli matrices in spin space are written as $\underline{\tau}_i$. The Green's functions also satisfy the normalization condition

$$\check{g} \otimes \check{g} = \check{1}. \tag{7}$$

The self-energies entering Eq. (6) must be solved in a self-consistent manner. For instance, a weak-coupling s-wave superconducting order parameter is obtained by

$$\Delta(\mathbf{R};t) = -\frac{\lambda}{4}\int_{-\omega_c}^{\omega_c} d\varepsilon \langle f^K_{\uparrow\downarrow}(\mathbf{p}_F, \mathbf{R}; \varepsilon, t)\rangle_{\hat{\mathbf{p}}_F}, \tag{8}$$

where ω_c is the cutoff energy, which may be eliminated in favor of the transition temperature. The notation $\langle \ldots \rangle$ is to be understood as an angular averaging over the Fermi surface. Once $\check{g}(\mathbf{p}_F, \mathbf{R}; \epsilon, t)$ has been determined, physical quantities of interest may be calculated, such as the electrical current

$$\mathbf{j}(\mathbf{R};t) = \frac{N_F e v_F}{4}\int d\varepsilon \ \mathrm{Tr}\{\langle \hat{\rho}_3 \mathbf{e}_F \hat{g}^K \rangle_{\hat{\mathbf{p}}_F}\}, \tag{9}$$

where N_F is the density of states (DOS) per spin at Fermi level. Equation (9) also includes the contribution to charge transport for holes, thus including processes such as Andreev reflection. In the special case of an equilibrium situation, one may express the Keldysh component in terms of the retarded and advanced Green's function by means of the relation

$$\hat{g}^K = (\hat{g}^R - \hat{g}^A)\tanh(\beta\varepsilon/2), \tag{10}$$

where $\beta = T^{-1}$ is inverse temperature. In nonequilibrium situations, one must derive kinetic equations for nonequilibrium distribution functions in order to specify the Keldysh part.[38]

The above equations suffice to completely describe for instance a single superconducting structure, but must be supplemented with boundary conditions when treating heterostructures such as F/S junctions. These boundary conditions take different forms depending on the physical properties of the interface, and we proceed to describe possible scenarios in this respect. Transport across interfaces in heterostructures may in general be characterized according to three particular properties: (i) the transmission of the interface, (ii) the resistivity of the compounds separated by the interface, and (iii) whether the interface is spin active or not. Let us clarify the distinction between the two first properties. The transmission of the barrier (assuming for simplicity a single open transport channel) determines whether one is dealing with a point contact or tunneling contact, which differ in terms of the likelihood of electron transport to occur across the interface. In the Blonder-Tinkham-Klapwijk language,[39] the point contact corresponds to low values of Z while the tunneling limit is obtained for high values of Z. On the other hand, the resistivity of the compounds separated by the interface is unrelated to the transmissivity of the interface, and one may have, for instance, a tunneling contact with electrodes attached to it that have either a large or small resistance.

The third property determines to what degree the interface discriminates between incoming quasiparticles with different spins. Zaitsev[40] derived boundary conditions for a clean N/S interface, while Kuprianov and Lukichev (KL)[41] worked out simplified boundary conditions in the dirty limit, valid for atomically sharp interfaces in the tunneling regime with a low barrier transparency. Although the KL boundary conditions are, strictly speaking, not valid for high transparency of the barrier, they may be used for qualitative predictions in that regime under certain conditions.[42] The most compact way of writing the boundary conditions for the Green's functions for arbitrary interfaces was introduced by Nazarov.[43] In all the preceding references, a nonmagnetic (spin-inactive) interface was assumed. The generalized boundary conditions for magnetically active interfaces have also been derived.[44] Let us make a final remark concerning the treatment of interfaces in the quasiclassical theory of superconductivity. We previously stated that the present theory is valid as long as characteristic energies of various self-energies and perturbations in the system are much smaller than the Fermi energy. At first glance, this might seem to be unreconcilable with the presence of interfaces, which represent strong perturbations varying on atomic length scales, clearly in stark contradiction to the regime of validity of quasiclassical theory. However, this problem may be overcome by including the interfaces as boundary conditions for the Green's functions rather than directly in the Eilenberger equation.

The KL boundary conditions may be applied for a dirty junction in the tunneling limit when the transparency of the interface is low, in correspondence with our assumption of a weak proximity effect. For the retarded part of the Green's function, they read

$$\begin{aligned} 2d\gamma(\hat{g}\partial_x\hat{g})|_{x=0} &= -[\hat{g}, \hat{g}_{F(V)}]|_{x=0}, \\ 2d\gamma(\hat{g}\partial_x\hat{g})|_{x=d} &= [\hat{g}, \hat{g}_S]|_{x=d}, \end{aligned} \tag{11}$$

where $F(V)$ corresponds to the $F/F/S$ (F/S) case of Fig. 1. The parameter γ models the interfacial transmission properties, and is given by $\gamma = R_I/R_F$, where R_I is the interface resistance per unit area, while R_F is the equivalent in the dirty ferromagnet. In this work, γ holds the status of a variational parameter. A low transparency of the interface amounts to the regime $\gamma \gg 1$. As previously mentioned, qualitative predictions may still be obtained using the linearized Usadel equations for $\gamma \simeq 1$, and even the quantitative aspects of the exact numerical solution may in some cases be very well modeled by this approximation.[45] Under the assumption of a weak proximity effect, we will neglect the depletion of the superconducting order parameter near the interface in order to facilitate the calculations and for the sake of obtaining analytical results. Moreover, we will use the bulk solution of the Green's function in the superconductor. This approximation is valid when the superconducting region is much less disordered than the ferromagnet.[1]

B. Green's functions

We will consider the dirty limit of the Eilenberger equation, Eq. (6), which leads to the Usadel equation.[46] This will

be an appropriate starting point for diffusive systems where the scattering time due to impurities satisfies $X\tau \ll 1$, where X is the energy scale of any other self-energy in the problem. For strong ferromagnets where h becomes comparable to ε_F, the stated inequality may, strictly speaking, not be valid for $X=h$. Hence, we will restrict ourselves to the regime $h \ll \varepsilon_F$. Below, we will mostly concern ourselves with the retarded part of $\check{g}(\mathbf{p}_F, \mathbf{R}; \varepsilon, t)$, since the advanced component may be found via the relation

$$\hat{g}^A = -(\hat{\rho}_3 \hat{g}^R \hat{\rho}_3)^\dagger. \tag{12}$$

The Keldysh component is calculated by means of Eq. (10) in a situation of local thermal equilibrium. For a nonequilibrium situation, the Keldysh component is found by

$$\hat{g}^K = \hat{g}^R \hat{\mathcal{F}} - \hat{\mathcal{F}} \hat{g}^A, \tag{13}$$

where $\hat{\mathcal{F}}$ is a matrix distribution function to be determined from kinetic equations, while Eq. (12) still holds. Equation (13) follows from the normalization condition of the Green's function, and the distribution function may be chosen as diagonal without any loss of generality. In general, we may write

$$\hat{\mathcal{F}} = \mathcal{F}_l \hat{1} + \mathcal{F}_t \hat{\rho}_3, \tag{14}$$

where comparison with Eq. (10) shows that in a thermal equilibrium one has $\mathcal{F}_l = \tanh(\beta\varepsilon/2)$, $\mathcal{F}_t = 0$.

By isotropizing the Green's function due to the assumed frequent impurity scattering, it is rendered independent of $\mathbf{p}_F$. This isotropic (in momentum space) Green's function satisfies the Usadel equation in the ferromagnet as follows:

$$D\boldsymbol{\nabla}(\check{g}\,\boldsymbol{\nabla}\,\check{g}) + i[\varepsilon\hat{\rho}_3 + \hat{M} - \check{\sigma}_{\mathrm{sf}}, \check{g}] = 0. \tag{15}$$

Above, the exchange energy h is accounted for by the matrix $\hat{M} = \mathrm{diag}(h\underline{\tau}_3, h\underline{\tau}_3)$, assuming a magnetization in the $\mathbf{z}$ direction, while the spin-flip self-energy reads

$$\check{\sigma}(\mathbf{R}; \varepsilon) = -\frac{i}{8\tau_{\mathrm{sf}}} \sum_i \hat{\alpha}_i \check{g}(\mathbf{R}; \varepsilon) \hat{\alpha}_i, \tag{16}$$

where τ_{sf} is the spin-flip scattering time. We have defined the matrices $\hat{\alpha}_i = \mathrm{diag}(\underline{\tau}_i, \underline{\tau}_i^T)$. The diffusion constant is given by $D = v_F^2 \tau/3$. Although the Usadel equation, in general, requires a numerical solution, an analytical approach is permissible under certain conditions. In the case of a weak proximity effect, one may effectively linearize Eq. (15). This is a valid treatment for low transparency interfaces or close to T_c. In this case, Eq. (15) is expanded around the bulk solution. To be definite, let us consider the retarded part of Eq. (15) which has the same form, namely,

$$D\boldsymbol{\nabla}(\hat{g}^R \boldsymbol{\nabla} \hat{g}^R) + i[\varepsilon\hat{\tau}_3 + \hat{M} - \hat{\sigma}_{\mathrm{sf}}, \hat{g}^R] = 0, \tag{17}$$

where $\hat{\sigma}_{\mathrm{sf}}$ is obtained from $\check{\sigma}_{\mathrm{sf}}$ simply by letting $\check{g} \to \hat{g}^R$. Omitting the superscript on the Green's function, we may expand it around the bulk solution $\hat{g}_0$ as $\hat{g} \simeq \hat{g}_0 + \hat{f}$, where $\hat{g}_0 = \mathrm{diag}(\underline{1}, -\underline{1})$ and

$$\hat{f} = \begin{pmatrix} \underline{0} & \underline{f}(\mathbf{R}; \varepsilon) \\ -[\underline{f}(\mathbf{R}; -\varepsilon)]^* & \underline{0} \end{pmatrix},$$

$$\underline{f}(\mathbf{R}; \varepsilon) = \begin{pmatrix} f_{\uparrow\uparrow}(\mathbf{R}; \varepsilon) & f^t_{\uparrow\downarrow}(\mathbf{R}; \varepsilon) + (^{t\to s}) \\ f^t_{\uparrow\downarrow}(\mathbf{R}; \varepsilon) - (^{t\to s}) & f_{\downarrow\downarrow}(\mathbf{R}; \varepsilon) \end{pmatrix}. \tag{18}$$

One may now multiply out the matrix equation, Eq. (17), only keeping the lowest order terms in the anomalous Green's functions $f_{\alpha\beta}(\mathbf{R}; \varepsilon)$. For more compact notation, we define the quantities

$$f^i_{\alpha\beta} \equiv f^i_{\alpha\beta}(\mathbf{R}; \varepsilon), \quad \{\alpha, \beta\} = \uparrow, \downarrow \quad \text{and} \quad f^{t(s)} \equiv f^{t(s)}_{\uparrow\downarrow}, \quad i = s, t. \tag{19}$$

We will proceed to consider the two distinct cases illustrated in Fig. 1. The Green's functions in the different reservoirs read

$$\hat{g}_V = \hat{0}, \quad \hat{g}_F = \begin{pmatrix} \underline{1} & \underline{0} \\ \underline{0} & \underline{1} \end{pmatrix}, \quad \hat{g}_S = \begin{pmatrix} \underline{1}c & i\underline{\tau}_2 s \\ i\underline{\tau}_2 s & -\underline{1}c \end{pmatrix}, \tag{20}$$

where we have defined $c \equiv \cosh(\vartheta)$, $s \equiv \sinh(\vartheta)$ with $\vartheta \equiv \mathrm{atanh}(|\Delta|/\varepsilon)$. Note that we have set the superconducting phase equal to zero, thus considering a gauge where the gap is a purely real quantity.

C. Odd-frequency pairing

Before moving on to the graphical presentation of our results, let us comment on the presence of the $S_z = 0$ triplet component of the anomalous Green's function in the ferromagnet. It is well known that even in the absence of spin-flip processes ($\tau_{\mathrm{sf}} \to \infty$), the triplet component is generated in the ferromagnet due to the presence of the exchange field h. We will later investigate how the magnitude of this triplet component is affected by including spin-flip processes. Also, it is of interest to investigate the symmetry properties of the singlet and triplet component. Since we are considering the isotropic part (with respect to momentum) of the Green's function due to the angular averaging in the dirty limit, one would naively expect that only the singlet component should be present. This is because the singlet anomalous Green's function is usually taken to be even under inversion of momentum, while the triplet components are taken to be odd under inversion of momentum. Recall that inversion of momentum amounts to an exchange of spatial coordinates for the field operators, since $\mathbf{p}$ is the Fourier transform of the relative coordinate $\mathbf{r} \equiv \mathbf{r}_1 - \mathbf{r}_2$. However, another possibility exists that permits the presence of triplet correlations in the ferromagnet, namely, a sign shift under inversion of energy. This type of pairing has been dubbed *odd-frequency pairing* in the literature, interpreting energy as a real frequency. Recall that inversion of energy is equivalent to an exchange of time coordinates for the field operators, since ε is the Fourier transform of the relative time coordinate $t \equiv t_1 - t_2$. For a detailed discussion of even- and odd-frequency pairing, the reader may consult Appendix B.

Let us in passing show that the singlet component is even in frequency, while the triplet component is odd in fre-

quency, by using the definition in Eq. (B16). To do this, we must first find the advanced Green's function f^A by exploiting Eq. (12). Direct matrix multiplication leads to

$$\hat{g}^A = \begin{pmatrix} -1 & 0 & 0 & -f_-^R(-\varepsilon) \\ 0 & -1 & -f_+^R(-\varepsilon) & \\ 0 & [f_-^R(\varepsilon)]^* & 1 & 0 \\ [f_+^R(\varepsilon)]^* & 0 & 0 & 1 \end{pmatrix}. \tag{21}$$

From this, one infers that $f_s^A(\varepsilon)=f_s^R(-\varepsilon)$ (even-frequency pairing) and $f_t^A(\varepsilon)=-f_t^R(-\varepsilon)$ (odd-frequency pairing). We have included this short paragraph on even- and odd-frequency pairing to emphasize that although even-frequency triplet correlations are destroyed in the dirty limit due to the isotropization stemming from impurity scattering, odd-frequency triplet correlations may persist since these do not vanish under angular averaging. Also, it is important to understand that the triplet pairing we are discussing in the present paper is then quite different from the triplet pairing in, for instance, Sr_2RuO_4. In the latter case, the triplet pairing is odd in momentum and therefore even in frequency.[47] As a consequence, superconductivity is highly sensitive to impurity scattering in Sr_2RuO_4 and only observed in very clean samples.

In the problem under consideration, the two important energies are the exchange energy h and the BCS gap $|\Delta|$. Associated with these energies are two typical length scales: the correlation length in the ferromagnet $\xi_F=\sqrt{D/h}$ and the superconducting coherence length $\xi_S=\sqrt{D/(2\pi T_c)}$, where the critical temperature in a weak-coupling superconductor is given by $|\Delta|\simeq 1.76T_c$. One may think of ξ_F as the penetration depth of the superconducting condensate into the dirty ferromagnet. In an experimental situation, one usually has $h\gg|\Delta|$ even for relatively weak ferromagnets, such that $\xi_F \ll \xi_S$. For the quasiclassical treatment to be valid, one must then have $|\Delta|\ll h\ll\varepsilon_F$. For a Fermi energy of 1 eV, it would then be reasonable to consider h in the neighborhood of 30 meV and $|\Delta|$ around 1 meV. The effect of D and d may be accounted for in the single parameter $\varepsilon_T=D/d^2$, named the Thouless energy. This is the relevant energy scale for the proximity effect in the case of highly transparent interfaces. In the following, we will, unless specifically stated otherwise, fix $h/|\Delta|=30$ to operate within the allowed boundaries of our approximations. Since one is often interested in investigating how various physical properties behave as a function of the thickness d of the ferromagnetic layer, it is useful to note that for $d/\xi_S=x$, one finds

$$\varepsilon_T=\frac{2\pi|\Delta|}{1.76x^2}. \tag{22}$$

III. RESULTS

We now provide the main results of this paper, namely, a study of how the triplet correlations and LDOS are affected by spin-flip scattering in a F/S and $F/F/S$ junction. When including scattering upon magnetic impurities in the sample, Eq. (15) yields the differential equations

$$D\partial_x^2(f_t\pm f_s)+2i(\varepsilon\pm h)(f_t\pm f_s)-\frac{1}{2\tau_{sf}}(f_t\pm 3f_s)=0,$$

$$D\partial_x^2 f_\sigma+\left(2i\varepsilon-\frac{1}{2\tau_{\rm sf}}\right)f_\sigma=0. \tag{23}$$

Note that we have here assumed an isotropic spin-flip disorder, in contrast to the uniaxial disorder considered in Refs. 30 and 48. We comment more on this in Sec. IV. Spin-flip processes in combination with a spatially homogeneous exchange field do not lead to equal-spin correlations in the ferromagnet, although the inclusion of a spin-active barrier will generate these components.[27,49] Therefore, for the present case of a nonmagnetic interface, we have that $f_\sigma=0$. For the $S_z=0$ triplet and singlet Green's functions, the general solution of Eq. (23) reads

$$f_t=c_1e^{-q_+x}+c_2e^{q_-x}+c_3e^{q_+x}+c_4e^{-q_-x},$$

$$f_s=\frac{i}{4\tau_{\rm sf}h}(c_1\kappa_-e^{-q_+x}+c_2\kappa_+e^{q_-x}+c_3\kappa_-e^{q_+x}+c_4\kappa_+e^{-q_-x}), \tag{24}$$

where we have defined

$$q_\pm=[-(4i\tau_{\rm sf}\varepsilon-2\pm\sqrt{1-16\tau_{\rm sf}^2h^2})/(2D\tau_{\rm sf})]^{1/2},$$

$$\kappa_\pm=1\pm\sqrt{1-16\tau_{\rm sf}^2h^2}. \tag{25}$$

The coefficients $\{c_i\}$ will be determined from the boundary conditions of the F/S and $F/F/S$ junctions. These are given by Eq. (11), which may be written in terms of the $f_\pm$ functions. For the F/S junction, we have

$$\text{(i)}\quad \partial_x f_\pm|_{x=0}=0,$$

$$\text{(ii)}\quad d\gamma\partial_x f_\pm|_{x=d}=\pm s-cf_\pm|_{x=d}. \tag{26}$$

Above, $s=\cosh(\vartheta)$, $s=\sinh(\vartheta)$, and $\vartheta=\operatorname{arctanh}(|\Delta|/\varepsilon)$. In the $F/F/S$ case, the condition (ii) is still valid while (i) must be replaced with

$$\text{(i)}\quad d\gamma\partial_x f_\pm|_{x=0}=f_\pm|_{x=0}. \tag{27}$$

Note that it is implicit here that $f_\pm=f_\pm^R$. The resulting analytical expressions or $\{c_i\}$ read as follows:

$$c_4=\frac{-2s(1+X_-/X_+)}{Y_--Y_+X_-/X_+},\quad c_3=(2s-c_4Y_+)/X_+,$$

$$c_2=Rc_4,\quad c_1=L_2c_2+L_3c_3+L_4c_4. \tag{28}$$

For convenience, we have defined the following quantities:

$$\mathcal{A}_\pm=1\pm i\kappa_-/(4\tau_{\rm sf}h),\quad \mathcal{B}_\pm=1\pm i\kappa_+/(4\tau_{\rm sf}h),$$

$$L_2=\frac{\mathcal{B}_+(\psi+q_-)}{\mathcal{A}_+(q_+-\psi)},\quad L_3=\frac{\psi+q_+}{q_+-\psi},$$

$$L_4 = \frac{\mathcal{B}_+(\psi - q_-)}{\mathcal{A}_+(q_+ - \psi)}, \quad R = \frac{q_- - \psi}{q_- + \psi}, \tag{29}$$

in addition to

$$X_\pm = \mathcal{A}_\pm[e^{q_+ d}(2c + 2\gamma d q_+) + e^{-q_+ d}L_3(2c - 2\gamma d q_+)],$$

$$Y_\pm = \mathcal{B}_\pm[e^{q_- d}R(2c + 2\gamma d q_-) + e^{-q_- d}(2c - 2\gamma d q_-)] + \mathcal{A}_\pm e^{-q_+ d}(L_4 + L_2 R)(2c - 2\gamma d q_+). \tag{30}$$

In the F/S case, $\psi=0$, while $\psi=(-\gamma d)^{-1}$ in the $F/F/S$ case. The knowledge of these coefficients completely determines the spatial and energy dependence of the anomalous Green's functions everywhere in the dirty ferromagnet. When applying the limit $\tau_{sf} \to \infty$, by making use of

$$\mathcal{A}_\pm \to 2\delta_{\pm,+}, \quad \mathcal{B}_\pm \to 2\delta_{\pm,-}, \quad q_\pm \to ik_\pm, \tag{31}$$

one regains well-known results for the scenario without spin-flip scattering. Also, it is worth noting that the triplet component vanishes for $h=0$, even in the presence of spin-flip scattering. Having calculated the Green's functions, we may now study the effect of spin-flip scattering on the LDOS. The spin-resolved LDOS is given by

$$N_\sigma(\mathbf{R};\varepsilon) = N_{F,\sigma}\,\mathrm{Re}\{(1 + [f_t(\varepsilon) + \sigma f_s(\varepsilon)] \times [f_t(-\varepsilon) - \sigma f_s(-\varepsilon)]^*)^{1/2}\}, \quad \sigma = \uparrow, \downarrow = \pm 1. \tag{32}$$

Above, $N_{F,\sigma}$ is the DOS at Fermi level for spin species σ ($N_F = \Sigma_\sigma N_{F,\sigma}$). The deviation δN from the bulk DOS inside the dirty ferromagnet may be defined as

$$\delta N \equiv \sum_\sigma [N_\sigma(\mathbf{R};\varepsilon) - N_{F,\sigma}]/N_{F,\sigma}. \tag{33}$$

We also define the normalized LDOS as $N = \Sigma_\sigma N_\sigma(\mathbf{R};\varepsilon)/(2N_{F,\sigma})$, such that in the absence of a proximity effect, $N=1$. The oscillations of the LDOS in a F/S junction was first reported by Buzdin,[50] and led to observable effects such as the nonmonotonic dependence of the critical temperature on the length d of a F/S bilayer[51–53] and the π-phase structures that occur in F/S hybrid systems.[11]

Consider first Fig. 2 for a plot of the correction δN to the LDOS as a function of position in the dirty ferromagnet. Although the maximum amplitude of δN is suppressed with increasing spin-flip scattering $\Gamma = 1/\tau_{sf}$, an interesting feature is that the magnitude of the correction ($|\delta N|$) is in some regions actually enhanced due to spin-flip scattering. This seems to be a result of the oscillatory behavior of the LDOS. In a N/S junction, where there is no oscillatory behavior of the LDOS, spin-flip scattering would simply cause a reduction of the correction δN. Thus, the role of spin-flip scattering in a F/S junction is more subtle than in a N/S junction where it simply amounts to a suppression of the LDOS.

It might seem counterintuitive that increasing spin-flip scattering should increase the correction to the LDOS, since the anomalous Green's functions should be suppressed for large Γ. We suggest the following resolvement of this phenomena. It is clear that the LDOS displays an oscillatory behavior due to the presence of an exchange field, both with and without the spin-flip scattering. However, in the presence of spin-flip processes, the period of these oscillations is modified. From Fig. 2, it is seen that the peak of the correction to δN is suppressed with increasing Γ. But even though this peak becomes smaller, the different periods of oscillation allows $|\delta N(\Gamma_1)|$ to outgrow $|\delta N(\Gamma_2)|$ at certain distances from the interface, even for $\Gamma_1 > \Gamma_2$. This is a subtle feature unique for F/S interfaces in the presence of spin-flip processes as compared to N/S junctions.

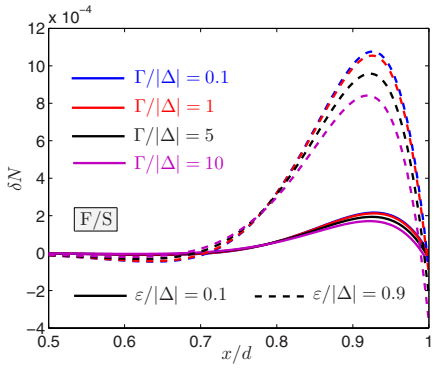

FIG. 2. (Color online) Spatial variation of the deviation from the LDOS (δN) for a F/S junction in the presence of spin-flip scattering. We have chosen $\varepsilon_T/|\Delta| = 1$ and $\gamma = 5$. The qualitative features are the same for the $F/F/S$ junctions for this particular set of parameters. It is seen that for a given energy, increasing spin-flip scattering $\Gamma = 1/\tau_{sf}$ will increase the oscillation length and reduce the amplitude of the Green's function.

It is interesting to investigate the role of spin-flip scattering with regard to the decay and oscillating lengths further. Very recently, some aspects of this topic were addressed in Ref. 54. We here examine in detail some features that occur when spin-flip scattering is included in a F/S junction, among them the *vanishing* of the characteristic oscillations of the anomalous Green's function $\hat{f}$ in a certain parameter regime. Consider first the case without spin-flip scattering, effectively letting $\tau_{sf} \to \infty$. From our previous equations, it is clear that if we write

$$k_\pm = \sqrt{2i(\varepsilon \pm h)/D} = k_{1,\pm} + ik_{2,\pm}, \tag{34}$$

then the real quantities $k_{1,\pm}$ and $k_{2,\pm}$ correspond to the oscillating part and decaying part of $f_\pm$, respectively. We ignore the ε term since we consider the regime $h \gg \varepsilon$, and write $|k_{1,\pm}| = 1/\xi_{osc}$, $|k_{2,\pm}| = 1/\xi_{dec}$. One readily obtains

$$\xi_{dec} = \xi_{osc} = \xi_F. \tag{35}$$

In other words, we recover the well-known fact that the oscillating and decaying length scales of the superconducting condensate in the absence of spin-flip scattering are equal.[2] Consider now a finite value of τ_{sf}, where we obtain

$$q_{\pm} = \sqrt{\frac{2 \mp \sqrt{1 - 16\tau_{sf}^2 h^2}}{2D\tau_{sf}}}. \tag{36}$$

We have neglected the energy term, assuming $\varepsilon\tau_{sf} \ll 1$. In this case, writing $q_{\pm} = q_{1,\pm} + iq_{2,\pm}$ means that $q_{1,\pm}$ and $q_{2,\pm}$ are associated with the decay and oscillating length, respectively. We may now distinguish between two cases. If the inequality

$$1 > 16\tau_{sf}^2 h^2 \tag{37}$$

is satisfied, then $q_{\pm}$ is purely real. In this case, there are *no oscillations* of the anomalous Green's function in the ferromagnet. Since we assumed that $\varepsilon\tau_{sf} \ll 1$, this means that the exchange field should be sufficiently weak for the vanishing of oscillations to take place. For instance, given a spin-flip energy of $\Gamma/|\Delta| = 20$ one would need $h/|\Delta| < 5$ for the oscillations to disappear. If the spin-flip energy becomes very large, then the oscillations would vanish even for moderate exchange fields. This prediction should have easily observable experimental consequences, manifested for instance in the behavior of the critical temperature as a function of junction width d, given that the required parameter regime may be experimentally realized. We comment further on this later in this paper.

In the case where $1 < 16\tau_{sf}^2 h^2$, $q_{\pm}$ is no longer purely real, and oscillations are again present in $f_{\pm}$. It is instructive to consider a plot of ξ_{osc} and ξ_{dec} as a function of spin-flip scattering to see how the oscillation and decay length are affected by these processes. This is done in Fig. 3, where the divergence of the oscillation length is clearly seen at the critical value $\Gamma_c = 4h$. Note that as $\Gamma \to 0$, ξ_{osc} and ξ_{dec} become equal, as previously stated. When Eq. (37) is satisfied, the decay length is different for the up and down spins. This may be seen by introducing $\xi_{dec}^{\pm} = 1/q_{\pm}$ as defined by Eq. (36). Our results for $\Gamma < \Gamma_c$ are consistent with Ref. 30, who reported that increased spin-flip scattering should increase the oscillation length and reduce the decay length. Let us consider how this effect is manifested in the LDOS, a directly measurable experimental quantity. In Fig. 3(b), we plot the spatial correction to the LDOS for $h/|\Delta| = 5$ for several values of the spin-flip energy. As seen, the oscillations vanish as Γ increases, and are completely absent when Eq. (37) is satisfied. The effect we predict should thus be measurable via scanning-tunneling microscopy (STM) measurements, by probing the LDOS.

We next consider a surface plot of the correction to the LDOS in the (x, ε) plane for a set of parameters that should correspond to an experimentally feasible F/S junction. We set $h/|\Delta| = 30$ and $\Gamma/|\Delta| = 0.3$. We use the analytical results for the F/S case, since the difference from a $F/F/S$ junction is small in the low transparency regime. As seen in Fig. 4, the LDOS peaks at $x = d$ with an amplitude that increases with energy. This peak vanishes upon increasing the spin-flip scattering parameter Γ, corresponding to the effect we predict—namely, that the oscillations seen in the LDOS of a F/S junction vanish above a critical value of the spin-flip scattering energy.

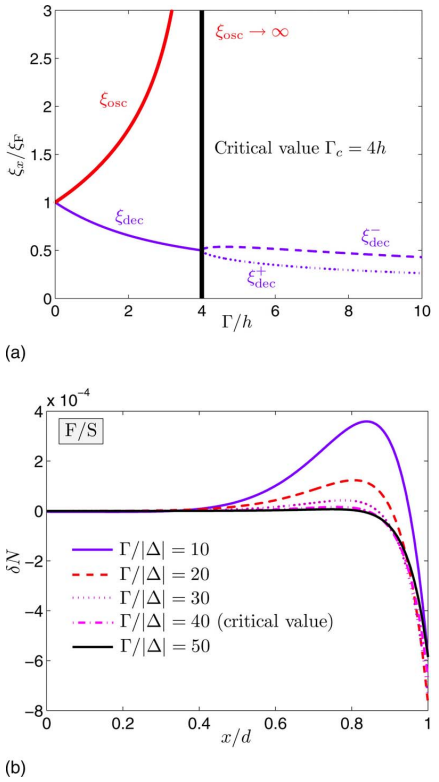

FIG. 3. (Color online) (a) Plot of the characteristic decay and oscillation lengths (ξ_x) of the anomalous Green's function in the presence of spin-flip scattering with $h/|\Delta| = 5$. (b) Spatial variation of the deviation from the LDOS (δN) for a F/S junction in the presence of spin-flip scattering. We have chosen $\varepsilon_T/|\Delta| = 1$, $\gamma = 5$, and $h/|\Delta| = 10$. The quasiparticle energy has been set to $\varepsilon/|\Delta| = 0.5$, but the qualitative behavior is identical for all $\varepsilon < |\Delta|$. As shown in (b), there are no oscillations of the Green's function in the ferromagnet in the parameter range $\Gamma/h > 4$ ($\Gamma = 1/\tau_{sf}$). Inclusion of the energy contribution ε brings small corrections to this result, but as seen from the figure the condition Eq. (37) is a very good approximation. This behavior is to be contrasted with the usual oscillations in F/S junctions as obtained without spin-flip scattering. Note that in (a), ξ_{osc} formally diverges near $\Gamma = \Gamma_c$, which separates the two parameter regimes where oscillations occur and where they do not occur.

IV. DISCUSSION

In F/S junctions without magnetic impurities, it is well known that the critical temperature of the superconductor exhibits a nonmonotonic dependence on the thickness of the ferromagnet layer d (for an extensive treatment of this topic, see the review by Buzdin[2]). The physical reason for the damped, oscillatory behavior of T_c in such systems is not completely understood. It seems reasonable to attribute this characteristic feature to the oscillatory behavior of the Green's functions in the ferromagnet, since this nonmono-

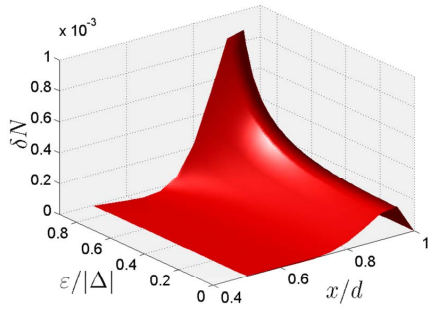

FIG. 4. (Color online) Correction to the LDOS (δN) for $\Gamma/h=0.01$ ($\Gamma=1/\tau_{sf}$). Surface plot of the deviation from the LDOS in the (x,ε) plane for a junction of width $d=2\xi_S$ and with transparency parameter $\gamma=5$ and exchange field $h/|\Delta|=30$. The most protruding feature is the peak emerging in the LDOS right at the F/S interface, followed by a dip structure at low energies.

tonic behavior of T_c is not observed in N/S junctions.[55] However, the transparency of the barrier may also play a key role in the manifestation of oscillations in T_c, as argued in, for instance, Ref. 56–58. In another experiment, a purely monotonic decay of T_c as a function of d was observed in a Pb/Ni junction.[59] Even though the physical picture is not fully resolved, it is highly plausible that the oscillations of $\hat{f}$ are intimately linked to the behavior of T_c. In this paper, we have shown that the presence of spin-flip scattering may significantly change the qualitative behavior of $\hat{f}$ in the ferromagnet. Specifically, the oscillations vanish at a critical value $\Gamma_c=4h$. Under the assumption that the characteristic behavior of $\hat{f}$ strongly influences the fashion in which T_c decays, it is then clear that one should observe a transition from a nonmonotonic (damped, oscillating) to a pure monotonic (damped) decay of T_c upon increasing the concentration of magnetic impurities in a sample. Our finding offers a new, possible explanation for the experiments where a monotonic decay of T_c was observed, namely, that the concentration of magnetic impurities was such that the critical value Γ_c was exceeded.

In this paper, we have assumed an isotropic spin-flip disorder, in contrast to the uniaxial magnetic disorder considered in Refs. 30 and 48. This leads to somewhat different equations for the proximity-induced anomalous Green's function in the ferromagnet. Since we have considered a strongly uniaxial exchange field, it is implicitly assumed that the presence of spin-flip scattering in the plane perpendicular to the exchange field still allows for the uniaxial field to be accommodated. In the case of strong uniaxial anisotropy, the first of the Usadel equations, Eq. (23), is replaced by[48]

$$D\partial_x^2(f_t \pm f_s) + 2i(\varepsilon \pm h)(f_t \pm f_s) - \frac{1}{2\tau_{sf}}(f_t \pm f_s) = 0. \quad (38)$$

Note how the factor 3 in the last term in Eq. (23) now is replaced by unity. Following the same line of reasoning that led to Eq. (36), we now obtain

$$q_\pm = \sqrt{\frac{1 \mp 4i\tau_{sf}h}{2D\tau_{sf}}}. \quad (39)$$

This quantity is always complex, and hence we always obtain (damped) oscillations and never a complete suppression of the oscillations. Thus, the model with isotropic scattering and strongly uniaxially anisotropic scattering are qualitatively different. The model with isotropic scattering, Eq. (23), is expected to be most relevant for a weak exchange field, while the model, Eq. (40), is expected to be most relevant for strong uniaxial anisotropy.[48] Clearly, it would also be interesting to investigate a model which interpolates between these two limits, in order to investigate at what maximum anisotropy in the scattering a complete suppression of oscillations can occur. One may consider this situation crudely by the following Usadel equation:

$$D\partial_x^2(f_t \pm f_s) + 2i(\varepsilon \pm h)(f_t \pm f_s) - \frac{1}{2\tau_{sf}}(f_t \pm \beta f_s) = 0, \quad (40)$$

where we have introduced the parameter β to account for the uniaxial ($\beta=1$) and the isotropic ($\beta=3$) case. Again, following the line of reasoning that led to Eq. (36), we now find

$$q_\pm = \sqrt{\frac{(1+\beta)/2 \mp \sqrt{(\beta-1)^2/4 - 16\tau_{sf}^2h^2}}{2D\tau_{sf}}}. \quad (41)$$

From this simple analysis, one would tentatively conclude that the case of strong uniaxial anisotropy is special, in that it is the only case where one cannot possibly obtain $(\beta-1)^2/4-16\tau_{sf}^2h^2=0$ for any finite τ_{sf} and h, which is the requirement for suppression of oscillations. For all other values of β, it would be possible to obtain a real q and hence complete suppression of oscillations. Clearly, this matter warrants further and detailed investigations.

In recent publications,[60,61] Crouzy *et al.* considered the interesting problem of a Josephson current in a $S/F/F'/S$ structure with noncollinear magnetizations in the ferromagnetic regions. It was shown that the misorientation angle between the ferromagnetic layers could be used to progressively shift the junction between a 0 and a π state. In deriving their results, effects such as spin-flip scattering and nonideal interfaces were omitted for simplicity. Our analytical results account for both of these effects, and may thus be useful to obtain a quantitatively better agreement for the Josephson effect with experimental data by including these phenomena in $S/F/F'/S$ structures. Work in this direction is now in progress.[62]

V. SUMMARY

In conclusion, we have investigated the role of spin-flip scattering and nonideal interfaces in dirty ferromagnet/superconductor (F/S) junctions. Our analytical results may serve as a basis for calculating other physical quantities of interest in F/S multilayers, such as the Josephson current. The main result of this paper is that we show analytically how the well-known oscillations of the anomalous Green's

function induced in the ferromagnet by the superconductor in F/S structures without magnetic impurities vanish completely above a critical value for the energy associated with spin-flip scattering, Γ. More precisely, we find that the oscillations are absent when the condition $\Gamma_c > 4h$ is fulfilled, where h is the exchange field. We have argued that this might be experimentally observable through a transition from a nonmonotonic (damped, oscillating) to a monotonic (damped) decrease of the critical temperature of the junction as a function of the thickness of the ferromagnet layer. As another consequence, we find that increasing spin-flip scattering may actually enhance the local density of states (LDOS) under certain conditions. This is a quite subtle effect that might seem counterintuitive at first glance. However, it may be understood by realizing that the anomalous Green's functions display an oscillatory behavior in the presence of an exchange field. The period of these oscillations is modified in the presence of spin-flip scattering. This means that although the amplitude of the oscillations decreases for increasing spin-flip scattering, the correction to the LDOS may in certain spatial intervals actually be greater for large spin-flip scattering than for weak spin-flip scattering. This finding may be of importance in order to correctly interpret LDOS spectra as obtained from, e.g., scanning-tunneling microscopy measurements.

ACKNOWLEDGMENTS

One of the authors (J.L.) is greatly indebted to J. P. Morten for providing him with a detailed introduction to the quasiclassical theory of superconductivity. D. Huertas-Hernando and H. J. Skadsem are also thanked for useful comments. This work was supported by the Norwegian Research Council Grants No. 158518/431, No. 158547/431, (NANOMAT), and No. 167498/V30 (STORFORSK).

APPENDIX A: DEFINING THE STAR PRODUCT

We here define the star product which enters the Eilenberger equation, Eq. (6). For any two functions A and B, we have

$$A \otimes B = e^{i(\partial_{T_A}\partial_{\varepsilon_B} - \partial_{\varepsilon_A}\partial_{T_B})/2} AB, \tag{A1}$$

where the differentiation operators denote derivation with respect to the variables T and ε in the mixed representation. Note that if there is no explicit time dependence in the problem, the star product reduces to regular multiplication.

APPENDIX B: EVEN- AND ODD-FREQUENCY PAIRING

Consider the anomalous Green's function with time-ordering operator $\mathcal{T}$,

$$f_{\alpha\beta}(\mathbf{r}_1,\mathbf{r}_2;t_1,t_2) = -i\mathcal{T}\{\langle \psi_\alpha(\mathbf{r}_1;t_1)\psi_\beta(\mathbf{r}_2;t_2)\rangle\}, \tag{B1}$$

which in the mixed representation may be written as

$$f_{\alpha\beta}(\mathbf{r}_1,\mathbf{r}_2;t_1,t_2) = f_{\alpha\beta}(\mathbf{R},\mathbf{r};T,t). \tag{B2}$$

The Pauli principle introduces restrictions on this correlation function for equal times $t_1 = t_2 = t'$, namely,

TABLE I. Symmetry classifications of the anomalous Green's function that are compatible with the Pauli principle. The "even" and "odd" terminology in the notation here points to the symmetry under a sign shift in energy, while "singlet" and "triplet" denotes the symmetry under exchange of spins. With these two properties in hand, the symmetry classification of momentum is given from the requirement that the entire function must be antisymmetric.

Spin	Momentum	Energy	Notation
Odd	Even	Even	Even singlet
Even	Odd	Even	Even triplet
Even	Even	Odd	Odd triplet
Odd	Odd	Odd	Odd singlet

$$f_{\alpha\beta}(\mathbf{r}_1,\mathbf{r}_2;t') = -f_{\beta\alpha}(\mathbf{r}_2,\mathbf{r}_1;t'). \tag{B3}$$

This follows directly from the anticommutation relation for the field operators in Eq. (B1), and reflects the fact that the fermionic two-particle anomalous Green's function must be antisymmetric under exchange of particle coordinates. Assume now for ease of notation that there is no explicit time dependence in the problem and that the system is homogeneous, which allows us to discard the dependence on the center-of-mass coordinates $\mathbf{R}$ and T. The following argumentation is valid even if this simplification may not be performed, and the equations then hold for each set of points $(\mathbf{R},T)$. By a Fourier transform, we now obtain

$$f_{\alpha\beta}(\mathbf{p};t) = \int d\mathbf{r}\, e^{-i\mathbf{p}\mathbf{r}} f_{\alpha\beta}(\mathbf{r};t). \tag{B4}$$

The Pauli-limitation equation (B3) then reads $f_{\alpha\beta}(\mathbf{p};0) = f_{\beta\alpha}(-\mathbf{p};0)$, since equal times give $t=0$. This seems to indicate that the Green's function must be odd under inversion of momentum or exchange of spin coordinates. However, another possibility exists, as may be seen by Fourier transforming

$$f_{\alpha\beta}(\mathbf{p};\varepsilon) = \int dt e^{i\varepsilon t} f_{\alpha\beta}(\mathbf{p};t). \tag{B5}$$

In terms of the momentum- and energy-dependent Green's functions, the Pauli principle now dictates that

$$\int d\varepsilon f_{\alpha\beta}(\mathbf{p};\varepsilon) = -\int d\varepsilon f_{\beta\alpha}(-\mathbf{p},\varepsilon). \tag{B6}$$

This gives us two possibilities that are still perfectly compatible with the equal-time restriction: either $f_{\alpha\beta}(\mathbf{p};\varepsilon) = -f_{\beta\alpha}(-\mathbf{p};\varepsilon)$ or $f_{\alpha\beta}(\mathbf{p};\varepsilon) = -f_{\beta\alpha}(-\mathbf{p};-\varepsilon)$. This is summarized in the equation

$$f_{\alpha\beta}(\mathbf{p};\varepsilon) = -f_{\beta\alpha}(-\mathbf{p};-\varepsilon), \tag{B7}$$

which contains all possible symmetry classifications for the Green's functions that are compatible with the Pauli principle. These are listed in Table I. Let us also make contact with the Matsubara formalism, where the anomalous Green's function is defined as

$$f^M_{\alpha\beta}(\mathbf{r}_1,\mathbf{r}_2;\tau_1,\tau_2) = -\mathcal{T}\{\langle\psi_\alpha(\mathbf{r}_1;\tau_1)\psi_\beta(\mathbf{r}_2;\tau_2)\rangle\}, \quad \text{(B8)}$$

and after a Fourier transformation to the mixed representation satisfies

$$f^M_{\alpha\beta}(\mathbf{p};i\omega_n) = \int_0^\beta d\tau e^{i\omega_n\tau} f^M_{\alpha\beta}(\mathbf{p};\tau),$$

$$f^M_{\alpha\beta}(\mathbf{p};\tau) = \frac{1}{\beta}\sum_n e^{-i\omega_n\tau} f^M_{\alpha\beta}(\mathbf{p};i\omega_n), \quad \text{(B9)}$$

with τ as a complex time, β as inverse temperature, and frequencies $\omega_n = (2n+1)\pi/\beta$. In this technique, one may apply the same procedure as for the real-time Green's functions and arrive at

$$\sum_n [f^M_{\alpha\beta}(\mathbf{p};i\omega_n) + f^M_{\beta\alpha}(-\mathbf{p};i\omega_n)] = 0, \quad \text{(B10)}$$

which also leads to the requirement that

$$f^M_{\alpha\beta}(\mathbf{p};i\omega_n) = -f^M_{\beta\alpha}(-\mathbf{p};-i\omega_n). \quad \text{(B11)}$$

The real-time retarded and advanced Green's functions may be obtained from the Matsubara Green's function by analytical continuation as follows ($\delta \to 0$):

$$\lim_{i\omega_n\to\varepsilon\pm i\delta} f^M_{\alpha\beta}(\mathbf{p};i\omega_n) = f^{R(A)}_{\alpha\beta}(\mathbf{p};\varepsilon). \quad \text{(B12)}$$

From Eq. (B7), one infers that a triplet correlation may be even under momentum inversion *if* it is odd under energy inversion. This scenario has been dubbed *odd-frequency* pairing in the literature. The Pauli principle can also be expressed by the retarded and advanced anomalous Green's functions by using Eq. (B11). To see this, we perform an analytical continuation on the right-hand side of Eq. (B11), yielding

$$\lim_{i\omega_n\to\varepsilon+i\delta} f^M_{\alpha\beta}(\mathbf{p};i\omega_n) = f^M_{\alpha\beta}(\mathbf{p};\varepsilon+i\delta) = f^R_{\alpha\beta}(\mathbf{p};\varepsilon), \quad \text{(B13)}$$

while the same operation on the left-hand side produces

$$\lim_{i\omega_n\to\varepsilon+i\delta} [-f^M_{\beta\alpha}(-\mathbf{p};-i\omega_n)] = -f^M_{\beta\alpha}(\mathbf{p};-\varepsilon-i\delta) = -f^A_{\beta\alpha}(-\mathbf{p};-\varepsilon). \quad \text{(B14)}$$

Equating the two sides, we finally arrive at

$$f^R_{\alpha\beta}(\mathbf{p};\varepsilon) = -f^A_{\beta\alpha}(-\mathbf{p};-\varepsilon). \quad \text{(B15)}$$

Actually, this information is embedded already in the definitions of the retarded and advanced Green's functions, and Eq. (B15) may be verified by direct Fourier transformation without going via Eq. (B11). It is also worth underscoring that the Matsubara technique is only valid for equilibrium situations, while the Keldysh formalism and the corresponding Green's function is viable also for nonequilibrium situations. The distinction between odd- and even-frequency correlations for the retarded and advanced Green's functions is now as follows:

$$\text{Odd frequency:} \quad f^R_{\alpha\beta}(\mathbf{p};\varepsilon) = -f^A_{\alpha\beta}(\mathbf{p};-\varepsilon),$$

$$\text{Even frequency:} \quad f^R_{\alpha\beta}(\mathbf{p};\varepsilon) = f^A_{\alpha\beta}(\mathbf{p};-\varepsilon). \quad \text{(B16)}$$

[1] F. S. Bergeret, A. F. Volkov, and K. B. Efetov, Rev. Mod. Phys. **77**, 1321 (2005).
[2] A. I. Buzdin, Rev. Mod. Phys. **77**, 935 (2005).
[3] A. Cottet and W. Belzig, Phys. Rev. B **72**, 180503(R) (2005).
[4] M. Zareyan, W. Belzig, and Yu. Nazarov, Phys. Rev. Lett. **86**, 308 (2001).
[5] M. Zareyan, W. Belzig, and Yu. V. Nazarov, Phys. Rev. B **65**, 184505 (2002).
[6] T. Yokoyama, Y. Tanaka, and A. A. Golubov, Phys. Rev. B **75**, 134510 (2007).
[7] V. L. Berezinskii, JETP Lett. **20**, 287 (1974); L. N. Bulaevskii, V. V. Kuzii, and A. A. Sobyanin, Pis'ma Zh. Eksp. Teor. Fiz. **25**, 314 (1977) [JETP Lett. **25**, 290 (1977)].
[8] A. V. Andreev, A. I. Buzdin, and R. M. Osgood, Phys. Rev. B **43**, 10124 (1991).
[9] F. S. Bergeret, A. F. Volkov, and K. B. Efetov, Phys. Rev. B **64**, 134506 (2001).
[10] F. S. Bergeret, A. F. Volkov, and K. B. Efetov, Phys. Rev. B **75**, 184510 (2007).
[11] V. V. Ryazanov, V. A. Oboznov, A. Yu. Rusanov, A. V. Veretennikov, A. A. Golubov, and J. Aarts, Phys. Rev. Lett. **86**, 2427 (2001).
[12] A. Bauer, J. Bentner, M. Aprili, M. L. Della-Rocca, M. Reinwald, W. Wegscheider, and C. Strunk, Phys. Rev. Lett. **92**, 217001 (2004).
[13] M. L. Kulic, C. R. Phys. **7**, 4 (2006); M. L. Kulic and I. M. Kulic, Phys. Rev. B **63**, 104503 (2001).
[14] I. Eremin, F. S. Nogueira, and R.-J. Tarento, Phys. Rev. B **73**, 054507 (2006).
[15] T. Champel, T. Löfwander, and M. Eschrig, arXiv:0706.3594 (unpublished).
[16] F. S. Bergeret, A. F. Volkov, and K. B. Efetov, Phys. Rev. Lett. **86**, 3140 (2001).
[17] A. A. Golubov, M. Yu. Kupriyanov, and Ya. V. Fominov, Pis'ma Zh. Eksp. Teor. Fiz. **75**, 223 (2002) [JETP Lett. **75**, 190 (2002)].
[18] X. Li, Z. Zheng, D. Y. Xing, G. Sun, and Z. Dong, Phys. Rev. B **65**, 134507 (2002).
[19] J. Linder and A. Sudbø, Phys. Rev. B **76**, 064524 (2007).
[20] M. S. Grønsleth, J. Linder, J.-M. Børven, and A. Sudbø, Phys. Rev. Lett. **97**, 147002 (2006).
[21] J. Linder, M. S. Grønsleth, and A. Sudbø, Phys. Rev. B **75**, 024508 (2007).
[22] L. N. Bulaevskii, V. V. Kuzii, and A. A. Sobyanin, Pis'ma Zh. Eksp. Teor. Fiz. **25**, 314 (1977) [JETP Lett. **25**, 290 (1977)].
[23] F. S. Bergeret, A. F. Volkov, and K. B. Efetov, Phys. Rev. Lett. **86**, 4096 (2001).
[24] A. F. Volkov, F. S. Bergeret, and K. B. Efetov, Phys. Rev. Lett. **90**, 117006 (2003).
[25] M. Eschrig, J. Kopu, J. C. Cuevas, and Gerd Schön, Phys. Rev. Lett. **90**, 137003 (2003).

[26] M. Eschrig, J. Kopu, A. Konstandin, J. C. Cuevas, M. Fogelstrm, and G. Schön, *Advances in Solid State Physics*, edited by B. Kramer (Springer Verlag, Heidelberg, 2004), Vol. 44, pp. 533–546.
[27] J. Kopu, M. Eschrig, J. C. Cuevas, and M. Fogelstrom, Phys. Rev. B **69**, 094501 (2004).
[28] Y. Asano, Y. Tanaka, and A. A. Golubov, Phys. Rev. Lett. **98**, 107002 (2007).
[29] R. S. Keizer, S. T. B. Goennenwein, T. M. Klapwijk, G. Miao, G. Xiao, and A. Gupta, Nature (London) **439**, 825 (2006).
[30] M. Faure, A. I. Buzdin, A. A. Golubov, and M. Yu. Kupriyanov, Phys. Rev. B **73**, 064505 (2006).
[31] D. Yu. Gusakova, A. A. Golubov, M. Yu. Kupriyanov, and A. Buzdin, Pis'ma Zh. Eksp. Teor. Fiz. **83**, 385 (2006).
[32] J. W. Serene and D. Rainer, Phys. Rep. **101**, 221 (1983).
[33] N. Kopnin, *Theory of Nonequilibrium Superconductivity* (Oxford University Press, New York, 2001).
[34] J. Rammer and H. Smith, Rev. Mod. Phys. **58**, 323 (1986).
[35] A. M. Zagoskin, *Quantum Theory of Many-Body Systems* (Springer, New York, 1998).
[36] J. P. Morten, m.s. thesis, Norwegian University of Science and Technology, 2003.
[37] G. Eilenberger, Z. Phys. **214**, 195 (1968).
[38] W. Belzig, F. K. Wilhelm, C. Bruder, G. Schön, and A. D. Zaikin, Superlattices Microstruct. **25**, 1251 (1999).
[39] G. E. Blonder, M. Tinkham, and T. M. Klapwijk, Phys. Rev. B **25**, 4515 (1982).
[40] A. V. Zaitsev, Sov. Phys. JETP **59**, 1163 (1984).
[41] M. Yu. Kupriyanov and V. F. Lukichev, Zh. Eksp. Teor. Fiz. **94**, 139 (1988) [Sov. Phys. JETP **67**, 1163 (1988)].
[42] C. J. Lambert, R. Raimondi, V. Sweeney, and A. F. Volkov, Phys. Rev. B **55**, 6015 (1997).
[43] V. Nazarov, Superlattices Microstruct. **25**, 1221 (1999).
[44] A. Millis, D. Rainer, and J. A. Sauls, Phys. Rev. B **38**, 4504 (1988).
[45] J. C. Hammer, J. C. Cuevas, F. S. Bergeret, and W. Belzig, Phys. Rev. B **76**, 064514 (2007).
[46] K. Usadel, Phys. Rev. Lett. **25**, 507 (1970).
[47] K. D. Nelson, Z. Q. Mao, Y. Maeno, and Y. Liu, Science **306**, 1151 (2004); K. Deguchi, Z. Q. Mao, H. Yaguchi, and Y. Maeno, Phys. Rev. Lett. **92**, 047002 (2004).
[48] V. A. Oboznov, V. V. Bol'ginov, A. K. Feofanov, V. V. Ryazanov, and A. I. Buzdin, Phys. Rev. Lett. **96**, 197003 (2006).
[49] J. Linder and A. Sudbø, Phys. Rev. B **75**, 134509 (2007).
[50] A. I. Buzdin, Phys. Rev. B **62**, 11377 (2000).
[51] L. Lazar, K. Westerholt, H. Zabel, L. R. Tagirov, Yu. V. Goryunov, N. N. Garifyanov, and I. A. Garifullin, Phys. Rev. B **61**, 3711 (2000).
[52] T. Kontos, M. Aprili, J. Lesueur, and X. Grison, Phys. Rev. Lett. **86**, 304 (2001).
[53] R. Fazio and C. Lucheroni, Europhys. Lett. **45**, 707 (1999).
[54] D. Yu. Gusakova, A. A. Golubov, and M. Yu. Kupriyanov, Pis'ma Zh. Eksp. Teor. Fiz. **83**, 487 (2006).
[55] W. L. McMillan, Phys. Rev. **175**, 537 (1968).
[56] J. S. Jiang, D. Davidović, D. H. Reich, and C. L. Chien, Phys. Rev. Lett. **74**, 314 (1995).
[57] F. Y. Ogrin, S. L. Lee, A. D. Hillier, A. Mitchell, and T.-H. Shen, Phys. Rev. B **62**, 6021 (2000).
[58] J. Aarts, J. M. E. Geers, E. Bruck, A. A. Golubov, and R. Coehoorn, Phys. Rev. B **56**, 2779 (1997).
[59] O. Bourgeois and R. C. Dynes, Phys. Rev. B **65**, 144503 (2002).
[60] B. Crouzy, S. Tollis, and D. A. Ivanov, Phys. Rev. B **75**, 054503 (2007).
[61] B. Crouzy, S. Tollis, and D. A. Ivanov, Phys. Rev. B **76**, 134502 (2007).
[62] J. Linder and A. Sudbø (unpublished).

Paper IX

Tunneling conductance in s- and d-wave superconductor-graphene junctions: Extended Blonder-Tinkham-Klapwijk formalism.

Physical Review B **77**, 064507 (2008).

Tunneling conductance in *s*- and *d*-wave superconductor-graphene junctions: Extended Blonder-Tinkham-Klapwijk formalism

Jacob Linder and Asle Sudbø
Department of Physics, Norwegian University of Science and Technology, N-7491 Trondheim, Norway
(Received 21 August 2007; revised manuscript received 1 November 2007; published 14 February 2008)

We investigate the conductance spectra of a normal-superconductor graphene junction using the extended Blonder-Tinkham-Klapwijk formalism, considering pairing potentials that are both conventional (isotropic *s*-wave) and unconventional (anisotropic *d*-wave). In particular, we study the full crossover from normal to specular Andreev reflection without restricting ourselves to special limits and approximations, thus expanding results obtained in previous work. In addition, we investigate in detail how the conductance spectra are affected if it is possible to induce an unconventional pairing symmetry in graphene—for instance, a *d*-wave order parameter. We also discuss the recently reported conductance oscillations that take place in normal-superconductor graphene junctions, providing both analytical and numerical results.

DOI: 10.1103/PhysRevB.77.064507 PACS number(s): 74.45.+c, 71.10.Pm, 73.23.−b, 74.78.Na

I. INTRODUCTION

A key issue in understanding low-energy quantum transport at the interface of a nonsuperconducting and superconducting material—e.g., a normal-superconductor (N-S) interface—is the process of Andreev reflection. Although the existence of a gap in the energy spectrum of a superconductor implies that no quasiparticle states may persist inside the superconductor for energies below that gap, physical transport of charge and spin is still possible at a N-S interface in this energy regime if the incoming electron is reflected as a hole with opposite charge. The remaining charge is transferred to the superconductor in the form of a Cooper pair at the Fermi level. The study of Andreev reflection and its signatures in experimentally observable quantities such as single-particle tunneling and the Josephson current has a long history (see, e.g., Ref. 1 and references therein). Only recently, however, has this field of research been the subject of investigation in *graphene* N-S interfaces.[2,3]

Graphene is a monoatomic layer of graphite with a honeycomb lattice structure, as shown in Fig. 1, and its recent experimental fabrication[4,5] has triggered a huge response in both the theoretical and experimental community over the last two years. The electronic properties of graphene display several intriguing features, such as the six-point Fermi surface and a Dirac-like energy dispersion, effectively leading to an energy-independent velocity and zero effective mass at the Fermi level. This obviously attracts the interest of the theorist, but graphene may also hold potential for technological applications due to its unique combination of a very robust carbon-based structural texture and its peculiar electronic features.

Condensed matter systems with such "relativistic" electronic structure properties as graphene constitute fascinating examples of low-energy emergent symmetries—in this case, Lorentz invariance. At half-filling, the Fermi level of graphene is exactly zero which renders the Fermi surface to be reduced to six single points due to the linear intersection of the energy bands (see Figs. 3 and 4 below). The linear dispersion relation is a decent approximation even for Fermi levels as high as 1 eV, such that the fermions in graphene behave like they are massless in the low-energy regime. The fact that the fermions around the Fermi level obey a Dirac-like equation at half-filling introduces Lorentz invariance as an emergent symmetry in the low-energy sector. Another example where Lorentz invariance appears for low-energy excitations is in one-dimensional interacting fermion systems, where phenomena like the breakdown of Fermi-liquid theory and spin-charge separation take place. When Lorentz invariance emerges in the low-energy sector of higher-dimensional condensed matter systems, it is bound to attract much interest from a fundamental physics point of view. Another interesting feature of graphene are the nodal fermions that are present at the Fermi level at half-filling. When moving away from half-filling by doping, the excitations at the Fermi level are no longer nodal. The nodal fermions of graphene hold certain similarities to, but also important differences from, the nodal Dirac fermions appearing in the low-energy sector of the pseudogap phase of *d*-wave superconductors such as the high-T_c cuprates. In contrast to graphene, the nodal fermions in the high-T_c cuprates track the Fermi level when these systems are doped and thus represent a more robust feature than in graphene. For an illustration of the latter scenario, consider Fig. 2 which contains a sketch of the Fermi surface in the cuprates when including terms up to next-nearest-neighbor hopping. The nodal lines of the $d_{x^2-y^2}$ gap intersect the Fermi surface at exactly four points, which per-

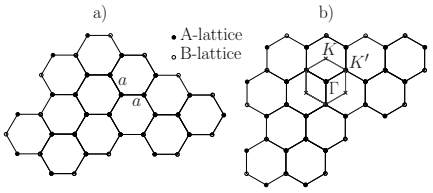

FIG. 1. (Color online) (a) Sketch of a real-space lattice of graphene, consisting of two hexagonal sublattices A and B. The interatomic distance a is equal between all lattice points. (b) $\mathbf{k}$-space (momentum-space) lattice of graphene, including the hexagonal Brillouin zone. Only two inequivalent points exist on the BZ boundary, termed K and K'.

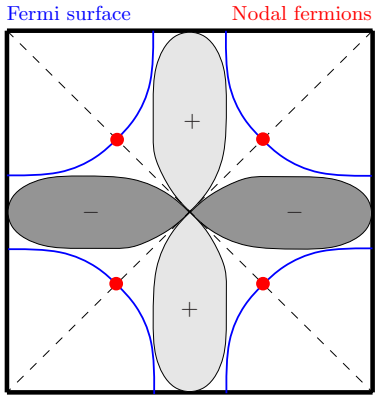

FIG. 2. (Color online) Sketch of the Fermi surface and anisotropic d-wave gap as believed to be present in high-T_c cuprate superconductors. The nodal fermions reside at the intersection of the nodal lines of the gap and the Fermi surface.

mits the existence of nodal fermions at those points in $\mathbf{k}$ space. However, in contrast to graphene, doping the system will in this case simply move the position of the Fermi arc with respect to the nodal line of the superconducting gap, such that the nodal fermions persist in the system.[6] Nonetheless, the existence of the Dirac cones in graphene represents an important example of emergent nontrivial symmetries at long distances and low energies in higher- (more than one) dimensional systems.

Although superconductivity does not appear intrinsically in graphene, it may be induced by means of the proximity effect by placing a superconducting metal electrode near a graphene layer.[7–11] Recent theoretical work[2,12] have considered coherent quantum transport in N-S and normal-insulator-superconductor (N-I-S) graphene junctions in the case where the pairing potential is isotropic—i.e., s-wave superconductivity. However, the hexagonal symmetry of the graphene lattice permits, in principle, for unconventional order parameters such as p-wave or d-wave parameters (characterized by a nonzero angular momentum of the Cooper pair). A complete classification of the possible pairing symmetries on a hexagonal lattice up to f-wave pairing ($l=3$) was given by Mazin and Johannes,[13] with the result given in Table I. We underline that the notation "insulator" in this context refers to a normal segment of graphene in which one experimentally induces an effective potential V_0. As we shall see, such a potential has a dramatically different impact upon the transport properties in graphene as compared to the metallic counterpart.

The intrinsic spin-orbit coupling in graphene is very weak, as dictated by the low value of the carbon atomic number, such that we will neglect it in this work. We will also disregard the electrostatic repulsion as mediated by the vector potential $\mathbf{A}$. At first sight, this might seem as an unphysical oversimplification since there is no metallic screening of the Coulomb interaction in graphene. In an ordinary metal, the renormalized Coulomb potential reads $V(r)=V_0(r)e^{-r/\lambda}$, where $\lambda \equiv [N(E_F)]^{-1/2}$ is the Thomas-Fermi

TABLE I. List of all superconducting pairing states allowed for a hexagonal lattice up to d-wave pairing, adapted from Ref. 13. An orbital angular momentum quantum number $l=0,1,2$ is denoted s,p,d wave, respectively. For the triplet states (p wave), the order parameter has multiple components and is conveniently represented as a vector $\mathbf{d}_\mathbf{k}$.

Pairing	Type	Pairing	Type
1	s	$(k_y,-k_x,0)$	p
$k_x^2+k_y^2$	s	$(0,0,k_z)$	p
k_z^2	s	$(k_x,k_y,0)$	p
$(0,0,k_x)$	p	$(k_x \pm ik_y, \pm ik_x - k_y, 0)$	p
$(0,0,k_y)$	p	$(k_x \pm ik_y)^2$	d
$(0,0,k_x \pm ik_y)$	p	k_xk_z	d
$(k_z,0,0)$	p	k_yk_z	d
$(0,k_z,0)$	p	$(k_x \pm ik_y)k_z$	d
$(k_z, \pm ik_z, 0)$	p	$k_x^2-k_y^2$	d
$(k_y,k_x,0)$	p	k_xk_y	d
$(k_x,-k_y,0)$	p		

screening length and $N(E_F)$ is the density of states (DOS) at the Fermi level. Since pure graphene has zero DOS at Fermi level, one might quite reasonably suspect that the screening of charge vanishes, and it might seem paradoxical that Coulomb interactions can be neglected. The resolution to this is found by realizing that one may disregard the Coulomb interaction if it is weak compared to the kinetic energy in the problem. Due to the linear dispersion, the kinetic energy is governed by the Fermi velocity v_F which formally diverges near Fermi level. The divergence is logarithmic and precisely due to the Coulomb interaction.[14,15] The limiting velocity in graphene (due to, e.g., umklapp processes) is nevertheless of order $\mathcal{O}(10^6)$ m/s; see, e.g., Ref. 16. This is roughly 100 times larger than in a normal metal, and it is thus safe to neglect the Coulomb interaction compared to the kinetic energy in graphene. In graphene, the Coulomb interaction self-destructs.

In this work, we will study in detail how an anisotropic order parameter induced in graphene will affect quantum transport in a N-S and N-I-S junction, extending the result of Ref. 17. In equivalent metallic junctions, it is well known[18] that the zero bias conductance peak (ZBCP) is an experimental signature of anisotropic superconductivity in clean superconductors with nodes in the gap. This is a consequence of bound surface states with zero energy at the interface that form due to a constructive phase interference between electron like and hole like transmissions into the superconductor.[19] In graphene junctions with superconductors, as we shall see, a new phenomenology comes into play with regard to the scattering processes that take place at the N-S interface. It is therefore desirable to clarify how anisotropic superconductivity is manifested in the conductance spectra of such a junction and in particular if the same condition for formation of a ZBCP holds for graphene junctions as well. As first shown in Ref. 17, we will demonstrate that in N-I-S graphene junctions, novel conductance oscillations as a function of bias voltage are present both for s-wave and

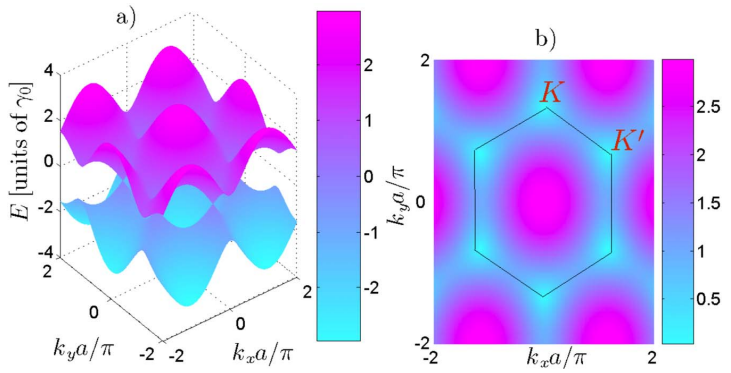

FIG. 3. (Color online) (a) The energy dispersion for graphene in the Brillouin zone. The upper band is the antibonding π orbital, while the lower band is the bonding π orbital. It is seen that the bands touch at Fermi level (E_F=0) at six discrete points, which constitutes the effective Fermi surface. (b) Contour plot of the dispersion relation, clearly showing the hexagonal structure of the Fermi points. The center of each red droplike structure represents either K or K'.

d-wave symmetries of the superconducting condensate due to the presence of low-energy "relativistic" nodal fermions on the N side. The period of the oscillations decreases with increasing width w of the insulating region and persists even if the Fermi energy in I is strongly shifted. This contrasts sharply with metallic N-I-S junctions, where the presence of a potential barrier causes the transmittance of the junction to go to zero with increasing w. The feature of conductance oscillations is thus unique to N-I-S junctions with low-energy Dirac-fermion excitations. Moreover, we contrast the N-S or N-I-S conductance spectra for the cases where s-wave and $d_{x^2-y^2}$-wave superconductors constitute the S side. The former has no nodes in the gap and lacks Andreev bound states. The latter has line nodes that always cross the Fermi surface in the gap and thus features in addition to Andreev bound states, also nodal relativistic low-energy Dirac fermions. The quantum transport properties in a heterostructure of two such widely disparate systems, both featuring a particular intriguing emergent low-energy symmetry, is of considerable importance.

This paper is organized as follows. In Sec. II, we establish the theoretical framework which we shall adopt in our treatment of the N-S graphene junction. The results are given in Sec. III, where we in particular treat the role of the barrier strength and doping with respect to how the conductance is influenced by these quantities. In addition, we investigate the role of a possible unconventional pairing symmetry induced in graphene. A discussion of our findings is given in Sec. V, and we summarize in Sec. VI. We will use a caret for 4×4 matrices and an inverted caret for 2×2 matrices, with boldface notation for three-dimensional row vectors.

II. THEORETICAL FORMULATION

A. General considerations

The Brillouin zone of graphene is hexagonal and the energy bands touch the Fermi level at the edges of this zone, amounting to six discrete points. Out of these, only two are inequivalent, which are conventionally dubbed K and K' and referred to as Dirac points. The band dispersion of graphene was first calculated by Wallace[20] and reads approximately

$$E = \pm \gamma_0 \left[1 + 4\cos\left(\frac{\sqrt{3}k_x a}{2}\right)\cos\left(\frac{k_y a}{2}\right) + 4\cos^2\left(\frac{k_y a}{2}\right)\right]^{1/2}, \tag{1}$$

where $\gamma_0 \simeq 2.5$ eV and the $\pm$ sign refers to the antibonding-bonding π orbital. The remaining three valence electrons are in hybridized sp^2 σ bonds. The energy dispersion in the Brillouin zone is plotted in Fig. 3, which reveals the conical structure of the conduction and valence bands at the six Fermi points. The cosinelike conduction and valence bands are made up by a mixture of the energy bands from the A and B sublattices in graphene (Fig. 1), which are linear near the Fermi level. This gives rise to the conical energy dispersion at the Dirac points K and K'.

In order to introduce the new phenomenology of scattering processes in N-S graphene junctions, it is instructive to compare it with the metallic N-S junction. This is done in Fig. 4. In the metallic case, an incident electron with energy $E<\Delta$ measured from the Fermi energy E_F cannot transmitted into the superconductor since there are no available quasiparticle states. Instead, it is reflected as a hole, represented as a quasiparticle with energy E in the holelike band, such that the leftover charge $2e$ is transferred into the superconductor as a Cooper pair at Fermi level. The hole has negative mass, energy, wave vector, and charge compared to the electron which is absent. Strictly speaking, only at $E=0$ are the wave vectors exactly related through $k_e=k_h$ since one in general has

$$k_e = \sqrt{2m(E_F + E)}, \quad k_h = \sqrt{2m(E_F - E)}. \tag{2}$$

At finite energies, the electron-hole coherence will therefore be lost after the hole has propagated a distance $L \sim 1/E$. At energies $E>\Delta$ above the gap, Andreev reflection is severly

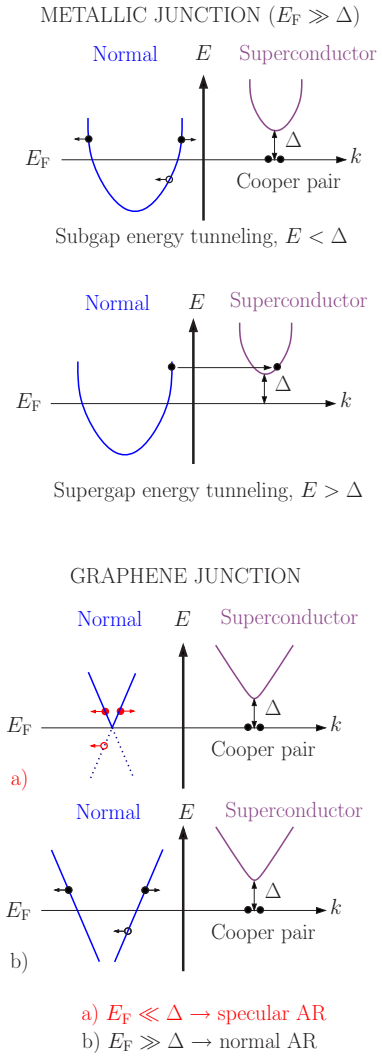

FIG. 4. (Color online) Graphical illustration of the different scattering processes that may take place at a (i) metallic and (ii) graphene N-S junction. While the Andreev reflected hole in case (i) retraces the trajectory of the incoming electron, the hole in case (ii) may be specularly reflected. This peculiar property is a result of the existence of two bands (conduction and valence) close to the Fermi energy in graphene. In the low-energy transport regime—i.e., quasiparticle energies E of order $\mathcal{O}(\Delta)$—retroreflection dominates if $E_F \gg \Delta$, while specular reflection dominates if $E_F \ll \Delta$.

suppressed since direct tunneling into quasiparticle states is now possible.

In graphene, a new phenomenology of Andreev reflection is at hand due to the band structure which effectively looks like that of a zero-gap semiconductor (see also Ref. 3). Since the conduction and valence bands touch at the Fermi energy $E_F=0$, one may distinguish between three important cases: (i) undoped graphene with $E_F=0$, (ii) doped graphene with $E_F>0$, and (iii) heavily doped graphene with $E_F \gg 0$. These different scenarios are shown in Fig. 4.

In undoped graphene, with $E_F \ll \Delta$, an incident electron with energy E is denied access as a quasiparticle into the superconductor, and physical transport across the junction is thus manifested through reflection as a hole. When Andreev reflection takes place, the transmitted Cooper pair is located at the Fermi level of the superconductor. Energy conservation then demands that the missing electron in the normal region that is reflected as a hole must be located at $-E$ due to the energy conservation—i.e., in the valence band. This is different from normal Andreev reflection, since in that case both the electron and hole belong to the same band (conduction). For specular Andreev reflection, however, they belong to *different* bands. The use of the term "specular" in order to characterize this type of Andreev reflection originates with the fact that the group velocity $\mathbf{v}_g$ and momentum $\mathbf{k}$ have the same sign for a valence band hole, while in contrast $\mathbf{v}_g$ and $\mathbf{k}$ have opposite signs for a conduction band hole. To see this, consider first a usual metallic parabolic dispersion $E=\mathbf{k}^2/2m-E_F$ for the electrons, such that one readily infers from $\mathbf{v}_g=\nabla_{\mathbf{k}}E$ that $\mathbf{v}_g=\mathbf{k}/m$. Therefore, a hole created at a given energy E will have $\mathbf{v}_g=-\mathbf{k}/m$, since holes have opposite group velocities of the electrons for a given wave vector $\mathbf{k}$. For normal Andreev reflection, the holes are located in the conduction band and therefore satisfy $\mathbf{v}_g \| -\mathbf{k}$.

In the case of specular Andreev reflection for undoped graphene ($E_F=0$), a hole is generated in the valence band. Since in the valence band, the electronic dispersion reads $E=-v_F|\mathbf{k}|$, the group velocity of electrons is opposite to their momentum. Conversely, the group velocity for valence holes is parallell to their momentum. This is the mechanism behind specular Andreev reflection. In doped graphene ($E_F>0$), the Andreev reflection can be normal or specular, depending on the energy of the incoming electron, as sketched in Fig. 4. In heavily doped graphene, ($E_F \gg \Delta$), only normal Andreev reflection (AR) is present for subgap energies since the distance from Fermi level to the valence band is too large for specular AR to occur. In the regime $E_F \in [0,\Delta]$, one has either normal or specular Andreev reflection, depending on the incident electron energy E.

We also comment on the effect of Fermi vector mismatch (FVM). Blonder and Tinkham[21] showed that in a metallic N-S junction, a FVM would act as a source for normal reflection, such that one could effectively account for it simply by choosing a higher value for the barrier strength Z. Interestingly, in a ferromagnet-superconductor junction the effect of a FVM could not be reproduced by simply shifting Z to a higher value, as discussed by Zutic and Valls.[22] In the absence of an exchange energy, however, the effect of FVM can be thought of as a reduction of the Fermi surface that participates in the scattering processes, as illustrated in Fig. 5. One may parametrize the FVM by the parameter $\kappa=k_F/q_F$ where k_F (q_F) is the Fermi momentum in the normal (superconducting) part of the system. In particular, it is seen that for $\kappa>1$, there is only a possible transmission of quasiparticles (although these decay exponentially) up to a critical angle less than $\pi/2$.[23]

Having established the states that participate in the scattering at the interface, we now turn to equations that describe these quasiparticle states.

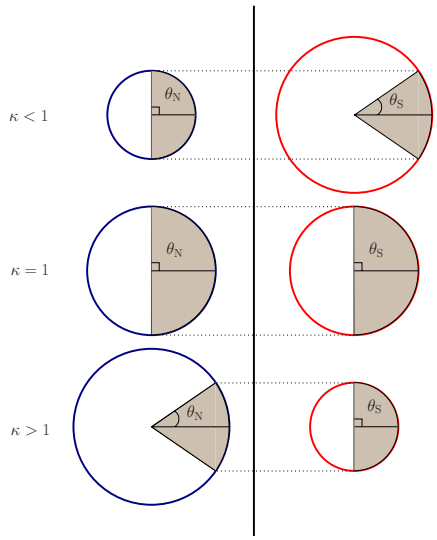

FIG. 5. (Color online) The effective impedance caused by FVM illustrated schematically for all possible cases of smaller, equal, and larger Fermi velocity in the normal part of the system. Except for the case when the Fermi velocities are identical in the normal and superconducting parts of the system ($\kappa=1$), parts of the Fermi surface does not participate in the scattering processes, resulting in a reduction in conductance. For instance, when $\kappa<1$, total reflection occurs at angles $\theta_N>\mathrm{asin}(\kappa)$, such that FVM effectively acts as a source of normal reflection (Ref. 23).

B. Scattering processes

Consider the case of zero external magnetic field. The full Bogoliubov–de Gennes (BdG) equation for the two-dimensional (2D) sheet graphene normal–*s*-wave-superconductor junction in the *xy* plane then reads[2,3]

$$\begin{pmatrix} \check{H} - E_F\check{1} & \Delta_{\mathbf{k}}\check{1} \\ \Delta_{\mathbf{k}}^{\dagger}\check{1} & E_F\check{1} - \check{T}\check{H}\check{T}^{-1} \end{pmatrix}\begin{pmatrix} u \\ v \end{pmatrix} = E\begin{pmatrix} u \\ v \end{pmatrix}, \tag{3}$$

where E is the excitation energy and $\{u,v\}$ denoting the electronlike and holelike exictations described by the wave function. Assuming that the superconducting region is located at $x>0$ and neglecting the decay of the order parameter in the vicinity of the interface,[24] we may write for the spin-singlet order parameter

$$\Delta_{\mathbf{k}} = \Delta(\theta)e^{i\vartheta}\Theta(x), \tag{4}$$

where $\Theta(x)$ is the Heaviside step function and ϑ is the phase corresponding the globally broken U(1) symmetry in the superconductor, while $\theta=\arctan(k_y/k_x)$ is the angle on the Fermi surface in reciprocal space (we have adopted the weak-coupling approximation with $\mathbf{k}$ fixed on the Fermi surface). Note that in contrast to previous work, we allow for the possibility of unconventional superconductivity in the graphene layer since $\Delta_{\mathbf{k}}$ now may be anisotropic. We have applied weak-coupling limit, the momentum $\mathbf{k}$ is fixed on the Fermi surface, such that $\Delta_{\mathbf{k}}$ only has an angular dependence. Since we employ a spin-singlet even-parity order parameter, the condition $\Delta(\theta)=\Delta(\pi+\theta)$ must be fulfilled. The single-particle Hamiltonian is given by

$$\check{H} = \begin{pmatrix} \hat{H}_+ & 0 \\ 0 & \hat{H}_- \end{pmatrix}, \quad \hat{H}_\pm = -iv_F(\hat{\sigma}_x\partial_x \pm \hat{\sigma}_y\partial_y). \tag{5}$$

Here, v_F is the energy-independent Fermi velocity for graphene, while $\hat{\sigma}_i$ denotes the Pauli matrices. For later use, we also define the Pauli matrix vector $\hat{\boldsymbol{\sigma}}=(\hat{\sigma}_x,\hat{\sigma}_y,\hat{\sigma}_z)$. These Pauli matrices operate on the sublattice space of the honeycomb structure, corresponding to the A and B atoms, while the $\pm$ sign refers to the two so-called *valleys* of K and K' in the Brillouin zone. The Dirac points earn their sobriquet as valleys from the geometrical resemblance of the band dispersion to the aforementioned. The spin indices may be suppressed since the Hamiltonian is time-reversal invariant. In addition to the spin degeneracy, there is also a valley degeneracy, which effectively allows one to consider either the one of the $\hat{H}_\pm$ set. Therefore, the 8-matrix BdG equation (3) reduces to a (4×4)-matrix BdG equation: namely,

$$\begin{pmatrix} \hat{H}_\pm - E_F\hat{1} & \Delta_{\mathbf{k}}\hat{1} \\ \Delta_{\mathbf{k}}^{\dagger}\hat{1} & E_F\hat{1} - \hat{H}_\pm \end{pmatrix}\begin{pmatrix} u \\ v \end{pmatrix} = E\begin{pmatrix} u \\ v \end{pmatrix}, \tag{6}$$

where have explicitly used that $\check{T}\check{H}=\check{H}\check{T}$. Let us then consider $\hat{H}_+$, such that one may write

$$\begin{pmatrix} \mathbf{p}\cdot\hat{\boldsymbol{\sigma}} - E_F\hat{1} & \Delta_{\mathbf{k}}\hat{1} \\ \Delta_{\mathbf{k}}^{\dagger}\hat{1} & E_F\hat{1} - \mathbf{p}\cdot\hat{\boldsymbol{\sigma}} \end{pmatrix}\begin{pmatrix} u \\ v \end{pmatrix} = E\begin{pmatrix} u \\ v \end{pmatrix}. \tag{7}$$

In the above Hamiltonian, we have only included diagonal terms in the gap matrix—i.e., $\hat{\Delta}_{\mathbf{k}}=\Delta_{\mathbf{k}}\hat{1}$. This corresponds to exclusively intraband pairing on each of the sublattices A and B. In recent work by Black-Schaffer and Doniach,[25] it was shown that by postulating interband spin-singlet hopping between the sublattices, one could achieve dominant *d*-wave pairing in intrinsic graphene. While an on-site attractive potential is sufficient to achieve *s*-wave pairing, leading to a diagonal gap matrix, nearest-neighbor interactions couple the two sublattices and should yield off-diagonal elements in the gap matrix. In this work, we restrict ourselves to anisotropic superconducting pairing with diagonal elements in the gap matrix, although one would have to take into account off-diagonal elements as well for a completely general treatment. We comment more on this later.

Consider an incident electron from the normal side of the junction ($x<0$) with energy E. For positive excitation energies $E>0$, the eigenvectors and corresponding momentum of the particles read

$$\psi_+^e = [1,e^{i\theta},0,0]^T e^{ip^e\cos\theta x}, \quad p^e = (E+E_F)/v_F, \tag{8}$$

for a right-moving electron at angle of incidence θ (see Fig. 6), while a left-moving electron is described by the substitution $\theta\to\pi-\theta$. If Andreev reflection takes place, a left-moving hole is generated with an energy E, angle of reflection θ_A, and corresponding wave function

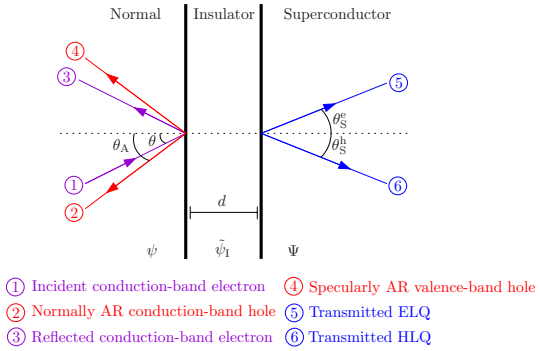

FIG. 6. (Color online) The scattering processes taking place at a N-S or N-I-S graphene junction. In the former case, the insulating region is completely absent, and only the six depicted processes take place. Note that only normal Andreev reflection *or* specular Andreev reflection takes place at any given energy E, never both. For a N-I-S graphene junction, there are transmitted and reflected electrons and holes in the insulating region corresponding to $\tilde{\psi}_{\mathrm{I}}$, not shown in the above figure.

$$\psi_{-}^{\mathrm{h}} = [0,0,1,e^{-i\theta_{\mathrm{A}}}]^{\mathrm{T}} e^{-ip^{\mathrm{h}}\cos\theta_{\mathrm{A}}x}, \quad p^{\mathrm{h}} = (E - E_{\mathrm{F}})/v_{\mathrm{F}}, \tag{9}$$

where the superscript "e" "(h)" denotes an electronlike (holelike) excitation. Since translational invariance in the $\hat{\mathbf{y}}$ direction holds, the corresponding component of momentum is conserved. This condition allows for determination of the Andreev reflection angle θ_{A} through $p^{\mathrm{h}}\sin\theta_{\mathrm{A}} = p^{\mathrm{e}}\sin\theta$. From this equation, one infers that there is no Andreev reflection ($\theta_{\mathrm{A}} = \pm\pi/2$), and consequently no subgap conductance, for angles of incidence above the critical angle

$$\theta_{\mathrm{c}} = \mathrm{asin}\left(\frac{|E - E_{\mathrm{F}}|}{E + E_{\mathrm{F}}}\right). \tag{10}$$

On the superconducting side of the system ($x > w$), the possible wave functions for transmission of a right-moving quasiparticle with a given excitation energy $E > 0$ read

$$\Psi_{+}^{\mathrm{e}} = (u(\theta^{+}), u(\theta^{+})e^{i\theta^{+}}, v(\theta^{+})e^{-i\phi^{+}}, v(\theta^{+})e^{i(\theta^{+}-\phi^{+})})^{\mathrm{T}}$$

$$\times e^{iq^{\mathrm{e}}\cos\theta^{+}x}, \quad q^{\mathrm{e}} = [E_{\mathrm{F}}' + \sqrt{E^2 - |\Delta(\theta^{+})|^2}]/v_{\mathrm{F}},$$

$$\Psi_{-}^{\mathrm{h}} = (v(\theta^{-}), v(\theta^{-})e^{i\theta^{-}}, u(\theta^{-})e^{-i\phi^{-}}, u(\theta^{-})e^{i(\theta^{-}-\phi^{-})})^{\mathrm{T}}$$

$$\times e^{iq^{\mathrm{h}}\cos\theta^{-}x}, \quad q^{\mathrm{h}} = [E_{\mathrm{F}}' - \sqrt{E^2 - |\Delta(\theta^{-})|^2}]/v_{\mathrm{F}}. \tag{11}$$

The coherence factors are, as usual, given by[26]

$$u(\theta) = \sqrt{\frac{1}{2}\left(1 + \frac{\sqrt{E^2 - |\Delta(\theta)|^2}}{E}\right)},$$

$$v(\theta) = \sqrt{\frac{1}{2}\left(1 - \frac{\sqrt{E^2 - |\Delta(\theta)|^2}}{E}\right)}. \tag{12}$$

Above, we have defined $\theta^{+} = \theta_{\mathrm{S}}^{\mathrm{e}}$, $\theta^{-} = \pi - \theta_{\mathrm{S}}^{\mathrm{h}}$, and $e^{i\phi^{\pm}} = e^{i\vartheta}\Delta(\theta^{\pm})/|\Delta(\theta^{\pm})|$. The transmission angles $\theta_{\mathrm{S}}^{(\mathrm{i})}$ for the electronlike (ELQ) and holelike (HLQ) quasiparticles are given by $q^{(\mathrm{i})}\sin\theta_{\mathrm{S}}^{(\mathrm{i})} = p^{\mathrm{e}}\sin\theta$, i=e,h. Note that for subgap energies $E < \Delta$, there is a small imaginary contribution to the wave vector, which leads to exponentional damping of the wave functions inside the superconductor. The physical reason for this is that there can be no transmission of quasiparticles into the superconductor for subgap energies. Note that for all wave functions listed in the equations above, we have for clarity not included a common phase factor $e^{ik_y y}$ which corresponds to the conserved momentum in the $\hat{\mathbf{y}}$ direction. A possible FVM between the normal and superconducting regions is accounted for by allowing for $E_{\mathrm{F}}' \neq E_{\mathrm{F}}$.The case $E_{\mathrm{F}}' \gg \Delta$ corresponds to a heavily doped superconducting region. It is also straightforward to obtain the eigenfunctions for the case when the gap matrix consists of off-diagonal elements, as opposed to the gap matrix treated here with diagonal elements. In particular, for

$$\hat{\Delta}_{\mathbf{k}} = \begin{pmatrix} 0 & \Delta(\theta)e^{i\vartheta} \\ \Delta(\theta)e^{i\vartheta} & 0 \end{pmatrix}, \tag{13}$$

the eigenfunctions may be obtained from Eq. (14) simply by switching the phase factors as follows:

$$\Psi_{+}^{\mathrm{e}} = (u(\theta^{+}), u(\theta^{+})e^{i\theta^{+}}, v(\theta^{+})e^{i(\theta^{+}-\phi^{+})}, v(\theta^{+})e^{-i\phi^{+}})^{\mathrm{T}}$$

$$\times e^{iq^{\mathrm{e}}\cos\theta^{+}x}, \quad q^{\mathrm{e}} = [E_{\mathrm{F}}' + \sqrt{E^2 - |\Delta(\theta^{+})|^2}]/v_{\mathrm{F}},$$

$$\Psi_{-}^{\mathrm{h}} = (v(\theta^{-}), v(\theta^{-})e^{i\theta^{-}}, u(\theta^{-})e^{i(\theta^{-}-\phi^{-})}, u(\theta^{-})e^{-i\phi^{-}})^{\mathrm{T}}$$

$$\times e^{iq^{\mathrm{h}}\cos\theta^{-}x}, \quad q^{\mathrm{h}} = [E_{\mathrm{F}}' - \sqrt{E^2 - |\Delta(\theta^{-})|^2}]/v_{\mathrm{F}}. \tag{14}$$

At this stage, it is appropriate to insert the restriction which will be used throughout the rest of this paper: namely, $\Delta \ll E_{\mathrm{F}}'$. Since we are using a mean-field approach to describe the superconducting part of the Hamiltonian, it is implicitly understood that phase fluctuations of the order parameter must be small.[39] For this criterion to be fulfilled, the superconducting coherence length ξ must be large compared to some characteristic length scale of the system.[27] Following Ref. 27, the critical temperature T_{K} at which long-range phase fluctuations of the order parameter destroy the ordering when approaching the critical temperature T_{c} from below is given by

$$T_{\mathrm{K}} = T_{\mathrm{c}}^{\mathrm{MF}}(1 - |\tau|), \tag{15}$$

where $|\tau| \sim \xi^{D}$, D is the dimensionality of the system, and $T_{\mathrm{c}}^{\mathrm{MF}}$ is the critical temperature predicted by mean-field theory. (For an extensive treatment of the effect of phase fluctuations in extreme type-II superconductors, see Ref. 28.) Thus, only for $|\tau| \ll 1$ is mean-field theory a viable option for describing superconductivity in the system, corresponding to a large coherence length ξ. Notice that the Ginzburg temperature T_{G}, which describes the regime where amplitude

fluctuations of the order parameter become important ($T > T_G$), satisfies $T_c^{MF} > T_G > T_K$. A natural choice of characteristic length scale for the system in the normal state is obviously the Fermi wavelength $\lambda_F' = 2\pi v_F'/E_F'$, such that the criterion for validity of mean-field theory reads $\xi/\lambda_F' \gg 1$, or equivalently, $E_F' \gg \Delta$.

The relevant scattering processes at the N-S graphene interface are shown in Fig. 6, in the two cases of zero barrier and an insulating region of width w. In the former case, the boundary conditions dictate that $\psi|_{x=0} = \Psi|_{x=0}$, where

$$\psi = \psi_+^e + r\psi_-^e + r_A\psi_-^h,$$

$$\Psi = t^e\Psi_+^e + t^h\Psi_-^h, \tag{16}$$

while in the latter case, one must match the wave functions at both interfaces:

$$\psi|_{x=0} = \tilde{\psi}_1|_{x=0}, \quad \tilde{\psi}_1|_{x=w} = \Psi_S|_{x=w}, \tag{17}$$

where we have defined the wave function in the insulating region

$$\tilde{\psi}_1 = \tilde{\tau}_1\tilde{\psi}_+^e + \tilde{\tau}_2\tilde{\psi}_-^e + \tilde{\tau}_3\tilde{\psi}_+^h + \tilde{\tau}_4\tilde{\psi}_-^h. \tag{18}$$

The wave functions $\tilde{\psi}$ differ from ψ in that the Fermi energy is shifted by means of, e.g., an external potential V_0, such that $E_F \to E_F - V_0$. Also, note that the trajectories of the quasiparticles in the insulating region, defined by the angles $\tilde{\theta}$ and $\tilde{\theta}_A$, differ by the same substitution, meaning

$$\sin\tilde{\theta}/\sin\theta = (E + E_F)/(E + E_F - V_0),$$

$$\sin\tilde{\theta}_A/\sin\theta = (E + E_F)/(E - E_F + V_0). \tag{19}$$

Finally, note that the subscript $\pm$ on the wave functions in the normal region indicates the direction of their group velocity, which *in general* is different from the direction of momentum, as discussed previously. Consequently, although the Andreev-reflected hole wave function carries a subscript "–" above, one should keep in mind that for normal Andreev reflection, the direction of momentum is opposite to the group velocity for the hole.

Before we go on to presenting results, we make one conceptual remark. The proximity effect means that an otherwise normal system becomes superconducting by virtue of having the superconducting wave function from a nearby superconductor leak into the normal system, thus making it superconducting in some region. This is a result of a boundary condition imposed on the normal system from the proximate host superconductor. The resulting wave function in the proximity region of the normal system is then a BCS-type wave function. Such a wave function unquestionably describes a system with a gapped Fermi surface (possibly with nodes on the Fermi surface). It matters not by what microscopic mechanism such a state was established, as long as it is there. The effective interaction giving rise to proximity-induced superconductivity in graphene close to the surface in contact with an intrinsically superconducting host system is obtained by considering the complete superconductor-graphene system and integrating out the electrons on the superconducting side. The electrons in graphene then experience an effective attractive interaction λ_{eff} giving rise to a gap by virtue of hopping into and out of the superconducting side. We thus have, by such tunneling processes, $\lambda_{eff} \neq 0$ even if $\lambda = 0$. Here, λ is the electron-electron coupling constant giving rise to superconductivity in graphene *per se*. Since graphene intrinsically is a normal system and is well approximated by noninteracting electrons, this coupling constant vanishes, $\lambda = 0$. The relationship between the gap in the normal region Δ and $\langle ff \rangle$ is thus $\Delta = \lambda_{eff}\langle ff \rangle$, and this gives a nonzero gap in the vicinity of the proximate host superconductor. Here, f are fermion annhilation operators and $\langle ff \rangle$ thus represents the pair amplitude induced in the normal graphene region. The proximity-induced gap vanishes rapidly as one goes away from the surface and into the bulk of graphene, since λ_{eff} vanishes rapidly as we move away from the proximate host superconductor. It would in principle be *incorrect* to assert that in the proximity region of graphene, we could have a nonzero anomalous Green's function $\langle ff \rangle$, but no gap Δ, by using a self-consistency relation of the type $\Delta = \lambda\langle ff \rangle$ with $\lambda = 0$.[29] Such a self-consistency relation does not exist in a normal system which does not superconduct by itself. However, in a situation where the intrinsic $\lambda = 0$, it could well turn out to be the case that λ_{eff} is small, leading to a gap which is very small.[24] In our paper, we have a thin film graphene system with a bulk superconductor in contact with the film, deposited on top of the film. If the thickness of the graphene film is smaller than the coherence length of the bulk superconductor, one obtains a proximity-induced superconducting gap throughout the film. This is similar to the situation realized in a planar superconductor/two-dimensional electron gas junction.[30,31] As we shall see, our results are quite sensitive to the presence of even a small induced gap in graphene.

III. CONDUCTANCE SPECTRA

In what follows, we describe how the conductance spectra of an N-S and N-I-S graphene junction may be obtained. According to the Blonder-Tinkham-Klapwijk (BTK) formalism,[32] the normalized conductance is given by

$$G(eV) = \frac{1}{G_N}\int_{-\pi/2}^{\pi/2} d\theta\cos\theta\left(1 - |r(eV,\theta)|^2 + \frac{\mathrm{Re}\, e^{i\theta_A}}{\cos\theta}|r_A(-eV,\theta)|^2\right), \tag{20}$$

where r and r_A are the reflection coefficients for normal and Andreev reflection,[40] respectively, while G_N is a renormalization constant corresponding to the N-N metallic conductance,[23]

$$G_N = \int_{-\pi/2}^{\pi/2} d\theta\cos\theta\frac{4\cos^2\theta}{4\cos^2\theta + Z^2}. \tag{21}$$

In this case, we have a zero intrinsic barrier such that $Z = 0$. We will apply the usual approximation $|r_A(-eV,\theta)|$

$=|r_A(eV,\theta)|$, which may be shown to hold for a quite general parameter regime. For perfect normal reflection ($|r|^2=1$), there is no conductance, while for perfect Andreev reflection ($|r_A|^2=1$), the conductance is doubled compared to the N-N case. In order to obtain these coefficients, we make use of the boundary conditions described in the previous section. The analytical solution and behavior of the conductance differs in the N-S and N-I-S cases, and we proceed with a separate treatment of these scenarios.

A. N-S junction

Solving the boundary conditions for the wave functions at the interface leads to the analytical expressions for the reflection coefficients:

$$r=\frac{2\cos\theta[\zeta_+v(\theta^+)v(\theta^-)e^{i(\phi^--\phi^+)}-\zeta_-u(\theta^+)u(\theta^-)]}{v(\theta^+)v(\theta^-)e^{i(\phi_--\phi_+)}Y_--u(\theta^+)u(\theta^-)Y_+}-1,$$

$$r_A=\frac{2e^{-i\phi^+}\cos\theta[\zeta_+u(\theta^-)v(\theta^+)-\zeta_-u(\theta^-)v(\theta^+)]}{v(\theta^+)v(\theta^-)e^{i(\phi_--\phi_+)}Y_--u(\theta^+)u(\theta^-)Y_+}, \quad (22)$$

where we have defined the auxiliary quantities $\zeta_\pm=e^{i\theta^\pm}-e^{-i\theta_A}$ and $Y_\pm=\zeta_\mp(e^{i\theta^\pm}+e^{-i\theta})$. The interplay between the different phases felt by the ELQ and HLQ in the superconductor in the case of an anisotropic order parameter enters above through the factor $e^{i(\phi^--\phi^+)}$. It remains, however, to be clarified how this interplay manifests itself in the tunneling conductance. Before investigating this in more detail, let us briefly consider the isotropic s-wave case first—i.e., $\Delta(\theta)=\Delta$—such that $e^{i(\phi^--\phi^+)}=1$.

1. Conventional s-wave pairing

For conventional superconducting pairing, Eq. (22) reduces to

$$r=\frac{2\cos\theta(\zeta_+v^2-\zeta_-u^2)}{v^2Y_--u^2Y_+}-1,$$

$$r_A=\frac{2\cos\theta uv(e^{i\theta^+}-e^{i\theta^-})}{v^2Y_--u^2Y_+}. \quad (23)$$

This case was first studied by Beenakker.[2] For consistency and completeness, we reproduce the results of Ref. 2 [see Fig. 7(a)]. We point out that Eqs. (23) are valid for any parameter range and not restricted to the heavily doped case treated in Ref. 2. To illustrate the difference, we consider the regime $E_F'=E_F$ shown in Fig. 7(b). In this case, the standard situation of perfect Andreev reflection for subgap energies is recovered, with a sharp drop at the gap edge corresponding to the onset of quasiparticle transmittance into the superconductor.

2. Anisotropic d-wave pairing

To treat an unconventional superconducting order parameter, we must revert to the general expressions in Eq. (22). In order to account for the effect of an anisotropic gap, we choose the $d_{x^2-y^2}$ gap from Table I, which in the weak-coupling approximation ($|\mathbf{k}|=k_F$) reads $\Delta(\theta)=\Delta\cos(2\theta-2\alpha)$. Here, α models the relative orientation of the gap in $\mathbf{k}$ space with respect to the interface normal as illustrated in Fig. 8.

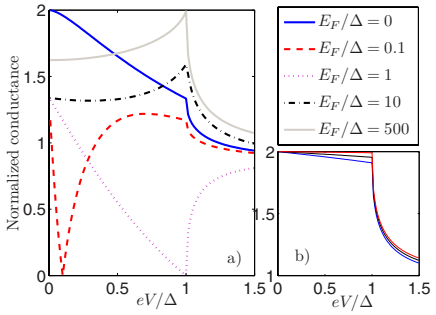

FIG. 7. (Color online) Conductance spectra for graphene in (a) with $E_F'/\Delta=10^3$ and in (b) with $E_F'=E_F$. The spectra in (a) are identical to the result of Ref. 2. In (b), the subgap conductance is always close to $2G_N$, but becomes more constant for increasing E_F since $\theta_c\to\pi/2$. We have plotted the ratios $\{50,100,1000\}$ of E_F/Δ in (b), from bottom to top.

We now proceed to investigate how the conductance spectra of a N-S graphene junction change when going from a s-wave to a d-wave order parameter in the superconducting part of the system. Consider Fig. 9 for the case of heavily doped graphene, where the orientation of the gap is such that the condition for perfect formation of zero energy states in a metallic N-S junction is fulfilled—i.e., $\Delta(\theta)=-\Delta(\pi-\theta)$. As shown by Tanaka and Kashiwaya,[19] this gives rise to a quasiparticle interference between the ELQ and HLQ since they feel different phases of the pairing potentials due to their different trajectories of transmittance into the superconductor. This results in a bound surface states with zero energy[18] close to the N-S interface. For the N-S graphene junction studied here, the explicit barrier potential is zero,

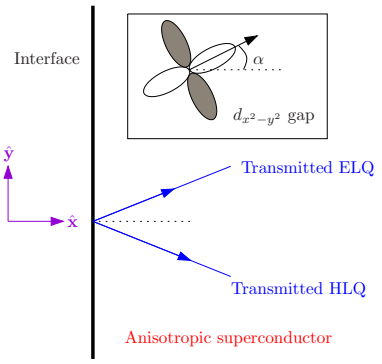

FIG. 8. (Color online) Sketch of a 2D N-S graphene junction with an anisotropic superconductor. The orientation of the gap in $\mathbf{k}$ space is modeled by the angle α.

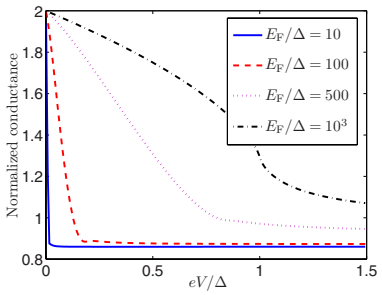

FIG. 9. (Color online) Conductance spectra for doped graphene in with $E_F'=10^4\Delta$ for a d-wave order parameter with orientation angle $\alpha=\pi/4$. A ZBCP is present for large FVM and becomes unobservable narrow for $E_F/\Delta<10$. For $\alpha=0$, the conductance spectra are essentially identical to those in Fig. 7.

while the FVM effectively acts as source of normal reflection. From Fig. 9, one may infer that a peak at zero bias is present in the presence of FVM, although the ZBCP does not increase in magnitude with increasing FVM. We will later study how the presence of an intrinsic barrier in the form of a thin, insulating region separating the normal and superconducting part affects the ZBCP.

Next, we plot the conductance spectra for doped graphene to see how they evolve upon a rotation of the gap. The behavior is quite distinct from that encountered in a N-S metallic junction. From Fig. 10(a), we see that the peak of the conductance shifts from $eV=\Delta$ to progressively lower values as α increases from 0 to $\pi/4$. In this respect, the conductance spectra actually mimicks a lower value of the gap than what is the case, if one were to infer the gap magnitude from the position of the singularity in the spectra. For a given

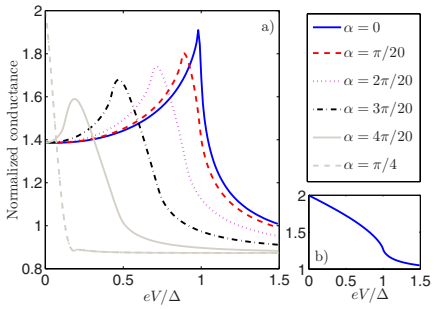

FIG. 10. (Color online) Conductance spectra for (a) doped graphene in with $E_F'=10^4\Delta$ for a d-wave order parameter and (b) undoped graphene with $E_F=E_F'$. In both cases, we have set $E_F/\Delta=100$ and investigate how the conductance spectra evolves upon rotating α from 0 to $\pi/4$ in steps of $\pi/20$. In (a), it is seen that the peak of the conductance shifts from $eV=\Delta$ to progressively lower values as α increases. This is in contrast to metallic N-S junctions. In (b), we plot the conductance for $\alpha=\pi/4$. We find virtually no difference between various orientations of the gap in this case, and the spectra are quite similar to the metallic N-S case with zero barrier.

FVM, determining the magnitude of the gap by the usual method of locating the characteristic feature in the conductance spectra is not as straight forward in N-S graphene junctions as in the metallic case. Indeed, multiple measurements with several different interface orientations would in general be required to obtain the correct value of the gap. This should be an unambigously observable feature in experiments and provides a direct way of testing our theory. Finally, we consider graphene in Fig. 10(b) with $E_F=E_F'$ for a d-wave order parameter. Upon varying α from 0 to $\pi/4$, there is now little distinction between different angles of orientation. The conductance spectra are in this case very resemblant to the metallic N-S case for zero barrier.[19]

B. N-I-S junction

We now consider the conductance of an N-I-S graphene junction, where I denotes an "insulating" (see Introduction) region modeled by a very large energy potential for the quasiparticles. Solving the boundary conditions introduced in Sec. II, we obtain analytical expression for r and r_A, which is all that is required in order to calculate the conductance. However, these expressions are unwieldy and the reader may consult the Appendix for their explicit form. In the following, we will not work exclusively in the thin-barrier limit $d\to 0, V_0\to\infty$ as in Ref. 12. Some aspects of including an insulation region of arbitrary width and strength were very recently discussed in Ref. 33, albeit only in the case of isotropic s-wave pairing. We now treat the two cases of s-wave and d-wave pairing separately.

1. Conventional s-wave pairing

This case was first studied by Bhattacharjee and Sengupta.[12] First, we briefly show that we are able to reproduce the qualitative findings of Ref. 12. As shown in the Appendix, it is convenient to introduce the parameter $\chi=V_0w/v_F$ in the thin-barrier limit. In this case, the reflection coefficients r and r_A exhibit an interesting oscillating behavior as a function of χ. To see this, consider Fig. 11 where we have plotted the voltage dependence of the normalized conductance for several values of χ. For $\chi=0$, we reproduce the result of Fig. 7(b). This is reasonable since the conductance of an N-I-S junction with $\chi=0$—i.e., zero width—should be the same as a N-S junction. The π periodicity is reflected in that the curves for $\chi=0$ and $\chi=\pi$ are identical. For $\chi\neq n\pi$, $n=0,1,2,\ldots$, there is a source of normal reflection at the interfaces due to the insulating region, and consequently the subgap conductance is reduced from its ballistic value $2G_N$. Even in the presence of a FVM, $E_F'\neq E_F$, the spectra of Fig. 11 retain their π periodicity. However, the FVM acts as a source of normal reflection such that one does not have nearly perfect Andreev reflection at subgap energies.

Our results differ slightly from those reported in Ref. 12. Although we obtain qualitatively exactly the same dependence on χ of the conductance, it is seen by comparing our Fig. 11 with Fig. 1 of Ref. 12 that our curves are phase shifted by $\pi/2$ in χ in comparison. As a consequence, we regain the N-S conductance result when $\chi=0$ instead of $\chi=\pi/2$ as reported in Ref. 12. Physically, this seems to be

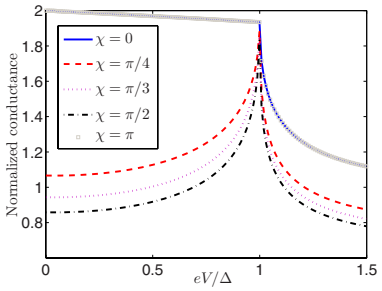

FIG. 11. (Color online) Conductance spectra for a N-I-S graphene junction with $E'_F/\Delta = E_F/\Delta = 100$, using s-wave pairing. We reproduce the same results as Ref. 12 with a π periodicity in the parameter χ. However, we obtain a phase shift of $\pi/2$ in χ compared to their results. We believe that this difference pertains to a minor sign error in the wave functions used in Ref. 12.

more reasonable since $\chi=0$ corresponds to the case of an absent barrier, a situation where there is no source of normal reflection besides the condition that momentum in the direction parallell to the barrier must be conserved. We have also verified that our $\chi=0$ result coincides with the results obtained using the full expressions (see the Appendix) without assuming a thin-barrier limit when we let both w and V_0 go to zero. We believe that this minor discrepancy between our results and the results of Ref. 12 stems from a sign error in their Eq. (5) and also in their expression for $k_b(k'_b)$ in the text above Eq. (5).

To unveil the periodicity even more clear, consider Fig. 12 for a plot of the zero-bias conductance as a function of χ. The cases $E'_F=E_F$ and $E'_F \neq E_F$ display a striking difference. The qualitative shape of the curves is equal, but the amplitude is diminished with increasing FVM. This may in similarity to the above discussion be attributed to the increased normal reflection that takes place at zero bias voltage, thus reducing the conductance.

2. Anisotropic d-wave pairing

We now contrast the s-wave case with an anisotropic pairing potential to see how the spectra are altered. Consider first

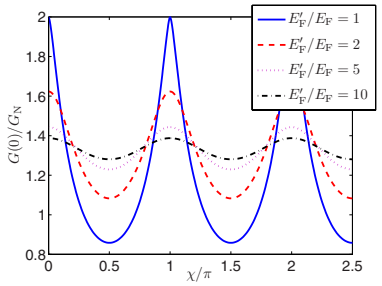

FIG. 12. (Color online) Plot of the zero-bias conductance as a function of χ with $E_F/\Delta = 100$ for a N-I-S graphene junctions with s-wave pairing.

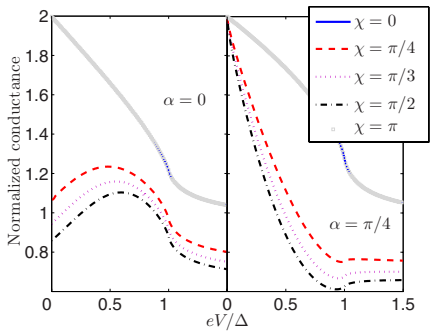

FIG. 13. (Color online) Conductance spectra for a N-I-S graphene junction with $E'_F/\Delta = E_F/\Delta = 100$, using d-wave pairing.

Fig. 13 for a plot of the tunneling conductance in the undoped case. We consider the two angles $\alpha=0$ and $\alpha=\pi/4$ as representatives for the two types of qualitative behavior that may be expected in a d-wave superconductor–normal-graphene junction. The latter corresponds to perfect formation of zero energy states (ZES) in the metallic counterpart junction. From the spectra, one infers that for $\alpha=0$, tunneling into the nodes of the superconducting gap destroys the nearly perfect Andreev reflection for subgap energies obtained in Fig. 11. When $\alpha=\pi/4$, one observes the formation of a ZBCP which peaks at twice the normal-state conductance. It is also interesting to note that the zero bias conductance remains unchanged upon increasing χ. Therefore, the equivalent of Fig. 12 in the present d-wave case is $G(0) \simeq 2G_N$, regardless of χ.

Introducing a FVM between the superconducting and normal parts of the system, the spectra are rendered less sensitive to any increase in χ, as seen in Fig. 14. For $\alpha=0$, the spectra are essentially identical to the doped s-wave case. For $\alpha=\pi/4$, it is seen that the formation of a ZBCP becomes even more protruding and that the zero bias conductance is still insensitive to any increase in χ. Therefore, one is led to conclude that the normalized zero bias conductance $G(0)/G_N$ in the $\alpha=\pi/4$ d-wave case is constantly equal to

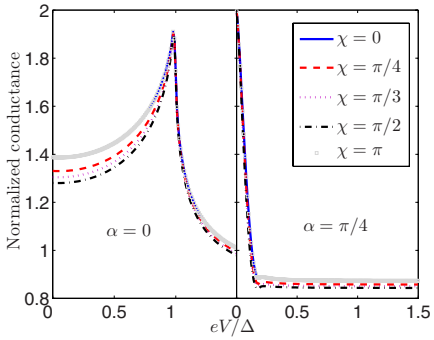

FIG. 14. (Color online) Conductance spectra for a N-I-S graphene junction with $E'_F/E_F = 10$ and $E_F/\Delta = 100$, using d-wave pairing.

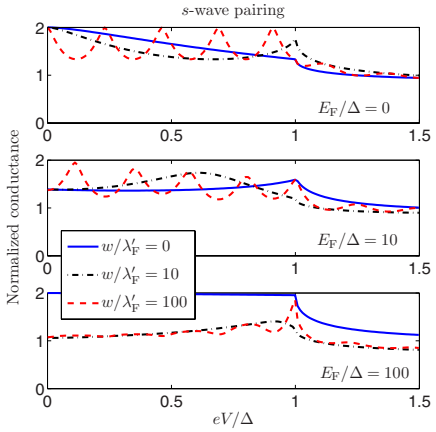

FIG. 15. (Color online) Tunneling conductance of a N-I-S graphene junction for s-wave pairing in the undoped and doped cases (see main text for parameter values). We have fixed $V_0/\Delta = 500$ and $E'_F/\Delta = 100$. It is seen that for increasing w, a novel oscillatory behavior of the conductance as a function of voltage is present in all cases.

nearly 2, regardless of χ *and* the magnitude of the FVM.

IV. CONDUCTANCE-OSCILLATIONS

In this section, we investigate a feature of the conductance spectra that is in common for both the s-wave and d-wave cases: an oscillatory behavior as a function of applied bias voltage. Consider first a N-I-S graphene junction. In the thin-barrier limit defined as $w \to 0$ and $V_0 \to \infty$ with s-wave pairing, Ref. 12 reported a π periodicity of the conductance with respect to the parameter $\chi = V_0 w / v_F$, as discussed in the previous section. We now show that by not restricting ourselves to the thin-barrier limit, new physics emerges from the presence of a finite-width doped region separating the N and S. We measure the width w of region I in units of λ'_F and the potential barrier V_0 in units of E'_F. The linear dispersion approximation is valid[20] up to $\simeq 1$ eV, and we will consider Fermi energies in graphene[4] ranging from the undoped case $E_F \approx 0$ meV to $E_F \approx 100$ meV in the doped case, setting the gap value to $\Delta = 1$ meV. Owing to the restriction of $E'_F \gg \Delta$, we fix $E'_F = 100\Delta$, and also set $V_0 = 500\Delta$ in order to model the effective potential in the region I.

Consider Fig. 15 where we plot the normalized tunneling conductance in case of s-wave pairing, for both a doped and undoped normal part of the system. The most striking new feature compared to the thin-barrier limit is the strong oscillations in the conductance as a function of eV. For subgap energies, we regain the N-S conductance for undoped graphene when $\chi = 0$, with nearly perfect Andreev reflection. The same oscillations are seen in the d-wave pairing case, shown in Fig. 16. To model the d-wave pairing, we have used the $d_{x^2-y^2}$ model $\Delta(\theta) = \Delta \cos(2\theta - 2\alpha)$ with $\alpha = \pi/4$. The parameter α effectively models different orientations of the gap in $\mathbf{k}$ space with regard to the interface, and $\alpha = \pi/4$

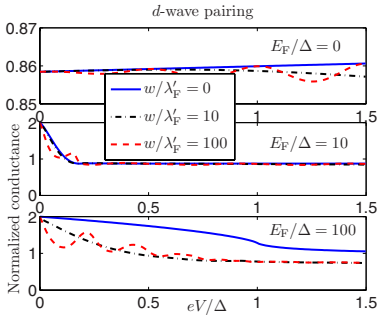

FIG. 16. (Color online) Same as Fig. 15, but now for d-wave pairing with $\alpha = \pi/4$. We have fixed $V_0/\Delta = 500$ and $E'_F/\Delta = 100$.

corresponds to perfect formation of ZES in N-S metallic junctions. For $\alpha = 0$, the d-wave spectra are essentially identical to the s-wave case, since the condition for formation of ZES is not fulfilled in this case.[19] It is seen that in all cases shown in Figs. 15 and 16 the conductance exhibits a novel oscillatory behavior as a function of applied bias voltage eV as the width w of the insulating region becomes much larger than the Fermi wavelength—i.e., $w \gg \lambda'_F$.

The oscillatory behavior of the conductance may be understood as follows. Nonrelativistic free electrons with energy E impinging upon a potential barrier V_0 are described by an exponentially decreasing nonoscillatory wave function e^{ikx} inside the insulating region if $E < V_0$, since the dispersion essentially is $k \sim \sqrt{E - V_0}$. Relativistic free electrons, on the other hand, have a dispersion $k \sim (E - V_0)$, such that the corresponding wave functions do not decay inside the insulating region. Instead, the transmittance of the junction will display an oscillatory behavior as a function of the energy of incidence E. In general, a kinetic energy given by $\sim k^\alpha$ will lead to a complex momentum $k \sim (E - V_0)^{1/\alpha}$ inside the tunneling region and hence damped oscillatory behavior of the wave function. Relativistic massless fermions are unique in the sense that only in this case ($\alpha = 1$) is the momentum purely real. Hence, the undamped oscillatory behavior at subgap energies appears as a direct manifestation of the relativistic low-energy Dirac fermions in the problem. This observation is also linked to the so-called Klein paradox which occurs for electrons with such a relativistic dispersion relation, which has been theoretically studied in normal graphene.[34]

We next discuss why the illustrated conductance spectra are different for s-wave and d-wave symmetries, in addition to comparing the doped and undoped case. The difference in doping level between the superconducting and normal part of the system may be considered as an effective FVM, acting as a source of normal reflection in the scattering processes. This is why the subgap conductance at thin barrier limit is reduced when $E'_F \neq E_F$. Moving away from the thin-barrier limit, it is seen that oscillations emerge in the conductance spectra. For s-wave pairing, the amplitude of the oscillations is larger for $E'_F \neq E_F$ than for the case of no FVM, but the period of oscillations remains the same. This period depends on w, while the amplitude of the oscillations is governed by the wave vectors in the regions I and S. The maximum value

of the oscillations occurs when $2w$ equals an integer number of wavelengths, corresponding to a constructive interference between the scattered waves. Physically, the amplitude dependence of the oscillations on the doping level originates with the fact that any FVM effectively acts as an increase in barrier strength. By making V_0 larger, one introduces a stronger source of normal reflection. When the resonance condition for the oscillations is not met, the incoming particles are reflected more efficiently. This is also the reason why increasing V_0 directly and increasing the FVM has the same effect on the spectra.

We now turn to the difference between the *s*-wave and *d*-wave symmetries. It is seen that the conductance is reduced in the *d*-wave case compared to the *s*-wave case and is actually nearly constant for $E_F=0$. One may understand the reduction in subgap conductance in the undoped case as a consequence of tunneling into the nodes of the gap, which is not present in the *s*-wave case. Hence, Andreev reflection, which significantly contributes to the conductance, is reduced in the *d*-wave case compared to the *s*-wave case. Moreover, we see that a ZBCP is formed when $E_{\mathrm{F}}' \neq E_{\mathrm{F}}$, equivalent to a stronger barrier, and this is interpreted as the usual formation of ZES leading to a transmission at zero bias with a sharp drop for increasing voltage.

V. DISCUSSION

By means of the proximity effect, Heersche *et al.* successfully induced superconductivity (see also Ref. 35) in a graphene layer.[7] This achievement opens up a vista of new, exciting physics due to the combination of the peculiar electronic features of graphene and the many interesting properties of superconductivity. For our theory to be properly tested experimentally, it is necessary to create N-S and N-I-S graphene junctions. Junctions involving normal graphene with insulating regions have recently been experimentally realized.[4,5] In our work, we have discussed novel conductance oscillations in a N-I-S graphene junction that arise when moving away from the thin-barrier limit discussed in Ref. 12. While reaching the thin-barrier limit might pose some difficulties from an experimental point of view, our predictions are manifested when using wide barriers, which should be technically easier to realize. In order to reach the doped regime, this could be achieved by either chemical doping or using a gate voltage to raise the Fermi level in the superconducting region.[34,36] The relevant magnitudes for the various physical quantities present in such an experimental setup has been discussed in the main text of this paper.

It is also worth mentioning that since we have assumed a homogeneous chemical potential in each of the normal, insulating, and superconducting regions, the experimental realization of the predicted effects require charge homogeneity of the graphene samples. This is a challenging criterion, since electron-hole puddles in graphene imaged by scanning single-electron transistors[37] suggest that such charge inhomogeneities probably play an important role in limiting the transport characteristics of graphene.[38] In addition, we have neglected the spatial variation of the superconducting gap near the N-S interfaces. The suppression of the order parameter is expected to least pronounced when there is a large FVM between the two regions. However, the qualitative results presented in this work are most likely unaffected by taken into account the reduction of the gap near the interface.

VI. SUMMARY

In summary, we have studied coherent quantum transport in normal-superconductor (N-S) and normal-insulator-superconductor (N-I-S) graphene junctions, investigating also the role of *d*-wave pairing symmetry on the tunneling conductance. We elaborate on the results obtained in Ref. 17: namely, a new oscillatory behavior of the conductance as a function of bias voltage for insulating regions that satisfy $w \gg \lambda_{\mathrm{F}}'$, which is present both for *s*- and *d*-wave pairing. This is a unique manifestion of the Dirac-like fermions in the problem. In the *d*-wave case, we have studied the conductance of N-S and N-I-S junctions in order to make predictions of what could be expected in experiments, providing both analytical and numerical results. We find very distinct behavior from metallic N-S junctions in the presence of a FVM: a rotation of α is accompanied by a progressive shift of the peak in the conductance, without any formation of a ZBCP except for $\alpha=\pi/4$. All of our predictions should be easily experimentally observable, which constitutes a direct way of testing our theory.

ACKNOWLEDGMENTS

The authors are indebted to Takehito Yokoyama for very useful comments, in addition to critical reading of the manuscript and the numerical code, and to Zlatko Tesanovic for helpful comunications. We have also benefited from discussions with Annica Black-Schaffer and Carlos Beenakker. This work was supported by the Norwegian Research Council Grants No. 158518/431 and No. 158547/431 (NANOMAT) and Grant No. 167498/V30 (STORFORSK). The authors also acknowledge the Center for Advanced Study at the Norwegian Academy of Science and Letters for hospitality.

APPENDIX: NORMAL- AND ANDREEV-REFLECTION COEFFICIENTS FOR N-I-S JUNCTIONS

Solving the boundary conditions, Eqs. (17), we obtain the following expressions for the normal-reflection coefficient r and the Andreev-reflection coefficient r_{A}:

$$r = t_{\mathrm{e}}(A + C) + t_{\mathrm{h}}(B + D) - 1,$$

$$r_{\mathrm{A}} = t_{\mathrm{e}}(A' + C') + t_{\mathrm{h}}(B' + D'), \tag{A1}$$

where the transmission coefficients read

$$t_{\mathrm{e}} = 2\cos\theta[e^{-i\theta_{\mathrm{A}}}(B' + D') - (B'e^{-i\tilde{\theta}_{\mathrm{A}}} - D'e^{i\tilde{\theta}_{\mathrm{A}}})]\rho^{-1},$$

$$t_{\mathrm{h}} = t_{\mathrm{e}}[e^{i\theta_{\mathrm{A}}}(A'e^{-i\tilde{\theta}_{\mathrm{A}}} - C'e^{i\tilde{\theta}_{\mathrm{A}}}) - A' - C']$$

$$\times[B' + D' - e^{i\theta_{\mathrm{A}}}(B'e^{-i\tilde{\theta}_{\mathrm{A}}} - D'e^{i\tilde{\theta}_{\mathrm{A}}})]^{-1}, \tag{A2}$$

with the definition

$$\rho = [e^{-i\theta_A}(B' + D') - (B'e^{-i\tilde{\theta}_A} - D'e^{i\tilde{\theta}_A})][e^{-i\theta}(A + C) + (Ae^{i\tilde{\theta}} - Ce^{-i\tilde{\theta}})] - [(De^{-i\tilde{\theta}} - Be^{i\tilde{\theta}}) - e^{-i\theta}(B + D)] \times [(A'e^{-i\tilde{\theta}_A} - C'e^{i\tilde{\theta}_A}) - e^{-i\theta_A}(A' + C')]. \quad \text{(A3)}$$

We have defined the auxiliary quantities

$$A = u_+ e^{i(q^+ - p^+)}[1 - (e^{i\tilde{\theta}} - e^{i\theta^+})(2\cos\tilde{\theta})^{-1}],$$

$$B = v_- e^{i(q^- - p^+)}[1 - (e^{i\tilde{\theta}} - e^{i\theta^-})(2\cos\tilde{\theta})^{-1}],$$

$$C = u_+ e^{i(p^+ + q^+)}(e^{i\tilde{\theta}} - e^{i\theta^+})(2\cos\tilde{\theta})^{-1},$$

$$D = v_- e^{i(p^+ + q^-)}(e^{i\tilde{\theta}} - e^{i\theta^-})(2\cos\tilde{\theta})^{-1}, \quad \text{(A4)}$$

and similarly introduced

$$A' = v_+ e^{i(q^+ + p^- - \phi^+)}[1 + (e^{i\theta^+} - e^{-i\tilde{\theta}_A})(2\cos\tilde{\theta}_A)^{-1}],$$

$$B' = u_- e^{i(q^- + p^- - \phi^-)}[1 + (e^{i\theta^-} - e^{-i\tilde{\theta}_A})(2\cos\tilde{\theta}_A)^{-1}],$$

$$C' = v_+ e^{i(q^+ - p^- - \phi^+)}(e^{-i\tilde{\theta}_A} - e^{i\theta^+})(2\cos\tilde{\theta}_A)^{-1},$$

$$D' = u_- e^{i(q^- - p^- - \phi^-)}(e^{-i\tilde{\theta}_A} - e^{i\theta^-})(2\cos\tilde{\theta}_A)^{-1}. \quad \text{(A5)}$$

For more compact notation, we have finally defined

$$q^+ = q^e\cos\theta^+ w, \quad q^- = q^h\cos\theta^- w,$$

$$p^+ = \tilde{p}^e\cos\tilde{\theta} w, \quad p^- = \tilde{p}^h\cos\tilde{\theta}_A w. \quad \text{(A6)}$$

In the thin-barrier limit defined as $w \to 0$ and $V_0 \to \infty$, one may set

$$\tilde{\theta} \to 0, \quad \tilde{\theta}_A \to 0, \quad q_\pm \to 0, \quad p_\pm \to \mp\chi, \quad \text{(A7)}$$

where $\chi = V_0 w / v_F$.

[1] G. Deutscher, Rev. Mod. Phys. **77**, 109 (2005).
[2] C. W. J. Beenakker, Phys. Rev. Lett. **97**, 067007 (2006).
[3] C. Beenakker, arXiv:0710.3848 (unpublished).
[4] K. S. Novoselov, A. K. Geim, S. V. Morozov, D. Jiang, Y. Zhang, S. V. Dubonos, I. V. Grigorieva, and A. A. Firsov, Science **306**, 666 (2004).
[5] Y. Zhang, Y.-W. Tan, H. L. Stormer, and P. Kim, Nature (London) **438**, 201 (2005).
[6] In the quantum domain at low temperatures and in the vicinity of the edge of the superconducting dome, the coupling between the nodal fermions in high-T_c superconductors and quantum critical phase-fluctuations of the superconducting order parameter (i.e., vortices) will lead to unusual behavior. This has important ramifications for constructing a viable theory of the so-called pseudogap phase of these systems. See M. Franz and Z. Tešanović, Phys. Rev. Lett. **87**, 257003 (2001); Z. Tešanović, O. Vafek, and M. Franz, Phys. Rev. B **65**, 180511(R) (2002); O. Vafek and Z. Tešanović, Phys. Rev. Lett. **91**, 237001 (2003).
[7] H. B. Heersche, P. Jarillo-Herrero, J. B. Oostinga, L. M. K. Vandersypen, and A. F. Morpurgo, Nature (London) **446**, 56 (2007).
[8] A. Yu. Kasumov, R. Deblock, M. Kociak, B. Reulet, H. Bouchiat, I. I. Khodos, Yu. B. Gorbatov, V. T. Volkov, C. Journet, and M. Burghard, Science **284**, 1508 (1999).
[9] A. F. Morpurgo, J. Kong, C. M. Marcus, and H. Dai, Science **286**, 263 (1999).
[10] M. R. Buitelaar, W. Belzig, T. Nussbaumer, B. Babić, C. Bruder, and C. Schönenberger, Phys. Rev. Lett. **91**, 057005 (2003).
[11] P. Jarillo-Herrero, J. A. van Dam, and L. P. Kouwenhoven, Nature (London) **439**, 953 (2006).
[12] S. Bhattacharjee and K. Sengupta, Phys. Rev. Lett. **97**, 217001 (2006).
[13] I. I. Mazin and M. D. Johannes, Nat. Phys. **1**, 91 (2005).
[14] J. González, F. Guinea, and M. A. H. Vozmediano, Phys. Rev. B **59**, R2474 (1999).
[15] C. L. Kane and E. J. Mele, Phys. Rev. Lett. **93**, 197402 (2004).
[16] K. S. Novoselov, A. K. Geim, S. V. Morozov, D. Jiang, M. I. Katsnelson, I. V. Grigorieva, S. V. Dubonos, and A. A. Firsov, Nature (London) **438**, 197 (2005).
[17] J. Linder and A. Sudbø, Phys. Rev. Lett. **99**, 147001 (2007).
[18] C.-R. Hu, Phys. Rev. Lett. **72**, 1526 (1994).
[19] Y. Tanaka and S. Kashiwaya, Phys. Rev. Lett. **74**, 3451 (1995).
[20] P. R. Wallace, Phys. Rev. **71**, 622 (1947).
[21] G. E. Blonder and M. Tinkham, Phys. Rev. B **27**, 112 (1983).
[22] I. Zutic and O. T. Valls, Phys. Rev. B **61**, 1555 (2000).
[23] S. Kashiwaya, Y. Tanaka, M. Koyanagi, and K. Kajimura, Phys. Rev. B **53**, 2667 (1996).
[24] C. Bruder, Phys. Rev. B **41**, 4017 (1990).
[25] A. M. Black-Schaffer and S. Doniach, Phys. Rev. B **75**, 134512 (2007).
[26] K. Fossheim and A. Sudbø, *Superconductivity: Physics and Applications* (Wiley, New York, 2004), Chap. 5.
[27] H. Kleinert, Phys. Rev. Lett. **84**, 286 (2000).
[28] Z. Tešanović, Phys. Rev. B **51**, 16204 (1995); **59**, 6449 (1999); A. K. Nguyen and A. Sudbø, *ibid.* **57**, 3123 (1998); **58**, 2802 (1998); **60**, 15307 (1999); Europhys. Lett. **46**, 780 (1999).
[29] F. S. Bergeret, A. F. Volkov, and K. B. Efetov, Rev. Mod. Phys. **77**, 1321 (2005); A. I. Buzdin, *ibid.* **77**, 935 (2005).
[30] A. F. Volkov, P. H. C. Magnee, B. J. van Wees, and T. M. Klapwijk, Physica C **242**, 261 (1995).
[31] G. Fagas, G. Tkachov, A. Pfund, and K. Richter, Phys. Rev. B **71**, 224510 (2005).
[32] G. E. Blonder, M. Tinkham, and T. M. Klapwijk, Phys. Rev. B **25**, 4515 (1982).
[33] S. Bhattacharjee, M. Maiti, and K. Sengupta, arXiv:0704.2760 (unpublished).
[34] M. I. Katsnelson, K. S. Novoselov, and A. K. Geim, Nat. Phys. **2**, 620 (2006).
[35] Xu Du, Ivan Skachko, and Eva Y. Andrei, arXiv:0710.4984 (unpublished).
[36] J. Milton Pereira, Jr., P. Vasilopoulos, and F. M. Peeters, arXiv:cond-mat/0702596 (unpublished).

[37] J. Martin, N. Akerman, G. Ulbricht, T. Lohmann, J. H. Smet, K. von Klitzing, and A. Yacoby, arXiv:0705.2180 (unpublished).
[38] E.-A. Kim and A. H. Castro Neto, arXiv:cond-mat/0702562 (unpublished).
[39] It is sufficient to demand that the phase fluctuations must be small, since it was shown by Kleinert (Ref. 27) that for any system exhibiting a second-order phase transition with a spontaneously broken O(N) ($N \geq 2$) symmetry at low temperatures, phase fluctuations destroy order before amplitude fluctations become important.
[40] Note that in Ref. 17, a factor $|p_h/p_e|$ was included as a prefactor of $|r_A(-eV,\theta)|^2$. While such a factor is present in the metallic case, it is absent for graphene junctions. Nevertheless, this does not affect the results of Ref. 17 in any manner since the case $E_F \gg (\Delta, \varepsilon)$ was considered there, implying $|p_h/p_e| \approx 1$.

Paper X

Heat transport by Dirac fermions in normal/superconducting graphene junctions.

Physical Review B **77**, 132503 (2008).

Heat transport by Dirac fermions in normal/superconducting graphene junctions

Takehito Yokoyama,[1] Jacob Linder,[2] and Asle Sudbø[2]
[1]*Department of Applied Physics, Nagoya University, Nagoya 464-8603, Japan*
[2]*Department of Physics, Norwegian University of Science and Technology, N-7491 Trondheim, Norway*
(Received 9 January 2008; published 21 April 2008)

We study heat transport in normal/superconducting graphene junctions. We find that while the thermal conductance displays the usual exponential dependence on temperature, reflecting the *s*-wave symmetry of the superconducting graphene, it exhibits an unusual oscillatory dependence on the potential height or the length of the barrier region. This oscillatory dependence stems from the emergent low-energy relativistic nature of fermions in graphene, essentially different from the result in conventional normal metal/superconductor junctions.

DOI: 10.1103/PhysRevB.77.132503 PACS number(s): 75.75.+a, 73.20.−r, 75.50.Xx, 75.70.Cn

The recent progress in practical fabrication techniques for a monatomic layer of graphite, called graphene, has allowed for experimental studies of this system, which in turn has triggered a tremendous interest.[1–7] Graphene is a two-dimensional system of carbon atoms, and the low-energy electrons in graphene are governed by the Dirac equation. Up to now, intensive studies on graphene have been conducted, for instance, quantum Hall effect,[6,8,9] minimum conductivity,[7] and bipolar supercurrent.[10]

From an applied physics point of view, graphene is also an important material. Graphene exhibits high mobility and carrier density controllable by gate voltage, which makes it well suited for achieving device applications.[5,6,11,12] In order to apply graphene to electric devices, it is an important issue to clarify characteristics of transport phenomena such as charge[5–7] and heat[13–16] transports in graphene.

In conventional normal metal/superconductor junctions, it is known that electric and thermal conductances reflect the magnitude or symmetry of the gap of the superconductor.[17,18] While the conductance in normal/superconductor graphene junction has been studied by several authors,[19–21] the thermal conductance in this junction has not yet been investigated—only the thermal conductance along the boundaries in a superconductor/normal/superconductor graphene junction has been treated previously.[22] Therefore, the study of the thermal conductance in normal/superconductor graphene junction will complement the study of the electrical conductance in this junction.

In this Brief Report, we study heat transport in normal/superconducting graphene junctions. We find that the thermal conductance has an exponential dependence on temperature, which reflects the *s*-wave symmetry of the superconducting graphene. However, it displays an oscillatory dependence on the potential height or the length of the barrier region. This oscillatory dependence stems from the linear dispersion relation in graphene and differs in an essential way from the result in the conventional normal metal/superconductor junctions.[17,18,29]

We briefly present the formalism to be used in this Brief Report by following Ref. 21. Consider a two dimensional normal/insulating/superconducting graphene junction[23] where the superconducting (normal) region is located in the semi-infinite regions $x>L$ ($x<0$). The proposed experimental setup of our model is shown in Fig. 1. By exploiting the valley degeneracy,[24] the Bogoliubov–de Gennes equation for the junction in the xy plane reads

$$\begin{pmatrix} H-E_F\hat{1} & \Delta\hat{1} \\ \Delta^{\dagger}\hat{1} & E_F\hat{1}-H \end{pmatrix}\begin{pmatrix} u \\ v \end{pmatrix} = E\begin{pmatrix} u \\ v \end{pmatrix}, \tag{1}$$

with $H=v_F(k_x\sigma_x+k_y\sigma_y)$ and Fermi energy E_F. The superconducting order parameter reads

$$\Delta = \Delta(T)e^{i\phi}\Theta(x-L), \tag{2}$$

where $\Theta(x)$ is the Heaviside step function, while ϕ is the phase corresponding to the globally broken U(1) symmetry in the superconductor. Also, $v_F\approx 10^6$ m/s is the energy-independent Fermi velocity for graphene, σ_i ($i=x,y$) denotes the Pauli matrices, E is the excitation energy, and u and v denote the electronlike and holelike excitations, respectively, described by the wave function. The Pauli matrices operate on the two triangular sublattice spaces of the honeycomb structure, corresponding to the A and B atoms. The linear dispersion relation is a reasonable approximation even for Fermi levels as high as 1 eV,[25] such that the fermions in graphene behave like massless Dirac fermions in the low-energy regime.

Let us consider an incident electron from the normal side of the junction ($x<0$) with energy E. For positive excitation energies $E>0$, the eigenvectors and corresponding momentum of the particles read

$$\psi_+^e = [1, e^{i\theta}, 0, 0]^{\mathcal{T}} e^{ip^e \cos\theta x}, \quad p^e = (E+E_F)/v_F, \tag{3}$$

for a right-moving electron at angle of incidence θ, while a left-moving electron is described by the substitution $\theta\rightarrow\pi$

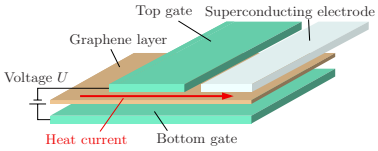

FIG. 1. (Color online) The proposed experimental setup to measure heat transport by Dirac fermions in a graphene normal/superconductor proximity structure. The top and bottom gates allow for the chemical potential in the middle region to be adjusted.

$-\theta$. The superscript $\mathcal{T}$ denotes the transpose. If Andreev reflection takes place, a left-moving hole with energy E and angle of reflection θ_A is generated with the corresponding wave function,

$$\psi_-^h = [0,0,1,e^{-i\theta_A}]^{\mathcal{T}} e^{-ip^h \cos\theta_A x}, \quad p^h = (E - E_F)/v_F, \quad (4)$$

where the superscript e (h) denotes an electronlike (holelike) excitation. Since translational invariance in the y direction holds, the corresponding component of momentum is conserved. This condition allows for the determination of the Andreev-reflection angle θ_A via $p^h \sin\theta_A = p^e \sin\theta$. From this equation, one infers that there is no Andreev reflection ($\theta_A = \pm\pi/2$) for angles of incidence above the critical angle,

$$\theta_c = \sin^{-1}[|E - E_F|/(E + E_F)]. \quad (5)$$

On the superconducting side of the system ($x > L$), the possible wave functions for transmission of a right-moving quasiparticle with a given excitation energy $E > 0$ read

$$\Psi_+^e = (u, ue^{i\theta^+}, ve^{-i\phi}, ve^{i(\theta^+ - \phi)})^{\mathcal{T}} e^{iq^e \cos\theta^+ x},$$
$$q^e = (E_F' + \sqrt{E^2 - \Delta^2})/v_F, \quad (6)$$

$$\Psi_-^h = (v, ve^{i\theta^-}, ue^{-i\phi}, ue^{i(\theta^- - \phi)})^{\mathcal{T}} e^{iq^h \cos\theta^- x},$$
$$q^h = (E_F' - \sqrt{E^2 - \Delta^2})/v_F, \quad (7)$$

where E_F' is the Fermi energy in the superconducting side. The coherence factors are given by[26]

$$u = \sqrt{\frac{1}{2}\left(1 + \frac{\sqrt{E^2 - |\Delta|^2}}{E}\right)}, \quad (8)$$

$$v = \sqrt{\frac{1}{2}\left(1 - \frac{\sqrt{E^2 - |\Delta|^2}}{E}\right)}. \quad (9)$$

Above, we have defined $\theta^+ = \theta_S^e$ and $\theta^- = \pi - \theta_S^h$. The transmission angles $\theta_S^{(i)}$ for the electronlike and holelike quasiparticles are given by $q^{(i)} \sin\theta_S^{(i)} = p^e \sin\theta$, $i = e, h$. Note that in all the wave functions listed above, for clarity, we have not included a common phase factor $e^{ik_y y}$, which corresponds to the conserved momentum in the y direction.

It is appropriate to insert the restriction which will be used throughout this Brief Report, namely, $\Delta \ll E_F'$. Since we are using a mean-field approach to describe the superconducting part of the Hamiltonian, phase fluctuations of the order parameter have to be small.[27]

We define the wave functions in the normal, insulating, and superconducting regions by ψ, $\tilde{\psi}_I$, and Ψ, respectively, with

$$\psi = \psi_+^e + r\psi_-^e + r_A\psi_-^h, \quad (10)$$

$$\tilde{\psi}_I = \tilde{t}_1\tilde{\psi}_+^e + \tilde{t}_2\tilde{\psi}_-^e + \tilde{t}_3\tilde{\psi}_+^h + \tilde{t}_4\tilde{\psi}_-^h, \quad (11)$$

$$\Psi = t^e\Psi_+^e + t^h\Psi_-^h. \quad (12)$$

The wave functions $\tilde{\psi}$ differ from ψ in that the Fermi energy is shifted by an external potential, such that $E_F \to E_F - U$, where U is the barrier height. Also, note that the trajectories of the quasiparticles in the insulating region, which are defined by the angles $\tilde{\theta}$ and $\tilde{\theta}_A$, differ by the same substitution,

$$\sin\tilde{\theta}/\sin\theta = (E + E_F)/(E + E_F - U), \quad (13)$$

$$\sin\tilde{\theta}_A/\sin\theta = (E + E_F)/(E - E_F + U). \quad (14)$$

Note that the subscript $\pm$ on the wave functions indicates the direction of momentum, which is, in general, different from the group velocity direction.

By matching the wave functions at both interfaces, $\psi|_{x=0} = \tilde{\psi}_I|_{x=0}$ and $\tilde{\psi}_I|_{x=L} = \Psi|_{x=L}$,[28] we obtain the following expressions for the normal reflection coefficient r and the Andreev-reflection coefficient r_A (Ref. 21):

$$r = t_e(A + C) + t_h(B + D) - 1, \quad (15)$$

$$r_A = t_e(A' + C') + t_h(B' + D'), \quad (16)$$

where the transmission coefficients read

$$t_e = 2\cos\theta[e^{-i\theta_A}(B' + D') - (B'e^{-i\tilde{\theta}_A} - D'e^{i\tilde{\theta}_A})]\rho^{-1}, \quad (17)$$

$$t_h = t_e[e^{i\theta_A}(A'e^{-i\tilde{\theta}_A} - C'e^{i\tilde{\theta}_A}) - A' - C']$$
$$\times[B' + D' - e^{i\theta_A}(B'e^{-i\tilde{\theta}_A} - D'e^{i\tilde{\theta}_A})]^{-1}, \quad (18)$$

$$\rho = [e^{-i\theta_A}(B' + D') - (B'e^{-i\tilde{\theta}_A} - D'e^{i\tilde{\theta}_A})][e^{-i\theta}(A + C)$$
$$+ (Ae^{i\tilde{\theta}} - Ce^{-i\tilde{\theta}})] - [(De^{-i\tilde{\theta}} - Be^{i\tilde{\theta}}) - e^{-i\theta}(B + D)]$$
$$\times[A'e^{-i\tilde{\theta}_A} - C'e^{i\tilde{\theta}_A} - e^{-i\theta_A}(A' + C')], \quad (19)$$

and we have introduced the auxiliary quantities,

$$A = ue^{i(q^+ - p^+)}[1 - (e^{i\tilde{\theta}} - e^{i\theta^+})(2\cos\tilde{\theta})^{-1}],$$

$$B = ve^{i(q^- - p^+)}[1 - (e^{i\tilde{\theta}} - e^{i\theta^-})(2\cos\tilde{\theta})^{-1}],$$

$$C = ue^{i(p^+ + q^+)}(e^{i\tilde{\theta}} - e^{i\theta^+})(2\cos\tilde{\theta})^{-1},$$

$$D = ve^{i(p^+ + q^-)}(e^{i\tilde{\theta}} - e^{i\theta^-})(2\cos\tilde{\theta})^{-1}, \quad (20)$$

$$A' = ve^{i(q^+ + p^- - \phi)}[1 + (e^{i\theta^+} - e^{-i\tilde{\theta}_A})(2\cos\tilde{\theta}_A)^{-1}],$$

$$B' = ue^{i(q^- + p^- - \phi)}[1 + (e^{i\theta^-} - e^{-i\tilde{\theta}_A})(2\cos\tilde{\theta}_A)^{-1}],$$

$$C' = ve^{i(q^+ - p^- - \phi)}(e^{-i\tilde{\theta}_A} - e^{i\theta^+})(2\cos\tilde{\theta}_A)^{-1},$$

$$D' = ue^{i(q^- - p^- - \phi)}(e^{-i\tilde{\theta}_A} - e^{i\theta^-})(2\cos\tilde{\theta}_A)^{-1}. \quad (21)$$

Here, we have defined

$$q^+ = q^e\cos\theta^+ L, \quad q^- = q^h\cos\theta^- L,$$

$$p^+ = \tilde{p}^e\cos\tilde{\theta} L, \quad p^- = \tilde{p}^h\cos\tilde{\theta}_A L. \quad (22)$$

In the thin-barrier limit defined as $L \to 0$ and $U \to \infty$, one gets

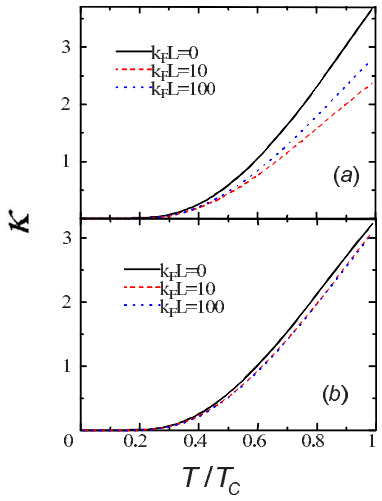

FIG. 2. (Color online) Thermal conductance as a function of T/T_C for various k_FL with $U/E_F=10$ and $E_F'=100\Delta_0$ at $E_F=100\Delta_0$ in (a) and $E_F=10\Delta_0$ in (b).

$$\tilde{\theta} \to 0, \quad \tilde{\theta}_A \to 0, \quad q_\pm \to 0, \quad p_\pm \to \mp\chi, \tag{23}$$

with $\chi=LU/v_F$. This indicates that thermal conductance is π periodic with respect to χ in this limit.

Finally, the normalized thermal conductance is given by[17,29]

$$\kappa = \int_0^\infty \int_{-\pi/2}^{\pi/2} dE d\theta \cos\theta \left(1 - |r(E,\theta)|^2 - \mathrm{Re}\left(\frac{\cos\theta_A}{\cos\theta}\right) \times |r_A(E,\theta)|^2\right) \frac{E^2}{\Delta_0 T^2 \cosh^2\left(\frac{E}{2T}\right)}, \tag{24}$$

with the gap at zero temperature, $\Delta_0 \equiv \Delta(0)$.

We next present our results for the normalized thermal conductance. Figure 2(a) shows thermal conductance as a function of T/T_C for various k_FL with $U/E_F=10$ and $E_F=E_F'=100\Delta_0$. Here, T_C is the transition temperature and $k_F \equiv E_F/v_F$. From Fig. 2(a), an exponential dependence of the thermal conductance on temperature is seen, which is similar to the conventional normal metal/superconductor junctions.[17] This exponential dependence reflects the s-wave symmetry of the superconducting graphene. However, the length dependence of the thermal conductance is nonmonotonic (oscillatory) and thus essentially different from the monotonic dependence in the conventional normal metal/superconductor junctions.[17,18,29] A similar plot for $E_F=10\Delta_0$ is shown in Fig. 2(b). We also find an exponential temperature dependence, but the dependence on L gets weaker. Therefore, the magnitude of the oscillation with respect to k_FL gets reduced with the increase of the Fermi wave vector mismatch.

Figure 3(a) depicts thermal conductance as a function of U/E_F for various lengths k_FL with $T/T_C=0.5$ and $E_F=E_F'=100\Delta_0$. An oscillatory dependence of the thermal conductance on U/E_F is seen. The period decreases with k_FL. Figure 3(b) displays thermal conductances as a function of k_FL for various U/E_F with $T/T_C=0.5$ and $E_F=E_F'=100\Delta_0$. We also find an oscillatory dependence on k_FL. The period also decreases with U/E_F. These features stem from the π periodicity of the thermal conductance with respect to $\chi=k_FLU/E_F$ in the limit of $U \gg E_F$ and $k_FL \ll 1$ similar to the junction conductance.[20,21,30] In other words, the damped oscillatory behavior of the thermal conductance is a direct manifestation of the relativistic low-energy Dirac fermions because this feature cannot be seen in the conventional normal metal/superconductor junctions.[17,18,29] Also, the presence of the insulating region is essential for the oscillatory behavior[20,21] since no such oscillation is seen without the insulating region.[19]

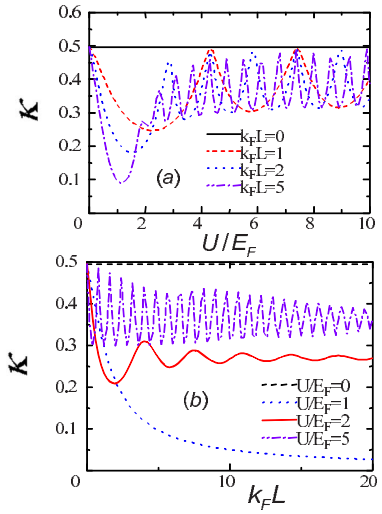

FIG. 3. (Color online) (a) Thermal conductance as a function of U/E_F for various k_FL with $T/T_C=0.5$ and $E_F=E_F'=100\Delta_0$. (b) Thermal conductance as a function of k_FL for various U/E_F with $T/T_C=0.5$ and $E_F=E_F'=100\Delta_0$.

We have neglected the spatial variation of the superconducting gap near the interface. The suppression of the order parameter near the interface is expected to be least pronounced when the sharp edge criteria are satisfied and there is a large Fermi-vector mismatch. In the present case, this is precisely the case, whence we do not expect our qualitative results to be affected by taking into account the reduction of the gap near the interface. Finally, we have assumed that there is no lattice mismatch at the interfaces and that these are smooth and impurity-free.[4] A more refined picture could be obtained by using more realistic models of the variation of the chemical potential, i.e., a continuous slope instead of a steplike variation.

In summary, we have studied heat transport in normal/superconducting graphene junctions. We found that the thermal conductance has an exponential dependence on temperature, which reflects the s-wave symmetry of the superconducting graphene but oscillatory dependence on the po-

tential height or the length of the barrier region. This oscillatory dependence stems from the relativistic dispersion in graphene, which is essentially different from the result in the conventional normal metal/superconductor junctions.

T.Y. acknowledges support by the JSPS. J.L. and A.S. were supported by the Research Council of Norway, Grants No. 158518/431 and No. 158547/431 (NANOMAT) and Grant No. 167498/V30 (STORFORSK).

[1] T. Ando, J. Phys. Soc. Jpn. **74**, 777 (2005).
[2] M. I. Katsnelson and K. S. Novoselov, Solid State Commun. **143**, 3 (2007).
[3] A. H. Castro Neto, F. Guinea, N. M. R. Peres, K. S. Novoselov, and A. K. Geim, arXiv:0709.1163v1, Rev. Mod. Phys. (to be published).
[4] C. W. J. Beenakker, arXiv:0710.3848, Rev. Mod. Phys. (to be published).
[5] K. S. Novoselov, A. K. Geim, S. V. Morozov, D. Jiang, Y. Zhang, S. V. Dubonos, I. V. Grigorieva, and A. A. Firsov, Science **306**, 666 (2004).
[6] Y. Zhang, Y.-W. Tan, H. L. Stormer, and P. Kim, Nature (London) **438**, 201 (2005).
[7] K. S. Novoselov, A. K. Geim, S. V. Morozov, D. Jiang, M. I. Katsnelson, I. V. Grigorieva, S. V. Dubonos, and A. A. Firsov, Nature (London) **438**, 197 (2005).
[8] K. S. Novoselov, E. McCann, S. V. Morozov, V. I. Fal'ko, M. I. Kastenelson, U. Zeitler, D. Jiang, F. Schedin, and A. K. Geim, Nat. Phys. **2**, 177 (2006).
[9] K. Yang, Solid State Commun. **143**, 27 (2007).
[10] H. B. Heersche, P. Jarillo-Herrero, J. B. Oostinga, L. M. K. Vandersypen, and A. F. Morpurgo, Nature (London) **446**, 56 (2007).
[11] J. Scott Bunch, Y. Yaish, M. Brink, K. Bolotin, and P. L. McEuen, Nano Lett. **5**, 287 (2005).
[12] C. Berger, Z. Song, X. Li, X. Wu, N. Brown, C. Naud, D. Mayou, T. Li, J. Hass, A. N. Marchenkov, E. H. Conrad, P. N. First, and W. A. de Heer, Science **312**, 1191 (2006).
[13] M. Trushin and J. Schliemann, Phys. Rev. Lett. **99**, 216602 (2007).
[14] T. Löfwander and M. Fogelström, Phys. Rev. B **76**, 193401 (2007).
[15] K. Saito, J. Nakamura, and A. Natori, Phys. Rev. B **76**, 115409 (2007).
[16] N. M. R. Peres, J. M. B. Lopes dos Santos, and T. Stauber, Phys. Rev. B **76**, 073412 (2007).
[17] A. F. Andreev, Sov. Phys. JETP **19**, 1228 (1964).
[18] G. E. Blonder, M. Tinkham, and T. M. Klapwijk, Phys. Rev. B **25**, 4515 (1982).
[19] C. W. J. Beenakker, Phys. Rev. Lett. **97**, 067007 (2006).
[20] S. Bhattacharjee and K. Sengupta, Phys. Rev. Lett. **97**, 217001 (2006); S. Bhattacharjee, M. Maiti, and K. Sengupta, Phys. Rev. B **76**, 184514 (2007).
[21] J. Linder and A. Sudbø, Phys. Rev. Lett. **99**, 147001 (2007); Phys. Rev. B **77**, 064507 (2008).
[22] M. Titov, A. Ossipov, and C. W. J. Beenakker, Phys. Rev. B **75**, 045417 (2007).
[23] We underline that the notation "insulator" in this context refers to a normal segment of graphene in which one experimentally induces an effective potential barrier.
[24] A. F. Morpurgo and F. Guinea, Phys. Rev. Lett. **97**, 196804 (2006).
[25] P. R. Wallace, Phys. Rev. **71**, 622 (1947).
[26] K. Fossheim and A. Sudbø, *Superconductivity: Physics and Applications* (Wiley, New York, 2004), Chap. 5.
[27] A. K. Nguyen and A. Sudbø, Phys. Rev. B **60**, 15307 (1999); H. Kleinert, Phys. Rev. Lett. **84**, 286 (2000).
[28] Note that these conditions are equivalent to $\hat{v}_x\psi|_{x=0} = \hat{v}_x\tilde{\psi}_I|_{x=0}$ and $\hat{v}_x\tilde{\psi}_I|_{x=L} = \hat{v}_x\Psi|_{x=L}$ with velocity operator $\hat{v}_x = \partial H/\partial k_x = v_F\sigma_x$ and, hence, the current is conserved at the interfaces.
[29] A. Bardas and D. Averin, Phys. Rev. B **52**, 12873 (1995).
[30] M. I. Katsnelson, K. S. Novoselov, and A. K. Geim, Nat. Phys. **2**, 620 (2006).

Paper XI

Quantum transport in a normal metal/odd-frequency superconductor junction.

Physical Review B **77**, 174505 (2008).

Quantum transport in a normal metal/odd-frequency superconductor junction

Jacob Linder,[1] Takehito Yokoyama,[2] Yukio Tanaka,[2] Yasuhiro Asano,[3] and Asle Sudbø[1]
[1]*Department of Physics, Norwegian University of Science and Technology, N-7491 Trondheim, Norway*
[2]*Department of Applied Physics, Nagoya University, Nagoya 464-8603, Japan, and CREST, Japan Science and Technology Corporation (JST), Nagoya 464-8603, Japan*
[3]*Department of Applied Physics, Hokkaido University, Sapporo 060-8628, Japan*
(Received 1 October 2007; revised manuscript received 4 February 2008; published 6 May 2008)

Recent experimental results indicate the possible realization of a bulk odd-frequency superconducting state in the compounds $CeCu_2Si_2$ and $CeRhIn_5$. Motivated by this, we present a study of the quantum transport properties of a normal metal/odd-frequency superconductor junction in a search for probes to unveil the odd-frequency symmetry. From the Eliashberg equations, we perform a quasiclassical approximation to account for the transport formalism of an odd-frequency superconductor with the Keldysh formalism. Specifically, we consider the tunneling charge conductance and the tunneling thermal conductance. We qualitatively find distinct behavior in the odd-frequency case compared to the conventional even-frequency case in both the electrical and thermal current. This serves as a useful tool to identify the possible existence of a bulk odd-frequency superconducting state.

DOI: 10.1103/PhysRevB.77.174505 PACS number(s): 74.45.+c, 74.20.Rp, 74.50.+r

I. INTRODUCTION

The symmetries of the superconducting order parameter with respect to orbital, time, and spin space are governed by the Pauli principle. A wave function describing two electronic states must be totally antisymmetric under the exchange of the particle coordinates. This leads to a finite number of allowed combinations for the symmetries of the wave function. In a wide variety of superconductors ranging from those described with Bardeen–Cooper–Schrieffer and/or Eliashberg theory via spin-triplet superconductivity in ^{3}He to strong-coupling superconductivity in high-T_c cuprates, the wave function of Cooper pairs is even in the frequency domain. For such even-frequency pairing, the wave function may be even or odd in space depending on whether the Cooper pairs form spin singlets or triplets. However, more exotic types of pairings than what is found in this wide range of materials are, in principle, permitted.

Recently, it was predicted that in a ferromagnet/superconductor structure, a so-called odd-frequency pairing could take place.[1] Thus, the Cooper-pair wave function is symmetric under the exchange of spatial and spin coordinates but antisymmetric under the exchange of time coordinates. This state was proposed to exist by Berezinskii[2] a few decades earlier in the context of liquid ^{3}He, and a strong experimental evidence for odd-frequency pairing now exists.[3] The study of such pairing in ferromagnet/conventional superconductor junctions has been addressed by a number of authors over the past few years.[4] Furthermore, it was very recently predicted[5–7] that due to a spatial variation of the pair potential near a normal/superconductor (N/S) junction, the odd-frequency pairing state can be induced even in a conventional ballistic N/S system without spin-triplet ordering. The generation of different symmetry components and their effect on electrical transport in a normal/superconductor interface has also been studied in the diffusive limit[8] in the context of the proximity effect in unconventional superconductors.[9,10]

An issue that arises in the context of the odd-frequency pairing state is if it can be realized in a bulk superconductor, i.e., without a proximity effect. There have been several theoretical proposals for this in strongly correlated systems up until now.[11,12] To explore an odd-frequency pairing state in the heavy-fermion superconductors is an interesting topic, and an assessment of the experimental properties of $CeCu_2Si_2$ and $CeRhIn_5$ concluded that an odd frequency pairing may be realized in these heavy-fermion compounds.[13]

However, only a very limited amount of studies have addressed the issue of identifying the odd-frequency pairing state in a bulk superconductor so far.[11,14,15] Hence, further clear-cut predictions are needed.

In this paper, we present the quantum transport properties of a normal metal/odd-frequency superconductor junction in the clean limit. We calculate the electrical and thermal conductances within the Blonder–Tinkham–Klapwijk (BTK) framework[16] by taking into account the anisotropy of the pair potential.[17] Our starting point is the Eliashberg equations that take into account the frequency dependence of the pair potential. This constitutes a wide range of experimental predictions, which are routinely used to characterize superconducting states.[18–21] Our main result is that the odd-frequency symmetry affects the charge (thermal) transport in an essential manner at low energies (temperatures). This provides a useful tool in identifying this highly unusual superconducting state.

To elucidate the physics in a transparent manner, we employ a simple two-dimensional calculation in the clean limit. We approximate the superconducting gap with a step function in space, which, in the isotropic even-parity *s*-wave case, should be an excellent approximation for low-transmission barriers. Since the low-transmission case is probably the most realistic scenario experimentally, we restrict our attention to this. In the anisotropic even-parity and odd-parity cases (corresponding, e.g., to the high-T_c superconductors and Sr_2RuO_4), the gap may undergo a severe depletion near the barrier even for low-transmission interfaces due to the formation of zero-energy states.[22] The method used in this paper may still capture qualitative fea-

tures of the transport properties even in those cases, just as in the case of the *d*-wave superconductors.[17] Our results are, in fact, consistent with recent findings[5] including a self-consistent solution of the spatial variation of the superconducting gap near the interface.

We will use boldface notation for three vectors, $\hat{\ldots}$ for 4×4 matrices, and $\underline{\ldots}$ for 2×2 matrices. Pauli matrices in particle-hole$\times$spin (Nambu) space are denoted as $\hat{\rho}_i$, while Pauli matrices in spin space are written as $\underline{\tau}_i$.

II. THEORETICAL FORMULATION

A. Equations for odd-frequency superconductivity

The frequency dependence of the superconducting order parameter may be naturally taken into account in the approach developed by Eliashberg,[23] where details of the electron-boson interaction are seriously taken. This contrasts with the usual weak-coupling picture where the pairing interaction is taken to be constant. For our purposes, the following Hamiltonian is an appropriate starting point:

$$\hat{H} = \sum_{\alpha} \int d\mathbf{r}\psi_{\alpha}(\mathbf{r})^{\dagger} H_f(\mathbf{r})\psi_{\alpha}(\mathbf{r}) + \int d\mathbf{r} b^{\dagger}(\mathbf{r}) H_b(\mathbf{r}) b(\mathbf{r}) + \sum_{\alpha} \int\int d\mathbf{r}d\mathbf{r}' \mathcal{V}(\mathbf{r}-\mathbf{r}')\psi_{\alpha}^{\dagger}(\mathbf{r})\psi_{\alpha}(\mathbf{r})[b(\mathbf{r}) + b^{\dagger}(\mathbf{r})], \quad (1)$$

where H_f is the Hamiltonian for free fermions, which we assume may be written as $H_f(\mathbf{r}) = -\frac{1}{2m}(\nabla - ie\mathbf{A})^2 - \mu$, while H_b is the Hamiltonian for free bosons. Above, α denotes the spin index, while ψ and b are fermion and boson operators, respectively. Introducing the Fourier transformation $b(\mathbf{r}) = \frac{1}{N}\Sigma_{\mathbf{q}} b_{\mathbf{q}} e^{-i\mathbf{q}\cdot\mathbf{r}}$, where $B_{\mathbf{q}} = b_{\mathbf{q}} + b_{-\mathbf{q}}^{\dagger}$, we obtain the Heisenberg equations of motion,

$$i\partial_t \psi_{\alpha}(\mathbf{r},t) = H_f(\mathbf{r})\psi_{\alpha}(\mathbf{r},t) + \sum_{\mathbf{q}} \zeta(\mathbf{r},t,\mathbf{q})\psi_{\alpha}(\mathbf{r}),$$

$$i\partial_t \psi_{\alpha}^{\dagger}(\mathbf{r},t) = -H_f^{*}(\mathbf{r})\psi_{\alpha}^{\dagger}(\mathbf{r},t) - \sum_{\mathbf{q}} \zeta(\mathbf{r},t,\mathbf{q})\psi_{\alpha}^{\dagger}(\mathbf{r}), \quad (2)$$

where $\zeta(\mathbf{r},t,\mathbf{q}) \equiv \mathcal{V}_{\mathbf{q}} B_{\mathbf{q}}(t) e^{-i\mathbf{q}\cdot\mathbf{r}}$ and $\mathcal{V}_{\mathbf{q}}$ is the Fourier transform of $\mathcal{V}(\mathbf{r}-\mathbf{r}')$. Note that $\mathcal{V}$ is not the effective pairing potential between electrons. Having obtained the time derivatives of the fermion operators, we may now calculate the equation of motion for Green's functions. This procedure is standard and covered, e.g., in Refs. 24–27. Explicitly taking into account the effect of the electron-boson interactions in the Hamiltonian naturally includes a frequency dependence of the effective electron-electron interaction,[23] which is obtained by integrating out the bosonic degrees of freedom in the partition function. The effective electron-electron interaction mediated by a boson excitation may, in general, be written as

$$V(\mathbf{q},\Omega) = \frac{2|\mathcal{V}_{\mathbf{q}}|^2 \omega_{\mathbf{q}}}{\Omega^2 - \omega_{\mathbf{q}}^2}, \quad (3)$$

where $\mathbf{q} = \mathbf{k} - \mathbf{k}'$ and $\Omega = \omega - \omega'$ are the momentum and energy transfers, respectively, of the interaction process. Above, $\omega_{\mathbf{q}}$ is the frequency of the boson propagator. Note that the pairing potential in Eq. (3) is even in Ω, i.e., $V(\mathbf{q},\Omega) = V(\mathbf{q},-\Omega)$. The self-consistency equation for the order parameter quite generally has the following structure:[11]

$$\Delta(\mathbf{k},\omega) \sim \sum_{\mathbf{k}'\omega'} \frac{V(\mathbf{k}-\mathbf{k}',\omega-\omega')\Delta(\mathbf{k}',\omega')}{\varepsilon_{\mathbf{k}}'^2 + \omega'^2}, \quad (4)$$

which may be rewritten as

$$\Delta(\mathbf{k},-\omega) \sim \sum_{\mathbf{k}'\omega'} \frac{V(\mathbf{k}-\mathbf{k}',\omega-\omega')\Delta(\mathbf{k}',-\omega')}{\varepsilon_{\mathbf{k}}'^2 + \omega'^2} \quad (5)$$

by exploiting $V(\mathbf{q},\Omega) = V(\mathbf{q},-\Omega)$. The above equations show that both $\Delta(\mathbf{k},\omega) = \Delta(\mathbf{k},-\omega)$ and $\Delta(\mathbf{k},\omega) = -\Delta(\mathbf{k},-\omega)$ are possible solutions of the gap equation. Therefore, although the pairing interaction is even in frequency, the gap Δ, in principle, may both be even and odd in frequency. In fact, in general, it is a superposition of even- and odd-frequency components.[11,28] However, assuming that the energy transfer is small compared to the term containing the momenta in Eq. (3), $|\Omega| \ll |\omega_{\mathbf{q}}|$, one obtains a part of the pairing potential which is linear in ω and ω' and one that is quadratic in the same quantities.[11] The former part is the necessary ingredient to obtain a superconducting order parameter that is odd in frequency. It is also possible to adopt a purely phenomenological approach to an odd-frequency superconductor by assuming the frequency dependence of the gap *a priori*.[29]

Let us now consider the structure of Green's function matrix for an odd-frequency superconductor. It is instructive to briefly mention the result for an ordinary BCS superconductor, which has an even frequency-singlet-even (ESE) parity symmetry. In the BCS case, one obtains

$$\left(i\frac{\partial}{\partial t_1}\hat{\rho}_3 - \hat{\xi} - \hat{\Delta}(\mathbf{r}_1)\right)\hat{G}^{\mathrm{R}}(1,2) = \delta(1-2)\check{1}. \quad (6)$$

Assuming a homogeneous and isotropic system where Green's function only depends on the relative coordinates $t = t_1 - t_2$ and $\mathbf{r} = \mathbf{r}_1 - \mathbf{r}_2$ and where $\hat{\Delta}(\mathbf{r}_1) = \hat{\Delta}$ is a constant, one may Fourier transform Eq. (6) according to $\hat{G}^R(\mathbf{p},\varepsilon) = \int\int d\mathbf{r}e^{-i\mathbf{p}\mathbf{r}} dt e^{i\varepsilon t}\hat{G}^R(\mathbf{r},t)$, where ε and $\mathbf{p}$ is the quasiparticle energy measured from the Fermi level and the momentum, respectively. We then obtain

$$(\varepsilon\hat{\rho}_3 - \hat{\xi}_{\mathbf{p}} - \hat{\Delta})\hat{G}^{\mathrm{R}}(\mathbf{p},\varepsilon) = \hat{1}, \quad (7)$$

which, upon matrix inversion, yields the well-known BCS solution. The quasiclassical Green's functions $\check{g}(\mathbf{p}_F,\mathbf{r};\varepsilon,t)$ is obtained from the Gor'kov Green's functions $\check{G}(\mathbf{p},\mathbf{r};\varepsilon,t)$ by integrating out the dependence on kinetic energy, assuming that $\check{G}$ is strongly peaked at the Fermi level,

$$\check{g}(\mathbf{p}_F,\mathbf{r};\varepsilon,t) = \frac{i}{\pi}\int d\xi_{\mathbf{p}}\check{G}(\mathbf{p},\mathbf{r};\varepsilon,t). \quad (8)$$

The above assumption is typically applicable to superconducting systems where the characteristic length scale of the perturbations present, namely, superconducting coherence length, is much larger than the Fermi wavelength. The cor-

responding characteristic energies of such phenomena must be much smaller than the Fermi energy ε_F. The quasiclassical Green's functions may be divided into advanced (A), retarded (R), and Keldysh (K) components, each of which has a 4×4 matrix structure in the combined particle-hole and spin spaces. One has

$$\check{g} = \begin{pmatrix} \hat{g}^R & \hat{g}^K \\ 0 & \hat{g}^A \end{pmatrix}, \tag{9}$$

where the elements of $\check{g}(\mathbf{p}_F, \mathbf{r}; \varepsilon, t)$ read

$$\hat{g}^{R,A} = \begin{pmatrix} \underline{g}^{R,A} & \underline{f}^{R,A} \\ -\underline{\tilde{f}}^{R,A} & -\underline{\tilde{g}}^{R,A} \end{pmatrix}, \quad \hat{g}^K = \begin{pmatrix} \underline{g}^K & \underline{f}^K \\ \underline{\tilde{f}}^K & \underline{\tilde{g}}^K \end{pmatrix}. \tag{10}$$

The quantities $\underline{g}$ and $\underline{f}$ are 2×2 spin matrices, with the structure

$$\underline{g} = \begin{pmatrix} g_{\uparrow\uparrow} & g_{\uparrow\downarrow} \\ g_{\downarrow\uparrow} & g_{\downarrow\downarrow} \end{pmatrix}. \tag{11}$$

Due to internal symmetry relations between these Green's functions, all of these quantities are not independent. In particular, the tilde operation is defined as

$$\tilde{f}(\mathbf{p}_F, \mathbf{r}; \varepsilon, t) = f(-\mathbf{p}_F, \mathbf{r}; -\varepsilon, t)^*. \tag{12}$$

For a bulk s-wave superconductor, the retarded part may be expressed in terms of the normal and anomalous Green's functions g and f as follows:

$$\hat{g}^R = \begin{pmatrix} g\underline{1} & fi\underline{\tau}_2 e^{i\chi} \\ fi\underline{\tau}_2 e^{-i\chi} & -g\underline{1} \end{pmatrix}, \tag{13}$$

Here, χ is the globally broken U(1) phase associated with the spontaneous symmetry breaking of the superconducting state. In the odd-frequency case, however, one finally arrives at

$$[\varepsilon\hat{\rho}_3 - \hat{\xi}_{\mathbf{p}} - \hat{\Delta}(\varepsilon)]\hat{G}^R(\mathbf{p}, \varepsilon) = \hat{1}, \tag{14}$$

where now $\hat{\Delta}(\varepsilon)$ is the odd-frequency gap matrix. Note that Eq. (14) is equivalent to the well-known Eliashberg equation. The structure of the Green's function for an odd-frequency superconductor may be different from Eq. (13) depending on the spin symmetry. For instance, the bulk Green's function matrix for an odd-frequency spin-triplet even-parity superconductor has the following structure:

$$\hat{g}^R = \begin{pmatrix} g\underline{1} & f\underline{\tau}_1 e^{i\chi} \\ -f\underline{\tau}_1 e^{-i\chi} & -g\underline{1} \end{pmatrix}. \tag{15}$$

Performing a quasiclassical approximation on Eq. (14) yields the Eilenberger equation, which reduces to the Usadel equation in the dirty limit. Note that for both even- and odd-frequency superconducting order parameters, the pairing interaction itself is always even in the frequency coordinate.

A quite general formalism for treating quantum transport in the nonuniform superconducting systems, e.g., normal/superconductor heterostructures, was developed by Tanaka *et al.*[30] For instance, the conductance spectra of a normal/superconductor junction may be obtained along the lines of Refs. 30 and 31 by numerically solving the Usadel equation using Nazarov's generalized boundary conditions.[10] Interestingly, taking the limit $R_d \to 0$ and $\theta \to 0$ in this formalism, where R_d represents the resistance of the normal metal region and θ is a measure of the proximity effect, leads to the well-known expression for the conductance obtained in the BTK formalism.[16] This may be specifically seen for the electrical conductance by consulting Eqs. (15) and (16) in Ref. 30, and for the thermal conductance in Eq. (19) of Ref. 31. Therefore, since the above treatment of the Eliashberg equation shows that the odd-frequency dependence of the gap may be taken into account simply by substituting $\Delta \to \Delta(\varepsilon)$, quantum transport for an odd-frequency superconductor can be treated in the BTK formalism by performing the same substitution. However, the derivation of the Bogolioubov–de Gennes equation for odd-frequency superconductivity is challenging since it is not obvious how to take into account the strong retardation effects of the pairing potential.

B. Transport formalism

We adopt the Keldysh formalism by using Nazarov's generalized boundary conditions[10] to obtain the electrical and thermal conductance for odd-frequency superconductors. We assume, without loss of generality, that the gap $\Delta(\varepsilon, \vartheta)$ has an opposite-spin pairing symmetry in both the singlet and triplet cases. To encompass accessible experimental techniques, we will focus on two experimentally accessible quantities that encode how the odd-frequency pairing symmetry is manifested in transport properties: namely, the normalized charge conductance $G(eV)$ for $T=0$ and the thermal conductance $\kappa(T)$. The procedure for obtaining these quantities is treated in detail in Refs. 30–32. In the limit of zero resistance in the normal part and vanishing proximity effect, one finds

$$G = \frac{1}{G_{\mathrm{N}}}\int_{-\pi/2}^{\pi/2} d\vartheta \cos\vartheta \Gamma_+(\mathrm{eV}, \vartheta),$$

$$\kappa = \int_{-\pi/2}^{\pi/2}\int_{-\infty}^{\infty} d\vartheta d\varepsilon \frac{\varepsilon^2\beta^2\Gamma_-(\mathrm{eV}, \vartheta)}{4\Delta_0 \cosh^2(\beta\varepsilon)(\cos\vartheta)^{-1}}, \tag{16}$$

where G_N is the normal-state conductance and we have defined

$$\Gamma_\alpha(\varepsilon, \vartheta) = 1 + \alpha\left|\frac{4\Omega_-\tilde{\Omega}_+ e^{-i\gamma_+}}{\Omega_+\Omega_-(4 - Z_\vartheta^2) + Z_\vartheta^2\tilde{\Omega}_+\tilde{\Omega}_- e^{i(\gamma_- - \gamma_+)}}\right|^2 - \left|\frac{2[\Omega_+\Omega_-(2 + Z_\vartheta) - Z_\vartheta\tilde{\Omega}_+\tilde{\Omega}_- e^{i(\gamma_- - \gamma_+)}]}{\Omega_+\Omega_-(4 - Z_\vartheta^2) + Z_\vartheta^2\tilde{\Omega}_+\tilde{\Omega}_- e^{i(\gamma_- - \gamma_+)}} - 1\right|^2. \tag{17}$$

Above, we have introduced $\vartheta_+ = \vartheta$, $\vartheta_- = \pi - \vartheta$, and $\Omega_\pm = \sqrt{(1 + \mathrm{sign}(\varepsilon)/g_\pm)/2}$, where $\mathrm{sign}(\varepsilon) \to -\mathrm{sign}(\varepsilon)$ for $\Omega \to \tilde{\Omega}$. The phase of the superconducting gap is contained in the factor $e^{i\gamma_\pm} = e^{i\chi(\vartheta_\pm)} = f_\pm/|f_\pm|$. The quantities $g_\pm$ and $f_\pm$ are the asymptotic values of the normal and anomalous Green's functions of the odd-frequency superconductor in a gauge where the superconducting order parameter is real: $g_\pm$

TABLE I. Overview of the specific gap forms will be considered in this paper. We model the temperature dependence of $A(T)$ with $A(T)=A_0 \tanh(1.74\sqrt{T_c/T-1})$ and $T_c=\Delta_0/1.76$.

Symmetry	Specific gap form $\Delta(\varepsilon,\vartheta,T)$
ESE	$A(T)\Delta_0$
OTE	$A(T)\varepsilon/[1+(\varepsilon/\Delta_0)^2]$
OSO	$A(T)\varepsilon\cos(\vartheta-\alpha)/[1+(\varepsilon/\Delta_0)^2]$
ETO	$A(T)\Delta_0\cos(\vartheta-\alpha)/[1+(\varepsilon/\Delta_0)^2]$

$=\varepsilon/\sqrt{\varepsilon^2-|\Delta(\varepsilon,\vartheta_\pm)|^2}$ and $f_\pm=\Delta(\varepsilon,\vartheta_\pm)/\sqrt{|\Delta(\varepsilon,\vartheta_\pm)|^2-\varepsilon^2}$. We have introduced $Z_\vartheta=-iZ/\cos\vartheta$, where Z denotes the strength of the scattering potential near the barrier. In what follows, we fix $Z=3$, which corresponds to a typical low-transparency barrier, which is experimentally realistic. Note that in the expression for κ, we have considered the linear response regime for a small temperature gradient in the system and introduced $\beta=1/T$, where T is the temperature of the reservoirs.

III. RESULTS AND DISCUSSION

Depending on the symmetries with respect to the sign inversion of frequency and momentum corresponding to $\varepsilon\to(-\varepsilon)$ and $\vartheta\to\pi+\vartheta$, the gap may be classified, as seen in Table I. In each case, we will model the gap $\Delta(\varepsilon,\vartheta,T)$, as illustrated in Table I. In the angular dependence of the odd-parity gaps, α denotes the misorientation angle between the antinodes and the interface normal (see Fig. 1). The motivation for modeling the frequency dependence of the superconducting gap, as we have done in Table I, is that it features the low-energy behavior, of the proximity-induced odd-frequency gap in dirty ferromagnet/superconductor structures[33] and that it exhibits a similar energy dependence to the gap seen in strongly correlated electron systems considered in Ref. 13.

Recently, it was demonstrated that the odd-frequency pairing is quite generally induced near the normal/superconductor interface by a fully self-consistent calculation of the superconducting correlations.[5] In an even-frequency-triplet-odd parity (ETO) superconductor with $\alpha=0$ corresponding to the perfect formation of zero-energy states, an odd-frequency-triplet-even parity (OTE) pairing is induced near the surface. Thus, the formation of zero-energy states may be reinterpreted as a manifestation of the odd-frequency superconductivity near the interface. The odd-frequency symmetry may permit the existence of gapless single-particle excitations at the Fermi level. On the other hand, when the nodal direction is parallel to the interface normal ($\alpha=\pi/2$), only the even-frequency states exist at the interface.

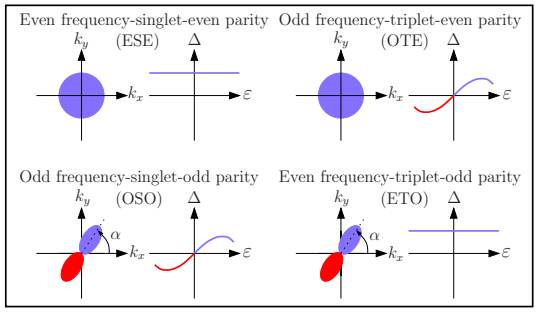

FIG. 1. (Color online) Overview of the different symmetry states will be considered in the superconducting part of the clean two-dimensional normal/superconductor junction.

In a similar manner, the odd-frequency-singlet-odd parity (OSO) pairing state can be induced near the interface of a clean normal/superconductor junction when the superconductor has an ESE symmetry. One may also apply this discussion to bulk odd-frequency superconducting states. In this scenario, the ETO (ESE) pairing can be induced at the interface for an OTE (OSO) bulk superconductor.[5] This should have clear observable consequences for the quantum transport properties of a normal/odd-frequency superconductor junction. We now proceed to investigate this in further detail.

Consider first the left column of Fig. 2 where we have plotted G as a function of bias voltage for the even-parity symmetries. In the even-frequency case, the usual singularity at $eV=A_0\Delta_0$ is present. In the odd-frequency case, we see a qualitatively different behavior of the conductance. First of all, G at low bias voltage is greatly enhanced compared to the even-frequency case for $A_0<1$, and the formation of a zero-bias conductance peak is clearly seen at $A_0=1$. For $A_0>1$, the conductance is similar to the even-frequency case for a reduced value of the gap. This may be understood as

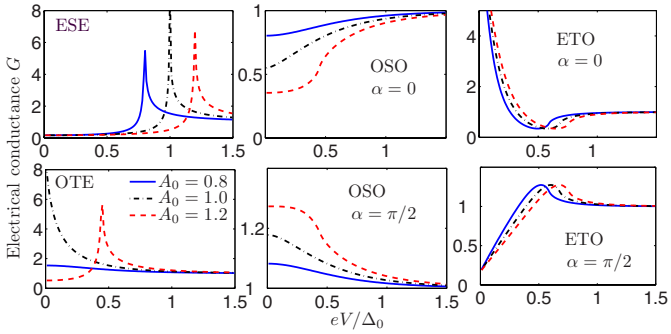

FIG. 2. (Color online) Plot of G for isotropic, even-parity superconductors, and odd-parity superconductors for both even- and odd-frequency pairing.

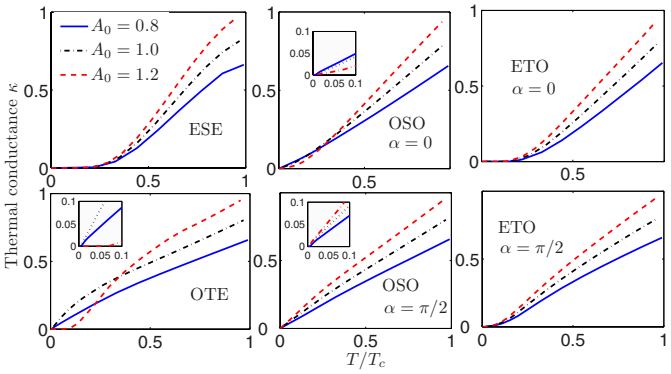

FIG. 3. (Color online) Plot of κ for isotropic, even-parity superconductors, and odd-parity superconductors for both even- and odd-frequency pairings. A power-law dependence with an exponent of $\simeq 1$ is observed for both of the odd-frequency symmetries (see insets).

follows. For $A_0 < 1$, the inequality $\varepsilon > \Delta(\varepsilon)$ is satisfied for all ε with our choice of gaps (Table I). This corresponds to gapless superconductivity. For $A_0 > 1$, the gap becomes larger than ε below a certain (finite) value of ε, which is similar to the BCS gap.

The middle and right columns of Fig. 2 shows G as a function of bias voltage for the odd-parity symmetries. In the OSO case, a gaplike structure is seen at $\alpha = 0$. This is because ESE pairing is induced near the interface due to the sign change of the pair potential.[5] This ESE pairing is responsible for the gaplike structure of the conductance spectra, which is similar to the ESE case in Fig. 2. In contrast, OSO pairing remains near the interface at $\alpha = \pi/2$. Thus, a zero-bias conductance peak is seen. On the other hand, in the ETO case at $\alpha = 0$, a zero-bias conductance peak appears due to the induced OTE pairing near the interface,[5] which is similar to the OTE case in Fig. 2. At $\alpha = \pi/2$, ETO pairing survives near the interface, and hence, the even frequency character of the pair amplitude results in a V-like shape of the spectra. Interestingly, OSO and ETO cases have the opposite tendency although their ϑ dependencies are the same. Furthermore, the sign change of the gap produces a qualitative difference in the spectra between OTE and OSO with $\alpha = 0$ junctions. Thus, G is phase sensitive not only in the even-frequency superconductor junctions[17] but also in odd-frequency superconductor junctions.

Next, we investigate the thermal conductance κ, as shown in Fig. 3. The left column corresponds to the even, parity case, where the usual exponential dependence on T is recovered for the ESE case.[34] In the OTE case, κ mimics the ESE case for $A_0 > 1$ as it does for the charge conductance. Otherwise, power-law dependence with exponent of $\simeq 1$ is observed due to the node of the gap at zero energy. Thus, the nodes in the frequency domain of an isotropic odd-frequency superconductor cause κ to behave as it does in an anisotropic even-frequency superconductor. In the middle and right columns of Fig. 3, we give κ in the odd-parity case. The well-known result of the exponential dependence for $\alpha = 0$ is recovered in the ETO case. The OSO case again displays power-law behavior that is similar to the OTE case for $A_0 < 1$. However, the exponential dependence again occurs for $A_0 > 1$ in the OSO case with $\alpha = 0$. When $\alpha = \pi/2$, there is an exclusively power-law dependence with exponent of $\simeq 1$. While the OTE case only has nodes in energy, the OSO case has both nodes in energy and in $\mathbf{k}$ space, but this does not appear to influence the exponent of the power-law dependence.

IV. SUMMARY

In summary, we have studied quantum transport in a normal metal/superconductor junction, by considering how a bulk odd-frequency symmetry in the superconductor is manifested in the electrical and thermal conductances of the junction. The odd-frequency symmetry is found to qualitatively display distinct behavior from the even-frequency case. This reflects the fact that the electrical conductance is sensitive to the presence of odd-frequency pairing at the interface, whereas the low temperature behavior of the thermal conductance reflects the node of the gap in the frequency domain. Moreover, one may distinguish the even- and odd-parity cases for an odd-frequency symmetry (OTE and OSO, respectively) by means of their different characteristic tunneling spectra. Our predictions should be useful for a wide range of experimental techniques and are thus a helpful tool in identifying the possible existence of the bulk odd-frequency superconductors with $CeCu_2Si_2$ and $CeRhIn_5$, which currently present themselves as the most promising candidates.

ACKNOWLEDGMENTS

J.L. and A.S. were supported by the Research Council of Norway under Grants No. 158518/431, No. 158547/431 (NANOMAT), and No. 167498/V30 (STORFORSK). T.Y. acknowledges support by JSPS. T.Y and Y.T were supported by Grant-in-Aid for Scientific Research (Grant No. 17071007) from the Ministry of Education, Culture, Sports, Science and Technology of Japan. The authors acknowledge A. Balatsky for helpful comments. Y.T. would like to thank K. Miyake, H. Kohno, and Y. Fuseya for their valuable discussions. J.L. acknowledges K. Yada for clarifying comments on the odd-frequency pairing potential.

[1] F. S. Bergeret, A. F. Volkov, and K. B. Efetov, Phys. Rev. Lett. **86**, 4096 (2001); A. F. Volkov, F. S. Bergeret, and K. B. Efetov, *ibid.* **90**, 117006 (2003).
[2] V. L. Berezinskii, JETP Lett. **20**, 287 (1974).
[3] R. S. Keizer, S. T. B. Goennenwein, T. M. Klapwijk, G. Miao, G. Xiao, and A. Gupta, Nature (London) **439**, 825 (2006); I. Sosnin, H. Cho, V. T. Petrashov, and A. F. Volkov, Phys. Rev. Lett. **96**, 157002 (2006).
[4] V. Braude and Yu. V. Nazarov, Phys. Rev. Lett. **98**, 077003 (2007); Y. Asano, Y. Tanaka, and A. A. Golubov, *ibid.* **98**, 107002 (2007).
[5] Y. Tanaka, A. A. Golubov, S. Kashiwaya, and M. Ueda, Phys. Rev. Lett. **99**, 037005 (2007).
[6] M. Eschrig, T. Lofwander, Th. Champel, J. C. Cuevas, and G. Schon, J. Low Temp. Phys. **147**, 457 (2007).
[7] Y. Tanaka, Y. Tanuma, and A. A. Golubov, Phys. Rev. B **76**, 054522 (2007).
[8] Y. Asano, Y. Tanaka, A. A. Golubov, and S. Kashiwaya, Phys. Rev. Lett. **99**, 067005 (2007).
[9] Y. Tanaka, Y. V. Nazarov, A. A. Golubov, and S. Kashiwaya, Phys. Rev. B **69**, 144519 (2004); Y. Tanaka and S. Kashiwaya, *ibid.* **70**, 012507 (2004); Y. Tanaka, S. Kashiwaya, and T. Yokoyama, *ibid.* **71**, 094513 (2005).
[10] Y. Tanaka, Yu. V. Nazarov, and S. Kashiwaya, Phys. Rev. Lett. **90**, 167003 (2003).
[11] A. Balatsky and E. Abrahams, Phys. Rev. B **45**, 13125 (1992); E. Abrahams, A. Balatsky, D. J. Scalapino, and J. R. Schrieffer, *ibid.* **52**, 1271 (1995).
[12] P. Coleman, E. Miranda, and A. Tsvelik, Phys. Rev. B **49**, 8955 (1994); P. Coleman, A. Georges, and A. M. Tsvelik, J. Phys.: Condens. Matter **9**, 345 (1997).
[13] Y. Fuseya, H. Kohno, and K. Miyake, J. Phys. Soc. Jpn. **72**, 2914 (2003); G. Q. Zheng, N. Yamaguchi, H. Kan, Y. Kitaoka, J. L. Sarrao, P. G. Pagliuso, N. O. Moreno, and J. D. Thompson, Phys. Rev. B **70**, 014511 (2004); S. Kawasaki, T. Mito, Y. Kawasaki, G.-q. Zheng, Y. Kitaoka, D. Aoki, Y. Haga, and Y. Onuki, Phys. Rev. Lett. **91**, 137001 (2003).
[14] Y. Tanaka and A. A. Golubov, Phys. Rev. Lett. **98**, 037003 (2007); Ya. V. Fominov, JETP Lett. **86**, 732 (2007) [Pis'ma v ZhETF **86**, 842 (2007)].
[15] J. Linder, T. Yokoyama, and A. Sudbø, arXiv:0712.0134, Phys. Rev. (to be published).
[16] G. E. Blonder, M. Tinkham, and T. M. Klapwijk, Phys. Rev. B **25**, 4515 (1982).
[17] Y. Tanaka and S. Kashiwaya, Phys. Rev. Lett. **74**, 3451 (1995); Y. Tanuma, Y. Tanaka, and S. Kashiwaya, Phys. Rev. B **64**, 214519 (2001).
[18] Y. Kasahara, Y. Nakajima, K. Izawa, Y. Matsuda, K. Behnia, H. Shishido, R. Settai, and Y. Onuki, Phys. Rev. B **72**, 214515 (2005).
[19] G. Seyfarth, J. P. Brison, M.-A. Méasson, J. Flouquet, K. Izawa, Y. Matsuda, H. Sugawara, and H. Sato, Phys. Rev. Lett. **95**, 107004 (2005).
[20] J. Y. T. Wei, N.-C. Yeh, D. F. Garrigus, and M. Strasik, Phys. Rev. Lett. **81**, 2542 (1998).
[21] E. V. Bezuglyi and V. Vinokur, Phys. Rev. Lett. **91**, 137002 (2003).
[22] L. J. Buchholtz and G. Zwicknagl, Phys. Rev. B **23**, 5788 (1981); J. Hara and K. Nagai, Prog. Theor. Phys. **74**, 1237 (1986); C.-R. Hu, Phys. Rev. Lett. **72**, 1526 (1994).
[23] G. M. Eliashberg, Zh. Eksp. Teor. Fiz. **38**, 966 (1960).
[24] J. W. Serene and D. Rainer, Phys. Rep. **101**, 221 (1983).
[25] N. Kopnin, *Theory of Nonequilibrium Superconductivity* (Oxford University Press, New York, 2001).
[26] J. Rammer and H. Smith, Rev. Mod. Phys. **58**, 323 (1986).
[27] A. M. Zagoskin, *Quantum Theory of Many-Body Systems* (Springer, 1998).
[28] M. Vojta and E. Dagotto, Phys. Rev. B **59**, R713 (1999).
[29] J. E. Bunder and K. B. Efetov, Phys. Rev. B **70**, 134522 (2004).
[30] Y. Tanaka, A. A. Golubov, and S. Kashiwaya, Phys. Rev. B **68**, 054513 (2003).
[31] T. Yokoyama, Y. Tanaka, A. A. Golubov, and Y. Asano, Phys. Rev. B **72**, 214513 (2005).
[32] T. Yokoyama, Y. Tanaka, A. A. Golubov, J. Inoue, and Y. Asano, Phys. Rev. B **71**, 094506 (2005).
[33] Ya. V. Fominov, A. F. Volkov, and K. B. Efetov, Phys. Rev. B **75**, 104509 (2007).
[34] A. F. Andreev, Sov. Phys. JETP **19**, 1228 (1964).

Paper XII

Identifying the odd-frequency superconducting state by a field-induced Josephson effect.

Physical Review B **77**, 174507 (2008).

PHYSICAL REVIEW B **77**, 174507 (2008)

Identifying the odd-frequency pairing state of superconductors by a field-induced Josephson effect

Jacob Linder,[1] Takehito Yokoyama,[2] and Asle Sudbø[1]
[1]*Department of Physics, Norwegian University of Science and Technology, N-7491 Trondheim, Norway*
[2]*Department of Applied Physics, Nagoya University, Nagoya 464-8603, Japan*
(Received 8 November 2007; revised manuscript received 14 April 2008; published 12 May 2008)

Superconducting order parameters that are odd under exchange of time coordinates of the electrons constituting a Cooper pair are potentially of great importance both conceptually and technologically. Recent experiments report that such an odd-frequency superconducting *bulk* state may be realized in certain heavy-fermion compounds. While the Josephson current normally only flows between superconductors with the same symmetries with respect to frequency, we demonstrate that an exchange field may induce a current between diffusive even- and odd-frequency superconductors. This suggests a way to identify the possible existence of bulk odd-frequency superconductors.

DOI: 10.1103/PhysRevB.77.174507 PACS number(s): 74.20.Rp, 74.25.Fy, 74.45.+c, 74.50.+r

I. INTRODUCTION

The prevalent symmetry in known superconductors may be described as odd under exchange of spin coordinates and even under an exchange of spatial coordinates or an exchange of time coordinates of the electrons constituting the Cooper pair. The latter condition corresponds to a sign change in frequency after Fourier transforming the time variables to a frequency representation. This symmetry may compactly be expressed as an even-frequency singlet even-parity superconducting state (hereafter referred to as the even-frequency state).

However, other types of pairing are also permitted. Among these is the so-called odd-frequency pairing state.[1] Such a state is potentially of great importance, both from a conceptual as well as a technological point of view. From a conceptual point of view, phase transitions involving pairing of fermions form centerpieces of physics in such widely disparate subdisciplines such as cosmology, astrophysics, physics of condensed matter, physics of extremely dilute ultracold atomic gases, and physics of extremely compressed quantum liquids. Extending the possible pairing states compatible with the Pauli principle will likely have impact on all of these disciplines and hence deserves attention. From a technological point of view, an odd-frequency pairing state would be a candidate for a robust superconducting pairing state capable of coexisting with ferromagnetism.[2] Such a material would be extremely important, since it would combine two functionalities of major importance, namely, magnetism and superconductivity.

The hope of experimentally detecting this type of pairing was raised by the prediction that an odd-frequency triplet even-parity (hereafter simply denoted as odd-frequency) pairing should be induced by the proximity effect in diffusive ferromagnet/conventional superconductor junctions.[3] Recently, odd-frequency states due to the proximity effect have been confirmed in experiments of diffusive ferromagnet/conventional superconductor junctions.[4] To date, no bulk odd-frequency superconductor has been unambiguously identified.

Currently, the heavy-fermion compounds $CeCu_2Si_2$ and $CeRhIn_5$ seem to be the most promising candidates for the realization of a bulk odd-frequency state.[5] It has also recently been argued[6] that this type of pairing could be realized in Na_xCoO_2, which is motivated by the band-structure calculations and the robustness of its superconductivity against impurities. However, the experimental reports on the Knight-shift data have shown evidence of both singlet[7] and triplet[8] pairings. To resolve the pairing issue, it would be desirable to make clear-cut theoretical predictions for experimentally measurable quantities that may distinguish the odd-frequency symmetry from the conventional even-frequency symmetry. Motivated by this, the conductance of a normal metal (N)/odd-frequency junction was very recently studied in both the diffusive[9] and clean[10] regimes.

It is well known that the Josephson current between superconductors with different symmetries is in general inhibited.[11] However, it was very recently shown that in the clean limit, such a Josephson coupling may be established between such superconductors by means of surface-induced pairing components of different symmetry than the bulk state in each superconductor.[12] In the dirty limit, it has been demonstrated that in the case of an s-wave even- or odd-frequency bulk superconductor, the proximity-induced pairing component in the N will have the same symmetry.[13] These results are valid in the absence of an exchange field. Due to the above mentioned properties, one would consequently expect that both the even- and odd-frequency symmetries are induced in the normal part of an even-frequency/N/odd-frequency junction. While this is true, the Josephson current is found to vanish in such a setup. If the N is replaced with a diffusive ferromagnet (F), the pairing components in the F will have the same symmetries as in the N case. Surprisingly, the Josephson current is *not* absent in this case.

In this paper, we report that a Josephson current may flow in a diffusive even-frequency/F/odd-frequency junction and argue that this should serve as a *smoking gun* to reveal the odd-frequency symmetry in a bulk superconductor. We also study the dependence of the Josephson current on the temperature and width of the F and show that 0-π transitions take place. In the following, we will use boldface notation for three vectors, $\check{\ldots}$ for 8×8 matrices, $\hat{\ldots}$ for 4×4 matrices, and $\underline{\ldots}$ for 2×2 matrices.

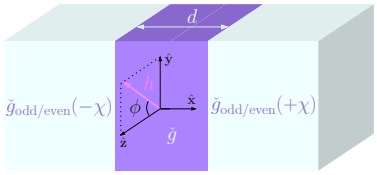

FIG. 1. (Color online) A diffusive metal, which may be either normal or ferromagnetic (with exchange field h) of width d, separates two superconductors with a phase difference 2χ, thus constituting a Josephson current. The individual superconductors have either an even-frequency or odd-frequency bulk symmetry. The exchange field may have any orientation in the yz plane, which is characterized by the angle ϕ.

II. THEORETICAL FRAMEWORK

In order to address this problem, we employ the quasiclassical theory of superconductivity by using the Keldysh formalism. The quasiclassical Green's functions may be divided into an advanced (A), a retarded (R), and a Keldysh (K) component, each of which has a 4×4 matrix structure in the combined particle hole and spin space. In thermal equilibrium, it suffices to consider the retarded component since the advanced component is obtained by $\hat{g}^A=-(\hat{\rho}_3\hat{g}^R\hat{\rho}_3)^\dagger$, while the Keldysh component is given by $\hat{g}^K=(\hat{g}^R-\hat{g}^A)\tanh(\beta\varepsilon/2)$, where β is inverse temperature. The Pauli matrices in particle hole $\times$ spin (Nambu) space are denoted as $\hat{\rho}_i$, while the Pauli matrices in spin space are written as $\underline{\tau}_i$, where $i=1,2,3$. As shown in Ref. 13, the symmetry of the anomalous Green's function induced in the N through the proximity effect by an odd-frequency superconductor is also odd-frequency and similarly for an even-frequency superconductor. We may write the retarded Green's function in the superconductors as

$$\hat{g}^R_{\mathrm{odd/even}}=\begin{pmatrix} c\underline{1} & se^{\mp i\chi}\underline{\tau}_1/se^{\mp i\chi}i\underline{\tau}_2 \\ -se^{\mp i\chi}\underline{\tau}_1/se^{\mp i\chi}i\underline{\tau}_2 & -c\underline{1}\end{pmatrix} \quad (1)$$

for an odd-frequency triplet even-parity s-wave symmetry/even-frequency singlet even-parity s-wave symmetry. Above, we have defined

$$c\equiv\cosh(\theta),\quad s\equiv\sinh(\theta),\quad \theta\equiv\operatorname{arctanh}[\Delta(\varepsilon)/\varepsilon], \quad (2)$$

where ε is the quasiparticle energy measured from the Fermi level, while χ is the superconducting phase associated with the broken $U(1)$ symmetry. The $\pm$ sign refers to the right and left sides of the F (Fig. 1). The retarded Green's function in the F satisfies the Usadel equation,[14]

$$D\nabla(\hat{g}^R\nabla\hat{g}^R)+i[\varepsilon\hat{\tau}_3+\hat{M},\hat{g}^R]=0,$$

$$\hat{M}=h\begin{pmatrix}\cos\phi\underline{\tau}_3+\sin\phi\underline{\tau}_2 & \underline{0} \\ \underline{0} & (\cos\phi\underline{\tau}_3+\sin\phi\underline{\tau}_2)^{\mathcal{T}}\end{pmatrix}, \quad (3)$$

where D is the diffusion constant, h is the exchange field, and $\mathcal{T}$ denotes the matrix transpose. An analytical of this equation is permissible when it may be linearized, which corresponds to a weak-proximity effect. This may be obtained in two limiting cases: (1) if the barriers have low transparency or (2) if the transmission is perfect (ideal interfaces) and the temperature in the superconducting reservoir is close to T_c, such that $|\Delta|$ is small. Here, we will mainly focus on the low-transparency case,[15] since it might be difficult to experimentally realize small and highly transparent junctions for observing the Josephson current. In this case, we make use of the standard Kupriyanov–Lukichev boundary conditions,[16]

$$2\gamma d(\hat{g}\partial_x\hat{g})=\pm[\hat{g},\hat{g}_{R(L)}(\pm\chi)]|_{x=d,0}, \quad (4)$$

where γ is a measure of the barrier strength and $\hat{g}_{R(L)}$ denotes the Green's function in the superconductor on the right ($x=d$) or left ($x=0$) side of the F, respectively. Defining the vector anomalous Green's function,

$$\mathbf{f}=[f_\downarrow-f_\uparrow,-\mathrm{i}(f_\uparrow+f_\downarrow),2f_t]/2. \quad (5)$$

and the matrix anomalous Green's function in spin space,

$$\underline{f}=(f_s+\mathbf{f}\cdot\underline{\tau})i\underline{\tau}_2=\begin{pmatrix}f_\uparrow & f_t+f_s \\ f_t-f_s & f_\downarrow\end{pmatrix}, \quad (6)$$

the linearized Green's function in the F reads in total

$$\hat{g}^R=\begin{pmatrix}\underline{1} & \underline{f}(\varepsilon) \\ -[\underline{f}(-\varepsilon)]^* & -\underline{1}\end{pmatrix}. \quad (7)$$

Note that Eq. (7) contains both equal-spin- and opposite-spin-pairing triplet components in general. In the special cases of $\phi=0$ and $\phi=\pi$, the equal-spin-pairing components f_σ ($\sigma=\uparrow,\downarrow$) vanish.

III. RESULTS

We now provide the analytical results for the Josephson current in an even-frequency/F/odd-frequency junction. To begin with, we will consider the case $\phi=0$ to emphasize our main result: namely, a *field-induced* Josephson effect. We will then investigate the effect of a change in orientation of the magnetization in the ferromagnetic layer. Changing the orientation, i.e., ϕ, in an even-frequency/F/even-frequency junction has no effect since the order parameters in the superconductors in that case are isotropic. However, for an odd-frequency triplet superconductor, the order parameter has a direction in spin space. Here, we consider an opposite-spin-pairing $S_z=0$ order parameter without loss of generality and then proceed to vary the orientation of the exchange field.

A. Field-induced Josephson current

For $\phi=0$, one readily finds that $f_\sigma=0$. The linearized version of equation Eq. (3) is then given by

$$D\partial_x^2 f_\pm+2i(\varepsilon\pm h)f_\pm=0, \quad (8)$$

with the general solution

$$f_\pm(x)=A_\pm e^{ik_\pm x}+B_\pm e^{-ik_\pm x},$$

$$k_{\pm} = \sqrt{2i(\varepsilon \pm h)/D}, \tag{9}$$

with the definition $f_{\pm}=f_t \pm f_s$. Employing the boundary conditions, one finds that the anomalous Green's function reads

$$f_{\pm} = \frac{B_{\pm}(c_L+\rho_{\pm}) \mp s_L e^{-i\chi}}{(\rho_{\pm}-c_L)e^{-ik_{\pm}x}} + B_{\pm}e^{-ik_{\pm}x}, \tag{10}$$

where we have introduced the auxiliary quantity

$$\begin{aligned} B_{\pm} = &[s_R e^{i\chi} \pm s_L e^{i(k_{\pm}d-\chi)}(\rho_{\pm}+c_R)/(\rho_{\pm}-c_L)] \\ &\times [e^{ik_{\pm}d}(\rho_{\pm}+c_L)(\rho_{\pm}+c_R)/(\rho_{\pm}-c_L) \\ &- e^{-ik_{\pm}d}(\rho_{\pm}-c_R)]^{-1}. \end{aligned} \tag{11}$$

Moreover, we have introduced $\rho_{\pm}=\gamma d i k_{\pm}$ while the subscripts L and R denote the left and right superconductors for the coefficients c and s. Once $\hat{g}^R$ has been obtained, the Josephson current may be calculated by the formula

$$\begin{aligned} \mathbf{j}(x) &= -(N_F e D \hat{\mathbf{x}}/4)\int d\varepsilon \ \mathrm{Tr}\{\hat{\rho}_3(\check{g}\partial_x \check{g})^K\} \\ &= -(N_F e D \hat{\mathbf{x}}/2)\int_{-\infty}^{\infty} d\varepsilon \ \mathrm{Re}\{M_+(\varepsilon)+M_-(\varepsilon)\} \times \tanh(\beta\varepsilon/2), \end{aligned} \tag{12}$$

with the definition

$$M_{\pm}(\varepsilon) = [f_{\pm}(-\varepsilon)]^* \partial_x f_{\mp}(\varepsilon) - f_{\pm}(\varepsilon)\partial_x [f_{\mp}(-\varepsilon)]^*. \tag{13}$$

The normalized current density is defined as

$$I(\chi)/I_0 = 4|\mathbf{j}(x,\chi)|/(N_F e D \Delta_0^2), \tag{14}$$

which is independent of x for $x \in [0,d]$, and the critical current is given by $I_c=I(\frac{\pi}{4})$.

At this point, we are in a position to compare the results for the even- and odd-frequency case against each other to investigate how the different symmetry properties alter the Josephson current. Similarly to Ref. 13, we will model the odd-frequency gap by

$$\Delta(\varepsilon) = \varepsilon/[1+(\varepsilon/\Delta_0)^n], \tag{15}$$

where $n=2,4,8,\ldots$, which exhibits the low-energy behavior considered in Ref. 9. We specifically choose $n=2$ and underline that none of our qualitative conclusions are altered by choosing $n=4,8$. It is natural to begin looking for signatures of the odd-frequency symmetry as probed by the Josephson current in the simplest case of an even-frequency/N/odd-frequency junction. The proximity-induced anomalous Green's function in the N will have a contribution from both the even- and odd-frequency symmetries.[13] However, we find that *no Josephson current may flow* in such a setup.

This may be understood by considering the boundary conditions at each interface (see Fig. 2). At the even-frequency/N interface, the odd-frequency triplet component of the proximity-induced Green's function is absent since penetration into the even-frequency superconductor is prohibited. Similarly, at the N/odd-frequency interface, the even-frequency singlet component of the Green's function vanishes for the same reason.

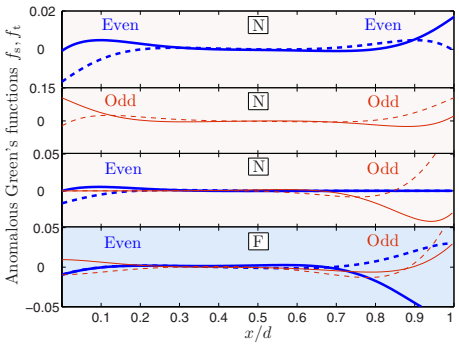

FIG. 2. (Color online) Plot of the singlet f_s (thick, blue lines) and triplet f_t (thin, red lines) anomalous Green's function induced in a N (upper panels) and F (lower panel) in proximity with an even-frequency and/or odd-frequency superconductors by using $\chi=\pi/4$ and $\varepsilon/\Delta_0=0.1$. The solid lines are the real parts of the anomalous Green's functions, while the dashed lines are the imaginary parts. To ensure that $f_{s,t} \ll 1$, we take $d/\xi=50$ in the N case and $d/\xi=2$, $h/\Delta_0=50$ in the F case. Here, $\xi=\sqrt{D/(2\pi T_c)}$ is the superconducting coherence length. While a Josephson current flows when the symmetries of the superconductors are equal in the N case, it vanishes when the superconductors have *different* symmetries. This is because the triplet and singlet components are absent at the interface of the even- and odd-frequency superconductors, respectively. Replacing the N with a F establishes a Josephson coupling between superconductors with different symmetries.

Therefore, the Josephson current is zero in this type of junction since the current-carrying Green's function in the N induced by the left superconductor is absent at the right superconductor, and vice versa. This is a direct result of the different symmetries of the even- and odd-frequency superconductors. The Josephson current can be divided into the individual contributions from f_s and f_t (cross terms vanish), and for each component, the coherence is lost since the even- and odd-frequency pairings cannot reach the opposite interface.

Analytically, one can confirm from Eqs. (10) and (11) that the Green's functions providing the critical current (at $\chi=\pi/4$) satisfy $f_{\pm}(\varepsilon)=if_{\pm}^*(-\varepsilon)$ for any x in the even-frequency/N/odd-frequency case, which upon insertion in Eq. (13) yields $\mathbf{j}(x)=0$. In even-frequency/N/even-frequency and odd-frequency/N/odd-frequency junctions, one can in a similar manner confirm that $A(\varepsilon)=A^*(-\varepsilon)e^{-ikd}$ and $B(\varepsilon)=B^*(-\varepsilon)e^{ikd}$, which leads to a finite value of the Josephson current. This may be seen, for instance, at $x=d/2$ upon substitution into Eq. (13), where $f_{\pm}(\varepsilon)=f_{\pm}^*(-\varepsilon)$ and $\partial_x f_{\pm}(\varepsilon)=-\partial_x f_{\pm}^*(-\varepsilon)$.

If we instead consider an even-frequency/F/odd-frequency junction, the proximity-induced anomalous Green's function in the F will have the same symmetries as in the N case. Remarkably, we find that in this case, however, *a Josephson current is allowed to flow* through the system. The reason for why a Josephson current is present when the N is replaced with a F is that the exchange field allows for both the singlet and triplet components to be induced throughout the F due to the mixing of singlet and triplet

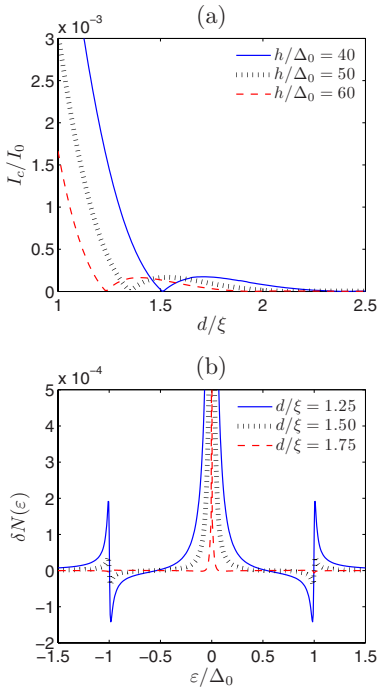

FIG. 3. (Color online) (a) The critical current ($\chi=\pi/4$) as a function of d/ξ for $T/T_c=0.001$. (b) Deviation from the LDOS at $x=d/2$ for an even-frequency/F/odd-frequency junction with $\chi=\pi/4$ and $h/\Delta_0=50$. The zero-energy peak is clearly discernible, which originates with the odd-frequency pairs.

components by breaking the symmetry in spin space, regardless of the internal symmetry of the superconductors,[17,18] as shown in Fig. 2. As a result, we suggest that as a way to unambiguously identify an odd-frequency superconductor, a coupling through a N to an ordinary even-frequency superconductor should not yield any Josephson current while replacing the N with an F should allow for the current to flow. One could argue that this is precisely the case also for even-frequency triplet odd-parity superconductors.[18] This symmetry is nevertheless easily distinguished from an odd-frequency s-wave symmetry since the former is highly sensitive to impurities while the latter does not suffer from this drawback.

We have investigated the behavior of the critical current when coupling an even- and odd-frequency superconductor through a F, and the results are shown in Fig. 3 for a representative choice of parameters. To make the numerical calculations stable, we have added a small imaginary number[19] in the quasiparticle energy, $\varepsilon \to \varepsilon + i\delta$, with $\delta=0.01\Delta_0$, and we fix $\gamma=5$ (also for Fig. 2). One observes the well-known 0-π transitions[20] upon increasing with the width d of the F [Fig. 3(a)]. Similarly, we also find that 0-π oscillations occur as a function of temperature. The current-phase relationship is sinusoidal as usual in the linearized treatment. The width of the junction is measured in units of the superconducting coherence length[21] $\xi=\sqrt{D/(2\pi T_c)}$.

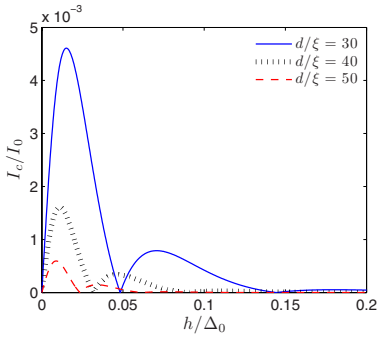

FIG. 4. (Color online) Field dependence of the critical current for several values of d/ξ with $T/T_c=0.001$.

As a further probe of the odd-frequency symmetry in a bulk superconductor, we investigate the local density of states (LDOS) in the F. The LDOS is altered from its normal-state value due to the proximity-induced anomalous Green's function in the F. Consider Fig. 3(b) for a plot of the deviation δN from the normal-state LDOS in an even-frequency/F/odd-frequency junction. The deviation is given by the formula

$$\delta N(\varepsilon) = \sum_{\sigma=\pm} (\mathrm{Re}\{\sqrt{1+f_\sigma(\varepsilon)[f_{-\sigma}(-\varepsilon)]^*}\}-1)/2 \quad (16)$$

under the assumption of a weak-proximity effect. As is seen, the LDOS is enhanced at $\varepsilon=0$ due to the presence of odd-frequency pairs,[13,22] and the usual peak arises at $\varepsilon=\Delta_0$. While the odd-frequency/F/odd-frequency case exhibits the first property, and the even-frequency/F/even-frequency case the latter, the even-frequency/F/odd-frequency junction is characterized by the fact that both of these features appear in δN. This could serve as an identifier of the odd-frequency symmetry in conjunction with the other properties we have analyzed here.

It is interesting to observe the field dependence of the critical current in an even-frequency/F/odd-frequency junction, as shown in Fig. 4. To gain access to the regime of a very weak or absent exchange field, we must choose the width d sufficiently large to ensure a weak-proximity effect. In Fig. 4, we plot the current as a function of h for several values of d/ξ. One observes that the critical current exactly goes to zero at $h=0$, while a current is induced for nonzero values of h. A maximum peak appears for very weak exchange fields, and the critical current oscillates with increasing field strength. Although the short-junction regime is not accessible for very weak exchange fields due to the linearized treatment, it follows from our analytical expressions that the current is absent for any choice of d as long as $h=0$.

B. Case with $\phi \neq 0$

We now proceed to consider the effect of rotating the exchange field in the ferromagnetic region. In effect, we allow for $\phi \neq 0$. Now, the equal-spin-pairing components f_σ are, in general, nonzero, and we find the following four coupled, linearized Usadel equations:[14]

$$D\partial_x^2 f_\pm + 2i(\varepsilon + h\cos\phi)f_\pm \pm h\sin\phi(f_\uparrow + f_\downarrow) = 0,$$

$$D\partial_x^2 f_\sigma + 2i\varepsilon f_\sigma - 2h\sin\phi f_s = 0, \quad \sigma = \uparrow,\downarrow. \tag{17}$$

The general solution for the anomalous Green's functions may be compactly written as

$$f_\pm(x) = A(x)(a_\uparrow + a_\downarrow) + B(x)(b_\uparrow + b_\downarrow) + c_5 R_+^\pm(x) + c_6 P_+^\pm(x) + c_7 R_-^\pm(x) + c_8 P_-^\pm(x),$$

$$f_\sigma = a_\sigma \cos L_0 x + b_\sigma \sin L_0 x + c_5(i\sin L_+ x\sin\phi) + c_6(i\cos L_+ x\sin\phi) + c_7(-i\sin L_- x\sin\phi) + c_8(-i\cos L_- x\sin\phi), \sigma = \uparrow,\downarrow. \tag{18}$$

In the above, $\{a_\sigma, b_\sigma, c_5, c_6, c_7, c_8\}$ are unknown coefficients to be determined from the boundary conditions in the problem. Also, we have introduced the following auxiliary quantities:

$$A(x) = \frac{i\cos L_0 x\sin\phi}{2\cos\phi}, \quad B(x) = \frac{i\sin L_0 x\sin\phi}{2\cos\phi},$$

$$R_\pm^\alpha(x) = \sin L_\pm x(\pm\cos\phi + \alpha), \quad \alpha = \pm 1,$$

$$P_\pm^\alpha(x) = \cos L_\pm x(\pm\cos\phi + \alpha), \quad \alpha = \pm 1,$$

$$L_0 = (1+i)\sqrt{\frac{\varepsilon}{D}}, \quad L_\pm = (i\pm 1)\sqrt{\frac{h\pm\varepsilon}{D}}. \tag{19}$$

When the left superconductor has an even-frequency symmetry and the right superconductor has an odd-frequency symmetry, the boundary conditions yield at $x=0$,

$$2\gamma d\partial_x f_\pm = 2f_\pm c_L \mp 2s_L e^{-i\chi},$$

$$2\gamma d\partial_x f_\sigma = 2f_\sigma c_L, \tag{20}$$

while at $x=d$, one obtains

$$2\gamma d\partial_x f_\pm = 2s_R e^{i\chi} - 2f_\pm c_R,$$

$$2\gamma d\partial_x f_\sigma = -2f_\sigma c_R. \tag{21}$$

The presence of equal-spin-pairing components slightly modifies expressions (12) and (16) for the density of states and the Josephson current, respectively. We now obtain

$$\delta N(\varepsilon) = \sum_\sigma [N_\sigma(\varepsilon) - 1]/2,$$

$$N_\sigma(\varepsilon) = \mathrm{Re}\{\{1 + f_\sigma(\varepsilon)f_\sigma^*(-\varepsilon) + [f_t(\varepsilon) + \sigma f_s(\varepsilon)] \times [f_t^*(-\varepsilon) - \sigma f_s^*(-\varepsilon)]\}^{1/2}\} \tag{22}$$

for the density of states, while the Josephson current is calculated according to

$$\mathbf{j}(x) = -(N_F e D\hat{\mathbf{x}}/2)\int_{-\infty}^{\infty} d\varepsilon\ \mathrm{Re}\{M_+(\varepsilon) + M_-(\varepsilon) + M_\uparrow(\varepsilon) + M_\downarrow(\varepsilon)\} \times \tanh(\beta\varepsilon/2), \tag{23}$$

with the definition ($\sigma = \uparrow,\downarrow$)

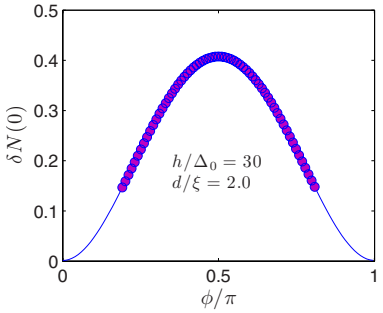

FIG. 5. (Color online) Plot of the deviation from the normal-state zero-energy density of states in the middle of the ferromagnetic region ($x/d=0.5$). The symbols denote approximately the region where the linearized treatment becomes less accurate, i.e., the anomalous Green's functions f no longer satisfy $|f| \ll 1$.

$$M_\sigma(\varepsilon) = [f_\sigma(-\varepsilon)]^*\partial_x f_\sigma(\varepsilon) - f_\sigma(\varepsilon)\partial_x[f_\sigma(-\varepsilon)]^*. \tag{24}$$

Let us first address the issue of how the zero-energy peak in the DOS treated earlier is affected by a rotation of the exchange field. In Fig. 5, we plot the deviation $\delta N(0)$ from the normal-state zero-energy DOS as a function of the misorientation ϕ for $d/\xi=2$ and $h/\Delta_0=30$. As ϕ is increased, it is seen that $\delta N(0)$ rapidly grows. As it becomes comparable to the normal-state DOS in magnitude, the linearized treatment of the Usadel equations[14] becomes less accurate, which was denoted by the symbols in Fig. 5. Nevertheless, the trend seems clear: the zero-energy DOS reaches a maximum at $\phi=\pi/2$. Also, we have demonstrated (not shown) that the characteristics in Fig. 3(b) remain the same for all ϕ. In particular, the zero-energy peak is not destroyed by changing ϕ.

Examining the magnitude of the anomalous Green's function numerically, we find that the weak-proximity effect assumption $|f| \ll 1$ becomes poor for energies close to zero when ϕ is close to $\pi/2$. Therefore, this parameter regime is strictly speaking inaccessible within our linearized treatment. Note that no such problem occurs when $\phi=0$. However, we will assume that the linearized treatment is still qualitatively correct when ϕ is close to $\pi/2$ in order to investigate how the critical current depends on the orientation of the exchange field orientation.

In Fig. 6, we plot the variation of the critical Josephson current as a function of the orientation ϕ of the exchange field. If the two superconductors have conventional even-frequency symmetry, the Josephson current is completely insensitive to the orientation of the exchange field. This is reasonable, since the superconducting order parameter in this case is spin singlet and has no orientation in spin space. Note that a magnetic flux threading a Josephson junction, in general, gives rise to a Fraunhofer modulation of the current as a function of the flux. Here, we neglect this modification by assuming that the flux constituted by the ferromagnetic region is sufficiently weak compared to the elementary flux quantum. This is the case for either a small enough surface area or weak enough magnetization (the energy *exchange splitting* may still be significant).

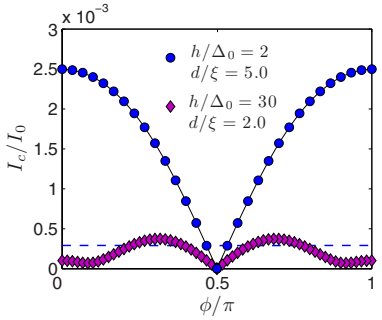

FIG. 6. (Color online) Plot of the modulation of the Josephson current with orientation ϕ of the exchange field in the ferromagnet. The symbols correspond to an even-frequency/F/odd-frequency junction, while the dashed line denotes an even-frequency/F/even-frequency junction with $h/\Delta_0=30$ and $d/\xi=2.0$.

The situation is quite different when one of the superconductors has an odd-frequency symmetry. In this case, the Josephson current is sensitive to the orientation ϕ of the exchange field and displays the behavior shown in Fig. 6. The reason for this is that the order parameter in the odd-frequency triplet case has a direction in spin space, here which is chosen as opposite-spin pairing (along the $\hat{\mathbf{z}}$ axis). For $\phi=0$, the Cooper pairs are opposite-spin paired relative to the exchange field, while for $\phi=\pi/2$, the Cooper pairs are equal-spin paired relative to the exchange field. Tuning the relative orientation of the exchange field and the superconducting order parameter in the odd-frequency superconductor is thus seen to lead to the possibility of controlling the magnitude of the Josephson current. In an experimental situation, only the orientation of the exchange field is probably alterable. In Fig. 7, we show the current-phase relationship for an even-frequency/F/odd-frequency Josephson junction for several values of ϕ to show that although it remains sinusoidal, it is shifted from $\sim\sin\phi$ to $\sim\sin[\phi+\alpha(\phi)]$, where $\alpha(\phi)$ is nonzero for $h\neq 0$.

Interestingly, for $\phi=\pi/2$, the current completely vanishes, as seen in Fig. 6, but it is nonzero otherwise. This can be understood by studying the contribution to the Josephson

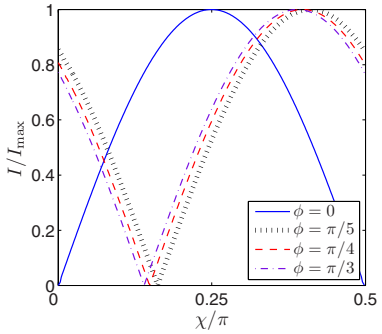

FIG. 7. (Color online) Plot of the current-phase relationship for several values of ϕ. We have chosen $h/\Delta_0=30$ and $d/\xi=2.0$.

current from each of the components of the anomalous Green's functions. One may rewrite Eq. (23) as

$$\mathbf{j}=\mathbf{j}_t+\mathbf{j}_s+\mathbf{j}_{\mathrm{ESP}}, \tag{25}$$

where $\{j_t,j_s,j_{\mathrm{ESP}}\}$ represent the contribution to the Josephson current from the $S_z=0$ triplet, the singlet, and the equal-spin-pairing anomalous Green's functions, respectively. These are defined as

$$j_t=-M_0\int_{-\infty}^{\infty}d\varepsilon\ \mathrm{Re}\{2M_t(\varepsilon)\}\tanh(\beta\varepsilon/2),$$

$$j_s=M_0\int_{-\infty}^{\infty}d\varepsilon\ \mathrm{Re}\{2M_s(\varepsilon)\}\tanh(\beta\varepsilon/2),$$

$$j_{\mathrm{ESP}}=-M_0\int_{-\infty}^{\infty}d\varepsilon\ \mathrm{Re}\{M_{\uparrow}(\varepsilon)+M_{\downarrow}(\varepsilon)\}\tanh(\beta\varepsilon/2), \tag{26}$$

with the definition $M_0=N_F eD/2$ and

$$M_j(\varepsilon)=[f_j(-\varepsilon)]^*\partial_x f_j(\varepsilon)-f_j(\varepsilon)\partial_x[f_j(-\varepsilon)]^*,\quad j=\{t,s\}. \tag{27}$$

Now, we get $\partial_x M_t=\partial_x(M_s-M_\sigma)=0(\sigma=\uparrow,\downarrow)$ for $\phi=\pi/2$ from Eq. (17). With Eq. (20), we have $M_t=0$ and similar $M_s-M_\sigma=0$ by virtue of Eq. (21) and the fact that $c_{L,R}(\varepsilon)=c_{L,R}^*(-\varepsilon)$. Therefore, the total Josephson current j becomes zero for $\phi=\pi/2$. In fact, an equivalent analytical approach is viable to show that the current vanishes in the case $h=0$. In that case, one finds that $\partial_x M_t=\partial_x M_s=0$ and $M_t=0$ at $x=0$ and $M_s=0$ at $x=d$ by means of the boundary conditions and the Usadel equation.[14]

At this point, it is important to underline that although the magnitude of the Josephson current in an even-frequency/F/odd-frequency Josephson junction depends on the orientation of the exchange field, our main message is that *no current* can flow in the absence of a field while the presence of an exchange field in general *induces a current* except for the special case where the exchange field is parallel to the spin of the Cooper pair, $\phi=\pi/2$.

IV. DISCUSSION

In our calculations, we have neglected the spatial variation of the pairing potential near the interfaces. This is permissible for either low-transmission interfaces or if the superconducting region is much less disordered than the F.[2] Also, we have considered nonmagnetic interfaces, which are routinely used in experiments. Including spin-flip scattering in the normal region is not expected to alter our qualitative conclusions since spin-flip scattering alone cannot induce triplet pairing in a normal metal in proximity to an even-frequency superconductor in the diffusive limit.[23] Our choice of studying the diffusive limit ensures that one may disregard the generation of possible odd-parity symmetry components of the superconducting gap,[13] which could have caused ambiguities in the interpretation of experimental results ob-

tained in our proposed setup. We expect that the predicted effect could be experimentally observed in disordered superconductor/ferromagnet/superconductor junctions by using superconductors with different symmetries with respect to frequency. The junction widths need to be a few coherence lengths, which is well within reach with present-day technology.

V. SUMMARY

In summary, we have proposed a method of identifying highly unusual superconducting states with the conceptually and technologically important property that the order parameter is odd under exchange of time coordinates of the electrons constituting a Cooper pair. Remarkably, we find that an exchange field quite generally induces a Josephson effect between even- and odd-frequency superconductors. This constitutes a clear-cut experimental test for such an unusual superconducting state. Since our qualitative findings rely on symmetry consideration alone, they are expected to be quite robust.

ACKNOWLEDGMENTS

The authors thank Y. Tanaka and I. B. Sperstad for useful discussions. J.L. and A.S. were supported by the Research Council of Norway under Grants No. 158518/432, No. 158547/431 (NANOMAT), and No. 167498/V30 (STORFORSK). T.Y. acknowledges support by the JSPS.

APPENDIX A: JOSEPHSON CURRENT WITH SPIN-DEPENDENT SCATTERING

Here, we provide some additional details of our calculations and also outline how spin-dependent scattering may be taken into account in the analytical expressions. We employ the linearized Usadel equations[14] under the assumption of a weak-proximity effect. This assumption is justified in the low-transparency regime (tunneling limit), where the depletion of the superconducting order parameter near the interface may also be disregarded. In the superconducting reservoirs, we employ the bulk solution that reads

$$\hat{g}_{\mathrm{SC}} = \begin{pmatrix} c_j & 0 & 0 & s_j e^{i\chi_j} \\ 0 & c_j & \alpha_j s_j e^{i\chi_j} & 0 \\ 0 & -\alpha_j s_j e^{-i\chi_j} & -c_j & 0 \\ -s_j e^{-i\chi_j} & 0 & 0 & -c_j \end{pmatrix}, \quad \text{(A1)}$$

where $c_j=\cosh\theta_j$, $s_j=\sinh\theta_j$, $\theta_j=\operatorname{arctanh}[\Delta_j(\varepsilon)/\varepsilon]$, and $j=L,R$ denotes the left and right superconducting regions. Here, χ_j denotes the broken $U(1)$ phase in superconductor j, and we use the convention $\chi_R=-\chi_L\equiv\chi$. For an odd-frequency superconductor on side j, we have $\alpha_j=1$ while for an even-frequency superconductor on side j, one has $\alpha_j=-1$.

The Kupriyanov–Lukichev[16] boundary conditions now read

$$2\gamma d\hat{g}\partial_x\hat{g} = -[\hat{g},\hat{g}_L]|_{x=0},$$

$$2\gamma d\hat{g}\partial_x\hat{g} = [\hat{g},\hat{g}_R]|_{x=d}. \quad \text{(A2)}$$

In the normal region, we may write the Green's function as

$$\hat{g}^R = \begin{pmatrix} \underline{1} & f_t^R(\varepsilon)\underline{\tau_1} + f_s^R(\varepsilon) i\underline{\tau_2} \\ -[f_t^R(-\varepsilon)\underline{\tau_1} + f_s^R(-\varepsilon) i\underline{\tau_2}]^* & -\underline{1} \end{pmatrix}, \quad \text{(A3)}$$

where the subscripts t and s denote the triplet and singlet parts of the anomalous Green's function. Note that the triplet part is odd in frequency. In the following, we will consider an exchange field $\mathbf{h}\|\hat{\mathbf{z}}$, i.e., perpendicular to the spin of the Cooper pair, such that there are no equal-spin-pairing components f_σ ($\sigma=\uparrow,\downarrow$) of the anomalous Green's function. Introducing $f_\pm=f_t\pm f_s$, we may write the boundary conditions more explicitly. At $x=0$, one obtains

$$2\gamma d\partial_x f_+ = 2f_+c_L - 2s_L e^{-i\chi},$$

$$2\gamma d\partial_x f_- = 2f_-c_L - 2\alpha_L s_L e^{-i\chi}, \quad \text{(A4)}$$

while the same procedure at $x=d$ yields

$$2\gamma d\partial_x f_+ = 2s_R e^{i\chi} - 2f_+c_R,$$

$$2\gamma d\partial_x f_- = 2\alpha_R s_R e^{i\chi} - 2f_-c_R. \quad \text{(A5)}$$

The linearized Usadel equations[14] in the normal region may be formally obtained by assuming that $|f_\pm|\ll 1$,[24–26]

$$\partial_x^2 f_t \pm \partial_x^2 f_s + A_\pm f_t \pm B_\pm f_s = 0, \quad \text{(A6)}$$

where we have introduced

$$A_\pm = \frac{1}{D}\left[2i(\varepsilon\pm h) - g_{\mathrm{so}} - \frac{g_{sf}S_z}{2}\right],$$

$$B_\pm = \frac{1}{D}\left[2i(\varepsilon\pm h) - \frac{g_{sf}(2S_{xy}+S_z)}{2}\right]. \quad \text{(A7)}$$

It is possible to find a general analytical solution for the functions $\{f_t,f_s\}$, and this can be written as

$$f_t = c_1 e^{-k_- x} + c_2 e^{k_- x} + c_3 e^{-k_+ x} + c_4 e^{k_+ x},$$

$$f_s = \frac{c_1 S_- e^{-k_- x} + c_2 S_- e^{k_- x} + c_3 S_+ e^{-k_+ x} + c_4 S_+ e^{k_+ x}}{2(B_- - B_+)}, \quad \text{(A8)}$$

where $\{c_i\}$ are constants to be determined from boundary conditions (A4) and (A5). Also, we have defined the auxiliary quantities,

$$k_\pm = \frac{1}{2}\sqrt{(-A_+ - A_- - B_+ - B_-) \pm R},$$

$$S_\pm = (A_+ + A_- - B_+ - B_-) \pm R,$$

$$R = [(A_+ + A_-)^2 + (B_+ + B_-)^2 - 4(A_+B_- + A_-B_+) + 2(A_+ - A_-)(B_+ - B_-)]^{1/2}. \quad \text{(A9)}$$

First, we note that

$$f_\pm = c_1 e^{-k_- x}(1 \pm L_-) + c_2 e^{k_- x}(1 \pm L_-) + c_3 e^{-k_+ x}(1 \pm L_+) + c_4 e^{k_+ x}(1 \pm L_+), \tag{A10}$$

with the definition $L_\pm = iDS_\pm/(8h)$. We also introduce

$$\delta_{L\pm} = \begin{cases} 1 & \text{for } + \\ \alpha_L & \text{for } - \end{cases} \tag{A11}$$

and similarly for $L \to R$. After lengthy calculations, we finally arrive at an explicit expression for the coefficients $\{c_i\}$,

$$c_4 = \frac{G_+ E_-/E_+ - G_-}{F_- - F_+ E_-/E_+},\ c_3 = -(G_+ + c_4 F_+)/E_+,\ c_2 = Y_0 + Y_3 c_3 + Y_4 c_4,\ c_1 = X_0 + X_2 c_2 + X_3 c_3 + X_4 c_4. \tag{A12}$$

We have defined the auxiliary quantities,

$$P = \frac{1 - L_-}{1 + L_-},\ X_0 = \frac{\delta_{L+} s_L e^{-i\chi}}{(1 + L_-)(c_L + \gamma d k_-)},\ X_2 = \frac{\gamma d k_- - c_L}{\gamma d k_- + c_L},$$

$$X_3 = -\frac{(1 + L_+)(c_L + \gamma d k_+)}{(1 + L_-)(c_L + \gamma d k_-)},\ X_4 = \frac{(1 + L_+)(\gamma d k_+ - c_L)}{(1 + L_-)(\gamma d k_- + c_L)}, \tag{A13}$$

$$Y_0 = \frac{s_L e^{-i\chi}(P\delta_{L+} - \delta_{L-})}{(c_L - \gamma d k_-)[P(1 + L_-) - (1 - L_-)]},$$

$$Y_3 = \frac{(1 - L_+)(c_L + \gamma d k_+) - (1 + L_+)(P c_L + P\gamma d k_+)}{(c_L - \gamma d k_-)[P(1 + L_-) - (1 - L_-)]},$$

$$Y_4 = \frac{(1 - L_+)(c_L - \gamma d k_+) - (1 + L_+)(P c_L - P\gamma d k_+)}{(c_L - \gamma d k_-)[P(1 + L_-) - (1 - L_-)]}, \tag{A14}$$

$$E_\pm = 2e^{-k_+ d}(1 \pm L_+)(c_R - \gamma d k_+) + 2(1 \pm L_-)[Y_3 e^{k_- d}(c_R + \gamma d k_-) + (X_2 Y_3 + X_3) e^{-k_- d}(c_R - \gamma d k_-)],$$

$$F_\pm = 2e^{k_+ d}(1 \pm L_+)(c_R + \gamma d k_+) + 2(1 \pm L_-)[Y_4 e^{k_- d}(c_R + \gamma d k_-) + (X_2 Y_4 + X_4) e^{-k_- d}(c_R - \gamma d k_-)],$$

$$G_\pm = -2\delta_{R\pm} s_R e^{i\chi} + 2(1 \pm L_-)[Y_0 e^{k_- d}(c_R + \gamma d k_-) + (X_2 Y_0 + X_0) e^{-k_- d}(c_R - \gamma d k_-)]. \tag{A15}$$

The above equations may be considerably simplified by considering only uniaxial spin-flip scattering. Setting the planar spin-flip and spin-orbit scattering rates to infinity, corresponding to the absence of such scattering processes, we obtain the anomalous Green's function as

$$f_\pm = c_{1\pm} e^{ik_\pm x} + c_{2\pm} e^{-ik_\pm x},\ k_\pm = \sqrt{\frac{4i(\varepsilon \pm h) - 3g_{\mathrm{sf}}}{2D}}, \tag{A16}$$

with the coefficients ($\rho_\sigma = \mathrm{i}\gamma d k_\sigma,\ \sigma = \pm$)

$$c_{2\sigma} = \frac{\delta_{L\sigma} s_L e^{-i\chi} e^{ik_\sigma d}(\rho_\sigma + c_R) + \delta_{R\sigma} s_R e^{i\chi}(\rho_\sigma - c_L)}{e^{ik_\sigma d}(\rho_\sigma + c_L)(\rho_\sigma + c_R) - e^{-ik_\sigma d}(\rho_\sigma - c_R)(\rho_\sigma - c_L)},$$

$$c_{1\sigma} = \frac{c_{2\sigma}(\rho_\sigma + c_L) - \delta_{L\sigma} s_L e^{-i\chi}}{\rho_\sigma - c_L},\ \sigma = \pm. \tag{A17}$$

Once $\hat{g}^R$ has been obtained, the Josephson current may be calculated according to the formulas in the main text.

APPENDIX B: PAULI MATRICES

In this paper, the Pauli matrices used are defined as

$$\underline{\tau_1} = \begin{pmatrix} 0 & 1 \\ 1 & 0 \end{pmatrix},\ \underline{\tau_2} = \begin{pmatrix} 0 & -i \\ i & 0 \end{pmatrix},\ \underline{\tau_3} = \begin{pmatrix} 1 & 0 \\ 0 & -1 \end{pmatrix},$$

$$\underline{1} = \begin{pmatrix} 1 & 0 \\ 0 & 1 \end{pmatrix},\ \hat{1} = \begin{pmatrix} \underline{1} & \underline{0} \\ \underline{0} & \underline{1} \end{pmatrix},\ \hat{\tau}_i = \begin{pmatrix} \underline{\tau_i} & \underline{0} \\ \underline{0} & \underline{\tau_i} \end{pmatrix},$$

$$\hat{\rho}_1 = \begin{pmatrix} \underline{0} & \underline{\tau_1} \\ \underline{\tau_1} & \underline{0} \end{pmatrix},\ \hat{\rho}_2 = \begin{pmatrix} \underline{0} & -i\underline{\tau_1} \\ i\underline{\tau_1} & \underline{0} \end{pmatrix},\ \hat{\rho}_3 = \begin{pmatrix} \underline{1} & \underline{0} \\ \underline{0} & -\underline{1} \end{pmatrix}. \tag{B1}$$

[1] V. L. Berezinskii, JETP Lett. **20**, 287 (1974).
[2] F. S. Bergeret, A. F. Volkov, and K. B. Efetov, Rev. Mod. Phys. **77**, 1321 (2005).
[3] F. S. Bergeret, A. F. Volkov, and K. B. Efetov, Phys. Rev. Lett. **86**, 4096 (2001); A. F. Volkov, F. S. Bergeret, and K. B. Efetov, *ibid.* **90**, 117006 (2003).
[4] R. S. Keizer, S. T. B. Goennenwein, T. M. Klapwijk, G. Miao, G. Xiao, and A. Gupta, Nature (London) **439**, 825 (2006); I. Sosnin, H. Cho, V. T. Petrashov, and A. F. Volkov, Phys. Rev. Lett. **96**, 157002 (2006).
[5] Y. Fuseya, H. Kohno, and K. Miyake, J. Phys. Soc. Jpn. **72**, 2914 (2003); G. Q. Zheng, N. Yamaguchi, H. Kan, Y. Kitaoka, J. L. Sarrao, P. G. Pagliuso, N. O. Moreno, and J. D. Thompson, Phys. Rev. B **70**, 014511 (2004); S. Kawasaki, T. Mito, Y. Kawasaki, G.-q. Zheng, Y. Kitaoka, D. Aoki, Y. Haga, and Y. Onuki, Phys. Rev. Lett. **91**, 137001 (2003).
[6] M. D. Johannes, I. I. Mazin, D. J. Singh, and D. A. Papaconstantopoulos, Phys. Rev. Lett. **93**, 097005 (2004).
[7] Y. Kobayashi, Hidekazu Watanabe, Mai Yokoi, Taketo Moyoshi, Yoshihiko Mori, and Masatoshi Sato, J. Phys. Soc. Jpn. **74**, 1800 (2005).
[8] Y. Ihara, Kenji Ishida, Kazuyoshi Yoshimura, Kazunori Takada, Takayoshi Sasaki, Hiroya Sakurai, and Eiji Takayama-Muromachi, J. Phys. Soc. Jpn. **74**, 2177 (2005).
[9] Ya. V. Fominov, JETP Lett. **86**, 732 (2007).
[10] J. Linder, T. Yokoyama, Y. Tanaka, Y. Asano, and A. Sudbø, arXiv:0712.0443, Phys. Rev. B (to be published).
[11] E. Abrahams, Alexander Balatsky, D. J. Scalapino, and J. R.

Schrieffer, Phys. Rev. B **52**, 1271 (1995).
[12] Y. Tanaka, Alexander A. Golubov, Satoshi Kashiwaya, and Masahito Ueda, Phys. Rev. Lett. **99**, 037005 (2007).
[13] Y. Tanaka and A. A. Golubov, Phys. Rev. Lett. **98**, 037003 (2007).
[14] K. Usadel, Phys. Rev. Lett. **25**, 507 (1970).
[15] For generalized boundary conditions, see Yu. V. Nazarov, Superlattices Microstruct. **25**, 1221 (1999); Y. Tanaka, Yu. V. Nazarov, and S. Kashiwaya, Phys. Rev. Lett. **90**, 167003 (2003).
[16] M. Yu. Kupriyanov and V. F. Lukichev, Zh. Eksp. Teor. Fiz. **94**, 139 (1988).
[17] Y. Tanaka and S. Kashiwaya, J. Phys. Soc. Jpn. **68**, 3485 (1999).
[18] T. Yokoyama, Y. Tanaka, and A. A. Golubov, Phys. Rev. B **75**, 094514 (2007).
[19] This may be understood as an effect of the finite quasiparticle lifetime due to inelastic scattering. See R. C. Dynes, V. Narayanamurti, and J. P. Garno, Phys. Rev. Lett. **41**, 1509 (1978).
[20] L. N. Bulaevskii, V. V. Kuzii, and A. A. Sobyanin, JETP Lett. **25**, 290 (1977); A. I. Buzdin, L. N. Bulaevskii, and S. V. Panjukov, *ibid.* **35**, 178 (1982); A. A. Golubov, M. Yu. Kupriyanov, and E. Il'ichev, Rev. Mod. Phys. **76**, 411 (2004).
[21] Some authors also use the definition $\xi=\sqrt{D/\Delta_0}$, which is of the same order of magnitude.
[22] V. Braude and Yu. V. Nazarov, Phys. Rev. Lett. **98**, 077003 (2007); T. Yokoyama, Y. Tanaka, and A. A. Golubov, Phys. Rev. B **75**, 134510 (2007); Y. Asano, Y. Tanaka, and A. A. Golubov, Phys. Rev. Lett. **98**, 107002 (2007).
[23] J. Linder and A. Sudbø, Phys. Rev. B **76**, 214508 (2007).
[24] E. A. Demler, G. B. Arnold, and M. R. Beasley, Phys. Rev. B **55**, 15174 (1997).
[25] M. Houzet, V. Vinokur, and F. Pistolesi, Phys. Rev. B **72**, 220506(R) (2005).
[26] J. Linder, T. Yokoyama, and A. Sudbø, Phys. Rev. B (to be published).

Paper XIII

Supercurrent switch in graphene π-junctions.

Physical Review Letters **100**, 187004 (2008).

Supercurrent Switch in Graphene π Junctions

Jacob Linder,[1] Takehito Yokoyama,[2] Daniel Huertas-Hernando,[1] and Asle Sudbø[1]

[1]*Department of Physics, Norwegian University of Science and Technology, N-7491 Trondheim, Norway*
[2]*Department of Applied Physics, Nagoya University, Nagoya, 464-8603, Japan*

(Received 18 January 2008; published 7 May 2008)

We study the supercurrent in a superconductor/ferromagnet/superconductor graphene junction. In contrast to its metallic counterpart, the oscillating critical current in our setup decays only weakly upon increasing the exchange field and junction width. We find an unusually large residual value of the supercurrent at the oscillatory cusps due to a strong deviation from a sinusoidal current-phase relationship. Our findings suggest a very efficient device for dissipationless supercurrent switching.

DOI: 10.1103/PhysRevLett.100.187004 PACS numbers: 74.45.+c, 74.50.+r

Graphene is a condensed matter system displaying an emergent low-energy ''relativistic'' electronic structure. For undoped graphene, the Fermi level reduces to six points, giving rise to nodal fermions at the edges of the Brillouin zone. Currently, it is of considerable interest, and potentially of great technological importance, to investigate how such unusual low-energy electronic structures manifest themselves in heterostructures where proximity effects are prominent. In particular, the potential for future applications in devices seems plausible if such proximity structures would combine two major functionalities in materials science: namely, magnetism and superconductivity.

Recently, there have been several experimental reports on proximity-induced *superconductivity* in graphene [1,2]. A measurable supercurrent was observed between regions of graphene under the influence of proximity-induced superconductivity in these works. Because of the massless nature and energy-independent velocity of the charge carriers, graphene offers a unique environment for the manifestation of a Josephson effect. Unusual behavior for the supercurrent in a superconductor/normal/superconductor (S/N/S) graphene setup has been predicted, including an anomalous scaling behavior with the length of the normal region in the undoped case [3] and an oscillatory behavior as a function of the gate voltage in the normal region [4].

Interestingly, it has also been shown [5,6] that *ferromagnetic* correlations may be induced in graphene nanoribbons by means of external electrical fields. A suggestion for a more conventional magnetic proximity effect has also been put forth [7,8], by means of exploiting a magnetic gate in contact with a graphene layer. The accompanying exchange splitting between the spin-$\uparrow$ and spin-$\downarrow$ electrons in graphene has been estimated [7] to lie around 5 meV for the magnetic insulator EuO. Precise estimates of the proximity-induced exchange splitting are difficult in this case, due to the strong effect of the proximity layer on the magnetization in EuO [9]. Nevertheless, it is known that the magnetization in the proximity EuO layer is tunable [10]. In applications, this is a great advantage, since it, in principle, offers the possibility of a tunable proximity-induced magnetization in graphene. Moreover, recent experiments on spin injection in a graphene layer show a rather long spin relaxation length ~ 1 μm at room temperature. This indicates that graphene is a promising material for spin transport [7,11].

The following question arises naturally: Do novel physical effects arise due to the peculiar electronic properties of graphene and simultaneously the interplay between ferromagnetic and superconducting correlations? The wide range of exotic phenomena that originate from the mutual interplay between magnetic and superconducting order include 0-π transitions [12,13], odd-frequency pairing [14], and even the intrinsic coexistence of ferromagnetism and superconductivity in the same material [15,16]. In particular, from the viewpoint of applications, the possibility of altering the fundamental Josephson current-phase relationship in a controlled fashion may bring about potential implications for their use in superconducting electronics as well as in (quantum) logic circuits based on superconductors [17].

In this Letter, we investigate the interplay between proximity-induced superconductivity and ferromagnetism in a graphene layer, resulting in an unusual behavior of the supercurrent through the system. The main results are that (i) the current-phase relationship deviates strongly from sinusoidal behavior, indicating a significant contribution from higher harmonics, and (ii) the critical current at the 0-π transition is finite and has a much larger value than the one observed in metallic systems. The latter result suggests a very efficient performance of the device as a supercurrent switch.

We envisage an experimental setup where superconductivity is induced in two parts of the graphene region by means of conventional superconductors, such as Nb or Al, in close proximity. Between the superconducting regions, an exchange splitting is induced in the graphene layer by means of, e.g., a magnetic insulating material. Instead of using a magnetic insulator such as EuO, where one, in principle, could tune the magnetization in the proximity

layer with an external magnetic field, one also could envision using a multiferroic (e.g., $BiFeO_3$) or piezomagnetic material (e.g., $Fe_xNi_yB_z$) in close proximity to the graphene layer. Both of these classes of materials would offer the opportunity of tuning the exchange field in the material by some external control parameter—the electric field due to the magnetoelectric coupling in the former case and pressure in the latter. Upon modifying the exchange field in the proximity layer of the material, it is reasonable to assume that the proximity-induced exchange field in graphene would also be altered. Materials in which the magnetoelectric coupling is substantial are currently attracting much interest due to their potential for novel technological applications [18]. In order to control the local Fermi level in the ferromagnetic (F) region, one could possibly use a normal gate on top of the magnetic insulator to create a tunable barrier [7]. The S regions are assumed to be heavily doped, such that the Fermi energy satisfies $\varepsilon_F \gg \Delta$, while the F region is taken be undoped, i.e., $\varepsilon_F' \simeq 0$. Moreover, we assume sharp edges for the region separating the F and S graphene regions and focus on the short-junction regime, which is experimentally feasible.

We will proceed to show that the Josephson current in an S/F/S graphene junction displays a strong oscillatory, nonmonotonic dependence on both the exchange field h and the width d of the junction. Most interestingly, we find a large residual value of the supercurrent at the cusps of these oscillations. This indicates a sign reversal of the current, and the considerable residual value of the supercurrent at these cusps suggests a very efficient device for dissipationless supercurrent switching. We now present our results in detail.

The F region separating the superconductors is taken to be undoped, such that the effective Fermi level is σh for spin-σ electrons. The regions S must be strongly doped to justify the mean-field treatment of superconductivity. We assume that this is comparable to the estimated exchange splitting in the F region [7,8]. Thus, we take $\varepsilon_F \simeq h$ to obtain analytically tractable results. To construct the scattering states that carry the supercurrent across the F region, we write down the Bogoliubov–de Gennes equations [19] in the presence of an exchange field h. The Bogoliubov–de Gennes equation essentially describes the eigenstates of quasiparticles in each of the graphene regions and their eigenvalues ε. It may be obtained by diagonalizing the full Hamiltonian and constitutes the foundation for constructing the scattering states which are involved in the transport formalism we use here. For the spin species σ, one finds that

$$\begin{pmatrix} H_0 - \sigma h(x) & \sigma\Delta(x) \\ \sigma\Delta^*(x) & -H_0 - \sigma h(x) \end{pmatrix} \begin{pmatrix} u^\sigma \\ v^{-\sigma} \end{pmatrix} = \varepsilon \begin{pmatrix} u^\sigma \\ v^{-\sigma} \end{pmatrix}. \quad (1)$$

Here we have made use of the valley degeneracy and defined $H_0 = v_F \mathbf{p} \cdot \boldsymbol{\sigma}$, where $\mathbf{p}$ is the momentum vector in the graphene plane and $\boldsymbol{\sigma}$ is a vector of Pauli matrices. The superconducting order parameter $\Delta(x)$ couples electron and hole excitations in the two valleys located at the two inequivalent corners of the hexagonal Brillouin zone. The u^σ spinor describes the electronlike part of the total wave function $\psi^\sigma = (u^\sigma, v^{-\sigma})^T$ and in this case reads $u^\sigma = (\psi^\sigma_{A,+}, \psi^\sigma_{B,+})^T$, while $v^{-\sigma} = \mathcal{T} u^\sigma$. Here ^{T} denotes the transpose, while $\mathcal{T}$ is the time-reversal operator. To capture the essential physics, we write $\Delta(x) = \Delta_0 e^{i\phi_{L,R}}$ in the left and right S regions and $\Delta(x) = 0$ otherwise. Similarly, we set $h(x) = h$ in the F region and $h = 0$ otherwise. The Josephson current is computed via the usual energy-current relation summed over projections of all paths perpendicular to the tunneling barrier [20]

$$I_J(\Delta\phi) = -\frac{2e}{\hbar} \sum_i \int_{-\pi/2}^{\pi/2} \frac{d\gamma \cos\gamma}{f^{-1}[\varepsilon_i(\Delta\phi)]} \frac{d\varepsilon_i(\Delta\phi)}{d\Delta\phi}, \quad (2)$$

where $\varepsilon_i(\Delta\phi)$ are the Andreev bound states carrying the current in the F region and $\Delta\phi = \phi_R - \phi_L$ is the macroscopic phase difference between the superconductors. The integration over angles γ takes into account all possible trajectories, and $f(x)$ is the Fermi-Dirac distribution function. We define the critical supercurrent as $I_c = |\max\{I_J(\Delta\phi)\}|$ and introduce $I_0 = 2e\Delta_0$. The procedure for obtaining $\varepsilon_i(\Delta\phi)$ is the same as in Ref. [3], and the details will be given elsewhere; here we give the main results. By introducing $T(\gamma, P) = 4\sin^2\gamma \sin^2(P\cos\gamma) + \cos^4\gamma$ and $\Phi(\gamma, P) = [2\sin^2(P\cos\gamma) - \cos^2\gamma] \times \cos^2\gamma \cos\Delta\phi - \cos^4\gamma - 4\sin^2\gamma \sin^2(P\cos\gamma)$, we find that the allowed bound states have energies $\pm\varepsilon_\sigma(\Delta\phi)$ ($\sigma = \pm$), with

$$\varepsilon_\sigma(\Delta\phi) = \frac{\Delta_0}{\sqrt{2T(\gamma, P)}} [\sigma\{\Phi(\gamma, P)^2 - 4T(\gamma, P) \times [\cos^2\gamma \cos^2(\Delta\phi/2) - \sin^2(P\cos\gamma)]^2\}^{1/2} - \Phi(\gamma, P)]^{1/2}. \quad (3)$$

The parameter $P = hd/v_F$ captures the effect of both the exchange field h and the length d of the junction. To understand the nature of these bound states, consider Fig. 1 for a representative plot of $\varepsilon_\pm(\Delta\phi)$, using

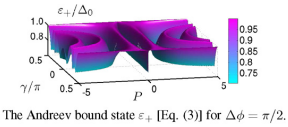

a) The Andreev bound state ε_+ [Eq. (3)] for $\Delta\phi = \pi/2$.

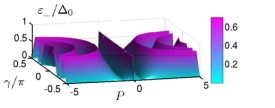

b) The Andreev bound state ε_- [Eq. (3)] for $\Delta\phi = \pi/2$.

FIG. 1 (color online). Contour plot of the Andreev bound states in the ferromagnetic region carrying the current between the superconductors.

$\Delta\phi = \pi/2$. As is seen from both plots, the bound state energies exhibit a strong oscillatory dependence on the parameter P. This indicates that similar oscillatory behavior may be expected in the supercurrent itself. Interestingly, the oscillations seen in Fig. 1 are not damped with increasing P. This directly reflects the Dirac-cone linear dispersion of the graphene electrons and is reminiscent of the weak damping of conductance oscillations at subgap energies in graphene-superconductor junctions [21,22].

Inserting the derivative of Eq. (3) into Eq. (2) provides the supercurrent. The current-phase relationship for the S/F/S graphene junction is shown in Fig. 2. With increasing P, the critical current gets suppressed, and finally the sign of the current is changed. Remarkably, the critical current never goes to zero. An interesting feature of the plot in Fig. 2(a) is that the discontinuity at $\Delta\phi = \pi$ for $P = 0$ is split for increasing P. The discontinuity of the current-phase relation originates with a crossing of Andreev levels in the normal graphene (F graphene with $h = 0$) region at $\Delta\phi = \pi$. For $\Delta\phi \in [0, \pi)$, only the 0-mode Andreev bound state carries the current. For $\Delta\phi \in (\pi, 2\pi]$, the π-mode Andreev bound state carries the current, such that there is an abrupt crossover exactly at $\Delta\phi = \pi$. The situation changes when $h \neq 0$, since the spin splitting doubles the number of Andreev bound states. Consequently, the crossover between different modes may occur at $\Delta\phi \neq \pi$, as a result of the superharmonic current-phase relationship. We have checked explicitly that the strong deviation from a sinusoidal current-phase relationship persists for larger d that do not satisfy $d/\xi \ll 1$. However, in this case one should strictly speaking also include the contribution to the current from the continuum of supergap states [20]. This requires a separate study, and we focus here on the short-junction regime.

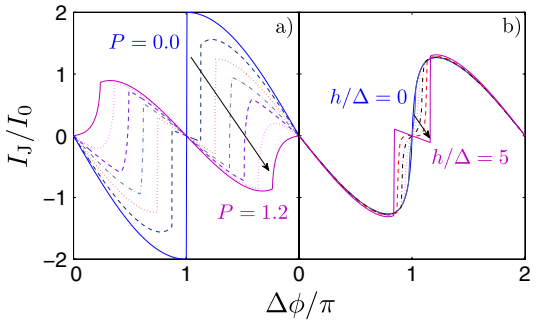

FIG. 2 (color online). (a) Current-phase relationship in the S/F/S graphene junction with an undoped F region. We have fixed $\varepsilon_F = h$ and set $\varepsilon'_F = 0$. We have used values of P in the interval [0.0, 1.2] in steps of 0.2. (b) Current-phase relationship in the S/F/S graphene junction with a doped F region. We have set $\varepsilon_F/\Delta_0 = 10$, $\varepsilon'_F/\Delta_0 = 15$, and $d/\xi = 0.05$ and vary h/Δ_0 in the range [0, 5] in steps of 1.

To show that the splitting of this discontinuity originates with the presence of an exchange field which separates the spin-$\uparrow$ and spin-$\downarrow$ bands, we have also numerically solved the current-phase relationship for a nonzero Fermi level in the ferromagnetic region. Although we have obtained analytical results in this regime, these are somewhat cumbersome and therefore are omitted here. The result is shown in Fig. 2(b), where we have chosen $\Delta_0 = 1$ meV, $\varepsilon_F = 10$ meV, $\varepsilon'_F = 15$ meV, and varying h in the range $[0, 5]$ meV. This ensures that there are no evanescent modes, such that only the Andreev bound states carry the current. We choose a junction with $d/\xi = 0.05$, where ξ is the superconducting coherence length, since the short-junction regime $d \ll \xi$ is the experimentally most relevant one. The figures in (a) and (b) correspond to two quite different regimes: In (a) the exchange field is much larger than the Fermi level, while in (b) the exchange field is much smaller than the Fermi level. The trend is nevertheless seen to be the same in both cases, namely, a progressive splitting of the discontinuity located at $\Delta\phi = \pi$ in the paramagnetic case.

By assuming a heavily doped superconducting region with $\varepsilon_F = 10$ meV and an effective gap Δ_0 of 1 meV, a mean-field treatment is justified by $\varepsilon_F \gg \Delta_0$. Moreover, the short-junction regime requires that $d \ll \xi$. By using $v_F \simeq 10^6$ m/s in graphene, we obtain from $\xi = v_F/\Delta$ that $d \ll 650$ nm is required. This condition has been met in at least two experimental studies of proximity-induced superconductivity in graphene [1,2]. The critical supercurrent I_c for an S/F/S graphene junction for $\varepsilon_F = h$ and $\varepsilon'_F = 0$ is shown in Fig. 3. The critical current shows oscillations with respect to P but decays weakly compared to the metallic case and never reaches $I_c = 0$ in the relevant regime. For instance, there is a factor $\simeq 100$ in reduction of the amplitude of the current right after the second cusp in the metallic case for $h \simeq 10\Delta_0$ (see Fig. 2 in Ref. [23]), while there is only a factor $\simeq 2$ in reduction of the amplitude in the present case. Right at the cusps located at $P \simeq \{0.8, 2.8, 4.4\}$, there is a large residual value of the supercurrent which should be experimentally detectable. This is very distinct from the usual sinusoidal current-phase rela-

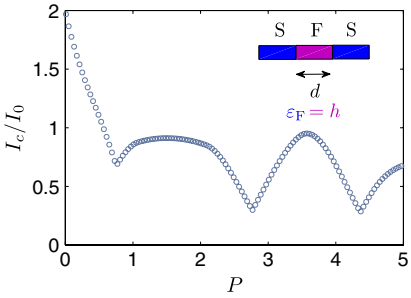

FIG. 3 (color online). The critical supercurrent in a proximity-induced S/F/S graphene junction for $\varepsilon_F = h$ and $\varepsilon'_F = 0$.

tionship for the Josephson current in which the supercurrent vanishes completely at the 0-π transition. The first switch occurs at a value $P = hd/v_F \approx 0.8$. For an exchange splitting of $h \simeq 10$ meV, this requires a junction width $d = 50$ nm. Alternatively, by employing a junction width of $d = 100$ nm [1,2], one would need an exchange splitting of $h \simeq 5$ meV [7].

In order to explain the appearance of cusps in the critical current dependent on the exchange field and junction width, it is instructive to draw parallels to the metallic S/F/S junction and the behavior of the supercurrent. In most experimental situations, the effective barriers separating the F and S regions are strong, leading to a current-phase relationship which is very nearly sinusoidal, i.e., $I_c = I_0 \sin\Delta\phi$ [24]. By tuning the temperature T and width of the junction d, one is able to switch the sign of the amplitude I_0, which necessarily means that one must have $I_0 = 0$ at some point. Precisely such behavior has been observed in several experiments [12,25]. In the present system, the current-phase relationship deviates strongly from sinusoidal behavior and contains a significant contribution from higher harmonics. By tracking the absolute value of the current with increasing P from Fig. 2, it is seen that I_c never becomes zero. Instead, it has a large residual value at the points where the current changes sign. While a small but finite value of the supercurrent at the 0-π transition also has been observed in metallic S/F/S junctions [26], the magnitude of the residual value of the supercurrent in the graphene case is huge compared to the metallic case. The relation between higher harmonics and a finite critical current at the 0-π transition has been discussed previously for ballistic Josephson S/F/S junctions with a scatterer in the F region [27].

Since we have assumed a homogeneous chemical potential in each of the S and F graphene regions, the experimental observation of the predicted effects requires charge homogeneity of the graphene samples. This is a challenge, since electron-hole puddles in graphene imaged by a scanning single electron transistor device [28] suggest that such charge inhomogeneities play an important role in limiting the transport characteristics of graphene close to the Dirac point [29]. In doped graphene, as considered here, we expect that the inhomogeneities should play a smaller role than in undoped graphene. Although we have neglected the spatial variation of the superconducting gap near the S/F interfaces, we do not expect our qualitative results to be affected by taking into account the reduction of the gap. Also, we have assumed that the junction d is short enough to neglect the orbital effect that the magnetic field constitutes on the electrons.

In summary, we have investigated the interplay between proximity-induced superconductivity and ferromagnetism in a graphene layer. In contrast to its metallic counterpart, the oscillating supercurrent in our setup decays only weakly upon increasing the exchange field and junction width. We find huge residual values of the supercurrent at the 0-π transition points where the supercurrent changes sign. If the exchange splitting could be adjusted by means of some external source, such as gate voltage or external electrical fields [5,6,18], these results imply that the supercurrent across the junction may be tuned in a controllable fashion. Specifically, a very efficient supercurrent switch may be realized by tuning the exchange field infinitesimally near the sign reversal points.

The authors thank K. Sengupta, M. Moiti, and P. Jarillo-Herrero for helpful communications. J. L. and A. S. were supported by the Norwegian Research Council Grants No. 158518/431, No. 158547/431 (NANOMAT), and No. 167498/V30 (STORFORSK). T. Y. was supported by the JSPS. D. H.-H. was supported by Norwegian Research Council Grants No. 162742/v00, No. 1585181/431, and No. 1158547/431.

[1] H. B. Heersche *et al.*, Nature (London) **446**, 56 (2007).
[2] X. Du *et al.*, arXiv:0710.4984 [Phys. Rev. B (to be published)].
[3] M. Titov and C. W. J. Beenakker, Phys. Rev. B **74**, 041401(R) (2006).
[4] M. Maiti and K. Sengupta, Phys. Rev. B **76**, 054513 (2007).
[5] Y.-W. Son *et al.*, Nature (London) **444**, 347 (2006).
[6] E.-J. Kan *et al.*, Appl. Phys. Lett. **91**, 243116 (2007).
[7] H. Haugen *et al.*, Phys. Rev. B **77**, 115406 (2008).
[8] Y. G. Semenov *et al.*, arXiv:0707.2966.
[9] T. Tokuyasu *et al.*, Phys. Rev. B **38**, 8823 (1988).
[10] P. M. Tedrow *et al.*, Phys. Rev. Lett. **56**, 1746 (1986).
[11] N. Tombros *et al.*, Nature (London) **448**, 571 (2007).
[12] V. V. Ryazanov *et al.*, Phys. Rev. Lett. **86**, 2427 (2001).
[13] A. I. Buzdin, Rev. Mod. Phys. **77**, 935 (2005).
[14] F. S. Bergeret *et al.*, Rev. Mod. Phys. **77**, 1321 (2005).
[15] S. S. Saxena *et al.*, Nature (London) **406**, 587 (2000).
[16] D. Aoki *et al.*, Nature (London) **413**, 613 (2001).
[17] J. J. A. Baselmans *et al.*, Nature (London) **397**, 43 (1999).
[18] R. Ramesh and N. A. Spaldin, Nat. Mater. **6**, 21 (2007); S.-W. Cheong and M. Mostovoy, Nat. Mater. **6**, 13 (2007).
[19] C. W. J. Beenakker, Phys. Rev. Lett. **97**, 067007 (2006).
[20] C. W. J. Beenakker and H. van Houten, Phys. Rev. Lett. **66**, 3056 (1991).
[21] J. Linder and A. Sudbø, Phys. Rev. Lett. **99**, 147001 (2007); Phys. Rev. B **77**, 064507 (2008).
[22] M. I. Katsnelson *et al.*, Nature Phys. **2**, 620 (2006).
[23] A. S. Vasenko *et al.*, Phys. Rev. B **77**, 134507 (2008).
[24] G. Mohammadkhani and M. Zareyan, Phys. Rev. B **73**, 134503 (2006).
[25] T. Kontos *et al.*, Phys. Rev. Lett. **89**, 137007 (2002); W. Guichard *et al.*, Phys. Rev. Lett. **90**, 167001 (2003).
[26] H. Sellier *et al.*, Phys. Rev. B **68**, 054531 (2003).
[27] N. M. Chtchelkatchev *et al.*, Pis'ma Zh. Eksp. Teor. Fiz. **74**, 357 (2001) [JETP Lett. **74**, 323 (2001)].
[28] J. Martin *et al.*, arXiv:0705.2180.
[29] E.-A. Kim and A. H. Castro Neto, arXiv:0702.562.

Paper XIV

Coexistence of itinerant ferromagnetism and a non-unitary superconducting state with line nodes: possible application to UGe_2.

Physical Review B **77**, 184511 (2008).

Coexistence of itinerant ferromagnetism and a nonunitary superconducting state with line nodes: Possible application to UGe_2

Jacob Linder,[1] Iver B. Sperstad,[1] Andriy H. Nevidomskyy,[2] Mario Cuoco,[3,4] and Asle Sudbø[1]
[1]*Department of Physics, Norwegian University of Science and Technology, N-7491 Trondheim, Norway*
[2]*Department of Physics and Astronomy, Rutgers University, Piscataway, New Jersey 08854-8019, USA*
[3]*Laboratorio Regionale SuperMat, CNR-INFM, Salerno, I-84081 Baronissi, Salerno, Italy*
[4]*Dipartimento di Fisica E.R. Caianiello, Università di Salerno, I-84081 Baronissi, Salerno, Italy*
(Received 25 February 2008; revised manuscript received 18 April 2008; published 19 May 2008)

We construct a mean-field theory for itinerant ferromagnetism coexisting with a nonunitary superconducting state, where only the majority-spin band is gapped and contains line nodes, while the minority-spin band is gapless at the Fermi level. Our study is motivated by recent experimental results, which indicate that this may be the physical situation realized in the heavy-fermion compound UGe_2. We investigate the stability of the mean-field solution of the magnetic and superconducting order parameters. Also, we provide theoretical predictions for experimentally measurable properties of such a nonunitary superconductor: the specific heat capacity, the Knight shift, and the tunneling conductance spectra. Our study should be useful for direct comparison with experimental results and also for further predictions of the physics that may be expected in ferromagnetic superconductors.

DOI: 10.1103/PhysRevB.77.184511 PACS number(s): 74.20.−z, 74.25.−q, 74.45.+c, 74.50.+r

I. INTRODUCTION

The interplay between ferromagnetic (FM) and superconducting (SC) long range order microscopically coexisting in the same material has attracted much interest during the last decade due to the discovery of superconductivity in ferromagnetic metals, UGe_2, URhGe, and UCoGe.[1–4] One possible route of investigation of such systems was adopted in early works,[5–7] which assumed a conventional *s*-wave superconducting condensate residing in a ferromagnetic background caused by localized spins or aligned magnetic impurities. It was shown that below a critical value of the magnetic coupling, which is comparable to the superconducting gap Δ itself, superconductivity and magnetism were able to coexist. It was also suggested that a finite-momentum pairing state, known as Fulde–Ferrell–Larkin–Ovchinnikov (FFLO) phase,[8] can appear in the presence of an external magnetic field or an intrinsic ferromagnetic order, and could thereby permit a larger threshold of the spin exchange energy to coexist with superconductivity.

On the other hand, it has been known since the early days of research on ^{3}He that alternative superconducting states, other than *s* wave, can be favored in a ferromagnetic background. The early theories of an equivalent phenomenon to occur in the solid state were formulated in the early 1980s,[9] despite the absence of any experimental example of a ferromagnetic superconductor at the time. With the discovery of superconductivity in UGe_2, especially given that the same electrons are believed to participate both in ferromagnetism and SC, this latter scenario had to be taken seriously to explain the microscopic coexistence between the two phases. In particular, the very large hyperfine magnetic molecular field in these materials, measured,[10] e.g., with Mössbauer spectroscopy, far exceeds the Pauli limit. This excludes any possibility of singlet-pairing superconductivity.

We should note that although the latter statement is true in UGe_2 and other ferromagnetic superconductors, one may still ask whether, in principle, a singlet-type superconductivity can coexist with ferromagnetism. Although some early theoretical studies[11] indicated that the answer to this question may be affirmative provided FM is weak, a more careful analysis concluded[12] that the coexistence state of spin-singlet pairing and ferromagnetism always turns out to be energetically unfavorable against the nonmagnetic superconducting state even if a finite-momentum pairing (FFLO) state is considered. Later, it was proposed[13] that the coexistence of metallic ferromagnetism and singlet superconductivity may be realized assuming that the magnetic instability is due to kinetic exchange. However, the coexistence of magnetism and spin-triplet superconductivity appears to be a more promising scenario, since the Cooper pairs may use their spin degree of freedom to align themselves with the internal magnetic field.

An experimental fact that is even more striking is that in all ferromagnetic superconductors known to date, the SC phase is only observed in a small part of the phase diagram otherwise occupied by ferromagnetism,[14] and it is the region where the magnetism appears to be at its weakest that SC sets in-on the boundary with paramagnetism when the Curie temperature is driven to zero (typically by applying pressure). This immediately raises the question of the microscopic origin of SC pairing, and whether ferromagnetic spin fluctuations play the role of a "glue" for Cooper pair formation very much as they do in superfluid ^{3}He. It is equally interesting what role the zero-temperature pressure-tuned phase transition plays in the formation of superconductivity and whether notions involving quantum criticality (provided the phase transitions are second order) are necessary to explain the phenomenon.

Although there is no universal answer to this question yet and the research efforts, both experimental and theoretical, are focused on this issue, it is interesting to note that in UGe_2 the ferromagnetic phase transition as a function of pressure becomes first order as the "critical pressure" is approached at

$T=0$. One cannot therefore straightforwardly apply a theory of quantum criticality (be it the Hertz–Millis[15] theory or one of its variations) given the absence of the quantum critical point as such. It is undeniable, however, that the point where Curie temperature goes to zero is of crucial importance to the formation of the SC state.

Drawing further parallels between triplet-pairing FM superconductors and the superfluid ^{3}He, one may wonder whether different symmetries of the SC gap can occur, as is the case in the different phases[16] of ^{3}He. For example, can the gap symmetry with point or line nodes be realized in the ferromagnetic superconductors? Very recently, experimental evidence has appeared, which suggests that the answer is "yes." Harada *et al.*[17] reported on ^{73}Ge nuclear-quadrupole-resonance experiments performed under pressure, in which the nuclear spin-lattice relaxation rate revealed an unconventional nature of superconductivity implying that the majority-spin band in UGe_2 was gapped with line nodes, while the minority-spin band remained gapless at the Fermi level.

Motivated by this, we present a mean-field model for coexisting ferromagnetism and spin-triplet superconductivity with a SC order parameter that displays line nodes in majority-spin channel and is gapless for minority spin. We first study the interplay between the magnetic and superconducting order parameters, and then proceed to make several predictions for experimentally relevant quantities: the specific heat capacity, Knight shift, and tunneling conductance. Let us briefly summarize our main results. We find that the low-temperature specific heat capacity C_V shows power-law behavior (to be contrasted with the conventional exponential decay in the *s*-wave case), and that the gapless minority spins dominate the contribution to C_V at low temperatures, giving rise to a linear T dependence. Also, the relative jump in C_V shows a strong dependence on the exchange splitting in the system. With regard to the Knight shift, we find that it is suppressed at $T=0$ with increasing exchange splitting of the majority- and minority-spin bands when the external field is applied perpendicular to the spin of the Cooper pairs in the system. In general, however, it depends strongly on the orientation of the field with respect to the crystallographic axes of the compound, indicative of the triplet pairing in the system. Finally, the normalized tunneling conductance spectra show a strong directional dependence with respect to the orientation of the superconducting order parameter in reciprocal space, but change very little upon modifying the exchange splitting in the system. Our findings should be useful for comparison with experimental studies, and could lead to further insights as regards the nature of the superconducting order parameter.

This paper is organized as follows. We first describe the phenomenological framework to be used in this work in Sec. II. We then present our theoretical model in Sec. III, and provide the results of the self-consistent mean-field treatment at both zero and finite temperatures in Sec. IV A. We then proceed to make predictions for experimentally accessible quantities in Sec. IV B, using the self-consistently obtained results from Sec. IV A. We discuss our findings in Sec. VI, and summarize in Sec. VII. We will use boldface notation for vectors, $\hat{\ldots}$ for operators, $\breve{\ldots}$ for 2×2 matrices, and $\hat{\ldots}$ for 4×4 matrices.

II. PHENOMENOLOGICAL FRAMEWORK

The issue of coexisting ferromagnetism and superconductivity dates back to half a century ago when the celebrated FFLO state was predicted[8] as a finite-momentum pairing state with real-space structure of the singlet SC order parameter that may develop under certain conditions close to the critical magnetic field H_{c2}. The conditions for the FFLO state are, however, very different from those observed in ferromagnetic superconductors such as UGe_2. In particular, as has already been emphasized above, the magnetic molecular field felt by Cooper pairs inside the ferromagnet is many times larger[10] than the Pauli limiting field necessary to destroy the singlet Cooper pairs. We shall therefore concentrate on triplet-type superconducting pairing.

Several remarks are in order. We note from the outset that the ferromagnetism observed in the uranium compounds is itinerant, Stoner-type in its nature. We shall therefore not discuss the topic of localized magnetic moments that would have, among other things, provided a pair-breaking mechanism in accord with the Abrikosov–Gor'kov theory[18] of magnetic scattering. Here, we will assume that the same electrons involved in the spontaneous SU(2) symmetry breaking associated with ferromagnetism also participate in the U(1) gauge symmetry breaking that characterizes a superconductor.

The idea of triplet pairing occurring between the same electrons that form the Stoner instability at the border of ferromagnetism goes back to Fay and Appel[9] (1980) who considered the exchange of magnetic spin fluctuations as a microscopic mechanism for Cooper pairing. More recently, the problem has been revisited[19–23] in the light of experimental findings in UGe_2 and other ferromagnetic superconductors.

In this paper, we shall take a phenomenological approach to superconductivity, leaving the intriguing and debated question of the microscopic mechanism for Cooper pairing aside. In particular, we shall consider systems where superconductivity appears at a lower temperature than the temperature at which onset of ferromagnetism is found. This is certainly the case experimentally and may be simply due to the fact that the energy scales for the two phenomena are quite different, with the exchange energy naturally being the largest. It may, however, also be due to the fact that superconductivity is dependent on ferromagnetism for its very existence. Such a suggestion has recently been put forth.[24]

A crucial issue to address in this context is whether superconductivity and ferromagnetism are phase separated (such as, e.g., solid and liquid phases coexisting at the melting point) or not. Fairly strong experimental evidence for non-phase-separated coexistence of ferromagnetism and superconductivity has recently been presented in UGe_2.[25] However, even if such non-phase-separated coexistence is established, there still remains the issue of whether the superconducting order parameters exhibits spatial variations, precisely due to its non-phase-separated coexistence with ferromagnetic order. One obvious candidate for such spatial variations[26] is a spontaneously formed Abrikosov vortex lattice, induced by the internal magnetization $\mathbf{M}$. As argued in Ref. 27, an important factor with respect to whether a vortex

lattice appears or not could be the magnitude of the internal magnetization $\mathbf{M}$. Specifically, Ref. 28 suggested that vortices may arise if $4\pi\mathbf{M} > \mathbf{H}_{c1}$, where $\mathbf{H}_{c1}$ is the lower critical field. It is conceivable that a weak ferromagnetic state coexisting with superconductivity may give rise to a domain structure, in the absence of an external field that is vortex-free. Therefore, we shall consider the non-phase-separated coexistence of the FM and SC order parameters from here on, as have other studies.[29] We will also leave the complications arising from the spatial variation of the superconducting order parameter originating with a putative spontaneously formed Abrikosov vortex lattice in the superconducting order parameter for future investigations.

Spin-triplet superconductors are characterized by a multicomponent order parameter, which for the simplest case of the p wave may be expressed in terms of three independent components of a $\mathbf{d}$ vector,

$$\mathbf{d}_{\mathbf{k}} = \left[\frac{\Delta_{\mathbf{k}\downarrow\downarrow} - \Delta_{\mathbf{k}\uparrow\uparrow}}{2}, \frac{-i(\Delta_{\mathbf{k}\downarrow\downarrow} + \Delta_{\mathbf{k}\uparrow\uparrow})}{2}, \Delta_{\mathbf{k}\uparrow\downarrow} \right]. \tag{1}$$

Note that $\mathbf{d}_{\mathbf{k}}$ transforms like a vector under spin rotations. In terms of the components of $\mathbf{d}_{\mathbf{k}}$, the order parameter itself is a 2×2 matrix that reads

$$\check{\Delta}_{\alpha\beta}(\mathbf{k}) \equiv \langle c_{\mathbf{k},\alpha} c_{\mathbf{k},\beta} \rangle = [i(\mathbf{d}_{\mathbf{k}} \cdot \boldsymbol{\sigma})\boldsymbol{\sigma}_y]_{\alpha\beta}, \tag{2}$$

where $\boldsymbol{\sigma}$ is the vector of Pauli matrices, and $c^{\dagger}_{\mathbf{k},\alpha}, c_{\mathbf{k},\alpha}$ are the usual electron creation-annihilation operators for momentum $\mathbf{k}$ and spin α.

The superconducting order parameter is characterized as *unitary* if the modulus of the gap is proportional to the unity matrix: $(\check{\Delta}\cdot\check{\Delta}^{\dagger}) \propto \check{1}$. Written in terms of the vector $\mathbf{d}_{\mathbf{k}}$, this condition is equivalent to the requirement that $\langle \mathbf{S}_{\mathbf{k}} \rangle = 0$, where we have introduced the net magnetic moment (or spin) of the Cooper pair,

$$\langle \mathbf{S}_{\mathbf{k}} \rangle \equiv i(\mathbf{d}_{\mathbf{k}} \times \mathbf{d}^{*}_{\mathbf{k}}). \tag{3}$$

The unitary triplet state thus has Cooper pairs with zero magnetic moment, whereas the *nonunitary* state is characterized by the nonzero value of $\langle \mathbf{S}_{\mathbf{k}} \rangle \neq 0$. The latter effectively means that time-reversal symmetry is spontaneously broken in the spin part of the Cooper pairs.[30] It is thus intuitively clear that having the spin of the Cooper pair aligned with the internal magnetic field of the ferromagnet can lower the energy of the resulting coexistence state. The above argument that the order parameter in the ferromagnetic superconductors must be nonunitary was put forward by Machida and Ohmi,[20] and others.[21,31] Distinguishing between unitary and nonunitary states in ferromagnetic superconductors is clearly one of the primary objectives in terms of identifying the correct SC order parameter. To this end, recent studies have focused on calculating transport properties of ferromagnetic superconductors.[32–37] There have also been investigations of identifying spin-triplet pairing in quasi-one-dimensional (quasi-1D) materials.[38–41]

Finally, we note that intersubband pairing is expected to be strongly suppressed in the presence of the Zeeman splitting between the $\uparrow,\downarrow$ conduction subbands. In other words, only electrons within the same subband will form Cooper pairs (the so-called *equal-spin pairing*) and we shall set $\Delta_{\uparrow\downarrow}=0$ in what follows. Moreover, the requirement of nonunitarity of the order parameter is then reduced to the requirement that the vector $\mathbf{d}_{\mathbf{k}}$ in Eq. (1) should have two nonzero components, i.e., $\Delta_{\uparrow\uparrow} \neq \Delta_{\downarrow\downarrow}$, which one would expect anyway in the presence of the Zeeman splitting between the two spin subbands. The spin of the Cooper pair is then $\langle S_z \rangle = \frac{1}{2}(|\Delta_{\uparrow\uparrow}|^2 - |\Delta_{\downarrow\downarrow}|^2)$ and is aligned along the magnetic field (with z being the spin quantization axis).

III. THEORY

We consider a model of a ferromagnetic superconductor described by uniformly coexisting itinerant ferromagnetism and nonunitary, spin-triplet superconductivity. We write down a weak-coupling mean-field theory Hamiltonian with equal-spin pairing Cooper pairs and a finite magnetization along the easy-axis similar to the model studied in Refs. 22 and 23, namely,

$$\hat{H} = \sum_{\mathbf{k}} \xi_{\mathbf{k}} + \frac{INM^2}{2} - \frac{1}{2}\sum_{\mathbf{k}\sigma} \Delta^{\dagger}_{\mathbf{k}\sigma\sigma} b_{\mathbf{k}\sigma\sigma} + \frac{1}{2}\sum_{\mathbf{k}\sigma} (\hat{c}^{\dagger}_{\mathbf{k}\sigma}\hat{c}_{-\mathbf{k}\sigma}) \times \begin{pmatrix} \xi_{\mathbf{k}\sigma} & \Delta_{\mathbf{k}\sigma\sigma} \\ \Delta^{\dagger}_{\mathbf{k}\sigma\sigma} & -\xi_{\mathbf{k}\sigma} \end{pmatrix} \begin{pmatrix} \hat{c}_{\mathbf{k}\sigma} \\ \hat{c}^{\dagger}_{-\mathbf{k}\sigma} \end{pmatrix}, \tag{4}$$

where $b_{\mathbf{k}\sigma\sigma} = \langle c_{-\mathbf{k}\sigma} c_{\mathbf{k}\sigma} \rangle$ is the nonzero expectation value of the pair of Bloch states. Applying a standard diagonalization procedure, we arrive at

$$\hat{H} = H_0 + \sum_{\mathbf{k}\sigma} E_{\mathbf{k}\sigma} \hat{\gamma}^{\dagger}_{\mathbf{k}\sigma} \hat{\gamma}_{\mathbf{k}\sigma},$$

$$H_0 = \frac{1}{2}\sum_{\mathbf{k}\sigma} (\xi_{\mathbf{k}\sigma} - E_{\mathbf{k}\sigma} - \Delta^{\dagger}_{\mathbf{k}\sigma\sigma} b_{\mathbf{k}\sigma\sigma}) + \frac{INM^2}{2}, \tag{5}$$

where $\{\hat{\gamma}_{\mathbf{k}\sigma}, \hat{\gamma}^{\dagger}_{\mathbf{k}\sigma}\}$ are new fermion operators and the eigenvalues read

$$E_{\mathbf{k}\sigma} = \sqrt{\xi^2_{\mathbf{k}\sigma} + |\Delta_{\mathbf{k}\sigma\sigma}|^2}. \tag{6}$$

It is implicit in our notation that $\xi_{\mathbf{k}} = \varepsilon_{\mathbf{k}} - E_F$ is measured from the Fermi level, where $\varepsilon_{\mathbf{k}}$ is the kinetic energy. The free energy is obtained through

$$F = H_0 - \frac{1}{\beta}\sum_{\mathbf{k}\sigma} \ln(1 + e^{-\beta E_{\mathbf{k}\sigma}}), \tag{7}$$

such that the gap equations for the magnetic and superconducting order parameters become[22]

$$M = -\frac{1}{N}\sum_{\mathbf{k}\sigma} \frac{\sigma\xi_{\mathbf{k}\sigma}}{2E_{\mathbf{k}\sigma}} \tanh(\beta E_{\mathbf{k}\sigma}/2),$$

$$\Delta_{\mathbf{k}\sigma\sigma} = -\frac{1}{N}\sum_{\mathbf{k}'} V_{\mathbf{k}\mathbf{k}'\sigma\sigma} \frac{\Delta_{\mathbf{k}'\sigma\sigma}}{2E_{\mathbf{k}'\sigma}} \tanh(\beta E_{\mathbf{k}'\sigma}/2). \tag{8}$$

Specifically, we now consider a model which should be of relevance to the ferromagnetic superconductor UGe_2, and possibly also for UCoGe and URhGe. In Ref. 17, it was

argued that the majority-spin (spin up in our notations) fermions were gapped and that the order parameter displayed line nodes, while the minority (spin-down) fermions remained gapless at the Fermi level in the heavy-fermion compound UGe_2. An obvious mechanism for suppressing the superconducting instability in the minority-spin channel as compared to the majority-spin channel is the difference in density of states (DOS) at the Fermi level. Indeed, from Fig. 1 in Ref. 22 (see also Fig. 4 in Ref. 23), it is seen that the critical temperature for pairing in the minority-spin subband, $T_c^{\downarrow}$, is predicted to be much smaller than the critical $T_c^{\uparrow}$ for the majority-spin subband, even for quite weak magnetic exchange splittings. Given the already quite low critical temperature T_c that is observed experimentally in ferromagnetic superconductors ($T_c \lesssim 1$ K), which we associate with $T_c^{\uparrow}$, we therefore conclude that it might indeed be very hard to observe experimentally the even smaller gap in the minority-spin subband. Therefore, it is permissible to only consider pairing in the majority-spin channel and neglect a small (if any) pairing between minority-spin electrons. In our notation this means setting $M \neq 0, \Delta_{\mathbf{k}\uparrow} \neq 0, \Delta_{\mathbf{k}\downarrow} = 0$.

We stress that the above statement, although intuitively attractive, may need further justification since we have so far neglected completely the spin-orbit interaction that is expected to be strong in uranium based compounds, such as UGe_2, URhGe, and UCoGe. The effect of the latter would be to provide some effective coupling between majority- and minority-spin subbands and would probably lead to induced SC order parameter in minority-spin channel. This issue is left for future study.[42]

To model the presence of line nodes in the order parameter, we choose

$$\Delta_{\mathbf{k}\uparrow} = \Delta_{\bar{\mathbf{k}}_F\uparrow\uparrow} = \Delta_0 \cos\,\theta, \tag{9}$$

where $\bar{\mathbf{k}}_F$ is the normalized Fermi wave vector, such that the gap only depends on the direction of the latter. This is the weak-coupling approximation. The above gap satisfies the correct symmetry requirement dictated by the Pauli principle, namely a sign change under inversion of momentum, $\theta \rightarrow \pi - \theta$. Here, θ is the azimuthal angle in the xy plane. Our choice of this particular symmetry for the p-wave superconducting gap is motivated by the experimental results of Harada *et al.*[17] The cos θ dependence is also in accord with the results of Ref. 43, which showed that the majority band at the Fermi level for UGe_2 is strongly anisotropic with a small dispersion along the k_y direction. We consider here a situation where the electrons are restricted from moving along the $\mathbf{z}$ axis. The motivation for this is that, strictly speaking, it seems plausible that uniform coexistence of ferromagnetic and superconducting order should only be realized in thin-film structures where the Meissner (diamagnetic) response of the superconductor is suppressed for in-plane magnetic fields. The thin-film structure would then also suppress the orbital effect of the field. In a bulk structure, as considered in Ref. 11, we expect that a spontaneous vortex lattice should be the favored thermodynamical state,[26] unless prohibited by a possible domain structure. Having said that, we point out that there is no firm experimental evidence for the presence of such a vortex phase in ferromagnetic superconductors such as UGe_2, and we therefore do not exclude some mechanism that would instead stabilize a truly uniform coexistence of the SC and FM in these materials. It should be mentioned that uniform coexistence of ferromagnetism and superconducting order have also been speculated to occur in quasi-1D and quasi-two-dimensional materials such as $RuSr_2GdCu_2O_8$.[44] In our model, the pairing potential may be written as

$$V(\theta, \theta') = -g \cos\,\theta \cos\,\theta', \tag{10}$$

where g is the weak-coupling constant. Conversion to integral equations is accomplished by means of the identity

$$\frac{1}{N}\sum_{\mathbf{k}} f(\xi_{\mathbf{k}\sigma}) = \int d\varepsilon N^{\sigma}(\varepsilon), \tag{11}$$

where $N^{\sigma}(\varepsilon)$ is the spin-resolved density of states. In three spatial dimensions, this may be calculated from the dispersion relation by using the formula

$$N^{\sigma}(\varepsilon) = \frac{V}{(2\pi)^3}\int_{\varepsilon_{\mathbf{k}\sigma}=\text{const}} \frac{\mathrm{d}S_{\varepsilon_{\mathbf{k}\sigma}}}{|\hat{\nabla}_{\mathbf{k}}\varepsilon_{\mathbf{k}\sigma}|}. \tag{12}$$

With the dispersion relation $\xi_{\mathbf{k}\sigma} = \varepsilon_{\mathbf{k}} - \sigma IM - E_F$, one obtains

$$N^{\sigma}(\varepsilon) = \frac{mV\sqrt{2m(\varepsilon + \sigma IM + E_F)}}{2\pi^2}. \tag{13}$$

In their integral form, Eqs. (8) for the order parameters read

$$M = -\frac{1}{4\pi}\sum_{\sigma}\sigma\int_0^{2\pi}\int_{-E_F-\sigma IM}^{\infty} d\theta d\varepsilon \frac{\varepsilon N^{\sigma}(\varepsilon)}{E_{\sigma}(\varepsilon,\theta)} \times \tanh[\beta E_{\sigma}(\varepsilon,\theta)/2],$$

$$1 = \frac{g}{4\pi}\int_0^{2\pi}\int_{-\omega_0}^{\omega_0} d\theta d\varepsilon \frac{N^{\uparrow}(\varepsilon)\cos^2\,\theta}{E_{\uparrow}(\varepsilon)} \tanh[\beta E_{\uparrow}(\varepsilon,\theta)/2]. \tag{14}$$

For ease of notation, we also define

$$\Delta_{\sigma}(\theta) = \begin{cases} \Delta_0 \cos\,\theta & \text{if } \sigma = \uparrow \\ 0 & \text{if } \sigma = \downarrow \end{cases},$$

$$E_{\sigma}(\varepsilon,\theta) = \begin{cases} \sqrt{\varepsilon^2 + \Delta_0^2 \cos^2\,\theta} & \text{if } \sigma = \uparrow \\ \varepsilon & \text{if } \sigma = \downarrow \end{cases}, \tag{15}$$

For the following treatment, we define $\tilde{M} = IM/E_F$, i.e., the exchange energy scaled on the Fermi energy. Moreover, we set $c = gN(0)/2$ to a typical value of 0.2 and $\tilde{\omega}_0 = \omega_0/E_F = 0.01$ as the typical spectral width of the bosons responsible for the attractive pairing potential. Finally, we define the parameter $\tilde{I} = IN(0)$ as a measure of the magnetic exchange coupling. As discussed below, only for $\tilde{I} > 1$ will a spontaneous magnetization appear in our model, in agreement with the Stoner criterion for itinerant ferromagnetism.

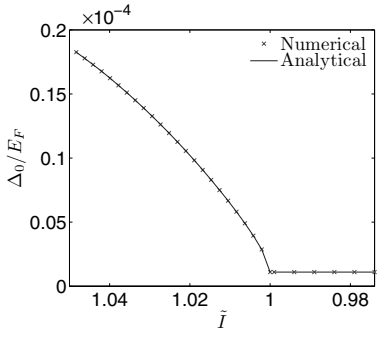

FIG. 1. (Color online) The gap dependence on the ferromagnetic exchange interaction parameter $\tilde{I}=IN(0)$. The gap remains constant for $\tilde{I}\in[0,1]$, which correspond to a unitary phase. The gap Δ_0 then starts growing with increasing $\tilde{I}$ for $\tilde{I}>1.0$, announcing the onset of a spontaneous magnetization. The analytical formula is based on Eq. (18).

IV. RESULTS: MEAN-FIELD MODEL FOR COEXISTENCE

A. Zero-temperature case

For zero temperature, the superconducting gap equation reads

$$1=\frac{g}{4\pi}\int_0^{2\pi}\int_{-\omega_0}^{\omega_0}d\theta d\varepsilon\frac{N^{\uparrow}(\varepsilon)\cos^2\theta}{\sqrt{\varepsilon^2+\Delta_0^2\cos^2\theta}}. \tag{16}$$

Under the assumption that $\omega_0\gg\Delta_0$, we obtain that

$$\frac{2}{c\sqrt{1+\tilde{M}}}=\ln\left(\frac{2\omega_0}{\Delta_0}\right)-\frac{1}{\pi}\int_0^{2\pi}d\theta\cos^2\theta\ln|\cos\theta|. \tag{17}$$

which may be solved to yield the zero-temperature gap

$$\Delta_0=2.426\omega_0\exp[-2/(c\sqrt{1+\tilde{M}})]. \tag{18}$$

By inserting Eq. (18) into the gap equation for the magnetization in Eq. (14), we have managed to decouple the self-consistency equations for M and Δ_0. Numerical evaluation reveals that the gap equation for M is completely unaffected by the presence of Δ_0, which physically means that the magnetization remains unaltered with the onset of superconductivity. This is reasonable in a model where the energy scale for the onset of magnetism is vastly different from the energy scale for superconductivity, such that by the time superconductivity sets in, the ordering of the spins essentially exhausts the maximum possible magnetization.

The dependence of Δ_0 on $\tilde{I}$ is shown in Fig. 1. The gap remains constant for $\tilde{I}\in[0,1]$, which is a unitary phase. In the unitary phase, there is no reason for the minority-spin band to remain ungapped when $M=0$, and hence we would expect two gaps $\Delta_{\uparrow}=\Delta_{\downarrow}$ of equal magnitude for $\tilde{I}<1$. Our model of gapping exclusively for the majority-spin band is therefore justified only for $\tilde{I}>1$, which is the regime we shall be concerned with throughout this paper. The onset of a spontaneous magnetization for $\tilde{I}>1$ is the well-known Stoner criterion for an isotropic electron gas, where the spin susceptibility may be written as[45]

$$\chi(\mathbf{q},\omega)=\frac{\chi_0(\mathbf{q},\omega)}{1-I\chi_0(\mathbf{q},\omega)},$$

$$\chi_0(\mathbf{q},\omega)=N_0\left(1-\frac{\mathbf{q}^2}{12k_F^2}+i\frac{\pi\omega}{2v_F|\mathbf{q}|}\right),$$

$$|\mathbf{q}|\ll 2k_F,\quad \omega\ll E_F. \tag{19}$$

For a parabolic band, the static susceptibility is maximal for $\mathbf{q}=0$ where

$$\chi(\mathbf{q}=0,\omega=0)=\frac{N_0}{1-IN(0)}=\frac{N_0}{1-\tilde{I}}. \tag{20}$$

The introduction of a ferromagnetic order is demarcated by the divergence of the susceptibility for $\tilde{I}=1$, which is precisely Stoner's criterion for itinerant ferromagnetism. In the absence of superconductivity, the self-consistency equation for the magnetization at $T=0$ reduces to

$$h=-\frac{\tilde{I}}{3\sqrt{E_F}}\sum_{\sigma}\sigma(E_F-\sigma h)^{3/2}, \tag{21}$$

where $h=IM$ is the exchange splitting of the majority and minority bands. Since the energy scales for the magnetic and superconducting order parameter differ so greatly in magnitude, Eq. (21) is an excellent approximation even in the coexistent state (we have verified this numerically).

B. Finite temperature case

The critical temperature for the superconducting order parameter is obtained in the standard way [setting $\Delta_0=0$ in Eq. (16)] to yield

$$T_c=1.134\omega_0\exp[-2/(c\sqrt{1+\tilde{M}})]. \tag{22}$$

In Fig. 2, we plot the temperature dependence of the self-consistently obtained solution of Δ_0 and compare it to the analytical mean-field temperature dependence

$$\Delta_0(T)=\Delta_0(0)\tanh[\gamma\sqrt{T_c/T-1}]. \tag{23}$$

The BCS result is $\gamma=1.74$, but we find a better fit for our numerical results using $\gamma=1.70$. Throughout the rest of this paper, we shall therefore make use of Eq. (23) with $\gamma=1.70$ to model the temperature dependence of the gap for $\tilde{I}=\{1.01,1.02,1.03\}$, since the agreement is excellent with the full numerical solution. As in the zero-temperature case, we find that the gap equations in Eq. (14) may be completely decoupled also at finite temperature. We have verified that the gap equation for the superconducting order parameter has a unique nontrivial solution, which guarantees that the system will prefer to be in the coexistent state of ferromagnetism and superconductivity.

The phase diagram of the model we are considering may be obtained numerically and is shown in Fig. 3. As seen, a

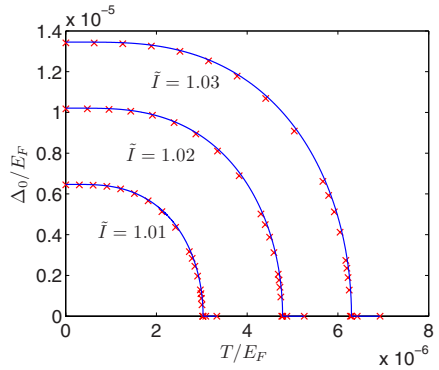

FIG. 2. (Color online) Self-consistently obtained solution for the superconducting gap Δ_0 (red symbols) compared to the analytical expression Eq. (23) with $\gamma=1.70$ (blue lines), modeling a BCS-type temperature dependence.

quantum phase transition may occur at $\tilde{I}=1.0$, separating the unitary superconducting state (see discussion in an earlier paragraph) from the ferromagnetic, nonunitary superconducting state. The critical temperature for the magnetic order parameter is orders of magnitudes larger than T_c for the superconductivity except for very close to $\tilde{I}=1.0$. The increase in T_c in the nonunitary phase as compared to the unitary phase is a result of the increase in density of states with magnetization for the majority spin.

Experimentally, one often maps out the T-p phase diagram, where T is temperature and p is pressure. Note that the value of $\tilde{I}$ may be controlled experimentally by adjusting the pressure on the sample. A change in pressure is accompanied by a change in the width of the electron bands, and therefore directly affects the density of states at the Fermi level: increasing the pressure on the samples reduces the density of

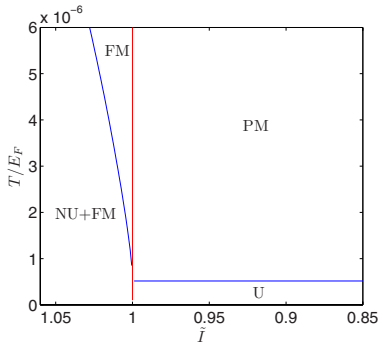

FIG. 3. (Color online) The phase diagram of our model in the T-$\tilde{I}$ plane. For $\tilde{I}>1.0$, a spontaneous magnetization arises and allows for the possible uniform coexistence of ferromagnetism and triplet superconductivity. Note that decreasing $\tilde{I}$ (going from left to right along the x axis) corresponds to an increasing external pressure p. The abbrevations stand for nonunitary (NU), unitary (U), ferromagnetic (FM), and paramagnetic (PM).

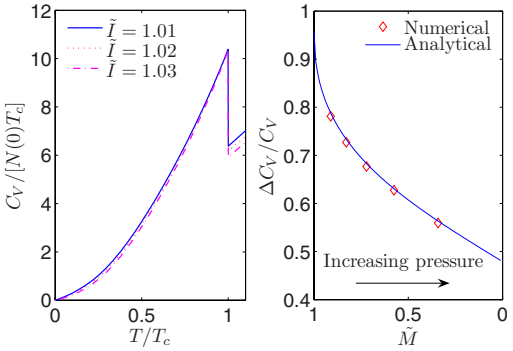

FIG. 4. (Color online) The left panel shows a plot of the specific heat capacity, using self-consistently obtained order parameters for three different values of $\tilde{I}$. The right panel shows relative jump (superconducting vs normal state) of the specific heat at the transition temperature as a function of the normalized exchange splitting between the spin bands, $\tilde{M}$. Numerically calculated values are shown in red; analytical results [Eq. (25)] using $\gamma\approx 1.70$ are shown in blue.

states, and hence also the effective coupling constant $\tilde{I}$.[46] A notable feature in the phase diagram for UGe_2 as determined experimentally, is that superconductivity only appears in the ferromagnetic phase, and not in the paramagnetic phase.

V. RESULTS: EXPERIMENTAL PREDICTIONS

We next proceed to using the self-consistently obtained solutions from the previous section to make predictions for three experimental quantities that are routinely used to study superconducting condensates: specific heat, Knight shift, and tunneling conductance spectra. We first consider the normalized heat capacity, which is defined as

$$C_V = \frac{\beta^2}{8\pi}\sum_\sigma \int_0^{2\pi}\int_{-E_F-\sigma IM}^{\infty} d\theta d\varepsilon \frac{N^\sigma(\varepsilon)}{\cosh^2[\beta E_\sigma(\varepsilon,\theta)/2]} \times \left[E_\sigma^2(\varepsilon,\theta) - T\left(\Delta_\sigma(\theta)\frac{\partial \Delta_\sigma(\theta)}{\partial T} - \sigma\varepsilon I\frac{\partial M}{\partial T}\right)\right]. \quad (24)$$

Since the critical temperature of M is much larger than the critical temperature for Δ_0 in our model, we may safely neglect $\partial M/\partial T$ in the low-temperature regime. Consider Fig. 4 for a plot of the specific heat capacity using three representative values for $\tilde{I}$. The general trend with increasing $\tilde{I}$ is an increase in the jump of C_V at $T=T_c$. The physical reason for this is that the majority-spin carriers will dominate the jump in specific heat stronger when the exchange splitting between the bands increases, which is in agreement with the results of Ref. 23. Analytically, the relative jump in specific heat may be expressed as

$$\left(\frac{\Delta C_V}{C_V}\right)\Bigg|_{T=T_c} \sim \left(1+\sqrt{\frac{1-h/E_F}{1+h/E_F}}\right)^{-1}. \tag{25}$$

It depends on the exchange splitting in the superconductor since the contribution from the majority-spin carriers will tend to dominate the specific heat when h increases. The low-temperature scaling with T bears witness of the line nodes in the gap and is to be contrasted with the more rapidly decaying s-wave case. Also note that the minority-spin fermions are in the normal state and give a significant contribution to the specific heat in form of a linear T dependence at low temperatures. If both spin species were gapped with line nodes, one would expect a T^2 dependence of the low temperature specific heat.

In the experimental study of the heat-capacity in UGe_2 conducted in Ref. 47, a peak of the heat-capacity associated with the superconducting transition was observed in a narrow pressure region $\Delta p \simeq 0.1$ GPa around p_x. Here, p_x is the pressure at which the superconducting transition temperature T_c shows a maximum value. Farther away from p_x, the heat capacity anomaly was smeared out. In particular, a substantial residual value of C_V/T was observed at $T \to 0$. Tateiwa *et al.*[47] argued that neither the minority-band density of states at the Fermi level nor the contribution from a self-induced vortex state would be appropriate to describe this residual value. Instead, it might stem from impurities that induce a finite density of states at the Fermi level. For an anisotropic superconductor such as UGe_2, the residual value would be highly sensitive to such impurities. It is also clear that the observation of sharp peaks, similar to the ones we obtain in Fig. 4, depend strongly on the applied pressure on the superconductor and, in particular, on how close it is to p_x.

We next consider the spin susceptibility, making use of the standard formula[48]

$$\chi(\mathbf{q},\omega) = -\frac{1}{2\beta}\sum_{\mathbf{k},i\omega_n} \mathrm{Tr}\{\hat{\mathcal{G}}(\mathbf{k},i\omega_n)\hat{\mathcal{G}}(\mathbf{k}+\mathbf{q},i\omega+i\omega_n)\}, \tag{26}$$

where $\hat{\mathcal{G}}$ is the matrix Green's function in particle hole and spin space, where $\omega_n = 2(n+1)\pi/\beta$ are fermionic Matsubara frequencies. In the static ($\omega=0$) and uniform ($q=0$) limit, Eq. (26) reduces to the Knight shift $\kappa \equiv \chi(0,0)$. We define the normalized Knight shift as

$$\frac{\kappa}{\kappa_0} = \frac{\beta}{8\pi}\sum_\sigma \int_0^{2\pi}\int_{-E_F-\sigma IM}^{\infty} \frac{d\theta d\varepsilon N_\sigma(\varepsilon)}{\cosh^2[\beta E_\sigma(\varepsilon,\theta)/2]}. \tag{27}$$

The Knight shift is a measure of the polarizability of the conduction electrons in the compound, and serves as a highly useful probe to distinguish between singlet and triplet superconductivity. For a singlet superconductor, the total spin S of the Cooper pair is zero, and the Knight shift therefore vanishes at $T=0$ since there are no quasiparticle excitations in the superconductor that may be polarized. The Knight shift vanishes regardless of the direction in which the external magnetic field is applied for a singlet superconductor. For a triplet superconductor, this is quite different. The Knight shift now may be anisotropic in terms of the direction in which the magnetic field is applied. By means of the $\mathbf{d_k}$-vector formalism [see Eq. (1)], one may infer that the Knight shift is unaltered even for $T<T_c$ when $\mathbf{d_k} \perp \mathbf{H}$ but is altered according to Eq. (27) when $\mathbf{d_k} \| \mathbf{H}$. This is valid as long as the $\mathbf{d_k}$ remains "pinned" in the material due to, e.g., spin-orbit coupling, and hence does not rotate with $\mathbf{H}$. Otherwise, the Knight shift would remain unaltered in any direction. Therefore, an anisotropic Knight shift is a strong signature of a vector character of the superconducting order parameter, and hence of a spin-triplet superconducting state.

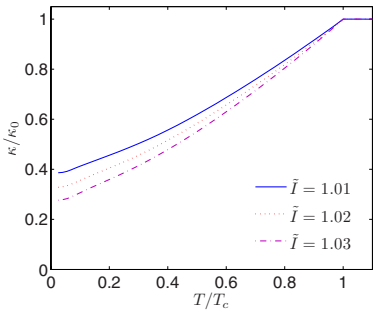

FIG. 5. (Color online) Knight shift for a ferromagnetic superconductor, using self-consistently obtained order parameters, for three different values of $\tilde{I}$. Here, the field is applied $\mathbf{H} \| \mathbf{d_k}$.

In Fig. 5, we plot the Knight shift for several values of $\tilde{I}$. It is interesting to note that $\kappa(0)$ is reduced with increasing $\tilde{I}$. Physically, this may be understood by realizing that the density of states of ungapped minority spins at the Fermi level decreases as the exchange splitting between the majority and minority bands increases. This results directly in a lower amount of polarizable quasiparticles, and hence the Knight shift becomes suppressed. For a fully polarized ferromagnet (half-metal), the Knight shift would therefore be identical to an s-wave singlet superconductor for an applied field satisfying $\mathbf{H} \| \mathbf{d_k}$. This fact emphasizes the importance of measuring the spin susceptibility along several directions to identify the proper spin symmetry of the superconductor.

As a final experimental probe for the interplay between ferromagnetism and superconductivity, we employ a Blonder–Tinkham–Klapwijk formalism[49] to calculate the tunneling between a normal metal and a ferromagnetic superconductor in the clean limit, using the self-consistently obtained values of the order parameters in the problem. From the results of Ref. 34, we find that the normalized tunneling conductance may be written as

$$\frac{G}{G_0} = \sum_\sigma \int_{-\pi/2}^{\pi/2} d\theta \cos\theta [1 + |r_\sigma^A(eV,\theta)|^2 - |r_\sigma^N(eV,\theta)|^2], \tag{28}$$

where G_0 is the normal-state conductance. Above, $r_\sigma^A(eV,\theta)$ and $r_\sigma^N(eV,\theta)$ designate the Andreev- and normal-reflection coefficients, respectively, and read

$$r_\sigma^N = -1 + \frac{2k_F \cos\theta [u_\sigma(\theta_{s+}^\sigma)u_\sigma(\theta_{s-}^\sigma)(\Upsilon_+^\sigma)^* + v_\sigma(\theta_{s-}^\sigma)v_\sigma(\theta_{s+}^\sigma)\gamma_\sigma(\theta_{s-}^\sigma)\gamma_\sigma^*(\theta_{s+}^\sigma)(\Upsilon_-^\sigma)^*]}{u_\sigma(\theta_{s+}^\sigma)u_\sigma(\theta_{s-}^\sigma)|\Upsilon_+^\sigma|^2 - v_\sigma(\theta_{s-}^\sigma)v_\sigma(\theta_{s+}^\sigma)\gamma_\sigma(\theta_{s-}^\sigma)\gamma_\sigma^*(\theta_{s+}^\sigma)|\Upsilon_-^\sigma|^2},$$

$$r_\sigma^A = \frac{4k_F \cos\theta q^\sigma \cos\theta_s^\sigma v_\sigma(\theta_{s+}^\sigma)u_\sigma(\theta_{s-}^\sigma)\gamma_\sigma^*(\theta_{s+}^\sigma)}{u_\sigma(\theta_{s+}^\sigma)u_\sigma(\theta_{s-}^\sigma)|\Upsilon_+^\sigma|^2 - v_\sigma(\theta_{s-}^\sigma)v_\sigma(\theta_{s+}^\sigma)\gamma_\sigma(\theta_{s-}^\sigma)\gamma_\sigma^*(\theta_{s+}^\sigma)|\Upsilon_-^\sigma|^2}. \quad (29)$$

We have defined $Z=2mV_0/k_F$ as a measure of the barrier strength, where m is the quasiparticle mass, V_0 is the scattering strength of the barrier, and k_F is the Fermi momentum. Moreover, θ is the angle of incidence of incoming electrons from the normal side and we have implicitly incorporated conservation of group velocity and conservation of momentum parallel to the barrier, i.e., $k_F \sin\theta = q^\sigma \sin\theta_s^\sigma$. Finally, we have introduced

$$\Upsilon_\pm^\sigma = q^\sigma \cos\theta_s^\sigma \pm k_F \cos\theta \pm ik_F Z \quad (30)$$

and $\gamma_\sigma(\theta)=\Delta_\sigma(\theta)/|\Delta_\sigma(\theta)|$, $\theta_{s+}^\sigma=\theta_s^\sigma$, $\theta_{s-}^\sigma=\pi-\theta_s^\sigma$. In the quasiclassical approximation $E_F \gg (\Delta_0, \varepsilon)$, the wave vectors read

$$k_F = \sqrt{2mE_F}, \quad q^\sigma = \sqrt{2m(E_F + \sigma IM)}, \quad (31)$$

while the spin-generalized coherence factors are

$$u_\sigma(\theta_{s\pm}^\sigma) = \frac{1}{\sqrt{2}}\{1 + \sqrt{1 - (|\Delta_\sigma(\theta_{s\pm}^\sigma)|/E)^2}\}^{1/2},$$

$$v_\sigma(\theta_{s\pm}^\sigma) = \frac{1}{\sqrt{2}}\{1 - \sqrt{1 - (|\Delta_\sigma(\theta_{s\pm}^\sigma)|/E)^2}\}^{1/2}. \quad (32)$$

In Fig. 6, we plot the conductance spectra of a normal/ferromagnetic superconductor junction. By writing the gap as $\Delta=\Delta_0\cos(\theta-\alpha)$, we allow for an arbitrary orientation of the gap with respect to the crystallographic axes. The features seen in the conductance spectra are qualitatively different for $\alpha=0$ and $\alpha=\pi/2$. In the first case, the electronlike and holelike quasiparticles entering the superconductor experience a constructive phase interference which gives rise to the formation of a zero-energy state that is bound to the surface of the superconductor. The resonance condition for the formation of such zero-energy states is $\Delta(\theta)=-\Delta(\pi-\theta)$,[50] and the bound states are manifested as a giant peak in the zero-bias conductance.[51] Note that such states exist even if the spatial depletion of the superconducting order parameter is not taken into account, which may be shown analytically.[52] Taking the reduction into account, one obtains the same qualitative features as the usual step-function approximation, with the exception of additional, smaller peaks at finite bias voltages due to nonzero bound states.[53] From Fig. 6, we see that the effect of increasing the exchange field amounts to sharper features in the conductance spectra. With increasing $\tilde{I}$, the zero-bias conductance peak becomes larger for $\alpha=0$, while the dip structure for $\alpha=\pi/2$ becomes more pronounced. Physically, this may be understood by the increased contribution from majority-spin carriers. The contribution from the minority-spin carriers is constant for the entire low-energy regime and leads to less pronounced features in the conductance. The effect of the barrier strength Z is seen in the left column of Fig. 6. For $\alpha=0$, increasing Z leads to a higher peak at zero bias, while increasing Z suppresses the conductance for $\alpha=\pi/2$.

It is also worth emphasizing the relation between the tunneling conductance and the bulk DOS of the superconductor. As is well known, the conductance of a normal/s-wave superconductor junction in the tunneling limit approaches the DOS of the bulk superconductor.[49] The same argument is valid for a $d_{x^2-y^2}$-wave superconductor.[51] One might be tempted to conclude that the tunneling conductance will always approach the bulk DOS of the superconductor in the strong barrier limit as long as there is no formation of zero-energy states. However, closer examination reveals that this is not necessarily so.

To illustrate this, we draw upon some results obtained in Ref. 54. In general, the conductance of an N/S junction in the tunneling limit may be written as

$$G(eV) \approx \frac{\int_{-\pi/2}^{\pi/2} d\theta_N \sigma_N \cos\theta_N \rho_S(eV)}{\int_{-\pi/2}^{\pi/2} d\theta_N \sigma_N \cos\theta_N}, \quad (33)$$

where σ_N is the normal-state conductance for a given angle of incidence θ_N and ρ_S is the surface DOS for the supercon-

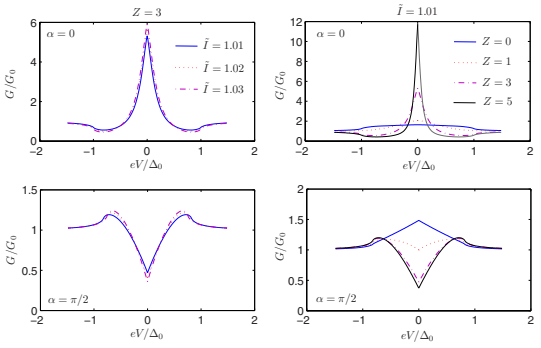

FIG. 6. (Color online) Plot of the tunneling conductance of a normal/ferromagnetic superconductor junction for $\alpha=0$ and $\alpha=\pi/2$, using self-consistently obtained solutions at $T=0$. In the left column, we fix the tunneling barrier strength $Z=2$ $mV_0/k_F=3$ and plot the conductance for several values of the Stoner interaction $\tilde{I}$. In the right column, we fix $\tilde{I}=1.01$ and plot the conductance for several values of Z.

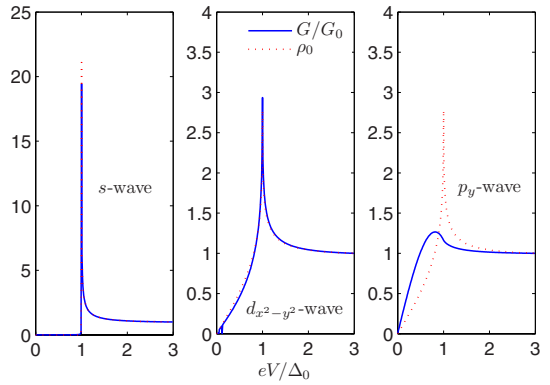

FIG. 7. (Color online) Illustration of the different symmetry states considered here and a qualitative sketch of the weighting factor $\sigma_N \cos\theta_N$.

ductor. In the absence of zero-energy states, the surface DOS coincides with the bulk DOS of the superconductor, i.e., $\rho_S = \rho_0$, where

$$\rho_0(eV) = \int_{-\pi/2}^{\pi/2} d\theta_N \, \mathrm{Re}\left\{ \frac{eV}{\sqrt{eV^2 - |\Delta(\theta_N)|^2}} \right\}. \tag{34}$$

An important consequence of the above equation is that the tunneling conductance may be interpreted as the expectation value of ρ_S with a weighting factor $\sigma_N \cos\theta_N$.

Let us now compare three different superconducting symmetries to illustrate the relation between the conductance and the DOS. We consider an s-wave, $d_{x^2-y^2}$-wave, and p_y-wave symmetry, none of which feature zero-energy surface states (Fig. 7). Naively, one might therefore expect that the conductance should converge toward ρ_0 in the tunneling limit. However, it turns out that the weighting factor $\sigma_N \cos\theta_N$, which is peaked around $\theta_N = 0$, plays a major role in this scenario. In Fig. 8, we plot both the tunneling conductance $G(eV)/G_0$ and the bulk DOS ρ_0 for these three symmetries and fix $Z = 20$. We regain the well-known results that $G(eV)/G_0 \to \rho_0$ for large Z in the s wave and $d_{x^2-y^2}$ case. However, the conductance and DOS differ in the p_y-wave case.

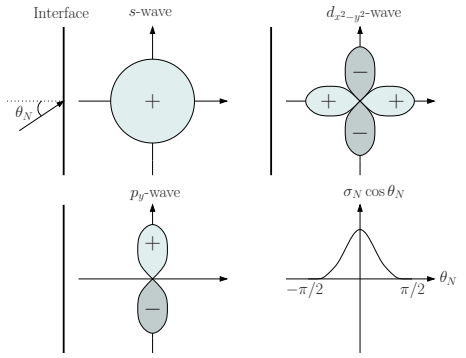

FIG. 8. (Color online) Plot of the normalized conductance G/G_0 and bulk DOS ρ_0 for three different symmetries of the superconducting state in the tunneling limit. Only in the p_y-wave case is there a difference between these two quantities.

The reason for the deviation between G/G_0 and ρ_0 in the p_y-wave case may be understood by consulting Fig. 7. As seen, the weighting factor is peaked around normal incidence $\theta_N = 0$. In the s wave and $d_{x^2-y^2}$ case, the gap magnitude is maximal at $\theta_N = 0$ and replacing the weighting factor in Eq. (33) with unity has little or no consequence. The situation is dramatically different in the p_y-wave case. Now, the gap magnitude is actually *zero* for normal incidence, and it is precisely this contribution that will dominate the integration over angles in Eq. (33). Therefore, replacing the weighting factor with unity, in order to obtain the DOS, has a nontrivial consequence in the p_y-wave case. This analysis illustrates how the conductance and bulk DOS in the absence of zero-energy states are not always the same in the tunneling limit. Note that the orientation of the interface with respect to the symmetry of the order parameter is crucial with regard to the measured conductance spectra and the surface DOS. For instance, even at $\alpha = \pi/4$ there is an appearance of a large zero-bias conductance peak for the p-wave pairing considered here, although the gap orientation does not satisfy the condition for perfect formation of zero-energy states.

VI. DISCUSSION

We have discussed a mean-field model where itinerant ferromagnetism coexists with nonunitary, triplet superconductivity, with a gap that contains line nodes. The precise symmetry of the order parameter in the ferromagnetic superconductors UGe_2, URhGe, and UCoGe is still under debate, although most experimental findings and theoretical considerations strongly point toward the realization of a triplet superconducting order parameter. It is plausible that such a superconducting order parameter is nonunitary, thus breaking time-reversal symmetry in the spin channel of the Cooper pair.

The orbital symmetry of the superconducting order parameter in ferromagnetic superconductors is a more subtle issue. In Ref. 23, a mean-field model for isotropic, chiral p-wave gaps in a background of itinerant ferromagnetism was constructed. In that work, pairing was assumed to occur both for majority and minority spins, resulting in, for instance, a double-jump structure in the specific heat capacity. An isotropic, chiral p-wave order parameter has a constant magnitude, which is favorable in terms of maximizing the condensation energy gained in the superconducting state. Assuming an isotropic density of states at the Fermi level and a separable pairing potential of the form $V_{\mathbf{k}\mathbf{k}'} = -g\lambda_{\mathbf{k}}\lambda_{\mathbf{k}'}$, the condensation energy gained at $T = 0$ in the superconducting state reads

$$E = -\frac{N(0)\Delta_0^2}{2}\langle|\lambda_{\mathbf{k}}|^2\rangle, \tag{35}$$

where Δ_0 is the maximum value of the gap and $\langle\ldots\rangle$ denotes the angular average over the Fermi surface. This clearly shows the advantage of an isotropic gap $|\lambda_{\mathbf{k}}| = 1$. The general

principle is well known: the system prefers to have the Fermi surface as gapped as possible. However, factors such as spin-orbit pinning energy and lattice structure may conspire to prevent a fully isotropic gap. We also note that in our model, the ferromagnetic ordering enters at a much higher temperature than the superconducting order unless $\tilde{I}$ is very close to unity. This is consistent[1,2] with the experimental findings for the ratio between the critical temperatures for ferromagnetic and superconducting order, $T_c^{\mathrm{FM}}/T_c^{\mathrm{SC}}$, except for UCoGe where the ratio is $\simeq 3$.[3]

The experiments performed so far are indicative of a single gap, or at least a strongly suppressed second gap, in the ferromagnetic superconductors. For instance, no double-jump features have been observed in the specific heat capacity[1] for UGe_2. This warrants the investigation of a single-gap model, possibly with line nodes as suggested by Harada *et al.*[17] Theoretically, the absence of the SC gap in the minority-spin subband can be justified by considering the effect of Zeeman splitting on the electronic density of states (see discussion in Sec. III and Ref. 22). In general, it should be possible to discern the presence of two gaps by analyzing specific heat or point-contact spectroscopy measurements, unless one of the gaps is very small.

Apart from this, another possible scenario, specific to UGe_2, can be invoked to explain the observed gapless behavior in the minority-spin subband. This is the *metamagnetic transition* that occurs inside the FM phase of UGe_2 and separates the two ferromagnetic phases with different values[47,55] of magnetization M. The reason this meta-magnetic transition in UGe_2 is of great importance is that the specific heat measurements clearly indicate[47] that the maximum of superconducting T_c occurs not at the FM to PM transition, but at some lower pressure $p_x \approx 12$ kbar that coincides precisely with the metamagnetic transition.[17,55]

One can think of this transition as a point where the value of low-temperature magnetization M sustains a jump. While the microscopic origin of this transition is not known, an idea has been put forward[56] that it may be due to a sharp change in the DOS due to the existence of a double peak in its structure close to the Fermi level. What happens according to this scenario is that applied pressure makes the Fermi level "sweep through" the double-peak structure in the DOS, thereby sharply increasing the density of states in the majority-spin channel. It follows from a simple Stoner instability argument that such an increase in the DOS would lead to a larger value of effective interaction $\tilde{I} \equiv IN(0)$ and thus higher magnetization M. However, this also means that the ratio of the DOS in the two spin channels, $N_\uparrow/N_\downarrow$, sharply increases at the metamagnetic transition. It follows from Eqs. (16), (18), and (22) that the ratio between the SC gaps in the two spin subbands

$$\frac{\Delta_\downarrow}{\Delta_\uparrow} \propto \frac{T_c^\downarrow}{T_c^\uparrow} = \frac{\exp(-1/gN_\downarrow)}{\exp(-1/gN_\uparrow)} \tag{36}$$

thus becomes very small, justifying the assumption $\Delta_\downarrow = 0$ made in this work.

We note in passing that from an experimental point of view, a complication with UGe_2 is that the superconductivity does not appear at ambient pressure, in contrast to URhGe and UCoGe. The necessity of considerable pressure restricts the use of certain experimental techniques, and this is clearly a challenge in terms of measuring, for instance, conductance spectra of UGe_2. Another experimental quantity which would be of high interest to obtain from for instance *ab initio* calculations, is the thermal expansion coefficient, which may be directly probed in high-pressure experiments.[57]

We also underline that in our model the magnetism is assumed to coexist uniformly with superconductivity. Depending on the geometry of the sample, it is likely that the intrinsic magnetization gives rise to a self-induced vortex phase. In a thin-film structure where the thickness t is smaller than the vortex radius λ, we expect that ferromagnetism and superconductivity may be realized in a vortex-free phase, similarly to a thin-film s-wave superconductor in the presence of an in-plane magnetic field. Further refinements leading to a more realistic model of a ferromagnetic superconductor should include the presence of spin-orbit coupling, which inevitably is present in heavy-fermion superconductors, in addition to the presence of vortices. Nevertheless, we believe that our model should capture important qualitative features of how the interplay between ferromagnetism and superconductivity may be manifested in experimentally accessible quantities. In particular, experiments on transport properties of ferromagnetic superconductors, such as the Josephson current and point-contact spectroscopy, would be of high interest to further illucidate the pairing symmetry realized in ferromagnetic superconductors.

VII. SUMMARY

In conclusion, we have constructed a mean-field theory of triplet superconductivity in the background of itinerant ferromagnetism, where the superconducting order parameter contains line nodes and the minority-spin band remains ungapped at the Fermi level. We have solved the self-consistent equations for the order parameters in the problem, and find that ferromagnetism enhances superconductivity, while the ferromagnetism itself is virtually unaffected by the presence of superconductivity. We have made several predictions for experimentally accessible quantities: heat capacity, Knight shift, and tunneling conductance spectra. Our results may be helpful in the interpretation of experimental data, and could provide tools concerning the issue of identifying the pairing symmetry of ferromagnetic superconductors.

ACKNOWLEDGMENTS

J.L. wishes to express his gratitude for the hospitality shown by Y. Tanaka at Nagoya University, where parts of this work were completed. N. Sato is also thanked for very useful discussions. This work was supported by the Norwegian Research Council under Grants No. 158518/431, No. 158547/431 (NANOMAT), and No. 167498/V30 (STORFORSK).

[1] S. S. Saxena, P. Agarwal, K. Ahilan, F. M. Grosche, R. K. W. Haselwimmer, M. J. Steiner, E. Pugh, I. R. Walker, S. R. Julian, P. Monthoux, G. G. Lonzarich, A. Huxley, I. Sheikin, D. Braithwaite, and J. Flouquet, Nature (London) **406**, 587 (2000).
[2] D. Aoki, A. Huxley, E. Ressouche, D. Braithwaite, J. Flouquet, J.-P. Brison, E. Lhotel, and C. Paulsen, Nature (London) **413**, 613 (2001).
[3] N. T. Huy, A. Gasparini, P. E. de Nijs, Y. Huang, J. C. P. Klaasse, T. Gortenmulder, A. de Visser, A. Hamann, T. Gorlach, and H. v. Lohneysen, Phys. Rev. Lett. **99**, 067006 (2007).
[4] Tetsuya Ohta, Yusuke Nakai, Yoshihiko Ihara, Kenji Ishida, Kazuhiko Deguchi, Noriaki K. Sato, and Isamu Satoh, arXiv:0712.1403, J. Phys. Soc. Jpn. (to be published).
[5] A. A. Abrikosov, and L. P. Gorkov, Zh. Eksp. Teor. Fiz. **39**, 1781 (1960) [Sov. Phys. JETP **12**, 1243 (1961)].
[6] A. M. Clogston, Phys. Rev. Lett. **9**, 266 (1962).
[7] B. S. Chandrasekhar, Appl. Phys. Lett. **1**, 7 (1962).
[8] P. Fulde and R. A. Ferrel, Phys. Rev. **135**, A550 (1964); A. I. Larkin, and Y. N. Ovchinnikov, Zh. Eksp. Teor. Fiz. **47**, 1136 (1964).
[9] D. Fay and J. Appel, Phys. Rev. B **22**, 3173 (1980).
[10] S. Tsutsui, M. Nakada, M. Saeki, S. Nasu, Y. Haga, E. Yamamoto, and Y. Onuki, Phys. Rev. B **60**, 37 (1999).
[11] N. I. Karchev, K. B. Blagoev, K. S. Bedell, and P. B. Littlewood, Phys. Rev. Lett. **86**, 846 (2001).
[12] R. Shen, Z. M. Zheng, S. Liu, and D. Y. Xing, Phys. Rev. B **67**, 024514 (2003).
[13] M. Cuoco, P. Gentile, and C. Noce, Phys. Rev. Lett. **91**, 197003 (2003).
[14] Although the superconductivity is observed at ambient pressure in URhGe (Ref. 2), UCoGe (Ref. 3), it is believed that it occurs on the border of ferromagnetism and that one could, in principle, suppress the Curie temperature to zero by applying pressure (sometimes a negative pressure would be required), making these compounds similar in this respect to UGe_2, where SC is observed (Ref. 1) in the vicinity of the pressure-tuned phase transition.
[15] J. A. Hertz, Phys. Rev. B **14**, 1165 (1976); A. J. Millis, *ibid.* **48**, 7183 (1993).
[16] A. J. Leggett, Rev. Mod. Phys. **47**, 331 (1975).
[17] A. Harada, S. Kawasaki, H. Mukuda, Y. Kitaoka, Y. Haga, E. Yamamoto, Y. Onuki, K. M. Itoh, E. E. Haller, and H. Harima, Phys. Rev. B **75**, 140502(R) (2007).
[18] A. A. Abrikosov and L. P. Gor'kov, Zh. Eksp. Teor. Fiz. **39**, 1781 (1960) [Sov. Phys. JETP **12**, 1243 (1961)].
[19] T. Ohmi and K. Machida, Phys. Rev. Lett. **71**, 625 (1993).
[20] K. Machida and T. Ohmi, Phys. Rev. Lett. **86**, 850 (2001).
[21] K. V. Samokhin and M. B. Walker, Phys. Rev. B **66**, 174501 (2002); K. V. Samokhin and M. B. Walker, *ibid.* **66**, 024512 (2002); M. B. Walker and K. V. Samokhin, Phys. Rev. Lett. **88**, 207001 (2002).
[22] A. H. Nevidomskyy, Phys. Rev. Lett. **94**, 097003 (2005).
[23] J. Linder and A. Sudbø, Phys. Rev. B **76**, 054511 (2007).
[24] J. Shi and Q. Niu, arXiv:cond-mat/0601531 (unpublished).
[25] H. Kotegawa, A. Harada, S. Kawasaki, Y. Kawasaki, Y. Kitaoka, Y. Haga, E. Yamamoto, Y. Onuki, K. M. Itoh, and E. E. Haller, J. Phys. Soc. Jpn. **74**, 705 (2005).
[26] S. Tewari, D. Belitz, T. R. Kirkpatrick, and J. Toner, Phys. Rev. Lett. **93**, 177002 (2004).
[27] V. P. Mineev, C. R. Phys. **7**, 35 (2006).
[28] V. P. Mineev and K. V. Samokhin, *Introduction to Unconventional Superconductivity* (Gordon and Breach, New York, 1999).
[29] D. V. Shopova and D. I. Uzunov, Phys. Rev. B **72**, 024531 (2005).
[30] Notice that time-reversal symmetry may be spontaneously broken in the orbital part (angular momentum) of the Cooper pair wave function even if the state is unitary.
[31] F. Hardy and A. D. Huxley, Phys. Rev. Lett. **94**, 247006 (2005).
[32] M. S. Grønsleth, J. Linder, J.-M. Børven, and A. Sudbø, Phys. Rev. Lett. **97**, 147002 (2006).
[33] J. Linder, M. S. Grønsleth, and A. Sudbø, Phys. Rev. B **75**, 024508 (2007).
[34] J. Linder, M. S. Grønsleth, and A. Sudbø, Phys. Rev. B **75**, 054518 (2007).
[35] T. Yokoyama and Y. Tanaka, Phys. Rev. B **75**, 132503 (2007).
[36] A. Brataas and Y. Tserkovnyak, Phys. Rev. Lett. **93**, 087201 (2004).
[37] Y. Zhao and R. Shen, Phys. Rev. B **73**, 214511 (2006).
[38] A. G. Lebed, Phys. Rev. B **59**, R721 (1999); A. G. Lebed, K. Machida, and M. Ozaki, *ibid.* **62**, R795 (2000).
[39] K. Sengupta, I. Zutic, H.-J. Kwon, V. M. Yakovenko, and S. Das Sarma, Phys. Rev. B **63**, 144531 (2001).
[40] C. J. Bolech and T. Giamarchi, Phys. Rev. Lett. **92**, 127001 (2004); C. J. Bolech and T. Giamarchi, Phys. Rev. B **71**, 024517 (2005).
[41] R. D. Duncan, C. D. Vaccarella, and C. A. R. Sade Melo, Phys. Rev. B **64**, 172503 (2001).
[42] J. Linder, A. Nevidomskyy, and A. Sudbø (unpublished).
[43] A. B. Shick and W. E. Pickett, Phys. Rev. Lett. **86**, 300 (2001).
[44] C. Bernhard, J. L. Tallon, E. Brucher, and R. K. Kremer, Phys. Rev. B **61**, R14960 (2000); J. L. Tallon, J. W. Loram, G. V. M. Williams, and C. Bernhard, *ibid.* **61**, R6471 (2000); A. Fainstein, E. Winkler, A. Butera, and J. Tallon, *ibid.* **60**, R12597 (1999).
[45] M. Sigrist, *Lectures on the Physics of Highly Correlated Electron Systems IX*, AIP Conf. Proc. No. 789 (AIP, New York, 2006), p. 165.
[46] E. P. Wohlfarth, Phys. Lett. **75A**, 141 (1979).
[47] N. Tateiwa, T. C. Kobayashi, K. Hanazono, K. Amaya, Y. Haga, R. Settai, and Y. Onuki, J. Phys.: Condens. Matter **13**, L17 (2001); N. Tateiwa, T. C. Kobayashi, K. Amaya, Y. Haga, R. Settai, and Y. Onuki, Phys. Rev. B **69**, 180513(R) (2004).
[48] J. R. Schrieffer, *Superconductivity*, 1st ed. (Benjamin/Cummings, Reading, 1964).
[49] G. E. Blonder, M. Tinkham, and T. M. Klapwijk, Phys. Rev. B **25**, 4515 (1982).
[50] C.-R. Hu, Phys. Rev. Lett. **72**, 1526 (1994).
[51] Y. Tanaka and S. Kashiwaya, Phys. Rev. Lett. **74**, 3451 (1995).
[52] T. Lofwander, V. S. Shumeiko, and G. Wendin, Supercond. Sci. Technol. **14**, R53 (2001).
[53] Y. S. Barash, A. A. Svidzinsky, and H. Burkhardt, Phys. Rev. B **55**, 15282 (1997).
[54] S. Kashiwaya, Y. Tanaka, M. Koyanagi, and K. Kajimura, Phys. Rev. B **53**, 2667 (1996).
[55] M. Uhlarz, C. Pfleiderer, and S. M. Hayden, Phys. Rev. Lett. **93**, 256404 (2004).
[56] K. G. Sandeman, G. G. Lonzarich, and A. J. Schofield, Phys. Rev. Lett. **90**, 167005 (2003).
[57] N. Sato (private communication).

Paper XV

The role of interface transparency and spin-dependent scattering in diffusive ferromagnet/superconductor heterostructures.

Physical Review B **77**, 174514 (2008).

Role of interface transparency and spin-dependent scattering in diffusive ferromagnet/superconductor heterostructures

Jacob Linder,[1] Takehito Yokoyama,[2] and Asle Sudbø[1]
[1]*Department of Physics, Norwegian University of Science and Technology, N-7491 Trondheim, Norway*
[2]*Department of Applied Physics, Nagoya University, Nagoya 464-8603, Japan*
(Received 8 January 2008; revised manuscript received 29 April 2008; published 28 May 2008)

We present a numerical study of the density of states in a ferromagnet/superconductor junction and the Josephson current in a superconductor/ferromagnet/superconductor junction in the diffusive limit by solving the Usadel equation with Nazarov's boundary conditions. Our calculations are valid for an arbitrary interface transparency and an arbitrary spin-dependent scattering rate, which allows us to explore the entire proximity-effect regime. We first investigate how the proximity-induced anomalous Green's function affects the density of states in the ferromagnet for three magnitudes of the exchange field h compared to the superconducting gap Δ: (i) $h \lesssim \Delta$, (ii) $h \gtrsim \Delta$, and (iii) $h \gg \Delta$. In each case, we consider the effect of the barrier transparency and allow for various concentrations of magnetic impurities. We clarify features that may be expected in the various parameter regimes accessible for the ferromagnetic film, with regard to thickness and exchange field. In particular, we address how the zero-energy peak and minigap observed in experiments may be understood in terms of the interplay between the singlet and the triplet anomalous Green's functions and their dependence on the concentration of magnetic impurities. Our results should serve as a useful tool for the quantitative analysis of experimental data. We also investigate the role of the barrier transparency and spin-flip scattering in a superconductor/ferromagnet/superconductor junction. We suggest that such diffusive Josephson junctions with large residual values of the supercurrent at the 0-π transition, where the first harmonic term in the current vanishes, may be used as efficient supercurrent-switching devices. We numerically solve for the Josephson current in such a junction to clarify to what extent this idea may be realized in an experimental setup. It is also found that uniaxial spin-flip scattering has a very different effect on the 0-π transition points depending on whether one considers the width or the temperature dependence of the current. Our theory takes into account vital elements that are necessary to obtain quantitative predictions of the supercurrent in such junctions.

DOI: 10.1103/PhysRevB.77.174514 PACS number(s): 74.45.+c, 74.20.Rp, 74.50.+r, 74.70.Kn

I. INTRODUCTION

Proximity structures consisting of ferromagnetic and superconducting materials are nowadays a very active research field. The interest in this type of systems has grown considerably over the last decade since they offer novel and interesting phenomena to explore from a fundamental physics point of view. In addition, it is hoped that future applications in low-temperature nanotechnology may emerge from this research field. Ferromagnetism is usually considered to be antagonistic to conventional superconductors since the exchange field acts as a depairing agent for spin-singlet Cooper pairs. However, closer examination reveals that the physical situation is more subtle than that. The proximity effect on a superconductor from a ferromagnet does not merely suppress the spin-singlet superconducting order parameter but may also under specific circumstances induce exotic features, such as odd-frequency pairing and long-ranged spin-triplet correlations.[1,2]

Various theoretical idealizations allow for a relatively simple approach to ferromagnet/superconductor (F/S) heterostructures within the quasiclassical framework. One of the most popular approaches in the literature employs the linearized Usadel[3] equations with the Kupriyanov–Lukichev boundary conditions,[4] which is a viable method in the case of a weak proximity effect. This is, for instance, permissible when the barrier transparency of the F/S interface is low. Although the linearized treatment clearly represents a special limit, much useful information has been obtained through this approach. Among these are the oscillations of the anomalous Green's function[5,6] for the ferromagnet due to the fact that the Cooper pair in the ferromagnet acquires a finite center-of-mass momentum $q=2h/v_F$, where h is the magnetic exchange energy and v_F is the Fermi velocity.[7] Although several other works have also considered various aspects of the density of states in both diffusive[8–15] and clean[16–18] ferromagnet/superconductor junctions, most of these rely on simplifying assumptions concerning the interface, that it is either perfectly transparent or strongly insulating.

From an experimental point of view, there has been several investigations of how the spin-splitting in energy level in a ferromagnet affects the proximity effect when placed in contact with superconductor.[19–22] Very recently, SanGiorgio *et al.*[23] reported an anomalous double peak structure in the density of states of a Nb/Ni tunneling junction. They attempted to capture the qualitative features of the unusual subgap structure of the density of states by using the Usadel equation but were not able to do so. This clearly warrants further investigation and serves as a motivation for employing more sophisticated models of a ferromagnet/superconductor interface, possibly including a domain structure in the ferromagnet.

Recently, a full numerical solution of the Usadel equation was employed by Gusakova *et al.*[24] including scattering on magnetic impurities but under the simplifying assumption

that the tunneling limit was reached at the F/S interface. It would clearly also be of interest to consider higher barrier transparencies to elucidate how these may influence the proximity effect. In this case, one should employ Nazarov's boundary conditions[25] instead of the Kupriyanov–Lukichev boundary conditions.[4] Yokoyama *et al.*[26,27] recently adopted this approach for the case without any magnetic impurities present. When comparing the theoretical models against quantitative aspects of the experimental data, the influence of magnetic impurities and barrier transparency clearly play a pivotal role. For instance, as argued in Ref. 28, the predicted amplitude of the critical current in a diffusive S/F/S junction is $\sim 10^3$ times larger than the actual measured curves. This may be attributed to the strong suppression of Andreev bound states due to spin-flip scattering processes, which are usually not taken into account in the theoretical treatment (see, however, Ref. 29). To date, there exists no study of the density of states in F/S structures that allows access to both the full range of barrier transparencies *and* the concentration of magnetic impurities.

In the present paper, we remedy this by employing a numerical solution of the Usadel equation in the ferromagnetic region, taking into account an arbitrary concentration of magnetic impurities as well as an arbitrary barrier transparency. This permits us to comprehensively study the local density of states (DOS) in a dirty ferromagnet/superconductor junction for experimentally realistic parameters. We study three cases for the size of the exchange field h as compared to the superconducting gap Δ: (i) $h \lesssim \Delta$, (ii) $h \gtrsim \Delta$, and (iii) $h \gg \Delta$. In each case, we compare the short-junction regime to the wide-junction regime to obtain the energy-resolved DOS. Among other things, we study the emergence of a zero-energy peak in the spectrum in a certain parameter range in addition to the transition from minigaps to peaks in the spectrum for increasing exchange field in the wide-junction regime. In particular, we investigate the interplay between the proximity-induced singlet and triplet anomalous Green's functions for the ferromagnet and how these are affected by spin-dependent scattering. Since our results take into account an arbitrary proximity effect and an arbitrary magnetic impurity concentration, they should serve as a useful tool for performing quantitative analysis of experimental data. We envision a ferromagnet/superconductor bilayer, shown in Fig. 1, which is virtually identical to the experimental setup used in Refs. 20 and 23.

Another interesting issue in the context of ferromagnet-superconductor is that there have been put forth suggestions of exploiting superconductor/ferromagnet/superconductor (S/F/S) Josephson junctions as qubits in quantum computers. By now, the 0-π oscillations that occur in S/F/S junctions are also well established both theoretically[30–37] and experimentally.[19,20,38–42]

As the fundamental understanding of the physics in an S/F/S junction begins to take shape, the next step to take should be a more sophisticated modeling of such systems in order to achieve better quantitative agreement between theory and experiment. Parameters such as barrier transparency and magnetic impurities become important in this respect, as they can have crucial impact on the behavior of the supercurrent in an S/F/S system. To this end, several recent

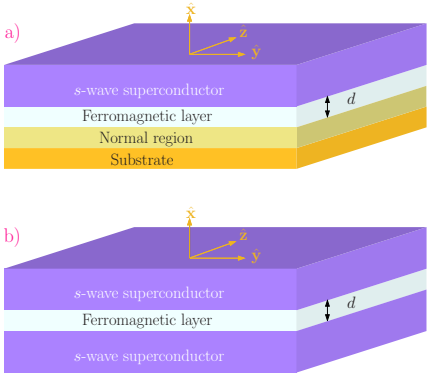

FIG. 1. (Color online) The ferromagnet/superconductor heterostructures investigated in this paper. In (a), a ferromagnet/superconductor bilayer setup is shown. We model the barrier region at the normal/ferromagnet interface to be very strong, mimicking a free edge boundary condition or insulating region. Our proposed experimental setup is thus equivalent to the ones employed in the experimental works in Refs. 20 and 23. In (b), we consider a superconductor/ferromagnet/superconductor junction. The superconductors are treated as reservoirs; thus, they are unaffected by the proximity effect. We will consider a ferromagnetic layer thickness ranging from $d/\xi=0.1$ to $d/\xi=1.0$, where ξ is the superconducting coherence length.

works investigated some aspects of the supercurrent by including magnetic impurities[29,43–48] but restricted themselves to the tunneling limit. Under the opposite simplifying assumption of transparent interfaces, the influence of spin-flip scattering has also been investigated.[49] The Josephson current in an S/F/S junction may under these circumstances be written with a good accuracy as $I=I_0 \sin \phi$, where ϕ is the macroscopic phase difference. As a direct result, the usual 0-π oscillations observed in S/F/S junctions do not exhibit any residual value of the supercurrent at the transition points where the current switches sign.

However, an interesting opportunity presents itself in the case wherein the current-phase relationship deviates strongly from its usual sinusoidal behavior. Higher harmonics in the Josephson current will lead to a finite residual value right at the cusps of the critical current oscillations with exchange field or temperature, and these cusps are indicative of a sign reversal of the supercurrent. This simple observation gives rise to a very interesting prospect. *If* the residual value of the current at the cusps were to be of considerable magnitude, one could exploit this effect to create a dissipationless current *switching* device. In this case, the direction of the Josephson current could be instantaneously flipped by some external control parameter when the system parameters are such that the junction is very close to the 0-π transition point.

Such an idea depends, however, on the possibility to actually obtain a large residual value of the current near the cusps. Early experiments[19,20,39–41] measuring the Josephson current in diffusive S/F/S systems showed that the critical current vanishes at these cusps. But recently, Sellier *et al.*[42]

observed a finite, albeit small, supercurrent at the 0-π transition point where the first harmonic term vanishes.

In Ref. 28, the magnitude of the residual value of the current at the cusps was investigated by solving the linearized Usadel equation[3] using Nazarov's boundary conditions.[25] However, this calculation was performed assuming two limiting circumstances: (i) no magnetic impurities and (ii) a weak proximity effect. The residual value was also analyzed in the clean limit in Ref. 50. It is definitely of much interest to go beyond these approximations and see how the physical picture is altered. As mentioned previously, a consequence of (i) is that the theoretically predicted magnitude of the critical current is a factor of 10^3 larger than the experimentally measured value. Even though highly valuable qualitative information may be obtained in approximations such as (i) and (ii), the progress on both the theoretical and experimental side of S/F/S Josephson junctions calls for a higher accuracy of the quantitative predictions. Obviously, this is also of paramount importance in the context of discussing a practical supercurrent-switch device.

We here develop a theory for the supercurrent in an S/F/S junction which takes into account an arbitrary concentration of magnetic impurities and an arbitrary transparency of the interfaces. Both of these are of vital importance in obtaining quantitative agreement with experimental findings. We numerically solve the Usadel equation and employ Nazarov's boundary condition. In the intermediate barrier transparency regime, we find that a finite but small residual value of the current is permitted at the 0-π transition points. However, the effect of spin-flip scattering is very different when comparing the width dependence against the temperature dependence of the current. The transition point is much more robust in the width dependence, although increasing the concentration of magnetic impurities reduces the residual value. On the other hand, increasing spin-flip scattering completely removes the 0-π transition point for the temperature dependence.

This paper is organized as follows: In Sec. II, we establish the theoretical framework which will serve as our tool to obtain both the density of states in the diffusive ferromagnet/superconductor bilayer and the Josephson current in the diffusive superconductor/ferromagnet/superconductor junction. In Secs. III and IV, we present and discuss our results. Finally, we summarize the results in Sec. V.

II. THEORETICAL FORMULATION

The central quantity in the quasiclassical theory of superconductivity is the quasiclassical Green's functions $\check{g}(\mathbf{p}_F,\mathbf{R};\varepsilon,t)$, which depends on the momentum at the Fermi level, $\mathbf{p}_F$; the spatial coordinate $\mathbf{R}$; the energy measured from the chemical potential, ε; and time t. A considerable literature covers the Keldysh formalism and nonequilibrium Green's functions.[51–56] Here, we only briefly sketch the theoretical structure for the sake of readability and for establishing notation. The quasiclassical Green's functions $\check{g}(\mathbf{p}_F,\mathbf{R};\varepsilon,t)$ is obtained from the Gor'kov Green's functions $\check{G}(\mathbf{p},\mathbf{R};\varepsilon,t)$ by integrating out the dependence on kinetic energy, assuming that $\check{G}$ is strongly peaked at Fermi level,

$$\check{g}(\mathbf{p}_F,\mathbf{R};\varepsilon,t)=\frac{i}{\pi}\int d\xi_p \check{G}(\mathbf{p},\mathbf{R};\varepsilon,t). \tag{1}$$

The above assumption is typically applicable to superconducting systems wherein the characteristic length scale of the perturbations present, namely, the superconducting coherence length, is much larger than the Fermi wavelength. The corresponding characteristic energies of such phenomena must be much smaller than the Fermi energy ε_F. The quasiclassical Green's functions may be divided into an advanced (A), a retarded (R), and a Keldysh (K) component, each of which has a 4×4 matrix structure in the combined particle-hole and spin space. Thus, one has

$$\check{g}=\begin{pmatrix}\hat{g}^R & \hat{g}^K\\ 0 & \hat{g}^A\end{pmatrix}, \tag{2}$$

where the elements of $\check{g}(\mathbf{p}_F,\mathbf{R};\varepsilon,t)$ read

$$\hat{g}^{R,A}=\begin{pmatrix}\underline{g}^{R,A} & \underline{f}^{R,A}\\ -\underline{\tilde{f}}^{R,A} & -\underline{\tilde{g}}^{R,A}\end{pmatrix},\quad \hat{g}^K=\begin{pmatrix}\underline{g}^K & \underline{f}^K\\ \underline{\tilde{f}}^K & \underline{\tilde{g}}^K\end{pmatrix}. \tag{3}$$

The quantities $\underline{g}$ and $\underline{f}$ are 2×2 spin matrices, with the structure

$$\underline{g}=\begin{pmatrix}g_{\uparrow\uparrow} & g_{\uparrow\downarrow}\\ g_{\downarrow\uparrow} & g_{\downarrow\downarrow}\end{pmatrix}. \tag{4}$$

Due to internal symmetry relations between these Green's functions, all of these quantities are not independent. In particular, the tilde operation is defined as

$$\tilde{f}(\mathbf{p}_F,\mathbf{R};\varepsilon,t)=f(-\mathbf{p}_F,\mathbf{R};-\varepsilon,t)^*. \tag{5}$$

The quasiclassical Green's functions $\check{g}(\mathbf{p}_F,\mathbf{R};\varepsilon,t)$ may be determined by solving the Eilenberger[57] equation

$$[\varepsilon\hat{\rho}_3-\hat{\Sigma},\check{g}]_\otimes+i\mathbf{v}_F\nabla\check{g}=0, \tag{6}$$

where $\hat{\Sigma}$ contains the self-energies in the system such as impurity scattering, superconducting order parameter, and exchange fields. The star product $\otimes$ is noncommutative and is defined in the Appendix. When there is no explicit time dependence in the problem, the star product reduces to normal multiplication. This is the case we will consider throughout the paper. The operation $\hat{\rho}_3\check{g}$ inside the commutator should be understood as $\hat{\rho}_3\check{g}\equiv\mathrm{diag}\{\hat{\rho}_3,\hat{\rho}_3\}\check{g}$. Pauli matrices in particle-hole $\times$ spin (Nambu) space are denoted as $\hat{\rho}_i$, while Pauli matrices in spin space are written as $\underline{\tau}_i$, all of which are defined in the Appendix. Green's functions also satisfy the normalization condition

$$\check{g}\otimes\check{g}=\check{1}. \tag{7}$$

In the special case of an equilibrium situation, one may

express the Keldysh component in terms of the retarded and the advanced Green's function by means of the relation

$$\hat{g}^K = (\hat{g}^R - \hat{g}^A)\tanh(\beta\varepsilon/2), \tag{8}$$

where $\beta=T^{-1}$ is inverse temperature. In nonequilibrium situations, one must derive the kinetic equations for nonequilibrium distribution functions in order to specify the Keldysh part.[58]

The above equations suffice to completely describe, for instance, a single superconducting structure but must be supplemented by boundary conditions when treating heterostructures such as F/S junctions. These boundary conditions take different forms depending on the physical properties of the interface. The Kupriyanov–Lukichev[4] boundary conditions may be applied for a dirty junction in the tunneling limit when the transparency of the interface is low, while an arbitrary interface transparency requires usage of the boundary conditions developed by Nazarov.[25] The boundary conditions for a spin-active interface have also been derived.[59,60]

We will consider the dirty limit of the Eilenberger equation [Eq. (6)], which leads to the Usadel equation.[3] Our motivation is that this is the experimentally most relevant situation. This will be an appropriate starting point for diffusive systems wherein the scattering time $\tau_{\rm imp}$ due to impurities satisfies $X\tau_{\rm imp}\ll 1$, where X is the energy scale of any other self-energy in the problem. For strong ferromagnets wherein h becomes comparable to ε_F, the stated inequality may strictly speaking not be valid for $X=h$. Hence, we will restrict ourselves to the regime $h/\varepsilon_F\ll 1$ and assume that[32] $h\tau_{\rm imp}\ll 1$. Below, we will mostly concern ourselves with the retarded part of $\check{g}(\mathbf{p}_F,\mathbf{R};\varepsilon,t)$ since the advanced component may be found via the relation

$$\hat{g}^A = -(\hat{\rho}_3\hat{g}^R\hat{\rho}_3)^\dagger. \tag{9}$$

By isotropizing Green's function due to the assumed frequent impurity scattering, it is rendered independent of $\mathbf{p}_F$. This isotropic (in momentum space) Green's function satisfies the Usadel equation in the ferromagnet,

$$D\nabla(\check{g}\nabla\check{g}) + i[\varepsilon\hat{\rho}_3 + \hat{M} - \check{\sigma}_{\rm sf} - \check{\sigma}_{\rm so},\check{g}] = 0. \tag{10}$$

Above, the exchange energy h is accounted for by the matrix $\hat{M}=\mathrm{diag}(h\underline{\tau_3},h\underline{\tau_3})$, assuming a magnetization in the $\mathbf{z}$ direction; while the spin-flip self-energy reads

$$\check{\sigma}_{\rm sf}(\mathbf{R};\varepsilon) = -\frac{i}{8\tau_{\rm sf}}\sum_i \hat{\alpha}_i\check{g}(\mathbf{R};\varepsilon)\hat{\alpha}_i S_i,$$

$$\check{\sigma}_{\rm so}(\mathbf{R};\varepsilon) = -\frac{i}{8\tau_{\rm so}}\sum_i \hat{\alpha}_i\hat{\rho}_3\check{g}(\mathbf{R};\varepsilon)\hat{\rho}_3\hat{\alpha}_i, \tag{11}$$

where $\tau_{\rm sf}$ is the spin-flip scattering time and S_i is a spin expectation value, while $\tau_{\rm so}$ is the spin-orbit scattering time. We have defined the matrices $\hat{\alpha}_i=\mathrm{diag}(\underline{\tau_i},\underline{\tau_i}^T)$. The diffusion constant is given by $D=v_F^2\tau_{\rm imp}/3$, where $\tau_{\rm imp}$ is the impurity scattering relaxation time. We will here consider either uniaxial spin-flip scattering, such that $S_3=1$ ($\hat{\mathbf{z}}$ direction) and zero otherwise, or isotropic spin-flip scattering, where $S_i=1$ for $i\in\{1,2,3\}$. For later use, we denote $S_{xy}\equiv S_1=S_2$ and $S_z=S_3$.

Let us now consider the retarded part of Eq. (10) which has the same form, namely,

$$D\nabla(\hat{g}^R\nabla\hat{g}^R) + i[\varepsilon\hat{\tau}_3 + \hat{M} - \hat{\sigma}_{\rm sf} - \hat{\sigma}_{\rm so},\hat{g}^R] = 0. \tag{12}$$

From now on, we will omit the superscript R of Green's function. Moreover, we will find it convenient to parametrize Green's function by exploiting the normalization condition. In an s-wave superconductor ($x>d$) and a normal metal ($x<0$), we use the bulk solutions

$$\hat{g}_S = \begin{pmatrix} g\underline{1} & fi\underline{\tau_2} \\ fi\underline{\tau_2} & -g\underline{1}\end{pmatrix}, \quad \hat{g}_N = \begin{pmatrix} \underline{1} & \underline{0} \\ \underline{0} & -\underline{1}\end{pmatrix}, \tag{13}$$

where $g\equiv\cosh(\theta_s)$, $f\equiv\sinh(\theta_s)$, and $\theta_s=\mathrm{atanh}(\Delta/\varepsilon)$. Green's function for the ferromagnet may conveniently be parametrized as[56]

$$\hat{g}_F = \begin{pmatrix} \cosh\theta_\uparrow(\varepsilon) & 0 & 0 & \sinh\theta_\uparrow(\varepsilon) \\ 0 & \cosh\theta_\downarrow(\varepsilon) & \sinh\theta_\downarrow(\varepsilon) & 0 \\ 0 & -\sinh\theta_\downarrow(\varepsilon) & -\cosh\theta_\downarrow(\varepsilon) & 0 \\ -\sinh\theta_\uparrow(\varepsilon) & 0 & 0 & -\cosh\theta_\uparrow(\varepsilon)\end{pmatrix}, \tag{14}$$

which satisfies $\hat{g}_F^2=\hat{1}$. We have made use of the symmetry $\theta_\uparrow(\varepsilon)=\theta_\downarrow^*(-\varepsilon)$ in obtaining Eq. (14). Note that for $h=0$, $\theta_\uparrow(\varepsilon)=-\theta_\downarrow(\varepsilon)$ is satisfied. Note that in Eq. (14), there is both a singlet and a triplet component of the anomalous Green's function. The triplet component is opposite-spin paired ($S_z=0$), and there are no equal-spin pairing ($S_z=\pm 1$) components in our system since we consider homogeneous magnetization and a spin-inactive barrier. The $S_z=0$ triplet component nevertheless plays a pivotal role in interpreting the behavior of the density of states, as we shall see later. This is because it has a special symmetry property referred to as odd in frequency, which will be elaborated upon in Sec. III A 4.

The Usadel equation [Eq. (12)] then yields the following for the majority and minority spins ($\sigma=\uparrow,\downarrow=\pm 1$) in the ferromagnet:

$$D\partial_x^2\theta_\sigma + 2i(\varepsilon + \sigma h)\sinh\theta_\sigma - \frac{\sigma S_{xy}}{2\tau_{sf}}\sinh(\theta_\uparrow - \theta_\downarrow) - \frac{S_z}{4\tau_{sf}}\sinh 2\theta_\sigma - \frac{1}{2\tau_{so}}\sinh(\theta_\uparrow + \theta_\downarrow) = 0. \quad (15)$$

We now use the generalized Nazarov boundary condition valid for the diffusive regime.[25] At $x=\{0,d\}$, it reads

$$2\gamma_{L,R}L\hat{g}_F\partial_x\hat{g}_F|_{x=\{0,d\}} = \mp\frac{4\tau[\hat{g}_F,\hat{g}_{L,R}]}{4+\tau(\{\hat{g}_F,\hat{g}_{L,R}\}-2)}\Bigg|_{x=\{0,d\}}, \quad (16)$$

where $[\ldots]$ and $\{\ldots\}$ denote the commutator and anticommutator, respectively, and $\hat{g}_{L,R}(=\hat{g}_{N,S})$ denotes Green's function for the left and right sides of the ferromagnet. The parameter $\gamma_{L,R}=R_B^{L,R}/R_F$ denotes the ratio between the resistance in the left/right barrier region, $R_B^{L,R}$, and the resistance in the F region, R_F. We have conventionally introduced the parameter τ, which is the transmissivity of the interface.[25] Giving an expression for τ in terms of microscopic parameters of the interface is not very practical, and we will therefore use τ as a phenomenological parameter to characterize the transparency of the interface, in complete analogy with Eq. 36 of Ref. 25. Here, $\tau=0$ corresponds to zero transmission of quasiparticles incident on the superconducting interface and $\tau=1$ corresponds to perfect transmission. Below, we will consider two values of τ, namely, 0.1, corresponding to low transmissivity; and $\tau=0.5$, corresponding to intermediate transmissivity. Note that the parameters τ and γ may be varied independently,[61] and one does not in general have $\gamma \sim \tau^{-1}$. The reason for this is that γ is related to the constriction area of the junction, which may be altered independently of the scattering strength proportional to τ^{-1}. Inserting Eqs. (13) and (14) into Eq. (16) yields the boundary conditions

$$\gamma_L d\partial_x\theta_\uparrow = \frac{2\tau\sinh\theta_\uparrow}{2-\tau+\tau\cosh\theta_\uparrow},$$

$$\gamma_L d\partial_x\theta_\downarrow = \frac{2\tau\sinh\theta_\downarrow}{2-\tau+\tau\cosh\theta_\downarrow}, \quad (17)$$

at the normal/ferromagnet (N/F) interface ($x=0$), while at the F/S interface ($x=d$) we have

$$\gamma_R d\partial_x\theta_\uparrow = \frac{2\tau(\cosh\theta_\uparrow f - \sinh\theta_\uparrow g)}{2-\tau+\tau(\cosh\theta_\uparrow g - \sinh\theta_\uparrow f)},$$

$$\gamma_R d\partial_x\theta_\downarrow = \frac{-2\tau(\cosh\theta_\downarrow f + \sinh\theta_\downarrow g)}{2-\tau+\tau(\cosh\theta_\downarrow g + \sinh\theta_\downarrow f)}. \quad (18)$$

For later use, we define the Thouless energy $\varepsilon_T=D/d^2$. As a measure of the strength of the spin-flip and spin-orbit scattering, which increases with decreasing spin relaxation time, we introduce $g_{sf}=\tau_{sf}^{-1}$ and $g_{so}=\tau_{so}^{-1}$. Also note that $S_z=S_{xy}=1$ for isotropic spin-flip scattering, while $S_z=3$ and $S_{xy}=0$ for uniaxial spin-flip scattering along the **z** direction. The spin-resolved and normalized DOS is obtained as

$$N_\uparrow = \mathrm{Re}\{\cosh\theta_\uparrow\}, \quad N_\downarrow = \mathrm{Re}\{\cosh\theta_\downarrow\}. \quad (19)$$

Furthermore, we define the total DOS as $N=\Sigma_\sigma N_\sigma/2$. Equations (15), (17), and (18) now constitute two coupled nonlinear second order differential equations supplemented with boundary conditions which may be solved numerically.

Before presenting our results for the DOS, we establish the theoretical framework for our treatment of the Josephson current in an S/F/S junction with spin-dependent scattering, following the notation in Ref. 62. The physical system studied here consists of a junction with two *s*-wave superconductors separated by a diffusive ferromagnet with a resistance R_F and a length d much larger than the mean free path. We here consider only uniaxial spin-flip scattering. The interface regions are characterized by a resistance R_B. The transparencies of the junction interfaces are given by $T=4\cos^2\varphi/(4\cos^2\varphi+Z^2)$, where Z is a measure of the barrier strength, and the barriers themselves are considered to be spin inactive and modeled by infinitely narrow insulating barriers $U(x)=(Zv_F/2)[\delta(x-d)+\delta(x)]$. Above, v_F is the Fermi velocity and φ is the injection angle measured from the interface normal to the junction. We employ the quasiclassical theory of superconductivity[51–56] and make use of the θ parametrization[58] of Green's function. The retarded part $\hat{g}^R$ may, due to symmetry requirements, be written as[62]

$$\underline{g} = \sin\theta(\cos\psi\underline{\tau_1} + \sin\psi\underline{\tau_2}) + \cos\theta\underline{\tau_3}. \quad (20)$$

From the Usadel equation, one obtains

$$D[\partial_x^2\theta - (\partial_x\psi)^2\cos\theta\sin\theta] + 2i(\varepsilon + \sigma h + i\gamma)\sin\theta = 0,$$

$$\partial_x[\sin^2\theta(\partial_x\psi)] = 0, \quad (21)$$

for $\sigma=\uparrow,\downarrow$ spins. Here, D is the diffusion constant, h is the exchange field, and γ is the self-energy associated with uniaxial spin-flip scattering. We employ the bulk solutions of Green's function for the superconducting regions, assuming that these are much less disordered than the ferromagnetic layer. To gain access to the full regime of different barrier transparencies, we again make use of Nazarov's boundary conditions,[25] which are valid for a nonmagnetic but otherwise arbitrary contact. These boundary conditions at $x=\{0,d\}$ may then in the present case be written as[62]

$$L(R_B/R_F)\partial_x\theta = \pm I_\pm[\mathcal{F}\cos\theta\cos(\psi\mp\phi/2) - \mathcal{G}\sin\theta],$$

$$L(R_B/R_F)\sin\theta\partial_x\psi = \mp I_\pm\mathcal{F}\sin(\psi\mp\phi/2), \quad (22)$$

where the upper (lower) sign is valid at $x=d$ ($x=0$). We have defined the following quantities:

$$I_\pm = \langle 4T/[A_\pm(1+\mathcal{F}^2+\mathcal{G}^2)]\rangle, \quad A_\pm = (2-T) + 2T[\mathcal{F}\sin\theta\cos(\psi\mp\phi/2) + \mathcal{G}\cos\theta]/(1+\mathcal{F}^2+\mathcal{G}^2). \quad (23)$$

and denoted the phase in the right and left superconductor as $\pm\phi/2$, giving rise to a total phase difference of ϕ. Above,

$$\mathcal{G} = \varepsilon/\sqrt{\varepsilon^2 - \Delta^2}, \quad \mathcal{F} = \Delta/\sqrt{\Delta^2 - \varepsilon^2} \tag{24}$$

denote components of the bulk Green's function for the superconductor. Equations (21) and (22) constitute two coupled, second order, nonlinear differential equations with boundary conditions and may be used to numerically solve for $\theta = \theta(x, \varepsilon)$. Once $\theta(x, \varepsilon)$ is obtained, the retarded Green's function is specified everywhere in the diffusive ferromagnet. The current density may then be calculated by

$$j = -(N_F|e|D/4)\int_{-\infty}^{\infty} d\varepsilon \, \mathrm{Tr}\{\hat{\rho}_3(\check{g}\partial_x\check{g})^K\}, \tag{25}$$

where N_F is the density of states at the Fermi level in the normal state, $|e|$ is the electronic charge, $\hat{\rho}_3$ is a Pauli matrix in particle-hole space, $\check{g}$ is the full Green's function in Keldysh $\otimes$ particle-hole $\otimes$ spin space, and the superscript K denotes the Keldysh component. The current is obtained by $I = jS_A$, where S_A is the surface area of the junction; and the critical current is defined as $I_c = \max\{I(\phi)\}$. The I_cR_N product can now be computed, where $R_N = 2R_B + R_F$. In the actual calculations and numerical implementation, we employ the Matsubara representation $\varepsilon \to i\omega$ and parametrize the quasiclassical Green's functions with the quantity Φ_ω as

$$f_\omega = g_\omega\Phi_\omega/\omega = \sin\theta e^{-i\psi}, \quad f^*_{-\omega} = \Phi^*_{-\omega}g_\omega/\omega = \sin\theta e^{i\psi},$$

$$g_\omega = \omega/\sqrt{\omega^2 + \Phi_\omega\Phi^*_{-\omega}} = \cos\theta. \tag{26}$$

We may now express Eqs. (21) and (22) in terms of the fermionic frequency $\omega = (2n+1)\pi/\beta$, where $n = 0, 1, 2, \ldots$, and Green's functions in Eq. (26).

For later purposes, we introduce dimensionless measures of the Thouless energy and inverse spin-flip scattering lifetime: $\mathcal{E} = \varepsilon_T/\Delta = D/(d^2\Delta)$ and $g = \gamma/\Delta$. For simplicity, we will also neglect the spatial depletion of the superconducting order parameter near the interfaces.

III. RESULTS

We now proceed to present our results for the DOS and the Josephson current in detail. In Sec. III A we consider a diffusive ferromagnet/superconductor bilayer, while in Sec. III B we investigate a diffusive superconductor/ferromagnet/superconductor junction.

A. Density of states in ferromagnet/superconductor junction

We will divide our results for the DOS into subsections to clarify the role of the spin-dependent scattering for different exchange fields and film thicknesses. In the spirit of Ref. 17, we will consider the cases (i) $h \lesssim \Delta$, (ii) $h \gtrsim \Delta$, and (iii) $h \gg \Delta$. For $h \gg \Delta$, the proximity effect in the ferromagnet is weak unless the Thouless energy is very high ($\varepsilon_T \gg \Delta$). Throughout the rest of this paper, we fix $\gamma_L = 100$ and $\gamma_R = 1$. This corresponds to a scenario wherein the normal metal reservoir effectively acts as a very strong insulating barrier, mimicking a vacuum boundary. Since the resistance of the N/F interface will constitute the largest contribution to the total resistance, the conductance of the junction will be equivalent to the DOS at the N/F interface in the tunneling limit. We will study an intermediate value $\tau = 0.5$ of the barrier transparency since this cannot be reached within the usual approximations of either a fully transparent interface ($\tau = 1$) or a tunneling barrier ($\tau \ll 1$), and contrast this to a strong barrier $\tau = 0.1$. These choices for the barrier strength are experimentally the most relevant ones. For each of cases (i)–(iii), we will investigate two different thicknesses of the ferromagnetic layer, namely, $d/\xi = \{0.1, 1.0\}$, corresponding to $\varepsilon_T/\Delta = \{100, 1\}$. Here, $\xi = \sqrt{D/\Delta}$ is the superconducting coherence length. We comment further on our choice of parameters in Sec. IV. For each type of spin-dependent scattering, we define the dimensionless parameter g as a measure of the inverse scattering time. For spin-flip scattering, we have $g_{so} = 0$ and $g = g_{sf}/\varepsilon_T$ with $S_z = 3$, $S_{xy} = 0$ in Eq. (15) for the uniaxial case, while $S_z = S_{xy} = 1$ in the isotropic case. For spin-orbit scattering, we have $g_{sf} = 0$ and $g = g_{so}/\varepsilon_T$. Unless otherwise specified, the DOS is calculated right at the interface between the normal metal and the ferromagnet, i.e., $x = 0$ (see Fig. 1). This corresponds precisely to the experimental situation in Ref. 20.

In what follows, we first present our numerical results for the DOS for cases (i)–(iii) described above. We then investigate and explain the features seen in each of those cases in separate subsections. One of the main conclusions in this section is that the distinction between different types of spin-dependent scattering, e.g., spin-flip and spin-orbit scattering, may actually become very important in terms of interpreting the DOS in a ferromagnet/superconductor bilayer. We relate this to the behaviors of the proximity-induced anomalous singlet and triplet Green's functions in Sec. III A 5.

1. Case (i): $h \lesssim \Delta$

We first consider the case of a very weak exchange field, $h/\Delta = 0.5$, which splits the DOS for spin-$\uparrow$ and spin-$\downarrow$ electrons. A peculiar feature that may arise in a ferromagnet/superconductor junction is the enhancement of the DOS at zero energy, manifested as a peak. This issue was addressed in Refs. 17, 26, and 27 and has also been experimentally observed in Ref. 20. As seen in Fig. 2, the ferromagnet becomes fully proximized by the superconductor in the thin-layer case $d/\xi = 0.1$, and the DOS is equivalent to the bulk of the superconductor (in the absence of spin-dependent scattering). In fact, the DOS is virtually unaltered compared with that in the paramagnetic case for the short-junction regime regardless of whether we consider the tunneling or intermediate transparency case. However, an important distinction between different types of spin-dependent scattering becomes evident in the thin-layer case $d/\xi = 0.1$. The effect of spin-flip scattering, whether it is uniaxial or isotropic, is that the DOS gap closes upon increasing g. However, increasing the spin-orbit scattering rate does not affect the DOS in any way. We investigate this issue in more details in Sec. III A 6.

The situation changes dramatically when going to a wider junction regime, here modeled by $d/\xi = 1.0$. In the tunneling limit, a minigaplike structure opens up in the DOS at energies $\varepsilon = \pm h$. This can be understood as a result of the exchange splitting in the ferromagnet which shifts the energies, and hence the density of states, for majority and minority

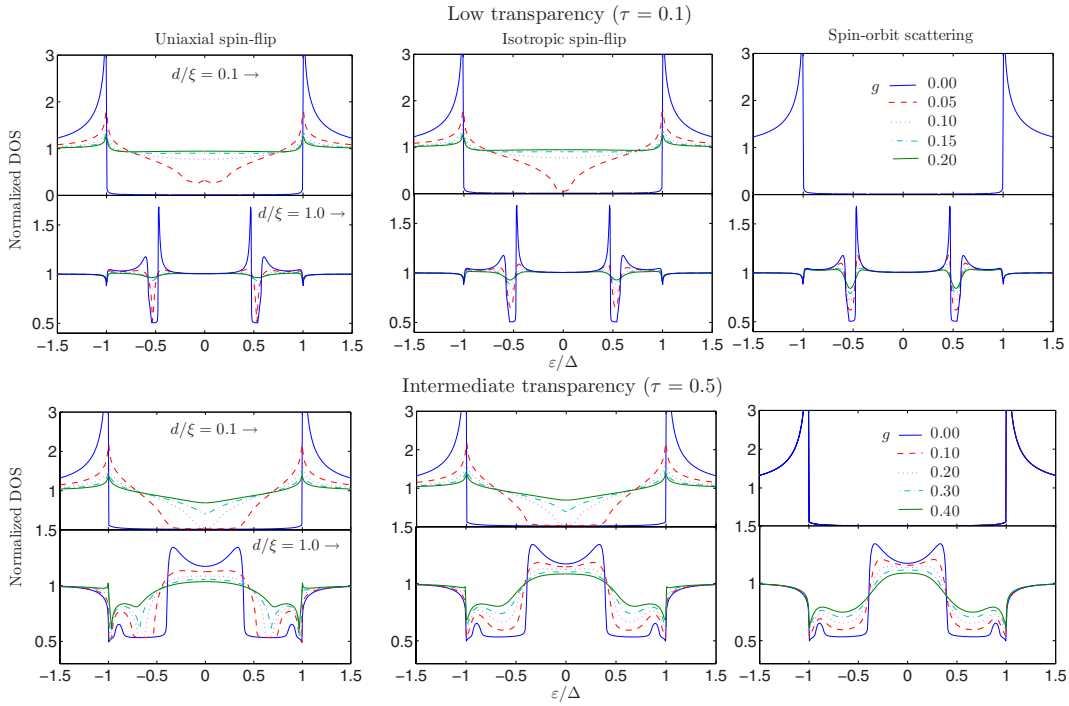

FIG. 2. (Color online) The local density of states at $x=0$ (see Fig. 1 for $h/\Delta=0.5$) For each thickness of the ferromagnetic layer and barrier transparency, we study the role of different types of spin-dependent scattering.

spins by $\pm h$. Increasing the barrier transparency to $\tau=0.5$, the minigaplike structure is retained and widened, which is reasonable since the proximity effect becomes larger and the minigap scales with τ. Another feature that is seen in the $d/\xi=1.0$ case is the appearance of a zero-energy peak (ZEP) in the DOS. The peak protrudes with increasing spin-flip scattering and is actually split into two in the absence of magnetic impurities. In Ref. 24, wherein the tunneling limit was applied to the F/S interface, no zero-energy peak was found to appear in the spectra. In the clean limit, however, a zero-energy peak was found to appear in the DOS for a wide range of parameters.[17] Although the appearance of a ZEP has been investigated in previous works, none of these considered the effect of spin-dependent scattering. In order to understand the ZEP feature seen in Fig. 2, we study the dependence of the anomalous Green's functions on spin-selective scattering in Sec. III A 5.

2. Case (ii): $h \gtrsim \Delta$

Next, we consider the case $h/\Delta=1.5$, shown in Fig. 3. As in the previous case, the DOS is almost unaffected by the presence of an exchange field in the short-junction regime $d/\xi=0.1$. Also, the gap in the DOS shows a remarkable resilience toward increasing the spin-orbit scattering. However, for $d/\xi=1.0$ the DOS is strongly modified and displays two peaks located at $\varepsilon=\pm\Delta$ and $\varepsilon=\pm h$. Increasing the concentration of magnetic impurities suppresses these peaks. In the clean limit, Zareyan *et al.*[17] found a similar development of the DOS with increasing Thouless energies (see Fig. 4 of Ref. 17). Note that the suppression of the proximity-induced features in the DOS due to the superconductor is now stronger for a given d/ξ compared to that in the case $h<\Delta$ (Fig. 2). In general, increasing the value of h leads to a smaller magnitude of the proximity-induced anomalous Green's functions (see also Fig. 7), which in turn causes the normalized DOS in the ferromagnetic layer to deviate less from unity.

3. Case (iii): $h \gg \Delta$

Finally, we investigate the case $h \gg \Delta$ in Fig. 4. If the ferromagnetic layer is an alloy of the type $Cu_{1-x}Ni_x$, a reasonable value of the exchange field may be found in the range $h=10$–50 meV. Here, we consider $h/\Delta=15$ and $h/\Delta=50$. With increasing value of the exchange field, the proximity effect becomes weaker. Therefore, we restrict our attention to the short-junction regime ($d/\xi=0.1$) with an intermediate barrier transparency ($\tau=0.5$) since the DOS deviates little from unity in the tunneling regime and for wide ferromagnetic layers.

For $h/\Delta=15$, the usual peak at $\varepsilon=\Delta$ is present and a minigap structure is seen in the absence of spin-flip scattering. Interestingly, increasing spin-flip scattering not only closes the minigap but actually causes the DOS to develop a peak at zero energy. This may be understood by considering

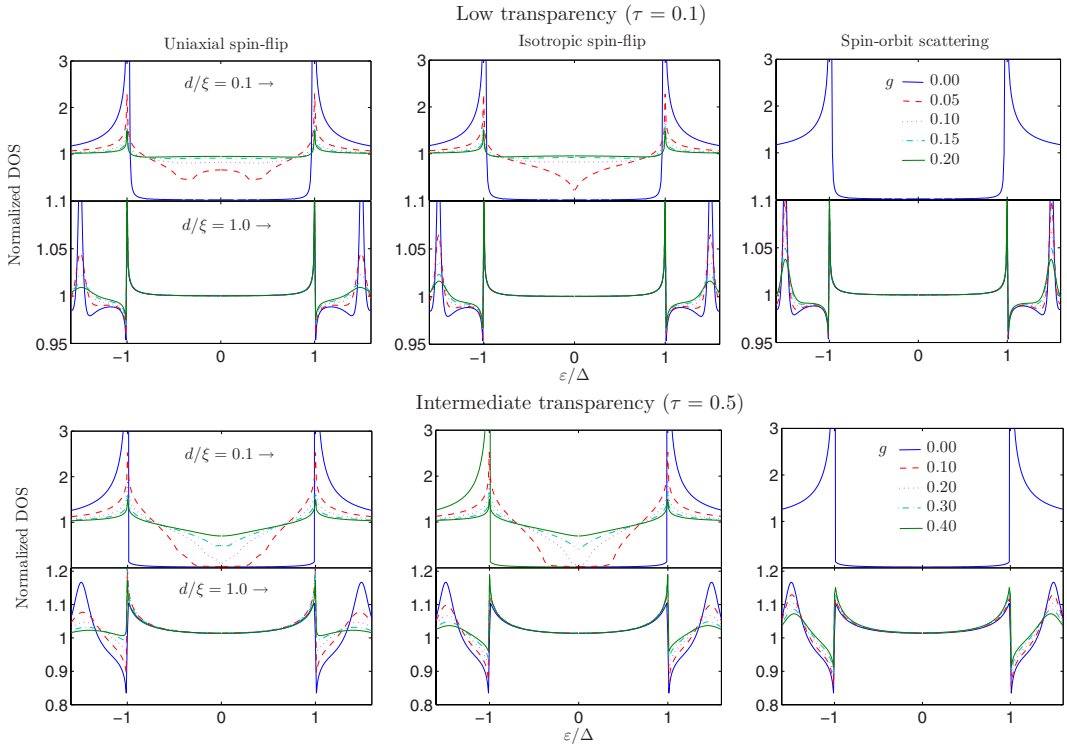

FIG. 3. (Color online) The local density of states at $x=0$ (see Fig. 1 for $h/\Delta=1.5$) For each thickness of the ferromagnetic layer and barrier transparency, we study the role of different types of spin-dependent scattering.

a subtle interplay between the singlet and triplet components of the proximity-induced anomalous Green's function for the ferromagnetic layer, and we delay a detailed explanation until Sec. III A 5.

For $h/\Delta=50$, all peaks and minigap features are now absent for $|\varepsilon|<\Delta$ and the only feature remaining in the spectrum is a dip at $\varepsilon=\Delta$. In this case, the qualitative effect of the different types of spin-dependent scattering is the same. Upon increasing d/ξ even further ($d/\xi \gg 1$), corresponding to a weaker proximity effect, one finds that the correction to the DOS oscillates upon increasing the spin-flip scattering rate, in contrast to the monotonous decay that might have been expected.[14] These oscillations are a result of the modified oscillation length of the proximity-induced anomalous Green's function in the F region.[1,2]

Also note that although the corrections to the normal-state DOS diminish rapidly for $h \gg \Delta$ upon increasing d/ξ, the combination of lock-in detection with an ultralow noise

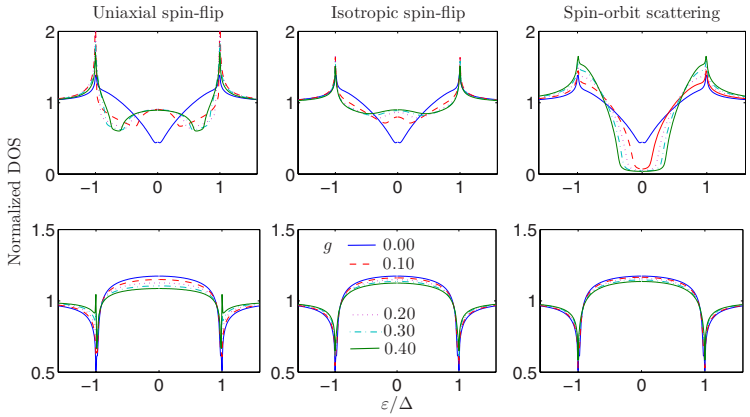

FIG. 4. (Color online) Local density of states at $x=0$ (see Fig. 1) for $h/\Delta=15$ (upper row) and $h/\Delta=50$ (lower row). Here, we have fixed $d/\xi=0.1$ and $\tau=0.5$ and study the role of different types of spin-dependent scattering.

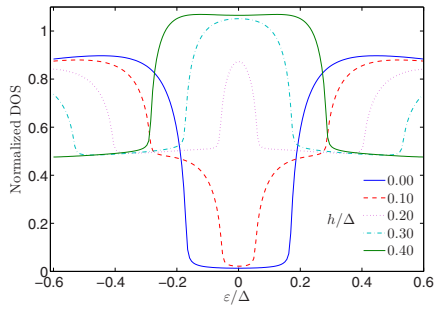

FIG. 5. (Color online) Plot of the DOS of a ferromagnet/superconductor junction with increasing exchange field h, using $d/\xi=1.0$ and $\tau=0.5$. Here, we have set the spin-dependent scattering to zero.

dc/ac mixer permits the resolution of structures in the DOS up to a factor of 10^{-4} smaller than the background conductance.[20]

4. Zero-energy peak

It is instructive to consider the development of the zero-energy peak in the DOS. In Fig. 5, we plot the DOS around zero energy for $d/\xi=1.0$ for increasing values of the exchange field h. The gradual formation of a zero-energy peak is clearly observed, and the peak flattens out when h becomes sufficiently large. The physical reason for this is intriguing. Yokoyama *et al.*[27] related this phenomenon directly to the proximity-induced odd-frequency pairing component of the anomalous Green's function in the ferromagnet (see also Refs. 63 and 64). In these works, it is shown that the DOS in the ferromagnet is enhanced due to the emergence of the proximity-induced odd-frequency pairing. Since we are considering the isotropic part (with respect to momentum) of Green's function due to the angular averaging in the dirty limit, one would perhaps naively expect that only the singlet component should be present. This is because the singlet anomalous Green's function is usually taken to be even under inversion of momentum, while the triplet components are taken to be odd under inversion of momentum. However, another possibility exists that allows for the presence of triplet correlations in the ferromagnet, involving a change in the sign of the superconducting order parameter under inversion of frequency. This type of pairing has been dubbed *odd-frequency pairing* in the literature.[1] The inversion of frequency is equivalent to an exchange of (relative) time coordinates for the field operators since ε is the Fourier transform of the relative time coordinate $t\equiv t_1-t_2$. Note that although even-frequency triplet correlations are destroyed in the dirty limit due to the isotropization stemming from impurity scattering, odd-frequency triplet correlations may persist since these do not vanish under angular averaging.

It remains to be clarified how the ZEP in a ferromagnet/superconductor junction is affected by spin-dependent scattering. To investigate this, we plot the DOS in Fig. 6 for a fixed exchange field $h/\Delta=0.3$, which gives a ZEP in the absence of spin-dependent scattering, and then successively increase the scattering rate. It is seen that the effect of increasing the spin-flip scattering rate (both uniaxial and isotropic) is a suppression of the proximity-induced features in the DOS. Qualitatively, the same occurs upon increasing the spin-orbit scattering rate (right panel of Fig. 6), but an interesting difference is that the peak is eventually transformed into a dip at $\varepsilon=0$. Increasing the spin-orbit scattering rate further ($g\gg 1$) leads to a fully developed minigap in the DOS. We propose an explanation of this peculiar phenomenon in the following section.

5. Anomalous Green's functions

In order to understand the interplay between the singlet and triplet components of the induced superconducting anomalous Green's function in the F region with regard to the zero-energy behavior of the DOS, consider the anomalous Green's functions defined as

$$f_s(\varepsilon,x)=[\sinh\,\theta_\uparrow(\varepsilon,x)-\sinh\,\theta_\downarrow(\varepsilon,x)]/2,$$

$$f_t(\varepsilon,x)=[\sinh\,\theta_\uparrow(\varepsilon,x)+\sinh\,\theta_\downarrow(\varepsilon,x)]/2. \quad (27)$$

At zero energy $\varepsilon=0$, one finds that $\mathrm{Re}\{f_s\}=\mathrm{Im}\{f_t\}=0$. The reader is reminded of the relation between the anomalous Green's functions and the DOS, which is a physical observable: the total DOS is given as $N=\Sigma_\sigma \mathrm{Re}\{\cosh\,\theta_\sigma\}/2$. Also note that the singlet and triplet components differ not only in their spin symmetries but also with respect to their energy dependences (even and odd, respectively), as noted in Sec. III A 4.

In Fig. 7, we plot $\mathrm{Im}\{f_s\}$ and $\mathrm{Re}\{f_t\}$ as measures of the singlet and triplet proximity-induced Green's functions for

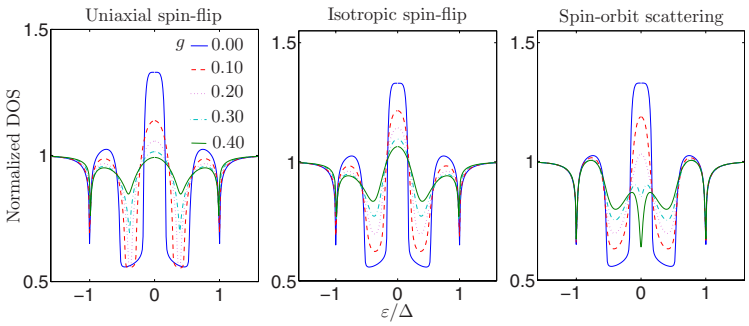

FIG. 6. (Color online) Plot of the DOS of a ferromagnet/superconductor junction for a fixed exchange field $h/\Delta=0.3$ which gives a ZEP in the absence of spin-dependent scattering. We fix $d/\xi=1.0$ and $\tau=0.5$.

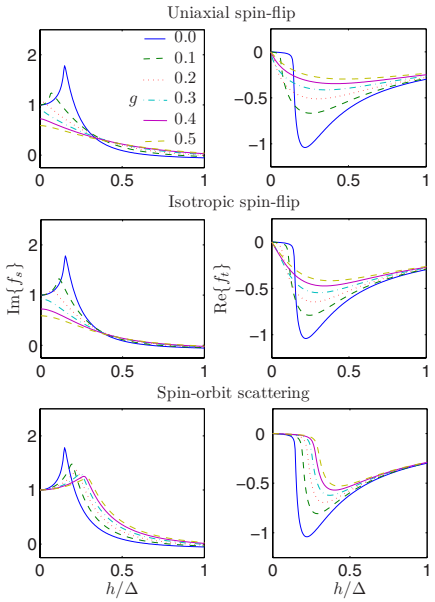

FIG. 7. (Color online) Plot of the singlet ($\mathrm{Im}\{f_s\}$) and the triplet ($\mathrm{Re}\{f_t\}$) anomalous Green's functions induced in the ferromagnet for $\varepsilon=0$ right at the N/F interface ($x=0$). We have used $\tau=0.5$ and $d/\xi=1.0$.

the ferromagnet right at the N/F interface ($x=0$). We consider the effect of each type of spin-dependent scattering separately. As seen, the peak in the singlet component occurring at a finite value of h vanishes upon increasing spin-flip scattering rate, and the decay eventually becomes monotonous for $g \gtrsim 0.3$. However, this is not the case for the triplet component: the maximum value of $|\mathrm{Re}\{f_t\}|$ occurs at a finite value of h even upon increasing the spin-dependent scattering rate. Therefore, the triplet component may become similar in magnitude to the singlet component even for weak exchange fields if the spin-flip scattering rate is sufficiently large. This explains the appearance of a zero-energy peak in the plot for $d/\xi=1.0$ in Fig. 3 upon increasing g.

Another interesting feature can be observed in Fig. 7. From the plots, it is seen that the anomalous Green's functions (both singlet and triplet) for a given exchange field may actually become larger upon increasing the rate of spin-flip scattering. This becomes evident at around $h/\Delta=0.1$ when comparing the lines for $g=0.0$ with those for $g=0.1$. Thus, we have at hand the opportunity to see an *enhanced proximity effect by spin-flip scattering* due to the increased magnitude of $|f_{s,t}|$ at low values of h. The enhanced proximity effect actually also becomes very pronounced sin the case of bulk odd-frequency superconductors.[65]

From Fig. 7, we may actually also find an explanation for the remarkable behavior of the DOS upon increasing the spin-orbit scattering rate in Fig. 6. For concreteness, let us first focus on the regime $h/\Delta \simeq 0.3$ corresponding to Fig. 6. Let us compare the plots for spin-flip and spin-orbit scattering. For both uniaxial and isotropic spin-flip scattering, it is

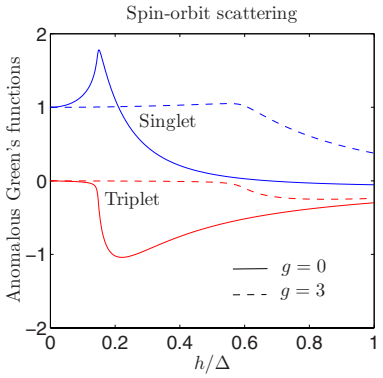

FIG. 8. (Color online) Plot of the singlet ($\mathrm{Im}\{f_s\}$) and the triplet ($\mathrm{Re}\{f_t\}$) anomalous Green's functions induced in the ferromagnet for $\varepsilon=0$ right at the N/F interface ($x=0$). We have used $\tau=0.5$ and $d/\xi=1.0$.

seen that the singlet component does not change much in magnitude, while the triplet component is suppressed. However, the singlet and triplet components are still comparable in magnitude for $g=0.5$, which accounts for the suppression of the minigap feature which is due to the singlet component. The situation is markedly different for the spin-orbit scattering. Now, the singlet component is actually enhanced in magnitude (for $h/\Delta \simeq 0.3$) while the triplet component is reduced very strongly. In fact, the triplet component becomes essentially zero for very large spin-orbit scattering rates, while the singlet component may still have a considerable magnitude. This explains the appearance of a minigap in Fig. 6 upon increasing the spin-orbit scattering rate: the singlet component, which is responsible for the minigap, increases; while the triplet component decreases.

The above discussion was restricted to $h/\Delta \simeq 0.3$ for concreteness, but the results nevertheless allude to a much more general principle: the spin-orbit scattering is much more detrimental for the triplet component than for the singlet component. To elucidate this feature, consider Fig. 8, wherein we compare the proximity-induced singlet and triplet components in the ferromagnetic layer. We set $d/\xi=1.0$ since for $d/\xi \ll 1$ the singlet component completely dominates the triplet component (see Figs. 2 and 3). Also, we set $\tau=0.5$, but we checked that the qualitative features are identical for lower barrier transparencies. As seen from Fig. 8, the singlet component is much more robust toward increased spin-orbit scattering than the triplet component. The latter only becomes appreciable in magnitude when the exchange field becomes of the same order or larger than Δ when the spin-orbit scattering range is large, $g \gg 1$. Note that in contrast, both the singlet and triplet components are strongly reduced with increasing spin-flip scattering.

In the absence of an exchange field, it is clear from Fig. 7 that the singlet component is completely independent of the rate of spin-orbit scattering. Although we have only shown this explicitly for $\varepsilon=0$, we have numerically confirmed that the magnitude of the singlet component at $h=0$ remains unchanged upon increasing g. On the other hand, the triplet

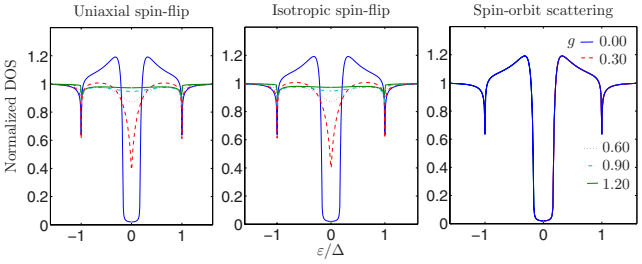

FIG. 9. (Color online) Plot of the DOS at $x=0$ for a normal metal/superconductor junction using $d/\xi=1.0$ and $\tau=0.5$. As seen, spin-flip scattering closes the minigap, whether it is uniaxial or isotropic. However, the minigap shows a strong resilience against increasing spin-orbit scattering.

component is always zero at $h=0$ but remains very close to zero upon increasing the exchange field h for high values of g. A natural question arises: why is the singlet component insensitive to spin-orbit scattering while the triplet component depends strongly on it?

The answer to this question is illuminated by considering the Usadel equations in the ferromagnetic region in limiting cases. From Eq. (15), we obtain several important properties.

(a) In the presence of uniaxial spin-flip scattering ($S_z=3, S_{xy}=0$), by taking the limit of $\tau_{sf}\to 0$ we get $\theta_\uparrow=\theta_\downarrow=0$. Then both the singlet and the triplet components are suppressed. This is also the case for isotropic spin-flip scattering ($S_z=S_{xy}=1$).

(b) With in-plane spin-flip scattering ($S_z=0$), we get $\theta_\uparrow=\theta_\downarrow$ when taking the limit $\tau_{sf}\to 0$. Then, the singlet component should vanish, as seen from the definition in Eq. (27).

(c) In the presence of pure spin-orbit scattering ($S_z=S_{xy}=0$), by taking limit of $\tau_{so}\to 0$ we get $\theta_\uparrow=-\theta_\downarrow$. Then, the triplet component should vanish, as seen from the definition in Eq. (27).

Therefore, we find that uniaxial and isotropic spin-flip scattering is harmful to both the singlet and the triplet components, while in-plane spin-flip scattering and spin-orbit scattering are detrimental to the singlet and the triplet components, respectively.

These properties are also obtained by using linearized Usadel equations in the ferromagnetic region, which may be formally obtained from Eq. (15) by letting $\theta_\sigma\to f_\sigma$, with $\sigma=\pm$, and assuming that $|f_\pm|\ll 1$ as follows:

$$\partial_x^2 f_t \pm \partial_x^2 f_s + A_\pm f_t \pm B_\pm f_s = 0, \tag{28}$$

where we have introduced

$$A_\pm = \frac{1}{D}\left[2i(\varepsilon \pm h) - g_{so} - \frac{g_{sf}S_z}{2}\right],$$

$$B_\pm = \frac{1}{D}\left[2i(\varepsilon \pm h) - \frac{g_{sf}(2S_{xy}+S_z)}{2}\right]. \tag{29}$$

As seen, the spin-orbit scattering rate enters only in the coefficient associated with the triplet component. Notice that in absence of an exchange field h, which renders $f_t=0$, the linearized Usadel equation is independent of the spin-orbit scattering rate. On a microscopic level, it is clear that the different dependences on spin-orbit scattering for the singlet and the triplet anomalous Green's functions originates from the fundamental symmetries of these wave functions. It should be emphasized that *both* the singlet and the triplet components are strongly affected by magnetic impurities, i.e., spin-flip scattering, as seen from Eq. (29).

The above analysis emphasizes the importance of distinguishing between different types of spin-dependent scattering in terms of understanding the behavior of the DOS in a ferromagnet/superconductor bilayer. In particular, we have shown that the effect of spin-orbit scattering may differ fundamentally from spin-flip scattering (originating, e.g., from magnetic impurities) and that this is manifested in the interplay between the singlet and the triplet anomalous Green's functions in the ferromagnetic layer.

6. Minigap and spin-orbit scattering

Finally, we consider the effect of spin-dependent scattering on the interesting manifestation of the proximity-induced superconducting correlations in a normal/superconductor junction: the minigap.[66] We first briefly recapitulate the results in the paramagnetic case. When a normal metal is placed in close proximity to a superconductor, a minigap Δ_g opens up in the DOS of the normal metal. This minigap roughly scales like $\Delta_g \sim \varepsilon_T\tau/\gamma_R$ and was originally studied by McMillan[66] in a tunneling model of a normal/superconductor junction. The minigap is defined as an almost complete suppression of the quasiparticle DOS in a given energy interval. The minigap is a consequence of the effective backscattering that quasiparticles incident on the superconducting interface from the normal side experience due to the presence of impurities. Consequently, the probability for transmission increases such that the DOS is nonzero for $\Delta_g<\varepsilon<\Delta$. For a nearly perfect transparency of the interface, Δ_g can become close to Δ in magnitude. For a tunneling barrier $\tau\ll 1$, the minigap becomes very small.

An interesting issue is how the minigap is affected by spin-dependent scattering. We provide numerical results to elucidate this question in Fig. 9. As seen from the plots, the influence of uniaxial spin-flip scattering is a gradual suppression of the proximity-induced features in the DOS, consistent with previous results.[67–71] The effect of isotropic spin-flip scattering is virtually identical to the uniaxial case. However, quite surprisingly, the minigap shows a strong resilience toward increasing spin-orbit scattering, as seen in Fig. 9. In fact, we find that even upon increasing g to values $\gg\Delta$, the minigap persists in the DOS as long as the exchange field is absent. Upon increasing the exchange field to values $h\gg\Delta$, the minigap slowly begins to close when the spin-orbit scat-

tering rate becomes large. This feature may be understood by again resorting to Fig. 7 and Fig. 8, wherein a detailed study of the singlet and the triplet components of the anomalous Green's function was conducted. In general, the spin-orbit scattering was shown to be detrimental for the triplet component while the singlet component still remained at a considerable magnitude, even for $g \gg 1$. However, the triplet component was strengthened upon increasing the exchange field h, which explains why the minigap would close for larger values of h upon increasing the scattering rate. This behavior should be contrasted with that of spin-flip scattering, whether it is isotropic or uniaxial, which invariably suppresses both the singlet and triplet components of the proximity-induced anomalous Green's function.

B. Josephson current

Having concluded our study of the DOS in the F/S bilayer, we now turn to the supercurrent in an S/F/S junction. In the following, we fix $R_B/R_F=5$, where R_B is the resistance of the barrier at the interfaces and R_F is the resistance of the diffusive ferromagnetic layer. Also, we consider an exchange field $h/\Delta=10$, which should correspond to a typical weak ferromagnetic alloy, such as $Cu_{1-x}Ni_x$. In the following, we are particularly interested in examining the possibility of obtaining a strong deviation from the usual sinusoidal current-phase relationship. This may lead to the opportunity of creating a supercurrent-switching device, which we elaborate on below. We remind the reader that all the quantities used below were introduced and defined in Sec. II.

Consider first the dependence of the I_cR_N product on the normalized junction width d/ξ, where $\xi=\sqrt{D/2\pi T_c}$ is the superconducting coherence length. We contrast the results obtained with barriers of intermediate transparency ($Z=0.5$) and of low transparency ($Z=5.0$) as the experimentally most relevant cases, shown in Fig. 10. As seen, the intermediate transparency allows for a finite residual value of the supercurrent at the 0-π transition point, where the first harmonic of the current-phase relationship vanishes. The effect of uniaxial spin-flip scattering is seen to be a reduction of the residual value of the supercurrent. Even for an intermediate transparency of the barrier, the residual current is reduced to immeasurable values for $g\sim 5$, where $g=\gamma/\Delta$ is a measure of the uniaxial spin-flip scattering. This issue has not been addressed previously in the literature and is useful to complement previous qualitative predictions with a more realistic quantitative analysis. Also, it is seen from Fig. 10 that the transition points are translated toward higher junction widths upon increasing g.

We next consider the temperature dependence of the I_cR_N product in Fig. 11. In the wide-junction regime $\mathcal{E}=\varepsilon_T/\Delta=0.05$, the magnitude of I_cR_N is quite small, and a 0-π transition occurs for zero spin-flip scattering at $T/T_c\approx 0.55$. However, increasing the value of g is seen to vanish the 0-π transition completely. This behavior is very distinct from the d/ξ dependence shown in Fig. 10, wherein increasing spin-flip scattering reduces the residual value of the supercurrent at the transition point but does not remove the transition completely. Consider now a shorter junction here modeled

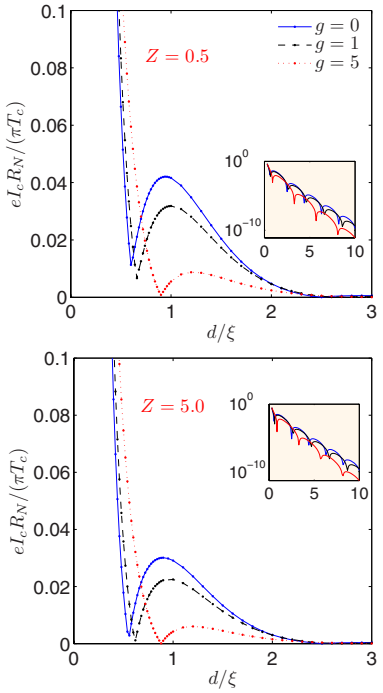

FIG. 10. (Color online) Plot of the junction-width dependence of the I_cR_N product for an S/F/S Josephson junction in the intermediate ($Z=0.5$) and low ($Z=5.0$) barrier transparency regimes. The temperature is fixed at $T/T_c=0.1$. For each case, the effect of increasing uniaxial spin-flip scattering is seen to severely reduce the residual value of the critical current at the 0-π transition points.

by $\mathcal{E}=9.0$, corresponding to $d/\xi\approx 0.6$, for an intermediate barrier transparency $Z=0.5$. Close examination of the transition point where the current changes sign reveals a small but finite residual value of the supercurrent, in this case for $T/T_c\approx 0.65$. At first sight, the effect of increasing g then appears to amount to a complete removal of the 0-π transition point, rather than a suppression of the residual value, as in Fig. 10. However, by increasing g in smaller steps as shown in Fig. 12(a) with $\mathcal{E}=10.0$, it is seen that the 0-π transition *gradually* vanishes. This means that the transition point when considering the temperature-dependence is much more sensitive to spin-flip scattering than the width dependence of Fig. 10. It should be noted that the 0-π oscillations vanish upon increasing g for the particular choice of the width d (corresponding to a certain $\mathcal{E}$) used here. For another choice of d, one might expect to have 0-π introduced upon increasing g. The main point is nevertheless that the temperature dependence of the critical current oscillations appear to be more sensitive to spin-flip scattering than the width dependence of the same oscillations is.

The origin of a residual value of the current at the sign-reversal point is a deviation from a purely sinusoidal current-phase relationship. To illustrate the strong deviation from a pure sinusoidal phase dependence for the $\mathcal{E}=9.0$ case, consider Fig. 12(b). The 0-π transition can clearly be discerned

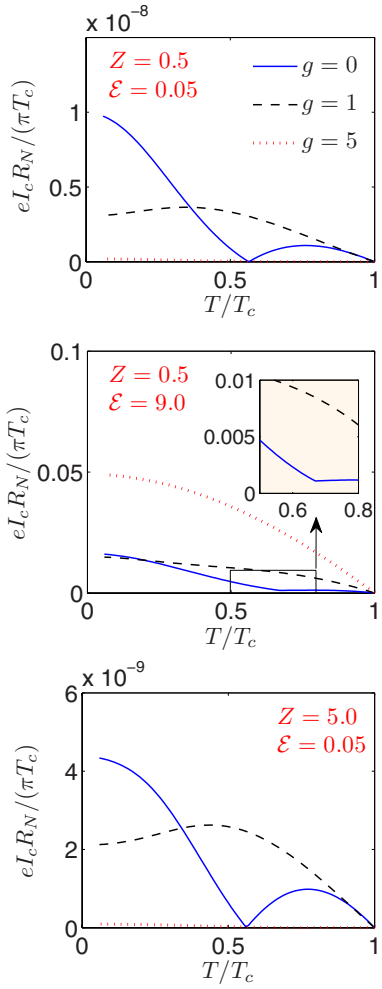

FIG. 11. (Color online) Plot of the temperature dependence of the I_cR_N product for an S/F/S Josephson junction in the intermediate (Z=0.5) and low (Z=5.0) barrier transparency regimes for different values of the normalized Thouless energy $\mathcal{E}$.

from the plot. Right before the transition (T/T_c=0.6), the maximum value of the current occurs at a negative value for I_cR_N. After the transition (T/T_c=0.7), the maximum value occurs for a positive value of I_cR_N. For comparison, we have plotted a pure sinusoidal phase dependence. Figure 12(b) shows that that higher harmonics [in this case, $\sin(2\phi)$] dominate near the sign-reversal point, giving rise to the residual value of the current.

IV. DISCUSSION

In our calculations, we have neglected the depletion of the superconducting and magnetic order parameter in the vicinity of the F/S interface. In the low transparency case, this is

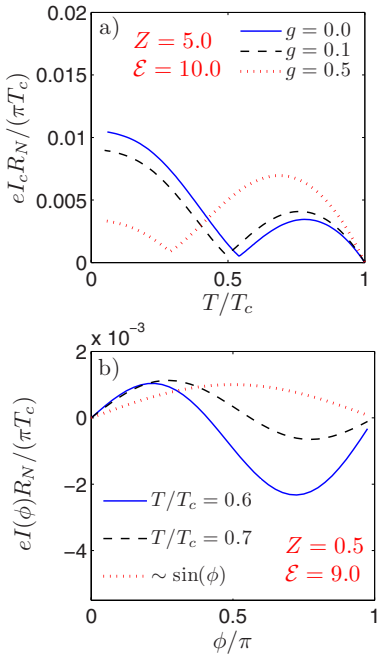

FIG. 12. (Color online) (a) Plot of the temperature-dependence of the I_cR_N product for weakly increasing spin-flip scattering. (b) Plot of the current-phase relationship for the I_cR_N product for an S/F/S Josephson junction, illustrating the strong deviation from the sinusoidal dependence and the 0-π transition.

permissible.[72] In the high transparency case, the depletion may be substantial. However, the qualitative features obtained in the DOS are known to be the same even if this depletion is taken into account—the characteristic features are often simply shifted in energy from the bulk value $\varepsilon = \Delta$ to a reduced value $\tilde{\Delta} < \Delta$. Our approximation consisting of using the bulk Green's function in the superconducting regions is well justified also if we assume that the superconducting region is much less disordered than the ferromagnetic layer. Also, we have employed an effectively one-dimensional model to account for the proximity effect. In the present system, we are concerned with isotropic order parameters (s-wave superconductivity), such that performing the same calculations in two or three dimensions will yield similar results since the averaging over angles will have virtually no effect.

Let us also comment on our choices of Thouless energy in the ferromagnetic region. The actual thicknesses employed in experiments on both F/S bilayers and S/F/S Josephson junctions vary greatly, but may in some cases be as small as <20 nm.[19,20] Now, the typical superconducting coherence length also varies a lot, ranging from 38 nm in Nb to 1600 nm in Al. Since the coherence length is defined as $\xi = \sqrt{D/\Delta}$ with the diffusion constant D in the ferromagnetic region, we find that if $\varepsilon_T/\Delta = x$, then the thickness d of the ferromagnetic region is given as $d = \xi/\sqrt{x}$. Assuming a superconducting material with ξ=100 nm, choosing ε_T/Δ=0.1

corresponds to $d \simeq 315$ nm. In order to make contact with the experimental situations that employ a ferromagnetic layer thickness of $d \simeq 20$ nm, we would then need a value of $x = 25$. This is the motivation for our choice of the large Thouless energy $\varepsilon_T/\Delta = 100$, corresponding to $d/\xi = 0.1$.

Finally, we discuss the possible realization of a supercurrent switch. The prospect of obtaining a dissipationless current-switching device relies on the opportunity to achieve sufficiently large residual values of the supercurrent at the 0-π transition points. As seen from our results, this may be obtained for the intermediate barrier transparency regime, which agrees with the qualitative conclusions in Ref. 28. However, the effect of uniaxial spin-flip scattering has a detrimental effect on this residual value. While the width dependence (Fig. 10) shows some resilience toward an increased concentration of magnetic impurities, the 0-π transition is highly sensitive to spin-flip scattering in temperature dependence (Fig. 11). To switch the sign of the current, one has to increase either the width or the temperature of the junction by an infinitesimal amount right at the transition point. Since only the temperature can be manipulated in this way in a realistic experiment, we arrive at the conclusion that the realization of a current-switch device in diffusive S/F/S junctions relies on samples with a high quality interface and very low amounts of magnetic impurities.

V. SUMMARY

In conclusion, we have numerically studied the local density of states in a proximity ferromagnet/superconductor structure in the dirty limit. Our results take into account an arbitrary rate of spin-flip scattering and an arbitrary interface transparency, focusing on a moderately transparent interface. This regime cannot be reached in the standard limiting cases of an ideal or tunneling interface. We have studied three cases for the size of the exchange field h compared to the superconducting gap Δ: (i) $h \lesssim \Delta$, (ii) $h \gtrsim \Delta$, and (iii) $h \gg \Delta$. In each case, we considered several values of the thickness of the ferromagnetic layer, barrier transparencies, and also different types of spin-dependent scattering to obtain the energy-resolved DOS. In doing so, we have clarified characteristic features that may be expected in the various parameter regimes accessible for the ferromagnetic film. Since our results take into account an arbitrary proximity effect and an arbitrary magnetic impurity concentration, they should serve as a useful tool for a quantitative analysis of experimental data. In particular, we investigated the effect of spin-dependent scattering on the zero-energy behavior observed in the DOS, which displayed the full range from a fully developed minigap to a peak structure. By analyzing in detail the singlet and the triplet parts of the anomalous Green's function, we come to the important conclusion that it is necessary to distinguish between different types of spin-dependent scattering in order to correctly interpret DOS measurements in ferromagnet/superconductor bilayers. Specifically, we find that the effect of spin-flip scattering (both uniaxial and isotropic) may differ fundamentally from the effect of spin-orbit scattering. The reason for this is that for weak exchange fields, the singlet component of the anomalous Green's function remains essentially unaltered by spin-orbit scattering, while the triplet component is strongly suppressed.

We have also investigated the supercurrent in diffusive superconductor/ferromagnet/superconductor junctions, allowing for arbitrary concentration of magnetic impurities and arbitrary interface transparency. We have investigated the effect of spin-flip scattering on the residual value of the supercurrent at the 0-π transition points and find a much weaker sensitivity to magnetic impurities in the width dependence compared with that for the temperature dependence of the $I_c R_N$ product. We have proposed that a finite and measurable residual value of the supercurrent may be obtained in the intermediate barrier transparency regime, although spin-flip scattering has a detrimental effect on this residual value. For samples with high quality interface and very low concentration of magnetic impurities, the residual value may be exploited to obtain efficient supercurrent-switching simply by altering the temperature of the system.

ACKNOWLEDGMENTS

The authors gratefully acknowledge Y. Tanaka for useful discussions. J.L. and A.S. were supported by the Norwegian Research Council Grants No. 158518/431, No. 158547/431 (NANOMAT), and No. 167498/V30 (STORFORSK). T.Y. acknowledges support by the JSPS.

APPENDIX

We here define the star product which enters the Eilenberger equation [Eq. (6)]. For any two functions A and B, we have

$$A \otimes B = e^{i(\partial_{T_A}\partial_{\varepsilon_B} - \partial_{\varepsilon_A}\partial_{T_B})/2} AB, \tag{A1}$$

where the differentiation operators denote derivation with respect to the variables T and ε in the mixed representation. Note that if there is no explicit time dependence in the problem, the star product reduces to regular multiplication.

The Pauli matrices used in this paper are defined as[56]

$$\underline{\tau}_1 = \begin{pmatrix} 0 & 1 \\ 1 & 0 \end{pmatrix}, \quad \underline{\tau}_2 = \begin{pmatrix} 0 & -i \\ i & 0 \end{pmatrix}, \quad \underline{\tau}_3 = \begin{pmatrix} 1 & 0 \\ 0 & -1 \end{pmatrix},$$

$$\underline{1} = \begin{pmatrix} 1 & 0 \\ 0 & 1 \end{pmatrix}, \quad \hat{1} = \begin{pmatrix} \underline{1} & \underline{0} \\ \underline{0} & \underline{1} \end{pmatrix}, \quad \hat{\tau}_i = \begin{pmatrix} \underline{\tau}_i & \underline{0} \\ \underline{0} & \underline{\tau}_i \end{pmatrix},$$

$$\hat{\rho}_1 = \begin{pmatrix} \underline{0} & \underline{\tau}_1 \\ \underline{\tau}_1 & \underline{0} \end{pmatrix}, \quad \hat{\rho}_2 = \begin{pmatrix} \underline{0} & -i\underline{\tau}_1 \\ i\underline{\tau}_1 & \underline{0} \end{pmatrix}, \quad \hat{\rho}_3 = \begin{pmatrix} \underline{1} & \underline{0} \\ \underline{0} & -\underline{1} \end{pmatrix}. \tag{A2}$$

[1] F. S. Bergeret, A. F. Volkov, and K. B. Efetov, Rev. Mod. Phys. **77**, 1321 (2005).
[2] A. I. Buzdin, Rev. Mod. Phys. **77**, 935 (2005).
[3] K. Usadel, Phys. Rev. Lett. **25**, 507 (1970).
[4] M. Yu. Kupriyanov and V. F. Lukichev, Zh. Eksp. Teor. Fiz. **94**, 139 (1988)[Sov. Phys. JETP **67**, 1163 (1988)].
[5] L. Lazar, K. Westerholt, H. Zabel, L. R. Tagirov, Yu. V. Goryunov, N. N. Garifyanov, and I. A. Garifullin, Phys. Rev. B **61**, 3711 (2000).
[6] A. I. Buzdin, Phys. Rev. B **62**, 11377 (2000).
[7] E. A. Demler, G. B. Arnold, and M. R. Beasley, Phys. Rev. B **55**, 15174 (1997).
[8] I. Baladie and A. Buzdin, Phys. Rev. B **64**, 224514 (2001).
[9] A. A. Golubov, M. Yu. Kupriyanov, and Ya. V. Fominov, JETP Lett. **75**, 223 (2002).
[10] V. N. Krivoruchko and E. A. Koshina, Phys. Rev. B **66**, 014521 (2002).
[11] F. S. Bergeret, A. F. Volkov, and K. B. Efetov, Phys. Rev. B **65**, 134505 (2002).
[12] M. Faure, A. I. Buzdin, A. A. Golubov, and M. Yu. Kupriyanov, Phys. Rev. B **73**, 064505 (2006).
[13] A. Cottet and W. Belzig, Phys. Rev. B **72**, 180503(R) (2005).
[14] J. Linder and A. Sudbø, Phys. Rev. B **76**, 214508 (2007).
[15] A. Cottet, Phys. Rev. B **76**, 224505 (2007).
[16] S. Pilgram, W. Belzig, and C. Bruder, Phys. Rev. B **62**, 12462 (2000).
[17] M. Zareyan, W. Belzig, and Yu. V. Nazarov, Phys. Rev. Lett. **86**, 308 (2001); Phys. Rev. B **65**, 184505 (2002).
[18] J. Kopu, M. Eschrig, J. C. Cuevas, and M. Fogelstrom, Phys. Rev. B **69**, 094501 (2004).
[19] V. V. Ryazanov, V. A. Oboznov, A. Yu. Rusanov, A. V. Veretennikov, A. A. Golubov, and J. Aarts, Phys. Rev. Lett. **86**, 2427 (2001).
[20] T. Kontos, M. Aprili, J. Lesueur, and X. Grison, Phys. Rev. Lett. **86**, 304 (2001).
[21] S. Reymond, P. SanGiorgio, M. R. Beasley, J. Kim, T. Kim, and K. Char, Phys. Rev. B **73**, 054505 (2006).
[22] L. Cretinon, A. K. Gupta, H. Sellier, F. Lefloch, M. Faure, A. Buzdin, and H. Courtois, Phys. Rev. B **72**, 024511 (2005).
[23] P. SanGiorgio, S. Reymond, M. R. Beasley, J. H. Kwon, and K. Char, arXiv:0712.1322 (unpublished).
[24] D. Yu. Gusakova, A. A. Golubov, M. Yu. Kupriyanov, and A. Buzdin, Pis'ma Zh. Eksp. Teor. Fiz. **83**, 385 (2006).
[25] V. Nazarov, Superlattices Microstruct. **25**, 1221 (1999).
[26] T. Yokoyama, Y. Tanaka, and A. A. Golubov, Phys. Rev. B **72**, 052512 (2005); **73**, 094501 (2006).
[27] T. Yokoyama, Y. Tanaka, and A. A. Golubov, Phys. Rev. B **75**, 134510 (2007).
[28] G. Mohammadkhani and M. Zareyan, Phys. Rev. B **73**, 134503 (2006).
[29] F. S. Bergeret, A. F. Volkov, and K. B. Efetov, Phys. Rev. B **75**, 184510 (2007).
[30] A. I. Buzdin, L. N. Bulaevsky, and S. V. Panyukov, JETP Lett. **35**, 178 (1982).
[31] L. N. Bulaevskii, V. V. Kuzii, and A. A. Sobyanin, Pis'ma Zh. Eksp. Teor. Fiz. **25**, 314 (1977)[JETP Lett. **25**, 290 (1977)].
[32] F. S. Bergeret, A. F. Volkov, and K. B. Efetov, Phys. Rev. B **64**, 134506 (2001).
[33] N. M. Chtchelkatchev, W. Belzig, Yu. V. Nazarov, and C. Bruder, JETP Lett. **74**, 323 (2001).
[34] J. Cayssol and G. Montambaux, Phys. Rev. B **71**, 012507 (2005).
[35] A. A. Golubov, M. Y. Kupriyanov, and E. Ilfichev, Rev. Mod. Phys. **76**, 411 (2004).
[36] J. Linder, T. Yokoyama, D. Huertas-Hernando, and A. Sudbø, Phys. Rev. Lett. **100**, 187004 (2008).
[37] Z. Nussinov, A. Shnirman, D. P. Arovas, A. V. Balatsky, and J. X. Zhu, Phys. Rev. B **71**, 214520 (2005).
[38] A. Bauer, J. Bentner, M. Aprili, M. L. Della-Rocca, M. Reinwald, W. Wegscheider, and C. Strunk, Phys. Rev. Lett. **92**, 217001 (2004).
[39] V. V. Ryazanov, V. A. Oboznov, A. V. Veretennikov, and A. Yu. Rusanov, Phys. Rev. B **65**, 020501(R) (2001).
[40] T. Kontos, M. Aprili, J. Lesueur, F. Genet, B. Stephanidis, and R. Boursier, Phys. Rev. Lett. **89**, 137007 (2002).
[41] H. Sellier, C. Baraduc, F. Lefloch, and R. Calemczuk, Phys. Rev. B **68**, 054531 (2003).
[42] H. Sellier, C. Baraduc, F. Lefloch, and R. Calemczuk, Phys. Rev. Lett. **92**, 257005 (2004).
[43] A. Buzdin, Phys. Rev. B **72**, 100501(R) (2005).
[44] M. Houzet, V. Vinokur, and F. Pistolesi, Phys. Rev. B **72**, 220506(R) (2005).
[45] A. S. Vasenko, A. A. Golubov, M. Yu. Kupriyanov, and M. Weides, Phys. Rev. B **77**, 134507 (2008).
[46] M. Faure, A. I. Buzdin, A. A. Golubov, and M. Yu. Kupriyanov, Phys. Rev. B **73**, 064505 (2006).
[47] O. Kashuba, Ya. M. Blanter, and Vladimir I. Fal'ko, Phys. Rev. B **75**, 132502 (2007).
[48] M. Mori, S. Hikino, S. Takahashi, and S. Maekawa, J. Phys. Soc. Jpn. **76**, 054705 (2007).
[49] V. A. Oboznov, V. V. Bolginov, A. K. Feofanov, V. V. Ryazanov, and A. I. Buzdin, Phys. Rev. Lett. **96**, 197003 (2006).
[50] Y. S. Barash and I. V. Bobkova, Phys. Rev. B **65**, 144502 (2002).
[51] J. W. Serene and D. Rainer, Phys. Rep. **101**, 221 (1983).
[52] N. Kopnin, *Theory of Nonequilibrium Superconductivity* (Oxford University Press, New York, 2001).
[53] J. Rammer and H. Smith, Rev. Mod. Phys. **58**, 323 (1986).
[54] A. M. Zagoskin, *Quantum Theory of Many-Body Systems* (Springer, New York, 1998).
[55] V. Chandrasekhar, in *The Physics of Superconductors*, edited by K.-H. Bennemann and J. B. Ketterson (Springer-Verlag, Berlin, 2004), Vol II; arXiv:cond-mat/0312507 (unpublished).
[56] We will use the notations and conventions of J. P. Morten, M.S. thesis, Norwegian University of Science and Technology, 2003, which in turn is closely similar to the notations used in Ref. 51.
[57] G. Eilenberger, Sov. Phys. JETP **214**, 195 (1968).
[58] W. Belzig, F. K. Wilhelm, C. Bruder, G. Schön, and A. D. Zaikin, Superlattices Microstruct. **25**, 1251 (1999).
[59] D. Huertas-Hernando, Yu. V. Nazarov, and W. Belzig, arXiv:cond-mat/0204116 (unpublished).
[60] A. Millis, D. Rainer, and J. A. Sauls, Phys. Rev. B **38**, 4504 (1988).
[61] Y. Tanaka, A. A. Golubov, and S. Kashiwaya, Phys. Rev. B **68**, 054513 (2003).
[62] T. Yokoyama, Y. Tanaka, A. A. Golubov, and Y. Asano, Phys. Rev. B **73**, 140504(R) (2006); T. Yokoyama, Y. Tanaka, and A. A. Golubov, *ibid.* **75**, 094514 (2007).
[63] V. Braude and Yu. V. Nazarov, Phys. Rev. Lett. **98**, 077003 (2007).
[64] Y. Asano, Y. Tanaka, and A. A. Golubov, Phys. Rev. Lett. **98**,

107002 (2007).
[65] J. Linder, T. Yokoyama, Y. Tanaka, and A. Sudbø (unpublished).
[66] W. L. McMillan, Phys. Rev. **175**, 537 (1968).
[67] W. Belzig, C. Bruder, and G. Schön, Phys. Rev. B **54**, 9443 (1996).
[68] A. A. Golubov and M. Yu. Kupriyanov, J. Low Temp. Phys. **70**, 83 (1988).
[69] A. F. Volkov, A. V. Zaitsev, and T. M. Klapwijk, Physica C **210**, 21 (1993).
[70] S. Yip, Phys. Rev. B **52**, 15504 (1995).
[71] T. Yokoyama, Y. Tanaka, A. A. Golubov, J. Inoue, and Y. Asano, Phys. Rev. B **71**, 094506 (2005).
[72] C. Bruder, Phys. Rev. B **41**, 4017 (1990).

Paper XVI

Strongly spin-polarized current generated in Zeeman-split unconventional superconductors.

Physical Review B **78**, 014516 (2008).

Strongly spin-polarized current generated in a Zeeman-split unconventional superconductor

Jacob Linder,[1] Takehito Yokoyama,[2] Yukio Tanaka,[2] and Asle Sudbø[1]
[1]*Department of Physics, Norwegian University of Science and Technology, N-7491 Trondheim, Norway*
[2]*Department of Applied Physics, Nagoya University, Nagoya 464-8603, Japan*
(Received 25 February 2008; revised manuscript received 26 June 2008; published 18 July 2008)

We consider a thin-film normal-metal/superconductor junction in the presence of an externally applied in-plane magnetic field for several symmetries of the superconducting order parameter. For *p*-wave superconductors, a strongly spin-polarized current emerges due to an interplay between the nodal structure of the superconducting order parameter, the existence or nonexistence of zero-energy surface states, and the Zeeman splitting of the bands which form superconductivity. Thus, the polarization depends strongly on the orbital symmetry of the superconducting state. Our findings suggest a mechanism for obtaining fully spin-polarized currents crucially involving zero-energy surface states, not present in *s*-wave superconductors.

DOI: 10.1103/PhysRevB.78.014516 PACS number(s): 74.20.Rp, 74.50.+r

I. INTRODUCTION

In recent years, spintronics[1–4] has grown enormously as a research field, based on the idea that the electron spin may form centerpiece in future technological applications. The main issues in this field are: (i) how may one obtain and manipulate the spin polarization of an electrical current and (ii) how may the spin polarization of an electrical current be detected? Concerning the first issue, suggestions so far (see Ref. 3 and references therein) have mostly revolved around the use of semiconducting materials. These materials have the potential of offering some control over the spin injection properties via the coupling between the spin degree of freedom and the electrons orbital motion. This coupling originates with the spin-orbit coupling that is present in such materials. Concerning the second question, detection of a spin current has been proposed in the form of spin accumulation[5–7] and that a spin current should generate electrical fields.[8]

In the search for functionalities utilizing ideas involving the spin of electrons (spintronics), a subfield known as *superspintronics* has emerged from its predecessor. The idea is to combine the useful properties of superconductors with spin generation and manipulation.[9–13] Most known superconductors have a spin-singlet symmetry, which means that the Cooper pair does not carry any net spin. For such superconductors, one relies mostly on strong magnetic sources such as half-metallic ferromagnets in concomitance with superconductors for obtaining strongly spin-polarized currents.

Recently, however, it was suggested in Ref. 14 that a thin-film *s*-wave superconductor subjected to an in-plane magnetic field may serve to strongly spin-polarize electrical currents in the tunneling limit. This actually follows from the results obtained by Meservey and Tedrow[19] who performed experiments in spin-polarized electron tunneling in thin-film *s*-wave superconductors subjected to an in-plane magnetic field. In Ref. 13, a proposal for an absolute spin-valve effect was put forward without assuming a thin-film structure of the spin-singlet superconductor. On the other hand, there now exist several superconductors exhibiting spin-triplet superconductivity,[15–18] and these systems are less antagonistic toward applied magnetic fields than what their spin-singlet counterparts are.

An intriguing situation may arise when an in-plane magnetic field is applied to a thin-film superconductor. If the thickness d of the superconducting film satisfies $d \ll \lambda$, where λ is the magnetic penetration depth, the field penetrates the superconducting film homogeneously and induces a Zeeman splitting of the bands. Experiments on such structures have clearly revealed a spin-split density of states in the superconductor,[19] and the problem was recently re-examined in Ref. 14.

A natural question arises in the context of *Zeeman-split superconductors*: what is the effect of the orbital symmetry of the superconducting order parameter on the polarization of the electrical current? In this work, we show that the *orbital symmetry* of the superconducting state strongly influences the *spin polarization* of the electrical current. We consider three different orbital symmetries for the superconductor and show how the polarization properties of the current differ greatly in each case, even though the spin structure is similar for each superconducting state. It follows from our results that the polarization properties of the current may be used not only as a tool for obtaining information about the orbital symmetry of the superconducting state, but that *the spin polarization may be controlled efficiently by a bias voltage due to an interplay between superconductivity and magnetism*.[13,14,19] The physics is that the Zeeman splitting of the bands leads to an onset of electrical currents of majority- and minority-spin species at distinct bias voltages. This phenomenon combines with a subtle enhancement of the conductance in a given spin channel, which is determined by a resonance condition that sensitively depends on the orbital symmetry of the superconducting order parameter. In this context, it will be shown that zero-energy surface states play a crucial role. We now proceed to present our results in detail.

II. THEORY

When an in-plane magnetic field is applied to a thin-film superconductor, there is an upper critical field associated with a first-order phase transition from the superconducting to paramagnetic state. The upper critical field may be determined by considering the argument in Ref. 20 and essentially

consists of balancing the free energies in the paramagnetic and superconducting states. Extending this argument to anisotropic superconductors, we find that the critical value for the exchange splitting h in the superconductor reads

$$h_c = \Delta_0 \sqrt{\langle |g_{\mathbf{k}}|^2 \rangle / 2}, \quad \Delta_{\mathbf{k}} = \Delta_0 g_{\mathbf{k}}. \tag{1}$$

Here, $\Delta_{\mathbf{k}}$ is the gap function with its magnitude Δ_0 and $\langle \cdots \rangle$ denotes angular average over the Fermi surface. We have $g_{\mathbf{k}}=1$ for s-wave superconductors, $g_{\mathbf{k}}=e^{i\theta}$ for chiral p-wave superconductors, and $g_{\mathbf{k}}=\cos\theta$ for p_x-wave superconductors, where θ is the azimuthal angle. Considering $T=0$, a self-consistent solution of the order parameter reveals that the value of the gap is constant up to $h=h_c$, at which a first-order phase transition occurs. Therefore, we fix $h/\Delta_0=0.3$ which satisfies $h<h_c$ for all symmetries considered. An important point in the context of p-wave superconductors is that the applied field $\mathbf{B}$ must be parallel to the $\mathbf{d}_{\mathbf{k}}$ vector to probe the Pauli limiting effect. In the present paper, both $\mathbf{B}$ and $\mathbf{d}_{\mathbf{k}}$ are assumed to lie in the plane of the thin-film superconductor. Note that the Zeeman-splitting of unconventional superconductors has been accomplished experimentally; see, e.g., Ref. 21 for the d-wave case.

To illustrate the physics in a simple manner, we employ a two-dimensional calculation in the clean limit using the framework developed in Ref. 22. Our calculations are done in the zero-temperature limit, $T\to 0$. We consider positive excitation energies of the incoming electrons from the normal side, which places the restriction that $h<\Delta_{\mathbf{k}}$ in the superconductor. For the s-wave and chiral p-wave symmetries, this translates to $h<\Delta_0$ which is satisfied for our choice $h/\Delta_0=0.3$. For the p_x-wave symmetry, we must have $h<\Delta\cos\theta$. Physically, the contribution to the current will be strongest for normal incidence of the quasiparticles with respect to the tunneling barrier, such that we may, to a good approximation, introduce an upper cutoff θ_c in the angular integration of the current. For $\theta_c \simeq 75°$, $h/\Delta_{\mathbf{k}}<0.3$ is satisfied for all angles of incidence in the p_x-wave case. For the s-wave and chiral p-wave case, we use $\theta_c=\pi/2$.

In this approach, the expression for the spin resolved tunneling current may be written as

$$I_\alpha(eV) = I_0 \int_{-\theta_c}^{\theta_c} \int_{-\infty}^{\infty} d\theta d\varepsilon \cos\theta [f(\varepsilon - eV) - f(\varepsilon)] \times [1 + |r_A^\alpha(\varepsilon,\theta)|^2 - |r_N^\alpha(\varepsilon,\theta)|^2], \tag{2}$$

with $\alpha=\uparrow,\downarrow$. The scattering coefficients $\{r_A, r_N\}$ may be obtained by exploiting the boundary conditions of the quasiparticle wave functions at the normal-metal/superconductor (N/S) interface. In line with Ref. 23, one finds that

$$r_a^\alpha = \frac{4u_-^\alpha v_+^\alpha e^{-i\gamma_+}}{u_+^\alpha u_-^\alpha (4 - Z_\theta^2) + Z_\theta^2 v_+^\alpha v_-^\alpha e^{i(\gamma_- - \gamma_+)}},$$

$$r_n^\alpha = -1 + \frac{2[u_+^\alpha u_-^\alpha (2 + Z_\theta) - Z_\theta v_+^\alpha v_-^\alpha e^{i(\gamma_- - \gamma_+)}]}{u_+^\alpha u_-^\alpha (4 - Z_\theta^2) + Z_\theta^2 v_+^\alpha v_-^\alpha e^{i(\gamma_- - \gamma_+)}}, \tag{3}$$

with the definition $Z_\theta = Z_0/(i\cos\theta)$, where $Z_0 = 2mV_0/k_F$ is a measure of the strength of the scattering potential at the interface. We have introduced the coherence factors $u_\pm^\alpha = u^\alpha(\varepsilon,\theta_\pm)$ and $v_\pm = v^\alpha(\varepsilon,\theta_\pm)$ with $\theta_+=\theta$, $\theta_-=\pi-\theta$, and

$$[u^\alpha(\varepsilon,\theta_\pm)]^2 = \left[\frac{1}{2} + \frac{\sqrt{(\varepsilon+\alpha h)^2 - |\Delta(\varepsilon,\theta_\pm)|^2}}{2(\varepsilon+\alpha h)}\right]^{1/2}, \tag{4}$$

with $[v^\alpha(\varepsilon,\theta_\pm)]^2 = 1 - [u^\alpha(\varepsilon,\theta_\pm)]^2$. The phase of the superconducting gap is contained in the factor

$$e^{i\gamma_\pm} = e^{i\gamma(\theta_\pm)} = \Delta(\varepsilon,\theta_\pm)/|\Delta(\varepsilon,\theta_\pm)|. \tag{5}$$

Also, we have made use of the quasiclassical approximation $\varepsilon_F \gg (\varepsilon,\Delta)$ such that the wave vector $k_\theta = k_F\cos\theta$ is the same on the normal and superconducting side. Moreover, the spin polarization of the current is given by

$$P = (I_\uparrow - I_\downarrow)/(I_\uparrow + I_\downarrow). \tag{6}$$

In what follows, we will compare an intermediate transparency barrier to a low transparency barrier, as these two cases are the most realistic scenarios experimentally. Note that for all symmetry states considered here, the spin part of the Cooper pair wave function has $S_z=0$. As we shall see, the spin polarization is nevertheless strongly affected by the differing orbital symmetries of the superconducting states.

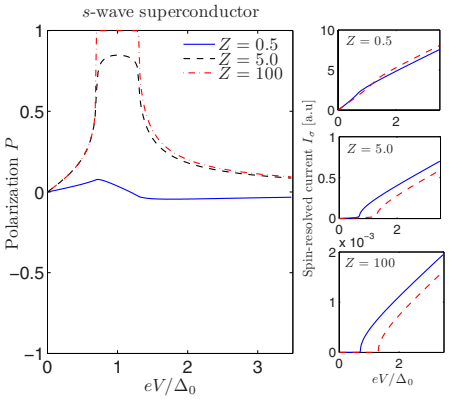

FIG. 1. (Color online) Plot of the spin polarization of the tunneling current for an s-wave symmetry. In the right panels, the full-drawn (dashed) line corresponds to majority (minority) spin.

III. RESULTS

We begin by commenting briefly on the s-wave symmetry, which was recently treated in Ref. 14 (see Fig. 1). By increasing the barrier strength Z, a fully spin-polarized current is generated in the regime $|eV-\Delta_0| \leq h$. This may be understood by the fact that the spin-$\uparrow$ and spin-$\downarrow$ currents begin to flow at different voltages, as experimentally verified in Ref. 19. Next, we consider a chiral p-wave symmetry in Fig. 2, believed to be realized in Sr_2RuO_4.[15] For an intermediate barrier transparency ($Z=0.5$), the polarization is similar to the s-wave case. Increasing the barrier strength to $Z=5.0$ and $Z=50$, however, the polarization actually becomes dominated by the minority-spin carriers. Before explaining the physics behind this unusual behavior, we consider the

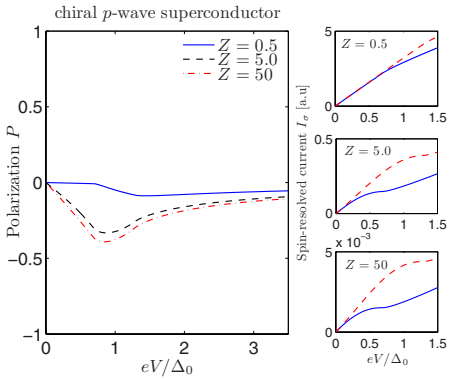

FIG. 2. (Color online) Plot of the spin polarization of the tunneling current for a chiral p-wave symmetry. In the right panels, the full-drawn (dashed) line corresponds to majority (minority) spin.

p_x-wave symmetry below. The result is shown in Fig. 3, in which case there is a formation of zero-energy Andreev bound states near the interface.[23,24] Such a pairing symmetry might be realized in the heavy fermion compound UGe_2.[18] Zero-energy states are also allowed to form in the chiral p-wave case, but only for angles of incidence θ=0. In the p_x-wave case, the effect of zero-energy states may therefore be expected to be much more pronounced since all quasiparticle trajectories contribute to the formation of these surface states. Comparing Figs. 2 and 3, one may immediately infer that this is so. Qualitatively, they are very similar, but the polarization is in general stronger in the p_x-wave case for a given value of Z. The most striking aspect of the polarization for both the chiral p-wave and p_x-wave symmetries is that it is exclusively negative, which means that the minority-spin carriers dominate the transport for positive voltage. In fact, the tendency of the polarization with increasing barrier strength is *opposite* to the s-wave case: a fully spin-polarized current consisting of minority-spin carriers is obtained in the

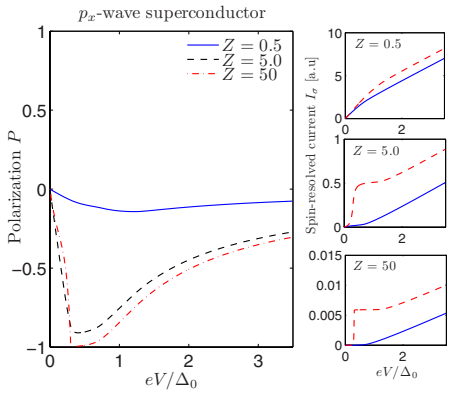

FIG. 3. (Color online) Plot of the spin-polarization of the tunneling current for a p_x-wave symmetry. In the right panels, the full-drawn (dashed) line corresponds to majority (minority) spin.

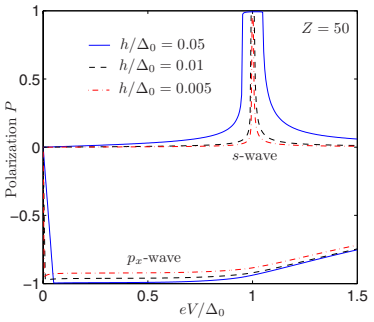

FIG. 4. (Color online) Comparing the s-wave and the p_x-wave symmetries for different exchange fields at Z=50.

tunneling limit. It is quite remarkable that the polarization actually favors the minority-spin carriers even though the majority-spin carriers benefit energetically from the presence of the exchange field. In order to understand this interesting behavior, recall that in the absence of a magnetic field there will be an immediate onset of electrical current at zero bias due to the formation of zero-energy states at the interface.[23,24] In the present case, the exchange field will split the spin bands such that the onset of the minority-spin current occurs at $eV=h$ instead of eV=0. The majority-spin current, on the other hand, will experience the sharp onset of current flow at $eV=-h$. Therefore, if the symmetry of the superconducting order parameter is such that it may accommodate zero-energy surface states, the tendency of the polarization will be toward being *negative* for positive voltages. Note that the polarization goes to zero at eV=0 for all symmetry states considered here. The same tendency was seen for the chiral p-wave case in Fig. 2.

Tuning the strength of the applied magnetic field permits full control over the induced exchange energy h. For very weak exchange energies $h/\Delta_0 \ll 1$, a major advantage of using superconductors with zero-energy states to obtain strongly polarized currents becomes evident. In Fig. 4, we compare the s-wave and p_x-wave symmetries against each other for Z=50. As seen, the width of the region of full spin-polarization in the s-wave case is $2h$, which becomes very narrow for decreasing h. In stark contrast, the current remains almost fully spin-polarized in the p_x-wave case over virtually the entire subgap energy regime. Also note that for $h/\Delta_0 \ll 1$, the effective angular integration range includes the entire half-circle $\theta \in [\pi/2, -\pi/2]$ even for the p_x-wave symmetry.

IV. DISCUSSION

Let us now discuss some aspects of our model. When the magnetic field splits the spin bands in a spin-singlet superconductor, the Cooper pair gains a finite center-of-mass momentum $q=2h/v_F$. This leads to the possibility of a spatially modulated superconducting order, known as the Fulde-Ferrel-Larkin-Ovchinnikov (FFLO) phase;[25] however this phase has not been unambiguously observed to date.[26]

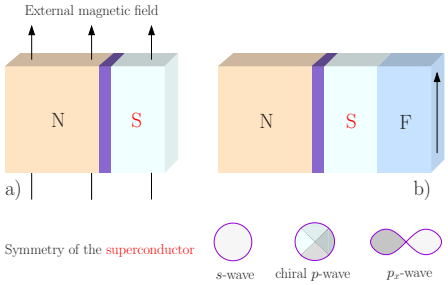

FIG. 5. (Color online) The experimental setup proposed in this paper. In (a), an in-plane magnetic field is applied to the junction. In (b), an exchange field is induced by a ferromagnetic film in close proximity. We will consider three different symmetries of the superconducting state, as shown above. In the chiral p-wave case, the gap has an intrinsic complex angular dependence and a constant magnitude. The system we consider is similar to that of Ref. 14.

Tanaka *et al.*[27] recently studied the tunneling conductance for the FFLO state. Here, we are considering homogeneous coexistence of the magnetic and superconducting orders which occur as long as one stays well below the Clogston limit[20] ($h/\Delta_0 < 1/\sqrt{2}$ for s-wave superconductors). It is also important to emphasize that we here consider electrical transport parallel to the film of the superconductor, which places restrictions on the resistances of the interfaces of our setup in Fig. 5. Specifically, the bias electrode should be connected to the edge of the superconducting film as opposed to the normal situation where the electrode is attached on top of the film. We not only underline that we have focused mainly on the *tunneling limit* ($Z \gg 1$), which is experimentally most feasible, but also contrasted this regime with a higher barrier transparency $Z=0.5$. The splitting of the zero-energy peak originating with the surface states in the p-wave case is less pronounced for low values of Z and thus yields a quantitatively reduced polarization compared to $Z \gg 1$, although the qualitative tendency is the same.

Although we have focused on the zero-temperature limit in this work, our results should not be affected by any finite temperature effects as long as T is not too close to T_c, i.e., $T/T_c \simeq 1$. As shown in Fig. 4 of Ref. 14, the finite temperature merely amounts to a smearing of the polarization curves for $T/T_c \ll 1$, while a reduction of the polarization properties is observed when T becomes similar to T_c in magnitude. Note that the existence of zero-energy surface states at the interface of a normal metal and unconventional superconductor does not depend on the temperature as long as $T < T_c$, such that the mechanism here proposed for generation of a strongly spin-polarized current should be a robust feature also at finite temperatures.

V. SUMMARY

In summary, we have investigated the tunneling current in a thin-film normal/superconductor junction in the presence of an external in-plane magnetic field. We have considered an s-wave, chiral p-wave, and p_x-wave symmetries for the superconductor. Remarkably, we find that even though the spin structure of the superconducting state is similar in all three cases ($S_z=0$, opposite-spin pairing), the spin polarization of the tunneling current is strongly modified by the orbital symmetry of the superconducting state. We find that the spin polarization may be substantial for tunneling barriers and that there is an unusual interplay between zero-energy states and the magnetic field that may result in a fully spin-polarized current for minority-spin carriers. We have studied the generation and manipulation of a strongly (and even possibly *fully*) spin-polarized current by applying of a weak static in-plane magnetic field to an N/S junction and then varying a bias voltage. Clearly, the main challenge in spintronics today is obtaining a clear-cut experimental technique of measuring the spin polarization of an electrical current. Our findings suggest an alternative approach to obtain fully spin-polarized currents which does not rely on strong magnetic fields or half-metallic compounds. We have pointed to two compounds, namely, Sr_2RuO_4 and UGe_2, as promising spin-triplet superconducting materials where these phenomenon should be particularly pronounced.

ACKNOWLEDGMENTS

J.L. and A.S. were supported by the Research Council of Norway, Grants No. 158518/431 and No. 158547/431 (NANOMAT) and Grant No. 167498/V30 (STORFORSK). T.Y. acknowledges support by JSPS.

[1] *Semiconductor Spintronics and Quantum Computation*, edited by D. D. Awschalom, D. Loss, and N. Samarth (Springer, Berlin, 2002).
[2] *Spin Dependent Transport in Magnetic Nanostructures*, edited by S. Maekawa and T. Shinjo (Taylor & Francis, London, 2002).
[3] I. Zutic, J. Fabian, and S. Das Sarma, Rev. Mod. Phys. **76**, 323 (2004).
[4] Y. Tserkovnyak, A. Brataas, G. E. W. Bauer, and B. I. Halperin, Rev. Mod. Phys. **77**, 1375 (2005).
[5] J. Martinek, J. Barnas, S. Maekawa, H. Schoeller, and G. Schon, Phys. Rev. B **66**, 014402 (2002).
[6] Y. K. Kato, R. C. Myers, A. C. Gossard, and D. D. Awschalom, Science **306**, 1910 (2004).
[7] J. Wunderlich, B. Kaestner, J. Sinova, and T. Jungwirth, Phys. Rev. Lett. **94**, 047204 (2005).
[8] Q. F. Sun, H. Guo, and J. Wang, Phys. Rev. B **69**, 054409 (2004).
[9] A. Brataas and Y. Tserkovnyak, Phys. Rev. Lett. **93**, 087201 (2004).
[10] I. Eremin, F. S. Nogueira, and R.-J. Tarento, Phys. Rev. B **73**, 054507 (2006).
[11] M. S. Grønsleth, J. Linder, J. M. Borven, and A. Sudbo, Phys.

Rev. Lett. **97**, 147002 (2006).
[12] T. Champel, T. Löfwander, and M. Eschrig, Phys. Rev. Lett. **100**, 077003 (2008).
[13] D. Huertas-Hernando, Yu. V. Nazarov, and W. Belzig, Phys. Rev. Lett. **88**, 047003 (2002).
[14] F. Giazotto and F. Taddei, Phys. Rev. B **77**, 132501 (2008).
[15] A. P. Mackenzie and Y. Maeno, Rev. Mod. Phys. **75**, 657 (2003).
[16] H. Tou, Y. Kitaoka, K. Ishida, K. Asayama, N. Kimura, Y. Onuki, E. Yamamoto, Y. Haga, and K. Maezawa, Phys. Rev. Lett. **80**, 3129 (1998).
[17] I. J. Lee, S. E. Brown, W. G. Clark, M. J. Strouse, M. J. Naughton, W. Kang, and P. M. Chaikin, Phys. Rev. Lett. **88**, 017004 (2001).
[18] A. Harada, S. Kawasaki, H. Mukuda, Y. Kitaoka, Y. Haga, E. Yamamoto, Y. Onuki, K. M. Itoh, E. E. Haller, and H. Harima, Phys. Rev. B **75**, 140502(R) (2007).
[19] R. Meservey and P. M. Tedrow, Phys. Rep. **238**, 173 (1994).
[20] A. M. Clogston, Phys. Rev. Lett. **9**, 266 (1962); B. S. Chandrasekhar, Appl. Phys. Lett. **1**, 7 (1962).
[21] M. Covington, M. Aprili, E. Paraoanu, L. H. Greene, F. Xu, J. Zhu, and C. A. Mirkin, Phys. Rev. Lett. **79**, 277 (1997).
[22] G. E. Blonder, M. Tinkham, and T. M. Klapwijk, Phys. Rev. B **25**, 4515 (1982).
[23] Y. Tanaka and S. Kashiwaya, Phys. Rev. Lett. **74**, 3451 (1995).
[24] C.-R. Hu, Phys. Rev. Lett. **72**, 1526 (1994).
[25] P. Fulde and R. A. Ferrell, Phys. Rev. **135**, A550 (1965); A. I. Larkin and Yu. N. Ovchinnikov, Sov. Phys. JETP **20**, 762 (1964).
[26] Y. Matsuda and H. Shimahara, J. Phys. Soc. Jpn. **76**, 051005 (2007).
[27] Y. Tanaka, Y. Asano, M. Ichioka, and S. Kashiwaya, Phys. Rev. Lett. **98**, 077001 (2007).

Paper XVII

Density of states near a vortex core in ferromagnetic superconductors: Application to STM measurements.

Physical Review B **78**, 064520 (2008).

Density of states near a vortex core in ferromagnetic superconductors: Application to STM measurements

Jacob Linder,[1] Takehito Yokoyama,[2] and Asle Sudbø[1]
[1]*Department of Physics, Norwegian University of Science and Technology, N-7491 Trondheim, Norway*
[2]*Department of Applied Physics, Nagoya University, Nagoya 464-8603, Japan*
(Received 3 June 2008; revised manuscript received 5 August 2008; published 28 August 2008)

We investigate numerically the local density of states (LDOS) in the vicinity of a vortex core in a ferromagnetic superconductor. Specifically, we investigate how the LDOS is affected by the relative weight of the spin bands in terms of the superconducting pairing and we also examine the effect of different pairing symmetries for the superconducting order parameter. Our findings are directly related to scanning tunneling microscopy measurements and may thus be highly useful to clarify details of the superconducting pairing in recently discovered ferromagnetic superconductors.

DOI: 10.1103/PhysRevB.78.064520 PACS number(s): 74.25.Ha, 74.25.Op, 74.25.Qt, 74.25.Jb

I. INTRODUCTION

Recently, UCoGe was added to the distinguished list of materials (already featuring UGe_2 and URhGe) that appear to display coexistence between ferromagnetism and superconductivity.[1–3] While ferromagnetism and conventional superconductivity may be shown to be antagonistic in terms of a bulk coexistent state,[4] several studies have pointed out the possibility of a nonunitary, spin-triplet superconducting state coexisting with itinerant ferromagnetism.[5–10] The synthesis of two important phenomena in condensed-matter physics, i.e., ferromagnetism and superconductivity, is not only interesting from the point of view of basic research but has also spawned hope of potential applications in low-temperature nanotechnology.

A number of questions arise concerning the nature of the coexistence of ferromagnetic and superconducting order. In particular, it is crucial to address (i) whether the two long-range orders are phase separated or not, (ii) whether the microscopic coexistence is spatially homogeneous or not, and (iii) what the symmetry of the superconducting order parameter is. Concerning the first question, the answer clearly appears to be "yes" since the onset of superconductivity appears inside the ferromagnetic part of the phase diagram.[6] The second question is, however, still open. Some authors have studied spatially uniform coexistence of ferromagnetic and superconducting order[7–11] while others have pointed out the intriguing possibility of a spontaneously formed vortex lattice state[12–14] due to the internal field. It has been argued[15] that a key factor with regard to whether such a spontaneous vortex phase appears or not is the magnitude of the internal magnetization $\mathbf{M}$. Finally, although the issue of pairing symmetry raised in the third question has not been established conclusively, the most likely option appears to be a nonunitary, spin-triplet superconducting state where the spin of the Cooper pair couples to the bulk magnetization through a third order term $\sim i(\mathbf{d}_{\mathbf{k}} \times \mathbf{d}_{\mathbf{k}}^*) \cdot \mathbf{M}$ in the Ginzburg-Landau free energy. Several studies[16–20] have addressed the means by which one may identify the pairing symmetry of the superconducting order parameter in a ferromagnetic superconductor (FMSC) mainly focusing on transport properties.

Clearly, it would be highly desirable to clarify experimental signatures of a possible spontaneous vortex lattice phase realized in a ferromagnetic superconductor. In this work, we present numerical results for the local density of states (LDOS) in the vicinity of a vortex core of a ferromagnetic superconductor. Our approach is based on the quasiclassical theory of superconductivity, and takes into account several crucial factors such as the depletion of the order parameter near the vortex core in addition to self-consistently obtained magnetic and superconducting order parameters. Our results are directly relevant to scanning tunneling microscopy (STM) measurements,[21] and may be useful to clarify signatures of the existence of a spontaneously formed vortex lattice and also the pairing symmetry of the superconducting order parameter.

This paper is organized as follows. In Sec. II, we establish the theoretical framework employed in this work. Namely, we use the quasiclassical approximation and solve the Eilenberger equation in the vicinity of the vortex core with appropriate boundary conditions. In Sec. III, we present our results for the spatial and energy dependences of the local density of states near the vortex core. Specifically, we investigate how the relative weight of the spin bands in terms of the superconducting pairing and different pairing symmetries for the superconducting order-parameter affect the density of states. In Secs. IV and V, we discuss and summarize the main results of the paper. We will use boldface notation for two vectors: $\hat{\ldots}$ for 4×4 matrices and $\underline{\ldots}$ for 2×2 matrices.

II. THEORETICAL FRAMEWORK

It is generally believed that the pairing symmetry in ferromagnetic superconductors may be classified as a nonunitary, spin-triplet state.[5,7,8] Our starting point is the quasiclassical Eilenberger equation[22] for such a system, which, in the clean limit, reads (see Appendix A for details)

$$i\mathbf{v}_F \cdot \nabla \hat{g}^R + [\varepsilon \hat{\rho}_3 + \hat{M} + \hat{\Delta}(\mathbf{p}_F), \hat{g}^R] = 0, \tag{1}$$

where ε is the quasiparticle energy measured from the Fermi level, $\mathbf{v}_F$ is the Fermi velocity, and $[\ldots]$ is a commutator. The exchange field h and the superconducting order parameters Δ_σ are contained in terms of $\hat{M}=h\ \mathrm{diag}(\underline{\tau_3}, \underline{\tau_3})$ in addition to

$$\hat{\Delta}(\mathbf{p}_F) = \begin{bmatrix} \underline{0} & \underline{\Delta}(\mathbf{p}_F) \\ -\underline{\Delta}^*(\mathbf{p}_F) & \underline{0} \end{bmatrix},$$

$$\underline{\Delta}(\mathbf{p}_F) = \begin{bmatrix} \Delta_\uparrow(\mathbf{p}_F) & 0 \\ 0 & \Delta_\downarrow(\mathbf{p}_F) \end{bmatrix}. \quad (2)$$

The matrices $\hat{\rho}_i$ and $\underline{\tau_i}$ are defined in Appendix A. The retarded part of the Green function, $\hat{g}^R$, will have the structure

$$\hat{g}^R = \begin{bmatrix} \underline{g}(\mathbf{r},\mathbf{p}_F,\varepsilon) & \underline{f}(\mathbf{r},\mathbf{p}_F,\varepsilon) \\ -\underline{f}^*(\mathbf{r},-\mathbf{p}_F,-\varepsilon) & -\underline{g}^*(\mathbf{r},-\mathbf{p}_F,-\varepsilon) \end{bmatrix},$$

and must satisfy the normalization condition $(\hat{g}^R)^2 = \hat{1}$. Due to the internal-symmetry relations between the components of $\hat{g}^R$, one may parametrize it very conveniently by means of a so-called Ricatti parametrization.[23,24] In the absence of interband scattering, the Eilenberger equation decouples into two 2×2 equations as follows:

$$i\mathbf{v}_F \cdot \nabla \underline{g_\sigma} + [\varepsilon \underline{\tau_3} + \sigma h \underline{\tau_0} + \underline{\Delta_\sigma}(\mathbf{p}_F), \underline{g_\sigma}] = 0, \quad (3)$$

where we have introduced

$$\underline{g_\sigma} = N_\sigma \begin{pmatrix} 1 - a_\sigma b_\sigma & 2a_\sigma \\ 2b_\sigma & -1 + a_\sigma b_\sigma \end{pmatrix}, \quad N_\sigma = (1 + a_\sigma b_\sigma)^{-1},$$

$$\underline{\Delta_\sigma}(\mathbf{p}_F) = \begin{bmatrix} 0 & \Delta_\sigma(\mathbf{p}_F) \\ -\Delta_\sigma^*(\mathbf{p}_F) & 0 \end{bmatrix}. \quad (4)$$

Note that the gap matrix in Eq. (4) is a 2×2 matrix in particle-hole space while the gap matrix in Eq. (2) is a 2×2 matrix in spin space. From Eq. (3), one obtains two decoupled differential equations for a_σ and b_σ:

$$i\mathbf{v}_F \cdot \nabla a_\sigma + 2a_\sigma \varepsilon - a_\sigma^2 \Delta_\sigma^*(\mathbf{p}_F) - \Delta_\sigma(\mathbf{p}_F) = 0,$$

$$i\mathbf{v}_F \cdot \nabla b_\sigma - 2b_\sigma \varepsilon - b_\sigma^2 \Delta_\sigma(\mathbf{p}_F) - \Delta_\sigma^*(\mathbf{p}_F) = 0. \quad (5)$$

Note that the above equations do not have any *explicit* dependence on the exchange splitting h. As we shall see later, the exchange splitting does however enter implicitly through the spin-dependent gaps Δ_σ. Note that the magnetic vector potential $\mathbf{A}$ may be incorporated above simply by a shift in the quasiparticle energies: $\varepsilon \to \varepsilon + e\mathbf{v}_F \cdot \mathbf{A}$. In a gauge that renders the superconducting gaps to be real, one finds that $e\mathbf{A} \to e\mathbf{A} - \nabla\Phi/2$, where Φ is the superconducting phase associated with the broken U(1) symmetry. Therefore, the total Doppler shift in the quasiparticle energies is $\varepsilon \to \varepsilon - em\mathbf{v}_F \cdot \mathbf{v}_s$, where the gauge-invariant superfluid velocity is $\mathbf{v}_s = (\nabla\Phi - 2e\mathbf{A})/(2m)$. Below, we keep the distribution of the superconducting phase in the order parameter and consider the case with Ginzburg-Landau parameter $\kappa \gg 1$, for which the magnetic vector potential $\mathbf{A}$ may be neglected. This follows since we are considering only one single vortex, i.e., the zero-field limit, such that only gauge-field fluctuations around zero could possibly be relevant. However, assuming that the superconductors are strongly type II with $\kappa \gg 1$, gauge-field fluctuations are suppressed.[25,26]

In order to solve the above Ricatti equations, we follow closely the procedure of Ref. 23. Let us consider the term with $\mathbf{v}_F \cdot \nabla$ in more detail. Assume that we have a cylindrically symmetric vortex situated at $r_a = r_b = 0$ with its axis along $\hat{\mathbf{c}}$. The position vector in this coordinate system then reads $\mathbf{r} = r_a\hat{\mathbf{a}} + r_b\hat{\mathbf{b}}$. Assuming that the transport of quasiparticles primarily takes place in the $\hat{\mathbf{a}}$-$\hat{\mathbf{b}}$ plane, we may define the Fermi velocity as

$$\mathbf{v}_F = v_F(\cos\theta\hat{\mathbf{a}} + \sin\theta\hat{\mathbf{b}}) \equiv v_F\hat{\mathbf{v}}, \quad (6)$$

and its orthogonal vector as $\hat{\mathbf{u}} = -\sin\theta\hat{\mathbf{a}} + \cos\theta\hat{\mathbf{b}}$. Thus, the position vector $\mathbf{r}$ may also be expressed as $\mathbf{r} = x\hat{\mathbf{v}} + y\hat{\mathbf{u}}$, where we have defined

$$x = r_a\cos\theta + r_b\sin\theta, \quad y = -r_a\sin\theta + r_b\cos\theta. \quad (7)$$

Using the coordinate system $\hat{\mathbf{v}}$-$\hat{\mathbf{u}}$, the Ricatti equations may be rewritten as

$$iv_F\partial_x a_\sigma + [2\varepsilon - \Delta_\sigma^* a_\sigma]a_\sigma - \Delta_\sigma = 0,$$

$$iv_F\partial_x b_\sigma - [2\varepsilon + \Delta_\sigma b_\sigma]b_\sigma - \Delta_\sigma^* = 0, \quad (8)$$

where $a_\sigma = a_\sigma(x,y)$ and $\Delta_\sigma = \Delta_\sigma(x,y)$. The above equations may be solved by imposing boundary conditions for $\{a_\sigma, b_\sigma\}$ in the bulk of the superconductor. The Ricatti equations with $\varepsilon > 0$ for a_σ and b_σ are stable for integration from $x \to (-\infty)$ and $x \to \infty$, respectively (opposite for $\varepsilon < 0$).[23] The boundary conditions then read as

$$a_\sigma[x \to (-\infty)] = (\varepsilon - \sqrt{\varepsilon^2 - |\Delta_\sigma|^2})/\Delta_\sigma^*,$$

$$b_\sigma(x \to \infty) = -(\varepsilon - \sqrt{\varepsilon^2 - |\Delta_\sigma|^2})/\Delta_\sigma. \quad (9)$$

The superconducting order parameter Δ_σ is now modeled in the presence of a vortex centered at $r_a = r_b = 0$. In general, the superconducting order parameter may be written as[27]

$$\Delta_\sigma(\mathbf{r},\theta,\varepsilon) = \Delta_{\sigma,0}\chi_\sigma(\theta,\varepsilon)F(r)e^{im\phi}, \quad (10)$$

assuming a vorticity m. Here, Δ_0 is the gap magnitude, $\chi(\theta,\varepsilon)$ is a symmetry factor for the gap (taking into account both anisotropicity and frequency dependence), $F(r)$ models the spatial depletion of the gap near the vortex core, and $\tan\phi = r_b/r_a$. We will here restrict our attention to an even frequency, p-wave symmetry, which is believed to be the most likely candidate for the order parameter in ferromagnetic superconductors. Assuming that the angular symmetry is the same for both the majority- and minority-spin gaps, and considering the usual case of $m = 1$, we explicitly have

$$\Delta_\sigma(\mathbf{r},\theta) = \Delta_{\sigma,0}\chi(\theta)\tanh\left(\frac{\sqrt{x^2+y^2}}{\xi}\right)\frac{x+iy}{\sqrt{x^2+y^2}}. \quad (11)$$

In what follows, we will compare the cases $\chi(\theta) = \cos\theta$ and $\chi(\theta) = e^{i\theta}$, and also investigate how the LDOS changes depending on the relative weight of the superconducting instability in both spin bands. The normalized LDOS for spin species σ is given by

$$N_\sigma(\mathbf{r},\varepsilon) = \int_0^{2\pi}\frac{d\theta}{2\pi}\mathrm{Re}[(1 - a_\sigma b_\sigma)/(1 + a_\sigma b_\sigma)], \quad (12)$$

and we introduce the total LDOS in the standard way as

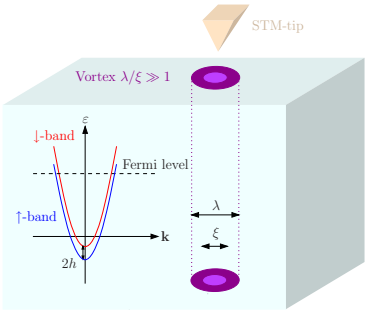

FIG. 1. (Color online) Schematic of the model.

$$N(\mathbf{r},\varepsilon) = \sum_{\sigma} N_{\sigma}(\mathbf{r},\varepsilon)/2. \tag{13}$$

To account for a finite quasiparticle lifetime τ, we let $\varepsilon \to \varepsilon + i\delta$, where $\delta \sim \tau^{-1}$. From now on, we fix $\delta = 0.1\Delta_{\uparrow,0}$ and comment further upon the role of inelastic scattering in Appendix B.

Even if the exchange field h is absent from the Eilenberger equation, the LDOS is not independent of the value of h. The reason for this is that the magnitude of the superconducting gaps depends on the strength of the exchange splitting. Following the approach of Refs. 8 and 9, we derive from a weak-coupling mean-field theory that the self-consistent solution of bulk superconducting gaps in the $T \to 0$ limit may be written as

$$\Delta_{\sigma,0}/\omega_0 = c\ \exp[-1/(g\sqrt{1+\sigma h/\mu})], \tag{14}$$

where the prefactor is equal to $c \simeq 2.43$ for a p_x-wave symmetry $[\chi(\theta) = \cos\theta]$ and $c = 2.00$ for a chiral p-wave symmetry $[\chi(\theta) = e^{i\theta}]$.[8,9] Here, $g = V_0 N_0$ is the weak-coupling constant, which we set to $g = 0.2$, and ω_0 is the typical frequency width around Fermi level for the bosons responsible for the superconducting pairing. Above, V_0 is the strength of the pairing interaction, N_0 is the LDOS at Fermi level in the normal state, and μ denotes the Fermi energy. The reader

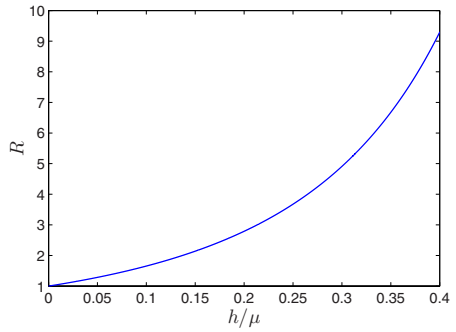

FIG. 2. (Color online) The ratio R between the majority- and minority-spin gaps as a function of h/μ as obtained from a self-consistent, mean-field solution [Eq. (15)].

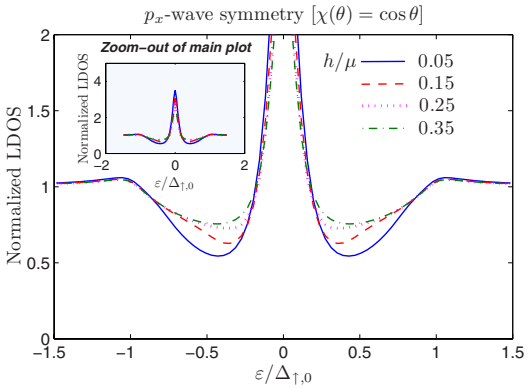

FIG. 3. (Color online) Normalized LDOS in the vortex core for a p_x-wave symmetry $[\chi(\theta) = \cos\theta]$ using several values of h/μ.

may consult Appendix C for a derivation of Eq. (14). We find that the ratio between the majority- and minority-spin gaps may be written as

$$\frac{\Delta_{\uparrow,0}}{\Delta_{\downarrow,0}} \equiv R(h/\mu) = \exp\left[\frac{\sqrt{1+h/\mu} - \sqrt{1-h/\mu}}{g\sqrt{1-(h/\mu)^2}}\right], \tag{15}$$

when assuming that $h/\mu \in [0,1)$ (shown in Fig. 1). In UGe_2, the energy splitting between the majority- and minority-spin bands was estimated[2] to lay around 70 meV, which yields $R \simeq 1.42$ when assuming $\mu = 1$ eV.

III. RESULTS

We begin by plotting the energy-resolved LDOS in the vortex core ($r_a = r_b = 0$) for an order parameter that has line nodes in momentum space. Such an order parameter was recently proposed to be realized in UGe_2 by Harada *et al.*[6] and it was argued that the superconducting pairing only took place in the majority-spin band. To investigate how the rela-

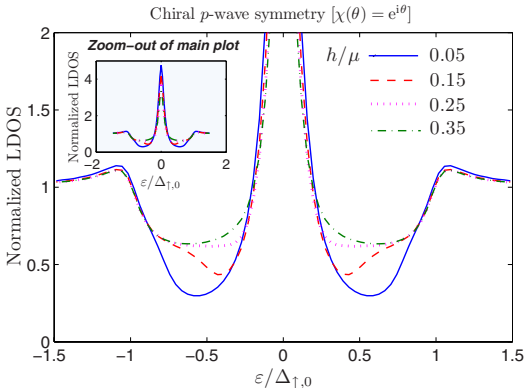

FIG. 4. (Color online) Normalized LDOS in the vortex core for a chiral p-wave symmetry $[\chi(\theta) = e^{i\theta}]$ using several values of h/μ.

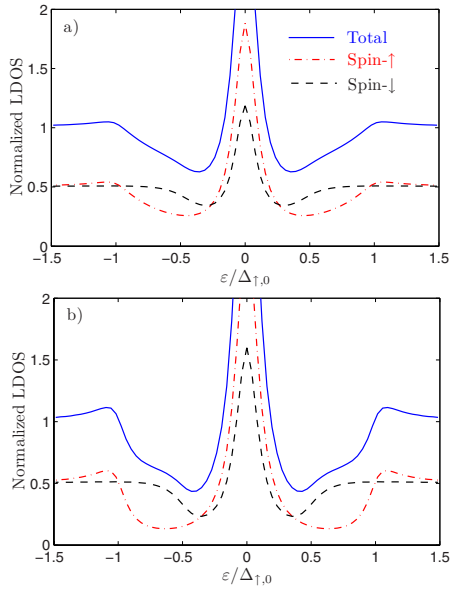

FIG. 5. (Color online) Total and spin-resolved LDOS in the vortex core for the (a) p_x-wave symmetry symmetry $[\chi(\theta)=\cos\theta]$ and the (b) chiral p-wave symmetry $[\chi(\theta)=e^{i\theta}]$. We have used $h/\mu=0.15$ here.

tive magnitudes of the majority- and minority-spin gaps (Fig. 2) affect the LDOS in the vortex core, we plot the LDOS for several values of the ratio h/μ in Fig. 3. As usual, the LDOS is strongly enhanced for subgap values due to the existence of bound states within the vortex core.[28] The presence of two gaps in the system should manifest itself in the form of nonmonotonous behavior in the subgap spectrum but it is not possible to discern such behavior unambiguously from Fig. 3. This effect may be masked by strong inelastic scattering, modeled here by the parameter δ, which effectively smears the LDOS. The effect of increasing the exchange field is seen to suppress the deviation from the normal-state LDOS. This may be understood by noting that the minority-spin gap is strongly reduced with increasing exchange field and that the corresponding increase in the majority-spin gap is not able to compensate for the suppressed regime of bound states within the core.

We next study the chiral p-wave symmetry analogous to the A2 phase in liquid ^{3}He and plot the energy-resolved LDOS for several values of h/μ in Fig. 4. Although the qualitative behavior is quite similar to Fig. 3, there are two important distinctions. First, one notices that the chiral symmetry appears to have a much more pronounced influence on the LDOS quantitatively, yielding a larger zero-energy peak and larger subgap dips. This is in fact *opposite* what one would have expected from tunneling conductance measurements of p_x-wave and chiral p-wave superconductors, respectively. For such measurements, the zero-energy peak becomes much larger in the p_x-wave case than in the chiral p-wave case. Second, the subgap features associated with the presence of two gaps were enhanced in Fig. 4 as compared to Fig. 3. The nonmonotonous behavior for subgap energies is present for all curves in Fig. 4 but the features indicative of multiple gaps are most clearly seen for $h/\mu=0.15$, manifested through an additional inflection point before the normal-state LDOS is recovered. These differences could be helpful in discriminating between different types of pairing symmetries in ferromagnetic superconductors.

In order to show more clearly the contribution from each spin band to the LDOS near the vortex core, consider Fig. 5 where we plot the total LDOS and the contribution from each spin band for (a) $\chi(\theta)=\cos\theta$ and (b) $\chi(\theta)=e^{i\theta}$. The rise of the LDOS following the gap edge $\Delta_{\sigma,0}$ of each spin band occurs at different energies due to the exchange splitting. This was revealed in the total LDOS as kinks located at two distinct energies, which offers the opportunity to obtain explicit information about the relative magnitude of the two gaps. The qualitative features are the same in Figs. 5(a) and 5(b) but they are quantitatively more pronounced in the chiral p-wave symmetry case. This may be due to the fact that the chiral p-wave gap has a constant magnitude ($|\chi(\theta)|=1$) while the p_x-wave gap varies in magnitude upon traversing

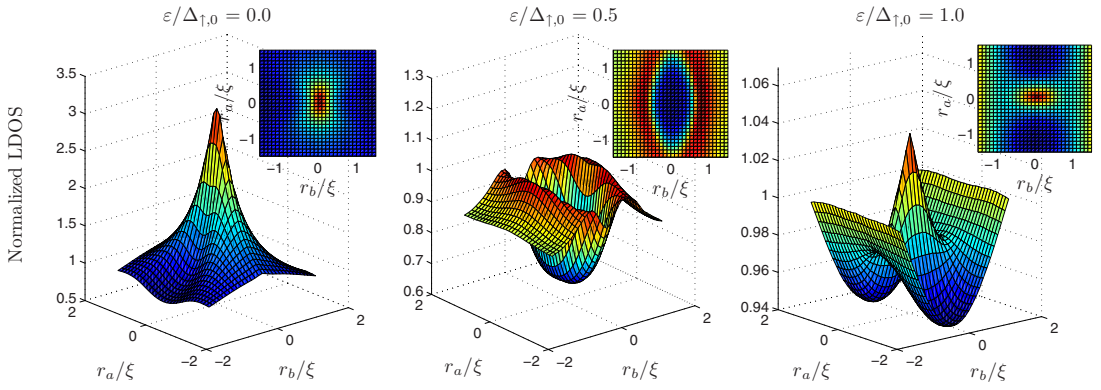

FIG. 6. (Color online) Normalized LDOS in the vicinity of the vortex core at three different quasiparticle energies, using $R=2$ with a p_x-wave symmetry $[\chi(\theta)=\cos\theta]$. A twofold symmetry is observed in agreement with the symmetry of the order parameter.

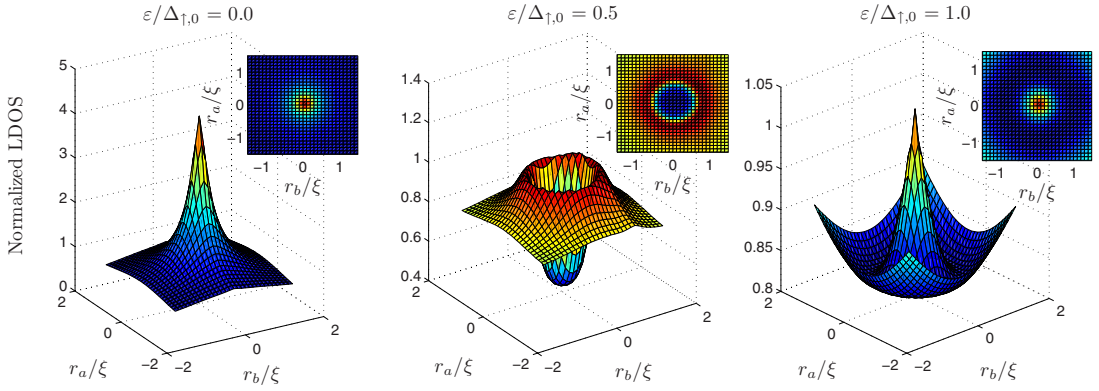

FIG. 7. (Color online) Normalized LDOS in the vicinity of the vortex core at three different quasiparticle energies, using $R=2$ with a chiral p-wave symmetry $[\chi(\theta)=e^{i\theta}]$. A circular symmetry is observed in agreement with the symmetry of the order parameter.

around the Fermi surface. Therefore, the LDOS is more strongly affected in the chiral p-wave case.

We now study the resolution of the LDOS in real space for a fixed energy in Fig. 6. We have chosen $R=2$, corresponding to $h/\mu \simeq 0.14$, and have also chosen the line node symmetry $\chi(\theta)=\cos\theta$. In all cases, the plots in Fig. 6 display a twofold spatial symmetry, in accordance with the superconducting order parameter.[23,29,30] The zero-energy peak present for $\varepsilon=0$ evolves into a dip structure at the vortex core upon increasing the quasiparticle energy. The deviation from the normal-state LDOS is still significant even at distances $\sim 2\xi$ away from the vortex core around $\varepsilon/\Delta_{\uparrow,0}=0.5$. The qualitative features are the same for the chiral p-wave symmetry in Fig. 7 although the symmetry is now circular due to the isotropy of the magnitude of the gap ($|\chi(\theta)|=1$).

IV. DISCUSSION

In our calculations, we have chosen a real gauge for both superconducting order parameters Δ_σ, where $\sigma=\uparrow,\downarrow$. If the two spin bands are completely independent, there is no phase locking between the order parameters, which fixes the relative phase $\Delta\nu=\nu_\uparrow-\nu_\downarrow$, where ν_σ is phase associated with the broken U(1) symmetry. The existence of two such phases would imply that a $U(1)\times U(1)$ symmetry is broken in a ferromagnetic superconductor and would in principle allow for two critical temperatures that may differ in magnitude. However, if the two spin bands do communicate by means of, e.g., spin-orbit coupling or impurity scattering, a term of the form $-\lambda\cos(\Delta\nu)$ will appear in the free energy describing the system. This corresponds to a phase locking scenario where the sign of λ determines whether $\Delta\nu=0$ or $\Delta\nu=\pi$ is the energetically preferred relative phase. Above, we have decoupled the two spin bands such that the relative phase of $\Delta_\uparrow$ and $\Delta_\downarrow$ is of no consequence. Taking into account scattering between the spin bands would require solving coupled Ricatti equations and investigating the effect of phase locking explicitly, which is beyond the scope of this paper.

In Fig. 5, we plotted the relative contribution from the two spin bands to the LDOS near the vortex core to clarify how the LDOS may give decisive clues about whether both spin bands partake in the superconducting pairing or not. In principle, it might be possible to probe explicitly the spin-resolved LDOS by using a strong ferromagnetic STM, and contrasting parallel and antiparallel relative configurations of the exchange fields in the FMSC and the ferromagnetic STM tip. The experimental realization of this particular proposal is nevertheless probably challenging.

V. SUMMARY

In summary, we have numerically studied the LDOS in the vicinity of a vortex core in a ferromagnetic superconductor. Specifically, we have investigated what influence the exchange field and the symmetry of the superconducting order parameter exhibit on both the spatially resolved and energy-resolved LDOS. The symmetry of the spatially resolved LDOS near the vortex core, as revealed by STM measurements, should give decisive clues about the orbital symmetry of the superconducting order parameter[23,29,30] while the energy-resolved LDOS could provide important information about the presence of multiple gaps in the system. Our results should be comparable to experimentally obtained data, both qualitatively and quantitatively, and may thus be helpful in clarifying the nature of the superconducting pairing in ferromagnetic superconductors.

ACKNOWLEDGMENTS

The authors acknowledge A. Nevidomskyy and I. B. Sperstad for useful discussions. J.L. and A.S. were supported by the Norwegian Research Council through Grants No. 158518/431, No. 158547/431, (NANOMAT), and No. 167498/V30 (STORFORSK). T.Y. acknowledges support by the JSPS.

APPENDIX A: MATRICES AND QUASICLASSICAL THEORY

The matrices used in this paper are defined as[31]

$$\underline{\tau}_1=\begin{pmatrix}0 & 1\\ 1 & 0\end{pmatrix},\quad \underline{\tau}_2=\begin{pmatrix}0 & -i\\ i & 0\end{pmatrix},\quad \underline{\tau}_3=\begin{pmatrix}1 & 0\\ 0 & -1\end{pmatrix},$$

$$\underline{1} = \begin{pmatrix} 1 & 0 \\ 0 & 1 \end{pmatrix}, \quad \hat{1} = \begin{pmatrix} \underline{1} & \underline{0} \\ \underline{0} & \underline{1} \end{pmatrix}, \quad \hat{\tau}_i = \begin{pmatrix} \underline{\tau_i} & \underline{0} \\ \underline{0} & \underline{\tau_i} \end{pmatrix},$$

$$\hat{\rho}_1 = \begin{pmatrix} \underline{0} & \underline{\tau_1} \\ \underline{\tau_1} & \underline{0} \end{pmatrix}, \quad \hat{\rho}_2 = \begin{pmatrix} \underline{0} & -i\underline{\tau_1} \\ i\underline{\tau_1} & \underline{0} \end{pmatrix}, \quad \hat{\rho}_3 = \begin{pmatrix} \underline{1} & \underline{0} \\ \underline{0} & -\underline{1} \end{pmatrix}. \tag{A1}$$

Let us briefly sketch the way to obtain the quasiclassical Eilenberger equations for a nonunitary, spin-triplet superconducting state coexisting with ferromagnetism. For further background information on the quasiclassical theory of superconductivity, the reader may consult, e.g., Refs. 32–36 for nice reviews. We follow here closely the notation of Ref. 31. Our starting point is the following Hamiltonian:

$$H = \sum_{\alpha\beta} \int d\mathbf{r} \psi_\alpha^\dagger(\mathbf{r},t) \left(-\frac{\nabla^2}{2m}\underline{1} - h\underline{\tau_3} \right)_{\alpha\beta} \psi_\beta(\mathbf{r},t)$$
$$- \sum_\sigma \int d\mathbf{r} d\mathbf{r}' [\Delta_\sigma(\mathbf{r},\mathbf{r}') \psi_\sigma^\dagger(\mathbf{r}) \psi_\sigma^\dagger(\mathbf{r})$$
$$+ \Delta_\sigma^*(\mathbf{r},\mathbf{r}') \psi_\sigma(\mathbf{r}') \psi_a(\mathbf{r})]. \tag{A2}$$

The Heisenberg equation of motion for the above Hamiltonian was obtained in the standard way:

$$\mathrm{i}\partial_t \hat{\rho}_3 \Psi(\mathbf{r},t) = \int d\mathbf{r}' \hat{H}(\mathbf{r},\mathbf{r}',t) \Psi(\mathbf{r},t),$$

$$\hat{H}(\mathbf{r},\mathbf{r}',t) = \hat{\xi}(\mathbf{r}) \delta(\mathbf{r}-\mathbf{r}') - \hat{\Delta}(\mathbf{r},\mathbf{r}'), \hat{\xi}(\mathbf{r}) = -\frac{\nabla_\mathbf{r}^2}{2m}\hat{1},$$

$$\hat{\Delta}(\mathbf{r},\mathbf{r}') = \begin{bmatrix} \underline{0} & \underline{\Delta}(\mathbf{r},\mathbf{r}') \\ \underline{\Delta}^*(\mathbf{r},\mathbf{r}') & \underline{0} \end{bmatrix},$$

$$\underline{\Delta}(\mathbf{r},\mathbf{r}') = \mathrm{diag}[\Delta_\uparrow(\mathbf{r},\mathbf{r}'), \quad \Delta_\downarrow(\mathbf{r},\mathbf{r}')]. \tag{A3}$$

For simplicity, we consider only the retarded component of the Green function G^R in what follows since the system is specified exclusively by G^R in an equilibrium situation. It is defined as

$$\underline{G}_{\alpha\beta}^\mathrm{R}(1,2) = -\mathrm{i}\Theta(t_1 - t_2) \langle [\psi_\alpha(1), \psi_\beta^\dagger(2)]_+ \rangle, \tag{A4}$$

where the notation [Eqs. (1) and (2)] refers to the spatial and time coordinates: $(1) \equiv (\mathbf{r}_1; t_1)$. We explicitly write the "+" sign as a subscript to denote an anticommutator; else it is implicitly understood that the notation $[\ldots]$ denotes a usual commutator. Similarly, the anomalous Green function is given by

$$\underline{F}_{\alpha\beta}^\mathrm{R}(1,2) = -\mathrm{i}\Theta(t_1 - t_2) \langle [\psi_\alpha(1), \psi_\beta(2)]_+ \rangle. \tag{A5}$$

One may construct 4×4 matrices in combined particle-hole and spin spaces, known as Nambu space, in the following manner:

$$\hat{G}^\mathrm{R}(1,2) = \begin{Bmatrix} \underline{G}^\mathrm{R}(1,2) & \underline{F}^\mathrm{R}(1,2) \\ [\underline{F}^\mathrm{R}(1,2)]^* & [\underline{G}^\mathrm{R}(1,2)]^* \end{Bmatrix}. \tag{A6}$$

Note that $G(1,2)$ is a generalized Gor'kov Green function, which contains information about processes occurring at length scales comparable to the Fermi wavelength. Such information is lost upon applying the quasiclassical approximation. Using the Heisenberg equation of motion Eq. (A3), we obtain

$$\left\{ i\partial_{t_1} [\hat{\rho}_3 \hat{G}^\mathrm{R}(1,2)]_{ij} - \int d\mathbf{r}' \sum_l [-\mathrm{i}\Theta(t_1 - t_2)] \hat{H}_{il}(\mathbf{r}_1, \mathbf{r}', t_1) \right.$$
$$\left. \times (\hat{\rho}_3)_{ll} \langle [\Psi_l(\mathbf{r}', t_1), \Psi_j^\dagger(\mathbf{r}_2, t_2)]_+ \rangle \right\} = \delta_{ij} \delta(1-2). \tag{A7}$$

To arrive at Eq. (1), it is convenient to introduce the mixed representation that shifts the frame of reference to a center-of-mass system. We define

$$\mathbf{R} = (\mathbf{r}_1 + \mathbf{r}_2)/2, \quad \mathbf{r} = \mathbf{r}_1 - \mathbf{r}_2,$$
$$T = (t_1 + t_2)/2, \quad t = t_1 - t_2, \tag{A8}$$

such that

$$\hat{G}^\mathrm{R}(1,2) = \hat{G}^\mathrm{R}\left(\mathbf{R} + \frac{\mathbf{r}}{2}, T + \frac{t}{2}, \mathbf{R} - \frac{\mathbf{r}}{2}, T - \frac{t}{2} \right). \tag{A9}$$

The Fourier transformation of Eq. (A9) yields

$$\hat{G}^\mathrm{R}(\mathbf{p},\mathbf{R};T,\varepsilon) = \int d\mathbf{r} \mathrm{e}^{-\mathrm{i}\mathbf{p}\mathbf{r}} \int dt \mathrm{e}^{\mathrm{i}t\varepsilon} \hat{G}^\mathrm{R}(1,2). \tag{A10}$$

An exact solution for $\hat{G}^\mathrm{R}(\mathbf{p},\mathbf{R};T,\varepsilon)$ is very hard to achieve but the situation is considerably simplified if one is willing to neglect all atomic-scale fine-structure effects that are included in $\hat{G}^\mathrm{R}$. These give rise to a rapidly oscillating part in the solution for $\hat{G}^\mathrm{R}$ and rewriting the Green function through Eq. (A10) allows us to integrate out this unnecessary information (at least for our purposes). This approximation may be expected to yield satisfactory results if the energy of the physical quantities involved in the problem, e.g., exchange field and superconducting order parameter, are much smaller than the Fermi energy. Assuming that only particles in the vicinity of Fermi level will take part in physical processes, one only needs to retain the direction of the momentum at Fermi level in the $\mathbf{p}$ coordinate.

As this Appendix is only meant as background information for the Eilenberger equation, we do not show all the details leading from Eq. (A7) to Eq. (1) here. The calculations are nevertheless fairly straightforward, and consist of first switching to a mixed representation, then Fourier transforming the variables, and finally performing the quasiclassical approximation

$$\hat{g}^\mathrm{R} = \frac{i}{\pi} \int d\xi_\mathbf{p} \hat{G}^\mathrm{R}, \quad \xi_\mathbf{p} = \frac{\mathbf{p}^2}{2m}. \tag{A11}$$

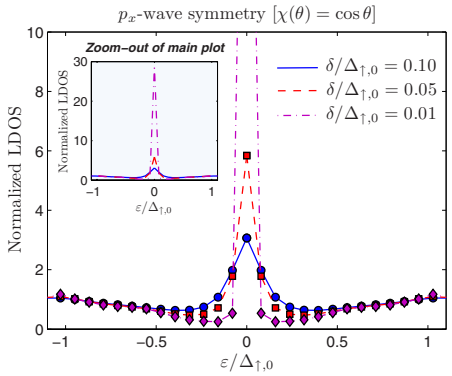

FIG. 8. (Color online) Normalized LDOS in the vicinity of the vortex core at three different values of the inelastic-scattering rate $\delta=\tau^{-1}$, using a p_x-wave symmetry with $h/\mu=0.15$.

APPENDIX B: INELASTIC SCATTERING

The choice of $\delta=0.1\Delta_{\uparrow,0}$ is motivated by the fact that the zero-energy peaks observed in experiments are usually limited from above to roughly a factor of five times the normal-state value of the LDOS, which we reproduce with this particular choice of δ. Choosing δ smaller (corresponding to a longer quasiparticle lifetime since $\delta=\tau^{-1}$) causes the zero-energy peak to grow substantially, as shown in Fig. 8. In general, the inelastic-scattering rate does not have to be proportional to the gap at all and our choice of $\delta=0.1\Delta_{\uparrow,0}$ is simply chosen to compare the scattering rate against a familiar quantity.

APPENDIX C: DERIVATION OF EQ. (14)

The gap equation may be obtained by starting out with a Hamiltonian assuming a nonunitary triplet pairing state coexisting with itinerant ferromagnetism,[7,18] namely

$$\hat{H}=\sum_{\mathbf{k}}\xi_{\mathbf{k}}+\frac{INM^2}{2}-\frac{1}{2}\sum_{\mathbf{k}\sigma}\Delta^{\dagger}_{\mathbf{k}\sigma\sigma}b_{\mathbf{k}\sigma\sigma}+\frac{1}{2}\sum_{\mathbf{k}\sigma}(\hat{c}^{\dagger}_{\mathbf{k}\sigma}\hat{c}_{-\mathbf{k}\sigma})\begin{pmatrix}\xi_{\mathbf{k}\sigma} & \Delta_{\mathbf{k}\sigma\sigma}\\ \Delta^{\dagger}_{\mathbf{k}\sigma\sigma} & -\xi_{\mathbf{k}\sigma}\end{pmatrix}\begin{pmatrix}\hat{c}_{\mathbf{k}\sigma}\\ \hat{c}^{\dagger}_{-\mathbf{k}\sigma}\end{pmatrix}. \quad \text{(C1)}$$

Here, I is the ferromagnetic exchange coupling constant, N is the number of lattice sites, M denotes the magnetic order parameter (dimensionless), and $b_{\mathbf{k}\sigma\sigma}$ is the Cooper pair expectation value. Diagonalization of this Hamiltonian produces:

$$\hat{H}=H_0+\sum_{\mathbf{k}\sigma}E_{\mathbf{k}\sigma}\hat{\gamma}^{\dagger}_{\mathbf{k}\sigma}\hat{\gamma}_{\mathbf{k}\sigma},$$

$$H_0=\frac{1}{2}\sum_{\mathbf{k}\sigma}(\xi_{\mathbf{k}\sigma}-E_{\mathbf{k}\sigma}-\Delta^{\dagger}_{\mathbf{k}\sigma\sigma}b_{\mathbf{k}\sigma\sigma})+\frac{INM^2}{2}, \quad \text{(C2)}$$

where $\{\hat{\gamma}_{\mathbf{k}\sigma},\hat{\gamma}^{\dagger}_{\mathbf{k}\sigma}\}$ are new fermion operators and the eigenvalues read

$$E_{\mathbf{k}\sigma}=\sqrt{\xi^2_{\mathbf{k}\sigma}+|\Delta_{\mathbf{k}\sigma\sigma}|^2}. \quad \text{(C3)}$$

Above, $\xi_{\mathbf{k}}$ is the kinetic energy measured from Fermi level. By minimizing the free energy, one obtains the gap equation for the superconducting order parameter:[7]

$$\Delta_{\mathbf{k}\sigma\sigma}=-\frac{1}{N}\sum_{\mathbf{k}'}V_{\mathbf{k}\mathbf{k}'\sigma\sigma}\frac{\Delta_{\mathbf{k}'\sigma\sigma}}{2E_{\mathbf{k}'\sigma}}\tanh(\beta E_{\mathbf{k}'\sigma}/2). \quad \text{(C4)}$$

Assuming that the gap is fixed on the Fermi surface in the weak-coupling limit, one may write in general

$$V_{\sigma\sigma}(\theta,\theta')=-V_0Y^{\sigma}(\theta)[Y^{\sigma}(\theta')]^*. \quad \text{(C5)}$$

where $Y^{\sigma}(\theta)$ are basis functions for the angular dependence of the interaction. To model p_x-wave and chiral p-wave pairing, respectively, we use $Y^{\sigma}(\theta)=-\sigma e^{i\sigma\theta}$ and $Y^{\sigma}(\theta)=\cos\theta$. Conversion to integral gap equations is accomplished by means of the identity

$$\frac{1}{N}\sum_{\mathbf{k}}f(\xi_{\mathbf{k}\sigma})=\frac{1}{4\pi}\int d\varepsilon d\Omega N^{\sigma}(\varepsilon)f(\varepsilon,\Omega), \quad \text{(C6)}$$

where $N^{\sigma}(\varepsilon)$ is the spin-resolved density of states. In three spatial dimensions, this may be calculated from the dispersion relation by using the formula

$$N^{\sigma}(\varepsilon)=\frac{V}{(2\pi)^3}\int_{\varepsilon_{\mathbf{k}\sigma}=\text{const}}\frac{dS_{\varepsilon_{\mathbf{k}\sigma}}}{|\hat{\nabla}_{\mathbf{k}}\varepsilon_{\mathbf{k}\sigma}|}. \quad \text{(C7)}$$

With the dispersion relation $\xi_{\mathbf{k}\sigma}=\varepsilon_{\mathbf{k}}-\sigma IM-\mu$, one obtains

$$N^{\sigma}(\varepsilon)=\frac{mV\sqrt{2m(\varepsilon+\sigma IM+\mu)}}{2\pi^2}. \quad \text{(C8)}$$

In their integral form, the gap equation reads

$$1=\frac{V_0}{4\pi}\sum_{\sigma}\int_{-\omega_0}^{\omega_0}\times\int 2\pi_0 d\varepsilon d\theta\frac{N^{\sigma}(\varepsilon)Y^{\sigma}(\theta)[Y^{\sigma}(\theta')]^*}{E_{\sigma}(\varepsilon)}\tanh[\beta E_{\sigma}(\varepsilon)/2]. \quad \text{(C9)}$$

Consider now $T=0$, where the integral may be done analytically to yield

$$\Delta_{\sigma,0}=c\omega_0 e^{-1/g\sqrt{1+\sigma\tilde{M}}}, \quad \sigma=\uparrow,\downarrow \quad \text{(C10)}$$

where we have defined $\tilde{M}=IM/\mu=h/\mu$, i.e., the exchange energy scaled by the Fermi energy. Moreover, c is a numerical prefactor which depends on that symmetry one considers (p_x wave or chiral p wave) while g is the weak-coupling constant. The important influence of the magnetization is that it modifies the density of states, which affects the superconductivity gaps. For $\tilde{M}=1$, i.e., an exchange splitting equal to the Fermi energy, the minority-spin gap is completely suppressed. Thus, the presence of magnetization reduces the available phase space for the minority-spin Cooper pairs, suppressing the gap and the critical temperature compared to the pure Bardeen-Cooper-Schrieffer case.

[1] N. T. Huy, A. Gasparini, D. E. de Nijs, Y. Huang, J. C. P. Klaasse, T. Gortenmulder, A. de Visser, A. Hamann, T. Gorlach, and H. v. Lohneysen, Phys. Rev. Lett. **99**, 067006 (2007).
[2] S. S. Saxena, P. Agarwal, K. Ahilan, F. M. Grosche, R. K. W. Haselwimmer, M. J. Steiner, E. Pugh, I. R. Walker, S. R. Julian, P. Monthoux, G. G. Lonzarich, A. Huxley, I. Sheikin, D. Braithwaite, and J. Flouquet, Nature (London) **406**, 587 (2000).
[3] D. Aoki, A. Huxley, E. Ressouche, D. Braithwaite, J. Flouquet, J.-P. Brison, E. Lhotel, and C. Paulsen, Nature (London) **413**, 613 (2001).
[4] R. Shen, Z. M. Zheng, S. Liu, and D. Y. Xing, Phys. Rev. B **67**, 024514 (2003).
[5] K. V. Samokhin and M. B. Walker, Phys. Rev. B **66**, 174501 (2002); **66**, 024512 (2002); M. B. Walker and K. V. Samokhin, Phys. Rev. Lett. **88**, 207001 (2002).
[6] A. Harada, S. Kawasaki, H. Mukuda, Y. Kitaoka, Y. Haga, E. Yamamoto, Y. Onuki, K. M. Itoh, E. E. Haller, and H. Harima, Phys. Rev. B **75**, 140502(R) (2007).
[7] A. H. Nevidomskyy, Phys. Rev. Lett. **94**, 097003 (2005).
[8] J. Linder and A. Sudbø, Phys. Rev. B **76**, 054511 (2007).
[9] J. Linder, I. B. Sperstad, A. H. Nevidomskyy, M. Cuoco, and A. Sudbø, Phys. Rev. B **77**, 184511 (2008).
[10] D. V. Shopova and D. I. Uzunov, Phys. Rev. B **72**, 024531 (2005).
[11] D. I. Uzunov, Europhys. Lett. **77**, 20008 (2007); Phys. Rev. B **74**, 134514 (2006).
[12] S. Tewari, D. Belitz, T. R. Kirkpatrick, and J. Toner, Phys. Rev. Lett. **93**, 177002 (2004).
[13] L. Radzihovsky, A. M. Ettouhami, K. Saunders, and J. Toner, Phys. Rev. Lett. **87**, 027001 (2001).
[14] A. Knigavko and B. Rosenstein, Phys. Rev. B **58**, 9354 (1998).
[15] V. P. Mineev, arXiv:cond-mat/0507572 (unpublished).
[16] A. Brataas and Y. Tserkovnyak, Phys. Rev. Lett. **93**, 087201 (2004).
[17] Y. Zhao and R. Shen, Phys. Rev. B **73**, 214511 (2006).
[18] M. S. Grønsleth, J. Linder, J.-M. Børven, and A. Sudbø, Phys. Rev. Lett. **97**, 147002 (2006); J. Linder, M. S. Grønsleth, and A. Sudbø, Phys. Rev. B **75**, 024508 (2007).
[19] J. Linder, M. S. Grønsleth, and A. Sudbø, Phys. Rev. B **75**, 054518 (2007).
[20] T. Yokoyama and Y. Tanaka, Phys. Rev. B **75**, 132503 (2007).
[21] H. F. Hess, R. B. Robinson, R. C. Dynes, J. M. Valles, Jr., and J. V. Waszczak, Phys. Rev. Lett. **62**, 214 (1989).
[22] G. Eilenberger, Z. Phys. **214**, 195 (1968).
[23] N. Schopohl and K. Maki, Phys. Rev. B **52**, 490 (1995); N. Schopohl, arXiv:cond-mat/9804064 (unpublished).
[24] M. Eschrig, Phys. Rev. B **61**, 9061 (2000).
[25] Z. Tesanovic, Phys. Rev. B **59**, 6449 (1999).
[26] A. K. Nguyen and A. Sudbø, Phys. Rev. B **60**, 15307 (1999); Europhys. Lett. **46**, 780 (1999).
[27] T. Yokoyama, Y. Tanaka, and A. A. Golubov, Phys. Rev. B **78**, 012508 (2008).
[28] C. Caroli, P. G. de Gennes, and J. Matricon, Phys. Lett. **9**, 307 (1964).
[29] H. F. Hess, R. B. Robinson, and J. V. Waszczak, Phys. Rev. Lett. **64**, 2711 (1990).
[30] M. Ichioka, N. Hayashi, N. Enomoto, and K. Machida, Phys. Rev. B **53**, 15316 (1996).
[31] We will use the notations and conventions of J. P. Morten, M.S. thesis, Norwegian University of Science and Technology, 2003, which in turn is close to the notations used in Ref. 32.
[32] J. W. Serene and D. Rainer, Phys. Rep. **101**, 221 (1983).
[33] N. Kopnin, *Theory of Nonequilibrium Superconductivity* (Oxford University Press, New York, 2001).
[34] J. Rammer and H. Smith, Rev. Mod. Phys. **58**, 323 (1986).
[35] A. M. Zagoskin, *Quantum Theory of Many-Body Systems* (Springer, New York, 1998).
[36] V. Chandrasekhar, in *The Physics of Superconductors*, edited by K.-H. Bennemann and J. B. Ketterson (Springer-Verlag, Berlin, 2004), Vol. II; arXiv:cond-mat/0312507 (unpublished).

Paper XVIII

Josephson current in diffusive multilayer superconductor/ferromagnet/superconductor junctions.

Physical Review B **78**, 104509 (2008).

Josephson current in diffusive multilayer superconductor/ferromagnet/superconductor junctions

Iver B. Sperstad, Jacob Linder, and Asle Sudbø
Department of Physics, Norwegian University of Science and Technology, N-7491 Trondheim, Norway
(Received 3 June 2008; revised manuscript received 23 July 2008; published 15 September 2008)

We calculate the Josephson current in a diffusive superconductor/ferromagnet/superconductor junction, where the ferromagnetic region contains multiple layers (or domains). In particular, we study a configuration where there are two layers with an arbitrary relative in-plane magnetization orientation and also include nonideal interfaces and arbitrary spin-flip scattering. We study the 0-π oscillations of the critical current for varying junction width d and find that the π state vanishes entirely when the magnetic misorientation angle of the two layers exceeds a critical angle ϕ_c. While $\phi_c \to \pi/2$ in the limit of high temperatures, we find that ϕ_c becomes smaller than $\pi/2$ at low temperatures compared to T_c. 0-π oscillations are also found when varying the temperature or the misorientation angle for fixed values of d, and we present phase diagrams that show qualitatively the conditions for the appearance of such oscillations. We also point out how one may obtain significant enhancement of the critical current in such a system by switching the magnetization for selected values of the junction width d, and comment on the necessary conditions for establishing a long-range triplet Josephson effect.

DOI: 10.1103/PhysRevB.78.104509 PACS number(s): 74.20.Rp, 74.50.+r, 74.70.Kn

I. INTRODUCTION

The topic of superconductor-ferromagnet heterostructures has been a subject of intense research for several years.[1,2] Not only do such systems constitute model systems for investigating the interplay between two fundamental condensed-matter phenomena, ferromagnetism (F) and superconductivity (S), but recent advances in fabrication techniques of such hybrid structures make applications increasingly attainable. Especially S/F based Josephson technology holds great promise in nanoelectronics, e.g., as a physical realization of the qubit of quantum computation.[3] Another possible device is in some sense analogous to a spin valve exhibiting giant magnetoresistance (GMR), i.e., strongly suppressing the current for opposite orientation of the magnetization[4] in two F layers separated by a normal metal (N). For our object of interest however, superconducting electrodes are used instead of ferromagnets and N is replaced with F, in which case the resistance effect of magnetization switching is known to be reversed compared to the spin valve.[5]

The proximity effect between a superconductor and a normal metal was predicted decades ago[6] and has since been investigated thoroughly both theoretically and experimentally. However, several new and interesting effects were predicted when the layer of normal metal was replaced with a ferromagnet due to spin-triplet correlations in the ferromagnet induced by the exchange field.[1,2] Much attention has been given to superconductor/ferromagnet/superconductor (SFS) structures, which are studied as a somewhat more exotic class of Josephson junctions. The most interesting emerging phenomenon in SFS junctions is the appearance of the so-called π state,[7,8] in which the difference in the superconducting phase across the junction is π in the ground state, in contrast to the conventional state with phase difference zero. The physical result of transitions between these states is usually a sign change in the critical Josephson current I_c through the junction, the observable manifestation of which being a nonmonotonic dependence of I_c on parameters such as temperature and junction width. Been predicted for decades, the experimental verification of this phenomenon some years ago[9,10] was one of the catalysts of the present activity on the field. Recently, the effect of magnetic impurities in SFS junctions was also investigated theoretically.[11,12]

It is well known that in simple S/F structures, the proximity effect will only induce opposite spin pairing (OSP) triplet correlations (spin projection $S_z=0$), and that equal spin pairing (ESP) triplet correlations ($S_z=\pm 1$) require inhomogeneous magnetization.[1] ESP components are in some contexts referred to as long-range triplet correlation (LRTC) components and are of special interest because they do not decay as rapidly in the ferromagnet as the other components, and may therefore evade the suppression of the supercurrent for increasing width of the ferromagnet. One way of achieving this in theory is to let the magnetization in the F layer have a helical structure.[13,14] A similar effect is also found by considering a superconductor/insulator/superconductor (SIS) junction where the S electrodes themselves exhibit a spiral magnetic order coexisting with the superconductivity.[15] Yet another alternative is layered S/F structures[16] with noncollinear magnetization or simply a SFS structure where F is replaced with several ferromagnets with different direction of magnetization.

Recent theoretical studies have been focusing on junctions with two ferromagnets sandwiched between the superconducting electrodes. There are two physical realizations of a system described by such a model. It may either describe a device with two distinct, consecutively placed F layers (a SF_1F_2S junction), constructed to achieve customized nonhomogeneous magnetization. Several works[5,17–22] have considered the Josephson current in such heterostructures. On the other hand, the model may describe the more realistic experimental situation of one ferromagnetic layer with several magnetic domains. Some models of the latter kind have included two or more in-plane magnetic domains,[23,24] and although this certainly is an interesting framework for understanding real heterostructures, the present paper considers the

two layers placed consecutively as a SF_1F_2S structure. The main motivation for this choice is that this configuration allows for much easier experimental control of the magnetization. The misorientation angle may be tuned by applying an external weak magnetic field to the interface between the ferromagnets if the magnetization axis is pinned in one layer while in the other one there is an in-plane easy axis.[18] To accomplish this experimentally, one would probably need some interlayer between the ferromagnetic films to avoid a locking between the corresponding magnetizations due to the interfilm exchange coupling.

Calculations on the models referred to here have predicted 0-π transitions upon varying the strength of the magnetic exchange field, the junction width, or the temperature, depending on the relative orientation of the magnetization in the two F layers.[5,17–22] For antiparallel magnetization, it is reported that the 0-π oscillations will vanish, rendering the π state impossible.[25] An enhancement of the critical current for the antiparallel orientation by increasing the exchange field was first reported by Bergeret *et al.*[5] and shortly after elaborated upon by others.[26,27] Much of the work has however been limited to the case of collinear magnetization,[25,27] but recently also SF_1F_2S systems with arbitrary misorientation angle for the magnetization have been analyzed.[17,18,28] In particular, Crouzy *et al.*[28] have shown how the π state of such a junction is suppressed for increasing misorientation angles, vanishing at a critical angle $\phi_c = \pi/2$ when the temperature is close to the critical temperature, i.e., $T/T_c \simeq 1$. One recent article[29] has even studied a corresponding ferromagnetic trilayer structure, but focused chiefly on the LRTC contribution to the Josephson current in such a structure. It should be noted that while the majority of the work in this field is carried out in the dirty limit, considering diffusive F/S systems, several of the relevant papers[17,18,29,30] study ballistic junctions as well.

Reference 28 points out the necessity of including additional effects to get a more accurate description of such systems. The present article may thus be viewed as an extension of their work by studying a SF_1F_2S junction with noncollinear domains where nonideal interfaces and magnetic impurities are also taken into consideration. For the latter, we will study the special cases where isotropic or uniaxial spin-flip scattering is present. Consequently, there are three questions addressed in this work which were not treated in Ref. 28: (i) how does spin-flip scattering influence the 0-π oscillations?; (ii) Do nonideal interfaces change the qualitative behavior of the system?; and (iii) How does the Josephson current for such a system depend on the temperature? The possibility of investigating the latter point is present in our model, as opposed to Ref. 28, which was restricted to temperatures close to T_c. The reason for this is that the regime of weak proximity effect is only attainable either if the S/F transparency is low or when transparency is high under the extra restriction that $T \approx T_c$, so that it is guaranteed that the influence of superconductivity is weak in either case.

For concreteness, we consider a diffusive Josephson junction with two ferromagnetic layers with arbitrary in-plane relative orientation of the magnetization, as shown in Fig. 1. Although we focus on this picture of distinct, controllable layers, the physically similar situation of magnetic domains will also be commented upon. The superconducting electrodes are two similar s-wave superconductors, and the interfaces between the superconductors and the ferromagnet are assumed to have low transparency.

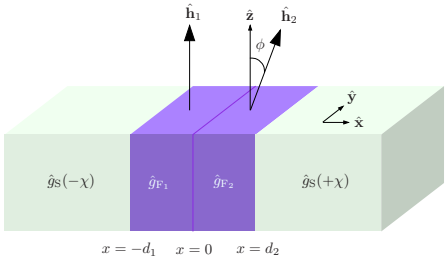

FIG. 1. (Color online) The experimental setup proposed in this paper. Two s-wave superconductors are separated by two ferromagnetic layers with an arbitrary relative orientation of the magnetizations. The ferromagnetic regions may model a domain structure of a single ferromagnetic layer or correspond directly to two distinctly deposited magnetic layers. This is similar to the setup considered in Ref. 28.

This paper is organized as follows: In Sec. II we will briefly sketch the theoretical framework and go on to obtain a solution for the proximity-induced anomalous Green's function in the ferromagnetic region of our SF_1F_2S system, from which an expression for the Josephson current can be calculated. In Sec. III we present the dependence of the Josephson current on the various parameters, analyze the resulting 0-π oscillations in the junction, and construct a corresponding phase diagram. We discuss the applicability of our findings in Sec. IV and furthermore present a discussion of the absence of the long-range Josephson effect in such SF_1F_2S systems. A summary and some final remarks are given in Sec. V. We will use boldface notation for three vectors, $\hat{\ldots}$ for 4×4 matrices, and $\underline{\ldots}$ for 2×2 matrices.

II. THEORETICAL FORMULATION

We address this problem by means of the Usadel equation in the quasiclassical approximation. This corresponds to integrating out the dependence on the kinetic energy of the Gor'kov Green's function, obtaining thus the quasiclassical Green's function $\hat{g}$ as the object used to describe our system. This approximation is valid as long as all relevant energy scales are much smaller than the Fermi energy ε_F, and correspondingly that all relevant length scales are much larger than the Fermi wavelength. The latter condition is reconciled with the presence of sharp interfaces in our model by introducing appropriate boundary conditions, as discussed below. The approach is based on the Keldysh formalism for nonequilibrium superconductors, which is convenient to work in also in the present limiting case of equilibrium. Here one operates with 8×8 matrix Green's functions, in which the retarded Green's function $\hat{g}^R$, the advanced Green's function $\hat{g}^A$, and the Keldysh Green's function $\hat{g}^K$ are 4×4 matrix components. As both the advanced and the Keldysh component of the matrix can easily be expressed by the retarded

component in our case, it will be implicitly assumed in the following that the Green's function under consideration is the retarded component $\hat{g}^R$.

We will desist from further discussion of quasiclassical theory and instead refer the reader to the considerable literature that covers the Keldysh formalism and nonequilibrium Green's functions.[31–35] We go on to write up the matrix structure of our quasiclassical Green's functions. In the bulk superconductors, the Green's function reads[31]

$$\hat{g}_S = \begin{pmatrix} \underline{1}c & i\underline{\tau_2}se^{\pm i\chi} \\ i\underline{\tau_2}se^{\mp i\chi} & -\underline{1}c \end{pmatrix}, \tag{1}$$

where $c \equiv \cosh(\theta)$, $s \equiv \sinh(\theta)$, and $\theta \equiv \operatorname{atanh}(\Delta_0/\varepsilon)$, with Δ_0 denoting the amplitude of the superconducting gap. The different signs of the phase χ above correspond to the left (lower sign) and right (upper sign) superconducting banks, respectively. When not being in proximity to a superconductor, the Green's function for a bulk ferromagnet reads

$$\hat{g}_{F,0} = \begin{pmatrix} \underline{1} & 0 \\ 0 & -\underline{1} \end{pmatrix}. \tag{2}$$

When being influenced by a superconductor, off-diagonal elements are introduced to this Green's function, and for weak proximity effect it is changed to $\hat{g}_F \approx \hat{g}_{F,0} + \hat{f}$. This perturbation can be expressed as[31]

$$\hat{f} = \begin{pmatrix} 0 & \underline{f}(\varepsilon) \\ -[\underline{f}(-\varepsilon)]^* & 0 \end{pmatrix}, \tag{3}$$

where the constituting anomalous Green's function can be written as a matrix in spin space on the form[36]

$$\underline{f} = \begin{pmatrix} f_\uparrow & f_t + f_s \\ f_t - f_s & f_\downarrow \end{pmatrix}. \tag{4}$$

Here, f_s denotes the singlet component, f_t the OSP triplet component, and $f_\uparrow$ and $f_\downarrow$ the ESP triplet components, and it is these anomalous Green's function that the Usadel equation is to be solved for.

In our calculations, we will account for the possibility of both uniaxial and isotropic spin-flip scatterings by the parameter η_{xy} and η_z as follows:

$$\text{Uniaxial spin-flip: } \eta_{xy} = 0, \quad \eta_z = 3,$$

$$\text{Isotropic spin-flip: } \eta_{xy} = 1, \quad \eta_z = 1. \tag{5}$$

The spin-relaxation time for spin-flip scattering will be denoted τ_{sf} and is to be considered as a phenomenological parameter in our approach.

In the ferromagnetic regions F_1 and F_2, the linearized Usadel[37] equations take the form

$$D\partial_x^2(f_t \pm f_s) + 2i(\varepsilon \pm h\cos\phi)(f_t \pm f_s) - \frac{1}{2\tau_{sf}}(\eta_z f_t \pm 3f_s) \pm h\sin\phi(f_\uparrow + f_\downarrow) = 0,$$

$$D\partial_x^2 f_\sigma + \left(2i\varepsilon - \frac{\eta_{xy}}{2\tau_{sf}}\right)f_\sigma - 2h\sin\phi f_s = 0; \quad \sigma = \uparrow,\downarrow, \tag{6}$$

with $\phi = 0$ in F_1. Equation (6) constitute a set of coupled, second-order, linear differential equations. Although an explicit analytical solution may be obtained for $\{f_s, f_t, f_\sigma\}$ by solving Eq. (6) brute force for nonzero ϕ, the resulting expressions are very large and cumbersome. We therefore proceed via an alternative but equivalent route. By a change of spin basis to a quantization axis which is aligned to the exchange field in F_2, one obtains the equations

$$D\partial_x^2(f_t' \pm f_s) + 2i(\varepsilon \pm h)(f_t' \pm f_s) - \frac{1}{2\tau_{sf}}(\eta_z f_t' \pm 3f_s) = 0,$$

$$D\partial_x^2 f_\sigma' + \left(2i\varepsilon - \frac{\eta_{xy}}{2\tau_{sf}}\right)f_\sigma' = 0. \tag{7}$$

The superscript $'$ denotes the new spin basis and the s-wave component transforms as a scalar under spin rotations $f_s' = f_s$. The general analytical solution for these equations in the case of isotropic spin-flip scattering was obtained in Ref. 38. In the present case, we obtain

$$f_t' = c_1 e^{-q_- x} + c_2 e^{q_- x} + c_3 e^{q_+ x} + c_4 e^{-q_+ x},$$

$$f_s = \frac{i}{8\tau_{sf}h}(c_1\kappa_+ e^{-q_- x} + c_2\kappa_+ e^{q_- x} + c_3\kappa_- e^{q_+ x} + c_4\kappa_- e^{-q_+ x}),$$

$$f_\sigma' = A_\sigma e^{ikx} + B_\sigma e^{-ikx}, \tag{8}$$

where we have defined

$$q_\pm = \sqrt{-D\tau_{sf}(\pm p - 3 - \eta_z + 8i\tau_{sf}\varepsilon)}/(2D\tau_{sf}),$$

$$\kappa_\pm = 3 - \eta_z \pm p, \quad p = \sqrt{(3-\eta_z)^2 - 64\tau_{sf}^2 h^2},$$

$$k = \sqrt{[2i\varepsilon - \eta_{xy}/(2\tau_{sf})]/D}. \tag{9}$$

Taking $\eta_z = \eta_{xy} = 1$, the above expressions reduce to those of Ref. 38. Once the $\{f_s', f_t', f_\sigma'\}$ have been obtained, one may transform them back to the original quantization axis $\|\hat{\mathbf{z}}$. If we write

$$\underline{f} = (f_s + \mathbf{f}\cdot\underline{\boldsymbol{\tau}})i\underline{\tau_2}, \tag{10}$$

one may from Eq. (4) identify the vector anomalous Green's function

$$\mathbf{f} = [f_\downarrow - f_\uparrow, \quad -i(f_\uparrow + f_\downarrow), \quad 2f_t]/2. \tag{11}$$

This is equivalent to the $\mathbf{d_k}$-vector formalism described in, for instance, Ref. 36. For future use, we define $f_\pm = f_t \pm f_s$. Finally, the transformation to the new spin basis is (see also Fig. 2)

$$(\mathbf{f}')^T = \begin{pmatrix} 1 & 0 & 0 \\ 0 & \cos\phi & -\sin\phi \\ 0 & \sin\phi & \cos\phi \end{pmatrix}(\mathbf{f})^T. \tag{12}$$

In general, the linearization of the Usadel equation is a valid approximation in the case of a weak proximity effect. This

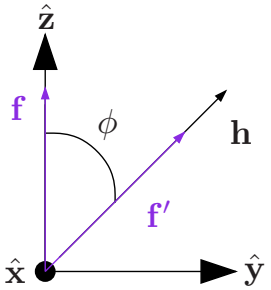

FIG. 2. (Color online) The change of spin basis from a quantization axis $\|\hat{\mathbf{z}}$ to a quantization axis $\|\mathbf{h}$.

may be obtained in two limiting cases: (i) the barriers have low transparency or (ii) the transparency is perfect (ideal interfaces) and the temperature in the superconducting reservoir is close to T_c, such that Δ_0 is small. An analytical approach is permissible in both scenarios, with differing boundary conditions. In case (i), the standard Kupriyanov-Lukichev (K-L) boundary conditions[39] are usually employed in the literature, while case (ii) implies continuity of the Green's function and its derivative. In an experimental situation, the barrier region can hardly be considered as fully transparent, such that the K-L boundary conditions are more realistic than continuity of the Green's function and its derivative. We will therefore employ the K-L boundary conditions in this paper.[40]

To obtain the anomalous Green's function, we must supplement the general solution in Eq. (8) with the K-L boundary conditions at three interfaces. At the S/F_i interfaces located at $x=-d_1$ and $x=d_2$, one obtains

$$2\gamma d_1 \hat{g}_{\mathrm{F}_1}\partial_x \hat{g}_{\mathrm{F}_1}|_{x=-d_1} = [\hat{g}_{\mathrm{S}}(-\chi), \hat{g}_{\mathrm{F}_1}]|_{x=-d_1},$$

$$2\gamma d_2 \hat{g}_{\mathrm{F}_2}\partial_x \hat{g}_{\mathrm{F}_2}|_{x=d_2} = [\hat{g}_{\mathrm{F}_2}, \hat{g}_{\mathrm{S}}(\chi)]|_{x=d_2}. \tag{13}$$

We have defined the parameter

$$\gamma = \frac{R_B}{R_{\mathrm{F}}}, \tag{14}$$

where R_B is the resistance of the barrier region and R_{F} is the resistance of in the diffusive ferromagnetic regions (assumed to be the same for both F_1 and F_2). For the F_1/F_2 interface, which denotes the separation of the ferromagnetic layers, we assume the resistance to be much smaller than at the S/F_i interfaces. Therefore, we model this by continuity of the Green's function and its derivative

$$g_{\mathrm{F}_1} = g_{\mathrm{F}_2}|_{x=0}, \quad \partial_x g_{\mathrm{F}_1} = \partial_x g_{\mathrm{F}_2}|_{x=0}. \tag{15}$$

Let us comment briefly on the case where F_1 and F_2 are two domains of a single layer. A domain-wall resistance may quite generally be defined as $R_w = R - R_0$, where R and R_0 are the electrical resistances with and without a domain wall (i.e., homogeneous magnetization), respectively. When the width of the domain wall increases, $R_w \to 0$ and vanishes all together when the width of the domain wall is much larger than the Fermi wavelength.[41] In the present paper, we consider an abrupt change in magnetization at the interface of the two domains, corresponding to a very thin domain wall, such that one would in general expect a finite contribution to the resistance of the junction. To reduce the number of parameters in the problem, however, we *assume* that this resistance is much smaller than at the S/F interfaces and effectively set it to zero. In the case where F_1 and F_2 are separate ferromagnetic layers, one may neglect the resistance at the interface between them by assuming a good electrical contact achieved during deposition of the layers.

The $\{f_{2\pm}, f_{2\sigma}\}$ anomalous Green's functions are related to a set of anomalous Green's functions in a rotated basis $\{f'_{2\pm}, f'_{2\sigma}\}$ via

$$f_{2\uparrow} = \frac{1}{2}[\cos\phi(f'_{2\downarrow} + f'_{2\uparrow}) + 2i\sin\phi f'_{2,t} + f'_{2\uparrow} - f'_{2\downarrow}],$$

$$f_{2\downarrow} = \frac{1}{2}[\cos\phi(f'_{2\downarrow} + f'_{2\uparrow}) + 2i\sin\phi f'_{2,t} - f'_{2\uparrow} + f'_{2\downarrow}],$$

$$f_{2,t} = \cos\phi f'_{2,t} + \frac{i\sin\phi}{2}(f'_{2\downarrow} + f'_{2\uparrow}), \tag{16}$$

where $\{f'_{2\pm}, f'_{2\sigma}\}$ have the general form as shown in Eq. (8). The complete anomalous Green's functions in the regions F_1 may be written as

$$f_{1\pm} = b_1 e^{-q_- x} L_+^{\pm}(0) + b_2 e^{q_- x} L_+^{\pm}(0) + b_3 e^{q_+ x} L_-^{\pm}(0) + b_4 e^{-q_+ x} L_-^{\pm}(0),$$

$$f_{1\sigma} = A_\sigma e^{ikx} + B_\sigma e^{-ikx}, \tag{17}$$

while in F_2 one finds

$$f_{2\pm} = c_1 e^{-q_- x} L_+^{\pm}(\phi) + c_2 e^{q_- x} L_+^{\pm}(\phi) + c_3 e^{q_+ x} L_-^{\pm}(\phi) + c_4 e^{-q_+ x} L_-^{\pm}(\phi) + \frac{i\sin\phi}{2}[(C_\uparrow + C_\downarrow)e^{ikx} + (D_\uparrow + D_\downarrow)e^{-ikx}],$$

$$f_{2\sigma} = \frac{1}{2}[e^{ikx}\{\cos\phi(C_\uparrow + C_\downarrow) + \sigma(C_\uparrow - C_\downarrow)\} + e^{-ikx}\{\cos\phi(D_\uparrow + D_\downarrow) + \sigma(D_\uparrow - D_\downarrow)\} + 2i\sin\phi(c_1 e^{-q_- x} + c_2 e^{q_- x} + c_3 e^{q_+ x} + c_4 e^{-q_+ x})]. \tag{18}$$

Above, we have defined $L_{\pm}^{\pm'}(\phi)=\cos\phi \pm' i\kappa_{\pm}/(8\tau_{\rm sf}h)$. Note that Eq. (18) reduces to exactly the same form as Eq. (17) for $\phi=0$ (parallel magnetization), as demanded by consistency. The remaining task is to determine the 16 unknown coefficients $\{b_i\},\{c_i\},\{A_\sigma,B_\sigma,C_\sigma,D_\sigma\}$. For clarity, we write out the boundary conditions explicitly. At $x=-d_1$, one has ($\sigma=\uparrow,\downarrow$),

$$\gamma d_1\partial_x f_{1\pm}=cf_{1\pm}\mp se^{-i\chi},\quad \gamma d_1\partial_x f_{1\sigma}=cf_{1\sigma}, \tag{19}$$

while at $x=d_2$ we find

$$\gamma d_2\partial_x f_{2\pm}=\pm se^{i\chi}-cf_{2\pm},\quad \gamma d_2\partial_x f_{2\sigma}=-cf_{2\sigma}. \tag{20}$$

Finally, at $x=0$ one obtains

$$f_{1\pm}=f_{2\pm},\quad \partial_x f_{1\pm}=\partial_x f_{2\pm},$$

$$f_{1\sigma}=f_{2\sigma},\quad \partial_x f_{1\sigma}=\partial_x f_{2\sigma}. \tag{21}$$

Inserting Eqs. (17) and (18) into Eqs. (19)–(21) yields a set of linear equations which may be represented by a 16×16 matrix, and the solution for the 16 coefficients is found numerically. Once the anomalous Green's functions have been obtained, one may calculate physical quantities of interest. In the present paper, we will be concerned with the Josephson current

$$\begin{aligned}\mathbf{j}(x)&=-(N_{\rm F}eD\hat{\mathbf{x}}/4)\int d\varepsilon\ {\rm Tr}\{\hat\rho_3(\hat g^R\partial_x\hat g^K-\hat g^K\partial_x\hat g^A)\}\\&=-(N_{\rm F}eD\hat{\mathbf{x}}/2)\int_{-\infty}^{\infty}d\varepsilon\ {\rm Re}\{M_+(\varepsilon)\\&\quad+M_-(\varepsilon)M_\uparrow(\varepsilon)+M_\downarrow(\varepsilon)\}\times\tanh(\beta\varepsilon/2),\end{aligned} \tag{22}$$

with the definitions ($\sigma=\uparrow,\downarrow$),

$$M_\sigma(\varepsilon)=[f_\sigma(-\varepsilon)]^*\partial_x f_\sigma(\varepsilon)-f_\sigma(\varepsilon)\partial_x[f_\sigma(-\varepsilon)]^*,$$

$$M_\pm(\varepsilon)=[f_\pm(-\varepsilon)]^*\partial_x f_\mp(\varepsilon)-f_\pm(\varepsilon)\partial_x[f_\mp(-\varepsilon)]^*. \tag{23}$$

The matrix $\hat\rho_3$ in the first line of Eq. (22) is defined by $\hat\rho_3={\rm diag}(1,1,-1,-1)$. The normalized current is defined as

$$I(\chi)/I_0=4|\mathbf{j}(x,\chi)|/(N_{\rm F}eD\Delta_0^2), \tag{24}$$

which is independent of x for $x\in[-d_1,d_2]$ (due to conservation of electrical current). The maximal supercurrent the system can support, known as the *critical current*, is given by $I_c=I(\frac{\pi}{4})$ in the case of a sinusoidal current-phase relation.

Before proceeding to disseminate our results, we briefly remind the reader (see, e.g., Refs. 2 and 42) of the qualitative physics that distinguishes S/F proximity structures from S/N systems, and thus gives rise to, e.g., 0-π oscillations of the critical current (which will be discussed in detail for our system in Sec. III). The fundamental difference between the proximity effect in a S/N structure as compared to a S/F structure is that the Cooper pair wave function acquires a finite center-of-mass momentum in the latter case due to the Zeeman-energy splitting between the $\uparrow$ and $\downarrow$ spins constituting the Cooper pair. The finite center-of-mass momentum of the Cooper pair implies that the condensate wave function in the ferromagnetic region displays oscillations in space, permitting it to change sign upon penetrating deeper into the ferromagnetic region. Quite generally, one may write that the Cooper pair wave function (order parameter) as $\Psi=\Psi_0e^{-k_sx}$ in a S/N structure while $\Psi=\Psi_0\cos(k_{f,1}x)e^{-k_{f,2}x}$ in a S/F structure, where $\{k_s,k_{f,1},k_{f,2}\}$ are wave vectors related to the decay and oscillation lengths of the proximity-induced condensate in the nonsuperconducting region.

The fact that the proximity-induced superconducting order parameter oscillates in the ferromagnetic region suggests that the energetically most favorable (ground-state) phase difference between the superconducting reservoirs might not always be zero, as in an S/N/S junction. For a very thin ferromagnetic layer, Ψ does not change much and there is no reason for why there should be an abrupt discontinuity in the phase at one of the F/S interfaces—hence, the system is in the 0 state. If the thickness of the ferromagnetic layer is comparable to the oscillation length of Ψ ($\sim1/k_{f,1}$ in our notation above), then Ψ may cross zero in the middle of the ferromagnetic region and display antisymmetric behavior. This is accompanied with a shift of sign of the order parameter in the, say, right bulk superconductor as compared to the left bulk superconductor. Under such circumstances, the energetically most favorable configuration corresponds to a phase difference of π between the superconductors, since $\Delta=\Delta_0$ in one of the superconductors and $\Delta=-\Delta_0=\Delta_0e^{i\pi}$ in the other superconductor.

This is related to 0-π oscillations of the critical current as follows. The energy of the Josephson junction may in the tunneling limit be well approximated by

$$\varepsilon_J\sim I_{J,0}(1-\cos2\chi), \tag{25}$$

where I_0 contains the magnitude and sign of the critical current while 2χ is the phase difference between the superconductors. Now, $I_{J,0}$ is closely related to the proximity-induced condensate wave function Ψ in the ferromagnetic region and may change sign depending on, for instance, the width of the ferromagnetic layer. Depending on its sign, the ground-state configuration corresponds to either $2\chi=0$ or $2\chi=\pi$, and the critical current supported by the system will change sign depending on which of these phases the system is in (although the critical current itself is given by $2\chi=\pi/2$).

III. RESULTS

Unless otherwise stated, we will fix $h/\Delta_0=10$ and $\gamma=5$ to model a realistic experimental setup with weak ferromagnets (the exchange field was estimated to 5–10 meV in Ref. 43.) The particular choice of γ is motivated by the fact that we expect the resistance of the barrier region to exceed the bulk resistance of the ferromagnets, and in addition to a low transparency of the S/F interfaces this clearly suggests that $\gamma\gg1$. This will ensure a weak proximity effect, as explained in Sec. II. In order to reduce the number of free parameters further, we in general set the widths of region F_1 and F_2 to be equal $d_1=d_2\equiv d$. The superconducting coherence length $\xi=\sqrt{D/\Delta_0}$ will be used as the unit in which the widths are measured. Where spin-flip scattering is included, we will use the parameter $g=1/(\tau_{sf}\Delta_0)$ as a measure of the strength of this effect.

We have numerically confirmed that the system follows a sinusoidal current-phase relation regardless of the direction of magnetization and all other variable parameters of our system. This allows us to focus on the state that supports the critical current, namely, $\chi=\pi/4$. A sinusoidal current-phase relation is moreover what should be expected for such systems with weak proximity effect[44] and where the bulk superconductors have the same symmetry.[45] We have also confirmed that the assumption of weak proximity effects holds by assuring that the value of the anomalous Green's function always obey $|f_{s,t,\sigma}| \ll 1$ for the parameter range we consider. To make the computation of the solutions to the Usadel equation numerically stable, we furthermore add a small imaginary term $i\delta$ to the excitation energy ε, where the value $\delta = 10^{-3}$ has been used. This can be motivated as a way to account for inelastic-scattering processes,[46] interpreting the term as the inverse (positive) quasiparticle lifetime.

A. Zero temperature

First, we will consider the case where the temperature is fixed to zero unless otherwise stated, i.e., the calculations are made with $T/T_c=0.001$. The critical current as a function of the junction width d is shown in Fig. 3 for uniaxial spin-flip scattering. Considering first the parallel case $\phi=0$, the well-known 0-π oscillations are reproduced, where the current change sign for certain values of d. It should however be noted that we have chosen to always plot the critical current as a positive quantity, as defined by Eq. (24), because this is what is most commonly measured in experiments.[2,9] We have confirmed that the oscillations are almost exactly periodic for the parameter range considered here. Increasing the effect of spin-flip scattering tends to move the transition points between the 0 state and the π state toward higher values of d. Throughout our investigations, we find no significant difference between isotropic and uniaxial spin-flip scatterings for the width dependence of the critical current. Thus, we consider only uniaxial spin-flip scattering whenever the role of magnetic impurities is studied.

The subplots of Fig. 3 show how increasing the relative angle of magnetization to $\phi=\pi/4$ shifts the first transition points to the right and the second to the left, reducing the width region in which the system is in the π state. For $\phi=\pi/2$, the oscillations have ceased entirely, leaving the junction in the 0 state for all values of d. These effects are shown more clearly in Fig. 4, which also shows that the oscillations do not return for $\phi \in [\pi/2, \pi]$. This can be expressed as a critical misorientation angle $\phi_c \lesssim \pi/2$ over which the π state is not realizable, which is in agreement with the findings of Ref. 28. Reference 28 claims that $\phi_c \equiv \pi/2$ independent of parameters as long as the system is near the critical temperature $T/T_c \simeq 1$. We find ϕ_c to have a somewhat lower value $\phi_c \simeq 0.46\pi < \pi/2$ in the present case of $T/T_c \ll 1$, but we will show in Sec. III B how this value approaches $\pi/2$ for increasing temperatures and how it changes for other values of the exchange field than our particular choice of $h/\Delta_0 = 10$. In light of the discussion concerning the qualitative physics involved in a S/F/S proximity structure, it seems reasonable to suggest that the vanishing of the 0-π transitions are directly linked to a strong modification of the Cooper-pair wave-function oscillation length inside the ferromagnet, which renders the π state inaccessible. Possible explanations will be discussed further in Sec. IV.

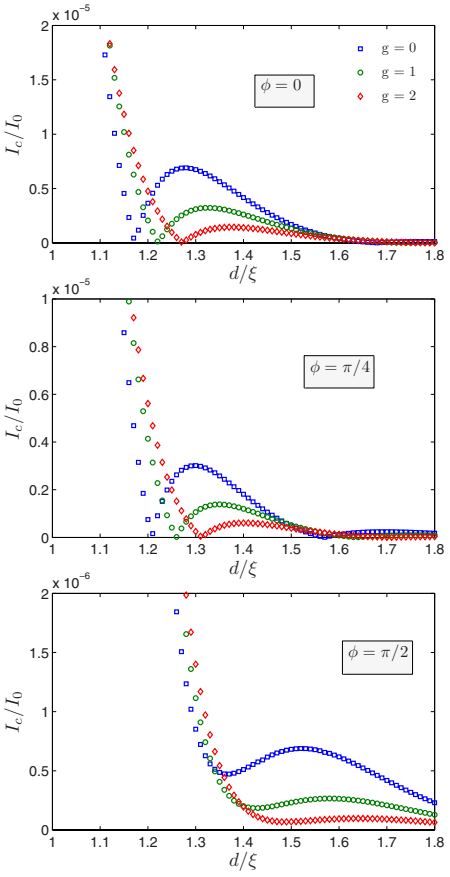

FIG. 3. (Color online) Plot of the width dependence of the critical current for several values of the spin-flip scattering rate, which is here taken to be uniaxial in spin space. We have defined the dimensionless parameter $g=1/(\tau_{sf}\Delta_0)$ as a measure of the spin-flip scattering rate. At $d/\xi=1.0$, the system is in the 0 state.

As stated in the introduction, several works have contrasted the cases of parallel and antiparallel orientations, while the intermediate angles have not been studied thoroughly (see, however, Refs. 18 and 28). We seek to remedy this by first presenting in Fig. 5 the dependence of the critical current on the misorientation angle. The three junction widths $d/\xi=\{1.0, 1.25, 1.5\}$ are chosen somewhat arbitrarily from the available range of values, but illustrate adequately the conditions for appearance of 0-π oscillations. First, we confirm the obvious fact that the critical current should be symmetric with respect to $\phi=\pi$. Therefore we will from now on only consider the interval $\phi \in [0, \pi]$, the maximum of the misorientation angle being the antiparallel orientation. Next, we see that no 0-π oscillations appear upon varying the mis-

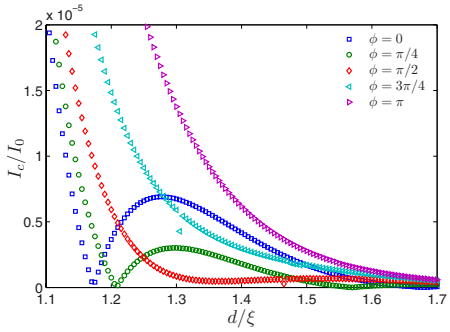

FIG. 4. (Color online) Plot of the width dependence of the critical current for several values of the misorientation angle ϕ, with spin-flip scattering turned off for simplicity (g=0).

orientation angle for d/ξ=1.0 fixed, which agrees with the observation from the previous figures that the junction appears to be in the 0 state for all angles at this junction width. For d/ξ=$\{1.25, 1.5\}$ however, the junction starts out in the π state for the parallel orientation, and we can see that a transition takes place to the 0 state for some angle $\phi < \pi/2$. This is in agreement with the result of Ref. 18 that a nonmonotonic dependence of the critical current on ϕ occurs when the π state is the equilibrium state of the junction for ϕ=0, and a similar statement was also made in Ref. 17.

A small effect of spin-flip scattering which may be mentioned here is that for $\phi > 0$ it may give the appearance of an effectively lowered misorientation angle with regard to the shift in the d values for 0-π crossover. As a result, for angles just above the critical angle, an increase of g may trigger the transition from complete absence of the π state to 0-π oscillations.

The evolution of the critical current for variable d and ϕ described in the previous paragraphs can be condensed to the phase diagram shown in Fig. 6. If only the sign of the Josephson current is of interest, each of the plots of $I_c(d)$ may be thought of as a horizontal sweep through the phase diagram for some fixed ϕ, while every plot of $I_c(\phi)$ is represented by a vertical sweep for some fixed d. As seen, the π state becomes impossible above a critical angle ϕ_c for the present case of $T \to 0$. We will contrast this with the finite-temperature case in Sec. III B.

B. Finite temperature

We proceed by considering the dependence of the Josephson current on the temperature. The superconducting electrodes were assumed to be conventional superconductors unaffected by the ferromagnetic layers, so the standard BCS temperature dependence of the superconducting gap will be employed

$$\Delta(T) = \Delta_0 \tanh(1.74\sqrt{T_c/T - 1}). \tag{26}$$

To illustrate how the critical angle ϕ_c for 0-π oscillations depends upon increasing the temperature, including also the dependence on the exchange field, we plot in Fig. 7 the critical angle as a function of the exchange splitting h for several values of T. As seen, ϕ_c remains less than $\pi/2$ up to $h/\Delta_0 \simeq 100$ in the $T \to 0$ limit. However, increasing the temperature only slightly to T/T_c=0.2, we see that ϕ_c rapidly approaches $\pi/2$. The trend is the same upon increasing the temperature even further, indicating the limit of $\phi_c = \pi/2$ for arbitrarily high values of h as $T \simeq T_c$. We conclude therefore that the critical angle above which 0-π oscillations cease to exist is equal to $\pi/2$ as long as the temperature is high ($T/T_c \simeq 1$). However, for low temperatures and weak exchange fields, we find that ϕ_c deviates noticeably from $\pi/2$.

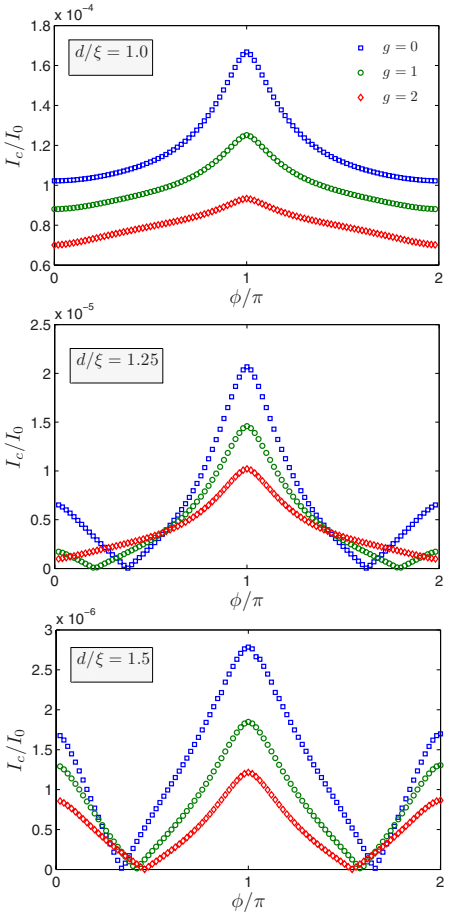

FIG. 5. (Color online) Plot of how the critical current is affected by a change in the relative orientation ϕ of the magnetizations for several values of the spin-flip scattering rate, which is here taken to be uniaxial in spin space.

Also by varying the temperature parameter 0-π oscillations may be found in the system, as shown in Fig. 8. This follows as a natural result if the critical values of junction width at which 0-π transitions were found in Sec. III A are temperature dependent. One difference from the plots of I_c as a function of d is the existence of no more than one transition

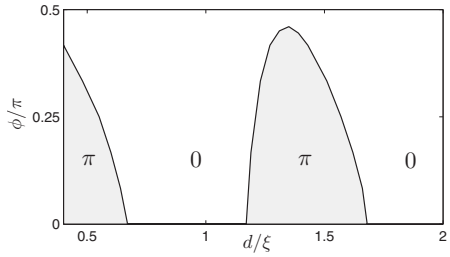

FIG. 6. Phase diagram of the Josephson junction for zero temperature, showing the regions occupied by the 0 state and the π state in width-misorientation parameter space. For the region given by $\phi \in [\pi/2, 3\pi/2]$, the π state is completely absent. We have set the spin-flip scattering strength to zero $g=0$.

point (for each value of g) before the Josephson current necessarily vanishes at $T=T_c$. For increasing ϕ, this transition point moves leftwards until vanishing at $T=0$ at some critical angle. By considering the dependence on misorientation angle more carefully, we found that this critical angle, over which the 0-π oscillations disappear for I_c as a function of T, differs from the corresponding critical angle for I_c as a function of d. This may be explained by going back to the phase diagram in Fig. 6 and noticing that (for $T/T_c \approx 0$) the maximum ϕ for the π phase region corresponds to a junction width $d/\xi \approx 1.35$ (up to periodicity). For any other junction width, e.g., $d/\xi = 1.25$ as used in the figures, the π state will be unrealizable at $T=0$ for even lower values of ϕ. This results in the inequality that ϕ_c for thermally induced oscillations is always less than or equal to ϕ_c for width-induced oscillations.

Another point on which the thermally induced 0-π oscillations differ from those obtained by varying the junction width or the misorientation angle is the remarkably stronger dependence on the spin-flip scattering rate. Increasing g shifts the transition point significantly to the left and furthermore strongly influence the ratios $I_c(g>0)/I_c(0)$. Similar findings were reported in Ref. 47.

So far, we have not considered the dependence of the critical current on the misorientation angle while simultaneously going away from the limiting case of $T=0$. In principle the phase diagrams presented might readily be generalized to a three-dimensional d-ϕ-T phase diagram, but we justify the omittance of this by arguing that the phase diagram of the system does not contain many interesting new features not already contained in the two-dimensional projection presented here. However, as is clearly visible in the phase diagram for $T/T_c = 0.5$ as shown in Fig. 9, the critical angle is exactly $\phi_c = \pi/2$, in full agreement with the analysis done in Ref. 28. Another development as T increases is the π region obtaining a more symmetric shape, also this in agreement with Ref. 28.

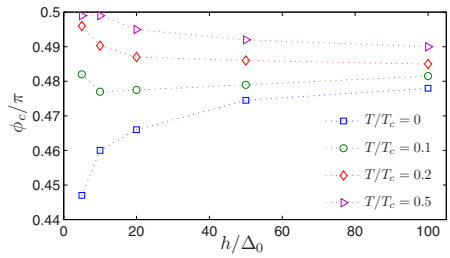

FIG. 7. (Color online) Plot of the critical angle ϕ_c at which the 0-π oscillations disappear, as a function of the exchange splitting h, for a number of temperatures. Spin-flip scattering is neglected for simplicity $g=0$.

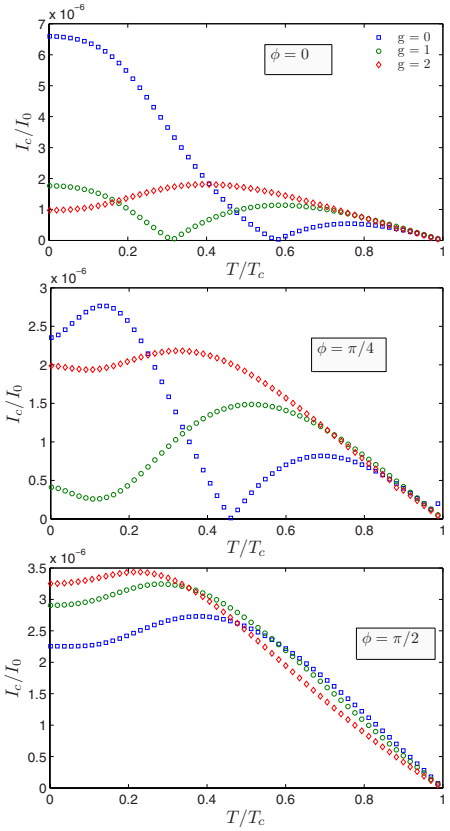

FIG. 8. (Color online) Plot of the temperature dependence of the critical current for several values of the spin-flip scattering rate, which is here taken to be uniaxial in spin space. The junction width is given by the value $d/\xi = 1.25$.

C. Enhancement effect

As was seen in Fig. 5, there is a significant difference between the current in the parallel configuration $\phi=0$ and the antiparallel $\phi=\pi$. The ratio between these two critical currents $I_c(\phi=\pi)/I_c(\phi=0)$ is plotted as a function of the junction width in Fig. 10. The fact that one always observes 0-π oscillations for varying d in the parallel case, but never in the antiparallel, leads to a divergence of the ratio at certain val-

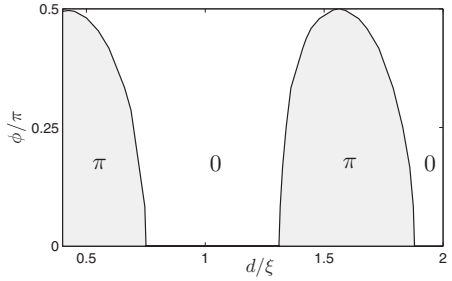

FIG. 9. Phase diagram of the Josephson junction for temperature $T/T_c=0.5$ showing the occupation of the 0 state and the π state in width-misorientation parameter space in a similar manner as Fig. 6 does for zero temperature. For the region given by $\phi \in [\pi/2, 3\pi/2]$, the π state is completely absent. We have here set the spin-flip scattering strength to zero $g=0$.

ues of the junction width, since $I_c(0)$ drops to zero at this transition point while $I_c(\pi)$ remains finite for all values of d. We note also that one will always have $I_c(\pi) > I_c(0)$, but the critical current is a monotonously increasing function of ϕ up to $\phi=\pi$ only in the case that the system is in the 0 state for $\phi=0$.

This enhancement of the Josephson current by switching the direction of magnetization may possibly be utilized in a device for controlling the magnitude of the current, if the junction is tuned to the vicinity of a transition point. A similar effect was mentioned by Golubov *et al.*[26] who considered the exchange field h as the variable parameter, but to our knowledge it has not yet been pointed out how this effect may be applied by tuning the junction width or the temperature.

IV. DISCUSSION

Above, we have neglected the spatial depletion of the superconducting order parameter near the S/F interfaces. This approximation is expected to be excellent in the case of a low-transparency interface.[48] Moreover, it is well known that a magnetic-flux threading in a Josephson junction in general gives rise to a Fraunhofer modulation of the current as a function of the flux.[49] We here neglect this modification by assuming that the flux constituted by the ferromagnetic region is sufficiently weak compared to the elementary flux quantum. This is the case for either a small enough surface area or weak enough magnetization, but neither of these preclude the possibility of having an appreciable energy *exchange splitting* between the majority and minority-spin bands.

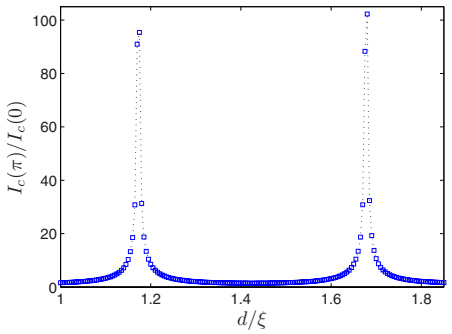

FIG. 10. (Color online) Plot of the ratio between the critical current in the antiparallel $[I_c(\phi=\pi)]$ and parallel $[I_c(\phi=0)]$ orientations as a function of width d. We have set $g=0$, but the behavior is qualitatively identical for $g>0$.

In the limit of antiparallel orientation, the π state will become disallowed because the effect of the ferromagnetic layers cancels, effectively giving a S/N/S junction. However, remembering the symmetry requirements around $\phi=\pi$ and the possibility that also partial cancellation is sufficient to render the sign change in $I_{J,0}$ impossible, we realize that 0-π oscillations may vanish for two intermediate angles $\phi = \pm \phi_c$ with $0 < \phi_c < \pi$. The partial cancellation of the exchange fields commences at $\phi \geq \pi/2$, which may provide a clue as to why the critical angle is always in the vicinity of $\phi=\pi/2$ as seen in Fig. 7. Note that although the 0-π oscillations vanish above the critical angle ϕ_c, it is evident from, e.g., Fig. 3 that the critical current does not decay monotonously even for $\phi > \phi_c$ as it would have in an S/N/S junction.

One interesting observation in our study is that although the critical angle varies, we never find $\phi_c > \pi/2$. This means that any choice of parameters that brings us away from the limit considered in Ref. 28 seems to lower ϕ_c but never increase it. A conjecture which may shed some more light on this phenomenon is that the magnetization component of the F_2 layer perpendicular to the magnetization of the F_1 layer can be viewed as an additional effective spin-flip scattering effect. It is known[38] that sufficiently strong spin-flip scattering may remove the oscillations in the anomalous Green's function entirely, thereby inhibiting 0-π oscillations. This effect will be at its strongest for $\phi \to \pi/2$, which may account for the somewhat surprising fact that ϕ_c always remains close to $\phi=\pi/2$. Combined with the effective cancellation of the magnetization described in the previous paragraph, this also serves as a possible explanation why the π state is forbidden for the orientations $\pi/2 < \phi < \pi$. To gain further understanding of the phase diagram of multilayer SFS junctions, we suggest to extend the study to a trilayer model similar as that studied in Ref. 29, but where the three layers have equal thicknesses. If one fixes the middle layer and varies the orientation of the leftmost and rightmost layers, the possible existence and value of a critical misorientation angle would give some hints to the origin of this phenomenon also in our bilayer system.

Finally, we would like to present a decomposition of the current to serve as the basis for a discussion on the long-range contributions to the Josephson current. It can be shown easily from the formula for the Josephson current in Eq. (22) that one may rewrite $M_+ + M_- = M_t - M_s$, where M_s and M_t are expressed exclusively by the components f_s and f_t of the Green's function, respectively. It can furthermore be shown that for the ESP components one gets $M_\uparrow = M_\downarrow \equiv M_\sigma$. One may in this manner decompose the current as

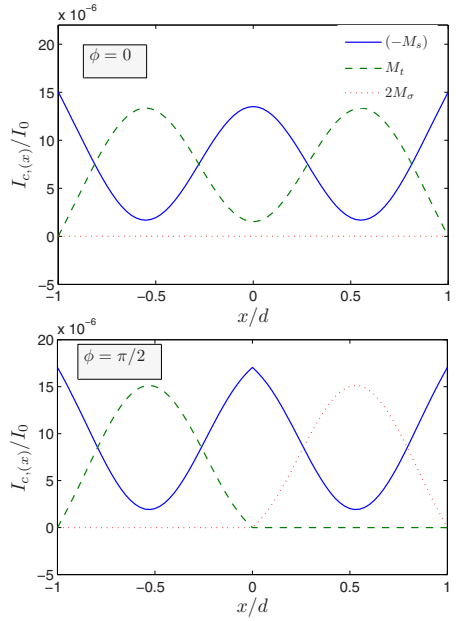

FIG. 11. (Color online) Spatial dependence through the ferromagnet for the separate contributions to the critical current, as decomposed in Eq. (27). $I_{c,(x)}$ refers to $I_{c,s}$, $I_{c,t}$, and $I_{c,\sigma}$, with contributions to the integrand from the components $[-M_s(\varepsilon)]$, $M_t(\varepsilon)$, and $2M_\sigma(\varepsilon)$, respectively. The current was evaluated for a junction width given by $d/\xi=1.0$ and temperature given by $T/T_c=0.4$, and spin-flip scattering is neglected for simplicity ($g=0$).

$$I_c/I_0 = (I_{c,s} + I_{c,t} + I_{c,\sigma})/I_0 = \int_{-\infty}^{\infty} d\varepsilon \, \mathrm{Re}\{[-M_s(\varepsilon)] + [M_t(\varepsilon)] + [2M_\sigma(\varepsilon)]\} \times \tanh(\beta\varepsilon/2). \quad (27)$$

While the total current is easily shown in our framework to be constant throughout the junction, the separate components given above need not be, and the spatial dependence of each contribution is plotted in Fig. 11 for selected parameter values. For parallel orientation, one naturally finds that the ESP correlations do not contribute to the current at all. For $\phi = \pi/2$, where the ESP contribution is naively expected to be at its maximum, we find that the OSP triplet contribution however, is exactly zero throughout F_2. That M_t and $2M_\sigma$ seem to change roles at $x=0$ can be explained in a natural way by remembering that ultimately, the quantization axis was taken to be $\|\hat{\mathbf{z}}$ for all x. For a quantization axis $\|\hat{\mathbf{y}}$, however, the components considered as ESP in the former case would here correspond to OSP components, having spin projection $S_y=0$.

The above argument may be used to clarify a point regarding the contribution to the current from LRTC. Reference 29 claims that a long-range component of the critical current does not appear in a SF_1F_2S structure even with noncollinear magnetizations, which seems at odds with our observation in Fig. 11 of a nonzero ESP component to the current in F_2. It is however important to maintain the distinction between the ESP contribution to the current and a LRTC contribution. As explained in the case of $\phi=\pi/2$, the total triplet contribution is equal for the two magnetic layers, but appears as an ESP component in F_2 only because of the choice of quantization axis. Therefore, the ESP contribution in F_2 is equivalent to the OSP contribution in F_1 and thus cannot be regarded as a true long-range component. A long-range Josephson effect is defined by the absence of the exchange field in the exponent for the relevant Green's functions, making its decay length in a ferromagnet comparable to that of a normal metal. Inspecting Eqs. (18) and (9), we see that this certainly is not the case for $\phi=\pi/2$.

The discussion concerning the different contributions to the Josephson current may also hold an important clue concerning the 0-π oscillations. When inspecting the symmetry components separately, we observed that there can be 0-π oscillations of both the singlet and the triplet components simultaneously. If this is generally the case, one idea is to investigate for which parameters these two contributions act constructively and for which they act destructively. In this way the relative interplay of the different symmetry components of I_c may offer an explanation of the behavior of the critical angle ϕ_c for which the 0-π oscillations of the total critical current disappear.

V. SUMMARY

In conclusion, we have investigated the 0-π oscillations of the critical current in a diffusive SF_1F_2S Josephson junction with noncollinear magnetization, where the effects of noncollinearity and spin-flip scattering have been studied in particular. The introduction of spin-flip scattering does not change the Josephson current dramatically, so the phase diagrams presented above for zero spin-flip scattering would therefore not be qualitatively changed much by setting $g>0$. Also, comparing isotropic and uniaxial spin-flip scatterings, we found that the effect of these was very similar both qualitatively and quantitatively.

Oscillations of the critical current for varying junction width disappear when the relative angle of magnetization passes a critical value ϕ_c, making the π state unattainable regardless of choice of the other parameters. This critical angle equals $\pi/2$ in the limit of relatively high temperatures ($T/T_c \simeq 1$), but is lowered below $\pi/2$ when the temperature is low *and* the exchange field is small simultaneously. These dependencies on the various parameters can rather easily be read out of phase diagrams of the kind we have presented. A straightforward analytical approach to the behavior of the critical angle is challenging due to the many variables in our system, but we have discussed several ways by which its origin can be better understood.

With regard to the effect of finite interface transparencies, we have not found any signs throughout our investigations implying that the results of Ref. 28 change in any significant way. Our mapping of the relevant parameter regimes does however serve as a starting point for looking for new inter-

esting effects that may appear upon varying the parameters kept fixed in our case, i.e., the transparency γ and the exchange field h in particular. A natural course for a continuation of this work would be expanding the system from a bilayer ferromagnet to a trilayer, similar to the Josephson junction considered in Ref. 29, where the relevant parameter regime for a significant LRTC contribution to the Josephson current was found. It might be interesting to see how LRTC manifests in our framework of symmetry components to I_c and to investigate for what region in parameter space the π state can be realized in such a system.

ACKNOWLEDGMENTS

J.L. thanks T. Yokoyama and M. Blamire for useful discussions. J.L. and A.S. were supported by the Research Council of Norway Grants No. 158518/432 and No. 158547/431 (NANOMAT), and Grant No. 167498/V30 (STORFORSK).

[1] F. S. Bergeret, A. F. Volkov, and K. B. Efetov, Rev. Mod. Phys. **77**, 1321 (2005).
[2] A. I. Buzdin, Rev. Mod. Phys. **77**, 935 (2005).
[3] L. B. Ioffe, V. B. Geshkenbein, M. V. Feigel'man, A. L. Fauchere, and G. Blatter, Nature (London) **398**, 679 (1999).
[4] G. Binasch, P. Grunberg, F. Saurenbach, and W. Zinn, Phys. Rev. B **39**, 4828 (1989); M. N. Baibich, J. M. Broto, A. Fert, F. Nguyen Van Dau, F. Petroff, P. Eitenne, G. Creuzet, A. Friederich, and J. Chazelas, Phys. Rev. Lett. **61**, 2472 (1988).
[5] F. S. Bergeret, A. F. Volkov, and K. B. Efetov, Phys. Rev. Lett. **86**, 3140 (2001).
[6] P. G. de Gennes, Rev. Mod. Phys. **36**, 225 (1964).
[7] L. N. Bulaevskii, V. V. Kuzii, and A. A. Sobyanin, Pis'ma Zh. Eksp. Teor. Fiz. **25**, 314 (1977) [JETP Lett. **25**, 290 (1977)].
[8] A. I. Buzdin, L. N. Bulaevskii, S. V. Panyukov, Pis'ma Zh. Eksp. Teor. Fiz. **35**, 147 (1982).
[9] V. V. Ryazanov, V. A. Oboznov, A. Yu. Rusanov, A. V. Veretennikov, A. A. Golubov, and J. Aarts, Phys. Rev. Lett. **86**, 2427 (2001).
[10] T. Kontos, M. Aprili, J. Lesueur, and X. Grison, Phys. Rev. Lett. **86**, 304 (2001).
[11] Yu. Gusakova, M. Yu. Kupriyanov, and A. A. Golubov, Pis'ma Zh. Eksp. Teor. Fiz. **83**, 487 (2006).
[12] F. S. Bergeret, A. F. Volkov, and K. B. Efetov, Phys. Rev. B **75**, 184510 (2007).
[13] F. S. Bergeret, A. F. Volkov, and K. B. Efetov, Phys. Rev. B **64**, 134506 (2001).
[14] T. Champel, T. Löfwander, and M. Eschrig, Phys. Rev. Lett. **100**, 077003 (2008).
[15] M. L. Kulic, C. R. Phys. **7**, 4 (2006); M. L. Kulic and I. M. Kulic, Phys. Rev. B **63**, 104503 (2001).
[16] A. F. Volkov, F. S. Bergeret, and K. B. Efetov, Phys. Rev. Lett. **90**, 117006 (2003).
[17] Z. Pajovic, M. Bozovic, Z. Radovic, J. Cayssol, and A. Buzdin, Phys. Rev. B **74**, 184509 (2006).
[18] Y. S. Barash, I. V. Bobkova, and T. Kopp, Phys. Rev. B **66**, 140503(R) (2002).
[19] J. Linder and A. Sudbø, Phys. Rev. B **76**, 064524 (2007).
[20] N. M. Chtchelkatchev, W. Belzig, and C. Bruder, JETP Lett. **75**, 642 (2002).
[21] X. Li, Z. Zheng, D. Y. Xing, G. Sun, and Z. Dong, Phys. Rev. B **65**, 134507 (2002).
[22] T. Löfwander, T. Champel, and M. Eschrig, Phys. Rev. B **75**, 014512 (2007).
[23] Ya. V. Fominov, A. F. Volkov, and K. B. Efetov, Phys. Rev. B **75**, 104509 (2007).
[24] B. Crouzy, S. Tollis, and D. A. Ivanov, Phys. Rev. B **76**, 134502 (2007).
[25] Y. M. Blanter and F. W. J. Hekking, Phys. Rev. B **69**, 024525 (2004).
[26] A. A. Golubov, M. Yu. Kupriyanov, and Ya. V. Fominov, Pis'ma Zh. Eksp. Teor. Fiz. **75**, 223 (2002) [JETP Lett. **75**, 190 (2002)].
[27] V. N. Krivoruchko and E. A. Koshina, Phys. Rev. B **64**, 172511 (2001).
[28] B. Crouzy, S. Tollis, and D. A. Ivanov, Phys. Rev. B **75**, 054503 (2007).
[29] M. Houzet and A. I. Buzdin, Phys. Rev. B **76**, 060504(R) (2007).
[30] Z. Radovic, N. Lazarides, and N. Flytzanis, Phys. Rev. B **68**, 014501 (2003).
[31] J. W. Serene and D. Rainer, Phys. Rep. **101**, 221 (1983).
[32] J. Rammer and H. Smith, Rev. Mod. Phys. **58**, 323 (1986).
[33] A. M. Zagoskin, *Quantum Theory of Many-Body Systems* (Springer, New York, 1998).
[34] W. Belzig, F. K. Wilhelm, C. Bruder, G. Schön, and A. D. Zaikin, Superlattices Microstruct. **25**, 1251 (1999).
[35] J. P. Morten, M.S. thesis, Norwegian University of Science and Technology, 2003.
[36] A. J. Leggett, Rev. Mod. Phys. **47**, 331 (1975).
[37] K. Usadel, Phys. Rev. Lett. **25**, 507 (1970).
[38] J. Linder and A. Sudbø, Phys. Rev. B **76**, 214508 (2007).
[39] M. Yu. Kupriyanov and V. F. Lukichev, Zh. Eksp. Teor. Fiz. **94**, 139 (1988) [Sov. Phys. JETP **67**, 1163 (1988)].
[40] It should be noted that the K-L boundary conditions may also be used in the special case of a barrier with perfect transparency, yielding continuity of the Green's function and its derivative.
[41] A. K. Nguyen, R. V. Shchelushkin, and A. Brataas, Phys. Rev. Lett. **97**, 136603 (2006).
[42] E. A. Demler, G. B. Arnold, and M. R. Beasley, Phys. Rev. B **55**, 15174 (1997).
[43] H. Sellier, C. Baraduc, F. Lefloch, and R. Calemczuk, Phys. Rev. Lett. **92**, 257005 (2004).
[44] A. A. Golubov, M. Yu. Kupriyanov, and E. Il'ichev, Rev. Mod. Phys. **76**, 411 (2004).
[45] J. Linder, T. Yokoyama, and A. Sudbø, Phys. Rev. B **77**, 174507 (2008).
[46] R. C. Dynes, V. Narayanamurti, and J. P. Garno, Phys. Rev. Lett. **41**, 1509 (1978).
[47] J. Linder, T. Yokoyama, and A. Sudbø, Phys. Rev. B **77**, 174514 (2008).
[48] C. Bruder, Phys. Rev. B **41**, 4017 (1990).
[49] K. Fossheim, and A. Sudbø, *Superconductivity: Physics and Applications* (Wiley, New York, 2004), Chap. 5.

Paper XIX

Nontrivial interplay of superconductivity and spin-orbit coupling in noncentrosymmetric ferromagnets.

Physical Review B **78**, 172502 (2008).

Nontrivial interplay of superconductivity and spin-orbit coupling in noncentrosymmetric ferromagnets

Jacob Linder,[1] Andriy H. Nevidomskyy,[2] and Asle Sudbø[1]
[1]*Department of Physics, Norwegian University of Science and Technology, N-7491 Trondheim, Norway*
[2]*Department of Physics and Astronomy, Rutgers University, Piscataway, New Jersey 08854-8019, USA*
(Received 29 August 2008; revised manuscript received 24 September 2008; published 5 November 2008)

Motivated by the recent discoveries of ferromagnetic and noncentrosymmetric superconductors, we present a mean-field theory for a superconductor that *both* lacks inversion symmetry and displays ferromagnetism, a scenario which is believed to be realized in UIr. We study the interplay between the order parameters to clarify how superconductivity is affected by the presence of ferromagnetism and spin-orbit coupling. One of our key findings is that the spin-orbit coupling seems to enhance both ferromagnetism and superconductivity in all spin channels. We discuss our results in the context of the heavy fermion superconductor UIr and analyze possible symmetries of the order parameter by the group theory method.

DOI: 10.1103/PhysRevB.78.172502 PACS number(s): 74.20.Rp, 74.20.Mn, 74.50.+r, 74.70.Tx

In the past decade, a number of superconductors have been discovered that are called "unconventional" as they fall outside the Bardeen-Cooper-Schrieffer (BCS) paradigm of electron-phonon mediated pairing with an isotropic gap. Of those, UPt_3 (Ref. 1) and Sr_2RuO_4 (Ref. 2) were the compounds to have been confirmed as triplet *p*-wave superconductors. More recently, a ferromagnetic (FM) superconductor was discovered in UGe_2 under pressure,[3] where the presence of an internal FM moment strongly suggests that only the equal-spin triplet pairing survives. In this latter example both the time-reversal and the gauge symmetry due to SC order are spontaneously broken, which made UGe_2, as well as its cousins URhGe (Ref. 4) and UCoGe (Ref. 5) an exciting avenue for theoretical and experimental research.

For spin-triplet pairing, Anderson noticed[6] that inversion symmetry is required to obtain a pair of degenerate states $c_{\mathbf{k}}^{\dagger}|0\rangle$ and $c_{-\mathbf{k}}^{\dagger}|0\rangle$ capable of forming a Cooper pair. It was therefore surprising that superconductivity was discovered in the heavy fermion compound $CePt_3Si$ which lacks inversion symmetry.[7] It soon became clear, however, that in the case of a noncentrosymmetric crystal, the spin-orbit coupling (SOC) mixes different spin states, so that the division into triplet and singlet symmetry of the SC order parameter becomes meaningless. A bulk of theoretical work exists that has provided a symmetry-based phenomenology to explain this in details.[8–12] The symmetry of the superconducting (SC) gap in this and other unconventional superconductors is presently a matter of intense investigation.[13–16]

An intriguing question is what happens if time-reversal symmetry is broken in a crystal that lacks a center of inversion. Can such a material become a superconductor? This question was answered affirmatively when superconductivity was discovered in the noncentrosymmetric ferromagnetic compound UIr under pressure.[17] The symmetry of the SC order parameter and its connection to FM nevertheless remains unclear, which motivates the present study. Spontaneous symmetry breaking in condensed-matter systems is conceptually of immense importance, as it may provide clues for what could be expected in systems belonging to vastly different areas of physics. The study of a condensed-matter system such as UIr with multiple broken symmetries is likely to have impact on a number of disciplines of physics, including such disparate phenomena as mass differences between elementary particles and extremely dilute ultracold atomic gases.

In this Brief Report, we study a model system of a noncentrosymmetric superconductor with substantial spin-orbit coupling, which at the same time exhibits itinerant ferromagnetism. The origin of the SOC may be either that the crystal structure lacks a center of inversion, such as in UIr, or due to a thin-film geometry where the breakdown of inversion symmetry near the surface induces transverse electrical fields, leading to the well-known Rashba SOC.[18] Our model should therefore be relevant both to the noncentrosymmetric and centrosymmetric heavy fermion compounds, since the SOC is considerable in any case due to the high atomic number. Specifically, materials that exhibit coexistence of SC and FM order and where SOC is large include UGe_2,[3] URhGe,[4] UCoGe,[5] and UIr.[17] For this model, we construct a mean-field theory, solve the saddle-point equations for the order parameters, and study the effect of spin-orbit coupling on the superconducting order parameters. Finally, we discuss application of this model to the case of UIr.

To label the SOC+FM split bands, it is possible to introduce a *pseudospin* basis in which the normal-state Hamiltonian is diagonalized. In the original spin basis, the SC matrix order parameter is characterized, in analogy to the *p*-wave state,[19] by a vector $\mathbf{d}_{\mathbf{k}}$ and a scalar $\mathbf{\Delta}_{\mathbf{s}}$ so that $\Delta_{\alpha\beta}(\mathbf{k}) = i\Delta_s\sigma_y + [(i\mathbf{d}_{\mathbf{k}}\cdot\boldsymbol{\sigma})\sigma_y]_{\alpha\beta}$. Note that, unlike the usual *p*-wave SC, a singlet component of the gap will also be present since antisymmetric SOC in general mixes the parity of the order parameter.

We now proceed to write down the effective Hamiltonian $\hat{H} = \hat{H}_N + \hat{H}_{\mathrm{SC}}$ for our system. In the normal state, the Hamiltonian in momentum-space reads[20]

$$\hat{H}_N = H_0 + \sum_{\mathbf{k}\alpha\beta} [c_{\mathbf{k}\alpha}^{\dagger}(\varepsilon_{\mathbf{k}}\hat{1} - h\hat{\sigma}_z + \hat{\boldsymbol{\sigma}}\cdot\mathbf{g}_{\mathbf{k}})_{\alpha\beta}c_{\mathbf{k}\beta}], \qquad (1)$$

where $H_0 = INM^2/2$. Above, the dispersion relation $\varepsilon_{\mathbf{k}}$ is measured from chemical potential μ, and the magnetization $M = |\mathbf{M}|$ is taken along the easy axis, while $h = IM$ is the

exchange splitting of the bands and $\mathbf{g}_\mathbf{k}$ is the SOC vector. When superconductivity coexists with FM, the SC pairing is generally believed to be nonunitary,[21] characterized by $\mathbf{d}_\mathbf{k}\times\mathbf{d}_\mathbf{k}^*\neq 0$. In such a scenario, the SC order parameter couples to the spontaneous magnetization $\mathbf{M}$ through a term $\gamma\mathbf{M}\cdot\mathbf{d}_\mathbf{k}\times\mathbf{d}_\mathbf{k}^*$ in the free energy, where the sign of γ is determined by the gradient of the DOS at Fermi level[22] and $\langle\mathbf{S}_\mathbf{k}\rangle = i\mathbf{d}_\mathbf{k}\times\mathbf{d}_\mathbf{k}^*$ is the spin associated with the Cooper pair. Thus, for $\gamma<0$ it is expected that a SC pairing state obeying $i\mathbf{d}_\mathbf{k}\times\mathbf{d}_\mathbf{k}^*\|\mathbf{M}$ is energetically favored, implying that $\mathbf{d}_\mathbf{k}$ must be complex valued. Our model captures broken time-reversal symmetry in addition to antisymmetric SOC. As shown by Anderson,[6] the presence of the latter is detrimental to spin-triplet SC pairing state, unless $\mathbf{d}_\mathbf{k}\|\mathbf{g}_\mathbf{k}$. In our case, it is obvious that a nonunitary SC pairing state cannot satisfy this condition since $\mathbf{d}_\mathbf{k}$ is complex, whereas $\mathbf{g}_\mathbf{k}$ must be real for the Hamiltonian to be Hermitian.

The SOC vector reads $\mathbf{g}_\mathbf{k}=-\mathbf{g}_{-\mathbf{k}}$, and we introduce $g_\mathbf{k}=\mathbf{g}_{\mathbf{k},x}-i\mathbf{g}_{\mathbf{k},y}$ for later use. We consider the SOC in the Rashba form, namely $\mathbf{g}_\mathbf{k}=\lambda(k_y,-k_x,0)$. This corresponds to a situation where an asymmetric potential gradient is present along the $\hat{\boldsymbol{z}}$ axis, and is also the scenario realized in noncentrosymmetric $CePt_3Si$.[11] We have introduced fermion operators $\{\hat{c}_{\mathbf{k}\sigma}\}$ in a basis $\hat{\varphi}_\mathbf{k}=[c_{\mathbf{k}\uparrow},c_{\mathbf{k}\downarrow}]^T$.

Diagonalizing the normal-state Hamiltonian yields the quasiparticle excitations $\tilde{E}_{\mathbf{k}\sigma}=\varepsilon_\mathbf{k}-\sigma\sqrt{h^2+\lambda^2k^2}$, which due to the SOC are characterized by the pseudospin $\sigma=\pm 1$. For later use, we define $\mathcal{N}_\mathbf{k}=[1+\lambda^2k^2/(h+\sqrt{h^2+\lambda^2k^2})^2]^{-1/2}$. The superconducting pairing is now assumed to occur between the excitations described by $\hat{\tilde{\varphi}}_\mathbf{k}$. Due to the presence of antisymmetric spin-orbit coupling, this automatically leads to a mixed-parity SC state in the original spin basis. To see this, we introduce

$$\hat{H}_{\mathrm{SC}}=\frac{1}{2N}\sum_{\mathbf{k}\mathbf{k}'\sigma}V_{\mathbf{k}\mathbf{k}'\sigma}\tilde{c}^\dagger_{\mathbf{k}\sigma}\tilde{c}^\dagger_{-\mathbf{k}\sigma}\tilde{c}_{-\mathbf{k}'\sigma}\tilde{c}_{\mathbf{k}'\sigma}, \tag{2}$$

and perform a standard mean-field decoupling, which after an additional diagonalization yields the total Hamiltonian in the superconducting state: $\hat{H}=H_0+\Sigma_{\mathbf{k}\sigma}(\tilde{E}_{\mathbf{k}\sigma}-E_{\mathbf{k}\sigma}-\tilde{\Delta}_{\mathbf{k}\sigma}\tilde{b}^\dagger_{\mathbf{k}\sigma}+2\eta^\dagger_{\mathbf{k}\sigma}\eta_{\mathbf{k}\sigma})/2$, where $E_{\mathbf{k}\sigma}=(\tilde{E}^2_{\mathbf{k}\sigma}+|\tilde{\Delta}_{\mathbf{k}\sigma}|^2)^{1/2}$ and $\{\eta^\dagger_{\mathbf{k}\sigma},\eta_{\mathbf{k}\sigma}\}$ are fermion operators in the new basis. The merit of this procedure is that we can now obtain simple self-consistency equations for the gaps $\tilde{\Delta}_{\mathbf{k}\sigma}$, which may then be transformed back to the gaps in the original spin-basis $\hat{\varphi}_\mathbf{k}$ by means of the unitary transformation $P_\mathbf{k}$. We assume a chiral p-wave symmetry for the gaps with a corresponding pairing potential $V_{\mathbf{k}\mathbf{k}'\sigma}=-g_{\mathrm{sc}}e^{i\sigma(\phi-\phi')}$, where $\tan\phi=k_x/k_y$. The motivation for this is that this choice ensures that the condition $\mathbf{d}_\mathbf{k}\|\mathbf{g}_\mathbf{k}$ is satisfied exactly for $h\to 0$, and corresponds to a fully gapped Fermi surface which favors the condensation energy. The gaps obtain the form $\tilde{\Delta}_{\mathbf{k}\sigma}=-\sigma\tilde{\Delta}_{\sigma,0}e^{i\sigma\phi}$ and we find a self-consistency equation of the standard BCS form with a cutoff ω on the pairing-fluctuation spectrum which we do not specify further. Moreover, $N^\sigma(\varepsilon)$ is the pseudospin-resolved density of states (DOS) for the $\tilde{E}_{\mathbf{k}\sigma}$ ($\sigma=\pm$) bands of the quasiparticle excitations.[23] Introducing the total DOS at the Fermi level for a normal metal $N_0=mV\sqrt{2m\mu}/\pi^2$ and defining $c=g_{\mathrm{sc}}N_0/2$, the analytical solution for the gaps reads $\tilde{\Delta}_{\sigma,0}=2\omega\exp\{-1/[cR_\sigma(0)]\}$, $R_\sigma(\varepsilon)=2N^\sigma(\varepsilon)/N_0$. With the analytical solution for $\tilde{\Delta}_{\sigma,0}$ in hand, we may exploit the unitary transformation $P_\mathbf{k}$ to express the superconducting gaps in the original spin basis as follows:

$$\begin{aligned}
\Delta_{\mathbf{k}\uparrow} &= -e^{i\phi}[\tilde{\Delta}_{\uparrow,0}(\mathcal{N}^\uparrow_\mathbf{k})^2+\tilde{\Delta}_{\downarrow,0}(\mathcal{N}^\downarrow_\mathbf{k})^2\lambda^2k^2_\downarrow(0)\Lambda^2_{\mathbf{k}\downarrow}],\\
\Delta_{\mathbf{k}\downarrow} &= e^{-i\phi}[\tilde{\Delta}_{\downarrow,0}(\mathcal{N}^\downarrow_\mathbf{k})^2+\tilde{\Delta}_{\uparrow,0}(\mathcal{N}^\uparrow_\mathbf{k})^2\lambda^2k^2_\uparrow(0)\Lambda^2_{\mathbf{k}\uparrow}],\\
\Delta_{\mathbf{k}\uparrow\downarrow} &= -\sum_\sigma\tilde{\Delta}_{\sigma,0}(\mathcal{N}^\sigma_\mathbf{k})^2\lambda|k_\sigma(0)|\Lambda_{\mathbf{k}\sigma},\quad \sigma=\pm 1,
\end{aligned} \tag{3}$$

where we have defined $\mathcal{N}^\sigma_\mathbf{k}=\mathcal{N}_{\mathbf{k}=\mathbf{k}\sigma(0)}$ and $\Lambda_{\mathbf{k}\sigma}=[h+\sqrt{h^2+\lambda^2k^2_\sigma(0)}]^{-1}$. Note that in the original spin basis, the superconducting order parameter is in general a mixture of triplet ($\Delta_{\mathbf{k}\sigma}$) and singlet ($\Delta_{\mathbf{k}\uparrow\downarrow}$) components. The self-consistency equation for the magnetization is

$$h+\frac{\tilde{I}}{4}\sum_\sigma\int\frac{\sigma d\varepsilon R^\sigma(\varepsilon)h\varepsilon}{\sqrt{[h^2+\lambda^2k^2_\sigma(\varepsilon)](\varepsilon^2+\tilde{\Delta}^2_{\sigma,0})}}=0, \tag{4}$$

where the integration is over the bandwidth and $\tilde{I}=IN_0$. Equations (3) and (4) are the main analytical results of this work.

Let us briefly investigate some important limiting cases of Eq. (3). In the absence of spin-orbit coupling ($\lambda\to 0$), one finds $\mathcal{N}^\sigma_\mathbf{k}\to 1$ and $\Delta_{\mathbf{k}\sigma}=\tilde{\Delta}_{\mathbf{k}\sigma}$ while $\Delta_{\mathbf{k}\uparrow\downarrow}=0$, such that we reproduce the results of Refs. 20 and 24. In the absence of an exchange energy ($h\to 0$), one finds that $\mathcal{N}^\sigma_\mathbf{k}\to 1/\sqrt{2}$ and $\Delta_{\mathbf{k}\uparrow}=-e^{i\phi}(\tilde{\Delta}_{\uparrow,0}+\tilde{\Delta}_{\downarrow,0})/2$, $\Delta_{\mathbf{k}\downarrow}=e^{-i\phi}(\tilde{\Delta}_{\uparrow,0}+\tilde{\Delta}_{\downarrow,0})/2$, and $\Delta_{\mathbf{k}\uparrow\downarrow}=(\tilde{\Delta}_{\downarrow,0}-\tilde{\Delta}_{\uparrow,0})/2$. As demanded by consistency, the triplet gaps are equal in magnitude since there is no exchange field and the singlet component is nonzero since $\tilde{\Delta}_{\uparrow,0}\neq\tilde{\Delta}_{\downarrow,0}$ in general. Finally, Eq. (4) reproduces the well-known Stoner criterion $\tilde{I}\geq 1$ for the onset of FM in the absence of SOC and superconductivity ($\lambda\to 0, g_{\mathrm{sc}}\to 0$).

We now focus on the general case in which $h\neq 0$ and $\lambda\neq 0$. First of all, we must specify the range of the parameters in the problem that corresponds to a physically realistic scenario. We allow h to range, in principle, from 0 to μ, the latter denoting a fully polarized ferromagnet. As a convenient measure of the strength of SOC, we introduce the dimensionless quantity $\alpha_{\mathrm{soc}}\equiv\sqrt{2\lambda^2m}/\mu$ which has a direct physical interpretation; namely, it is the ratio of the SOC (at E_F) to the Fermi energy μ. The parameter α_{soc} is allowed to vary from 0 to δ, where δ denotes a fraction of the Fermi energy. We take $\delta=0.5$ as a sensible upper limit. Note that generically, the SOC strength at the Fermi level is different for the two quasiparticle bands, and moreover depends on h. For a given value of h, one may derive that $\lambda\leq\delta\mu/[2\mu m+\sqrt{2m^2(h^2+\delta^2\mu^2)}]^{1/2}$ ensures that the spin-orbit energy is less than $\delta\times\mu$ for both quasiparticle bands.

In Figs. 1(a)–1(d), we present the self-consistent solutions for the order parameters in Eqs. (3) and (4) as a function of

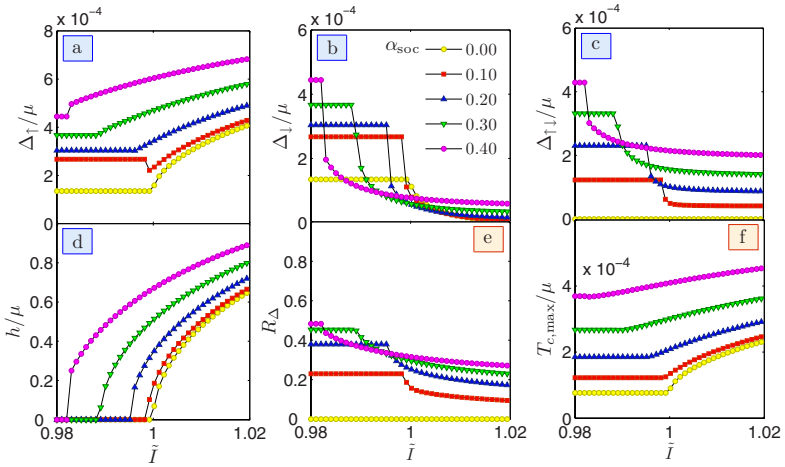

FIG. 1. (Color online) Self-consistent solution of the order parameters [(a)–(d)] as a function of the FM exchange parameter $\tilde{I}$, the ratio between the singlet and triplet gaps (e) $R_\Delta=\Delta_{\uparrow\downarrow}/(\Delta_\uparrow+\Delta_\downarrow)$, and the maximal critical temperature (f) $T_{c,\max}$ as a function of the FM exchange parameter $\tilde{I}$.

the FM exchange parameter $\tilde{I}$ for several values of $\alpha_{\rm soc}$. We have defined $\Delta_\sigma=|\Delta_{\mathbf{k}\sigma}|$ and $\Delta_{\uparrow\downarrow}=|\Delta_{\mathbf{k}\uparrow\downarrow}|$, and fixed $\omega/\mu=0.01$ and $m/\mu=5\times10^4$ with $c=0.2$, which are standard choices. For $\alpha_{\rm soc}=0$, the onset of FM occurs at $\tilde{I}=1.0$ which lifts the degeneracy of $\Delta_\uparrow$ and $\Delta_\downarrow$, while $\Delta_{\uparrow\downarrow}$ is always zero. Upon increasing $\alpha_{\rm soc}$, it is interesting to note that the PM-FM transition occurs at lower values of $\tilde{I}$, indicating that spin-orbit coupling favors ferromagnetic ordering. For $\alpha_{\rm soc}\neq0$, it is seen that $\Delta_{\uparrow\downarrow}$ is also nonzero, although it becomes suppressed at the onset of ferromagnetism. A common feature for all gaps is that they increase with $\alpha_{\rm soc}$ in the absence of ferromagnetism *and* deep inside the ferromagnetic phase $\tilde{I}\geq1.02$. In the intermediate regime, there are crossovers between the gaps for different values of $\alpha_{\rm soc}$ due to the different onsets of ferromagnetic order. By comparing the behavior between the gaps for increasing $\tilde{I}$ with $\alpha_{\rm soc}\neq0$, one infers that $\Delta_\downarrow$ and $\Delta_{\uparrow\downarrow}$ eventually saturate at a constant nonzero value, while $\Delta_\uparrow$ continues to increase steadily. This is quite different from the case when $\alpha_{\rm soc}=0$, where the minority spin-gap goes to zero rapidly with increasing $\tilde{I}$. This seems to suggest that the presence of spin-orbit coupling in the system ensures the survival of the minority-spin gap $\Delta_\downarrow$ and the singlet gap $\Delta_{\uparrow\downarrow}$ even though the FM exchange energy becomes strong.

In Figs. 1(e) and 1(f), we plot the ratio of the singlet and triplet gaps, defined as $R_\Delta=\Delta_{\uparrow\downarrow}/(\Delta_\uparrow+\Delta_\downarrow)$, and the maximal critical temperature $T_{c,\max}$ for the onset of superconductivity. It is seen from the left panel that R_Δ increases with $\alpha_{\rm soc}$ in the PM regime, suggesting that the singlet component becomes more prominent in the system as compared to the triplet gaps. However, at the onset of FM order, R_Δ decreases since the singlet component becomes suppressed by the Zeeman splitting. In the right panel, one observes that $T_{c,\max}$ increases both with $\alpha_{\rm soc}$ and $\tilde{I}$. Our findings suggest that the presence of antisymmetric SOC, originating from, e.g., noncentrosymmetricity of the crystal structure, *enhances both* the tendency toward ferromagnetism and the magnitude of the SC gaps in all spin channels. In the absence of spin-orbit coupling, it was shown in Ref. 20 that the simultaneous coexistence of FM and nonunitary triplet superconductivity is the thermodynamically favored state as compared to the pure normal, FM, or SC state. Since the presence of spin-orbit coupling is seen to enhance both the FM and SC order parameters, it is reasonable to expect that the coexistent state is still thermodynamically the most favorable one even when $\alpha_{\rm soc}\neq0$.

Out of the known noncentrosymmetric superconductors, UIr is the only compound that is also a ferromagnet. This material, which is ferromagnetic at ambient pressure, develops superconductivity in a narrow pressure region around $P\sim2.6$ GPa right next to the FM-PM quantum phase transition, with a maximum SC transition temperature $T_{\rm SC}\sim0.14$ K.[17] At this pressure, the saturated magnetic moment was measured to be $0.07\mu_B$ per U atom, and such a small value clearly indicates the itinerant character of the ferromagnetism, presumably due to $5f$ electrons of uranium. UIr crystallizes in the monoclinic structure (space group $P2_1$) which lacks inversion symmetry, and the FM moment is Ising-like, oriented along the $[10\bar{1}]$ direction in the (ac) plane.

Given the proximity of the SC state in UIr to the PM transition, one may probably consider the magnetization h as a perturbation on top of the SOC-split bands. Neglecting the effect of the former, it is known[12] that even in the case of noncentrosymmetric superconductors (and $h=0$), the band energies still satisfy the relation $\varepsilon_\beta(\mathbf{k})=\varepsilon_\beta(-\mathbf{k})$ due to the time-reversal symmetry of the single-electron Hamiltonian. As a consequence, the SC order parameter on the βth sheet of the Fermi surface transforms according to one of the irreducible representations of the normal state point group. In the case of UIr, the point group $\mathbf{C}_2$ has two one-dimensional irreducible representations, denoted A and B. Then the SC order parameter is an odd function $\Delta(-\mathbf{k})=-\Delta(\mathbf{k})$ given by[25] $\Delta_\beta^{A,B}(\mathbf{k})\propto t(\mathbf{k})\phi_\beta^{A,B}(\mathbf{k})$, where $t(\mathbf{k})$ is an odd phase factor[26] and the basis functions $\phi^{A,B}$ are even in $\mathbf{k}$. Denoting the rotation axis of the $\mathbf{C}_2$ group as z (this actually corresponds to b axis in case of UIr), the even functions ϕ_A and ϕ_B can then be cast in the following form: $\phi_A(\mathbf{k})=(k_z^2+C)u_1(\mathbf{k})$, and $\phi_B(\mathbf{k})=k_z[k_xu_2(\mathbf{k})+k_yu_3(\mathbf{k})]$,

where C is some constant and $\{u_i(\mathbf{k})\}$ are arbitrary even functions of k_x, k_y, k_z. Function ϕ_A generically has no nodes, whereas ϕ_B has two point nodes at the poles ($k_x=k_y=0$) and a line of nodes at the equator. The symmetry argument does not allow one to determine which pairing channel is realized, however, the experimental observation of the strong pair-breaking effect due to disorder[17] indicates that the gap must be anisotropic, possibly favoring the gap with the nodes such as $\Delta_B(\mathbf{k})$.

One way of experimentally probing the symmetry of the superconducting order parameter in UIr would be by means of transport properties such as Josephson tunneling or point-contact spectroscopy. In particular, it has recently been shown that the presence of multiple gaps in superconductors with broken inversion symmetry should manifest itself through clear signatures at bias voltages corresponding to the sum and difference of the singlet and triplet components.[20,27,28] We expect similar behavior in the present case, at least when the ferromagnetism is weak, and point-contact spectroscopy data could then be compared with the predictions for R_Δ in Fig. 1(e). Alternatively, it should be possible to directly probe the spin texture of the superconducting order parameter by studying the effect of an externally applied magnetic field when the paramagnetic limitation dominates, e.g., in a thin-film structure, where the orbital mechanism of destroying superconductivity is suppressed.[29]

In summary, we have developed a mean-field model for a superconductor lacking inversion symmetry and displaying itinerant ferromagnetism. Specifically, we have investigated the interplay between ferromagnetism and asymmetric spin-orbit coupling and how these affect superconducting order, which in general is a mixture of a singlet and triplet components. Our main results are the analytical expression Eqs. (3) and (4) and the belonging discussion. We find that spin-orbit coupling may *enhance* superconductivity in both the singlet and triplet channels in addition to favoring the Stoner criterion for the ferromagnetic instability. We have applied these considerations to the heavy fermion superconductor UIr, together with group-theoretical analysis of the symmetry of the SC order parameter.

The authors are grateful to M. Dzero for bringing Ref. 10 to our attention. A.H.N. was supported by the U.S. NSF Grant No. DMR 0605935. J.L. and A.S. were supported by the Norwegian Research Council Grants No. 158518/431 and No. 158547/431 (NANOMAT), and Grant No. 167498/V30 (STORFORSK).

[1] R. A. Fisher, S. Kim, B. F. Woodfield, N. E. Phillips, L. Taillefer, K. Hasselbach, J. Flouquet, A. L. Giorgi, and J. L. Smith, Phys. Rev. Lett. **62**, 1411 (1989).

[2] Y. Maeno, H. Hashimoto, K. Yoshida, S. Nishizaki, T. Fujita, J. G. Bednorz, and F. Lichtenberg, Nature (London) **372**, 532 (1994).

[3] S. S. Saxena, P. Agarwal, K. Ahilan, F. M. Grosche, R. K. W. Haselwimmer, M. J. Steiner, E. Pugh, I. R. Walker, S. R. Julian, P. Monthoux, G. G. Lonzarich, A. Huxley, I. Sheikin, D. Braithwaite, and J. Flouquet, Nature (London) **406**, 587 (2000).

[4] D. Aoki, A. Huxley, E. Ressouche, D. Braithwaite, J. Flouquet, J.-P. Brison, E. Lhotel, and C. Paulsen, Nature (London) **413**, 613 (2001).

[5] N. T. Huy, A. Gasparini, D. E. de Nijs, Y. Huang, J. C. P. Klaasse, T. Gortenmulder, A. de Visser, A. Hamann, T. Gorlach, and H. v. Lohneysen, Phys. Rev. Lett. **99**, 067006 (2007).

[6] P. W. Anderson, J. Phys. Chem. Solids **11**, 26 (1959).

[7] E. Bauer, G. Hilscher, H. Michor, C. Paul, E. W. Scheidt, A. Gribanov, Y. Seropegin, H. Noel, M. Sigrist, and P. Rogl, Phys. Rev. Lett. **92**, 027003 (2004).

[8] M. M. Salomaa and G. E. Volovik, Rev. Mod. Phys. **59**, 533 (1987).

[9] H. Shimahara, Phys. Rev. B **62**, 3524 (2000).

[10] L. P. Gor'kov and E. I. Rashba, Phys. Rev. Lett. **87**, 037004 (2001).

[11] P. A. Frigeri, D. F. Agterberg, A. Koga, and M. Sigrist, Phys. Rev. Lett. **92**, 097001 (2004).

[12] K. V. Samokhin, E. S. Zijlstra, and S. K. Bose, Phys. Rev. B **69**, 094514 (2004).

[13] K. D. Nelson, Z. Q. Mao, Y. Maeno, and Y. Liu, Science **306**, 1151 (2004).

[14] H. Q. Yuan, D. F. Agterberg, N. Hayashi, P. Badica, D. Vandervelde, K. Togano, M. Sigrist, and M. B. Salamon, Phys. Rev. Lett. **97**, 017006 (2006).

[15] A. G. Lebed, Phys. Rev. Lett. **96**, 037002 (2006).

[16] I. Zutic and I. Mazin, Phys. Rev. Lett. **95**, 217004 (2005).

[17] T. Akazawa, H. Hidaka, H. Kotegawa, T. C. Kobayashi, T. Fujiwara, E. Yamamoto, Y. Haga, R. Settai, and Y. Onuki, J. Phys.: Condens. Matter **16**, L29 (2004); J. Phys. Soc. Jpn. **73**, 3129 (2004).

[18] E. I. Rashba, Sov. Phys. Solid State **2**, 1109 (1960).

[19] A. J. Leggett, Rev. Mod. Phys. **47**, 331 (1975).

[20] J. Linder and A. Sudbø, Phys. Rev. B **76**, 054511 (2007).

[21] K. V. Samokhin and M. B. Walker, Phys. Rev. B **66**, 174501 (2002); F. Hardy and A. D. Huxley, Phys. Rev. Lett. **94**, 247006 (2005).

[22] K. Machida and T. Ohmi, Phys. Rev. Lett. **86**, 850 (2001).

[23] We find that $N^\sigma(\varepsilon)=\frac{mVk_\sigma(\varepsilon)(2\pi^2)^{-1}}{1-\sigma m\lambda^2/\sqrt{\hbar^2+\lambda^2k_\sigma^2(\varepsilon)}}$, $k_\sigma(\varepsilon)=[2(\varepsilon+\mu)_m+2\lambda^2m^2+2\sigma\sqrt{\lambda^4m^4+2\lambda^2m^3(\varepsilon+\mu)+h^2m^2}]^{1/2}$.

[24] A. H. Nevidomskyy, Phys. Rev. Lett. **94**, 097003 (2005).

[25] K. V. Samokhin, E. S. Zijlstra, and S. K. Bose, Phys. Rev. B **70**, 069902(E) (2004); I. A. Sergienko and S. H. Curnoe, *ibid.* **70**, 214510 (2004).

[26] The nontrivial phase factor $t(\mathbf{k})=-t(\mathbf{k})$ is defined such that $T|\mathbf{k}\rangle=t(\mathbf{k})|-\mathbf{k}\rangle$, where T is the time-reversal operator.

[27] K. Børkje and A. Sudbø, Phys. Rev. B **74**, 054506 (2006).

[28] C. Iniotakis, N. Hayashi, Y. Sawa, T. Yokoyama, U. May, Y. Tanaka, and M. Sigrist, Phys. Rev. B **76**, 012501 (2007).

[29] Experimentally, the measurements on a single crystal of UIr so far indicate that the orbital effects of the magnetic field dominate.

Paper XX

Theory of Andreev reflection in junctions with iron-based high-T_c superconductors.

Physical Review. B **79**, 020501(R) (2009)

PHYSICAL REVIEW B **79**, 020501(R) (2009)

Theory of Andreev reflection in junctions with iron-based high-T_c superconductors

Jacob Linder and Asle Sudbø
Department of Physics, Norwegian University of Science and Technology, N-7491 Trondheim, Norway
(Received 3 October 2008; published 7 January 2009)

We construct a theory for low-energy quantum transport in normal|superconductor junctions involving the recently discovered iron-based high-T_c superconductors. We properly take into account both Andreev bound surface states and the complex Fermi-surface topology in our approach and investigate the signatures of the possible order-parameter symmetries for the FeAs lattice. Our results could be helpful in determining the symmetry of the superconducting state in the iron-pnicitide superconductors.

DOI: 10.1103/PhysRevB.79.020501 PACS number(s): 74.20.Rp, 74.50.+r, 74.70.Dd

I. INTRODUCTION

Very recently, a family of iron-based superconductors with high transition temperatures was discovered with a concomitant avalanche of both experimental and theoretical activities.[1–12] The highest T_c measured so far in this class of materials is 55 K, and many experimental reports indicate signatures of unconventional superconducting pairing. However, it remains to be clarified what the exact symmetry is for both the orbital and spin parts of the Cooper pair wave function—there has, for instance, been reports of both nodal[11] and fully gapped[10] order parameters (OPs) in the literature up to now.

Probing the low-energy quantum transport properties of superconducting materials has proven itself as a highly useful tool to access information about the symmetry of the superconducting OP.[13] The conductance spectra of normal|superconductor (N|S) junctions often contain important and clear signatures of the orbital structure of the OP. For instance, when the OP contains nodes in the tunneling direction with a sign change across the nodes on each side of the Fermi surface, the conductance will display a large zero-bias conductance peak (ZBCP) due to the presence of Andreev surface bound states.[14]

Two recent studies[10,11] utilized the method of point-contact spectroscopy in order to study the symmetry of the superconducting OP in $LaFeAsO_{0.9}F_{0.1-\delta}$ and $SmFeAsO_{0.85}F_{0.15}$, respectively. The findings were in stark contrast. Namely, the large ZBCP found in $LaFeAsO_{0.9}F_{0.1-\delta}$ gave evidence of a nodal order parameter, while the data of $SmFeAsO_{0.85}F_{0.15}$ clearly indicated a nodeless OP. In both these studies, the Blonder-Tinkham-Klapwijk[15] (BTK) framework was used to analyze the data theoretically using the extension to anisotropic pairing by Tanaka and Kashiwaya.[16] In this model, one considers a cylindrical or spherical Fermi surface with a free-electron dispersion relation, which does not account for the nontrivial multiband Fermi-surface topology and dispersion relation in the iron pnicitides. One might argue that the extended BTK model nevertheless may suffice to describe the transport properties of these materials qualitatively, but this statement clearly warrants a detailed investigation.

In this Rapid Communication, we construct a theory of low-energy quantum transport properties of the iron-based high-T_c superconductors by considering a N|S junction relevant for point-contact spectroscopy and scanning-tunneling-microscopy measurements. In doing so, we model fairly accurately the Fermi-surface topology and the associated quasiparticle dispersions in order to see how this affects the results as compared with the usual BTK paradigm. We consider several possible OP symmetries which may be realized in the iron pnicitides. We organize this work as follows. In Sec. II, we introduce the theoretical framework which is used to obtain the tunneling conductance. In Sec. III, we present our main results and a discussion of these. Finally, we summarize in Sec. IV.

II. THEORY

We adopt the minimal two-band model derived in Ref. 8 [Fig. 1(a)], in which the normal-state Hamiltonian reads

$$H_N = \sum_{\mathbf{k}\sigma} \phi^\dagger_{\mathbf{k}\sigma} \begin{pmatrix} \epsilon_{\mathbf{k}x} - \mu & \epsilon_{\mathbf{k}xy} \\ \epsilon_{\mathbf{k}xy} & \epsilon_{\mathbf{k}y} - \mu \end{pmatrix} \phi_{\mathbf{k}\sigma}, \tag{1}$$

where the fermion basis $\phi_{\mathbf{k}\sigma}=[d_{\mathbf{k}x\sigma}, d_{\mathbf{k}y\sigma}]^T$ contains the annihilation operators for electrons in the d_{xz} and d_{yz} orbitals with spin σ and wave vector $\mathbf{k}$, respectively. We have also defined $\epsilon_{\mathbf{k}x}=-2t_1c_x-2t_2c_y-4t_3c_xc_y$, $\epsilon_{\mathbf{k}xy}=-4t_4s_xs_y$, and $\epsilon_{\mathbf{k}y}=-2t_2c_x-2t_1c_y-4t_3c_xc_y$, with $c_j=\cos(k_ja)$, $s_j=\sin(k_ja)$, $j=x,y$, and a the lattice constant. By diagonalizing the above Hamiltonian, one obtains

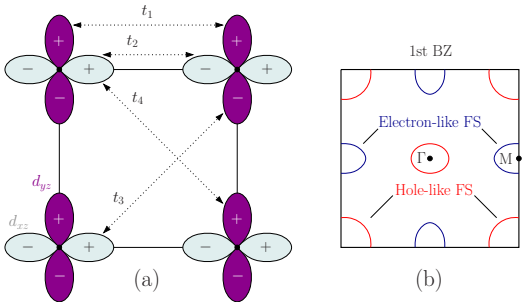

FIG. 1. (Color online) (a) Illustration of the two-dimensional FeAs plane with the d_{xz} and d_{yz} orbitals and hopping between them, as proposed in Ref. 8. (b) Sketch of the Fermi-surface topology for the long-lived quasiparticle excitations in a minimal two-band model (see main text for parameter values).

$$H_N = \sum_{\mathbf{k}\sigma} \tilde{\phi}^\dagger_{\mathbf{k}\sigma} \mathrm{diag}\{\Omega^+_{\mathbf{k}}, \Omega^-_{\mathbf{k}}\} \tilde{\phi}_{\mathbf{k}\sigma},$$

$$\Omega^\pm_{\mathbf{k}} = (\epsilon_{\mathbf{k}x} + \epsilon_{\mathbf{k}y})/2 - \mu \pm \sqrt{(\epsilon_{\mathbf{k}x} - \epsilon_{\mathbf{k}y})^2/4 + \epsilon^2_{\mathbf{k}xy}}, \quad (2)$$

where the new basis $\tilde{\phi}_{\mathbf{k}\sigma} = [\gamma^+_{\mathbf{k}\sigma}, \gamma^-_{\mathbf{k}\sigma}]^T$ consists of new fermion quasiparticle operators in the bands + and − which are hybrids of the d_{xz} and d_{yz} orbitals. The Fermi-surface topology is given by $\Omega^\pm_{\mathbf{k}} = 0$ and gives an electronlike band (+) and holelike band (−) shown in Fig. 1(b) for the choice $t_1 = -1$, $t_2 = 1.3$, $t_3 = t_4 = -0.85$, and $\mu = 1.54$, all measured in units of $|t_1|$. Our choice of parameter set is motivated by the fact that it reproduces the same Fermi-surface structure as the local-density approximation (LDA) band-structure calculations,[17] and it was also employed in Refs. 18 and 19. The new fermion operators are related to the old basis $\phi_{\mathbf{k}\sigma}$ by

$$\zeta_{\mathbf{k}} = \epsilon_{\mathbf{k}xy} / [(\epsilon_{\mathbf{k}x} - \epsilon_{\mathbf{k}y})/2 + \sqrt{(\epsilon_{\mathbf{k}x} - \epsilon_{\mathbf{k}y})^2/4 + \epsilon^2_{\mathbf{k}xy}}],$$

$$\phi^\dagger_{\mathbf{k}\sigma} P_{\mathbf{k}} = \tilde{\phi}^\dagger_{\mathbf{k}\sigma}, \quad P_{\mathbf{k}} = (1 + \zeta^2_{\mathbf{k}})^{-1/2} \times \begin{pmatrix} 1 & -\zeta_{\mathbf{k}} \\ \zeta_{\mathbf{k}} & 1 \end{pmatrix}. \quad (3)$$

We now introduce a superconducting pairing between the long-lived quasiparticles $\gamma^\lambda_{\mathbf{k}\sigma}$, with $\lambda = \pm$, which then automatically accounts for both interband and intraband pairings in the original fermion basis $\phi_{\mathbf{k}}$,

$$H_{\mathrm{SC}} = \sum_{\mathbf{k}\lambda} [\Delta^\lambda_{\mathbf{k}} (\gamma^\lambda_{\mathbf{k}\uparrow})^\dagger (\gamma^\lambda_{-\mathbf{k}\downarrow})^\dagger + \mathrm{H.c.}]. \quad (4)$$

In this way, we may diagonalize the total Hamiltonian $H = H_N + H_{\mathrm{SC}}$ by introducing a final fermion basis $\eta^\lambda_{\mathbf{k}} = [c^\lambda_{\mathbf{k}\uparrow}, c^\lambda_{-\mathbf{k}\downarrow}]^T$ describing the quasiparticle excitations in the superconducting state. After discarding unimportant constants, we find that

$$H = \sum_{\mathbf{k}\sigma\lambda} \sigma E^\lambda_{\mathbf{k}} (c^\lambda_{\mathbf{k}\sigma})^\dagger c^\lambda_{\mathbf{k}\sigma}, \quad E^\lambda_{\mathbf{k}} = [(\Omega^\lambda_{\mathbf{k}})^2 + |\Delta^\lambda_{\mathbf{k}}|^2]^{1/2}. \quad (5)$$

This result is formally identical to a two-band superconductor with gaps $\Delta^\lambda_{\mathbf{k}}$ and normal-state dispersions $\Omega^\lambda_{\mathbf{k}}$, with $\lambda = \pm$. The belonging wave functions which describe the quasiparticle excitations read

$$\Psi^\lambda_{\mathbf{k}} = \{[u^\lambda_{\mathbf{k}}, v^\lambda_{\mathbf{k}} e^{-i\phi^\lambda_{\mathbf{k}}}]^T e^{i\lambda \mathbf{k}^\lambda \cdot \mathbf{r}}, [v^\lambda_{\mathbf{k}} e^{i\phi^\lambda_{\mathbf{k}}}, u^\lambda_{\mathbf{k}}]^T e^{-i\lambda \mathbf{k}^\lambda \cdot \mathbf{r}}\},$$

$$(u^\lambda_{\mathbf{k}})^2 = 1 - (v^\lambda_{\mathbf{k}})^2 = \frac{1}{2}(1 + \sqrt{E^2 - |\Delta^\lambda_{\mathbf{k}}|^2}/E), \quad (6)$$

for quasiparticles with positive excitation energies $E \geq 0$. Here, $\mathbf{k}^\lambda$ denotes the Fermi momentum for band λ while $e^{i\phi^\lambda_{\mathbf{k}}} = \Delta^\lambda_{\mathbf{k}} / |\Delta^\lambda_{\mathbf{k}}|$.

We have now effectively described the superconducting state as a two-band model with gaps $\Delta^\pm_{\mathbf{k}}$ and normal-state dispersions $\Omega^\pm_{\mathbf{k}}$. This has allowed us to obtain a simple form for the wave functions in Eq. (6) that are to be used in the scattering problem below. The trade off for this advantage, however, is that the $\mathbf{k}$ dependence of the gap functions $\Delta^\pm_{\mathbf{k}}$ in general will become quite complicated. To see this, we may transform Eq. (4) back to the original fermion basis $\phi_{\mathbf{k}}$ by means of our expression for $P_{\mathbf{k}}$ in Eq. (3) to find that

$$H_{\mathrm{SC}} = \sum_{\mathbf{k}} [\Delta_{\mathbf{k}x} d^\dagger_{\mathbf{k}x\uparrow} d^\dagger_{-\mathbf{k}x\downarrow} + \Delta_{\mathbf{k}y} d^\dagger_{\mathbf{k}y\uparrow} d^\dagger_{-\mathbf{k}y\downarrow} + \Delta_{\mathbf{k}xy} (d^\dagger_{\mathbf{k}x\uparrow} d^\dagger_{-\mathbf{k}y\downarrow} - d^\dagger_{\mathbf{k}y\uparrow} d^\dagger_{-\mathbf{k}x\downarrow}) + \mathrm{H.c.}], \quad (7)$$

where $\Delta_{\mathbf{k}x}$ and $\Delta_{\mathbf{k}y}$ are the intraorbital gaps while $\Delta_{\mathbf{k}xy}$ is the interorbital gap. They are defined as

$$\Delta_{\mathbf{k}x} = (\Delta^+_{\mathbf{k}} + \zeta^2_{\mathbf{k}} \Delta^-_{\mathbf{k}})/\nu^+_{\mathbf{k}}, \quad \Delta_{\mathbf{k}y} = (\Delta^-_{\mathbf{k}} + \zeta^2_{\mathbf{k}} \Delta^+_{\mathbf{k}})/\nu^+_{\mathbf{k}},$$

$$\Delta_{\mathbf{k}xy} = \zeta_{\mathbf{k}} (\Delta^+_{\mathbf{k}} - \Delta^-_{\mathbf{k}})/\nu^+_{\mathbf{k}}, \quad \nu^\pm_{\mathbf{k}} = (1 \pm \zeta^2_{\mathbf{k}}). \quad (8)$$

We see that the interorbital pairing vanishes in the case where $\Delta^+_{\mathbf{k}} = \Delta^-_{\mathbf{k}}$. However, we emphasize that our model accounts for interorbital pairing $\Delta_{\mathbf{k}xy}$ in the original fermion basis and that $\Delta_{\mathbf{k}xy} \neq 0$ whenever $\Delta^+_{\mathbf{k}} \neq \Delta^-_{\mathbf{k}}$. We do not consider any interband pairing in the new diagonalized fermion basis. Assuming spin-singlet and even-frequency pairing, there are three possible s-wave symmetries $\{\Delta_0, \Delta_0(c_x + c_y), \Delta_0 c_x c_y\}$ and two possible d-wave symmetries $\{\Delta_0(c_x - c_y), \Delta_0 s_x s_y\}$ for the superconducting order parameters $\Delta_{\mathbf{k}x}$ and $\Delta_{\mathbf{k}y}$ in terms of the square lattice harmonics. The gaps in the $\pm$ quasiparticle hybridized bands are then obtained as $\Delta^+_{\mathbf{k}} = (\Delta_{\mathbf{k}x} - \zeta^2_{\mathbf{k}} \Delta_{\mathbf{k}y})/\nu^-_{\mathbf{k}}$ and $\Delta^-_{\mathbf{k}} = (\Delta_{\mathbf{k}y} - \zeta^2_{\mathbf{k}} \Delta_{\mathbf{k}x})/\nu^-_{\mathbf{k}}$. Note that the extended s-wave symmetry $\sim c_x c_y$ changes sign on the electron and hole Fermi surfaces, similar to the $s_\pm$ scenario suggested in Refs. 5 and 19.

III. RESULTS AND DISCUSSION

We are now in a position to evaluate the conductance of the system. The presence of a Fermi-vector mismatch between the normal and superconducting sides of the junction is assumed to be manifested through an effective decrease in the junction transmission. Since the Fermi velocity may be different in the two bands with normal-state dispersions $\Omega^\pm_{\mathbf{k}}$, we allow different barrier parameters $Z^\pm$ in the two bands. For a specified pairing symmetry, there are then four fitting parameters present: the barrier strength Z^λ and gap magnitude Δ^λ_0 for band $\lambda = \pm$. By generalizing the results of Refs. 15 and 16 to a two-band model which also takes into account the nontrivial Fermi-surface topology in Fig. 1(a), we obtain the following expression for the normalized tunneling conductance: $G(eV)/G_0 = \Sigma_{\lambda,k_y} f(k_y) \sigma^\lambda_S(eV) / [2 f(k_y) \sigma^\lambda_N]$, where $\sigma^\lambda_N = [1 + (Z^\lambda)^2]^{-1}$ and

$$\sigma^\lambda_S(eV) = \{\sigma^\lambda_N [1 + \sigma^\lambda_N |\Gamma^\lambda_+(\mathbf{k}, eV)|^2 + (\sigma^\lambda_N - 1) \times |\Gamma^\lambda_+(\mathbf{k}, eV) \Gamma^\lambda_-(\mathbf{k}, eV)|^2]\} / [|1 + (\sigma^\lambda_N - 1) \times \Gamma^\lambda_+(\mathbf{k}, eV) \Gamma^\lambda_-(\mathbf{k}, eV) \rho^\lambda(\mathbf{k})|^2],$$

$$\Gamma^\lambda_\pm(\mathbf{k}, eV) = \frac{eV - \sqrt{(eV)^2 - |\Delta(\pm \lambda k_x, k_y)|^2}}{|\Delta^\lambda(\pm \lambda k_x, k_y)|},$$

$$\rho^\lambda(\mathbf{k}) = \frac{\Delta^\lambda(-\lambda k_x, k_y)[\Delta^\lambda(\lambda k_x, k_y)]^*}{|\Delta^\lambda(-\lambda k_x, k_y) \Delta^\lambda(\lambda k_x, k_y)|}, \quad (9)$$

where $f(k_y) = \cos(k_y a/2)$ is a weighting function that models the directional dependence of the incoming quasiparticles.

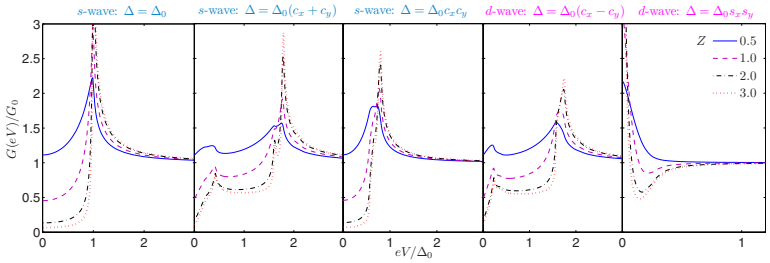

FIG. 2. (Color online) Plot of the conductance spectra for tunneling along the (100) axis in an iron-pnicitide N|S junction for several possible order-parameter symmetries. Only in the d_{xy}-wave case $\Delta=\Delta_0 s_x s_y$ is there a considerable ZBCP. Note the different scale on the voltage axis for this case due to the narrowness of the ZBCP. High (low) values of the parameter Z denote low (high) transmissivity interfaces.

The strategy is now to sum the conductance over the allowed values $k_y \in [-\pi/a, \pi/a]$ for the electronlike ($\lambda=1$) and holelike ($\lambda=-1$) Fermi surfaces and solve for k_x from Eq. (2) by $\Omega_{\mathbf{k}}^{\lambda}=0$ for a given k_y. In what follows, we choose an equal value for the barrier transparencies $Z^+=Z^-\equiv Z$ and gap magnitudes $\Delta_0^+=\Delta_0^-\equiv\Delta_0$ in the two bands for simplicity and add a small imaginary number δ to the quasiparticle energy to model inelastic scattering $eV\rightarrow eV+i\delta$, where $\delta/\Delta_0=10^{-2}$.

As in Ref. 18, we choose $\Delta_0=0.1$. Clearly, it is possible to study a rich variety of interplays between the two quasiparticle bands in terms of different symmetries for the d_{xz} and d_{yz} orbitals and with different gap magnitudes. Here, however, our main aim is to investigate how the conductance spectra are influenced by the nontrivial Fermi-surface topology and dispersion relations and see how this compares with the cylindrical/spherical Fermi surface and free-particle dispersion scenario employed in the usual BTK paradigm. In particular, this is relevant to the interpretation of the point-contact spectroscopy measurements of Refs. 10 and 11. There is, however, an important caveat with regard to which conclusion one may draw with regard to the symmetry of the superconducting OP from the tunneling data of Refs. 10 and 11. In these works, polycrystalline samples were used, while the orbital/nodal structure of the OP can only be convincingly probed in single-crystal specimens. This is because tunneling into polycrystalline samples may lead to intrinsic averaging effects which distort the contribution from anisotropic OPs.

In Fig. 2, we plot the conductance for tunneling along the (100) direction for several OP symmetries. As seen, the d_{xy}-wave case stands out from the rest as it features a considerable ZBCP. Comparing with the experimental data of Ref. 11, we would conclude that a nodal d-wave OP is likely to be realized in $LaFeAsO_{0.9}F_{0.1-\delta}$. The results of Ref. 10 seem to be most consistent with either s-wave or extended s-wave pairing, as only one gap is seen in the spectra. For the s-wave and d_{xy}-wave cases, the standard BTK approach appears to suffice in order to qualitatively say something about the OP symmetry. However, the results are quite different from the usual BTK approach when considering the extended s-wave and $d_{x^2-y^2}$-wave symmetries. More specifically, we find satellite features at subgap energies, including sharp peaks. These features most likely pertain to the specific band structure which we consider here (see Fig. 1) and are thus not possible to capture within the conventional BTK treatment with the cylindrical Fermi-surface approximation. In fact, the density of states (DOS) in our minimal two-band model is a highly nonmonotonic function of energy and contains two Van Hove singularities.[8,17]

Let us also consider the case where there is one fully gapped OP and one nodal OP to see what fingerprints this combination leaves in the conductance spectra. In Fig. 3, we plot the conductance for the case where $\Delta_{\mathbf{k}x}$ is fully gapped, while $\Delta_{\mathbf{k}y}$ has a nodal symmetry. For concreteness, we consider s-wave+d_{xy}-wave pairing and $d_{x^2-y^2}$-wave+d_{xy}-wave pairing in Figs. 3(a) and 3(b), respectively. As seen, the nodal OP gives rise to a ZBCP while there are several satellite features in addition to the large coherence peak at the gap edge. The plots are qualitatively similar regardless of whether the fully gapped OP is s wave or $d_{x^2-y^2}$ wave, while the features in the conductance are qualitatively more pronounced in the s-wave case due to the better gapping of the Fermi surface. Finally, we consider the evolution of the con-

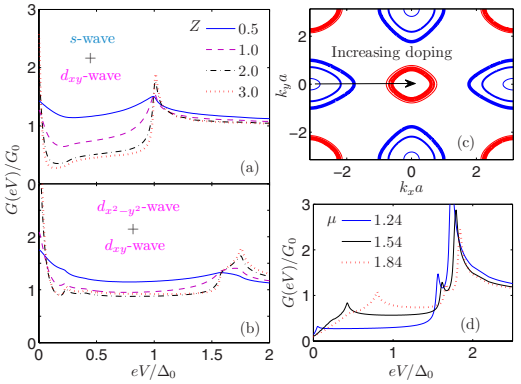

FIG. 3. (Color online) [(a) and (b)] Plot of the conductance spectra for tunneling along the (100) axis in an iron-pnicitide N|S junction for the case of one fully gapped OP and one nodal OP. (c) Evolution of the Fermi-surface topology for $\mu=\{1.24, 1.54, 1.84\}$ in the direction of the arrow. (d) Conductance spectra for the c_x+c_y symmetry with $Z=3$ for different doping levels.

ductance spectra upon changing the doping level μ. The Fermi-surface topology evolves with a change in μ as shown in Fig. 3(c); the electron pockets increase in size while the hole pockets decrease in size upon increasing μ. To see how the subgap features obtained in Fig. 2 evolve upon modifying μ, consider Fig. 3(d) where we provide results for the c_x+c_y symmetry with $Z=3$. As seen, the satellite features shown in Fig. 2 are still present and qualitatively the same, but they are shifted to different bias voltages.

IV. SUMMARY

In summary, we have developed a theory for Andreev reflection in the iron-based high-T_c superconductors. Starting with a tight-binding model on a square lattice to model the puckered FeAs planes, we have investigated several OP symmetries and the resulting conductance spectra. Fully taking into account the Fermi-surface topology and the quasiparticle dispersion relation, we have investigated scenarios where the symmetry of the superconducting OP in both bands is the same and where it is different, i.e., one is fully gapped and the other is nodal. We find that the standard BTK formalism should give qualitatively correct results for the case where the OP symmetries on both bands are either isotropic s wave or d wave. However, the results differ considerably for the extended s-wave symmetries, as we find satellite features at subgap energies which are absent within the usual BTK treatment. Our results may be useful in the context of analyzing quantum transport data of tunneling in normal|superconductor junctions involving the iron pnicitides.

ACKNOWLEDGMENTS

T. Yokoyama is thanked for useful discussions. J.L. and A.S. were supported by the Research Council of Norway under Grants No. 158518/431, No. 158547/431 (NANOMAT), and No. 167498/V30 (STORFORSK).

[1] Y. Kamihara, T. Watanabe, M. Hirano, and H. Hosono, J. Am. Chem. Soc. **130**, 3296 (2008).
[2] H. H. Wen, G. Mu, L. Fang, H. Yang, and X. Y. Zhu, Europhys. Lett. **82**, 17009 (2008).
[3] X. H. Chen, T. Wu, G. Wu, R. H. Liu, H. Chen, and D. F. Fang, Nature (London) **453**, 761 (2008).
[4] Z. A. Ren, J. Yang, W. Lu, W. Yi, G.-C. Che, X.-L. Dong, L.-L. Sun, and Z.-X. Zhao, Mater. Res. Innovations **12**, 105, (2008); Z. A. Ren, G.-C. Che, X.-L. Dong, J. Yang, W. Lu, W. Yi, X.-L. Shen, Z.-C. Li, L.-L. Sun, F. Zhou, and Z.-X. Zhao, Europhys. Lett. **83**, 17002 (2008).
[5] I. I. Mazin, D. J. Singh, M. D. Johannes, and M. H. Du, Phys. Rev. Lett. **101**, 057003 (2008).
[6] R. H. Liu, G. Wu, T. Wu, D. F. Fang, H. Chen, S. Y. Li, K. Liu, Y. L. Xie, X. F. Wang, R. L. Yang, L. Ding, C. He, D. L. Feng, and X. H. Chen, Phys. Rev. Lett. **101**, 087001 (2008).
[7] V. Cvetkovic and Z. Tesanovic, arXiv:0804.4678 (unpublished).
[8] S. Raghu, X.-L. Qi, C.-X. Liu, D. J. Scalapino, and S.-C. Zhang, Phys. Rev. B **77**, 220503(R) (2008).
[9] A. J. Drew, F. L. Pratt, T. Lancaster, S. J. Blundell, P. J. Baker, R. H. Liu, G. Wu, X. H. Chen, I. Watanabe, V. K. Malik, A. Dubroka, K. W. Kim, M. Rössle, and C. Bernhard, Phys. Rev. Lett. **101**, 097010 (2008).
[10] T. Y. Chen, Z. Tesanovic, R. H. Liu, X. H. Chen, and C. L. Chien, Nature (London) **453**, 1224 (2008).
[11] L. Shan, Y. Wang, X. Zhu, G. Mu, L. Fang, C. Ren, and H.-H. Wen, Europhys. Lett. **83**, 57004 (2008).
[12] V. Stanev, J. Kang, and Z. Tesanovic, Phys. Rev. B **78**, 184509 (2008).
[13] G. Deutscher, Rev. Mod. Phys. **77**, 109 (2005).
[14] C.-R. Hu, Phys. Rev. Lett. **72**, 1526 (1994); J. Yang and C.-R. Hu, Phys. Rev. B **50**, 16766 (1994).
[15] G. E. Blonder, M. Tinkham, and T. M. Klapwijk, Phys. Rev. B **25**, 4515 (1982).
[16] Y. Tanaka and S. Kashiwaya, Phys. Rev. Lett. **74**, 3451 (1995); S. Kashiwaya, Y. Tanaka, M. Koyanagi, and K. Kajimura, Phys. Rev. B **53**, 2667 (1996).
[17] G. Xu, W. Ming, Y. Yao, X. Dai, S. Zhang, and Z. Fang, Europhys. Lett. **82**, 67002 (2008).
[18] M. M. Parish, J. Hu, and B. A. Bernevig, Phys. Rev. B **78**, 144514 (2008).
[19] K. Seo, B. A. Bernevig, and J. Hu, Phys. Rev. Lett. **101**, 206404 (2008).

Paper XXI

Tunneling conductance and local density of states in time-reversal symmetry breaking superconductors under the influence of an external magnetic field.

Physical Review B **79**, 054508 (2009)

Tunneling conductance and local density of states in time-reversal symmetry breaking superconductors under the influence of an external magnetic field

Mihail A. Silaev,[1] Takehito Yokoyama,[2] Jacob Linder,[3] Yukio Tanaka,[2] and Asle Sudbø[3]
[1]*Institute for Physics of Microstructures, Russian Academy of Sciences, 603950 Nizhny Novgorod GSP-105, Russia*
[2]*Department of Applied Physics, Nagoya University, Nagoya, 464-8603, Japan and CREST, Nagoya, 464-8603, Japan*
[3]*Department of Physics, Norwegian University of Science and Technology, N-7491 Trondheim, Norway*
(Received 1 November 2008; published 10 February 2009)

We consider different effects that arise when time-reversal symmetry breaking superconductors are subjected to an external magnetic field, thus rendering the superconductor to be in the mixed state. We focus in particular on two time-reversal symmetry breaking order parameters which are believed to be realized in actual materials: $p+ip'$ wave and $d+is$ or $d+id'$ wave. The first-order parameter is relevant for Sr_2RuO_4, while the latter order parameters have been suggested to exist near surfaces in some of the high-T_c cuprates. We investigate the interplay between surface states and vortex states in the presence of an external magnetic field and their influence on both the tunneling conductance and the local density of states. Our findings may be helpful to experimentally identify the symmetry of unconventional time-reversal symmetry breaking superconducting states.

DOI: 10.1103/PhysRevB.79.054508 PACS number(s): 74.45.+c, 74.20.Rp, 74.25.−q

I. INTRODUCTION

Recently, considerable attention has been devoted to the chiral superconducting phase which is believed to be realized in the p-wave triplet superconductor[1] Sr_2RuO_4. The chiral state of a p-wave superconductor corresponds to a nonzero projection $l_z=\pm 1$ of the Cooper pairs angular momentum $\mathbf{l}$ along the z axis, and thus breaks time-reversal symmetry (TRS). The spatially homogeneous triplet order parameter (OP) $\hat{\Delta}=\Delta_0(\mathbf{d}\cdot\hat{\sigma})i\hat{\sigma}_y$ is described by the vector[1] $\mathbf{d}(\mathbf{p})=(0,0,p_x+i\chi p_y)$, which depends on the direction of electron momentum $\mathbf{p}$. Here Δ_0 is the bulk value of the order parameter, $\hat{\sigma}=(\hat{\sigma}_x,\hat{\sigma}_y,\hat{\sigma}_z)$ is the vector of Pauli matrices of conventional spin operators, and $\chi=\pm 1$ corresponds to the two possible values of chirality. Also, chiral superconducting states can be associated with an admixture of two order parameters corresponding to different irreducible representations of crystal point group. Different order parameter components can naturally coexist in the vicinity of interfaces between superconductors and surfaces due to the broken symmetry of the crystal group.[2–5] Among the possibilities of subdominant order parameter symmetries,[2] there are states which break time-reversal symmetry.[3–5] The coexistence of order parameters shows up in the local density of states,[6–9] as well as in the generation of spontaneous currents flowing along the surfaces in the time-reversal symmetry breaking cases.[7,8]

Time-reversal symmetry breaking order parameters have been proposed to exist near surfaces[10] and within vortex cores[11] in high-T_c superconductors. This proposal stems from the observation of a split zero-bias conductance peak in the *absence* of any applied magnetic field. In this case, it has been suggested that the relevant order parameter is either $d+is$ or $d+id'$ wave. The gap may then be written as $\Delta=\Delta_0 g(\theta_p)+i\Delta_s$ or $\Delta=\Delta_0 g(\theta_p)+i\Delta_d g_1(\theta_p)$, respectively, where Δ_0 is an amplitude of the main component and the admixture of another pairing symmetry is denoted by the amplitudes Δ_s and Δ_d. Here, θ_p is a polar angle in momentum space $\mathbf{p}=p(\cos\theta_p,\sin\theta_p)$; $g(\theta_p)=\cos(2\theta_p+\alpha)$ and $g_1(\theta_p)=\sin(2\theta_p+\alpha)$, where $\alpha/2$ is an angle measuring the disorientation of crystalline symmetry axes and coordinate axes. One obtains $d_{x^2-y^2}$-wave symmetry of the main order-parameter component for $\alpha=0$ and d_{xy}-wave pairing for $\alpha=\pi/2$. While the experimental data so far clearly indicate an order parameter which breaks time-reversal symmetry, the question of whether the symmetry is $d+is$ or $d+id'$ wave remains unsolved. Clearly, experimental signatures that may distinguish these two types of pairings would be highly desirable.

One of the important features of unconventional superconductors is the possibility for the existence of surface Andreev bound states.[12–14] They occur in the vicinity of the scattering interface between a superconductor and an insulator if the incident and reflected quasiparticles (QPs) with different momentum directions see different phases of the order parameter. The consequence of the Andreev bound-state formation is an increase in the local density of states (DOS) (LDOS) at the surface resulting in zero-bias conductance peak anomaly observed[15] in tunneling spectroscopy of high-T_c cuprates with d-wave symmetry of superconducting pairing as well as in the p-wave triplet superconductor Sr_2RuO_4.[16] Also, the Andreev bound states determine the anomalous low-temperature behavior of the London penetration length[17] and the Josephson critical current in d-wave[18] and chiral superconductors.[19]

Under the influence of an applied magnetic field, screening currents and vortices may be generated in a superconductor. As a result, the spectrum of surface states acquires a Doppler shift, leading to a splitting of the zero-bias conductance peak.[10] Abrikosov vortices located near a superconducting surface generate an essentially inhomogeneous superfluid velocity field, which leads to a nontrivial electronic structure of the surface-bound states.[20–22] Also, it was recently[22] proposed that the same Doppler-shift effect should lead to a chirality-selective influence of the magnetic field on the surface states in a p-wave chiral superconductor with broken time-reversal invariance. The quasiparticle DOS near

a flat surface was shown to depend on the orientation of magnetic field with respect to the chirality as well as on the vorticity in the case where the Abrikosov vortex is pinned near the surface of superconductor. Additionally, in superconductors featuring gap nodes, such as in the case in pure $d_{x^2-y^2}$-symmetric superconducting cuprates, a vanishing pair potential in nodal directions results in important ramifications for the physics of the system.[11,23–26]

To understand the effect of an externally applied magnetic field on the surface DOS, let us consider a spectrum of Andreev bound states near a flat surface of a time-reversal symmetry breaking superconductor occupying the half-space $x>0$. Below, we focus on the $p+ip$-, $d_{xy}+is$-, and $d_{xy}+id_{x^2-y^2}$-wave cases for concreteness. We consider a model situation assuming spatially homogeneous gap function, having the following form in momentum space:

$$\Delta = \Delta_0 e^{i\chi\theta_p} \tag{1}$$

for $p+ip$-wave,

$$\Delta = \Delta_0 \sin(2\theta_p) + i\Delta_s \tag{2}$$

for $d_{xy}+is$-wave, and

$$\Delta = \Delta_0 \sin(2\theta_p) + i\Delta_d \cos(2\theta_p) \tag{3}$$

for $d_{xy}+id_{x^2-y^2}$-wave superconductors.

Assuming that the QPs are specularly reflected at the surface of the superconductor within a Doppler-shift approach,[27] the spectrum of the surface states can be expressed as follows:[19,28] $\varepsilon_a=\varepsilon_{a0}+\epsilon_D$, where ε_{a0} is a position of energy level in zero magnetic field and $\epsilon_D=\hbar\mathbf{k}_F\mathbf{v}_s$ is the Doppler-shift energy which is determined by a local field of superfluid velocity. The superfluid velocity $\mathbf{v}_s$ near a surface has only a tangential component, directed along the y axis $\mathbf{v}_s=(0,v_{sy},0)$, and can be related to the density of supercurrent flowing along the surface $\mathbf{j}_s=en\mathbf{v}_s$, where e is the electron charge and n is the concentration of Cooper pairs. The magnetic field is screened in a superconductor at the London length λ as follows: $B=He^{-x/\lambda}$, where H is the value of magnetic field outside the superconductor. Therefore, the superfluid velocity is $v_{sy}=-(2e/mc)\lambda H$.

If the magnetic field is absent, the spectrum of surface states is given by[12,29]

$$\varepsilon_{0a} = \chi\Delta_0 k_y/k_F \tag{4}$$

for a chiral p wave,

$$\varepsilon_{a0} = \Delta_s \operatorname{sgn}(k_y) \tag{5}$$

for a $d_{xy}+is$ wave, and

$$\varepsilon_{a0} = \Delta_d \operatorname{sgn}(k_y)\cos(2\theta_p) \tag{6}$$

for a $d_{xy}+id_{x^2-y^2}$ wave. Here k_y is the projection of QP momentum along the surface. The above spectra may be formally obtained by solving[13]

$$\frac{\Delta(\theta_p)}{\varepsilon_{a0} - i\sqrt{|\Delta(\theta_p)|^2 - \varepsilon_{a0}^2}} = \frac{\Delta(\pi-\theta_p)}{\varepsilon_{a0} + i\sqrt{|\Delta(\pi-\theta_p)|^2 - \varepsilon_{a0}^2}}. \tag{7}$$

In the $d_{x^2-y^2}+is$-wave case, one finds that $\varepsilon_{a0}=\sqrt{\Delta_0^2\cos^2(2\theta_p)+\Delta_s^2}$, from which one infers that there are no subgap surface states. This is qualitatively different from the $d_{xy}+is$-wave case. The interesting effects occur in the latter case, so we focus on the $d_{xy}+is(d)$-wave symmetry in the following, corresponding to $\alpha=\pi/2$.

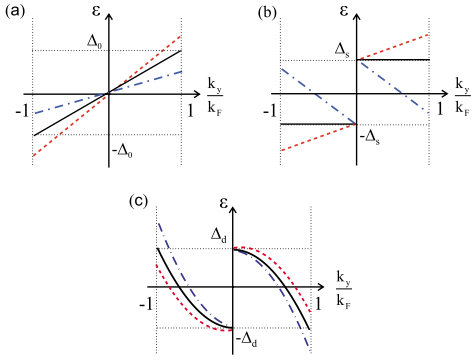

FIG. 1. (Color online) Plot of the surface states spectrum for (a) chiral $p+ip$-wave, (b) $d+is$-wave, and (c) $d+id$-wave superconductors. Spectrum in zero magnetic field is shown by solid lines. Blue (dash-dotted) and red (dotted) lines correspond to the spectrum transformation due to magnetic field directed along and opposite the z axis correspondingly.

The transformation of these spectra due to the Doppler-shift effect is shown in Fig. 1. To be definite we assume that $\Delta_s>0$, $\Delta_d>0$, and $\chi=1$. Considering the DOS at Fermi level, $\nu=|\partial\varepsilon_a/\partial k_y|^{-1}_{\varepsilon=0}$, in a chiral p-wave superconductor one can see that its dependence on the magnetic field is monotonic: it either increases or decreases for different field directions [see Fig. 1(a)] as discussed in Ref. 22.

Another behavior of the DOS occurs in the case of a $d+is$-wave superconductor. From Fig. 1(b) it follows that for a certain field direction there are no states at the Fermi level $\varepsilon=0$ [red dashed lines in Fig. 1(b)]. For the opposite field direction [blue dashed-dotted lines in Fig. 1(b)], intersections of spectral branches with the Fermi level appear when the superfluid velocity is large enough, $|v_{sy}|>\Delta_s/p_F$, so that the value of momentum projection at the intersection point is smaller than the Fermi momentum $|k_y^*|<k_F$. Thus, one can expect that the DOS at the Fermi level should be zero when $H<H^*$, where H^* is the magnetic field value providing the condition $|v_{sy}|=|\Delta_s|/p_F$ to be fulfilled.

On the contrary, in the $d+id$-wave case the DOS at the Fermi level is nonzero even in the absence of a magnetic field. As can be seen from Fig. 1(c) (black solid lines) the spectral branches intersect the level $\varepsilon=0$ at $k_y^*=\pm k_F/\sqrt{2}$. The transformation of the spectrum due to the magnetic field of different directions is shown in Fig. 1(c) by red dashed lines ($H>0$) and by blue dashed-dotted lines ($H<0$). Then, it can be easily seen that for $H>0$ the coordinates of the intersection points k_y^* shift toward $\pm k_F$ and for a certain value of the magnetic field $H>H^*$ the DOS at the Fermi level $\varepsilon=0$ disappears.

In the presence of an Abrikosov vortex near the surface of chiral superconductor a nontrivial structure of the local density of states distribution appears which depends on the vor-

tex orientation.[22] Along with the Doppler-shift effect,[22] an important modification of the quasiparticle spectrum and the DOS can be obtained due to the overlapping of the surface states and the low-energy QP states localized within the vortex core found in the pioneering work by Caroli, de Gennes, and Matricon (CdGM).[30] It was shown that QP states with energy lower than the bulk superconducting gap value Δ are localized within the vortex core at the characteristic scale of the order of coherence length ξ and have a discrete spectrum $\varepsilon_v(\mu)$ as a function of the quantized (half-integer) angular momentum μ. At small energies $|\varepsilon| \ll \Delta$ the spectrum for a vortex with vorticity M is given by

$$\varepsilon_v(\mu) \approx -M\mu\omega, \tag{8}$$

where $k_F = p_F/\hbar$ and $\omega \sim \Delta_0/k_F\xi$. For most of superconducting materials, including Sr_2RuO_4, the interlevel spacing ω is much less than the superconducting gap Δ since $k_F\xi \gg 1$. Therefore, the CdGM spectrum may be considered as a continuous function of the impact parameter of the quasiclassical trajectory $b = -\mu/k_F$ and the direction of QP momentum θ_p as in the following form:

$$\varepsilon_v(b, \theta_p) \approx M\Delta(b/\xi). \tag{9}$$

In the case of a chiral p-wave superconductor, the spectrum of vortex core states differs from the CdGM result and is given by Eq. (8) with integer μ. For the $d+is$- and $d+id$-wave superconductors the quasiclassical spectrum of vortex core states is given by Eq. (9) with $\Delta(\theta_p) = \sqrt{\Delta_0^2 g^2(\theta_p) + \Delta_s^2}$ and $\Delta(\theta_p) = \sqrt{\Delta_0^2 g^2(\theta_p) + \Delta_d^2 g_1^2(\theta_p)}$. The discrete spectrum is obtained by applying the Bohr-Sommerfeld quantization rule to the canonical variables $\mu = -k_F b$ and θ_p.[23,31] It should be noted that when the superconducting order parameter contains nodes, the quasiclassical expression (9) is invalid near the nodal directions since energy states near the vortex core are not truly localized but rather "leak" out through the gap nodes.[11,23–26] This is not the case for us since we consider superconducting order parameters which are gapped over the entire Fermi surface.

To study the interaction between vortex and surface states, let us consider an example of vortex positioned near a flat surface of chiral $p+ip$-wave superconductor. Comparing the energies of surface ε_a (4) and vortex ε_v (9) states one can see that for certain QP trajectories the condition of resonance $\varepsilon_a = \varepsilon_v$ is realized. Thus the spectrum transformation in such almost degenerate two-level system is given by a secular equation

$$(\varepsilon - \varepsilon_a)(\varepsilon - \varepsilon_v) = J^2. \tag{10}$$

Since we consider a low-energy spectrum $|\varepsilon| \ll \Delta_0$, the trajectories should pass close to the vortex center for the spectrum modification (10) to be effective. Then, the interaction of surface and vortex states is determined by the overlap integral $J \approx \Delta \exp(-\tilde{a}/\xi)$, where $\tilde{a} = a/\cos\theta_p$ and a is the distance from the vortex to the surface. Taking a certain point at the surface [see point A in Fig. 2(a)] of the superconductor one can obtain a relation between the angles and impact parameters of trajectories passing through this point as follows: $b = \tilde{a}\sin(\theta - \theta_p)$. Thus the energy of vortex core states can be written as $\varepsilon_v = M(\tilde{a}/\xi)\Delta_0 \sin(\theta - \theta_p)$. Then, from Eq. (10) we obtain the spectrum transformation shown qualitatively in Fig. 2 for the particular case of $\theta = 0$. It is easy to see that for equal values of vorticity and chirality [Fig. 2(b)] there appears a minigap in quasiparticle spectrum near the Fermi level and therefore the zero-energy DOS is suppressed. On the other hand, in the case of opposite vorticity and chirality [Fig. 2(c)] there is no minigap and the DOS is not suppressed.

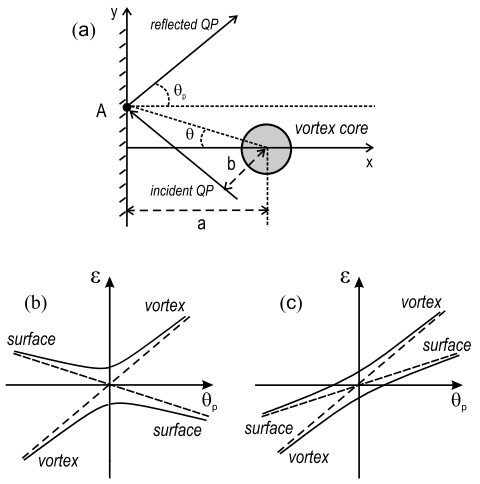

FIG. 2. (a) Sketch of QP trajectories forming surface and vortex states and qualitative plot of spectrum transformation due to the interaction of surface and vortex states in the case of a chiral p-wave superconductor; vorticity and chirality have (b) equal and (c) opposite values.

In $d+is$- and $d+id$-wave superconductors, the interaction between vortex and surface states can also lead to noticeable effects, which will be discussed later in the present paper. Recently, it was pointed out that tunneling of quasiparticles into vortex core states leads to a resonant enhancement of subgap conductance of normal-metal/superconductor (N/S) junction.[32] In the case of chiral superconductors, such a tunneling effect can lead to either stimulation or suppression of conductance, depending on the direction of vorticity. We will show that if vortices are located far from the N/S interface, the conductance follows the behavior expected from the Doppler-shift approach. On the other hand, when the distance from the vortex to the interface becomes comparable with coherence length ξ the tunneling into vortex core states comes into play, leading to the peculiar nonmonotonic conductance dependence on the vortex coordinate with respect to the superconducting surface.

This paper is organized as follows. In Sec. II, we give an overview of the theoretical framework which is employed in this work, namely, a Bogoliubov approach and a quasiclassical Eilenberger approach. In Sec. III, we present our main results for the influence of magnetic field on bound surface states spectra and local density of states near the surface. We discuss the transformation of surface states in the Meissner state of superconductor as well as the effects of interplay between surface and vortex core states. We give our conclusions in Sec. IV.

II. THEORETICAL APPROACH

Our further considerations are based on the Bogoliubov–de Gennes (BdG) equations for particlelike (u) and holelike (v) parts of the wave function, which have the following form:

$$-\frac{1}{2m}\left(\hat{\mathbf{p}}-\frac{e}{c}\mathbf{A}\right)^2 u+\hat{\Delta}v=(\varepsilon+\varepsilon_F)u,$$

$$\frac{1}{2m}\left(\hat{\mathbf{p}}+\frac{e}{c}\mathbf{A}\right)^2 v+\hat{\Delta}^{\dagger}u=(\varepsilon-\varepsilon_F)v. \tag{11}$$

Here $\hat{\Delta}$ is the gap operator, $\mathbf{A}$ is the vector potential, $\hat{\mathbf{p}}=-i(\partial/\partial_x,\partial/\partial_y)$, and $\mathbf{r}=(x,y)$ is the radius vector in the plane perpendicular to the anisotropy plane. Hereafter we assume the Fermi surface to be cylindrical along the z axis and consider a motion of QPs only in xy plane.

In the case of unconventional superconductors, the gap potential $\hat{\Delta}$ is a nonlocal operator, so the BdG system effectively becomes a very complicated integrodifferential equation. Another complexity arises from the broken spatial invariance of the superconducting gap in the presence of vortices near the N/S interface. A simplification can be obtained if one considers a quasiclassical approximation, assuming that the wavelength of quasiparticles is much smaller than the superconducting coherence length (see, e.g., Ref. 33). Within such an approximation, QPs move along linear trajectories, i.e., straight lines along the direction of QP momentum $\mathbf{n}=\mathbf{k}_F k_F^{-1}=(\cos\theta_p,\sin\theta_p)$. Generally, the quasiclassical form of the wave function can be constructed as follows: $(u,v)=e^{i\mathbf{k}_F\cdot\mathbf{r}}(U,V)$, where $(U(\mathbf{r}),V(\mathbf{r}))$ is a slowly varying envelope function. Then system (11) reduces to a system of first-order differential equations along the linear trajectories defined by the direction of the QP momentum $\mathbf{n}=\mathbf{k}_F k_F^{-1}=(\cos\theta_p,\sin\theta_p)$. Introducing the coordinate along trajectory $x'=(\mathbf{n}\cdot\mathbf{r})=r\cos(\theta_p-\theta)$, we arrive at the following form of the quasiclassical equations:

$$\left(-i\hbar v_F\partial_{x'}+\mathbf{v}_F\cdot\frac{e}{c}\mathbf{A}\right)U+\Delta V=\varepsilon U,$$

$$\left(i\hbar v_F\partial_{x'}+\mathbf{v}_F\cdot\frac{e}{c}\mathbf{A}\right)V+\Delta^{\dagger}U=\varepsilon V, \tag{12}$$

where the Fermi velocity is $\mathbf{v}_F=\mathbf{n}\hbar k_F/m$. The pairing potential in Eq. (12) may generally be written as

$$\Delta(\mathbf{r},\theta_p)=\Delta(\theta_p)\Psi(\mathbf{r}), \tag{13}$$

where $\Delta(\theta_p)$ describes the orbital symmetry of the superconducting order parameter in momentum space, while $\Psi(\mathbf{r})$ describes its spatial dependence both magnitudewise and phasewise.

The LDOS can be expressed through the eigenfunctions of the BdG equation (11) in the following form:[34]

$$N(\varepsilon,\mathbf{r})=\sum_n |u_n(\mathbf{r})|^2\delta(\varepsilon-\varepsilon_n), \tag{14}$$

where $u_n(\mathbf{r})$ is electron component of quasiparticle eigenfunction corresponding to an energy level ε_n. The eigenfunction has to be normalized; $\int\int_{-\infty}^{\infty}|u_n(\mathbf{r})|^2+|v_n(\mathbf{r})|^2 d^2r=1$.

We will also later employ the quasiclassical Eilenberger approach to study the spatially resolved DOS. Let us here sketch the framework of the treatment which makes use of the Eilenberger equation, following the notation of Refs. 35 and 36. It is now convenient to solve the Eilenberger equation along trajectories along the Fermi momentum and to introduce a Ricatti parametrization for the Green's function.[36] In this way, one obtains[20]

$$\hbar v_F\partial_{x'}a(x')+[2\tilde{\omega}_n+\Delta^{\dagger}a(x')]a(x')-\Delta=0,$$

$$\hbar v_F\partial_{x'}b(x')-[2\tilde{\omega}_n+\Delta b(x')]b(x')+\Delta^{\dagger}=0, \tag{15}$$

where $i\tilde{\omega}_n=i\omega_n+m\mathbf{v}_F\cdot\mathbf{v}_s$ is a Doppler-shifted Matsubara frequency and

$$\mathbf{v}_s=\frac{1}{2m}\left(\hbar\nabla\Phi-\frac{2e}{c}\mathbf{A}\right)$$

is a gauge-invariant superfluid velocity where $\Phi(\mathbf{r})$ is a gap function phase; $\Psi(\mathbf{r})=|\Psi|e^{i\Phi}$. The LDOS may be expressed through the scalar coherence functions a and b as follows:[20]

$$N(\varepsilon)=\int_0^{2\pi}\frac{d\theta}{2\pi}\mathrm{Re}\left\{\frac{1-ab}{1+ab}\right\}_{i\omega_n\to\varepsilon+i\delta}, \tag{16}$$

where ε is the quasiparticle energy measured from Fermi level and δ is a scattering parameter which accounts for inelastic scattering.

To investigate the transport properties of N/S junction, we employ an approach similar to what was used in work by Blonder *et al.*[37] The expression for the dimensionless zero-bias conductance of the N/S junction measured in terms of the conductance quantum $e^2/\pi\hbar$ can be written as follows:

$$G=\frac{G_{\mathrm{Sh}}}{2}\int_{-\pi/2}^{\pi/2}[1-R_n(\theta_0)+R_a(\theta_0)]\cos\theta_0 d\theta_0, \tag{17}$$

where $R_n(\theta_0)$ and $R_a(\theta_0)$ are the probabilities of normal and Andreev reflections respectively, θ_0 is the incident angle, $\mathbf{k}_F=k_F(\cos\theta_0,\sin\theta_0)$, characterizing the propagation direction of quasiparticles coming from the normal-metal region. The Sharvin conductance $G_{\mathrm{Sh}}=k_F L_y/\pi$ equals the total number of propagating modes determined by the channel width L_y.

The problem of quasiparticle scattering at the N/S interface is formulated within the BdG theory (11).[38] An interfacial barrier separating the N and S regions can be modeled by repulsive delta function potential $W(x)=W_0\delta(x)$ parametrized by a dimensionless barrier strength $Z=W_0/\hbar v_F$. The boundary conditions at the N/S interface then read[39]

$$[f(0)]=0,\quad [\partial_x f(0)]=2k_F Z f(0), \tag{18}$$

where $f=(u,v)$ and $[f(x)]=f(x+0)-f(x-0)$.

Considering a zero-bias problem we will have to analyze only zero-energy excitations with $\varepsilon=0$. For wave functions in S region corresponding to subgap quasiparticles, the following representation can be used: (U,V)

$=e^{\zeta}(e^{i(\eta+\Phi)/2}, e^{-i(\eta+\Phi)/2})$, where $\zeta=\zeta(s,b)$ and $\eta=\eta(s,b)$ are real-valued functions. Then, the quasiclassical equation (12) can be written as follows:

$$\partial_{x'}\eta + 2|\Delta|\cos\eta + 2\epsilon_D = 0,$$

$$\partial_{x'}\zeta + 2|\Delta|\sin\eta = 0. \tag{19}$$

where $\epsilon_D(\mathbf{r})=\hbar\mathbf{k}_F\mathbf{v}_s$ is the Doppler-shift energy. For wave functions decaying at the different ends of trajectory $(U,V)(x'=\pm\infty)=0$ from Eq. (19) we obtain

$$\eta(x'=\pm\infty)=\pm\pi/2. \tag{20}$$

The boundary conditions (18) model the specularly reflecting N/S interface, coupling the waves with wave vectors $\mathbf{k}_F=k_F(\cos\theta_0,\sin\theta_0)$ and $\mathbf{k}'_F=k_F[\cos(\pi-\theta_0),\sin(\pi-\theta_0)]$. Therefore if the incident electron wave is $u_i=e^{i\mathbf{k}_F\cdot\mathbf{r}}$, then the reflected electron u_r and hole v_r waves will have the form

$$u_r = U_r e^{i\mathbf{k}'_F\cdot\mathbf{r}}, \quad v_r = V_r e^{i\mathbf{k}_F\cdot\mathbf{r}},$$

where U_r and V_r are the envelope functions. Thus, each point $(0,y)$ at the N/S interface lies on the intersection of two quasiclassical trajectories characterized by the angles $\theta_p=\theta_0$ and $\theta_p=\pi-\theta_0$. Let us denote the distribution of phases $\eta(x')$ along these trajectories as $\eta_+(x')$ and $\eta_-(x')$ correspondingly. Using the boundary conditions we obtain the following expression for the conductance:[32]

$$G = \frac{N_0}{2}\int_{-L_y/2}^{L_y/2}\int_{-\pi/2}^{\pi/2} g(y,\theta_0)\cos\theta_0 d\theta_0 dy, \tag{21}$$

where $g(y,\theta_0)$ is given by

$$g(y,\theta_0) = \frac{2}{(\tilde{Z}^4+\tilde{Z}^2)|1-e^{i\rho}|^2+1} \tag{22}$$

with $\tilde{Z}=Z/\cos\theta_0$ and $\rho(y,\theta_0)=\eta_- - \eta_+$ is determined by the difference of phases $\eta_-(x')$ and $\eta_+(x')$ at the intersection point $(0,y)$. To evaluate the conductance, one needs to find the factor $e^{i\rho}$ in Eq. (22) and then the reflection probabilities by solving numerically Eq. (19) with the boundary conditions in Eq. (20).

III. RESULTS

To illustrate the basic effect of how the interplay between the Doppler shift and the time-reversal symmetry breaking of the superconducting order parameter is manifested, we consider a situation where an external magnetic field is applied near the surface of the superconductor along the $\hat{\mathbf{z}}$ axis, thus inducing a vector potential $\mathbf{A}$ in the superconductor which drives the shielding supercurrent. In order to proceed analytically, we make the simplifying assumption that the superfluid velocity field is nearly homogeneous and that the spatial variation in the superconducting order parameter near the interface is small. Choosing a real gauge, we then find that the Ricatti functions a and b in Eq. (15) may be written as[20,22]

$$a(\theta)=s(\theta)\Delta(\theta), \quad b(\theta)=s(\theta)\Delta^*(\theta),$$

$$s(\theta)=1/\{\tilde{\omega}_n(\theta)+\sqrt{[\tilde{\omega}_n(\theta)]^2+|\Delta(\theta)|^2}\}, \tag{23}$$

where $\tilde{\omega}_n$ depends on θ through the Doppler shift. To evaluate the LDOS in Eq. (16) at the surface, we need to take into account proper boundary conditions at $x=0$. Assuming an impenetrable surface with perfect reflection, these boundary conditions read

$$a_{\text{surface}}(\theta)=a(\pi-\theta), \quad b_{\text{surface}}(\theta)=b(\theta). \tag{24}$$

Inserting these into the expression for the LDOS, we obtain

$$N(\varepsilon) = 2\,\mathrm{Re}\left\{\left\langle\frac{1}{1+a(\pi-\theta)b(\theta)}\right\rangle\right\}_{i\omega_n\to\varepsilon+i\delta} - 1. \tag{25}$$

$\langle\cdots\rangle$ denotes angular averaging, which we restrict to angles $-\pi/2\le\theta\le\pi/2$ due to the surface. It may be shown that, for a chiral p-wave superconductor,[22] the zero-energy DOS at the surface reads

$$N(0) = 1 + \frac{\hbar k_F v_{sy}}{\Delta_0} + \cdots, \tag{26}$$

while for pure s- or d-wave superconductors one finds

$$N(0) = C_1 + C_2 v_{sy}^2 + \cdots, \tag{27}$$

where C_1 and C_2 are arbitrary constants. From numerical investigations of Eq. (25) at $\varepsilon=0$, we find that the zero-energy DOS may quite generally be written as

$$N(0) = C_1 + C_2 v_{sy} + \cdots \tag{28}$$

whenever the superconducting order parameters (i) break time-reversal symmetry and (ii) support the presence of subgap surface-bound states. This is the case both for the p_x+ip_y-wave pairing which is believed to be realized in Sr_2RuO_4, as well as the $d+is$-wave and $d+id$-wave pairings that are relevant for the cuprates. In particular, tunneling spectroscopy measurements have indicated the presence of such a time-reversal symmetry breaking order parameter near surfaces by a split zero-bias conductance peak that was observed in the *absence* of an external field in several experiments.[10]

In Ref. 35, it was pointed out that the neglect of the gradient term in the Eilenberger equation is expected to be a reasonable approximation as long as the Doppler-shift energy $m\mathbf{v}_F\cdot\mathbf{v}_s$ is small compared to the local gap energy $\Delta(\theta)$. This approximation would then fail close to the vortex core or gap nodes of $\Delta(\theta)$. Nevertheless, in the model case of spatially homogeneous gap function and superfluid velocity field, the gradient terms in the —Eilenberger equation can be neglected in the whole range of Doppler-shift energies. However considering a model situation the above discussion nevertheless serves to illustrate our main qualitative argument, namely, that chirality-sensitive effects should be expected in superconductors with order parameters that (i) break time-reversal symmetry and (ii) support the presence of subgap surface-bound states. We now proceed to discuss the cases of p_x+ip_y-wave and $d+is(d)$-wave pairings in more detail since these are relevant to actual materials.

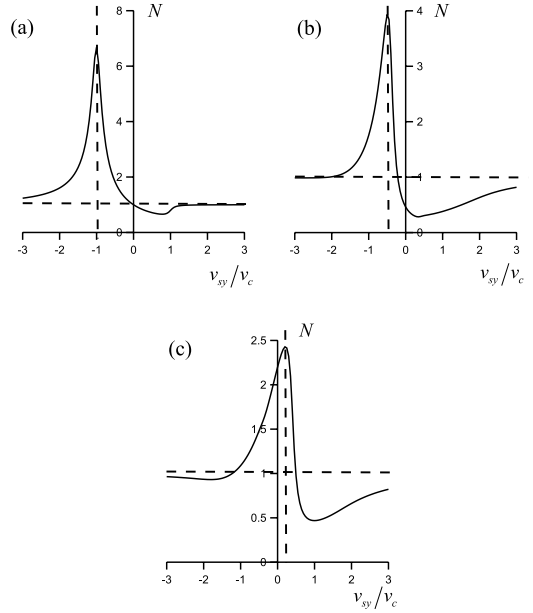

FIG. 3. Plot of the normalized zero-energy LDOS $N(0)$ for (a) p-wave superconductor with $\chi=1$, (b) $d+is$-wave case with $\Delta_s=0.4\Delta_0$, and (c) $d+id$-wave case with $\Delta_d=0.4\Delta_0$. Dashed lines are guides for eyes. The vertical ones denote positions of LDOS peaks and the horizontal ones correspond to the level of normal-metal DOS N_0.

A. Surface states in $p+ip$ and $d+is(d)$ superconductors under the influence of magnetic field

In Fig. 3, we show numerical plots of the surface LDOS given by Eq. (25) for the chiral p-wave [Fig. 3(a)], $d+is$-wave [Fig. 3(b)], and $d+id$-wave [Fig. 3(c)] cases in a wide domain of superfluid velocities. The structure of gap functions is chosen in the form of Eqs. (1)–(3) and the parameter characterizing inelastic scattering in Eq. (16) is chosen as $\delta=0.1\Delta_0$. We introduce the following notations for the different critical velocities: $v_c=\Delta_0/\hbar k_F$, $v_{cs}=|\Delta_s|/\hbar k_F$ and $v_{cd}=|\Delta_d|/\hbar k_F$.

As seen, the surface LDOS has sharp peaks at a certain value of the superfluid velocity in all cases. We will show below that peaked structure of LDOS is provided by bound surface states. Another contribution to the LDOS comes from the delocalized states corresponding to the continuous part of QP spectrum. A delocalized state with zero energy $\varepsilon=0$ exists provided that (i) $|v_{sy}|>v_c$ in case of chiral p-wave superconductor and (ii) $|v_{sy}|>v_{cs}$ and (iii) $|v_{sy}|>v_{cd}$ in cases of $d+is$-wave and $d+id$-wave superconductors correspondingly. Condition (i) is unlikely to be realized because it means that the superfluid velocity is larger than the critical depairing value. Conditions (ii) and (iii) can be realized because the values v_{cs} and v_{cd} can be well below the critical depairing velocity if the amplitude of additional order-parameter components is small enough.

To analyze the contribution to LDOS provided by the bound surface states we will consider the domain of low energies $|\varepsilon|\ll\Delta_0$. By neglecting small deviations of the electron and hole momenta, the normalized wave function of QP localized near the boundary can be written as

$$\begin{pmatrix} u \\ v \end{pmatrix} = \begin{pmatrix} 1 \\ i \end{pmatrix} \sqrt{\frac{2}{\tilde{\xi}|\cos\theta_p|}} e^{ik_y y} \sin(k_x x) e^{-x/(\tilde{\xi}\cos\theta_p)},$$

where $(k_x,k_y)=k_F(\cos\theta_p,\sin\theta_p)$. This wave-function decay in the superconducting side $x>0$ at a characteristic localization scale $\tilde{\xi}$ is given by $\tilde{\xi}=\hbar v_F/\Delta_0$ for chiral p wave and $\tilde{\xi}=\hbar v_F/|\Delta_0\sin(2\theta_p)|$ for $d+is$- and $d+id$-wave superconductors correspondingly with gap functions given by Eqs. (2) and (3). The spectrum of the Andreev bound states, shifted by the superfluid velocity, is given by

$$\varepsilon_a = \chi\Delta_0 k_y/k_F + \hbar v_{sy} k_y \tag{29}$$

for the p-wave case,

$$\varepsilon_a = \Delta_s \,\mathrm{sgn}(k_y) + \hbar v_{sy} k_y \tag{30}$$

for $d+is$-wave case, and

$$\varepsilon_a = \Delta_d \,\mathrm{sgn}(k_y)\cos(2\theta_p) + \hbar v_{sy} k_y \tag{31}$$

for $d+id$-wave case. Consequently, the contribution from Andreev bound states to the zero-energy LDOS at the surface of a chiral p-wave superconductor is given by

$$N_a = N_0 \frac{1}{|v_{sy}/v_c + \chi|},$$

where $N_0=m/2\pi\hbar^2$ is the normal-metal LDOS per one spin direction. For a chiral $d+is$ superconductor, the behavior of the LDOS is more complicated. Assuming that $\Delta_s>0$, we obtain that the LDOS is zero for $v_{sy}>-\Delta_s/\hbar k_F$. Otherwise, it is given by

$$N_a = 4N_0 \frac{v_{cs} v_c}{v_{sy}^2}.$$

On the contrary, for the $d+id$ case the LDOS is zero if $v_{sy}>\Delta_d/\hbar k_F$ (for $\Delta_d>0$) and otherwise it is given by

$$N_a = N_0 \frac{\Delta_0}{|\Delta_d|}\left(1+\frac{v_{cd}}{\sqrt{v_{sy}^2+8v_{cd}^2}}\right).$$

It can be seen that these contributions to LDOS have peaks at $v_{sy}=v_c$ for p-wave case. For $d+is$-wave and $d+id$-wave superconductors the peaks are positioned at $v_{sy}=-\mathrm{sgn}(\Delta_s)v_{cs}$ and $v_{sy}=\mathrm{sgn}(\Delta_d)v_{cd}$ correspondingly. Even though the position of the peaks are different, the dependencies of the surface LDOS on the superfluid velocity (and consequently on magnetic field) are very similar for $d+is$- and $d+id$-wave superconductors. Therefore, it might be difficult to distinguish which case is realized experimentally.

On the other hand the considered model with a spatially homogeneous gap function $\Psi(\mathbf{r})=1$ is adequate only when the applied magnetic field is not too large. When the magnetic field is large enough, it breaks the Meissner state and generates vortices near the surface of superconductor. Therefore, we investigate the influence of vortices on the LDOS distribution near a superconducting surface as well as on the

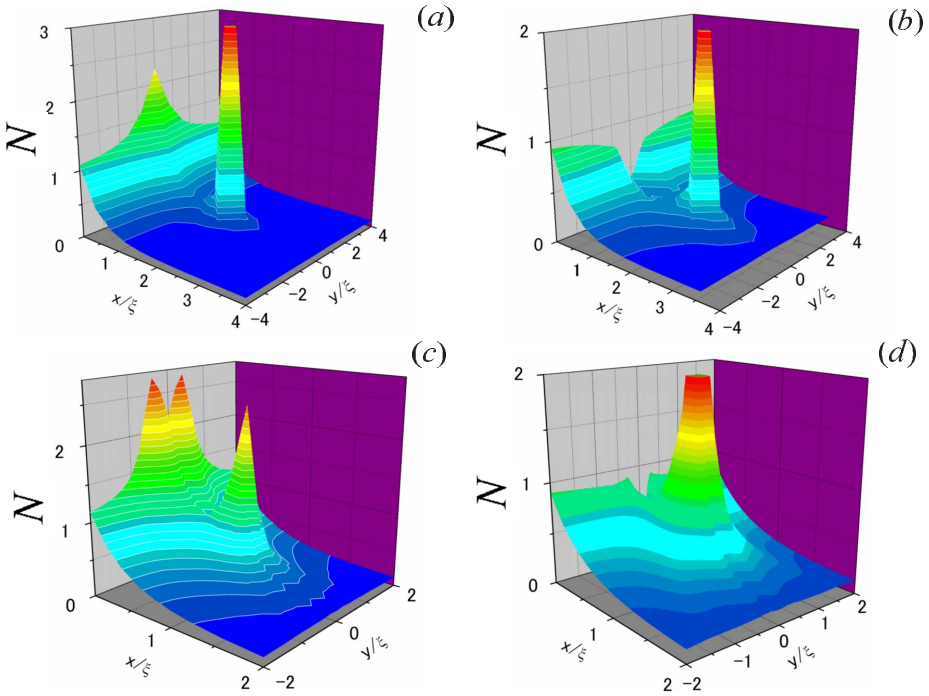

FIG. 4. (Color online) Plot of the normalized zero-energy LDOS $N(0)$ in the presence of a vortex near the surface of a chiral p-wave superconductor. (a) and (c) correspond to equal vorticity and chirality and (b) and (d) correspond to opposite vorticity and chirality. The distance from vortex to the surface is $a=2\xi$ for (a) and (b) and $a=\xi$ for (c) and (d).

conductance of normal-metal/superconducting junctions. We will show that vortices have different effects on the conductance in $d+is$ and $d+id$ cases.

B. Interplay between vortex and surface states in chiral superconductors

A chirality-sensitive LDOS transformation due to vortices situated near the surface of a chiral p-wave superconductor was considered in Ref. 22. It was shown that depending on the chirality and vorticity values, the surface LDOS near is either enhanced or suppressed upon decreasing the distance from the vortex to the surface. In the case of $d+is(d)$ superconductors the transformation of LDOS profile is also sensitive to the value of vorticity. Similar behavior is expected for a conductance of normal-metal/chiral superconductor junction in the presence of vortices.

To investigate the influence of a single vortex on the LDOS profile and conductance, we assume that at $x>0$ (superconducting region) the coordinate dependence of the order parameter may be written as follows:

$$\Psi(\mathbf{r}) = e^{i\Phi}. \tag{32}$$

Here, we consider a model situation where the magnitude of the order parameter is constant. The phase distribution $\Phi(\mathbf{r})$ consists of a singular part $\Phi_v(\mathbf{r})=\arg(\mathbf{r}-\mathbf{r}_v)$ and a regular part $\Phi_r(\mathbf{r})$ determined by the particular metastable vortex lattice configuration realizing near the boundary. We assume that the regular part of the phase distribution is $\Phi_r(\mathbf{r})=-\arg(\mathbf{r}-\mathbf{r}_{\mathbf{av}})$ corresponding to the image vortex situated at the point $\mathbf{r}_{\mathbf{av}}=(-2a,0,0)$ behind the N/S interface.

1. $p+ip$ wave

In Fig. 4 we show the LDOS profile near the surface of a chiral p-wave superconductor in the presence of a single vortex positioned at some distance a from the surface. When the vortex is positioned far from the surface $a\geq 2\xi$ the LDOS profile follows the behavior, as expected from the picture of local Doppler shift.[22] Depending on the relative values of vorticity and chirality, the surface LDOS is either increased [Fig. 4(a)] or decreased [Fig. 4(b)]. An analytical estimate with the help of spectrum (33) yields the following estimation of the amplitude of LDOS peak in Fig. 4(a): $\Delta N/N_0=(1+M\chi a)^{-1}$. At smaller distances $a\leq 2\xi$, the behavior of LDOS changes drastically. In the case of opposite vorticity and chirality, the surface LDOS grows at $a\leq 2\xi$, obviously due to the overlapping with the peak of vortex core states. In the case of equal vorticity and chirality the same overlapping occurs, but on the contrary it leads to reduction in DOS, as it was discussed in Sec. I. The peak of the LDOS at the surface discussed in Ref. 22 transforms into a dip-and-peak structure as the vortex comes close to the surface.

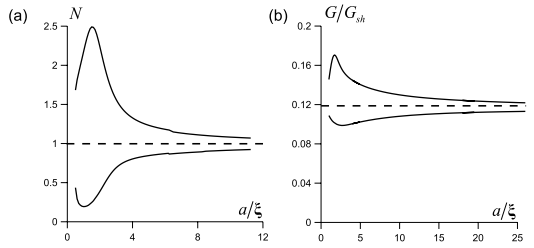

FIG. 5. (a) Plot of the normalized zero-energy LDOS at the point on the surface which is closest to the vortex core. Different curves correspond to different vorticities. (b) Plot of the vortex-induced conductance in chiral $p+ip$-wave superconductor for equal and opposite values of vorticity and chirality. The strength of interface barrier is $Z=5$. Large-distance asymptotes for N and G are shown by dash lines.

This is illustrated in Fig. 5(a), where we plot the LDOS at the surface point (0,0), which is the nearest point to the vortex in Fig. 4. At large distances $a \gg \xi$ the LDOS is a monotonic function of a, either increasing or decreasing depending on the relation between vorticity and chirality. At smaller distances $a \leq 2\xi$, the extremum of LDOS appears. In the case of opposite vorticity and chirality [lower curve in Fig. 5(a)], the surface LDOS grows at $a \leq 2\xi$ due to the overlapping with the peak of vortex core states. In the case of equal vorticity and chirality [upper curve in Fig. 5(a)] the same overlapping leads to reduction in LDOS.

To investigate the influence of vortices on the transport properties of normal-metal/chiral p-wave superconductor junction we solve the generic problem of the influence of a single vortex near the N/S surface on the zero-bias conductance of the junction. A numerical plot of the conductance G as a function of a distance of vortex to the junction interface is shown by the solid lines in Fig. 5(b) for equal (upper curve) and opposite (lower curve) values of chirality and vorticity. The conductance is normalized to the value of Sharvin conductance $G_{\mathrm{Sh}}=k_F L_y/\pi$.

At large distances $a \gg \xi$ an analytical estimation of conductance can be obtained by using a local Doppler-shift approximation on the quasiparticle spectrum. Indeed, the modification of the surface states energy due to a supercurrent flowing along the boundary of superconductor can be written as

$$\varepsilon_a \approx (\chi\Delta_0 + \hbar v_{sy} k_F) k_y / k_F, \tag{33}$$

where k_y is the quasiparticle momentum along the surface, $\chi=\pm 1$ is the chirality value, and $v_{sy}=(M\hbar/m)a/(y^2+a^2)$ is the projection on the surface plane of superfluid velocity generated by the vortex and image antivortex, where M is the vorticity value and m is the electron mass. It follows from Eq. (33) that the Doppler-shift effect leads to a change in the slope of anomalous branch. It is easy to obtain that in this case the function $g(y,\theta_0)$ in expression (22) takes the following form:

$$g(y,\theta_0) = \frac{2}{4(\tilde{Z}^4+\tilde{Z}^2)(\varepsilon_a/\Delta_0)^2+1}. \tag{34}$$

The straightforward integration in Eq. (21) yields $G=G_0+\delta G$, where $G_0=G_{\mathrm{Sh}}(\pi/Z^2)$ is the conductance without vortex and

$$\delta G/G_{\mathrm{Sh}} = \pm \frac{2\pi\xi}{Z^2 L_y} \arctan(L_y/2a) \tag{35}$$

is the vortex-induced conductance shift, where the upper (lower) sign corresponds to equal (opposite) vorticity and chirality.

At distances smaller than 2ξ, an extremum of the conductance appears. Upon placing the vortex closer to the surface, an opposite effect occurs: one obtains a conductance suppression instead of enhancement and vice versa. The origin of the conductance extremum is a tunneling of quasiparticles into the vortex core states or, in other words, the overlapping of vortex and surface-bound states. Comparing Figs. 5(a) and 5(b) one can see that the conductance in general follows the behavior of the surface DOS.

2. d+is and d+id waves

In chiral $d+is$ and $d+id$ superconductors the LDOS transformation appears to also be vorticity sensitive. In Fig. 6 we show the profile of zero-energy LDOS in the case where the vortex is placed at a distance of $a=2\xi$ from a flat boundary of a $d+is$-wave superconductor characterized by a gap function in momentum space given by Eq. (2). In this section, we use the notation $\xi=\hbar v_F/\Delta_0$.

One can see that for one sign of vorticity the surface LDOS shows two peaks which are symmetric with respect to the vortex position. As we have shown above, the large peaks in surface LDOS appear when the energy coincides with the position of bound-state level. For a different sign of the vorticity, there are no surface states at the Fermi level and the LDOS along the surface is a flat function. A nonzero level of LDOS in this case is provided by inelastic scattering which leads to the smearing of the QP energy levels. Applying a local Doppler-shift approach, which holds if the distance from vortex to surface is rather large ($a \gg \xi$), one can interpret the results shown in Fig. 6.

The coordinates y^* of surface LDOS peaks can be estimated from the relation $v_{sy}=\Delta_s/p_F$, where $v_{sy}=(M\hbar/m)a/(y^2+a^2)$ is the projection on the surface plane of superfluid velocity generated by the vortex with vorticity M and image antivortex. It can be seen that for $a>\xi(\Delta_0/|\Delta_s|)$ the peak is situated at $y^*=0$, i.e., at the surface point nearest to the vortex. Otherwise, we obtain $y^*=\pm a\sqrt{1-(a/\xi)(|\Delta_s|/\Delta_0)}$. Comparing this estimation with the numerical results in Fig. 6, one observes a minor difference. For example, it follows from the estimation that the LDOS peaks should be positioned at $y^*=\pm 2.4\xi$ for $\Delta_s=0.2\Delta_0$, but in Fig. 6 they are located at $y^*=\pm 2.0\xi$. This discrepancy can be attributed to the complex shift of the energy $\varepsilon \to \varepsilon + i\delta$ due to the effective scattering parameter $\delta=0.1\Delta_0$ which was

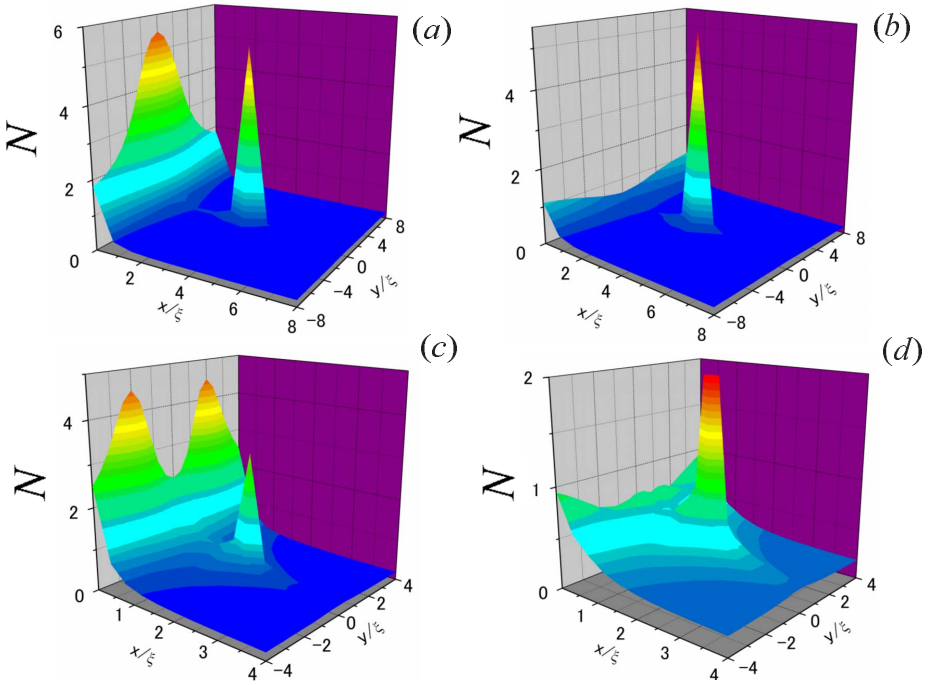

FIG. 6. (Color online) Plot of the normalized zero-energy LDOS profile $N(0)$ in the presence of vortex near the surface of chiral $d+is$-wave superconductor with $\Delta_s=0.2\Delta_0$. (a)–(d) correspond to different vortex orientations with respect to the z axis. The distance from vortex to the surface is $a=4\xi$ for (a) and (b) and $a=2\xi$ for (c) and (d).

used in the numerical calculations. If we increase the distance from vortex to surface, a, the LDOS peaks will merge when $a>\xi(\Delta_0/|\Delta_s|)$ (see Fig. 6).

In Fig. 7, we show the LDOS profile modulated by a vortex placed at a distance of $a=2\xi$ from a flat boundary of $d+id$ superconductor. The structure of the gap function was chosen in the form (3). Applying the approach based on the local Doppler shift we obtain the similar expression for the coordinates of the peaks of surface LDOS: $y^*=\pm a\sqrt{1-(a/\xi)(|\Delta_d|/\Delta_0)}$. For the particular values of parameters $\Delta_d=0.2\Delta_0$ and $a=2\xi$ this estimation yields $y^*=\pm 2.4\xi$, which is much less than obtained from numerical plot in Fig. 7 ($y^*\approx\pm 4\xi$). This discrepancy can also be attributed to the effect of inelastic scattering, which appears to have a larger effect in $d+id$-wave case than in discussed above $d+is$-wave case.

A numerical plot of the N/S junction conductance as a function of distance from vortex to surface is shown in Fig. 8 for the $d+is$ and $d+id$ cases. The conductance is normalized to the Sharvin conductance $G_{\mathrm{Sh}}=k_F L_y/\pi$. Comparing Figs. 8(a) and 8(b) one can see that the conductance behavior is qualitatively different for s- and d-wave symmetries of the additional gap function component. For $d+is$ wave, the conductance has a sharp peak for one vortex orientation [upper curve in Fig. 8(a)] and it is a flat function of a for another vortex orientation [lower curve in Fig. 8(a)]. The origin of the conductance enhancement is a formation of Andreev bound states at the Fermi level which are localized near the superconducting surface. As was discussed in Sec. I [see Fig. 1(b)], the zero-energy Andreev bound states can appear only for a certain direction of superfluid velocity flowing along the superconducting surface and if the value of the superfluid velocity is larger than a critical value $|v_{sy}|>|\Delta_s|/\hbar k_F$. For a high interface barrier $Z\gg 1$, applying the approximate analytical expression (35), we find that a sharp increase in conductance in Fig. 8(a) can be described by the following expression:

$$G/G_{\mathrm{Sh}}=\frac{16\pi}{3Z^2}\frac{\xi}{L_y}\frac{\Delta_0}{|\Delta_s|}\left(1-\frac{a}{a^*}\right)^{3/2}+\lambda Z^{-4},$$

where $a^*=\xi(\Delta_0/|\Delta_s|)$ and $\lambda\sim 1$. Otherwise, if $a>a^*$ the conductance is much smaller since $Z\gg 1$,

$$G/G_{\mathrm{Sh}}\approx\left(\frac{\Delta_0}{\Delta_s}\right)^2\frac{4}{3Z^4}.$$

When the distance a is decreased further, the conductance is suppressed [see Fig. 8(a), upper curve]. The decrease in conductance can be attributed to the gap at the Fermi level which appears due to the interaction of vortex and surface states in a similar way as for the $p+ip$-wave case discussed in Sec. III B 1.

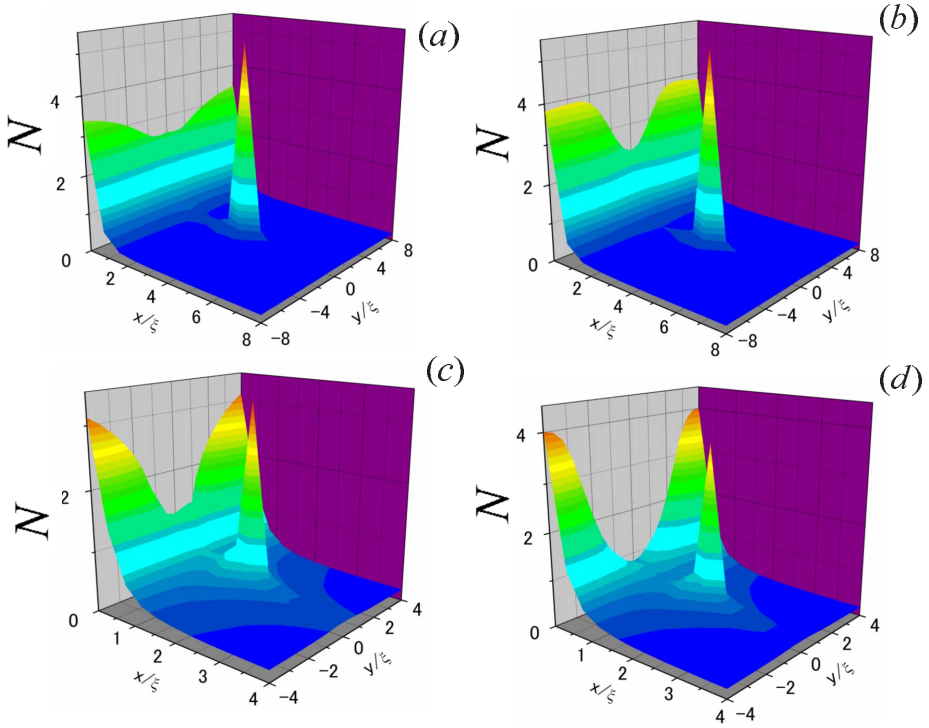

FIG. 7. (Color online) Plot of the normalized zero-energy LDOS profile $N(0)$ in the presence of vortex near the surface of chiral $d+id$-wave superconductor with $\Delta_d=0.2\Delta_0$ (a)–(d) correspond to different vortex orientations with respect to the z axis. The distance from vortex to the surface is $a=4\xi$ for (a) and (b) and $a=2\xi$ for (c) and (d).

In a $d+id$-wave superconductor, zero-energy Andreev bound states may exist even in the absence of vortex. An asymptotic value of the conductance G_0 at $a \gg \xi$ can be obtained using expression (35) as follows:

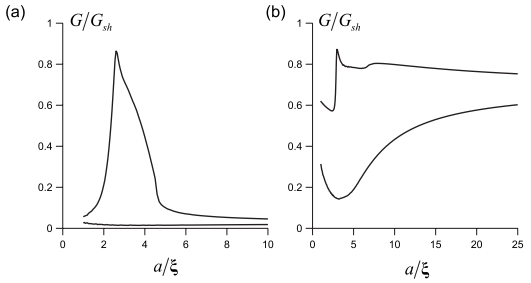

FIG. 8. Plots of the vortex-induced conductance in cases of (a) chiral $d+is$ superconductor for $\Delta_s=0.2\Delta_0$ and (b) $d+id$ superconductor for $\Delta_d=0.2\Delta_0$. The strength of interface barrier is $Z=5$. Different curves on each plot correspond to different vortex orientations with respect to the z axis.

$$G_0/G_{\mathrm{Sh}} = \left(\frac{\Delta_0}{|\Delta_d|}\right)\frac{\pi}{2\sqrt{2}Z^2}.$$

When the vortex approaches the superconducting surface, the conductance is either suppressed [lower curve in Fig. 8(b)] or slightly enhanced [upper curve in Fig. 8(b)]. This behavior can be understood by again using the Eq. (35) with the Doppler-shifted spectrum of Andreev bound states (6). The decrease (increase) in conductance corresponds to the transformation of spectrum shown qualitatively in Fig. 1(c) by dashed (dashed-dotted) lines. It is possible to obtain an analytical expression for the vortex-induced conductance shift at $a \gg \xi$ in the following form:

$$\delta G/G_{\mathrm{Sh}} = \pm\frac{\pi}{2Z^2}\left(\frac{\Delta_0}{\Delta_d}\right)^2\frac{\xi}{L_y}\arctan\left(\frac{L_y}{2a}\right),$$

where the upper and lower signs correspond to the different vortex orientations. As the vortex approaches the surface further, there appears an extremum of the conductance. Such behavior can be explained by a conductance enhancement due to the tunneling of QP into the vortex core states discussed in Ref. 32. A sharp decrease in the upper curve in Fig. 8(b) can be attributed to the opening of an energy gap at the

Fermi level due to the interaction of vortex and surface states.

IV. SUMMARY

In summary, we have investigated how the tunneling conductance and the local density of states (LDOS) in superconductors are affected by the influence of an external magnetic field when the superconducting OP breaks TRS. This is directly relevant for both Sr_2RuO_4, where chiral $p+ip$-wave pairing is believed to be realized, and for the high-T_c cuprates, where a $d+is$- or $d+id$-wave OP has been suggested to exist near surfaces. In addition to breaking TRS, all of these OPs feature surface-bound zero-energy states at surfaces under appropriate circumstances (e.g., a dominant d-wave OP in the $d+is$-wave case).

We have shown how the Doppler shift conspires with an interaction of vortex and surface states to produce a considerable qualitative modification of both the tunneling conductance and the LDOS. When the vortex is located at distances well above a coherence length ξ from the surface, the Doppler shift produces an enhancement or suppression of the LDOS depending on the relative sign of the vorticity and the chirality of the superconducting OP. This effect may be directly probed by first applying an external magnetic field in a direction while measuring the LDOS and then reversing the field direction and measuring again. When the vortex is located very close to the surface (a distance on the order of ξ or smaller), there is an overlap between the vortex and surface states which effectively causes a dramatic change in the tunneling conductance and LDOS. This effect is also sensitive to the relative signs of the vorticity and the chirality of the superconducting OP. The overlap between these two sets of states results in either a strongly enhanced or suppressed tunneling conductance/LDOS at zero-bias voltage/zero energy.

We have demonstrated the aforementioned effects both qualitatively and quantitatively for $p+ip$-, $d+is$-, and $d+id$-wave symmetries. Experimentally, the distance from the surface to the closest vortex can be altered by modifying the field strength. All of our predictions should be possible to test experimentally with present-day techniques.

ACKNOWLEDGMENTS

M.A.S. is grateful to Alexander S. Mel'nikov for numerous stimulating discussions. This work was supported in part by Russian Foundation for Basic Research, by Program "Quantum Macrophysics" of RAS, and by Russian Science Support and "Dynasty" Foundations. J.L. and A.S. were supported by the Norwegian Research Council Grants No. 158518/431, No. 158547/431 (NANOMAT), and No. 167498/V30 (STORFORSK). T.Y. acknowledges the support by JSPS.

[1] Y. Maeno, H. Hashimoto, K. Yoshida, S. Nishizaki, T. Fujita, J. G. Bednorz, and F. Lichtenberg, Nature (London) **372**, 532 (1994); K. Ishida, H. Mukuda, Y. Kitaoka, K. Asayama, Z. Q. Mao, Y. Mori, and Y. Maeno, *ibid.* **396**, 658 (1998); G. M. Luke, Y. Fudamoto, K. M. Kojima, M. I. Larkin, J. Merrin, B. Nachumi, Y. J. Uemura, Y. Maeno, Z. Q. Mao, Y. Mori, H. Nakamura, and M. Sigrist, *ibid.* **394**, 558 (1998); A. P. Mackenzie and Y. Maeno, Rev. Mod. Phys. **75**, 657 (2003); K. D. Nelson, Z. Q. Mao, Y. Maeno, and Y. Liu, Science **306**, 1151 (2004); Y. Asano, Y. Tanaka, M. Sigrist, and S. Kashiwaya, Phys. Rev. B **67**, 184505 (2003); **71**, 214501 (2005).

[2] L. J. Buchholtz, M. Palumbo, D. Rainer, and J. A. Sauls, J. Low Temp. Phys. **101**, 1079 (1995).

[3] M. Matsumoto and H. Shiba, J. Phys. Soc. Jpn. **64**, 3384 (1995).

[4] K. Kuboki and M. Sigrist, J. Phys. Soc. Jpn. **65**, 361 (1996).

[5] M. Sigrist, Prog. Theor. Phys. **99**, 899 (1998).

[6] L. J. Buchholtz, M. Palumbo, D. Rainer, and J. A. Sauls, J. Low Temp. Phys. **101**, 1099 (1995).

[7] M. Matsumoto and H. Shiba, J. Phys. Soc. Jpn. **64**, 4867 (1995).

[8] M. Fogelstrom, D. Rainer, and J. A. Sauls, Phys. Rev. Lett. **79**, 281 (1997).

[9] Y. Tanuma, Y. Tanaka, M. Ogata, and S. Kashiwaya, J. Phys. Soc. Jpn. **67**, 1118 (1998); Phys. Rev. B **60**, 9817 (1999).

[10] M. Covington, M. Aprili, E. Paraoanu, L. H. Greene, F. Xu, J. Zhu, and C. A. Mirkin, Phys. Rev. Lett. **79**, 277 (1997); A. Biswas, P. Fournier, M. M. Qazilbash, V. N. Smolyaninova, H. Balci, and R. L. Greene, *ibid.* **88**, 207004 (2002); Y. Dagan and G. Deutscher, *ibid.* **87**, 177004 (2001); A. Sharoni, O. Millo, A. Kohen, Y. Dagan, R. Beck, G. Deutscher, and G. Koren, Phys. Rev. B **65**, 134526 (2002); A. Kohen, G. Leibovitch, and G. Deutscher, Phys. Rev. Lett. **90**, 207005 (2003); M. Aprili, E. Badica, and L. H. Greene, *ibid.* **83**, 4630 (1999); R. Krupke and G. Deutscher, *ibid.* **83**, 4634 (1999).

[11] M. Franz and Z. Tesanovic, Phys. Rev. Lett. **80**, 4763 (1998).

[12] C. R. Hu, Phys. Rev. Lett. **72**, 1526 (1994).

[13] J. Yang and C.-R. Hu, Phys. Rev. B **50**, 16766 (1994).

[14] Y. Tanaka and S. Kashiwaya, Phys. Rev. Lett. **74**, 3451 (1995); S. Kashiwaya and Y. Tanaka, Rep. Prog. Phys. **63**, 1641 (2000).

[15] J. Y. T. Wei, N. C. Yeh, D. F. Garrigus, and M. Strasik, Phys. Rev. Lett. **81**, 2542 (1998).

[16] Z. Q. Mao, K. D. Nelson, R. Jin, Y. Liu, and Y. Maeno, Phys. Rev. Lett. **87**, 037003 (2001).

[17] L. Alff, S. Kleefisch, U. Schoop, M. Zittartz, T. Kemen, T. Bauch, A. Marx, and R. Gross, Eur. Phys. J. B **5**, 423 (1998); H. Walter, W. Prusseit, R. Semerad, H. Kinder, W. Assmann, H. Huber, H. Burkhardt, D. Rainer, and J. A. Sauls, Phys. Rev. Lett. **80**, 3598 (1998); Yu. S. Barash, M. S. Kalenkov, and J. Kurkija¨rvi, Phys. Rev. B **62**, 6665 (2000); A. Carrington, F. Manzano, R. Prozorov, R. W. Giannetta, N. Kameda, and T. Tamegai, Phys. Rev. Lett. **86**, 1074 (2001).

[18] Y. Tanaka and S. Kashiwaya, Phys. Rev. B **53**, R11957 (1996); Yu. S. Barash, H. Burkhardt, and D. Rainer, Phys. Rev. Lett. **77**, 4070 (1996); R. A. Riedel and P. F. Bagwell, Phys. Rev. B **57**, 6084 (1998); E. Il'ichev, M. Grajcar, R. Hlubina, R. P. J. IJsselsteijn, H. E. Hoenig, H. G. Meyer, A. Golubov, M. H. S. Amin, A. M. Zagoskin, A. N. Omelyanchouk, and M. Y. Kupriyanov,

Phys. Rev. Lett. **86**, 5369 (2001).
[19] Yu. S. Barash, A. M. Bobkov, and M. Fogelstrom, Phys. Rev. B **64**, 214503 (2001).
[20] S. Graser, C. Iniotakis, T. Dahm, and N. Schopohl, Phys. Rev. Lett. **93**, 247001 (2004).
[21] C. Iniotakis, S. Graser, T. Dahm, and N. Schopohl, Phys. Rev. B **71**, 214508 (2005).
[22] T. Yokoyama, C. Iniotakis, Y. Tanaka, and M. Sigrist, Phys. Rev. Lett. **100**, 177002 (2008).
[23] N. B. Kopnin and G. E. Volovik, JETP Lett. **64**, 690 (1996).
[24] Y. Morita, M. Kohmoto, and K. Maki, Phys. Rev. Lett. **78**, 4841 (1997).
[25] M. Franz and Z. Tesanovic, Phys. Rev. Lett. **87**, 257003 (2001); O. Vafek, A. Melikyan, M. Franz, and Z. Tesanovic, Phys. Rev. B **63**, 134509 (2001); O. Vafek, A. Melikyan, and Z. Tesanovic, *ibid.* **64**, 224508 (2001); A. Melikyan and Z. Tesanovic, *ibid.* **76**, 094509 (2007).
[26] A. S. Mel'nikov, Phys. Rev. Lett. **86**, 4108 (2001).
[27] M. Tinkham, *Introduction to Superconductivity*, 2nd ed. (McGraw-Hill, New York, 1996), Chap. 10.
[28] J. Goryo and M. Sigrist, J. Phys.: Condens. Matter **12**, L599 (2000).
[29] G. E. Volovik, JETP Lett. **70**, 609 (1999).
[30] C. Caroli, P. G. de Gennes, and J. Matricon, Phys. Lett. **9**, 307 (1964).
[31] N. B. Kopnin, Phys. Rev. B **57**, 11775 (1998).
[32] M. A. Silaev, Phys. Rev. B **77**, 014504 (2008).
[33] J. Bardeen, R. Kummel, A. E. Jacobs, and L. Tewordt, Phys. Rev. **187**, 556 (1969).
[34] G. D. Mahan, *Many-Particle Physics*, 2nd ed. (Plenum, New York, 1993), Chap. 9.
[35] T. Dahm, S. Graser, C. Iniotakis, and N. Schopohl, Phys. Rev. B **66**, 144515 (2002).
[36] N. Schopohl and K. Maki, Phys. Rev. B **52**, 490 (1995); N. Schopohl, arXiv:cond-mat/9804064 (unpublished).
[37] G. E. Blonder, M. Tinkham, and T. M. Klapwijk, Phys. Rev. B **25**, 4515 (1982).
[38] R. Krupke and G. Deutscher, Phys. Rev. Lett. **83**, 4634 (1999).
[39] A. Sharoni, G. Koren, and O. Millo, Europhys. Lett. **54**, 675 (2001).

Paper XXII

Proximity effect in ferromagnet/superconductor hybrids: From diffusive to ballistic motion.

Physical Review B **79**, 064514 (2009)

Proximity effect in ferromagnet/superconductor hybrids: From diffusive to ballistic motion

Jacob Linder,[1] Malek Zareyan,[2] and Asle Sudbø[1]
[1]*Department of Physics, Norwegian University of Science and Technology, N-7491 Trondheim, Norway*
[2]*Institute for Advanced Studies in Basic Sciences (IASBS), P. O. Box 45195-1159, Zanjan 45195, Iran*
(Received 12 August 2008; revised manuscript received 11 December 2008; published 12 February 2009)

We present an analytical study of the proximity effect in ferromagnet/superconductor (F/S) heterostructures, allowing for an arbitrary magnetic exchange energy as well as arbitrary impurity and spin-flip scattering rates within a quasiclassical approach. While previous studies mainly have focused on the clean or dirty limits, our results grant access to the regime of intermediate impurity concentrations, thus allowing us to probe the crossover from the clean to the dirty limit. We find that in the crossover regime, all possible symmetry correlations of the proximity-induced anomalous Green's function are induced in the ferromagnet. We also point out that the local density of states oscillates spatially not only for an F/S bilayer but also for a normal/superconductor (N/S) bilayer in the diffusive limit, a fact which appears to have gone unnoticed in the literature. Within the weak proximity-effect regime, we present compact analytical expressions valid for arbitrary exchange fields and impurity-scattering rates for (i) the local density of states in an F/S bilayer, (ii) the Josephson current in an S/F/S junction, and (iii) the critical temperature in an F/S/F multilayer. For all cases, we study in particular the crossover regime between diffusive and ballistic motion. Our results may be useful for analyzing experimental data in cases when the dirty limit is not fully reached, thus invalidating the use of the Usadel equation.

DOI: 10.1103/PhysRevB.79.064514 PACS number(s): 74.25.Fy, 74.45.+c, 74.50.+r, 74.62.−c

I. INTRODUCTION

The interest in ferromagnet/superconductor (F/S) heterostructures has increased much during the last decade.[1–3] This may probably be attributed to advances in experimental fabrication/deposition techniques as well as intriguing theoretical predictions. The main hope is that future devices and applications will rely on manipulation of not only the electron charge but also its *spin*. Based on this idea, a new research area known as superspintronics has emerged, aiming at utilization of charge and spin transport in ferromagnet/superconductor heterostructures. For instance, several authors have investigated the possibility of dissipationless currents of spin and charge in magnetically ordered superconductors.[4–11] A large number of other studies related to spin degrees of freedom in superconducting systems has also appeared in the literature.[12–15]

A considerable amount of attention has been devoted to the arguably simplest experimental laboratory where the interplay between ferromagnetism and superconductivity may be studied, namely a F/S bilayer. The two long-range-order phenomena mix close to the interface, giving rise to interesting effects both from a basic physics perspective and in terms of potential applications. These effects include induction of unusual superconducting symmetry correlations and a highly nonmonotonic behavior of various physical quantities on the size of the system. The latter is a result of the nonuniform superconducting correlations that are induced in the ferromagnetic layer by means of the proximity effect.

As a natural extension of the F/S bilayer, there has also been much focus on S/F/S systems and F/S/F systems, where the influence of ferromagnetism on the Josephson current and the critical temperature has been studied, respectively. The large majority of works related to these systems assumed that the diffusive limit was reached. In this case, elastic scattering on impurities renders the Green's function to be isotropic in space while it may still retain a complicated spin structure. From an experimental point of view, the diffusive regime is certainly relevant but there are nevertheless some complications. One point bears upon the theoretical framework used to study the physics in the diffusive regime. The quasiclassical Usadel[16] equation is widely employed to study the proximity effect in F/S heterostructures and is valid under two main assumptions. First, the Fermi energy is much larger than any other energy scale and the essential physics is governed by fermions at Fermi level, and second, the inverse impurity-scattering rate is much larger than any other energy scale except for the Fermi energy. For strong ferromagnets such as Co or Ni, the second condition may be violated. In that case, one must revert to the more general Eilenberger[17] equation, which is only subject to the first condition.

The Eilenberger equation is more complicated to solve analytically than the Usadel equation, although some special limits permit fairly simple analytical expressions. Let h denote the exchange energy of the ferromagnet while τ_{imp} denotes the inverse impurity-scattering rate. The Usadel equation is then obtained from the Eilenberger equation by demanding $h\tau_{\mathrm{imp}} \ll 1$, while the case of a strong and clean ferromagnet is obtained in the limit $h\tau_{\mathrm{imp}} \gg 1$. We assume that $h \gg \Delta$ is fulfilled. In Ref. 18, some aspects of the density of states (DOS) in F/S heterostructures were considered to leading order in the parameter $(h\tau_{\mathrm{imp}})^{-1}$, corresponding to a strong ferromagnet which falls outside the range of applicability of the Usadel equation. In Ref. 19, the Josephson current in an S/F/S structure was also investigated for the case of a strong ferromagnet, $h\tau_{\mathrm{imp}} \gg 1$. Some authors have also considered F/S heterostructures where the impurity-scattering rate was disregarded or assumed to be small, corresponding to the ballistic regime.[20–27]

Although the agreement between theory and experiment in this research area has proven to be satisfactory in many

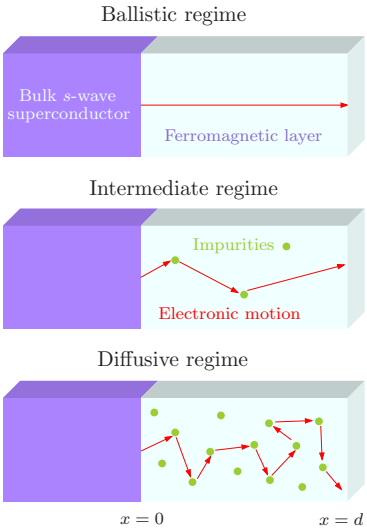

FIG. 1. (Color online) Overview of the superconductor/ferromagnet heterostructure that we study in this paper. We take into account an arbitrary strength of the exchange field as well as an arbitrary rate of nonmagnetic and magnetic scatterings within a quasiclassical approach.

cases, there are still discrepancies to be accounted for. For instance, the Usadel equation has failed to account quantitatively for the critical temperature in F/S/F spin valves. Furthermore, anomalous features in the DOS for a very thin F/S bilayer that could not be accounted for, even qualitatively, were reported in Ref. 28. Moreover, the Usadel equation approach fails from the start when addressing systems with strong ferromagnets.

All of this points to the need of taking the role of impurity scattering more seriously. In this paper, we aim at doing precisely so by solving the Eilenberger equation analytically and studying the *crossover* regime between ballistic and diffusive motion (see Fig. 1). To illustrate how various physical quantities behave in this crossover regime, we study (i) the local density of states (LDOS) in an F/S bilayer, (ii) the Josephson current in an S/F/S junction, and (iii) the critical temperature in an F/S/F multilayer for *arbitrary* values of h and τ (within the quasiclassical approach). In each case, we present compact analytical formula to facilitate comparison to experimental data in cases where the diffusive limit may not be fully warranted or where strong ferromagnets are involved.

This paper is organized as follows. In Sec. II, we establish the theoretical framework which is employed in this work. In Sec. III, we present our main results with their corresponding discussions: the DOS of an F/S bilayer in Sec. III B, the Josephson current in an S/F/S multilayer in Sec. III C, and finally the critical temperature in an F/S/F multilayer in Sec. III D. Equations (25), (32), and (37) are the main analytical results of this work. We conclude in Sec. IV. Below, we will use boldface notation for vectors, $\underline{\ldots}$ for 2×2 matrices, and $\hat{\ldots}$ for 4×4 matrices. The reader may consult the Appendix for a definition of the generalized Pauli matrices we employ in this paper.

II. THEORETICAL FORMULATION

The Eilenberger equation reads[17]

$$i\mathbf{v}_F\cdot\nabla\hat{g}+[\varepsilon\hat{\rho}_3+\hat{M}-\hat{V}_{\mathrm{imp}}-\hat{S}_{\mathrm{flip}}+\hat{\Delta},\hat{g}]=0, \tag{1}$$

where $\hat{g}\equiv\hat{g}^R(\mathbf{R},\varepsilon,\mathbf{p}_F)$ is the retarded part of the Green's function. Here, ε is the quasiparticle energy, $\mathbf{R}$ is the center-of-mass coordinate, and $\mathbf{p}_F$ ($\mathbf{v}_F$) is the Fermi momentum (velocity) vector. The self-energies that enter Eq. (1) are the magnetic exchange energy $\hat{M}=h\,\mathrm{diag}\{\underline{\tau}_3,\underline{\tau}_3\}$, the impurity scattering $\hat{V}_{\mathrm{imp}}=-[i/(2\tau_{\mathrm{imp}})]\langle\hat{g}\rangle$, the (uniaxial) spin-flip scattering $\hat{S}_{\mathrm{flip}}=-[i/(2\tau_{\mathrm{flip}})]\hat{\rho}_3\langle\hat{g}\rangle\hat{\rho}_3$, and the superconducting order parameter

$$\hat{\Delta}=\begin{pmatrix}\underline{0} & i\underline{\tau}_2\Delta\\ i\underline{\tau}_2\Delta^* & \underline{0}\end{pmatrix}.$$

All matrices used above $(\hat{\rho}_i,\underline{\tau}_i)$ are defined in the Appendix [Eq. (A1)]. The brackets $\langle\ldots\rangle$ denote an angular average over the Fermi surface. Also, h is the exchange splitting while $\tau_{\mathrm{imp(flip)}}$ is the scattering time associated with impurity (spin-flip) scattering. We may conveniently rewrite Eq. (1) as

$$i\mathbf{v}_F\cdot\nabla\underline{g}_\sigma+\left[(\varepsilon+\sigma h)\underline{\tau}_3+\sigma\underline{\Delta}+\frac{i}{2\tau_{\mathrm{imp}}}\langle\underline{g}_\sigma\rangle+\frac{i}{2\tau_{\mathrm{sf}}}\underline{\tau}_3\langle\underline{g}_\sigma\rangle\underline{\tau}_3,\underline{g}_\sigma\right]=0,\quad \sigma=\uparrow,\downarrow=\pm 1 \tag{2}$$

where the superconducting order-parameter matrix $\underline{\Delta}$ reads

$$\underline{\Delta}=\begin{pmatrix}0 & \Delta\\ -\Delta^* & 0\end{pmatrix},\quad \Delta=\Delta_0e^{i\chi}, \tag{3}$$

upon letting χ denote the phase corresponding to the globally broken $U(1)$ symmetry in the superconducting state. The brackets $\langle\ldots\rangle$ denote angular averaging over the Fermi surface. We employ the Ricatti parametrization[29] of the Green's function

$$\underline{g}_\sigma=\mathcal{N}_\sigma\begin{pmatrix}1-a_\sigma b_\sigma & 2a_\sigma\\ 2b_\sigma & -1+a_\sigma b_\sigma\end{pmatrix},\quad \mathcal{N}_\sigma=(1+a_\sigma b_\sigma)^{-1}. \tag{4}$$

Here, a_σ and b_σ are two unknown functions used to parametrize the Green's functions. They will be determined by solving the Eilenberger equation with appropriate boundary conditions. A general treatment of the Eilenberger equation calls for a numerical solution. In the case of a weak proximity effect, however, the Eilenberger equation may be linearized in the anomalous part of the Green's function which permits an analytical approach. The assumption of a weak proximity effect corresponds mathematically to a scenario where higher-order terms of $\{a_\sigma,b_\sigma\}$ are disregarded in the Eilenberger equation, i.e., one assumes that $|a_\sigma|\ll 1$ and $|b_\sigma|\ll 1$. In an experimental situation, a weak proximity effect in F/S heterostructures may be expected whenever the

tunneling limit is reached and the number of conducting channels at the interface is low. Also, assuming a superconducting reservoir, the proximity effect becomes weaker in magnitude upon increasing the thickness of the ferromagnetic layer.

The spatial depletion of the superconducting order parameter near the S/F interface will be disregarded. This is an excellent approximation in the corresponding low-transparency regime, which will be considered throughout this paper except for Sec. III D, where this issue is discussed further. At the S/F interface ($x=0$) we use the boundary conditions of Zaitsev.[30] Define the symmetric and antisymmetric parts of the Green's function as

$$\underline{\mathcal{S}_{\sigma,i}} = \frac{1}{2}(\underline{g_{\sigma,i}}^{+} + \underline{g_{\sigma,i}}^{-}), \quad \underline{\mathcal{A}_{\sigma,i}} = \frac{1}{2}(\underline{g_{\sigma,i}}^{+} - \underline{g_{\sigma,i}}^{-}), \tag{5}$$

where the $\pm$ superscript on the Green's function denotes right-going/left-going quasiparticle excitations and the subscript i denotes the ferromagnetic or superconducting region. The first of the boundary conditions of Zaitsev[30] demands continuity of the antisymmetric part $\underline{\mathcal{A}_{\sigma,i}}$ of the Green's function. The second one relates the Green's functions in the ferromagnetic and superconducting regions to the interface transparency. We obtain

$$\underline{\mathcal{A}_{\sigma,F}}\left[\mathcal{R}(1-\underline{\mathcal{A}_{\sigma,F}}^{2}) + \frac{\mathcal{T}}{4}(\underline{\mathcal{S}_{\sigma,S}} - \underline{\mathcal{S}_{\sigma,F}})^{2}\right] = \frac{\mathcal{T}}{4}[\underline{\mathcal{S}_{\sigma,F}}, \underline{\mathcal{S}_{\sigma,S}}]_{-}, \tag{6}$$

where $\mathcal{R}$ and $\mathcal{T}$ are the reflection and transmission coefficients satisfying $\mathcal{R}+\mathcal{T}=1$, and $[\ldots]_{-}$ denotes a commutator. High- and low-transparency interfaces correspond to $\mathcal{T}\simeq 1$ and $\mathcal{T}\ll 1$, respectively. Although Eq. (6) is expressed rather compactly, a general solution for arbitrary $\mathcal{T}$ and $\mathcal{R}$ is very hard to obtain. In the experimentally relevant situation, one may assume that $\mathcal{T}\ll\mathcal{R}$. For a low-transparency barrier and a weak proximity effect, Eq. (6) simplifies greatly to

$$\underline{\mathcal{A}_{\sigma,F}}|_{x=0} = \gamma[\underline{\mathcal{S}_{\sigma,F}}, \underline{\mathcal{S}_{\sigma,S}}]_{-}|_{x=0}, \tag{7}$$

where $\gamma=\mathcal{T}/(4\mathcal{R})$ is a measure of the barrier transparency. At the end of the ferromagnetic layer, we demand $\underline{\mathcal{A}_{\sigma,F}}|_{x=d}=\underline{0}$.

We consider here an effective one-dimensional calculation, which should provide sound results due to the isotropic nature of the ferromagnetic and superconducting order parameters. We do not expect any qualitative differences from a two-dimensional or three-dimensional model, since the superconducting gap and the magnetic exchange field do not depend on the quasiparticle momenta and there are no surface-bound states[31] at the interfaces of the systems we consider. Thus, it should be possible to capture the essential physics by studying an effective one-dimensional model, which permits us to proceed analytically. This point of view is supported by the fact that, as seen later in this work, we reproduce in limiting cases previous results obtained in the literature which employed a two-dimensional calculation.

Under the assumption of a weak proximity effect, the Eilenberger equations in the ferromagnetic region take the form

$$\begin{aligned}
&\alpha i v_F \partial_x a_\sigma + 2a_\sigma(\varepsilon+\sigma h) + \frac{i}{2\tau_{\mathrm{imp}}}(a_\sigma^{\alpha} - a_\sigma^{-\alpha}) + \frac{i}{2\tau_{\mathrm{sf}}}(3a_\sigma^{\alpha} + a_\sigma^{-\alpha}) \\
&= 0, \\
&\alpha i v_F \partial_x b_\sigma - 2b_\sigma(\varepsilon+\sigma h) - \frac{i}{2\tau_{\mathrm{imp}}}(b_\sigma^{\alpha} - b_\sigma^{-\alpha}) - \frac{i}{2\tau_{\mathrm{sf}}}(3b_\sigma^{\alpha} + b_\sigma^{-\alpha}) \\
&= 0,
\end{aligned} \tag{8}$$

where $\alpha=\pm$ denotes right- and left-going quasiparticles, respectively. It is necessary to take into account the direction of the quasiparticles at Fermi level due to the term $\mathbf{v}_F\cdot\nabla\hat{g}$ in Eq. (1). Thus, σ denotes the spin direction while α denotes the direction of motion in a_σ^α and likewise for b_σ^α. The impurity and spin-flip scattering self-energies enter Eq. (8) by means of the matrices $\hat{V}_{\mathrm{imp}}$ and $\hat{S}_{\mathrm{flip}}$ in Eq. (1), which both depend on the Fermi-surface averaged Green's function. For a weak proximity effect, we have

$$\langle\underline{g_\sigma}\rangle = \begin{pmatrix} 1 & a_\sigma^{+} + a_\sigma^{-} \\ b_\sigma^{+} + b_\sigma^{-} & -1 \end{pmatrix}. \tag{9}$$

For a bulk ferromagnet, the solution is $a_\sigma^{\pm}=b_\sigma^{\pm}=0$.

In Ref. 18, the DOS in a S/F bilayer was studied by neglecting both spin-flip scattering ($\tau_{\mathrm{sf}}\to\infty$) and the coupling term between the right- and left-going excitations in Eq. (8). In this case, one finds that Eq. (8) reduces to

$$\begin{aligned}
&\pm i v_F \partial_x a_\sigma^{\pm} + \left[2(\varepsilon+\sigma h) + \frac{i}{2\tau_{\mathrm{imp}}}\right] a_\sigma^{\pm} = 0, \\
&\pm i v_F \partial_x b_\sigma^{\pm} - \left[2(\varepsilon+\sigma h) + \frac{i}{2\tau_{\mathrm{imp}}}\right] b_\sigma^{\pm} = 0.
\end{aligned} \tag{10}$$

The decaying solution for $x\to\infty$ of the above equations reads

$$\begin{aligned}
&a_\sigma^{+} = k_{a\sigma}\exp[-\kappa_\sigma x/l], \quad b_\sigma^{-} = k_{b\sigma}\exp[-\kappa x/l], \\
&\kappa_\sigma = 1 - 2i(\varepsilon+\sigma h)\tau_{\mathrm{imp}}, \quad l = v_F\tau_{\mathrm{imp}},
\end{aligned} \tag{11}$$

while $a_\sigma^{-}=b_\sigma^{+}=0$. Above, $k_{a\sigma}$ and $k_{b\sigma}$ are constants to be determined from the boundary condition at $x=0$, and the structure of the Green's function becomes

$$\underline{\mathcal{S}_{\sigma,F}} = \begin{pmatrix} 1 & a_\sigma^{+} \\ b_\sigma^{-} & -1 \end{pmatrix}, \quad \underline{\mathcal{A}_{\sigma,F}} = \begin{pmatrix} 0 & a_\sigma^{+} \\ -b_\sigma^{-} & 0 \end{pmatrix}. \tag{12}$$

This shows how the decay length of the proximity-induced anomalous Green's function in the ferromagnet is governed by the mean-free path l and that it is independent of the exchange field in this main approximation. We now present a more rigorous solution by fully taking into account the coupling term in Eq. (8). To solve this problem, we note that Eq. (8) may be written as a matrix differential equation,

$$\partial_x \mathbf{a}_\sigma = \underline{M_{a\sigma}} \mathbf{a}_\sigma, \quad \mathbf{a}_\sigma = [a_\sigma^+ a_\sigma^-]^T,$$

$$\underline{M_{a\sigma}} = \frac{1}{v_F}\begin{pmatrix} r_\sigma & g \\ -g & -r_\sigma \end{pmatrix}, \tag{13}$$

where T denotes matrix transpose, and we have defined the auxiliary quantities

$$r_\sigma = 2i(\varepsilon + \sigma h) - (g_{\rm imp} + 3g_{\rm sf})/2,$$

$$g = (g_{\rm imp} - g_{\rm sf})/2, \quad g_{\rm imp(sf)} \equiv \tau_{\rm imp(sf)}^{-1}. \tag{14}$$

Diagonalizing $\underline{M_\sigma}$ according to $\underline{D_\sigma} = \underline{P_\sigma}^{-1}\underline{M_\sigma P_\sigma}$, we obtain the trivial set of decoupled differential equations

$$\partial_x \tilde{\mathbf{a}}_\sigma = \underline{D_\sigma}\tilde{\mathbf{a}}_\sigma, \quad \tilde{\mathbf{a}}_\sigma = \underline{P_\sigma}^{-1}\mathbf{a}_\sigma. \tag{15}$$

From the above, we find that

$$\tilde{a}_\sigma^\pm = C_{a,\sigma}^\pm e^{\pm\lambda_\sigma x}, \quad \lambda_\sigma = v_F^{-1}\sqrt{r_\sigma^2 - g^2}, \tag{16}$$

while the diagonalization matrix $\underline{P_\sigma}$ reads

$$\underline{P_\sigma} = \begin{pmatrix} p_{1\sigma} & p_{2\sigma} \\ p_{2\sigma} & p_{1\sigma} \end{pmatrix}, \quad G_\sigma = g/(v_F\lambda_\sigma + r_\sigma),$$

$$p_{1\sigma} = N_\sigma, \quad p_{2\sigma} = -N_\sigma G_\sigma, \quad N_\sigma = (1 + |G_\sigma|^2)^{-1/2}. \tag{17}$$

In the superconducting region, we employ the bulk solution under the assumption that the interface transparency is low and that the ferromagnetic layer is much more disordered than the superconductor.[1] In this main approximation, we may employ the bulk solution of the Green's function in the superconductor

$$\underline{g_\sigma^\pm} = \begin{pmatrix} c(\theta) & \sigma s(\theta) \\ -\sigma s(\theta) & -c(\theta) \end{pmatrix}$$

with the definitions $c(\theta)=\cosh(\theta)$, $s(\theta)=\sinh(\theta)$, and $\theta = \operatorname{atanh}(\Delta/\varepsilon)$. Once the expression for the Green's function in the ferromagnet has been obtained, one may calculate various physical quantities of interest. By approximating $\underline{\mathcal{S}_{\sigma,F}} \simeq \underline{\tau_3}$ in Eq. (7) in accordance with a weak proximity effect, we obtain, for the case where the impurity-scattering coupling between the Ricatti equations is ignored,

$$\underline{g_{\sigma,F}^\pm} = \underline{\tau_3} + 2\gamma\sigma s(\theta)\exp(-\kappa_\sigma x/l)(\underline{\tau_1} \pm i\underline{\tau_2}), \tag{18}$$

which is precisely the result of Ref. 18 for two semi-infinite superconducting and ferromagnetic layers in contact. When the coupling is properly taken into account, in addition to the vacuum boundary condition at $x=d$, we find that

$$\underline{g_{\sigma,F}^\pm} = \begin{pmatrix} 1 & 2a_\sigma^\pm \\ 2b_\sigma^\pm & -1 \end{pmatrix},$$

upon defining

$$a_\sigma^\pm = p_\sigma^\pm C_{1\sigma}(\lambda_\sigma) + p_\sigma^\mp C_{2\sigma}(\lambda_\sigma),$$

$$b_\sigma^\pm = p_\sigma^\pm C_{1\sigma}(-\lambda_\sigma) + p_\sigma^\mp C_{2\sigma}(-\lambda_\sigma),$$

$$C_{1\sigma} = \frac{2\gamma\sigma s(\theta)e^{\lambda_\sigma x}}{p_\sigma^+ - p_\sigma^-}\left[1 - \frac{e^{\lambda_\sigma d}}{2\sinh(\lambda_\sigma d)}\right],$$

$$C_{2\sigma} = -\frac{\gamma\sigma s(\theta)e^{\lambda_\sigma(d-x)}}{(p_\sigma^+ - p_\sigma^-)\sinh(\lambda_\sigma d)}, \tag{19}$$

and $p_\sigma^\pm = p_{1,2\sigma}$. Note that in the diffusive limit where $g_{\rm imp} \gg \{h, \varepsilon, \Delta_0, g_{\rm sf}\}$, one would expect that the distinction between right-going and left-going particles is removed such that $\underline{g_{\sigma,F}}^+ = \underline{g_{\sigma,F}}^-$. This is easily shown by exploiting

$$\lim_{g_{\rm imp} \gg \{h,\varepsilon,\Delta_0,g_{\rm sf}\}} (v_F\lambda_\sigma + r_\sigma) = -g_{\rm imp}/2, \tag{20}$$

as seen from the previous equations. We also want to compare the results for $g_{\rm imp} \gg \{h, \varepsilon, \Delta_0, g_{\rm sf}\}$ with those obtained when using the linearized Usadel equation. The Usadel equation in a diffusive ferromagnet then reads

$$D\partial_x^2 f_\pm + 2i(\varepsilon + ig_{\rm sf} \pm h)f_\pm = 0, \tag{21}$$

where $f_\pm = f_t \pm f_s$ and f_t is the odd-frequency triplet anomalous Green's function while f_s is the even-frequency singlet anomalous Green's function (both are isotropic in momentum space). We obtain that the only physically acceptable (decaying for $x \to \infty$) solution is

$$f_+ = f_0 e^{ik_+ x} \quad \text{if } \varepsilon > 0, \quad f_- = f_0 e^{-ik_- x} \quad \text{if } \varepsilon < 0,$$

$$k_\pm = \sqrt{2i(\varepsilon + ig_{\rm sf} \pm h)/D}, \tag{22}$$

where f_0 is a constant to be determined from the boundary conditions. Above, D is the diffusion constant. For consistency, we should be able to obtain the same decaying solution from Eq. (19) when $g_{\rm imp} \gg \{h, \varepsilon, \Delta_0, g_{\rm sf}\}$. Focusing on the wave vector, we see that in this limit

$$\lambda_\sigma \to v_F^{-1}\sqrt{-2i(\varepsilon + \sigma h)g_{\rm imp} + 2g_{\rm imp}g_{\rm sf}}$$
$$= \sqrt{-2i(\varepsilon + \sigma h + ig_{\rm sf})/D}, \tag{23}$$

where $D = v_F^2\tau_{\rm imp}$ is the diffusion constant in one dimension (in three dimensions, $D = v_F^2\tau_{\rm imp}/3$). Equation (23) is then consistent with the form of Eq. (22).

With a complete description of the behavior of the Green's function in the ferromagnetic region, we now investigate the influence of the proximity effect on the LDOS and also study the singlet and triplet superconducting order parameters induced in the ferromagnet. The normalized LDOS as obtained from the solution of the Eilenberger equation may be written as

$$N(\varepsilon, x) = \frac{1}{2}\sum_\sigma \langle \mathrm{Re}\{1 + 4a_\sigma(\varepsilon, x)b_\sigma(\varepsilon, x)\}\rangle \tag{24}$$

for a weak proximity effect. In the normal state, the normalized DOS is $N_0 = 1$. Inserting the expressions for $a_\sigma^\pm$ and $b_\sigma^\pm$ into the above equation yields

TABLE I. The proximity-induced anomalous Green's functions in a normal metal, in contact with a conventional BCS superconductor, which has an even-frequency spin-singlet even-parity symmetry. Below, the quasiballistic limit regime is characterized by a vanishing or small value of the impurity-scattering rate, while the diffusive limit is characterized by an impurity-scattering rate which dominates all other energy scales in the problem (except for the Fermi energy).

Symmetry	$h\neq 0$, quasiballistic	$h=0$, quasiballistic	$h\neq 0$, diffusive	$h=0$, diffusive
Even-frequency spin-singlet even-parity (ESE)	√	√	√	√
Odd-frequency spin-singlet odd-parity (OSO)	√	√		
Even-frequency spin-triplet odd-parity (ETO)	√			
Odd-frequency spin-triplet even-parity (OTE)	√		√	

$$N(x,\varepsilon)=1-\mathrm{Re}\left\{\sum_{\sigma}\frac{2\gamma^2 s^2(\theta)}{\sinh(\lambda_\sigma d)(1+G_\sigma)^2}\left\{1+G_\sigma^2-2G_\sigma\left[2\sinh(\lambda_\sigma d-2\lambda_\sigma x)+\frac{\cosh(2\lambda_\sigma x)}{\sinh(\lambda_\sigma d)}\right]\right\}\right\}. \tag{25}$$

Equation (25) is the first of our three main analytical results in this work. Within the weak proximity-effect regime, it provides a general expression for the DOS, taking into account an arbitrary exchange field and impurity-scattering rate. As seen, the correction to the normal-state DOS $N_0=1$ is zero for a vanishing interface transparency ($\gamma=0$). While the weak proximity restriction only allows access to variations from the normal state of DOS of around 10%, this seems to be sufficient for the experimentally relevant situation. For instance, the deviation from the normal-state DOS due to the superconducting proximity effect was of the order of 1% in Ref. 32.

In order to study the superconducting correlations inside the ferromagnetic region, first note that the full structure of the retarded Green's function is

$$\hat{g}^R=\begin{pmatrix}\underline{g} & \underline{f}\\ -\underline{\tilde{f}} & -\underline{\tilde{g}}\end{pmatrix}, \tag{26}$$

where the spin structure reads

$$\underline{f}=\begin{pmatrix}f_{\uparrow\uparrow} & f_{\uparrow\downarrow}\\ f_{\downarrow\uparrow} & f_{\downarrow\downarrow}\end{pmatrix}, \tag{27}$$

and we have defined $f_{\alpha\beta}=f_{\alpha\beta}(\mathbf{p}_F,\varepsilon,x)$ and $\tilde{f}(\mathbf{p}_F,\varepsilon,x)=f(-\mathbf{p}_F,-\varepsilon,x)^*$. From the Ricatti parametrization, we may define the different symmetry components of the anomalous Green's functions as follows:

$$f_{\mathrm{ESE}}=\sum_\sigma\sigma(a_\sigma^+ + a_\sigma^-),\quad f_{\mathrm{OSO}}=\sum_\sigma\sigma(a_\sigma^+ - a_\sigma^-),$$

$$f_{\mathrm{ETO}}=\sum_\sigma(a_\sigma^+ - a_\sigma^-),\quad f_{\mathrm{OTE}}=\sum_\sigma(a_\sigma^+ + a_\sigma^-). \tag{28}$$

Here, the abbreviations are explained in Table I. Note that in the general case of finite h and τ_{imp}, *all possible symmetry components* of the anomalous Green's function are induced in the nonsuperconducting region. In the case of $h=0$, one may confirm from Eq. (19) that $a_\sigma^\pm\rightarrow\sigma a^\pm$, where $a^\pm$ is independent of σ, such that $f_{\mathrm{OTE}}=f_{\mathrm{ETO}}=0$. Physically, the induction of other symmetry components than f_{ESE}, corresponding to the bulk superconductor, may be explained as follows.[33,34] In a normal (N)-metal/superconductor junction, the translational symmetry is broken at the interface separating the two regions. This causes even-parity and odd-parity components of the Green's function to mix near the interface. Since the Pauli principle must be satisfied at all times, a change in the parity symmetry of the Green's function must be accompanied by a change in either spin or frequency symmetry. In the absence of an exchange field, nothing breaks the spin symmetry, such that only the frequency symmetry may be altered indirectly by the broken translational symmetry. However, if the spin symmetry is also broken by replacing the normal metal with a ferromagnet, the spin symmetry of the Green's function may also be altered. These considerations are summarized in Table I. The possibility of a *bulk* odd-frequency superconducting state was discussed in Refs. 35 and 36, and there has very recently been some predictions made concerning characteristic transport properties of such a bulk odd-frequency superconducting state.[33,37–39]

III. RESULTS AND DISCUSSION

A. Anomalous Green's functions

The linearized Eilenberger equations allow us to study the direct crossover from the diffusive to the ballistic regime of quasiparticle transport, and hence dependence of the different symmetry components on the impurity scattering. In the experimental situation, one usually probes the DOS at the F/I interface $x=d$, although in principle it is possible to obtain a spatially resolved DOS in the entire ferromagnetic region by using local scanning tunneling microscopy (STM) measurements. Let us first focus on $x=d$ and consider the ballistic limit, in which case simple and transparent analytical expressions may be obtained from Eq. (28). In the case $h\neq 0$, we obtain

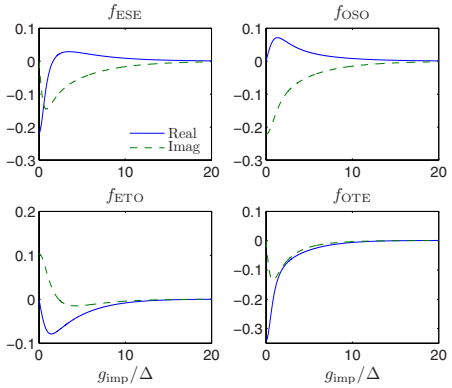

FIG. 2. (Color online) Plot of the proximity-induced anomalous Green's functions in the middle of the ferromagnetic region $(x/d=0.5)$ using $h/\Delta=15$ and $\varepsilon/\Delta_0=0.5$.

$$f_{ESE} = \sum_{\sigma} [-2\gamma s(\theta)]/\sinh(\lambda_\sigma d), \quad f_{OSO} = 0,$$

$$f_{ETO} = 0, \quad f_{OTE} = \sum_{\sigma} [-2\sigma\gamma s(\theta)]/\sinh(\lambda_\sigma d). \quad (29)$$

Note that for $h=0$, λ_σ becomes independent of σ, leading to $f_{OTE}=0$. At first glance, this appears to be in contradiction to Table I since the odd-parity components are absent even in the ballistic limit. However, evaluation of Eq. (28) for $x \neq d$ reveals that these components are in general induced as they should be. It is remarkable that the odd-parity components vanish exactly right at the F/I interface. In the presence of a finite exchange field $h \neq 0$, however, the odd-frequency component f_{OTE} survives at $x=d$, and its influence on physical quantities such as the DOS may be directly probed there. These results suggest that in order to investigate the influence of the odd-frequency superconducting correlations f_{ETO} and f_{OSO}, one would have to measure the DOS also at several positions in the ferromagnetic region and not only at the F/I interface. In Fig. 2, we plot the different symmetry components of the anomalous Green's function in the ferromagnet and their dependence on the impurity level.

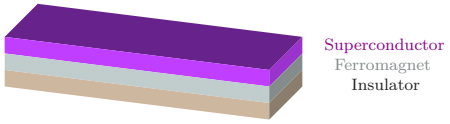

FIG. 3. (Color online) Setup for our study of the density of states.

B. Density of states

To demonstrate the applicability of Eq. (25), we study in particular how the DOS depends on the crossover from the ballistic $(g_{imp}=0)$ to the diffusive limit $(g_{imp} \gg \{h, \varepsilon, \Delta_0, g_{sf}\})$. We will fix $\gamma=0.05$ and $h/\Delta_0=15$ to model a realistic experiment, corresponding to a weak ferromagnetic alloy such as $Cu_{1-x}Ni_x$ or $Pd_{1-x}Ni_x$. The setup is shown in Fig. 3. It is well known that the DOS oscillates in space upon penetration deeper into the ferromagnetic region[40] due to the presence of an exchange field, a feature which is robust both in the clean and dirty limits. However, the energy dependence of the DOS in the presence of an arbitrary impurity concentration has not received much attention so far. This is because most works concerned themselves with the simplified Usadel equation (diffusive limit) or the Eilenberger equation in the absence of impurities (clean limit).

In Ref. 18, corrections to the normal-state DOS as induced by the proximity effect were calculated under the assumption that $h\tau_{imp} \gg 1$. This case corresponds to a ferromagnet where the exchange field is considerably larger than the self-energy associated with the impurity scattering. This

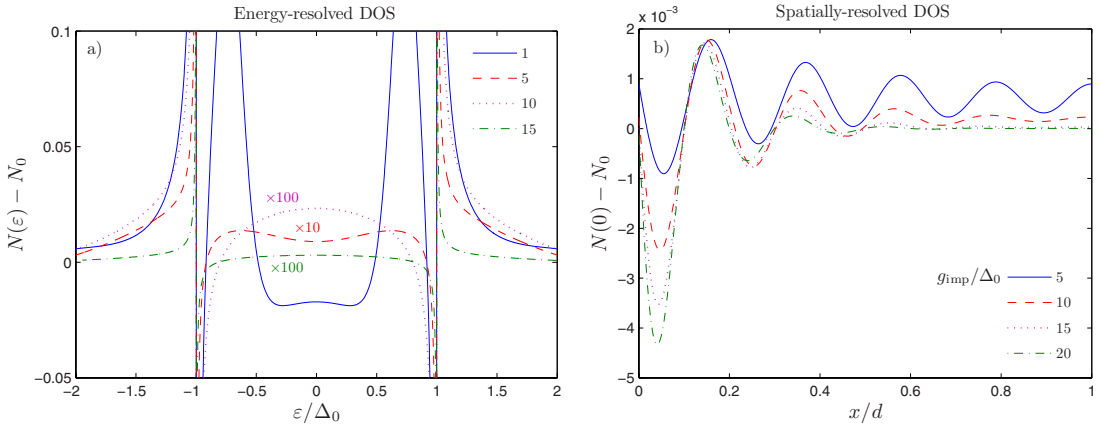

FIG. 4. (Color online) Plot of the (a) energy-resolved DOS at $x=d$ and (b) spatially resolved DOS at $\varepsilon=0$ for several values of the impurity-scattering rate. Here, the exchange field is set to $h/\Delta_0=15$ and $d/\xi=0.5$.

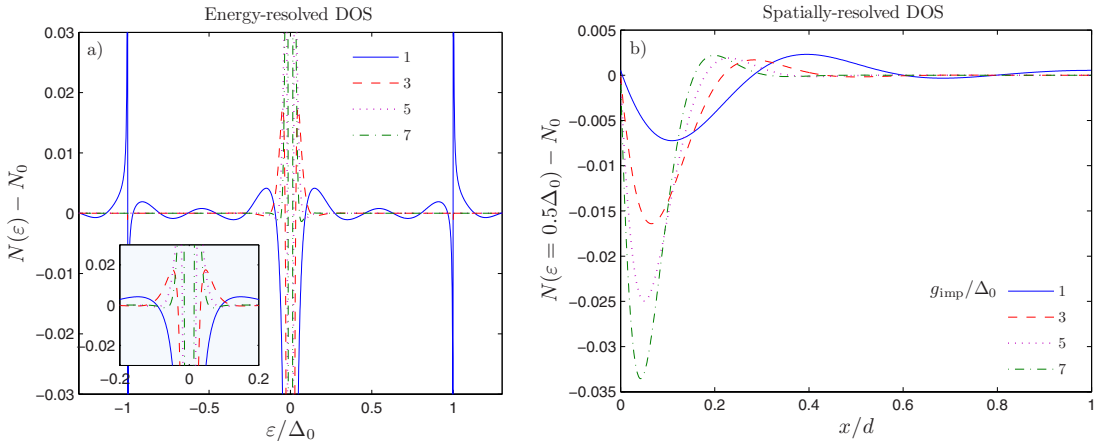

FIG. 5. (Color online) Plot of the (a) energy-resolved DOS at $x=d$ and (b) spatially resolved DOS at $\varepsilon/\Delta_0=0.5$ for several values of the impurity-scattering rate. Here, the exchange field is set to zero, corresponding to a normal metal, and $d/\xi=5.0$.

may describe either a strong ferromagnet (one must still demand $h \ll \varepsilon_F$) or a weak ferromagnet with weak impurity scattering. Neither of these cases is possible to treat with the Usadel equation. In the present work, however, we do not impose any restrictions on the parameter $h\tau_{\rm imp}$, which allows us to study the full crossover regime. This may be important in order to obtain a larger degree of consistency between theory and experimental data in the case when the diffusive limit is not fully reached.

In Fig. 4(a), we study the energy-resolved DOS for an intermediate range of impurity scattering. As a measure of the junction width, we use the superconducting coherence length in the clean limit $\xi_S=v_F/\Delta_0$. To isolate the role of the impurity scattering, we fix the junction width at $d/\xi_S=0.5$. For a superconductor with $v_F=10^5$ m/s and $\Delta_0=1$ meV, this corresponds to $d \simeq 30$ nm, which is experimentally relevant. As seen, the DOS exhibits a slightly oscillating behavior as a function of energy when the impurity-scattering rate $g_{\rm imp}$ is comparable in magnitude to the superconducting gap. This effect becomes more obvious for wider junctions $d/\xi_S \gg 1$ and is attributed to bound states appearing in the ferromagnetic film. We discuss this in more detail below. As $g_{\rm imp}$ increases, however, the DOS becomes featureless for subgap energies, although one may still observe an alternating positive and negative correction to the zero-energy DOS upon increasing $g_{\rm imp}$. In Fig. 4(b), we plot the spatially resolved DOS at $\varepsilon=0$ for various rates of the impurity scattering including the case when $h\tau_{\rm imp} \sim 1$. As seen, the oscillations of the zero-energy DOS are reduced with increasing impurity scattering. We have also investigated the effect of spin-flip scattering for an intermediate value of the impurity concentration. The spin-flip scattering, here taken to be uniaxial, is pair breaking and thus suppresses the proximity effect induced by the superconductor. This aspect agrees with Ref. 41, which found that both the triplet and singlet components are suppressed with uniaxial and/or isotropic spin-flip scattering. For other types of magnetic scattering, such as planar spin-flip or spin-orbit scattering, the singlet and triplet components are affected very differently.[41]

The oscillations of the DOS in S/F junctions are usually attributed to the oscillating decay of the Cooper pair wave function in the ferromagnetic region. In an S/N junction, this decay is monotonous, and hence one would not expect to see any oscillations in the DOS. However, we underline that the impurity scattering plays an important role in this respect. In the ballistic case $g \to 0$, the proximity of the superconductor induces Andreev-bound states with well-defined trajectories which propagate in the normal part of the system. The statistical distribution of all possible trajectories is peaked at given lengths, typically at trajectories corresponding to the first and second reflection processes at the interface. As a result, the DOS in a *clean* S/N junction acquires oscillations both as a function of energy and coordinate inside the normal region as seen in Fig. 5 upon averaging over all possible trajectories. This effect is known as Tomasch oscillations.[42] The influence of impurity scattering on the minigap of a N/S junction was investigated in Ref. 43.

However, there is another point which appears to have been overlooked in the literature, namely, that the spatial oscillations of the DOS in a S/N junction at finite energies *do not vanish* in the diffusive limit. Hence, the oscillating DOS as a function of distance penetrated into the nonsuperconducting region is not a feature pertaining uniquely to F/S junctions, as have been implied in some works.[44] To see this, we plot the spatially resolved DOS both for F/S and N/S junctions in Fig. 6 in the diffusive regime. The curves are obtained by using the framework of Ref. 41, and thus correspond to a full numerical solution of the Usadel equation without restricting ourselves to the weak proximity-effect regime. The oscillations of the DOS in the N/S case may be understood by noting that the induced superconducting Green's function in the normal region has a finite center-of-mass momentum $q=2\varepsilon/v_F$. This is typically much smaller than the center-of-mass momentum acquired in a ferromagnet, $q=2h/v_F$, which means that the corresponding oscillation length is much larger but still present. Such spatial oscillations of the DOS in N/S junctions can be inferred

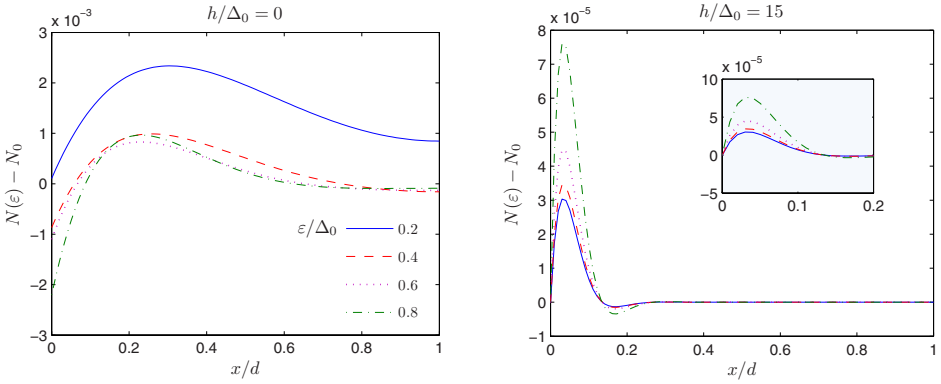

FIG. 6. (Color online) Plot of the spatially resolved DOS for a diffusive N/S and F/S junctions, respectively. In both cases, oscillations of the DOS are seen at finite energies. We have here fixed $d/\xi=3.0$ and $\tau=0.2$ using the notation of Ref. 41 (here, $\xi=\sqrt{D/\Delta_0}$ while τ denotes the barrier transparency).

indirectly from the results of Refs. 45 and 46, although they were not explicitly mentioned there.

Having stated this, it should be noted that the oscillating nature of the anomalous Green's function does not necessarily imply that the critical temperature dependence or the Josephson current in N/S multilayers is nonmonotonuous, e.g., displaying 0-π oscillations, since the energy dependence of the Green's functions is integrated out when obtaining the critical temperature or critical current. For an F/S junction, on the other hand, the Cooper pair wave function may retain its oscillating character even after the energy integration since the center-of-mass momentum depends on the exchange field h.

C. Josephson current

We now evaluate the Josephson current in an SFS junction for an arbitrary impurity concentration with a setup as shown in Fig. 7. Denoting the phase at the left (right) superconductor as $+\chi$ $(-\chi)$, the total phase difference is given by $\varphi=2\chi$. The current through the junction is evaluated by

$$\mathbf{I}_J = \frac{N_F S_0 e v_F}{4} \int d\varepsilon \, \tanh(\beta\varepsilon/2) \mathrm{Tr}\{\langle \hat{\rho}_3 \mathbf{e}_F (\hat{g}^R - \hat{g}^A)\rangle\} \quad (30)$$

under the assumption of equilibrium distribution functions. Here, S_0 is the effective area of the contact through which the current flows, while $\beta=1/T$ is the inverse temperature. Experimentally, one measures the current that flows through the junction, corresponding to the x direction here. We employ the following boundary conditions:

$$\underline{\mathcal{A}_{\sigma,F}}|_{x=0} = \gamma[\underline{\mathcal{S}_{\sigma,F}}, \underline{\mathcal{S}^{\mathrm{Left}}_{\sigma,S}}]_-|_{x=0},$$

$$\underline{\mathcal{A}_{\sigma,F}}|_{x=d} = -\gamma[\underline{\mathcal{S}_{\sigma,F}}, \underline{\mathcal{S}^{\mathrm{Right}}_{\sigma,S}}]_-|_{x=d}, \quad (31)$$

and approximate $\underline{\mathcal{S}_{\sigma,F}}=\underline{\tau_3}$ as in Sec. III B, in accordance with our assumption of a weak proximity effect. After some calculations, we arrive at the following expression for the Josephson current:

$$I_J = 4\gamma^2 N_F S_0 e v_F I_c \sin\varphi, \quad \text{with the definition}$$

$$I_c = \int_{-\infty}^{\infty} d\varepsilon \sum_\sigma \mathrm{Re}\left\{ \frac{s^2(\theta)(1-G_\sigma)\tanh(\beta\varepsilon/2)}{i(1+G_\sigma)\sinh(\lambda_\sigma d)} \right\}. \quad (32)$$

The reader is reminded of the definitions

$$G_\sigma = g/(\sqrt{r_\sigma^2 - g^2} + r_\sigma),$$

$$r_\sigma = 2i(\varepsilon + \sigma h) - (g_{\mathrm{imp}} + 3g_{\mathrm{sf}})/2,$$

$$g = (g_{\mathrm{imp}} - g_{\mathrm{sf}})/2, \quad g_{\mathrm{imp(sf)}} \equiv \tau^{-1}_{\mathrm{imp(sf)}}. \quad (33)$$

Equation (32) is the second of our three main analytical results in this work. It is probably the most compact way of expressing the Josephson current for arbitrary exchange fields and impurity-scattering rates within the quasiclassical framework. It is thus suitable both for the case of a weak ferromagnet (such as the alloy $Cu_{1-x}Ni_x$) and for strong ferromagnets (such as Co or Fe) regardless of whether they are clean or dirty. In experiments performed with such strong ferromagnets, where the exchange field may be of the order of 100 meV ($\gg T_c$), the Usadel equation is not valid at the same time as the clean limit may not be fully reached. In this case, one has to use an expression valid for the crossover regime, which emphasizes the importance of Eq. (32).

Below, we will study how impurity scattering affects both the width and temperature dependences of the critical current, as well as its corresponding 0-π phase diagram. Bergeret *et al.*[19] investigated this in the limiting cases of

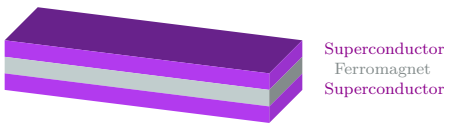

FIG. 7. (Color online) Setup for our study of the Josephson current.

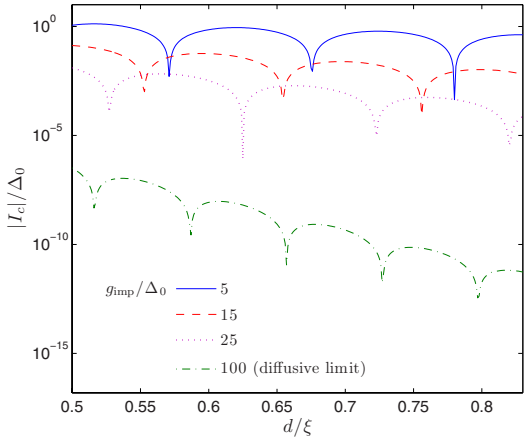

FIG. 8. (Color online) Plot of the critical current as a function of junction width d. We have used $T/T_c=0.2$.

$h\tau_{\rm imp}\ll 1$ and $h\tau_{\rm imp}\gg 1$, while the majority of studies so far considered exclusively the limiting case of diffusive motion. The possibility of 0-π oscillations in clean and strong ferromagnets was recently studied in Refs. 47 and 48. We here pay particular attention to the crossover between the ballistic and diffusive sector, which has not been investigated previously. To model inelastic scattering, we add a small imaginary number to the quasiparticle energy $\varepsilon\rightarrow\varepsilon+i\delta$, where $\delta=10^{-3}$.

In Fig. 8, we plot the width dependence of the critical current for a temperature $T/T_c=0.2$. As seen, increasing impurity scattering suppresses the magnitude of the current and also reduces the oscillation length $l_{\rm osc}$. The dependence of the latter on impurity scattering is shown explicitly in Fig. 9. Using the Usadel equation, it is predicted that the oscillation length of the critical current in the dirty limit should depend on the impurity-scattering rate like $\sqrt{hl_{\rm imp}}\sim\sqrt{\tau_{\rm imp}}$ (for a discussion of the characteristic decay and oscillation lengths in the clean and dirty limits, see Table I in Ref. 2). We obtain a good fit with this in Fig. 9 when $g_{\rm imp}\gg\Delta$. For values of $g_{\rm imp}$ comparable to Δ, however, the oscillation length saturates at a finite value. In the ballistic limit, the oscillation length is known to depend on the exchange field like $1/h$. We have also confirmed this for several values of h when $g_{\rm imp}\sim\Delta$.

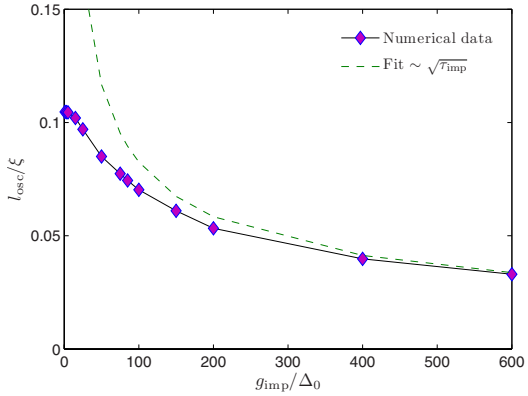

FIG. 9. (Color online) Plot of the oscillation length of the critical current as a function of the impurity-scattering strength $g_{\rm imp}$. We have used $T/T_c=0.2$.

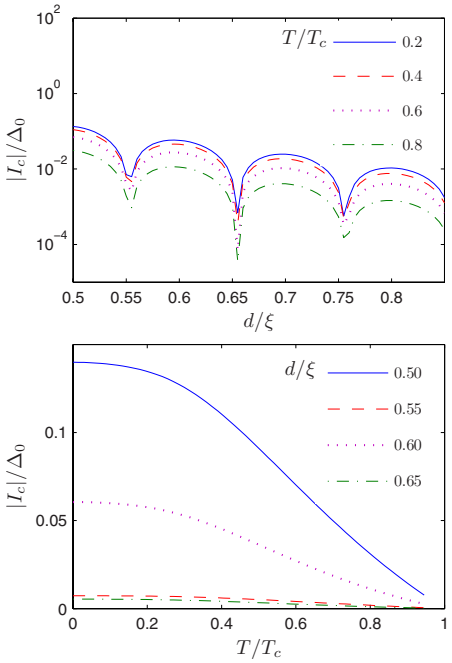

FIG. 10. (Color online) Plot of the d dependence and the T dependence of the critical current for $g_{\rm imp}/\Delta_0=15$, corresponding to $h\tau_{\rm imp}=1$.

Also, one notes from Fig. 8 that the decay length of the current increases with the concentration of impurities. It should be noted that the measure ξ used as a length unit in this context is *independent* of the impurity-scattering rate since we are using $\xi=v_F/\Delta_0$. This way, we ensure that the effects observed are really due to the increased impurity scattering. If we for instance had used the mean-free path $l_{\rm mfp}=v_F\tau_{\rm imp}$ as a measure for the junction width, the scale would have been different for each value of $g_{\rm imp}$ in Fig. 8. We also underline that the dirty limit condition is $\xi/l_{\rm mfp}\gg 1$, while the size d of the sample may be either smaller or larger than ξ as long as that condition is fulfilled.

In Fig. 10, we pay particular attention to the case $h\tau_{\rm imp}=1$ which is inaccessible in the Usadel framework. As seen, nothing qualitatively new shows up in the d dependence or the T dependence of the critical current as compared to the diffusive limit, although the decay rate is considerably lower. We also investigate how the 0-π phase diagram of the Josephson junction is affected by impurity scattering. This is most conveniently plotted in the d-T plane. In Fig. 11, one observes several features. First, it is clear that

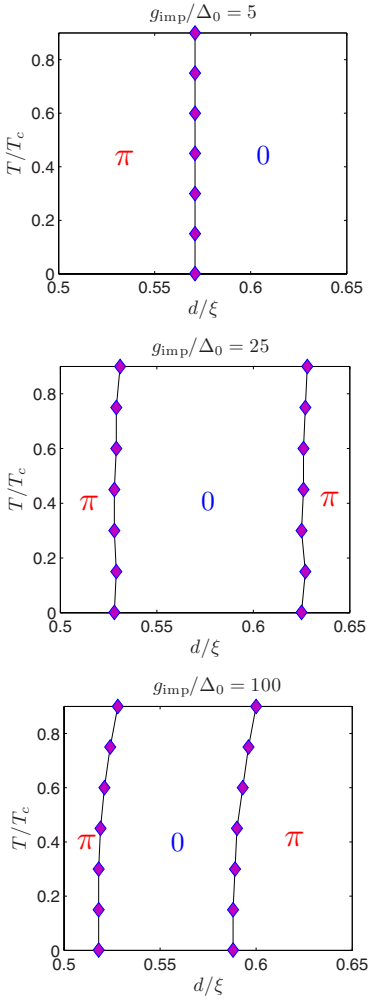

FIG. 11. (Color online) Phase diagram in the d-T plane for the 0-π transitions of the critical current for several values of the impurity concentration.

the area occupied by the 0 and π phases, respectively, diminishes with increasing g_{imp}, in agreement with the shortened oscillation length of Fig. 9. Second, it is seen that thermal 0-π transitions are (practically speaking) impossible to observe for scattering rates satisfying $g_{\mathrm{imp}} \leq h$. As the scattering rate is increased, however, the thermal transitions become possible when $g_{\mathrm{imp}} \gg h$ or equivalently $h\tau_{\mathrm{imp}} \ll 1$. In this regime, the Usadel equation is valid and we obtain consistency with previous results. At all scattering rates, the width-induced transitions are possible.

D. Critical temperature

Finally, we investigate F/S/F layers where the critical temperature of the superconductor is sensitive to the relative

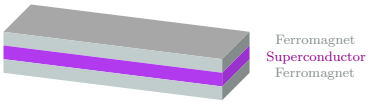

FIG. 12. (Color online) Setup for our study of the critical temperature.

orientation of magnetization of the two F layers. This effect is usually dubbed to a *spin-switch* effect in the literature. Our setup is shown in Fig. 12. Tagirov[49] was the first to point out the interesting opportunity to "activate" superconductivity simply by means of switching the direction of the magnetization in one of the ferromagnetic layers. Since then, a number of works have elaborated on the spin-switch effect both experimentally[50–52] and theoretically.[40,53–55] In particular, a convincing numerical approach was developed in Ref. 54. So far, however, almost all theoretical works focused on the dirty limit, in which the critical temperature may be conveniently calculated by using the Usadel equation in the Matsubara frequency representation. Although the obtained results compare well qualitatively with experimental data, an unsolved factor so far is the discrepancy of 2 orders of magnitude of the predicted effect. Recently, it was proposed and investigated[56] if an asymmetry in the interface transparencies of the F/S/F junctions could be responsible for this; in effect one of the interfaces was much less transparent than the other. The authors of Ref. 56 concluded that this was not the case. At present, the single ferromagnet F/S/F devices to have been examined so far have used strong ferromagnets, which falls outside the range of applicability of the Usadel equation.[50–52] In light of this, it would be interesting to go beyond the usual treatment with the Usadel equation and solve the more general Eilenberger equation to investigate the role of the impurity scattering.

A general analytical solution for arbitrary proximity effect and barrier transparency is hardly achievable, as pointed out previously. Nevertheless, it is reasonable to expect that one may capture the essential physics in the weak proximity-effect regime. In order to calculate the critical temperature for the parallel (P) and antiparallel (AP) alignments, we assume that the temperature is close to T_c, which allows us to write the Green's function in the superconductor as follows:

$$\underline{g}_\sigma = \begin{pmatrix} 1 & 2a_\sigma \\ 2b_\sigma & -1 \end{pmatrix}, \tag{34}$$

since $\lim_{\Delta \to 0} c(\theta) = 1$. For the normal part of the Green's function matrix, this means that $(1 - a_\sigma b_\sigma)/(1 + a_\sigma b_\sigma) \simeq 1$, while for the anomalous Green's function one thus has $2a_\sigma/(1 + a_\sigma b_\sigma) \simeq 2a_\sigma$. The self-consistency equation for the superconducting gap reads in general[57]

$$\Delta = \frac{N_F \lambda}{8} \mathrm{Tr}\left\{ \left(\frac{\hat{\rho}_1 - i\hat{\rho}_2}{2} \right) \hat{\tau}_3 \int d\varepsilon \langle \hat{g}^K \rangle \right\}, \quad \lambda > 0, \tag{35}$$

where λ is the attractive interaction and $\hat{g}^K$ is the Keldysh part of the Green's function. For an equilibrium situation $[\hat{g}^K = (\hat{g}^R - \hat{g}^A)\tanh(\beta\varepsilon/2)]$ in the weak proximity-effect regime with a temperature very close to T_c, this reduces to

$$\Delta = \frac{N_F\lambda}{8}\int d\varepsilon \tanh\left(\frac{\varepsilon}{2T_c}\right)\sum_{\pm}\sum_{\sigma}\sigma[a_\sigma^{\pm} - (b_\sigma^{\pm})^*]. \quad (36)$$

Once the anomalous Green's functions $\{a_\sigma^{\pm}, b_\sigma^{\pm}\}$ have been obtained, one may solve Eq. (37) numerically to obtain T_c in the P and AP configurations. Using boundary conditions explained below, we solve for the anomalous Green's functions in both the ferromagnetic and superconducting regions and obtain the following equation determining the critical temperature:

$$1 - N_F\lambda\int_0^{\omega} d\varepsilon \tanh\left(\frac{\varepsilon}{2T_c}\right)\varepsilon^{-1}\left[1 - \cos(2\varepsilon x/v_F) - \sum_{\sigma,\pm}\mathrm{Re}\left\{\frac{L_\sigma^{\pm}e^{\pm 2i\varepsilon x/v_F}\sum_\alpha \alpha R_\sigma^\alpha(1 - e^{2\alpha i\varepsilon d_S/v_F})}{4\sum_\alpha \alpha e^{2\alpha i\varepsilon d_S/v_F}L_\sigma^\alpha R_\sigma^\alpha}\right\}\right] = 0, \quad (37)$$

with the cutoff energy ω, $\alpha = \pm$, and finally

$$L_\sigma^{\pm} = e^{\pm\lambda_\sigma^{\mathrm{Left}}d_F} - G_\sigma^{\mathrm{Left}}e^{\mp\lambda_\sigma^{\mathrm{Left}}d_F},$$

$$R_\sigma^{\pm} = e^{\pm\lambda_\sigma^{\mathrm{Right}}d_F} - G_\sigma^{\mathrm{Right}}e^{\mp\lambda_\sigma^{\mathrm{Right}}d_F}. \quad (38)$$

Equation (37) is the third of our three main analytical results in this work. It gives an expression for the critical temperature in an F/S/F junction for arbitrary exchange fields and impurity-scattering rates within the framework of quasiclassical theory in the weak proximity-effect regime.

In order to find $\{a_\sigma^{\pm}, b_\sigma^{\pm}\}$, we must introduce proper boundary conditions at each of the interfaces in the setup (Fig. 12). The left ferromagnet is assumed to occupy the region $-d_F < x < 0$, the superconductor is located at $0 < x < d_S$, while the right ferromagnet occupies the space $d_S < x < d_S + d_F$. Thus, the ferromagnetic layers are assumed to have the same thickness d_F while the superconductor has thickness d_S. Due to the complexity of the problem, we will assume rigid boundary conditions at the superconductor/ferromagnet interfaces, which amount to continuity of the Green's function. Although the low-transparency limit is probably more realistic, it is reasonable to expect qualitatively correct results in this approach. Moreover, since we already assume a temperature close to T_c, the proximity effect would be almost completely absent if we (in addition) incorporated tunneling interfaces. In general, high-transparency interfaces cause a depletion of the superconducting order parameter near the interface, which means that one should (strictly speaking) solve for the spatial depletion of the gap self-consistently. In our approach, we do not incorporate this depletion since we are aiming for analytical results. A full numerical approach would, however, doubtlessly improve the accuracy of the results presented below but at the prize of losing the analytical information.

At the ends of the ferromagnetic layers, we impose vacuum boundary conditions. In total, the boundary conditions then read

$$x = -d_F: \underline{\mathcal{A}_{\sigma,F}^{\mathrm{Left}}} = \underline{0},$$

$$x = 0: \underline{g_{\sigma,F}^{\mathrm{Left}}} = \underline{g_\sigma},$$

$$x = d_S: \underline{g_\sigma} = \underline{g_{\sigma,F}^{\mathrm{Right}}},$$

$$x = d_S + d_F: \underline{\mathcal{A}_{\sigma,F}^{\mathrm{Right}}} = \underline{0}. \quad (39)$$

After straightforward calculations, we obtain an expression for $\{a_\sigma^{\pm}, b_\sigma^{\pm}\}$ in the superconductor. A few comments with regard to the expression Eq. (37) are in order. First, it should be noted that the expression for the critical temperature in Eq. (37) depends on the position x in the superconductor through the spatial dependence of the anomalous Green's function. This dependence is of course artificial and a result of the approximations we have made in the calculations; in a real experimental sample, T_c is a property for the entire layer and does not depend on the position in the superconductor. The reason why we obtain an artificial x dependence in the expression for the critical temperature is because we have neglected the spatial modification of the order parameter Δ in the layer. Employing a fully self-consistent calculation would remove the spatial dependence of T_c in the gap equation. However, for thin superconducting layers $d_S/\xi \ll 1$, our approximation is expected to be good. A similar procedure has been used in several other works which calculated T_c by means of the Usadel equation. In those works, it was assumed that the anomalous Green's function in the superconductor varied very little as long as $d_S/\xi \ll 1$ was satisfied, and hence one could ignore the spatial dependence of the Green's function once it had been found. More precisely, T_c was evaluated in the middle of the superconducting region. In our case, we will use the same approximation since our approach is analytical in nature. The main contribution to the integral in Eq. (37) comes from energies $\varepsilon \leq \Delta$, for which the terms including the coordinate x on the right-hand side of the equation change very little as long as $d_S/\xi \ll 1$. We will focus on the difference between the critical temperature in the P and AP alignments defined as

$$\Delta T_c \equiv T_c^{\mathrm{AP}} - T_c^{\mathrm{P}}. \quad (40)$$

We will normalize all temperatures on T_c^0, which is the bulk critical temperature of the superconductor in the absence of a proximity effect. As demanded by consistency, the critical temperature approaches T_c^0 when $d_F \to 0$. We choose the cutoff frequency as $\omega/\Delta_0 = 30$.

With the analytical solution in hand, we now present a study of the critical temperature in the P and AP configurations, investigating in particular the role of impurity scattering. First, we plot the critical temperature as a function of ferromagnetic layer thickness with a fixed superconducting layer thickness of $d_S/\xi = 0.03$ in Fig. 13. Using a superconductor with $\xi = 200$ nm, this would correspond to a thickness $d_S = 6$ nm. To ensure the validity of our assumption that the anomalous Green's functions vary little with x throughout the superconducting layer, we plot the critical temperature both at $x/d_S = 0.50$ (symbols) and $x/d_S = 0.01$ (dashed lines). As seen, the difference is negligible. From Fig. 13, one may

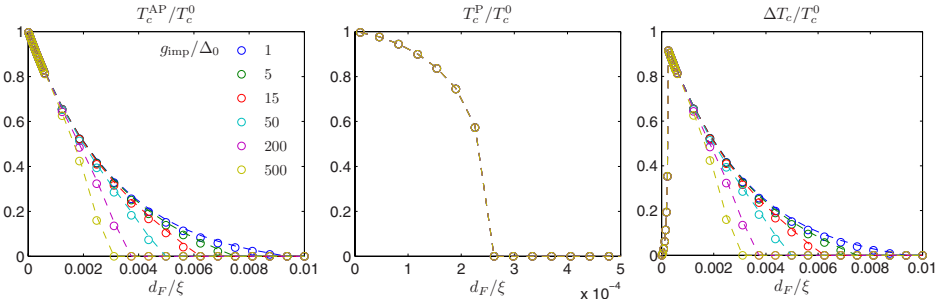

FIG. 13. (Color online) Plot of the critical temperature in an F/S/F structure as a function of the ferromagnetic layer thickness d_F for fixed d_S/ξ=0.03. Note the different scale for d_F in the middle panel. The symbols denote the result for x/d_S=0.50 while the dashed lines correspond to x/d_S=0.01.

infer that the critical temperature in the P configuration goes to zero much faster than in the AP configuration as a function of the ferromagnetic layer thickness d_F. This supports the notion that the antiparallel configuration favors superconductivity in the middle layer. The effect of impurity scattering is seen to suppress the critical temperature in general.

One may understand intuitively why the antiparallel alignment is favorable compared to the parallel alignment, since the average exchange field cancels in the former case. Qualitatively, our results are consistent with the monotonic decay found for a high barrier transparency when using the Usadel equation.[2] However, a more realistic scenario would be to invoke low barrier transparency boundary conditions at the S/F interfaces. Due to the complexity of the problem upon including an arbitrary amount of impurities, we have used perfectly transparent interfaces here as a first approximation. It would nevertheless be quite interesting to extend this formalism to low-transparency interfaces to investigate the role of impurity scattering under those circumstances. Especially, the role of g_{imp} with regard to the re-entrant behavior of T_c would be worth investigating. Our analytical results may serve as a basis for extending this formalism to low-transparency interfaces in the case of an arbitrary value for $h\tau_{imp}$, as opposed to $h\tau_{imp} \ll 1$ in the Usadel regime.

IV. SUMMARY

We have investigated various aspects of the physics resulting from the proximity effect in ferromagnet/superconductor (F/S) bilayers. In contrast to previous works, which were limited to either the clean or dirty limit, we have taken into account an arbitrary scattering rate for both nonmagnetic and magnetic impurities. This has allowed us to access the crossover regime from the ballistic to diffusive regime of the proximity effect. We have derived analytical formula for (i) the proximity-induced DOS of an F/S bilayer, (ii) the Josephson current in an S/F/S junction, and (iii) the critical temperature of an F/S/F structure. Our results are valid for an arbitrary ratio of the parameter $h\tau_{imp}$ and are thus applicable both to weak ferromagnetic alloys as well as Permalloys in either the diffusive or clean limit.

ACKNOWLEDGMENTS

J.L. acknowledges T. Yokoyama, A. Cottet, F. S. Bergeret, and Ya. Fominov for useful discussions. H. Skadsem and M. Thaule are also thanked for valuable input. J.L. and A.S. were supported by the Norwegian Research Council under Grants No. 158518/431, No. 158547/431 (NANOMAT), and No. 167498/V30 (STORFORSK). M.Z. thanks A. Brataas and A. Sudbø for their hospitality and support during his visit to the Centre for Advanced Study, Oslo.

APPENDIX

The Pauli matrices used in this paper are defined as

$$\underline{\tau}_1 = \begin{pmatrix} 0 & 1 \\ 1 & 0 \end{pmatrix}, \quad \underline{\tau}_2 = \begin{pmatrix} 0 & -i \\ i & 0 \end{pmatrix}, \quad \underline{\tau}_3 = \begin{pmatrix} 1 & 0 \\ 0 & -1 \end{pmatrix},$$

$$\underline{1} = \begin{pmatrix} 1 & 0 \\ 0 & 1 \end{pmatrix}, \quad \hat{1} = \begin{pmatrix} \underline{1} & \underline{0} \\ \underline{0} & \underline{1} \end{pmatrix}, \quad \hat{\tau}_i = \begin{pmatrix} \underline{\tau}_i & \underline{0} \\ \underline{0} & \underline{\tau}_i \end{pmatrix},$$

$$\hat{\rho}_1 = \begin{pmatrix} \underline{0} & \underline{\tau}_1 \\ \underline{\tau}_1 & \underline{0} \end{pmatrix}, \quad \hat{\rho}_2 = \begin{pmatrix} \underline{0} & -i\underline{\tau}_1 \\ i\underline{\tau}_1 & \underline{0} \end{pmatrix}, \quad \hat{\rho}_3 = \begin{pmatrix} \underline{1} & \underline{0} \\ \underline{0} & -\underline{1} \end{pmatrix}. \tag{A1}$$

[1] F. S. Bergeret, A. F. Volkov, and K. B. Efetov, Rev. Mod. Phys. **77**, 1321 (2005).
[2] A. I. Buzdin, Rev. Mod. Phys. **77**, 935 (2005).
[3] Yu. A. Izyumov, Yu. N. Proshin, and M. G. Khusainov, Phys. Usp. **45**, 109 (2002).
[4] M. L. Kulić and I. M. Kulić, Phys. Rev. B **63**, 104503 (2001).
[5] F. S. Bergeret, A. F. Volkov, and K. B. Efetov, Phys. Rev. Lett. **86**, 3140 (2001).

[6] I. Eremin, F. S. Nogueira, and R.-J. Tarento, Phys. Rev. B **73**, 054507 (2006).
[7] Y. Zhao and R. Shen, Phys. Rev. B **73**, 214511 (2006).
[8] M. S. Grønsleth, J. Linder, J.-M. Børven, and A. Sudbø, Phys. Rev. Lett. **97**, 147002 (2006); J. Linder, M. S. Grønsleth, and A. Sudbø, Phys. Rev. B **75**, 024508 (2007).
[9] Y. Asano, Phys. Rev. B **74**, 220501(R) (2006).
[10] P. M. R. Brydon, B. Kastening, D. K. Morr, and D. Manske, Phys. Rev. B **77**, 104504 (2008).
[11] T. Champel, T. Löfwander, and M. Eschrig, Phys. Rev. Lett. **100**, 077003 (2008).
[12] A. Brataas and Y. Tserkovnyak, Phys. Rev. Lett. **93**, 087201 (2004).
[13] D. Huertas-Hernando, Yu. V. Nazarov, and W. Belzig, Phys. Rev. Lett. **88**, 047003 (2002).
[14] F. Giazotto and F. Taddei, Phys. Rev. B **77**, 132501 (2008).
[15] J. Linder, T. Yokoyama, Y. Tanaka, and A. Sudbø, Phys. Rev. B **78**, 014516 (2008).
[16] K. Usadel, Phys. Rev. Lett. **25**, 507 (1970).
[17] G. Eilenberger, Z. Phys. **214**, 195 (1968).
[18] F. S. Bergeret, A. F. Volkov, and K. B. Efetov, Phys. Rev. B **65**, 134505 (2002).
[19] F. S. Bergeret, A. F. Volkov, and K. B. Efetov, Phys. Rev. B **64**, 134506 (2001).
[20] M. Zareyan, W. Belzig, and Yu. V. Nazarov, Phys. Rev. B **65**, 184505 (2002); Phys. Rev. Lett. **86**, 308 (2001).
[21] J. Kopu, M. Eschrig, J. C. Cuevas, and M. Fogelström, Phys. Rev. B **69**, 094501 (2004).
[22] K. Halterman, O. T. Valls, and P. H. Barsic, Phys. Rev. B **77**, 174511 (2008); K. Halterman, P. H. Barsic, and O. T. Valls, Phys. Rev. Lett. **99**, 127002 (2007); K. Halterman and O. T. Valls, Phys. Rev. B **66**, 224516 (2002).
[23] J. Linder and A. Sudbø, Phys. Rev. B **75**, 134509 (2007).
[24] A. I. Buzdin, L. N. Bulaevskii, and S. V. Panyukov, Pis'ma Zh. Eksp. Teor. Fiz. **35**, 147 (1982) [JETP Lett. **35**, 178 (1982)].
[25] M. Fogelström, Phys. Rev. B **62**, 11812 (2000).
[26] N. M. Chtchelkatchev, W. Belzig, Yu. V. Nazarov, and C. Bruder, JETP Lett. **74**, 323 (2001).
[27] I. V. Bobkova and Yu. S. Barash, Phys. Rev. B **71**, 144510 (2005).
[28] P. SanGiorgio, S. Reymond, M. R. Beasley, J. H. Kwon, and K. Char, Phys. Rev. Lett. **100**, 237002 (2008).
[29] N. Schopohl and K. Maki, Phys. Rev. B **52**, 490 (1995); N. Schopohl, arXiv:cond-mat/9804064 (unpublished).
[30] A. V. Zaitsev, Sov. Phys. JETP **59**, 1163 (1984).
[31] C.-R. Hu, Phys. Rev. Lett. **72**, 1526 (1994); J. Yang and C.-R. Hu, Phys. Rev. B **50**, 16766 (1994).
[32] T. Kontos, M. Aprili, J. Lesueur, and X. Grison, Phys. Rev. Lett. **86**, 304 (2001).
[33] Y. Tanaka, A. A. Golubov, S. Kashiwaya, and M. Ueda, Phys. Rev. Lett. **99**, 037005 (2007).
[34] T. Yokoyama, Y. Tanaka, and A. A. Golubov, Phys. Rev. B **78**, 012508 (2008).
[35] V. L. Berezinskii, JETP Lett. **20**, 287 (1974).
[36] E. Abrahams, A. Balatsky, D. J. Scalapino, and J. R. Schrieffer, Phys. Rev. B **52**, 1271 (1995).
[37] J. Linder, T. Yokoyama, and A. Sudbø, Phys. Rev. B **77**, 174507 (2008).
[38] Ya. V. Fominov, JETP Lett. **86**, 732 (2007).
[39] J. Linder, T. Yokoyama, Y. Tanaka, Y. Asano, and A. Sudbø, Phys. Rev. B **77**, 174505 (2008).
[40] I. Baladie and A. Buzdin, Phys. Rev. B **64**, 224514 (2001).
[41] J. Linder, T. Yokoyama, and A. Sudbø, Phys. Rev. B **77**, 174514 (2008).
[42] W. J. Tomasch, Phys. Rev. Lett. **15**, 672 (1965).
[43] S. Pilgram, W. Belzig, and C. Bruder, Phys. Rev. B **62**, 12462 (2000).
[44] A. Buzdin, Phys. Rev. B **62**, 11377 (2000).
[45] W. Belzig, C. Bruder, and G. Schön, Phys. Rev. B **54**, 9443 (1996).
[46] W. Belzig, F. K. Wilhelm, C. Bruder, G. Schön, and A. D. Zaikin, Superlattices Microstruct. **25**, 1251 (1999).
[47] F. Konschelle, J. Cayssol, and A. I. Buzdin, Phys. Rev. B **78**, 134505 (2008).
[48] R. Zikic, L. Dobrosavljević-Grujić, and B. Vujičić, Phys. Rev. B **79**, 052503 (2009).
[49] L. R. Tagirov, Physica C **307**, 145 (1998); L. R. Tagirov, Phys. Rev. Lett. **83**, 2058 (1999).
[50] A. Yu. Rusanov, S. Habraken, and J. Aarts, Phys. Rev. B **73**, 060505(R) (2006).
[51] I. C. Moraru, W. P. Pratt, Jr., and N. O. Birge, Phys. Rev. Lett. **96**, 037004 (2006).
[52] I. C. Moraru, W. P. Pratt, Jr., and N. O. Birge, Phys. Rev. B **74**, 220507(R) (2006).
[53] A. I. Buzdin, A. V. Vedyayev, and N. V. Ryzhanova, Europhys. Lett. **48**, 686 (1999).
[54] Ya. V. Fominov, N. M. Chtchelkatchev, and A. A. Golubov, Phys. Rev. B **66**, 014507 (2002).
[55] T. Löfwander, T. Champel, and M. Eschrig, Phys. Rev. B **75**, 014512 (2007).
[56] P. Cadden-Zimansky, Ya. B. Bazaliy, L. M. Litvak, J. S. Jiang, J. Pearson, J. Y. Gu, Chun-Yeol You, M. R. Beasley, and S. D. Bader, Phys. Rev. B **77**, 184501 (2008).
[57] We have here notations and conventions close to the ones of J. P. Morten, M.Sc. thesis, Norwegian University of Science and Technology, 2003. These in turn are similar to J. W. Serene and D. Rainer, Phys. Rep. **101**, 221 (1983).

Paper XXIII

Superconducting/ferromagnetic diffusive bilayer with a spin-active interface: A numerical study.

Physical Review B **79**, 054518 (2009)

Superconducting/ferromagnetic diffusive bilayer with a spin-active interface: A numerical study

Audrey Cottet[1,2] and Jacob Linder[3]

[1]*Ecole Normale Supérieure, Laboratoire Pierre Aigrain, 24 rue Lhomond, 75005 Paris, France*

[2]*CNRS UMR8551, Laboratoire associé aux universités Pierre et Marie Curie et Denis Diderot, France*

[3]*Department of Physics, Norwegian University of Science and Technology, N-7491 Trondheim, Norway*

(Received 2 October 2008; revised manuscript received 3 December 2008; published 17 February 2009)

We calculate the density of states (DOS) in a diffusive superconducting/ferromagnetic bilayer with a spin-active interface. We use a self-consistent numerical treatment to make a systematic study of the effects of the spin dependence of interfacial phase shifts (SDIPS) on the self-consistent superconducting gap and the DOS. Strikingly, we find that the SDIPS can induce a double gap structure in the DOS of the ferromagnet, even when the superconducing layer is much thicker than the superconducting coherence length. We thus obtain DOS curves which have interesting similarities with those of SanGiorgio*et al.* [Phys. Rev. Lett. **100**, 237002 (2008)].

DOI: 10.1103/PhysRevB.79.054518 PACS number(s): 73.23.−b, 74.20.−z, 74.50.+r

I. INTRODUCTION

Superconducting/ferromagnetic (S/F) hybrid structures give rise to a fascinating interplay between two antagonist electronic orders. The ferromagnetic exchange field E_{ex} privileges one spin direction while standard superconductivity favors singlet correlations. This leads to a rich behavior which has triggered an intense activity in the last years (see, e.g., Refs. 1 and 2). In particular, the "superconducting proximity effect," i.e., the propagation of the superconducting correlations in ferromagnets, has been widely studied. This propagation is accompanied by spatial oscillations of the superconducting order parameter because E_{ex} induces an energy shift between electrons and holes. As a result, one can build electronic devices with new functionalities, such as Josephson junctions with negative critical currents,[3] which could find applications in the field of superconducting circuits.[4,5] From a fundamental point of view, it is very instructive to study the density of states (DOS) of S/F structures. So far, this quantity has been less measured[6–10] than critical temperatures or supercurrents. However, this way of probing the superconducting proximity effect is very interesting because it provides spectroscopic information. One striking consequence of the spatial oscillations of the order parameter in the F layer is that the zero-energy DOS can become larger than in the normal state for certain ferromagnet thicknesses.[6]

The behavior of S/F hybrid circuits depends crucially on the properties of the interfaces between the S and F materials. In this paper, we focus on the case of diffusive structures. Diffusive S/F interfaces have been initially described with spin-independent boundary conditions.[11] It has been found that the amplitude of the superconducting proximity effect directly depends on the tunnel conductance G_T of an interface (see, e.g., Ref. 1). Later, spin-dependent boundary conditions have been introduced in the limit of a weakly polarized ferromagnet.[12,13] Due to the spin dependence of interfacial phase shifts (SDIPS),[14–16] one has to take into account new conductance parameters G_ϕ^F and G_ϕ^S at the F and S sides of the interface, respectively. It has been shown that G_ϕ^F and G_ϕ^S can significantly affect the behavior of S/F hybrid circuits. For instance, G_ϕ^F can shift the spatial oscillations of the superconducting order parameter.[13] More recently, it has been found that G_ϕ^S can induce an effective Zeeman splitting Δ_Z^{eff} in a superconducting layer with a thickness d_S smaller than the superconducting coherence length scale ξ_S.[17] This induces a double gap structure (DGS) in the S and F densities of states. However, in practice, the regime $d_S \geq \xi_S$ is frequently reached (see, e.g., Refs. 18 and 19). Remarkably, DGSs have been recently observed at the F side of Ni/Nb bilayers with d_S much larger than ξ_S,[10] although Ref. 17 has found that Δ_Z^{eff} scales with d_S^{-1} in the low-d_S regime. Whether a DGS persists in the large-d_S regime is therefore an important question, especially in the light of this recent experiment.

In this paper, we study how G_ϕ^F and G_ϕ^S modify the DOS of a S/F bilayer. We use a numerical treatment to explore a wider parameter range than in previous works. In particular, we can reach the limit of thick superconductors and larger values of G_ϕ^S. We find that G_ϕ^S shifts the spatial oscillations of the superconducting order parameter in F, similarly to G_ϕ^F. It can also significantly affect the amplitude of the superconducting gap. When d_S increases, the SDIPS-induced DGS becomes narrower, in agreement with Ref. 17. Nevertheless, it can surprisingly persist in the large-d_S limit. Indeed, in a distance of the order of ξ_S near the S/F interface, the resonance energies of the S spectrum remain spin dependent because quantum interferences make the superconducting correlations sensitive to the SDIPS. This behavior is transmitted to the whole F layer due to the superconducting proximity effect. We thus obtain, at the F side of S/F bilayers, DOS curves which have interesting similarities with those of Ref. 10, although $d_S \gg \xi_S$. More generally, our results could be useful for interpreting experiments.

This paper is organized as follows. Section II defines the S/F bilayer problem studied in this paper. Section III explains the principle of our numerical treatment. Section IV presents a detailed study of the SDIPS-induced DGS. Section V shows the effects of the SDIPS on the self-consistent superconducting gap and on the oscillations of the zero-energy DOS with the thickness of F. Section VI discusses the data of Ref. 10. Section VII concludes.

II. DESCRIPTION OF THE S/F BILAYER

We consider a diffusive S/F bilayer consisting of a standard BCS superconductor S for $-d_S<x<0$ and a ferromagnet F for $0<x<d_F$. We characterize the normal quasiparticle excitations and the superconducting condensate of pairs with the Usadel normal and anomalous Green's functions $G_{n,\sigma}=\mathrm{sgn}(\omega_n)\cos(\theta_{n,\sigma})$ and $F_{n,\sigma}=\sin(\theta_{n,\sigma})$, with $\theta_{n,\sigma}(x)$ as the superconducting pairing angle, which depends on the spin direction $\sigma\in\{\uparrow,\downarrow\}$, $\omega_n(T)=(2n+1)\pi k_B T$ as the Matsubara frequency, and x as the spatial coordinate.[20] The Usadel equations describing the spatial evolution of $\theta_{n,\sigma}$ write

$$\xi_S^2\frac{\partial^2\theta_{n,\sigma}}{\partial x^2}=\frac{|\omega_n|}{\Delta_0}\sin(\theta_{n,\sigma})-\frac{\Delta(x)}{\Delta_0}\cos(\theta_{n,\sigma}) \tag{1}$$

in S and

$$\xi_F^2\frac{\partial^2\theta_{n,\sigma}}{\partial x^2}=k_{n,\sigma}^2\sin(\theta_{n,\sigma}) \tag{2}$$

in F with

$$k_{n,\sigma}=\sqrt{2[i\sigma\,\mathrm{sgn}(\omega_n)+(|\omega_n|/E_{\mathrm{ex}})]}. \tag{3}$$

In the above equations, Δ_0 denotes the bulk gap of the S material, $\xi_S=(\hbar D_S/2\Delta_{\mathrm{BCS}})^{1/2}$ is the superconducting coherence length scale, $\xi_F=(\hbar D_F/E_{\mathrm{ex}})^{1/2}$ is the magnetic coherence length scale, $D_{F(S)}$ is the diffusion constant in $F(S)$, and E_{ex} is the ferromagnetic exchange field of F. The self-consistent superconducting gap $\Delta(x)$ occurring in Eq. (1) can be expressed as

$$\Delta(x)\log\left[\frac{T}{T_c^0}\right]=\frac{\pi k_B T}{2}\sum_{\substack{\sigma\in\{\uparrow,\downarrow\}\\ |\omega_n|\le\Omega_D}}\left[\sin(\theta_{n,\sigma})-\frac{\Delta(x)}{|\omega_n|}\right] \tag{4}$$

with Ω_D as the Debye frequency of S, $T_c^0=\Delta_0\exp(\mathcal{E})/\pi k_B$ as the bulk transition temperature of S, k_B as the Boltzmann constant, T as the temperature, and $\mathcal{E}$ as the Euler constant. The above equations must be supplemented with a description of the boundaries of S and F. We use $\partial\theta_{n,\sigma}/\partial x|_{x=-d_S^+}=\partial\theta_{n,\sigma}/\partial x|_{x=d_F^-}=0$ for the external sides of the bilayer. For the S/F interface, we use the spin-dependent boundary conditions[12,17]

$$\xi_F\frac{\partial\theta_{n,\sigma}}{\partial x}\bigg|_{x=0^+}=\gamma_T\sin[\theta_{n,\sigma}^F-\theta_{n,\sigma}^S]+i\gamma_\phi^F\sigma\,\mathrm{sgn}(\omega_n)\sin[\theta_{n,\sigma}^F] \tag{5}$$

and

$$\xi_S\frac{\partial\theta_{n,\sigma}}{\partial x}\bigg|_{x=0^-}=\gamma\gamma_T\sin[\theta_{n,\sigma}^F-\theta_{n,\sigma}^S]-i\gamma_\phi^S\sigma\,\mathrm{sgn}(\omega_n)\sin[\theta_{n,\sigma}^S] \tag{6}$$

with $\theta_{n,\sigma}^F=\theta_{n,\sigma}(x=0^+)$ and $\theta_{n,\sigma}^S=\theta_{n,\sigma}(x=0^-)$. These equations involve the reduced conductances $\gamma_T=G_T\xi_F/A\sigma_F$ and $\gamma_\phi^{F(S)}=G_\phi^{F(S)}\xi_{F(S)}/A\sigma_{F(S)}$, the barrier asymmetry coefficient $\gamma=\xi_S\sigma_F/\xi_F\sigma_S$, the normal-state conductivity $\sigma_{F(S)}$ of the $F(S)$ material, and the junction area A. Note that we have used a definition of γ_ϕ^S which differs from that of Ref. 17 to ensure a symmetric treatment of γ_ϕ^F and γ_ϕ^S in Eqs. (5) and (6). The term G_T corresponds to the usual tunnel conductance of the interface. Like G_T, the terms G_ϕ^F and G_ϕ^S can be defined microscopically from the scattering parameters of the S/F interface (see definitions in Ref. 17). The terms G_ϕ^F and G_ϕ^S can be finite only in case of a SDIPS. The SDIPS results from the fact that the scattering phases picked up by electrons upon scattering by the S/F interface can depend on spin due to the ferromagnetic exchange field or to a spin-dependent interface potential. Thus, in principle, any kind of S/F interface can have a finite SDIPS. However, the exact values of G_ϕ^F and G_ϕ^S are difficult to predict because they depend on the detailed microscopic structure of the interface. One possible approach is to consider G_ϕ^F and G_ϕ^S as fitting parameters which have to be determined from proximity-effect measurements. Note that the derivation of the boundary conditions (5) and (6) assumes a weak transmission probability per channel (tunnel limit), which seems reasonable considering the band-structure mismatch between most S and F materials. It furthermore assumes that the system is weakly polarized. However, there is no fundamental constraint on the amplitudes of G_T, G_ϕ^F, and G_ϕ^S because these parameters consist of a sum of contributions from numerous conducting channels.

In S/F circuits, long-range triplet correlations (between equal spins) can occur when the circuit includes several F electrodes or domains with noncolinear magnetizations.[21] Recently, it has been found that this effect can also arise in S/F circuits with spin-active interfaces due to spin-flip interfacial coupling terms which are due, e.g., to some misaligned local moments at the S/F interface.[22] In our work, we consider interfaces which are "spin active" in the sense that the SDIPS is finite. However, we assume that there is no interfacial spin-flip coupling and that F is uniformly polarized. Hence, we do not obtain any long-range triplet component with our model. Note that we also disregard spin-flip and spin-orbit scattering occurring inside the S and F layers (see, for instance, Refs. 23 and 24).

III. NUMERICAL TREATMENT OF THE PROBLEM

Equations (1)–(6) have already been solved numerically with a self-consistent procedure in the case $\gamma_\phi^S=\gamma_\phi^F=0$ (see, e.g., Ref. 24). In this paper, we study the cases of finite γ_ϕ^S and γ_ϕ^F using a numerical treatment based on a relaxation method. This treatment is divided into two steps. We first calculate the values of $\Delta(x)$ and $\theta_{n,\sigma}$ self-consistently with a relaxation method in imaginary times. Then, we determine the pairing angle $\theta_\sigma(\varepsilon,x)$ corresponding to the calculated $\Delta(x)$ by using a similar relaxation method in real times, i.e., we use $\omega_n=-i\varepsilon+\Gamma$ and $\mathrm{sgn}(\omega_n)=1$ in Eqs. (1)–(6), with as ε the energy and $\Gamma=0.05\Delta_0$ as a rate which accounts for inelastic processes.[25] Finally we obtain the DOS $N(\varepsilon,x)=\Sigma_\sigma N_\sigma(\varepsilon,x)$ at position x by using $N_\sigma(\varepsilon,x)=(N_0/2)\mathrm{Re}\{\cos[\theta_\sigma(\varepsilon,x)]\}$, with $N_0/2$ as the normal DOS per spin direction. Throughout this numerical treatment, we use a discretized space, with a step of $0.001\xi_{S(F)}$ in $S(F)$. In the following, we mainly focus on $N_F(\varepsilon)=N(\varepsilon,x=d_F^-)$. Reference 17 studied analytically S/F bilayers with $d_S\le\xi_S/2$, $\gamma_\phi^S\ll1$, $\gamma_T\ll1$, and $d_F\ge\xi_F$. Our approach allows one to go

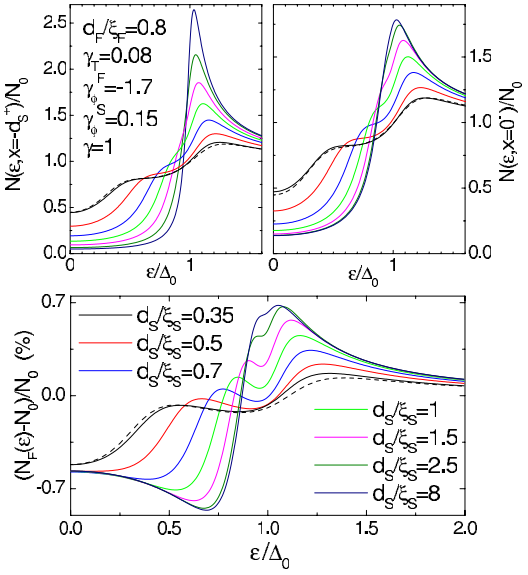

FIG. 1. (Color online) Densities of states $N(\varepsilon,x=-d_S^+)$ (top left panel) and $N(\varepsilon,x=0^-)$ (top right panel) at the left and right sides of the superconductor, respectively, and density of states $N_F(\varepsilon)$ at the right side of the ferromagnet (bottom panel) plotted vs ε for different values of d_S. The full lines correspond to our numerical results. The black dashed lines correspond to the analytical predictions of Ref. 17 for $d_S/\xi_S=0.35$.

beyond this regime. Note that in Figs. 1–5, the results are shown for $E_{ex}=100\Delta_0$, $\Omega_D=601k_BT$, and $k_BT=0.1\Delta_0$.

IV. SDIPS-INDUCED DOUBLE GAP STRUCTURE

A. Variations of the bilayer spectrum with the thickness of S

The left and right top panels of Fig. 1 show the densities of states $N(\varepsilon,x=-d_S^+)$ and $N(\varepsilon,x=0^-)$ at the left and right

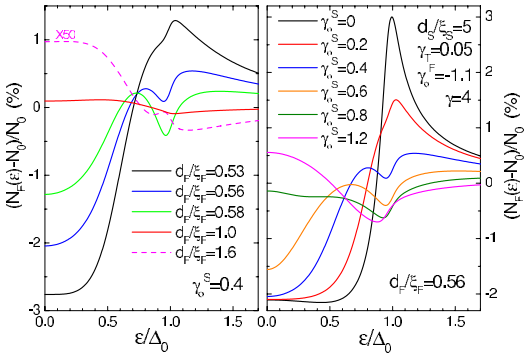

FIG. 2. (Color online) Density of states $N_F(\varepsilon)$ at the right side of the ferromagnet plotted vs ε for different values of d_F (left panel) and different values of γ_ϕ^S (right panel). In the left panel, for $d_F/\xi_F=1.6$, we have multiplied $[N_F(\varepsilon)-N_0]/N_0$ by a factor of 50 for visibility of the curve.

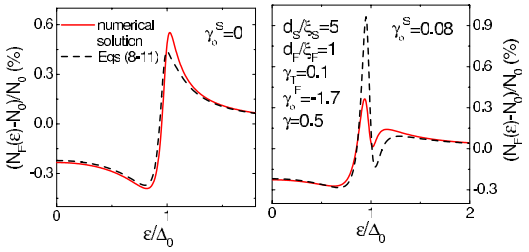

FIG. 3. (Color online) Density of states $N_F(\varepsilon)$ at the right side of the ferromagnet plotted vs ε for $\gamma_\phi^S=0$ (left panel) and γ_ϕ^S finite (right panel). The solid lines are calculated from Eqs. (8)–(11) and the black dotted lines correspond to the self-consistent numerical resolution of Eqs. (1)–(6).

sides of the superconductor, respectively, for different values of d_S and the bottom panel of Fig. 1 shows the corresponding DOS $N_F(\varepsilon)$ at the right side of F. For $d_S=0.35\xi_S$, the curves calculated with our numerical code (black full lines) are in close agreement with the analytical solution given in Ref. 17 (black dashed lines). The DOS is similar at the two sides of S and displays a DGS which reveals the existence of an effective Zeeman splitting of the form

$$\Delta_Z^{\text{eff}} = 2\Delta_0 \frac{\xi_S}{d_S}\gamma_\phi^S = E_{\text{Th}}^S \frac{G_\phi^S}{G_S} \tag{7}$$

with $E_{\text{Th}}^S=\hbar D_S/d_S^2$ as the Thouless energy of the S layer and $G_S=\sigma_S A/d_S$ as its normal-state conductance. The DGS is also visible in $N_F(\varepsilon)$ due to the proximity effect. It becomes narrower when d_S increases, in agreement with Eq. (7), which indicates that Δ_Z^{eff} scales with d_S^{-1}. For very large values of d_S, the DOS $N(\varepsilon,x=-d_S^+)$ at the left side of S tends to the bulk value $\text{Re}\{\cos[\theta_0(\varepsilon)]\}$, with $\theta_0(\varepsilon)=\arctan[\Delta_0/(-i\varepsilon+\Gamma)]$. However, a DGS remains clearly visible in $N_F(\varepsilon)$, a result which is quite counterintuitive considering the low-d_s expression Eq. (7) (see bottom panel, full line). Note that in the S layer, with the parameters of Fig. 1, $d_S \gg \xi_S$ and $\varepsilon=0$ $[\varepsilon=\Delta_0]$, $N(\varepsilon,x)$ decays from its bulk value to $N(\varepsilon,x=0^-)$ in a distance on the order of ξ_S $[2\xi_S]$ near the interface (not shown). In the large-d_S limit, the DOS $N(\varepsilon,x=0^-)$ at the left side of the S/F interface does not show a clear DGS for the

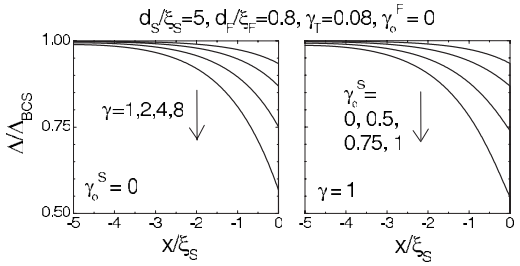

FIG. 4. Self-consistent superconducting gap $\Delta(x)$ vs the spatial coordinate x for different values of γ (left panel) and γ_ϕ^S (right panel).

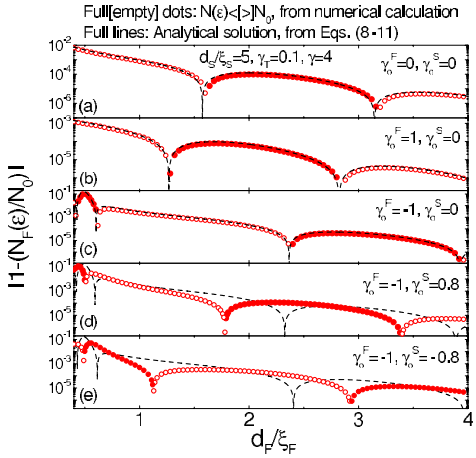

FIG. 5. (Color online) Zero-energy density of states $N_F(\varepsilon=0)$ at the right side of F versus the thickness d_F of F. The density of states calculated numerically is shown with dots. The full and empty dots correspond to $N_F(\varepsilon=0)<0$ and $N_F(\varepsilon=0)>0$, respectively. The density of states given by Eqs. (8)–(11) is shown with black dashed lines. Panel (a) corresponds to a case with no SDIPS ($\gamma_\phi^F=\gamma_\phi^S=0$). Panels (b) and (c) show the effect of a finite γ_ϕ^F. Panels (d) and (e) show the effect of a finite γ_ϕ^S, in comparison with panel (c) where $\gamma_\phi^S=0$. With the parameters used here, Eqs. (8)–(11) are in agreement with our numerical code only when $\gamma_\phi^S=0$.

weak value of γ_ϕ^S used in Fig. 1 because of the strong DOS peak at $\varepsilon=\Delta_0$. However, a DGS would appear more clearly in $N(\varepsilon,x=0^-)$ for larger values of γ_ϕ^S, e.g., using $\gamma_\phi^S=0.4$ (not shown). The DGS thus seems to persist at large values of d_S due to an effect which involves a S area with thickness $\sim\xi_S$ near the S/F interface and the whole F.

B. Variations of the bilayer spectrum with the thickness of F

Due to the ferromagnetic exchange field E_{ex}, the zero-energy DOS $N_F(\varepsilon=0)$ oscillates around its normal-state value N_0 when d_F increases.[6,26–28] In the large-d_S limit, we find that the DGS can occur at the F side for both an ordinary $[N_F(\varepsilon=0)>N_0]$ and a reversed $[N_F(\varepsilon=0)<N_0]$ DOS. However, its visibility varies with d_F like in the limit $d_S\leq\xi_S/2$ of Ref. 17. Figure 2, left panel, shows N_F versus ε for different values of d_F and $d_S/\xi_S=5$. From $d_F=0.53\xi_F$ to $0.58\xi_F$, $N_F(\varepsilon=0)-N_0$ is positive and the visibility of the DGS increases (see black, blue, and green full lines). For $d_F=\xi_F$, $N_F(\varepsilon=0)-N_0$ is negative and the DGS is not visible anymore (see red full line). For $d_F=1.6\xi_F$, the DGS is visible again, with both the inner and outer peaks of the DOS inverted due to $N_F(\varepsilon=0)-N_0<0$ (see dashed line).

C. Variations of the bilayer spectrum with G_ϕ^S

In the parameters range investigated by us (with in particular $E_{ex}\gg\Delta$, $0.35\leq d_S/\xi_S\leq 10$, and $0.4\leq d_F/\xi_F\leq 4$), no DGS occurs when $\gamma_\phi^S=0$. The DGS studied in this paper thus seems to be a direct consequence of $\gamma_\phi^S\neq 0$ for large d_S/ξ_S as well as small d_S/ξ_S. Figure 2, right panel, shows the variations of $N_F(\varepsilon)$ with γ_ϕ^S, for a constant value of d_F. For $\gamma_\phi^S=0$, no DGS appears. For a very small γ_ϕ^S (see full line, corresponding to $\gamma_\phi^S=0.2$ or $G_\phi^S=G_T$), $N_F(\varepsilon)$ shows a change in slope which corresponds to a smoothed DGS, near $\varepsilon=\Delta_0$ (from Sec. IV B, this DGS occurs only for certain values of d_F). When γ_ϕ^S becomes sufficiently large, $N_F(\varepsilon)$ shows a clear DGS, i.e., two peaks, one above and one below $\varepsilon=\Delta_0$, while a local minimum is visible for $\varepsilon\sim\Delta_0$. The distance between the two peaks of $N_F(\varepsilon)$ increases with γ_ϕ^S. In Fig. 2, when γ_ϕ^S becomes too large ($\gamma_\phi^S\geq 0.8$), the sign of $N_F(\varepsilon=0)-N_0$ changes. This suggests that γ_ϕ^S does not only induce DGSs but also shifts the oscillations of $N_F(\varepsilon)$ with d_F. This last effect will be investigated in more details for $\varepsilon=0$ in Sec. V. With the parameters of Fig. 2, the DGS is not visible anymore when γ_ϕ^S becomes larger than approximately 1. In the general case, this threshold strongly depends on the different parameters characterizing the S/F bilayer.

D. Analytical description of the thick superconductor limit

In order to have a better insight on the persistence of the SDIPS-induced DGS at large values of d_S, we provide in this section an analytical description of the case where S is semi-infinite. For simplicity, we assume that the superconducting gap is only weakly affected by the presence of the F layer, i.e., $\Delta(x)=\Delta_0$. We furthermore assume that the proximity effect is weak, i.e., $\theta_{n,\sigma}(x\in F)\ll 1$ and $\theta_{n,\sigma}(x\in S)-\theta_n^0\ll 1$, with $\theta_n^0=\arctan(\Delta_0/|\omega_n|)$. In this case, the Usadel equations (1) and (2) lead to

$$\theta_{n,\sigma}(x)=\theta_{n,\sigma}^F\cosh\left[\frac{(x-d_F)k_{n,\sigma}}{\xi_F}\right]\Big/\cosh\left(\frac{d_Fk_{n,\sigma}}{\xi_F}\right) \quad (8)$$

for $x\in F$ and

$$\theta_{n,\sigma}(x)=\theta_n^0+\delta\theta_{n,\sigma}^S\exp\left(\frac{x\eta_n}{\xi_S}\right) \quad (9)$$

for $x\in S$, with $\eta_n=[1+(\omega_n/\Delta_0)^2]^{1/4}$. We have introduced in the above equations $\delta\theta_{n,\sigma}^S=\theta_{n,\sigma}(x=0^-)-\theta_n^0$ and $\theta_{n,\sigma}^F=\theta_{n,\sigma}(x=0^+)$. The linearization of the boundary conditions (5) and (6) with respect to these two quantities leads to

$$\theta_{n,\sigma}^F=\frac{\gamma_T[\sin(\theta_n^0)+\cos(\theta_n^0)\delta\theta_\sigma^S]}{\gamma_T\cos(\theta_n^0)+i\gamma_\phi^F\sigma\,\mathrm{sgn}(\omega_n)+B_{n,\sigma}} \quad (10)$$

and

$$\delta\theta_{n,\sigma}^S=-\frac{\gamma\gamma_T+i\gamma_\phi^S\sigma\,\mathrm{sgn}(\omega_n)}{\eta_n^3+[\gamma\gamma_T+i\gamma_\phi^S\sigma\,\mathrm{sgn}(\omega_n)]\dfrac{|\omega_n|}{\Delta_0}} \quad (11)$$

with $B_{n,\sigma}=k_{n,\sigma}\tanh[d_Fk_{n,\sigma}/\xi_F]$. Importantly, Eqs. (8)–(11) are valid provided $\delta\theta_{n,\sigma}^S\ll 1$ and $\theta_{n,\sigma}^F\ll 1$, which requires $\gamma_T\ll 1$, $\gamma_\phi^S\ll 1$, and $d_F\geq\xi_F$. We have used these hypotheses to simplify Eq. (11). The validity of the approximation $\Delta(x)=\Delta_0$ will be discussed in Sec. V.

Figure 3 shows $N_F(\varepsilon)$ calculated from the analytical continuation of Eqs. (8)–(11) (black dashed lines) and from our numerical code (red full lines) for a weak value of γ and

$\gamma_\phi^S=0$ (left panel) or $\gamma_\phi^S\neq 0$ (right panel). The two calculations are in relatively good agreement.[29] For the parameters used in Fig. 3, we have checked numerically that the approximation $\Delta(x)=\Delta_0$ gives results in very good agreement with the full resolution of Eqs. (1)–(6). At $\varepsilon\sim\Delta_0$, small discrepancies arise between the predictions of the numerical code and of Eqs. (8)–(11) due to resonance effects which make $\delta\theta_{n,\sigma}^S$ and $\theta_{n,\sigma}^F$ larger than for $\varepsilon=0$ or $\varepsilon\gg\Delta_0$. Equations (8)–(11) allow one to recover the fact that a DGS can appear in $N_F(\varepsilon)$ due to $\gamma_\phi^S\neq 0$ (right panel). In the limit $d_S\gg\xi_S$, the pairing angle of the system cannot be put under the form $\theta_\sigma(x,\varepsilon)=\theta(x,\varepsilon-(\sigma\Delta_Z^{\text{eff}}/2))$, contrarily to what has been found for $d_S\leq\xi_S/2$. Therefore, the notion of SDIPS-induced effective Zeeman splitting is not valid for thick S layers. Nevertheless, from Eqs. (9) and (11), near the S/F interface, the resonance energies of the S spectrum can be spin dependent because quantum interferences make the superconducting correlations sensitive to the SDIPS on a distance on the order of ξ_S/η_n near the S/F interface. From Eqs. (8) and (10), this behavior is transmitted to the whole F layer due to the proximity effect. From Eq. (11), the energy scale related to the occurrence of the DGS has the form

$$\Delta_{\text{SDIPS}}=2\Delta_0\frac{G_\phi^S}{\widetilde{G_S}} \tag{12}$$

with $\widetilde{G_S}=\sigma_S A/\xi_S$ as the normal-state conductance of a slab of thickness ξ_S of the S material. Interestingly, this expression has a form similar to Eq. (7), with d_S replaced with ξ_S (one has $2\Delta_0=\hbar D_S/\xi_S^2=\widetilde{E_{\text{Th}}^S}$). Note that for a ballistic S/F single-channel contact, the SDIPS also produces a spin-dependent resonance effect.[30] However, in this case, one does not obtain a DGS but rather a subgap resonance in the conductance and the zero-frequency noise of the system.

V. SELF-CONSISTENT SUPERCONDUCTING GAP AND ZERO-ENERGY DOS OF F

For completeness, we now discuss the effects of the SDIPS on the self-consistent superconducting gap $\Delta(x)$ and the zero-energy DOS $N_F(\varepsilon=0)$ versus d_F. It is already known that the amplitude of $\Delta(x)$ decreases when γ_T or γ increases, similarly to what happens in a S/normal-metal bilayer.[31] Figure 4 compares the effects of γ (left panel) and γ_ϕ^S (right panel) on $\Delta(x)$ (it only shows the effect of $\gamma_\phi^S>0$, but the effect of $\gamma_\phi^S<0$ is similar). One can see that $\Delta(x)$ significantly decreases when $|\gamma_\phi^S|$ increases. Similarly, in a clean superconductor connected to a ferromagnetic insulator (FI), $\Delta(x)$ has been predicted to decrease due to the spin dependence of the reflection phases against FI.[32] In contrast, in the regime of parameters investigated by us, γ_ϕ^F has a negligible effect on the value of $\Delta(x)$ because it does not occur directly in boundary condition (11) at the S side of the interface. From this brief study of $\Delta(x)$, we conclude that the approximation $\Delta(x)=\Delta_0$ used in Sec. IV D is valid only for sufficiently small values of γ_T, γ, and γ_ϕ^S.

Figure 5 presents the effects of γ_ϕ^F and γ_ϕ^S on the variations of $N_F(\varepsilon=0)$ with d_F. The DOS calculated numerically is shown with symbols and the DOS given by Eqs. (8)–(11) is shown with full lines. In panels (a)–(c), we have used $\gamma_\phi^S=0$, so that the two calculations are in close agreement. In panels (d) and (e), the two calculations strongly differ because γ_ϕ^S is too large for the hypotheses leading to Eqs. (8)–(11) to be valid. We recover the fact that, in the regime $d_F\geq\xi_F$, $N_F(\varepsilon=0)$ shows exponentially damped oscillations with d_F.[6,26] In the regime $d_F\leq\xi_F$, the oscillations of $N_F(\varepsilon=0)$ with d_F are less regular. This can be understood from the analytical description of Sec. IV D. For $d_F\geq\xi_F$, one has $B_{n,\sigma}\sim k_{n,\sigma}$, so that $N_F(\varepsilon=0)$ depends on d_F through the $\cosh(d_F k_{n,\sigma}/\xi_F)$ term of Eq. (8) only. For $d_F\leq\xi_F$, $B_{n,\sigma}$ and thus $\theta_{n,\sigma}^F$ strongly depend on d_F, which complicates the variations of $N_F(\varepsilon=0)$ with d_F and leads to more irregular oscillations. Reference 13 already showed that γ_ϕ^F can shift the oscillations of $N_F(\varepsilon=0)$ with d_F. Panels (b) and (c) confirm this result and also show that a positive (negative) γ_ϕ^F decreases (increases) the amplitude of $N_F(\varepsilon=0)$. From panels (d) and (e), γ_ϕ^S can also significantly shift the oscillations of $N_F(\varepsilon=0)$ with d_F, in agreement with Fig. 2, right panel. For the parameters used in Fig. 5, γ_ϕ^S does not modify spectacularly the amplitude of $N_F(\varepsilon)$. For larger values of $|\gamma_\phi^S|$, the amplitude of the superconducting proximity effect would significantly decrease due to a reduction in $\Delta(x)$ (not shown).

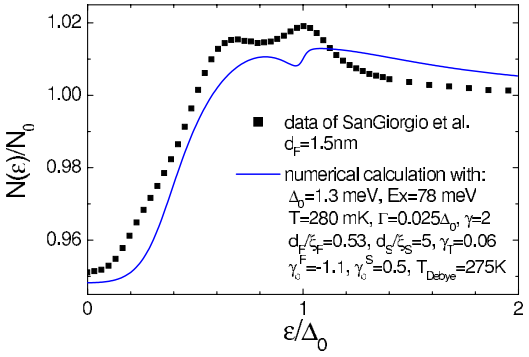

FIG. 6. (Color online) Comparison between the data of SanGiorgio *et al.* (Ref. 10) for $d_s=1.5$ nm and our numerical calculation with $\Delta_0=1.3$ meV, $E_{\text{ex}}=78$ meV, $k_BT=280$ mK, $d_F/\xi_F=0.53$, $d_S/\xi_S=5$, $\gamma_T=0.06$, $\gamma_\phi^F=-1.1$, $\gamma_\phi^S=0.5$, $\gamma=2$, $T_D=275$ K, and $\Gamma=0.025\Delta_0$.

VI. DISCUSSION ON THE DATA OF REFERENCE 10

We now consider the DOS measurements realized by SanGiorgio *et al.*[10] for Nb/Ni bilayers with $d_S=50$ nm. From Ref. 18 which considers samples fabricated by the same team, one has $\xi_S\sim 10$ nm, so that $d_S/\xi_S\sim 5$. However, double gap structures have been observed by SanGiorgio *et al.*, which motivates a comparison with our model.

Figure 6 compares the data measured for $d_F=1.5$ nm (black squares) with our numerical calculation (full line). Our calculation reproduces almost quantitatively the experimental curve. We have used $d_F=1.5$ nm, $d_S/\xi_S=5$, and $T=280$ mK, in agreement with Refs. 10 and 18. We have also used the exchange field $E_{\text{ex}}=78$ meV, estimated by Ref. 10,

and the Debye temperature $T_D=275$ K of Nb, taken from Ref. 33. We have assumed $\xi_F=2.83$ nm, $\gamma_T=0.06$, $\gamma_\phi^F=-1.1$, $\gamma_\phi^S=0.5$, and $\Gamma=0.025\Delta_0$. Note that from Ref. 18, one has $\sigma_S^{-1}\sim 15.9\ \mu\Omega$ cm and $\sigma_F^{-1}\sim 9.7\ \mu\Omega$ cm, so that one should have $\gamma=\xi_S\sigma_F/\xi_F\sigma_S\sim 2.9$ with the above values of ξ_S and ξ_F. In Fig. 6, we have used a value $\gamma=2$, which is in relatively good agreement with this estimate. The values of γ_T, γ_ϕ^F, γ_ϕ^S, and γ used in the fit yield $G_\phi^F/G_T\sim 18$ and $G_\phi^S/G_T\sim 4$. A theoretical prediction of these ratios is very difficult because they depend on the detailed microscopic structure of the Nb/Ni interface. However, with a simple delta function barrier model, it is already possible to find situations where G_ϕ^S and G_ϕ^F are larger than G_T (see Appendix A and Fig. 6 of Ref. 17). Therefore, we think that the SDIPS parameters used by us are possible.

We cannot reproduce quantitatively the data obtained by SanGiorgio *et al.* for all values of d_F with the same set of parameters as for $d_F=1.5$ nm. We think that this might be due to the fact that some characteristics of the samples such as, e.g., $E_{\rm ex}$ and thus ξ_F, γ_ϕ^F, γ_ϕ^S, and γ can vary with d_F.[34] In the data of SanGiorgio *et al.*, from $d_F=1.5$ nm to $d_F=3.0$ nm, the distance between the two peaks of the DGS increases like in our model (see Fig. 2, left panel). However, the outer peak of the DGS remains very close to $\varepsilon\sim\Delta_0$, which seems difficult to reproduce with our model. Note that in Ref. 10, for $d_F=3.5$ nm, the outer peaks of the DOS are inverted, whereas a sharp dip occurs at low energies, which can give the impression that the inner peaks of the DOS persist but are not inverted, in contrast to what we find (see Sec. IV B). However, we think that the observation of this zero-bias dip is not totally reliable. Indeed, SanGiorgio *et al.* explained that, in the DOS of their thickest samples (for $d_F>3.5$ nm), "the zero-bias peak is due to the steep voltage dependence of the background conductance and is therefore a by-product of the data normalization procedure." The zero-bias dip of the $d_F=3.5$ nm sample occurs on the same energy scale as these zero-bias peaks, and it goes together with a strange zero-bias singularity similar to those shown by the thickest samples. Therefore, we are not sure whether a proper interpretation of the data of Ref. 10 must take into account this feature. Reference 35 suggests that the DGS observed by SanGiorgio *et al.* could be due to triplet correlations. However, it is difficult to know whether this interpretation can be more satisfying than ours because Ref. 35 does not show any quantitative interpretation of the data and does not discuss, for instance, the evolution of the inner and outer peak positions with d_F.

VII. CONCLUSION

In summary, we have calculated the density of states (DOS) in a diffusive S/F bilayer with a spin-active interface. We have used a self-consistent numerical treatment to make a systematic study of the effects of the SDIPS. We characterize the SDIPS with two conductance-like parameters G_ϕ^S and G_ϕ^F, which occur in the boundary conditions describing the S and F sides of the interface, respectively. We find that the amplitude of $\Delta(x)$ significantly decreases if G_ϕ^S is too strong, whereas it is almost insensitive to G_ϕ^F. In contrast, both G_ϕ^S and G_ϕ^F can shift the oscillations of the zero-energy DOS of F with the thickness of F. Remarkably, we find that the SDIPS can produce a double gap structure in the DOS of F, even when the S layer is much thicker than the superconducting coherence length. This leads to DOS curves which have striking similarities with those of Ref. 13. More generally, our results could be useful for interpreting future experiments on superconducting/ferromagnetic diffusive hybrid structures.

ACKNOWLEDGMENTS

We acknowledge interesting discussions with A. A. Golubov, T. Kontos, M. Yu. Kuprianov, and N. Regnault. We thank P. SanGiorgio and M. Beasley for discussions and for sending us their data. J.L. was supported by the Research Council of Norway under Grants No.158518/431, No. 158547/431 (NANOMAT), and No. 167498/V30 (STORFORSK).

[1] A. A. Golubov, M. Yu. Kupriyanov, and E. Il'ichev, Rev. Mod. Phys. **76**, 411 (2004).
[2] A. I. Buzdin, Rev. Mod. Phys. **77**, 935 (2005).
[3] W. Guichard, M. Aprili, O. Bourgeois, T. Kontos, J. Lesueur, and P. Gandit, Phys. Rev. Lett. **90**, 167001 (2003).
[4] L. B. Ioffe, V. B. Geshkenbein, M. V. Feigel'man, A. L. Fauchère, and G. Blatter, Nature (London) **398**, 679 (1999).
[5] T. Yamashita, K. Tanikawa, S. Takahashi, and S. Maekawa, Phys. Rev. Lett. **95**, 097001 (2005).
[6] T. Kontos, M. Aprili, J. Lesueur, and X. Grison, Phys. Rev. Lett. **86**, 304 (2001).
[7] T. Kontos, M. Aprili, J. Lesueur, X. Grison, and L. Dumoulin, Phys. Rev. Lett. **93**, 137001 (2004).
[8] L. Crétinon, A. K. Gupta, H. Sellier, F. Lefloch, M. Fauré, A. Buzdin, and H. Courtois, Phys. Rev. B **72**, 024511 (2005).
[9] S. Reymond, P. SanGiorgio, M. R. Beasley, J. Kim, T. Kim, and K. Char, Phys. Rev. B **73**, 054505 (2006).
[10] P. SanGiorgio, S. Reymond, M. R. Beasley, J. H. Kwon, and K. Char, Phys. Rev. Lett. **100**, 237002 (2008).
[11] M. Yu. Kuprianov and V. F. Lukichev, Sov. Phys. JETP **67**, 1163 (1988).
[12] D. Huertas-Hernando, Y. V. Nazarov, and W. Belzig, arXiv:cond-mat/0204116 (unpublished); D. Huertas-Hernando, Ph.D. thesis, Delft University of Technology, The Netherlands, 2002; D. Huertas-Hernando, Y. V. Nazarov, and W. Belzig, Phys. Rev. Lett. **88**, 047003 (2002).
[13] A. Cottet and W. Belzig, Phys. Rev. B **72**, 180503(R) (2005).
[14] The SDIPS is called by some other authors "spin-mixing angle" or "spin-rotation angle." However, in our case, we consider a single ferromagnet which is uniformly polarized, so that the notions of mixing or rotation are not relevant.

[15] The effects of the SDIPS on S/F systems have been initially studied in the ballistic case (see, e.g., Refs. 16 and 32).
[16] A. Millis, D. Rainer, and J. A. Sauls, Phys. Rev. B **38**, 4504 (1988).
[17] A. Cottet, Phys. Rev. B **76**, 224505 (2007).
[18] J. Kim, J. H. Kwon, K. Char, H. Doh, and H.-Y. Choi, Phys. Rev. B **72**, 014518 (2005).
[19] Th. Mühge, K. Westerholt, H. Zabel, N. N. Garif'yanov, Yu. V. Goryunov, I. A. Garifullin, and G. G. Khaliullin, Phys. Rev. B **55**, 8945 (1997).
[20] N. B. Kopnin, *Theory of Nonequilibrium Superconductivity* (Clarendon, Oxford, 2001); W. Belzig, F. K. Wilhelm, C. Bruder, G. Schön, and A. D. Zaikin, Superlattices Microstruct. **25**, 1251 (1999).
[21] F. S. Bergeret, A. F. Volkov, and K. B. Efetov, Rev. Mod. Phys. **77**, 1321 (2005).
[22] M. Eschrig, J. Kopu, J. C. Cuevas, and Gerd Schön, Phys. Rev. Lett. **90**, 137003 (2003); Y. Asano, Y. Sawa, Y. Tanaka, and A. A. Golubov, Phys. Rev. B **76**, 224525 (2007); A. V. Galaktionov, M. S. Kalenkov, and A. D. Zaikin, *ibid.* **77**, 094520 (2008); M. Eschrig and T. Lofwander, Nat. Phys. **4**, 138 (2008).
[23] E. A. Demler, G. B. Arnold, and M. R. Beasley, Phys. Rev. B **55**, 15174 (1997); S. Oh, Y.-H. Kim, D. Youm, and M. R. Beasley, *ibid.* **63**, 052501 (2000); L. Crétinon, A. K. Gupta, H. Sellier, F. Lefloch, M. Fauré, A. Buzdin, and H. Courtois, *ibid.* **72**, 024511 (2005); M. Fauré, A. I. Buzdin, A. A. Golubov, and M. Yu. Kupriyanov, *ibid.* **73**, 064505 (2006); F. S. Bergeret, A. F. Volkov, and K. B. Efetov, *ibid.* **75**, 184510 (2007); J. Linder, T. Yokoyama, and A. Sudbo, *ibid.* **77**, 174514 (2008).
[24] D. Yu. Gusakova, A. A. Golubov, M. Yu. Kupriyanov, and A. Buzdin, JETP Lett. **83**, 327 (2006).
[25] W. Belzig, Ph.D. thesis, Karlsruhe University, 1999.
[26] A. Buzdin, Phys. Rev. B **62**, 11377 (2000); I. Baladié and A. Buzdin, *ibid.* **64**, 224514 (2001).
[27] M. Zareyan, W. Belzig, and Yu. V. Nazarov, Phys. Rev. Lett. **86**, 308 (2001); Phys. Rev. B **65**, 184505 (2002).
[28] F. S. Bergeret, A. F. Volkov, and K. B. Efetov, Phys. Rev. B **65**, 134505 (2002).
[29] For the parameters of Figs. 1 and 2, Eqs. (8)–(11) are not in good agreement with our numerical results because the hypotheses leading to these equations are not satisfied (see Sec. V).
[30] A. Cottet and W. Belzig, Phys. Rev. B **77**, 064517 (2008).
[31] A. A. Golubov and M. Yu. Kuprianov, Sov. Phys. JETP **69**, 805 (1990).
[32] T. Tokuyasu, J. A. Sauls, and D. Rainer, Phys. Rev. B **38**, 8823 (1988).
[33] N. W. Ashcroft and N. D. Mermin, *Solid State Physics* (Saunders College, Philadelphia, 1976).
[34] T. Kontos, Ph.D. thesis, Université Paris-Sud, Orsay, France, 2002.
[35] A. F. Volkov and K. B. Efetov, Phys. Rev. B **78**, 024519 (2008).

Paper XXIV

Theory of superconducting and magnetic proximity effect in S/F structures with inhomogeneous magnetization textures and spin-active interfaces .

Physical Review B **79**, 054523 (2009)

PHYSICAL REVIEW B **79**, 054523 (2009)

Theory of superconducting and magnetic proximity effect in S/F structures with inhomogeneous magnetization textures and spin-active interfaces

Jacob Linder,[1] Takehito Yokoyama,[2] and Asle Sudbø[1]
[1]*Department of Physics, Norwegian University of Science and Technology, N-7491 Trondheim, Norway*
[2]*Department of Applied Physics, Nagoya University, Nagoya 464-8603, Japan*
(Received 27 October 2008; published 20 February 2009)

We present a study of the proximity effect and the inverse proximity effect in a superconductor|ferromagnet bilayer, taking into account several important factors which mostly have been ignored in the literature so far. These include spin-dependent interfacial phase shifts (spin-DIPS) and inhomogeneous textures of the magnetization in the ferromagnetic layer, both of which are expected to be present in real experimental samples. Our approach is numerical, allowing us to access the full proximity effect regime. In Sec. II of this work, we study the superconducting proximity effect and the resulting local density of states in an inhomogeneous ferromagnet with a nontrivial magnetic texture. Our two main results in Sec. II are a study of how Bloch and Néel domain walls affect the proximity-induced superconducting correlations and a study of the superconducting proximity effect in a conical ferromagnet. The latter topic should be relevant for the ferromagnet Ho, which was recently used in an experiment to demonstrate the possibility to generate and sustain long-range triplet superconducting correlations. In Sec. III of this work, we investigate the inverse proximity effect with emphasis on the induced magnetization in the superconducting region as a result of the "leakage" from the ferromagnetic region. It is shown that the presence of spin-DIPS modifies conclusions obtained previously in the literature with regard to the induced magnetization in the superconducting region. In particular, we find that the spin-DIPS can trigger an antiscreening effect of the magnetization, leading to an induced magnetization in the superconducting region with *the same sign* as in the proximity ferromagnet.

DOI: 10.1103/PhysRevB.79.054523 PACS number(s): 74.20.Rp, 74.50.+r

I. INTRODUCTION

The interplay between ferromagnetism and superconductivity has over the past decade attracted much interest from the condensed-matter physics community. Research on superconductor|ferromagnet (S|F) heterostructures continues to benefit from great interest, which is fueled by the exciting phenomena arising from a fundamental physics point of view in addition to the prospect of harvesting functional devices in low-temperature nanotechnology.

There is currently intense activity in this particular research area (see, e.g., Refs. 1 and 2 and references therein). The interest in S|F hybrid structures was boosted at the beginning of this millenium, primarily due to the theoretical proposition of proximity-induced odd-frequency correlations[3] and the experimental observation of 0-π oscillations in S|F|S Josephson junctions.[4] A large amount of work has been devoted to odd-frequency pairing (see, e.g., Refs. 5–21) and the physics of 0-π oscillations (see, e.g., Refs. 22–38) in S|F heterostructures. The concept of odd-frequency pairing dates back to Refs. 39–42 and was recently re-examined in Ref. 43.

So far, the proximity effect has received much more attention than the inverse proximity effect. In S|F bilayers, the proximity effect causes superconducting correlations to penetrate into the ferromagnetic region.[1] Similarly, the inverse proximity effect induces ferromagnetic correlations in the superconducting region near the interface region.[44–47,76] Often, the bulk solution is employed in the superconducting region, such that both the induced magnetic correlations and the self-consistency of the superconducting order parameter are neglected. However, it was shown in Ref. 48 that the induction of an odd-frequency triplet component would lead to a finite magnetization in the superconducting region close to the S|F interface. Prior to this finding, some experimental groups had reported findings which pointed toward precisely such a phenomenon.[49,50] Very recently, Xia *et al.*[51] presented an experimental observation of the inverse proximity effect in Al/(Co-Pd) and Pd/Ni bilayers by measuring the magneto-optical Kerr effect. Their data could be roughly fitted to the predictions of Ref. 48, and other experiments[44,45,49,50,52] have also addressed aspects of the inverse proximity effect S|F bilayers.

In Ref. 53, the authors investigated the proximity-induced magnetization in the superconducting region of a S|F bilayer and found that the magnetization would oscillate in the clean limit (see also Ref. 54) and decay monotonously in the diffusive limit, with a sign opposite to the magnetization in the bulk of the ferromagnet. The reason for this screening behavior in the superconductor was attributed to a scenario in which the spin-↑ electron of a Cooper pair near the interface would prefer to be located in the ferromagnetic region, while its spin-↓ partner would remain in the superconducting region, thus creating a magnetization with an opposite sign compared to the ferromagnet. By considering the weak-proximity effect regime in the diffusive limit, both Refs. 48 and 53 arrived at this conclusion. However, it would be desirable to go beyond the approximation of a weak-proximity effect employed in previous work to investigate if this may alter how the induced magnetization in the superconducting region behaves.

Moreover, none of the above works on the inverse proximity effect have properly included an important property which is intrinsic to S|F interfaces, namely, the spin-

dependent interfacial phase shifts (spin-DIPS) that occur at the interface. The spin-DIPS have been shown to exert an important influence on various experimentally observable quantities in S|F bilayers[28,55,56] and should be taken into account. For instance, the anomalous double-peak structure in the local density of states (LDOS) in a diffusive S|F bilayer reported very recently by San Giorgio *et al.*[57] was reproduced theoretically in Ref. 58 by using a numerical solution of the Usadel equation when including the effect of the spin-DIPS.

So far, due to the complexity of the problem, several assumptions have been usually made when treating S|F hybrid structures. For instance, since the quasiclassical equations become quite complicated for inhomogeneous ferromagnets, they have been linearized in most of the previous works. However, presently, the direction of this research field tends toward a more realistic description of S|F structures than the simplified models that mostly have been employed up to now. It is obvious that this is a necessary step in order to reconcile the theoretical predictions with experimentally observed data.

Our motivation for this work is to examine the effect of inhomogeneous magnetization textures and spin-DIPS on both the proximity effect and the inverse proximity effect in S|F bilayers. This is directly relevant to two recent experimental studies[51,59] which studied the superconducting proximity effect in the conical ferromagnet Ho and the inverse proximity effect in the superconducting region of a S|F bilayer, respectively. As we shall show in this work, nontrivial magnetization textures and spin-DIPS have profound influence on the physical properties of S|F bilayers, suggesting that their role must be taken seriously.

We divide this work into two parts which are devoted to the proximity effect in the ferromagnetic region (Sec. II) and the inverse proximity effect in the superconducting region (Sec. III). In Sec. II, we present results where we treat the role of magnetic properties at the interface and the possibility of inhomogeneous magnetization thoroughly. We study the proximity-induced density of states (DOS) in a S|F bilayer which takes into account the presence of spin-DIPS at the interface and also the possibility of having a nontrivial magnetization texture (such as a domain wall) in the ferromagnetic region. In order to access the full proximity effect regime, we do not restrict ourselves to any limiting cases. Rather, we employ a full numerical solution of the DOS by means of the quasiclassical theory of superconductivity. We apply our theory to two cases of ferromagnets with an inhomogeneous magnetic texture, namely, on one hand ferromagnets with domain walls and on the other hand conical ferromagnets.

In Sec. III, we study numerically and self-consistently the inverse proximity effect in a S|F bilayer of finite size upon taking properly into account the spin-DIPS that occurs at the S|F interface. Our main objective is to study the influence exerted on the inverse proximity effect by the spin-DIPS. Surprisingly, we find that the spin-DIPS may invert the sign of the proximity-induced magnetization in the superconducting layer compared to the predictions of Refs. 48 and 53. Consequently, the spin-DIPS can trigger an antiscreening effect of the magnetization, which suggests that their role must be taken seriously in any attempt to construct a theory for the inverse proximity effect in S|F bilayers. We also explain the basic mechanism behind the sign-inversion induced by the spin-DIPS.

This paper is organized as follows. In Sec. II A, we present the theoretical framework we use to perform our computations in Sec. II, namely, the quasiclassical theory of superconductivity in the diffusive limit for an inhomogeneous ferromagnet using the Ricatti parametrization. In Sec. II B, we present our numerical results for proximity-effect and the local density of states for the two cases of ferromagnets with domain walls and with conical magnetic textures. In Sec. II C, we present a discussion of our results obtained in Sec. II. Moving on to Sec. III of this work, we introduce a slightly different notation and parametrization for the Green's function in Sec. III A, which is easier to implement for a homogeneous S|F bilayer. In Sec. III B, we present our results for the inverse proximity effect manifested through an induced magnetization in the superconducting region and in particular how it is influenced by the presence of spin-DIPS. The results for Sec. III are discussed in Sec. III C, and we conclude with final remarks in Sec. IV. Throughout the paper, we will use boldface notation for three-vectors, $\hat{\ldots}$ for 4×4 matrices and $\underline{\ldots}$ for 2×2 matrices.

II. PROXIMITY EFFECT IN A S|F BILAYER WITH AN INHOMOGENEOUS MAGNETIZATION TEXTURE

A. Theoretical framework

In the first part of our work, we shall consider the proximity effect in the ferromagnetic region of an S|F bilayer when the magnetization texture is inhomogeneous. This is the case, e.g., in the presence of a domain-wall structure or conical ferromagnetism, which both will be treated below. We will use the quasiclassical theory of superconductivity[60] and consider the diffusive limit described by the Usadel equation.[61]

1. Quasiclassical theory and Green's functions

To account for an inhomogeneous magnetization in the ferromagnet, it is convenient to parametrize the Green's function to obtain a simpler set of equations to solve. One possibility is to use a generalized θ-parametrization[62] as follows:

$$\hat{g} = \begin{pmatrix} M_0 c\underline{\sigma_0} + (\boldsymbol{M}\cdot\underline{\boldsymbol{\sigma}})s & \underline{\rho}^{+} \\ \underline{\rho}^{-} & -M_0 c\underline{\sigma_0} - (\boldsymbol{M}\cdot\underline{\boldsymbol{\sigma}})^{*}s \end{pmatrix},$$

$$\underline{\rho}^{\pm} = c\left[i(M_z\underline{\sigma_2} - M_y\underline{\sigma_3}) \pm M_x\underline{\sigma_0}\right] \pm M_0\underline{\sigma_1}s, \tag{1}$$

where $\underline{\sigma_j}$ are the identity ($j=0$) and Pauli ($j=1,2,3$) matrices and

$$\underline{\boldsymbol{\sigma}} = (\underline{\sigma_1}, \underline{\sigma_2}, \underline{\sigma_3}). \tag{2}$$

Also, $s \equiv \sinh(\theta)$ and $c \equiv \cosh(\theta)$. The Green's function is then completely determined by the complex functions θ, M_0, and $\boldsymbol{M}$ with the additional constraint $M_0^2 - \boldsymbol{M}^2 = 1$ in order to satisfy $\hat{g}^2 = \hat{1}$.

However, for our purpose we find it both more convenient and elegant to use a Ricatti-parametrization of the Green's function[63,64] as follows:

$$\hat{g} = \begin{pmatrix} \underline{\mathcal{N}}(\underline{1} - \underline{\gamma}\underline{\tilde{\gamma}}) & 2\underline{\mathcal{N}}\underline{\gamma} \\ 2\underline{\tilde{\mathcal{N}}}\underline{\tilde{\gamma}} & \underline{\tilde{\mathcal{N}}}(-\underline{1} + \underline{\tilde{\gamma}}\underline{\gamma}) \end{pmatrix}. \tag{3}$$

This parametrization facilitates the numerical computations and also ensures that $\hat{g}^2 = \hat{1}$. The unknown functions $\underline{\gamma}$ and $\underline{\tilde{\gamma}}\underline{\gamma}$ are key elements in this parametrization of the Green's function and will be solved for below. Here, $\underline{\ldots}$ denotes a 2×2 matrix and

$$\underline{\mathcal{N}} = (1 + \underline{\gamma}\underline{\tilde{\gamma}})^{-1}\underline{\tilde{\mathcal{N}}} = (1 + \underline{\tilde{\gamma}}\underline{\gamma})^{-1}. \tag{4}$$

In order to calculate the Green's function $\hat{g}$, we need to solve the Usadel equation with appropriate boundary conditions at $x=0$ and $x=d_F$. The two natural length scales associated with each of the long-range orders are the superconducting and ferromagnetic coherence lengths,

$$\xi_S = \sqrt{D_S/\Delta_0}, \quad \xi_F = \sqrt{D_F/h_0}, \tag{5}$$

where Δ_0 and h_0 denote the bulk values of the gap and the exchange field. We set $D_F = D_S = D$ for simplicity. The Usadel equation reads

$$D\,\partial(\hat{g}\,\partial\hat{g}) + i\{\varepsilon\hat{\rho}_3 + \mathrm{diag}[\boldsymbol{h}\cdot\boldsymbol{\underline{\sigma}}, (\boldsymbol{h}\cdot\boldsymbol{\underline{\sigma}})^T], \hat{g}\} = 0 \tag{6}$$

and is supplemented with the boundary conditions,[28,55]

$$2\zeta d_F \hat{g}\,\partial\hat{g} = [\hat{g}_{\mathrm{BCS}}, \hat{g}] + i(G_\phi/G_T)[\mathrm{diag}(\underline{\tau_3}, \underline{\tau_3}), \hat{g}] \tag{7}$$

at $x=0$ where the interface is spin polarized along the z axis and $\hat{g}\,\partial\hat{g} = \hat{0}$ at $x=d_F$. Here, $\partial \equiv \frac{\partial}{\partial x}$, and we define

$$\zeta = R_B/R_F \tag{8}$$

as the ratio between the resistance of the barrier region and the resistance in the ferromagnetic film (note that $R_B = G_T^{-1}$). The barrier conductance is given by[28]

$$G_T = G_Q \sum_n^N T_n, \tag{9}$$

where $G_Q = e/h$ and T_n is the transmission coefficient for channel n. The boundary conditions Eqs. (22) and (23) are derived under the assumption that $T_n \ll 1$, but this does not necessarily mean that the barrier conductance is small since there may be a large total number of channels N through which transport may take place. The parameter G_ϕ describes the spin-DIPS taking place at the F side of the interface.[65] Since its exact value depends on the microscopic properties of the barrier region, they are here treated phenomenologically. We finally underline that the boundary conditions above are valid for planar diffusive contacts.

Since we employ a numerical solution, we have access to study the full proximity effect regime and also an, in principle, arbitrary spatial modulation $h = h(x)$ of the exchange field. This is desirable in order to clarify effects associated with nonuniform ferromagnets, such as spiral magnetic ordering or the presence of domain walls. Inserting Eq. (3) into Eq. (21), we obtain the transport equation for the unknown function $\underline{\gamma}$ (and hence $\underline{\tilde{\gamma}}\underline{\gamma}$),

$$D[\partial^2\underline{\gamma} + (\partial\underline{\gamma})\underline{\tilde{\mathcal{F}}}(\partial\underline{\gamma})] + i[2\varepsilon\underline{\gamma} + \boldsymbol{h}\cdot(\boldsymbol{\underline{\sigma}}\underline{\gamma} - \underline{\gamma}\boldsymbol{\underline{\sigma}}^*)] = 0, \tag{10}$$

with $\underline{\tilde{\mathcal{F}}} = -2\underline{\tilde{\mathcal{N}}}\underline{\tilde{\gamma}}$. The boundary condition at $x=0$ reads as

$$2\zeta d_F \partial_x\underline{\gamma} = [2c\underline{\gamma} - si\underline{\tau_2} + \underline{\gamma}(si\underline{\tau_2})\underline{\gamma}] + i(G_\phi/G_T)(\underline{\tau_3}\underline{\gamma} - \underline{\gamma}\underline{\tau_3}), \tag{11}$$

while $\partial_x\underline{\gamma} = 0$ at $x=d$. For $\underline{\tilde{\gamma}}$, we obtain

$$D[\partial^2\underline{\tilde{\gamma}} + (\partial\underline{\tilde{\gamma}})\underline{\mathcal{F}}(\partial\underline{\tilde{\gamma}})] + i[2\varepsilon\underline{\tilde{\gamma}} + \boldsymbol{h}\cdot(\underline{\tilde{\gamma}}\boldsymbol{\underline{\sigma}} - \boldsymbol{\underline{\sigma}}^*\underline{\tilde{\gamma}})] = 0, \tag{12}$$

with the corresponding boundary condition,

$$2\zeta d_F \partial_x\underline{\tilde{\gamma}} = [2c\underline{\tilde{\gamma}} - si\underline{\tau_2} + \underline{\tilde{\gamma}}(si\underline{\tau_2})\underline{\tilde{\gamma}}] - i(G_\phi/G_T)(\underline{\tau_3}\underline{\tilde{\gamma}} - \underline{\tilde{\gamma}}\underline{\tau_3}). \tag{13}$$

We have defined $\underline{\mathcal{F}} = -2\underline{\mathcal{N}}\underline{\gamma}$. Note that we use the bulk solution in the superconducting region, which is a good approximation when assuming that the superconducting region is much less disordered than the ferromagnet and when the interface transparency is small, as considered here (see detailed discussion in Sec. II C). One finds that

$$\underline{\gamma}_{\mathrm{BCS}} = \underline{\tilde{\gamma}}_{\mathrm{BCS}} = \begin{pmatrix} 0 & s/(1+c) \\ -s/(1+c) & 0 \end{pmatrix}. \tag{14}$$

The normalized DOS is finally evaluated by

$$N(\varepsilon)/N_0 = \mathrm{Tr}\{\mathrm{Re}[\underline{\mathcal{N}}(1 - \underline{\gamma}\underline{\tilde{\gamma}})]\}/2. \tag{15}$$

In what follows, we will omit the effect of spin-flip and spin-orbit scattering to reduce the number of parameters in the problem. In comparison with real experimental data, however, the effects of these pair-breaking mechanisms are easily included in our framework by adding two terms $\hat{\sigma}_{\mathrm{sf}}$ and $\hat{\sigma}_{\mathrm{so}}$ in Eq. (21) (see, e.g., Ref. 20 for a detailed treatment). In this paper, we will focus on the role of the phase shifts obtained at the interface due to the spin-split bands and the inhomogeneity of the exchange field in the ferromagnet.

2. Inhomogeneous magnetization

We will consider three types of inhomogeneous magnetic structures: Bloch walls, Néel walls, and conical ferromagnets (see Fig. 1). An example of the latter is the rare-earth heavy fermion elemental magnet Ho although we hasten to add that while Ho features strong ferromagnetism, we will consider the weakly ferromagnetic case. These structures are shown in Fig. 1 and are to be contrasted with the usual assumption of a homogeneous exchange field in the ferromagnetic region. For the first two cases, the domain wall has a width d_W and is taken to be located at the center of the ferromagnetic region ($x = d_F/2$). The Bloch wall is thus modeled by

$$\mathbf{h} = h(\cos\theta\hat{\mathbf{y}} + \sin\theta\hat{\mathbf{z}}), \tag{16}$$

while $\hat{\mathbf{y}} \to \hat{\mathbf{x}}$ for the Néel wall. Here, we have defined

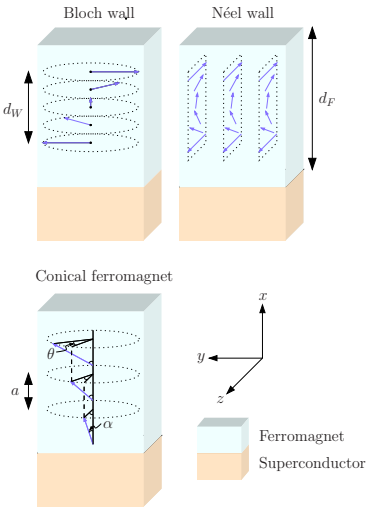

FIG. 1. (Color online) The three types of inhomogeneous ferromagnets we will consider in this work: Bloch walls, Néel walls, and conical ferromagnets (such as Ho).

$$\theta = -\arctan[(x - d_F/2)/d_W], \tag{17}$$

similarly to Ref. 64.

In the case of a conical ferromagnet, cf. Fig. 1, the magnetic moment belongs to a cone. In Ho, the opening angle is $\alpha = 4\pi/9$ and the magnetic moment then rotates like a helix along the c axis with a turning angle $\theta = \pi/6$ per interatomic layer with distance a (see Ref. 59 for a further discussion). Above 21 K, the conical ferromagnetic structure transforms into a spiral antiferromagnetic structure. Instead of using an abrupt change in the magnetization direction at each interatomic layer, we will model this transition smoothly since the effective field felt between the layers probably should be a weighed superposition of the exchange fields from the two closest layers. In the ferromagnetic phase, the spatial variation in the exchange field may thus be written as

$$\mathbf{h} = h\left[\cos\alpha\hat{\mathbf{x}} + \sin\alpha\left\{\sin\left(\frac{\theta x}{a}\right)\hat{\mathbf{y}} + \cos\left(\frac{\theta x}{a}\right)\hat{\mathbf{z}}\right\}\right]. \tag{18}$$

B. Results

In what follows, we will choose the parameters of our model, corresponding to a realistic experimental setup in order to make our study directly relevant for experiments on S|F bilayers. The numerical treatment makes use of built-in routines in MATLAB for a two-point boundary value problem for an ordinary differential equation. More specifically, we use a finite difference code which implements a three-stage Lobatto-Illa formula. An initial guess for the Ricatti matrices is supplied with fixed boundary conditions, and the Usadel equation is then solved in the entire ferromagnetic region.

In Sec. II B 1, we will study the effect of domain walls in weak ferromagnets. Weak ferromagnetic alloys such as PdNi or CuNi are commonly employed in experiments, and the corresponding exchange field h depends on the concentration of Ni, reaching up to tens of meV. The modification of the DOS is most dramatic in the case when the energy scales for the superconductivity and the ferromagnetism are of the same order, $h \sim \Delta$. This scenario appears to have been realized in Ref. 4 where $Cu_{1-x}Ni_x$, with $x = 0.44$ was used. The diffusion constant in the weakly ferromagnetic alloys is usually of order $D \sim 10^{-4}$ m^2/s. The superconducting region is considered to act as a reservoir with thickness $d_S \gg \xi_S$, while we fix the thickness of the ferromagnetic region at $d_F/\xi_S = 0.5$. This typically corresponds to a thickness of the ferromagnetic layer ~ 10 nm. The remaining parameters are then the domain-wall thickness d_W and the term G_ϕ accounting for the spin-dependent phase shifts at the interface. Below, we will contrast a thin domain wall ($d_W \ll d_F$) with a thick domain wall ($d_W \simeq d_F$) and investigate the role of G_ϕ. In what follows, we choose $\zeta = 5$ corresponding to a situation where $R_B \gg R_F$.

In Sec. II B 2, we will study conical ferromagnetism, of a similar kind to that realized in the heavy rare-earth element holmium (Ho) under certain conditions. Recently, it was strongly suggested by experimental data that a long-range triplet superconducting component was generated and sustained in a superconductor|Ho proximity structure.[59] The experimental samples used in Ref. 59 did not appear to fall into the diffusive motion regime since Ho is a strong ferromagnet. More specifically, it was estimated that $h\tau \simeq 10$ in Ref. 59, suggesting that one would have to revert to the more general Eilenberger equation in order to study the proximity effect in Ho. In this work, we will study a conical ferromagnet under the assumption that the diffusive limit is reached. For the actual structure of the magnetization, we choose the same parameters for Ho as those reported in Ref. 59: $\alpha = 4\pi/9$, $\theta = \pi/6$, and $a = 0.526$ nm (see Fig. 1). However, we choose the exchange field much weaker than in Ho, in order to justify the Usadel approach. Thus, our results may not be directly applicable to Ho. While in Ref. 59 it was estimated that $h \sim 1$ eV, corresponding to an exchange field comparable in magnitude with the Fermi energy, we choose $h/\Delta_0 = 5$ in our study of conical ferromagnetism to ensure the validity of the quasiclassical approach. Assuming that $\xi_S = 20$ nm, which should be reasonable for a moderately disordered conventional superconductor, we obtain $a/\xi_S = 0.0263$.

1. Domain wall

Before proceeding to a dissemination of our results, it should be noted that we find identical results for the Bloch and Néel wall cases. This seems reasonable since the only difference between those two cases is that the y component of the magnetization is exchanged with the x component. The long-range triplet component comes about as long as only one of these is nonzero, and it does not matter which one it is. It is also necessary for the magnetization to vary directionally with the x coordinate in order to generate the inhomogeneity required for the long-range triplet component. Note that the z component of the magnetization is the same for the Bloch and Néel walls. In what follows, we only

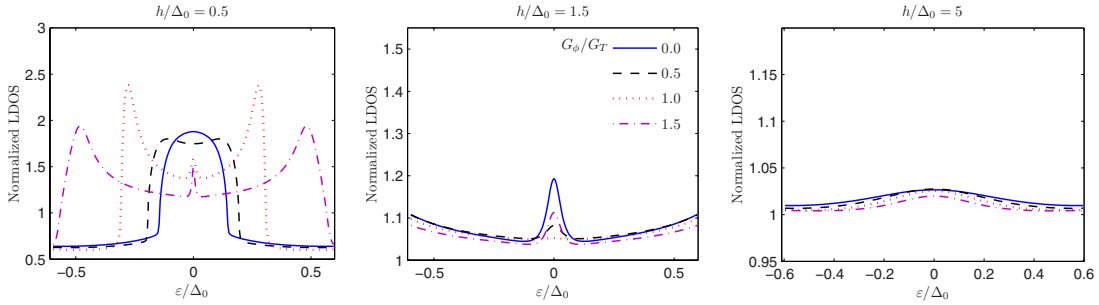

FIG. 2. (Color online) Plot of the energy-resolved LDOS evaluated at $x/d_F=0.5$ in the case of a thin domain wall $d_W/d_F=0.2$. We consider three values of the exchange field h and also investigate how the LDOS changes with the phase shift G_ϕ at the interface.

consider the Bloch wall configuration since the results for the Néel wall are identical. We also note that in our study, the magnetization is always inhomogeneous in the direction perpendicular to the interface, i.e., upon penetrating into the ferromagnetic region. In the case where the inhomogeneity of the magnetization is in the transverse direction (parallel to the interface), i.e., there is no variation in the x direction, the proximity effect does not become long ranged even if equal-spin correlations may be generated.[35] The general condition for a long-range proximity effect is that there exists a misalignment between the triplet anomalous Green's-function vector and the exchange field.

We first study the thin-domain-wall case $d_W/d_F=0.2$. To begin with, we shall consider the energy-resolved DOS in the center of the domain wall ($x=d_F/2$) for several values of the exchange field. This is shown in Fig. 2. As seen, the zero-energy DOS is enhanced in all cases due to the presence of odd-frequency correlations.[8,9,12,66] The influence of the spin-DIPS (G_ϕ) seems to be an induction of additional peak features in the subgap regime. This effect is most pronounced at low exchange fields (in particular $h/\Delta_0=0.5$ in Fig. 2). A possible physical explanation for the additional peak features in the LDOS may be the fact that G_ϕ acts as an effective exchange field in both the superconducting and ferromagnetic layers.[55] It thus conspires with the intrinsically existing exchange field in the ferromagnetic layer to yield a modified value of the total exchange field. This explanation is consistent with the fact that the position of the peaks change upon increasing G_ϕ. More specifically, the spin-DIPS appear to enhance the exchange field since the peaks move outwards toward the gap edge.

Next, we investigate the thick-domain-wall case and choose $d_W/d_F=0.8$. In Fig. 3, we again consider the energy-resolved LDOS in the middle of the ferromagnetic layer ($x/d_F=0.5$) for three different values of the exchange field. Upon comparison with Fig. 2, it is seen that the general trend upon increasing the domain-wall thickness is an overall enhancement of the proximity effect. The qualitative features in Fig. 3 are very similar to those in the thin-domain-wall case, but the enhancement at zero energy tends to be larger particularly so for large values of h/Δ_0. Again, it is seen that the effect of the spin-DIPS is a modification of the total exchange field, amounting to a double-peak structure at subgap energies in the LDOS.

It is also interesting to consider the spatial dependence of the zero-energy DOS in the ferromagnetic region. By using local STM-techniques, it is possible to probe the DOS at (in principle) any location in the ferromagnetic film. The specific choice of $\varepsilon=0$ is particularly interesting in terms of the DOS since it is strongly influenced by the presence of odd-frequency correlations. As pointed out in Refs. 12 and 20, the behavior of the DOS at $\varepsilon=0$ may be interpreted as a competition between spin-singlet even-frequency and spin-triplet odd-frequency correlations. The former tend to give a mini-

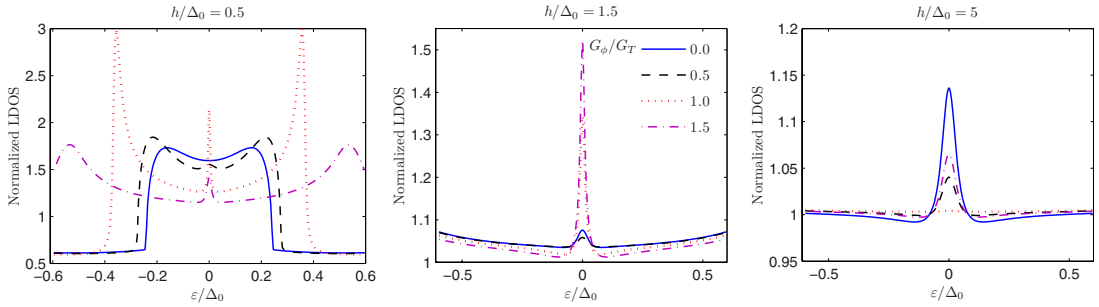

FIG. 3. (Color online) Plot of the energy-resolved LDOS evaluated at $x/d_F=0.5$ in the case of a thick domain wall, $d_W/d_F=0.8$. We consider three values of the exchange field h and also investigate how the LDOS changes with the phase shift G_ϕ at the interface.

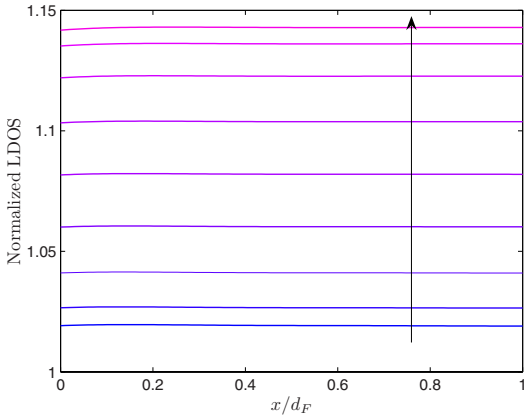

FIG. 4. (Color online) Plot of the zero-energy LDOS induced in the ferromagnet for $h/\Delta_0=5$ and $d_F/\xi_S=0.5$. The lines correspond to d_W/d_F in the range [0.1,0.9] in steps of 0.1 along the arrow. Here, G_ϕ is set to zero.

gap in the DOS for subgap energies, while the latter yields a zero-energy peak in the DOS. Clearly, these two effects are competing with each other since they have a destructive interplay. In the present case, one would expect that the domain-wall structure should favor the generation of the odd-frequency triplet components, thus enhancing the LDOS. This conjecture is supported by Figs. 2 and 3.

In Fig. 4, we plot the spatially resolved LDOS at $\varepsilon=0$ for several values of d_W to probe directly how the odd-frequency correlations are affected by the domain-wall thickness. As compared to Figs. 2 and 3, we normalize the LDOS on its value at $x=0$ in Fig. 4 for easier comparison between different values of d_W and choose $G_\phi=0$. From the plot, it is clear that the thicker the domain wall, the more strongly enhanced the zero-energy DOS. This also supports the notion that the magnetically inhomogeneous structure favors the generation of odd-frequency triplet components. The concomitant enhancement of the DOS may then be seen at increasingly larger penetration depths in the ferromagnet when the domain-wall thickness is increased.

2. Conical ferromagnetism

We now turn to a study of how the superconducting proximity effect is manifested in a ferromagnet with a conical magnetization such as Ho. We fix the exchange field at $h/\Delta_0=5$ and study how the DOS changes upon increasing the ferromagnetic layer thickness. The motivation for this is to obtain a better understanding of how the DOS changes when only the long-range triplet components are present in the sample. In an inhomogeneous ferromagnet, the singlet component and the $S_z=0$ triplet component are short ranged and penetrate in a distance $\xi_F=\sqrt{D/h}$ into the ferromagnet. The $S_z=\pm 1$ triplet components, however, are not subject to the pair-breaking effect originating with the Zeeman splitting and can thus penetrate a much longer distance $\xi_N=\sqrt{D/T}$ into the ferromagnet, where T is temperature. Therefore, by making the ferromagnetic layer thick enough, one can be certain that there is no contribution from either the singlet or $S_z=0$ triplet components. Since we have chosen $h/\Delta_0=5$, we find that the penetration depth of these components in the ferromagnetic layer should be $0.44\xi_S$.

We next turn to a study of the proximity-induced LDOS. In Fig. 5, we plot the energy-resolved LDOS for three layer thicknesses: (i) $d/\xi_S=0.1$, (ii) $d/\xi_S=0.5$, and (iii) $d/\xi_S=0.9$. In case (i), both short-ranged and long-ranged components should contribute significantly to the LDOS. In case (ii), the long-ranged components should dominate over the short-ranged ones, while finally in case (iii) only long-ranged components remain. This is because we evaluate the energy-resolved DOS at the $F|I$ interface, $x=d_F$, as was also done in the experiment of Refs. 57 and 67.

As seen in case (ii) and (iii), a pronounced zero-energy peak is present, bearing witness of the odd-frequency correlations in the system. The peak is more pronounced with increasing thickness since the long-range triplet correlations dominate over the even-frequency singlet Green's function as the thickness increases. However, case (i) is qualitatively different from the two other thicknesses. In this case, the low-energy LDOS is completely suppressed in the regime $G_\phi/G_T<1$ and suddenly reappears for $G_\phi/G_T>1$. It is very interesting to note that the same effect was recently discovered for an $S|N$ junction with a magnetically active interface,[68] but in that case the effect was completely independent on the junction thickness.

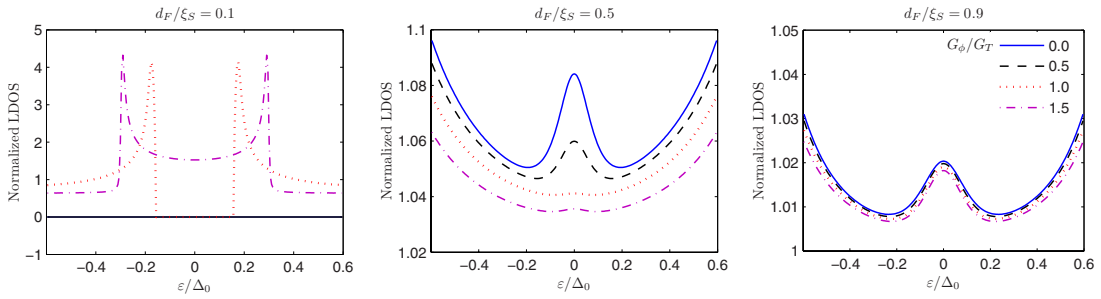

FIG. 5. (Color online) Plot of the LDOS at $x=d_F$ for a conical ferromagnet with $h/\Delta_0=5$ for several values of the ferromagnetic layer thickness d_F. In each case, we investigate the role of the spin-DIPS (G_ϕ) at the S|F interface.

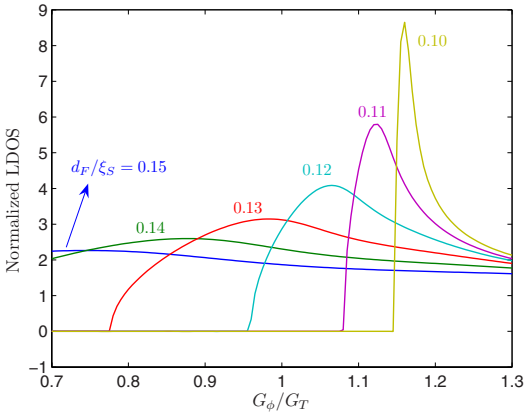

FIG. 6. (Color online) Plot of the zero-energy LDOS at $x=d_F$ for a conical ferromagnet with $h/\Delta=5$ as a function of the normalized spin-DIPS parameter G_ϕ/G_T. Below a critical value for d_F, a qualitatively different behavior is observed for the LDOS.

In order to investigate this effect further, we focus on the zero-energy LDOS in the thin junction case in Fig. 6. As seen, for sufficiently thin layers $d_F/\xi_S \ll 1$, an abrupt crossover takes place at a critical value of G_ϕ/G_T, qualitatively altering the LDOS at zero energy. Remarkably, we find that a similar transition takes place upon increasing the ferromagnetic layer thickness. Consider a plot of the zero-energy LDOS in Fig. 7 as a function of d_F/ξ_S. As seen, at a critical layer thickness, the zero-energy LDOS rises abruptly from zero and acquires the usual oscillating behavior. To see how the full energy-resolved LDOS evolves with increasing G_ϕ for a fixed thickness $d_F/\xi_S=0.1$, consider Fig. 8. As seen, the LDOS changes qualitatively above a critical value of $G_\phi/G_T \simeq 1.14$.

To summarize the findings of Figs. 6–8, we have found that there is an abrupt crossover from a fully suppressed

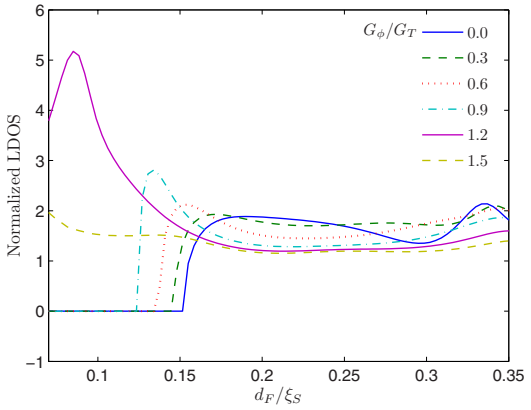

FIG. 7. (Color online) Plot of the zero-energy LDOS at $x=d_F$ as a function of d_F/ξ_S for several values of G_ϕ. As seen, there is a critical thickness at which the zero-energy LDOS becomes nonzero. We have used $h/\Delta_0=5$.

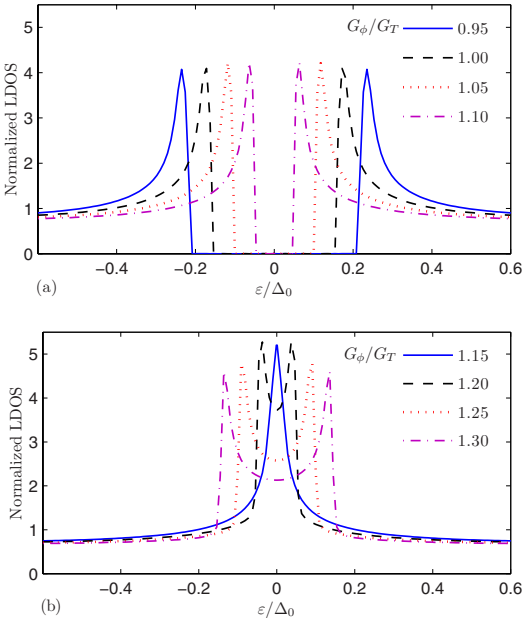

FIG. 8. (Color online) Plot of the LDOS at $x=d_F$ for a conical ferromagnet with $h/\Delta_0=5$ and $d_F/\xi_S=0.1$ for several values of the spin-DIPS (G_ϕ) at the S|F interface. In (a), G_ϕ/G_T is below the critical value, while in (b) G_ϕ/G_T is larger than the critical value.

LDOS to a finite LDOS which appears at a critical thickness of the ferromagnetic layer, and the particular value of the critical thickness depends on the value of G_ϕ. In a similar way, we find that there is an abrupt change appearing at a critical value of G_ϕ for sufficiently thin layers. The natural question is: what is the reason for these changes? An important clue is found in the fact that when the LDOS is fully suppressed, the odd-frequency correlations must be zero.[12] The presence of odd-frequency correlations will in general lead to an enhancement of the LDOS at zero energy, which at present is one of the main suggestions put forth in the literature with regard to the issue of how to obtain clear experimental signatures of this exotic type of superconducting pairing. Therefore, the abrupt transition from a fully suppressed LDOS to a LDOS which is enhanced even compared to the normal-state value is a strong indicator of a symmetry transition from the usual even-frequency correlations to a state of mixed even-frequency and odd-frequency correlations or possibly even pure odd-frequency correlations. It is therefore clear that the spin-DIPS occurring at the interface have paramount consequences with regard to the symmetry properties of the induced superconducting correlations in the ferromagnet. Due to the complexity of the problem, it is unfortunately not possible to give an exact analytical treatment of the influence of G_ϕ on the symmetry properties of the anomalous Green's function.

In the remaining part of the discussion of conical ferromagnets, we wish to focus on how the proximity-induced LDOS depends on the structure of the magnetic texture,

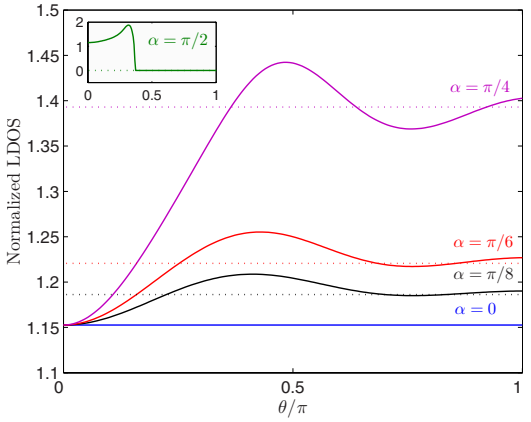

FIG. 9. (Color online) Plot of the zero-energy LDOS at $x=d_F$ as a function of θ for several values of α. We have fixed $h/\Delta_0=5$, $d_F/\xi_S=0.5$, and $G_\phi=0$ to focus on the effect of the magnetic structure. The dotted lines give the result for $h_y=h_z=0$, which corresponds to the saturating behavior when θ increases since the average value of h_y and h_z vanishes in this limit. The inset shows the case $\alpha=\pi/2$ corresponding to $h_x=0$. For increasing θ, the ferromagnetic layer effectively acts as a normal metal, thus causing a complete suppression of the zero-energy LDOS.

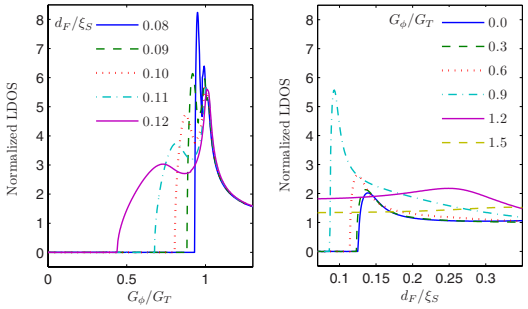

FIG. 10. (Color online) Self-consistent solution for the spatial profile of the superconducting order parameter using the approach described in Sec. III of this paper. The choice for parameter values are specified in the main text. To add stability to the numerical calculations, we added a small imaginary number $i\eta$ to the quasiparticle energies ε, with $\eta=0.05\Delta_0$, effectively modeling inelastic scattering.

which is determined by the parameters $\{a,\alpha,\theta\}$ in Fig. 1. We here focus on the role of α and θ, which control, respectively, the direction and the speed of rotation of the magnetization upon entering the ferromagnetic layer. Thus, we keep a/ξ_S fixed at $a/\xi_S=0.0263$. In Fig. 9, we present results for the zero-energy LDOS at $x=d_F$ as a function of θ for several values of α. The LDOS displays oscillations as a function of θ and eventually seems to sature upon increasing θ. This may be understood microscopically by realizing that when the rotation of the magnetization texture becomes faster, i.e., increasing θ, the effective magnetization felt by the Cooper pair averages out to zero for the rotating components. For our setup, this would mean that only the h_x component should remain nonzero, while $h_y=h_z=0$. To verify this scenario, we have also plotted the results in the $h_y=h_z=0$ case in Fig. 9 (dotted lines) for each value of α, which is seen to coincide with the limiting behavior in the high-θ case. It is interesting to note that for $\alpha=\pi/2$, the LDOS vanishes completely above a critical value for θ. This may be understood by noting that $h_x=0$ when $\alpha=\pi/2$. Thus, when θ increases, we have $\langle h_x\rangle=\langle h_y\rangle=0$, causing the ferromagnetic layer to act as a normal metal.

C. Discussion

The main approximation that we have made in our calculations is to use the bulk solution for the order parameter of the superconductor. Although this approximation is expected to be satisfactory in the regime $d_S\gg\{\xi_S,d_F\}$, such that the superconductor acts as a reservoir, there are two aspects which are lost upon doing so. One aspect is the depletion of the superconducting order parameter near the interface. The depletion may be disregarded in the tunneling limit[69] (low barrier transparency), and we do not expect that an inclusion of the spatial profile of the superconducting order parameter near the interface should have any qualitative influence upon our results, as long as the superconducting order parameter is not dramatically reduced at the interface.

The assumption of a step-function superconducting order parameter is commonly employed in the literature, but let us for the sake of clarity here examine a bit more carefully under which circumstances this is truly warranted. In the present work, we have considered a superconducting reservoir of size $d_S\gg\xi_S$ and a ferromagnetic film of size $d_F\leq\xi_S$. For a weak ferromagnet considered here, the ferromagnetic coherence length ξ_F is comparable in size to ξ_S. Also, we have considered the case where $\zeta=R_B/R_F\gg1$, corresponding to a low barrier transparency, which should be experimentally relevant. To investigate quantitatively how much the superconducting order parameter is suppressed near the interface, let us fix $h/\Delta_0=10$, $d_S/\xi_S=5$, $d_F/\xi_F=1$, and $\zeta=5$. Using a numerical approach for S|F bilayer with a homogeneous exchange field as employed in Sec. III of our paper, we obtain the gap self-consistently with the result shown in Fig. 10. It is also necessary to introduce the barrier asymmetry factor $\gamma=\xi_S\sigma_F/(\xi_F\sigma_S)$, where $\sigma_{F(S)}$ is the conductivity in the F (S) layer. Here, we set $\gamma=1$. As seen, the depletion of the gap is quite insensitive to the value of G_ϕ, and we have verified that the depletion of the gap is virtually the same even up to ferromagnetic layer thicknesses of $d_F/\xi_F=4$. As recently pointed out in Ref. 58, the step-function approximation breaks down for low values of ζ and/or high values of γ, and if the spin-DIPS G_ϕ^S induced on the superconducting side are large in magnitude compared to the tunneling conductance G_T, the suppression of the gap becomes more pronounced.

The second aspect which is lost is the inverse proximity effect in the superconductor. The inverse proximity effect is, in similarity to the depletion of the order parameter, expected to be small when the interface transparency is low and $d_S\gg d_F$. Nevertheless, the presence of the spin-DIPS at the in-

terface, modeled through the parameter G_ϕ, could have some nontrivial impact on the correlations in the superconductor. Cottet showed that this may indeed be so in Ref. 56, at least when the superconducting layer is quite thin. The full effect exerted on the LDOS by the presence of spin-DIPS on both sides of the interfaces was recently investigated numerically in an S|F bilayer.[58] However, no study so far have investigated how the proximity-induced magnetization in the superconducting region is affected by spin-DIPS. We will proceed to investigate this particular issue in detail in Sec. III of this work.

Above, we have considered the diffusive limit $\xi_S/l_{\mathrm{imp}} \gg 1$, where $l_{\mathrm{imp}}=v_F\tau$ is the mean-free path. The diffusive limit was also considered in Ref. 77, where the critical supercurrent through a conical ferromagnet was calculated. Although the magnetic texture we have considered in the second part is identical that of the conical ferromagnet Ho, one important difference is that Ho is a strong ferromagnet, contrary to the case studied here. This means that the diffusive limit condition $h\tau \ll 1$ is not fulfilled for Ho, and it was in fact estimated in Ref. 59 that $h\tau \simeq 10$. This calls for a treatment with the more general Eilenberger equation, which allows for a study where the energy scale of the Zeeman splitting is comparable or larger than the self-energy associated with impurity scattering. A natural continuation of this work would therefore be to study a proximity structure of a superconductor|conical ferromagnet for an arbitrary ratio of the parameter $h\tau$. Such an endeavor would nevertheless be quite challenging unless a weak-proximity effect is assumed. In the present work, we have not restricted ourselves to any limits with regard to the barrier transparency or the proximity effect. Although the exchange field considered for the conical ferromagnet in this paper is smaller than the one realized in Ho, we expect that our results may be qualitatively relevant for STM measurements in superconducting junctions with Ho. In general, increasing the exchange field amounts to a quantitative reduction in the magnitude of the proximity effect.

Finally, we show that the zero-energy DOS for the domain-wall case exhibits a similar crossover behavior as the conical ferromagnetic case upon varying G_ϕ and d_F when $d_F/\xi_S \ll 1$. In Fig. 11, the zero-energy DOS is plotted for the thick-domain-wall case to illustrate this effect—the results are very similar even for $d_W/d_F \ll 1$ when $d_F/\xi_S \ll 1$. Once again, it should be noted that a complete suppression of the DOS amounts to pure even-frequency superconducting correlations induced in the ferromagnetic region, since the presence of odd-frequency correlations enhances the zero-energy DOS. The exact microscopic mechanism behind the abrupt crossover occurring at critical values of G_ϕ and d_F, respectively, remains somewhat unclear. A possible resolution to this behavior is the observation that the spin-DIPS may conspire with the proximity-induced minigap in the ferromagnetic region for sufficiently thin layers $(d_F/\xi_S \ll 1)$ and yield a zero-energy DOS of the form $N(0) \sim 1/\sqrt{G_\phi^2 - G_T^2}$, as noted in Ref. 55. In this case, a scenario similar to the one of a thin-film superconductor in the presence of an in-plane magnetic field is realized, where the spin-resolved DOS experiences a quasiparticle energy-shift with $\pm h$. In this case, the role of the exchange field is played by G_ϕ, while the role

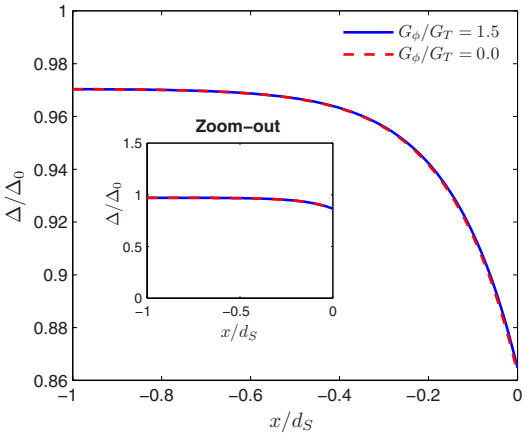

FIG. 11. (Color online) Plot of the zero-energy LDOS at $x=d_F$ in the case of a Bloch domain wall with $h/\Delta_0=5$. In (a) and (c), we plot the LDOS as a function of the spin-DIPS G_ϕ, while in (b) and (d) we plot it as a function of the ferromagnetic layer thickness d_F. For thin layers $d_F/\xi_S \ll 1$, one observes an abrupt transition from a fully suppressed DOS to a nonzero DOS at a critical value for either G_ϕ or d_F.

of the superconducting gap is played by G_T. We do not observe the effects shown in Fig. 11 for larger values of d_F, which is consistent with the fact that the minigap is completely absent in this regime since the proximity effect becomes weaker.

III. INVERSE PROXIMITY EFFECT IN A S|F BILAYER WITH A HOMOGENEOUS MAGNETIZATION TEXTURE

In this part of the paper, we will consider the inverse proximity effect of an S|F bilayer, where the exchange field is fixed and parallel to the z axis, manifested through an induced magnetization near the interface of the superconducting region. We will again employ the quasiclassical theory of superconductivity[60] and consider the diffusive limit described by the Usadel equation,[61] as this is experimentally the most relevant case. Our approach will be to solve the Usadel equation and the gap equation for the superconducting order parameter self-consistently everywhere in the system shown in Fig. 12.

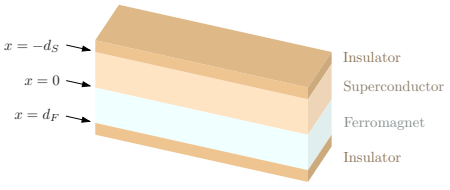

FIG. 12. (Color online) The experimental setup proposed in this paper: a superconductor|ferromagnet bilayer.

A. Theory

We will use the conventions and notation of Ref. 20, which also allows for an inclusion of magnetic impurities and spin-orbit coupling if desirable. To facilitate the numerical implementation, we employ the following parametrization of the Green's functions:

$$\hat{g}_j = \begin{pmatrix} c_{\uparrow,j} & 0 & 0 & s_{\uparrow,j} \\ 0 & c_{\downarrow,j} & s_{\downarrow,j} & 0 \\ 0 & -s_{\downarrow,j} & -c_{\downarrow,j} & 0 \\ -s_{\uparrow,j} & 0 & 0 & -c_{\uparrow,j} \end{pmatrix}, \quad j=\{S,F\}, \quad (19)$$

where we have introduced

$$s_{\sigma,j} = \sinh(\theta_{\sigma,j}), \quad c_{\sigma,j} = \cosh(\theta_{\sigma,j}). \quad (20)$$

Note that $(\hat{g}_j)^2 = \hat{1}$ is satisfied. The parameter $\theta_{\sigma,j}$ is a measure of the proximity effect, and obeys the Usadel equation,

$$D_j \partial_x^2 \theta_{\sigma,j} + 2i(\varepsilon + \sigma h)\sinh(\theta_{\sigma,j}) - 2i\sigma\Delta\cosh(\theta_{\sigma,j}) = 0, \sigma = \{\uparrow,\downarrow\}, \quad (21)$$

in the superconducting ($h=0, j=S$) and ferromagnetic ($\Delta=0, j=F$) layer, respectively. Above, D_S and D_F denote the diffusion constants in the two layers, ε is the quasiparticle energy, Δ is the pair potential, and h is the exchange field. The two latter are in general subject to a depletion close to the S|F interface.

The boundary condition for the ferromagnetic Green's function, $\hat{g}_F$, reads as[55]

$$2\xi_F \hat{g}_F \partial_x \hat{g}_F = \gamma_T[\hat{g}_S, \hat{g}_F] + i\gamma_{\phi,F}[\hat{\alpha}_3, \hat{g}_F] \quad (22)$$

at $x=0$ and $\hat{g}_F \partial_x \hat{g}_F = \hat{0}$ at $x=d_F$. Here, $\hat{\ldots}$ denotes a 4×4 matrix in spin $\otimes$ particle-hole space. Also,. For the superconducting Green's function, $\hat{g}_S$, we have

$$2(\xi_S/\gamma)\hat{g}_S \partial_x \hat{g}_S = -\gamma_T[\hat{g}_F, \hat{g}_S] - i\gamma_{\phi,S}[\hat{\alpha}_3, \hat{g}_S] \quad (23)$$

at $x=0$ and $\hat{g}_S \partial_x \hat{g}_S = \hat{0}$ at $x=-d_S$. Above, we have defined

$$\gamma_T = G_T \xi_F/(A\sigma_F), \quad \gamma_{\phi,F(S)} = G_{\phi,F(S)}\xi_F/(A\sigma_F), \quad (24)$$

and the barrier asymmetry factor,

$$\gamma = \xi_S \sigma_F/(\xi_F \sigma_S). \quad (25)$$

Moreover, A is the tunneling contact area, while $\sigma_{F(S)}$ are the normal-state conductivities. Note that

$$A\sigma_{F(S)} = d_{F(S)}/R_{F(S)}, \quad (26)$$

where $d_{F(S)}$ is the thickness of the layer and $R_{F(S)}$ is the normal-state resistance.

In total, the interface between the S and F regions is thus characterized by three parameters: the normalized barrier conductance γ_T, the spin-DIPS $\gamma_{\phi,S}$, and $\gamma_{\phi,F}$ on each side of the interface. In what follows, we will study the mutual influence of superconductivity and ferromagnetism on each other instead of assuming the bulk solution for $\hat{g}_S$ in the superconducting region, as is usually done in the literature. We solve the Usadel equation self-consistently in both the S and F layers, supplementing it with the gap equation:

$$\Delta = \frac{N_F\lambda}{2}\int_0^\omega d\varepsilon \tanh(\beta\varepsilon/2)\sum_\sigma \sigma \,\mathrm{Re}\{\sinh(\theta_\sigma)\}, \quad (27)$$

where we choose the weak coupling-constant and cut-off energy to be $N_F\lambda=0.2$ and $\omega/\Delta_0=75$. When obtaining the Green's functions, a number of interesting physical quantities may be calculated. For instance, the normalized LDOS is obtained according to

$$N(\varepsilon)/N_0 = \mathrm{Re}\{\cosh\,\theta_\uparrow + \cosh\,\theta_\downarrow\}/2. \quad (28)$$

Experimentally, the LDOS may be probed at $x=-d_S$ in the superconducting layer and $x=d_F$ in the ferromagnetic layer by performing tunneling spectroscopy through the insulating layer. In principle, it is also possible to obtain the LDOS at any position x by using spatially resolved scanning tunneling microscopy.

The quantity of interest which we shall focus on in this work is the proximity-induced magnetization in the superconducting region. A few words about the sign of the magnetization in the problem are appropriate. First, recall that the magnetic moment μ of an electron is directed *opposite* to its spin $\mathbf{S}$, namely, $\mu \simeq -(e/m_e)\boldsymbol{S}$, where $e=|e|$ and m_e is the electron charge and mass. Therefore, if the exchange energy h favors spin-$\uparrow$ electrons energetically, the resulting magnetization $\boldsymbol{M}$ of the ferromagnet will be directed in the opposite direction, $\boldsymbol{M} \| (-z)$.

In the absence of a proximity effect, we have $\boldsymbol{M}=0$ in the superconducting region and $\boldsymbol{M}=M_0\hat{z}$ in the ferromagnetic region, where

$$M_0 \simeq -\mu_B N_0 h \quad (29)$$

in the quasiclassical approximation $h \ll \varepsilon_F$. Now, the change in magnetization due to the proximity effect may be calculated according to

$$\delta\boldsymbol{M} = -\mu_B \hat{z}\sum_\sigma \sigma\langle\psi_\sigma^\dagger \psi_\sigma\rangle \quad (30)$$

in both the superconducting and ferromagnetic regions. Using a quasiclassical approach, the above expression translates into a normalized change in magnetization,

$$\delta M/M_0 = -\int_0^\infty \frac{d\varepsilon}{h}\sum_\sigma \sigma\,\mathrm{Re}\{\cosh\theta_\sigma\}\tanh(\beta\varepsilon/2). \quad (31)$$

In the ferromagnetic region, the normalized magnetization M/M_0 is therefore $1+\delta M_F/M_0$, while in the superconducting region we have an induced magnetization $\delta M_S/M_0$, where $\delta M_{F(S)}$ is determined by Eq. (31) on the ferromagnetic (superconducting) side of the interface.

Although we shall be concerned with a full numerical solution when presenting our results in Sec. III B, let us for completeness sketch how an analytical solution may be obtained under the assumption of a weak-proximity effect. Including the spin-DIPS, the analytical results obtained here are thus a natural extension of the results in Ref. 48, where the spin-DIPS were neglected. We remind the reader that spin-DIPS occur whenever there is a finite spin polarization in the ferromagnetic region or when the barrier itself is magnetic.

In the weak-proximity regime, the Usadel equation in the ferromagnetic region becomes

$$D_F\partial_x^2\delta\theta_\sigma^F + 2i(\varepsilon+\sigma h)\delta\theta_\sigma^F = 0, \tag{32}$$

where the linearization of Eqs. (19) and (21) amounts to $\theta_{\sigma,F}\rightarrow\delta\theta_\sigma^F$ where $|\delta\theta_\sigma^F|\ll 1$. The general solution is readily obtained as

$$\delta\theta_\sigma^F = A_\sigma(e^{ik_\sigma x} + e^{-ik_\sigma x+2ik_\sigma d_F}), \tag{33}$$

upon taking into account the vacuum boundary condition $\partial_x\delta\theta_\sigma^F=0$ at $x=d_F$ and defining

$$k_\sigma^2 = 2i(\varepsilon+\sigma h)/D_F. \tag{34}$$

In the superconducting region, we obtain the Usadel equation,

$$D_S\partial_x^2\delta\theta_\sigma^S + 2i(\varepsilon c_{\rm BCS} - \Delta s_{\rm BCS})\delta\theta_\sigma^S = 0, \tag{35}$$

under the assumption that the superconducting order parameter is virtually unaltered from the bulk case. This is a valid approximation for $\{\gamma,\gamma_T\}\ll 1$ and not too large $\gamma_{\phi,S}$ (typically $\gamma_{\phi,S}<1$), which we have verified by using the full numerical solution. Here, $\delta\theta_\sigma^S$ is the deviation from the bulk BCS solution, i.e., $\theta_{\sigma,S}\rightarrow\sigma\theta_{\rm BCS}+\delta\theta_\sigma^S$ with $|\delta\theta_\sigma^S|\ll 1$ and

$$c_{\rm BCS} = \cosh(\theta_{\rm BCS}), \quad s_{\rm BCS} = \sinh(\theta_{\rm BCS}),$$

$$\theta_{\rm BCS} = \operatorname{atanh}(\Delta/\varepsilon). \tag{36}$$

In this case, the general solution reads as

$$\delta\theta_\sigma^S = B_\sigma(e^{i\kappa x} + e^{-i\kappa x-2i\kappa d_S}), \tag{37}$$

when incorporating the vacuum boundary condition $\partial_x\delta\theta_\sigma^S=0$ at $x=-d_S$ upon defining

$$\kappa^2 = (\varepsilon c_{\rm BCS} - \Delta s_{\rm BCS})/D_S. \tag{38}$$

The remaining task is to determine the unknown coefficients $\{A_\sigma,B_\sigma\}$. Linearizing the boundary conditions Eqs. (22) and (23), we obtain at $x=0$

$$\xi_S\partial_x\delta\theta_\sigma^S/\gamma = \gamma_T(c\,\delta\theta_\sigma^F - \sigma s_{\rm BCS} - c_{\rm BCS}\delta\theta_\sigma^S) - \sigma i\gamma_{\phi,S}(\sigma s_{\rm BCS} + c_{\rm BCS}\delta\theta_\sigma^S),$$

$$\xi_F\partial_x\delta\theta_\sigma^F = \gamma_T(c\,\delta\theta_\sigma^F - \sigma s_{\rm BCS} - c_{\rm BCS}\delta\theta_\sigma^S) + \sigma i\gamma_{\phi,F}\delta\theta_\sigma^F. \tag{39}$$

From these boundary conditions, one derives that

$$A_\sigma = \frac{z_4^\sigma}{z_3^\sigma}\frac{s_{\rm BCS}[z_3^\sigma(\gamma_T a + i\gamma_{\phi,S}) - z_1^\sigma\sigma\gamma_T]}{z_2^\sigma z_3^\sigma - z_1^\sigma z_4^\sigma} - \sigma s_{\rm BCS}\gamma_T,$$

$$B_\sigma = \frac{s_{\rm BCS}[z_1^\sigma\sigma\gamma_T - z_3^\sigma(\gamma_T\sigma + i\gamma_{\phi,S})]}{z_2^\sigma z_3^\sigma - z_1^\sigma z_4^\sigma}. \tag{40}$$

Here, we have defined the auxiliary quantities:

$$z_1^\sigma = -\gamma_T c_{\rm BCS}(1+e^{2ik_\sigma d_F}),$$

$$z_2^\sigma = \frac{i\kappa\xi_S(1-e^{-2i\kappa d_S})}{\gamma} + c_{\rm BCS}(\gamma_T + i\sigma\gamma_{\phi,S})(1+e^{-2i\kappa d_S}),$$

$$z_3^\sigma = ik_\sigma\xi_F(1-e^{2ik_\sigma d_F}) - (\gamma_T c_{\rm BCS} + \sigma i\gamma_{\phi,F})(1+e^{2ik_\sigma d_F}),$$

$$z_4^\sigma = c_{\rm BCS}\gamma_T(1+e^{-2i\kappa d_S}). \tag{41}$$

Equations (33), (37), and (40) constitute a closed analytical solution for the Green's functions in the entire S|F bilayer. To use this analytical solution, one should verify that $|\delta\theta_\sigma^{F,S}|\ll 1$ for the relevant parameter regime. Spin-flip and spin-orbit scatterings may also be accounted for in the analytical solution of the Green's function by adding appropriate terms to the Usadel equation. The calculation is then performed along the lines of Refs. 20 and 70.

B. Results

We are now in a position to evaluate the proximity-induced magnetization numerically. The full (nonlinearized) Usadel equation will be employed, such that we are not restricted to the weak-proximity effect regime. To stabilize the numerical calculations, we add a small imaginary number to the quasiparticle energy, $\varepsilon\rightarrow\varepsilon+i\eta$, with $\eta=0.05\Delta_0$. We focus on the results reported very recently by Xia *et al.*[51] and take $d_S/\xi_S=0.2$, $d_F/\xi_F=1.0$, and $h/\Delta_0=15$ as a reasonable set of parameters which should be relevant to this experiment. Also, we assume that the junction conductance was low, $\gamma_T=0.1$, and set the barrier asymmetry factor to $\gamma=0.2$, corresponding to a scenario where the superconducting region is much less disordered than the ferromagnetic one. We will also investigate the case $d_S/\xi_S=1.0$ to see how the properties of the system changes when going away from the limit $d_S/\xi_S\ll 1$. We underline that our main objective in this work is to investigate the influence of the spin-DIPS on the proximity-induced magnetization in the system, such that we mainly vary $\gamma_{\phi,F}$ and $\gamma_{\phi,S}$ while keeping the other parameters fixed.

Let us first consider the temperature dependence of the proximity-induced magnetization in the superconducting region in Fig. 13. To clarify the role of the spin-DIPS on each side of the interface, we plot $\delta M_S/M_0$ for several values of $\gamma_{\phi,S}$ in Fig. 13(a) while keeping $\gamma_{\phi,F}=0$ fixed. Conversely, we plot $\delta M_S/M_0$ for several $\gamma_{\phi,F}$ in Fig. 13(b) with $\gamma_{\phi,S}=0$. In both cases, we plot the proximity-induced magnetization at $x=-d_S$. One obvious difference between these two scenarios is that the spin-DIPS on the superconducting side, $\gamma_{\phi,S}$, influence the proximity-induced magnetization much stronger than $\gamma_{\phi,F}$. The same thing is true with regard to the influence of spin-DIPS on the superconducting order parameter: $\gamma_{\phi,S}$ influences the spatial profile of Δ much more than what $\gamma_{\phi,F}$ does. From Fig. 13, it is clearly seen how the proximity-induced magnetization may switch sign upon increasing the magnitude of the spin-DIPS $\gamma_{\phi,S}$. We have checked numerically that this effect also takes upon increasing $\gamma_{\phi,F}$ when keeping $\gamma_{\phi,S}=0$. Thus, increasing either $\gamma_{\phi,S}$ or $\gamma_{\phi,F}$ can lead to a sign change in the proximity-induced magnetization in the superconducting region. It is then clear that the conclusion of Ref. 53 that only spin screening is possible in diffusive S|F bilayers does not hold in general since the presence of spin-DIPS alters the screening effect. In what follows, we focus on the role of $\gamma_{\phi,S}$ since its impact on

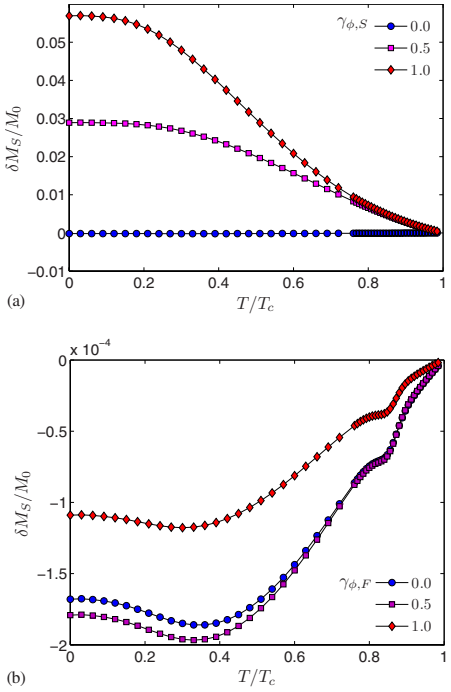

FIG. 13. (Color online) (a) Plot of the proximity-induced magnetization for $\gamma_{\phi,F}=0$ upon varying the spin-DIPS $\gamma_{\phi,S}$ on the superconducting side. (b) Plot of the proximity-induced magnetization for $\gamma_{\phi,S}=0$ upon varying the spin-DIPS $\gamma_{\phi,F}$ on the ferromagnetic side. We have used $d_S/\xi_S=0.2$, and the other parameter values are discussed and provided in the main text. Note that the lines with a (blue) circle marker are equal in (a) and (b), corresponding to $\gamma_{\phi,S}=\gamma_{\phi,F}=0$. As seen, $\gamma_{\phi,S}$ affects $\delta M_S/M_0$ much more strongly than $\gamma_{\phi,F}$. In (b), the magnetization switches sign upon increasing $\gamma_{\phi,F}$ further (for the present parameters, the sign switch occurs around $\gamma_{\phi,F}\simeq 1.3$).

$\delta M_S/M_0$ is much greater than that of $\gamma_{\phi,F}$. In Fig. 14, we consider the case $d_S/\xi_S=1.0$ to show that the sign change in the magnetization persists when going away from the limit $d_S/\xi_S \ll 1$. The spatial profile of the total magnetization in the F and S regions are shown for the case $d_S/\xi=0.2$ with $\gamma_{\phi,S}=0.0$ in Fig. 15 and $\gamma_{\phi,S}=1.0$ in Fig. 16. It is seen that the magnetization decreases in a monotonic fashion toward the superconducting region and reaches its bulk value deep inside the ferromagnetic region. In the superconductor, magnetization is induced near the interface and decays with the distance from the interface.

C. Discussion

We propose the following explanation for the antiscreening effect observed upon increasing $\gamma_{\phi,S}$. The effect of the spin-DIPS in the case of a thin superconducting layer $d_S \ll \xi_S$ in Ref. 56 was shown to be equivalent to an internal magnetic exchange splitting h_{eff} in the superconducting region. Therefore, the magnitude of the magnetization in the superconductor should essentially grow with an increasing value of $\gamma_{\phi,S}$. If this is the case, the proximity-induced magnetization should also be sensitive to the sign of $\gamma_{\phi,S}$, as the opposite spin species would be energetically favored when comparing the case $\gamma_{\phi,S}$ with $(-\gamma_{\phi,S})$. To test this hypothesis, we plot in Fig. 17 the proximity-induced magnetization at $T=0$ as a function of the spin-DIPS on the superconducting side, $\gamma_{\phi,S}$ (keeping $\gamma_{\phi,F}=0$). The results confirm our hypothesis—it is seen that $\delta M_S/M_0$ is an antisymmetric function of $\gamma_{\phi,S}$. The influence of $\gamma_{\phi,S}$ can also be seen directly in the LDOS in the superconducting region. For $\gamma_{\phi,S} \neq 0$, we obtain a double-peak structure in the LDOS at $x=-d_S$ in agreement with Refs. 56 and 58, while the superconducting order parameter depletes very little close to the interface for the chosen parameter values. In general, the depletion of the superconducting order parameter is found to be small as long as $\{\gamma_T, \gamma\} \ll 1$ and $\gamma_{\phi,S} \simeq 1$ or smaller.

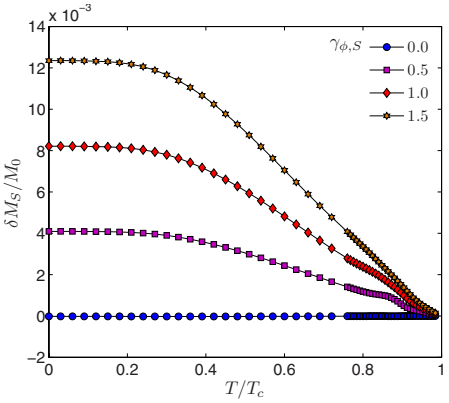

FIG. 14. (Color online) Plot of the proximity-induced magnetization for $\gamma_{\phi,F}=0$ upon varying the spin-DIPS $\gamma_{\phi,S}$ on the superconducting side using $d_S/\xi_S=1.0$.

In Ref. 48, the inverse proximity effect of an S|F bilayer was studied without taking into account the presence of spin-

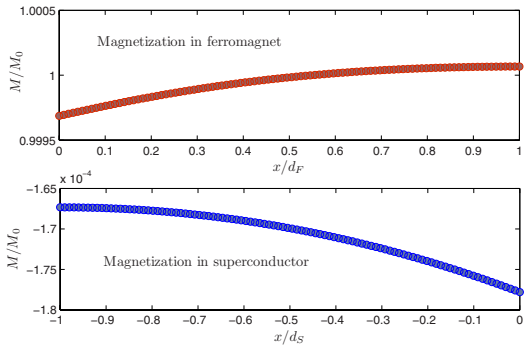

FIG. 15. (Color online) Plot of the spatial dependence of the total magnetization at zero temperature for $d_S/\xi_S=0.2$ and $\gamma_{\phi,F}=\gamma_{\phi,S}=0.0$.

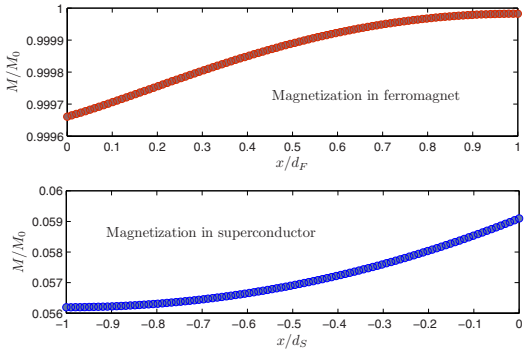

FIG. 16. (Color online) Plot of the spatial dependence of the total magnetization at zero temperature for d_S/ξ_S=0.2, $\gamma_{\phi,F}$=0.0, and $\gamma_{\phi,S}$=1.0.

DIPS, with the result that the proximity-induced magnetization in the superconducting region would have the opposite sign of the proximity ferromagnet, i.e., a screening effect. It was proposed in Ref. 48 that this behavior could be understood physically by considering the contribution to the magnetization from Cooper pairs which were close to the interface: the spin-↑ electron would prefer to be in the ferromagnetic region due to the exchange energy, while the spin-↓ electron remaining in the superconducting region then would give rise to a magnetization in the opposite direction of the proximity ferromagnet. However, it is clear from the present study that this simple picture must be modified when properly considering the spin-DIPS $\gamma_{\phi,S}$ on the superconducting side of the junction since they act as an effective exchange field inside the superconductor.

In this paper, we have evaluated the proximity-induced magnetization in the vicinity of the interface without taking into account the Meissner response of the superconductor. This should be permissible in a thin-film geometry as the one employed in Ref. 51, where the screening currents are suppressed. In particular, for a field in the plane of the superconducting film (see Fig. 12), the Meissner effect should be strongly suppressed[71] for $d_S/\xi_S \ll 1$.

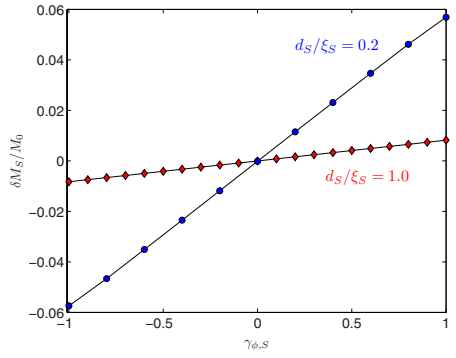

FIG. 17. (Color online) Plot of the proximity-induced magnetization at T=0 as a function of $\gamma_{\phi,S}$ for two different values of d_S/ξ_S.

IV. SUMMARY

In conclusion, we have in Sec. II of this work investigated the proximity effect in a superconductor|inhomogeneous ferromagnet junctions. Proper boundary conditions which take into account the spin-dependent phase shifts experienced by the reflected and transmitted quasiparticles were employed. As an application of our model, we have studied the LDOS in the ferromagnet in the presence of domain walls and a conical magnetic structure. We find that the presence of a domain wall enhances the odd-frequency correlations induced in the ferromagnet manifested through a zero-energy peak in the LDOS. For the conical ferromagnet, we show that the spin-dependent phase shifts originating with the interface have a strong qualitative effect on the LDOS, especially for thin layers. In particular, we find an abrupt crossover from a fully suppressed LDOS to a finite LDOS which appears at a critical thickness of the ferromagnetic layer, and the particular value of the critical thickness depends on the value of G_ϕ. In a similar way, we find that there is an abrupt change appearing at a critical value of G_ϕ for sufficiently thin layers. We speculate that the reason for this could be a symmetry transition from even-frequency to odd-frequency correlations for the proximity amplitudes in the ferromagnetic region. The theory developed in the present paper takes into account both the phase shifts acquired by scattered quasiparticles at the interface due to the presence of ferromagnetic correlations and also an arbitrary inhomogeneity of the magnetic texture on the ferromagnetic side. Our results for the conical ferromagnetic structure should be relevant for the material Ho, which was used in Ref. 59 to indicate the presence of long-range superconducting correlations.

In Sec. III of this work, we have investigated numerically and self-consistently the inverse proximity effect in a superconductor|ferromagnet (S|F) bilayer manifested through an induced magnetization in the superconducting region. We find that the interface properties play a crucial role in this context, as the spin-dependent interfacial phase-shifts (spin-DIPS) may invert the sign of the proximity-induced magnetization. This finding modifies previous conclusions obtained in the literature and suggests that the influence of the spin-DIPS should be properly accounted for in a theory for the inverse proximity effect in S|F bilayers.

ACKNOWLEDGMENTS

J.L. acknowledges M. Eschrig and A. Cottet for very useful discussions. J.L. and A.S. were supported by the Research Council of Norway under Grants No. 158518/432 and No. 158547/431 (NANOMAT), and Grant No. 167498/V30 (STORFORSK). T.Y. acknowledges support by JSPS.

APPENDIX: SPIN-ACTIVE BOUNDARY CONDITIONS

To facilitate and encourage use of the spin-active boundary conditions required for an S|F interface, we here write down their explicit form in the diffusive limit for the case of a magnetization in the z direction, following Refs. 55 and 56. Consider a junction consisting of two regions 1 and 2, as shown in Fig. 18. The regions have widths d_j and bulk elec-

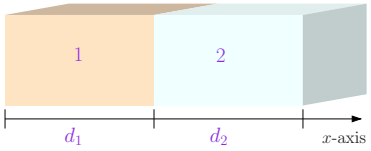

FIG. 18. (Color online) Junction consisting of two regions 1 and 2 with an interface perpendicular to the $\boldsymbol{x}$ axis.

trical resistances R_j. The matrices used below are 4×4 matrices in particle-hole $\otimes$ spin space using a basis

$$\psi(\boldsymbol{r},t)=\begin{pmatrix}\psi_\uparrow(\boldsymbol{r},t)\\ \psi_\downarrow(\boldsymbol{r},t)\\ \psi_\uparrow^\dagger(\boldsymbol{r},t)\\ \psi_\downarrow^\dagger(\boldsymbol{r},t)\end{pmatrix}.$$

Introducing $\hat{\alpha}=\mathrm{diag}(1,-1,1,-1)=\mathrm{diag}(\underline{\sigma}_3,\underline{\sigma}_3)$, where $\underline{\sigma}_3$ is the third Pauli matrix in spin-space, we may write the boundary conditions as follows:

$$2(d_1/R_1)\hat{g}_1\partial_x\hat{g}_1=G_T[\hat{g}_1,\hat{g}_2]-iG_{\phi,1}[\hat{\alpha},\hat{g}_1],$$

$$2(d_2/R_2)\hat{g}_2\partial_x\hat{g}_2=G_T[\hat{g}_1,\hat{g}_2]+iG_{\phi,2}[\hat{\alpha},\hat{g}_2]. \quad \text{(A1)}$$

Here, G_T is the conductance of the junction, while $G_{\phi,j}$ are the phase shifts on side j of the interface. The parameters $\{G_T,G_{\phi,j}\}$ may be calculated by relating them to microscopic transmission and reflection probabilities within, e.g., a Blonder-Tinkham-Klapwijk (BTK) (Ref. 72) framework. Explicitly spin-active barriers were considered in ballistic S|F bilayers using the BTK approach for both s-wave[73] and d-wave[74] superconductors. In the absence of spin-DIPS ($G_{\phi,j}\to0$), Eq. (A1) reduce to the Kupriyanov-Lukichev nonmagnetic boundary conditions.[75] Let us make a final remark concerning the treatment of interfaces in the quasiclassical theory of superconductivity. We previously stated that the application of the present theory requires that the characteristic energies of various self-energies and perturbations in the system are much smaller than the Fermi energy ε_F. At first glance, this might seem to be irreconcilable with the presence of interfaces, which represent strong perturbations varying on atomic length scales. However, this problem may be overcome by including the interfaces as boundary conditions for the Green's functions rather than directly as self-energies in the Usadel equation.

[1] F. S. Bergeret, A. F. Volkov, and K. B. Efetov, Rev. Mod. Phys. **77**, 1321 (2005).
[2] A. I. Buzdin, Rev. Mod. Phys. **77**, 935 (2005).
[3] F. S. Bergeret, A. F. Volkov, and K. B. Efetov, Phys. Rev. Lett. **86**, 4096 (2001).
[4] V. V. Ryazanov, V. A. Oboznov, A. Yu. Rusanov, A. V. Veretennikov, A. A. Golubov, and J. Aarts, Phys. Rev. Lett. **86**, 2427 (2001).
[5] A. F. Volkov, F. S. Bergeret, and K. B. Efetov, Phys. Rev. Lett. **90**, 117006 (2003).
[6] F. S. Bergeret, A. F. Volkov, and K. B. Efetov, Phys. Rev. B **68**, 064513 (2003).
[7] M. Eschrig, J. Kopu, J. C. Cuevas, and G. Schön, Phys. Rev. Lett. **90**, 137003 (2003).
[8] V. Braude and Yu. V. Nazarov, Phys. Rev. Lett. **98**, 077003 (2007).
[9] Y. Asano, Y. Tanaka, and A. A. Golubov, Phys. Rev. Lett. **98**, 107002 (2007); Y. Asano, Y. Sawa, Y. Tanaka, and A. A. Golubov, Phys. Rev. B **76**, 224525 (2007).
[10] R. S. Keizer, S. T. B. Goennenwein, T. M. Klapwijk, G. Miao, G. Xiao, and A. Gupta, Nature (London) **439**, 825 (2006).
[11] Ya. V. Fominov, A. F. Volkov, and K. B. Efetov, Phys. Rev. B **75**, 104509 (2007).
[12] T. Yokoyama, Y. Tanaka, and A. A. Golubov, Phys. Rev. B **75**, 134510 (2007).
[13] Y. Asano, Y. Tanaka, A. A. Golubov, and S. Kashiwaya, Phys. Rev. Lett. **99**, 067005 (2007).
[14] K. Halterman, P. H. Barsic, and O. T. Valls, Phys. Rev. Lett. **99**, 127002 (2007).
[15] Y. Tanaka and A. A. Golubov, Phys. Rev. Lett. **98**, 037003 (2007).
[16] M. Eschrig, T. Lofwander, T. Champel, J. C. Cuevas, J. Kopu, and G. Schön, J. Low Temp. Phys. **147**, 457 (2007).
[17] J. Linder, T. Yokoyama, and A. Sudbø, Phys. Rev. B **77**, 174507 (2008); J. Linder, T. Yokoyama, Y. Tanaka, Y. Asano, and A. Sudbø, *ibid.* **77**, 174505 (2008).
[18] M. Eschrig and T. Löfwander, Nat. Phys. **4**, 138 (2008).
[19] K. Halterman, O. T. Valls, and P. H. Barsic, Phys. Rev. B **77**, 174511 (2008).
[20] J. Linder, T. Yokoyama, and A. Sudbø, Phys. Rev. B **77**, 174514 (2008).
[21] K. Yada, S. Onari, Y. Tanaka, and K. Miyake, arXiv:0806.4241 (unpublished).
[22] L. N. Bulaevskii, V. V. Kuzii, and A. A. Sobyanin, Pis'ma Zh. Eksp. Teor. Fiz. **25**, 314 (1977); JETP Lett. **25**, 290 (1977).
[23] A. I. Buzdin, L. N. Bulaevskii, and S. V. Panyukov, Pis'ma Zh. Eksp. Teor. Fiz. **35**, 147 (1982).
[24] E. Koshina and V. Krivoruchko, Phys. Rev. B **63**, 224515 (2001).
[25] T. Kontos, M. Aprili, J. Lesueur, F. Genet, B. Stephanidis, and R. Boursier, Phys. Rev. Lett. **89**, 137007 (2002).
[26] A. Buzdin and A. E. Koshelev, Phys. Rev. B **67**, 220504(R) (2003).
[27] M. Houzet, V. Vinokur, and F. Pistolesi, Phys. Rev. B **72**, 220506(R) (2005).
[28] A. Cottet and W. Belzig, Phys. Rev. B **72**, 180503(R) (2005).
[29] J. W. A. Robinson, S. Piano, G. Burnell, C. Bell, and M. G. Blamire, Phys. Rev. Lett. **97**, 177003 (2006).
[30] G. Mohammadkhani and M. Zareyan, Phys. Rev. B **73**, 134503 (2006).
[31] T. Yokoyama, Y. Tanaka, and A. A. Golubov, Phys. Rev. B **75**, 094514 (2007).
[32] M. Houzet and A. I. Buzdin, Phys. Rev. B **76**, 060504(R) (2007).

[33] B. Crouzy, S. Tollis, and D. A. Ivanov, Phys. Rev. B **75**, 054503 (2007); **76**, 134502 (2007).
[34] J. Linder, T. Yokoyama, D. Huertas-Hernando, and A. Sudbø, Phys. Rev. Lett. **100**, 187004 (2008).
[35] T. Champel and M. Eschrig, Phys. Rev. B **71**, 220506(R) (2005); T. Champel and M. Eschrig, *ibid.* **72**, 054523 (2005); T. Champel, T. Löfwander, and M. Eschrig, Phys. Rev. Lett. **100**, 077003 (2008).
[36] P. M. R. Brydon, B. Kastening, D. K. Morr, and D. Manske, Phys. Rev. B **77**, 104504 (2008).
[37] I. B. Sperstad, J. Linder, and A. Sudbø, Phys. Rev. B **78**, 104509 (2008).
[38] A. F. Volkov and K. B. Efetov, Phys. Rev. B **78**, 024519 (2008).
[39] V. L. Berezinskii, JETP Lett. **20**, 287 (1974).
[40] A. Balatsky and E. Abrahams, Phys. Rev. B **45**, 13125 (1992).
[41] P. Coleman, E. Miranda, and A. Tsvelik, Phys. Rev. Lett. **70**, 2960 (1993).
[42] E. Abrahams, A. Balatsky, D. J. Scalapino, and J. R. Schrieffer, Phys. Rev. B **52**, 1271 (1995).
[43] D. Solenov, I. Martin, and D. Mozyrsky, arXiv:0812.1055 (unpublished).
[44] J. Y. Gu, J. A. Caballero, R. D. Slater, R. Loloee, and W. P. Pratt, Jr., Phys. Rev. B **66**, 140507(R) (2002).
[45] M. A. Sillanpaa, T. T. Heikkila, R. K. Lindell, and P. J. Hakonen, Europhys. Lett. **56**, 590 (2001).
[46] F. S. Bergeret, A. L. Yeyati, and A. Martin-Rodero, Phys. Rev. B **72**, 064524 (2005).
[47] J. P. Morten, A. Brataas, G. E. W. Bauer, W. Belzig, and Y. Tserkovnyak, Europhys. Lett. **84**, 57008 (2008)..
[48] F. S. Bergeret, A. F. Volkov, and K. B. Efetov, Phys. Rev. B **69**, 174504 (2004).
[49] Th. Mühge, N. N. Garif'yanov, Yu. V. Goryunov, K. Theis-Bröhl, K. Westerholt, I. A. Garifullin, and H. Zabel, Physica C **296**, 325 (1998).
[50] I. A. Garifullin, D. A. Tikhonov, N. N. Garif'yanov, M. Z. Fattakhov, K. Theis-Bröhl, K. Westerholt, and H. Zabel, Appl. Magn. Reson. **22**, 439 (2002).
[51] J. Xia, V. Shelukhin, M. Karpovski, A. Kapitulnik, and A. Palevski, arXiv:0810.2605 (unpublished).
[52] R. I. Salikhov, I. A. Garifullin, N. N. Garif'yanov, L. R. Tagirov, K. Theis-Bröhl, K. Westerholt, and H. Zabel, arXiv:0806.4104 (unpublished).
[53] M. Yu. Kharitonov, A. F. Volkov, and K. B. Efetov, Phys. Rev. B **73**, 054511 (2006).
[54] K. Halterman and O. T. Valls, Phys. Rev. B **69**, 014517 (2004).
[55] D. Huertas-Hernando, Yu. V. Nazarov, and W. Belzig, Phys. Rev. Lett. **88**, 047003 (2002); D. Huertas-Hernando and Yu. V. Nazarov, Eur. Phys. J. B **44**, 373 (2005).
[56] A. Cottet, Phys. Rev. B **76**, 224505 (2007).
[57] P. SanGiorgio, S. Reymond, M. R. Beasley, J. H. Kwon, and K. Char, Phys. Rev. Lett. **100**, 237002 (2008).
[58] A. Cottet and J. Linder, arXiv:0810.0904 (unpublished).
[59] I. Sosnin, H. Cho, V. T. Petrashov, and A. F. Volkov, Phys. Rev. Lett. **96**, 157002 (2006).
[60] See, e.g., J. W. Serene and D. Rainer, Phys. Rep. **101**, 221 (1983).
[61] K. Usadel, Phys. Rev. Lett. **25**, 507 (1970).
[62] D. A. Ivanov and Ya. V. Fominov, Phys. Rev. B **73**, 214524 (2006).
[63] N. Schopohl and K. Maki, Phys. Rev. B **52**, 490 (1995); N. Schopohl, arXiv:cond-mat/9804064 (unpublished).
[64] A. Konstandin, J. Kopu, and M. Eschrig, Phys. Rev. B **72**, 140501(R) (2005).
[65] A. Brataas, Yu. V. Nazarov, and G. E. W. Bauer, Phys. Rev. Lett. **84**, 2481 (2000); Eur. Phys. J. B **22**, 99 (2001); A. Brataas, G. E. W. Bauer, and P. J. Kelly, Phys. Rep. **427**, 157 (2006).
[66] T. Yokoyama, Y. Tanaka, and A. A. Golubov, Phys. Rev. B **72**, 052512 (2005); **73**, 094501 (2006).
[67] T. Kontos, M. Aprili, J. Lesueur, and X. Grison, Phys. Rev. Lett. **86**, 304 (2001).
[68] J. Linder, T. Yokoyama, A. Sudbø, and M. Eschrig (unpublished).
[69] C. Bruder, Phys. Rev. B **41**, 4017 (1990).
[70] J. Linder and A. Sudbø, Phys. Rev. B **76**, 214508 (2007).
[71] R. Meservey and P. M. Tedrow, Phys. Rep. **238**, 173 (1994).
[72] G. E. Blonder, M. Tinkham, and T. M. Klapwijk, Phys. Rev. B **25**, 4515 (1982).
[73] J. Linder and A. Sudbø, Phys. Rev. B **75**, 134509 (2007).
[74] S. Kashiwaya, Y. Tanaka, N. Yoshida, and M. R. Beasley, Phys. Rev. B **60**, 3572 (1999).
[75] M. Yu. Kupriyanov and V. F. Lukichev, Zh. Eksp. Teor. Fiz. **94**, 139 (1988); Sov. Phys. JETP **67**, 1163 (1988).
[76] T. Lofwander, T. Champel, J. Durst, and M. Eschrig, Phys. Rev. Lett. **95**, 187003 (2005).
[77] G. B. Halasz, J. W. A. Robinson, M. G. Blamire, and J. F. Annett, arXiv:0901.2024 (unpublished).

Paper XXV

Pairing symmetry transition induced by spin-active interfaces in superconducting junctions.

Accepted for publication in Physical Review Letters.

Pairing symmetry conversion by spin-active interfaces in superconducting junctions

Jacob Linder,[1] Takehito Yokoyama,[2] Asle Sudbø,[1] and Matthias Eschrig[3]

[1]*Department of Physics, Norwegian University of Science and Technology, N-7491 Trondheim, Norway*
[2]*Department of Applied Physics, Nagoya University, Nagoya, 464-8603, Japan*
[3]*Institut für Theoretische Festkörperphysik and DFG-Center for Functional Nanostructures, Universität Karlsruhe, D-76128 Karlsruhe, Germany*

(Dated: Received February 19, 2009)

We study the proximity-induced superconducting correlations in a normal metal connected to a superconductor when the interface between them is spin-active and the normal metal is ballistic or diffusive. Remarkably, for any interface spin polarization there is a critical interface resistance, above which the conventional even-frequency proximity component vanishes completely at the chemical potential, while the odd-frequency component remains finite. We propose a way to unambiguously observe the odd-frequency component.

PACS numbers: 74.20.Rp, 74.50.+r, 74.20.-z

Superconductivity and superfluidity are hallmarks of the wave-like character of matter, and manifest themselves in vastly different systems, from ultracold dilute gases via cold metals and fluids, to extremely dense protonic and neutronic matter. In all these contexts, the symmetry of the order parameter is of profound importance. Over the last decades, the possibility of superconducting order parameters that changes sign under a *time-coordinate* exchange of the two fermions comprising the Cooper-pair, has emerged in addition to the by now well studied varieties of orbital symmetries [1–5]. This so-called odd-frequency superconductivity [6] is distinct from the traditional even-frequency pairing in the Bardeen-Cooper-Schrieffer paradigm, and may be induced by proximity effects in hybrid structures of superconductors and magnets [1].

In a broader context, proximity systems offer the possibility of controlling the physics of competing broken symmetries. The fundamental heterostructure for studying proximity induced superconductivity is the superconductor/normal metal (S|N) bilayer, where the normal metal or the interface may have magnetic properties. Among possible triplet pair correlations, in the diffusive limit odd-frequency pairs are favored [7], whereas in ballistic hybrid systems both odd- and even-frequency amplitudes compete [3, 4]. As all known superconductors to date exhibit an even-frequency order parameter, the observation of proximity induced effects that are particular to odd-frequency pairing would be of utmost interest.

There are two major difficulties associated with the detection of the odd-frequency state in superconductor/ferromagnet (S|F) bilayers. One is the usually short penetration depth into the ferromagnetic region, limited by the magnetic coherence length ξ_F, much less than the superconducting coherence length ξ_S [1]. Another problem is that odd-frequency pairs are only well defined when even-frequency correlations vanish in the ferromagnet. Clear-cut signatures of the former are therefore only accessible in a limited parameter regime [8].

The majority of work on superconducting proximity-structures so far has been restricted to the diffusive limit and spin-inactive interfaces [9]. For a non-magnetic bilayer, a minigap appears in the density of states of the normal metal. It scales with the Thouless energy of the normal layer and with the transmission probability of the interface. Such minigap structures are readily accessible experimentally [10]. For a spin-active interface, the transmission properties of spin-↑ and spin-↓ electrons into a metal are different, and this gives rise to both spin-dependent conductivities and spin-dependent phase shifts at the interface [11–15]. In this Letter we show that a spin-active interface in an S|N bilayer produces clear signatures of purely odd-frequency triplet pairing amplitudes that can be tested experimentally.

We consider the system shown in Fig. 1. The superconductor is conventional (even-frequency s-wave) while the interface is magnetic. We find that there is a dramatic change in the nature of proximity correlations when the spin-dependent phase shifts exceed the tunneling probability of the interface. The spin-active interface in an S|N bilayer causes the even-frequency correlations to vanish at zero excitation energy, while odd-frequency correlations appear. At the same time, the minigap, one of the hallmarks of the conventional proximity effect, is replaced by a low-energy band with enhanced density of states. We focus on the density of states (DOS) in the normal region, which can be probed by tunneling experiments. Our findings suggest that it should be possible to detect the odd-frequency amplitude without any in-

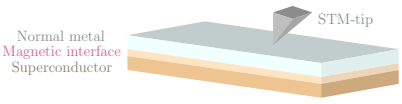

FIG. 1: (Color online) Proposed experiment for observation of the odd-frequency component in a diffusive N|S junction.

terfering effects of even-frequency correlations. Since the exchange field is absent in the normal metal, this resolves the two main difficulties associated with the experimental detection of odd-frequency correlations mentioned above.

We adopt the quasiclassical theory of superconductivity [18], where information about the physical properties of the system is embedded in the Green's function. For equilibrium situations, it suffices to consider the retarded Green's function, $\hat{g}$, that is parameterized conveniently in the normal (N) region by a parameter θ_σ, allowing for both singlet and triplet correlations [8]. In the superconducting (S) region, we employ the bulk solution $\hat{g}_S = c \cdot \underline{\tau_3} \otimes \underline{\sigma_0} + s \cdot \underline{\tau_1} \otimes (\mathrm{i}\underline{\sigma_2})$, with $c = \cosh(\theta)$, $s = \sinh(\theta)$, $\theta = \mathrm{atanh}(\Delta/\varepsilon)$, $\underline{\tau_i}$ and $\underline{\sigma_i}$ being Pauli matrices in particle-hole and spin space, respectively.

We use the formalism described in Ref. [8], and consider first the diffusive limit. Then, the orbital symmetry for all proximity amplitudes is reduced to s-wave and hence the singlet component always has an even-frequency symmetry while the triplet component has an odd-frequency symmetry. The Green's functions are subject to boundary conditions, which assume at the S|N interface in the tunneling limit the form [13, 15]: $2\gamma d\hat{g}_N\partial_x\hat{g}_N = [\hat{g}_S, \hat{g}_N] + \mathrm{i}(G_\phi/G_T)[\underline{\tau_0}\otimes\underline{\sigma_3}, \hat{g}_N]$, and at the outer interface read $\partial_x\hat{g}_N = \hat{0}$. Here, $\gamma = R_B/R_N$ where R_B (R_N) is the resistance of the barrier (normal region), and d is the width of the normal region, while G_T is the junction conductance in the normal-state. The boundary condition above contains an additional term G_ϕ compared to the usual non-magnetic boundary conditions in Ref. [9]. This term is due to spin-dependent phase shifts of quasiparticles being reflected at the interface. G_ϕ may be non-zero even if the transmission $G_T \to 0$, corresponding to a ferromagnetic insulator [13]. We define the superconducting coherence length $\xi_S = \sqrt{D/\Delta}$ and Thouless energy $\varepsilon_{\mathrm{Th}} = D/d^2$, where D is the diffusion constant, and assume that the inelastic scattering length, l_{in}, is sufficiently large, such that $d \ll l_{\mathrm{in}}$.

The Usadel equation [19] reads $D\partial_x^2\theta_\sigma + 2\mathrm{i}\varepsilon\sinh\theta_\sigma = 0$, with boundary condition $\gamma d\partial_x\theta_\sigma = (cs_\sigma - \sigma sc_\sigma) + \mathrm{i}\sigma s_\sigma \frac{G_\phi}{G_T}$ at $x = 0$ and $\partial_x\theta_\sigma = 0$ at $x = d$. Here, $c_\sigma = \cosh(\theta_\sigma)$ and $s_\sigma = \sinh(\theta_\sigma)$. For $\varepsilon = 0$ we find pairing amplitudes that are either purely (odd-frequency) triplet for $|G_\phi| > G_T$,

$$f_s(0) = 0, \quad f_t(0) = G_T \cdot \mathrm{sgn}(G_\phi)/\sqrt{G_\phi^2 - G_T{}^2}, \quad (1)$$

or purely (even-frequency) singlet for $|G_\phi| < G_T$,

$$f_s(0) = \mathrm{i} \cdot G_T/\sqrt{G_T{}^2 - G_\phi^2}, \quad f_t(0) = 0. \quad (2)$$

Thus, the presence of G_ϕ induces an odd-frequency component in the normal layer. The remarkable aspect of Eqs. (1) and (2) is that they are valid for any value of the width d below the inelastic scattering length, and for any interface parameter γ. Thus, the vanishing of the singlet component is a robust feature in S|N structures with spin-active interfaces, as long as $|G_\phi| > G_T$. Without loss of generality, we focus on positive values of G_ϕ from now on. The DOS is given as $N(\varepsilon)/N_0 = \sum_\sigma \mathrm{Re}\{c_\sigma\}/2$, yielding $N(0)/N_0 = \mathrm{Re}\{G_\phi/\sqrt{G_\phi^2 - G_T{}^2}\}$. At zero-energy, the DOS vanishes when $G_\phi < G_T$, which means that the usual minigap in S|N structures survives. However, the zero-energy DOS is enhanced for $G_\phi > G_T$ since the singlet component vanishes there.

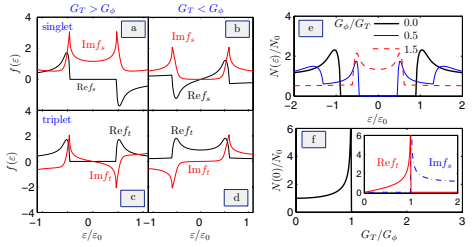

FIG. 2: (Color online) The singlet and triplet proximity amplitudes induced in the normal metal are shown for $G_\phi/G_T < 1$ [in a) and c)] and $G_\phi/G_T > 1$ [in b) and d)]. In e), we plot the energy-resolved DOS for several values of G_ϕ/G_T. Finally, f) shows the zero-energy DOS as a function of G_T/G_ϕ, with the proximity amplitudes shown in the inset.

The full energy-dependence of the DOS may only be obtained numerically. To model a realistic experimental setup, we fix $\gamma = 10$ and $d/\xi_S = 1.0$, although our qualitative results are independent of these particular choices. As a measure of the relevant energy scale, we define $\varepsilon_0 = \varepsilon_{\mathrm{Th}}/(2\gamma)$. The results are shown in Fig. 2 to investigate the effect of the spin-dependent phase shifts. The low-energy DOS is strongly enhanced due to the odd-frequency amplitude when $G_\phi/G_T > 1$ ($G_\phi/G_T = 1.5$ in the figure). Conversely, the DOS develops a minigap around $\varepsilon = 0$ when $G_\phi/G_T < 1$ ($G_\phi/G_T = 0.5$ in the figure). The ratio G_ϕ/G_T depends on the microscopic barrier properties [15]. In the tunneling limit, one finds that G_ϕ can be considerably larger than G_T.

We suggest the following qualitative explanation for the mechanism behind the separation between even- and odd-frequency correlations. The superconductor induces a minigap $\propto G_T$ in the normal metal, while the spin-active barrier induces an effective exchange field $\propto G_\phi$. The situation in the normal metal then resembles that of a thin-film conventional superconductor in the presence of an in-plane external magnetic field [22], with the role of the gap and field played by G_T and G_ϕ, respectively. In that case, it is known that superconductivity is destroyed above the Clogston-Chandrasekhar limit [23], as the spin-singlet Cooper-pairs break up. In the present case, we observe coexistence of the exchange field and spin-singlet even-frequency superconductivity as long as G_ϕ is below the critical value of $G_\phi = G_T$. At the critical point, the DOS varies as $1/\sqrt{|\epsilon|}$ and diverges at $\epsilon = 0$. However, for $G_\phi > G_T$ spin-singlet pairing is no longer possible

at the chemical potential. It is then replaced by spin-triplet pairing, which must be odd in frequency due to the isotropization of the gap in the diffusive limit. Thus, there is a natural separation between even-frequency and odd-frequency pairing in the normal metal at a critical value of the effective exchange field G_ϕ.

The same effect occurs in the ballistic limit, as we now show. In this case, we can obtain the retarded Green's function using the formalism described in Refs. [14, 16]. The Eilenberger equation in the normal region reads $iv_{Fx}\partial_x\hat{g} + [\varepsilon\underline{\tau_3}\otimes\underline{\sigma_0}, \hat{g}] = \hat{0}$. For the boundary conditions, we use a scattering matrix describing the magnetic interface between the superconductor and the normal metal,

$$\hat{S} = \begin{pmatrix} \underline{r}_S \cdot \exp\left(\frac{i}{2}\vartheta_S\underline{\sigma_3}\right) & \underline{t}_{SN} \cdot \exp\left(\frac{i}{2}\vartheta_{SN}\underline{\sigma_3}\right) \\ \underline{t}_{NS} \cdot \exp\left(\frac{i}{2}\vartheta_{NS}\underline{\sigma_3}\right) & -\underline{r}_N \cdot \exp\left(\frac{i}{2}\vartheta_N\underline{\sigma_3}\right) \end{pmatrix}, \quad (3)$$

with real reflection and transmission spin matrices $\underline{r}_S$, $\underline{r}_N$, $\underline{t}_{SN}$, and $\underline{t}_{NS}$. The spin mixing angles ϑ_S, ϑ_N, ϑ_{SN}, and ϑ_{NS} describe spin dependent scattering phases [11]. Neglecting spin flip scattering, the transmission and reflection amplitudes are diagonal in spin space, and the relations $\underline{r}_S = \underline{r}_N \equiv \mathrm{diag}\,[r_\uparrow, r_\downarrow]$, $\underline{t}_{NS} = \underline{t}_{SN} \equiv \mathrm{diag}\,[t_\uparrow, t_\downarrow]$, $r_\uparrow^2 + t_\uparrow^2 = r_\downarrow^2 + t_\downarrow^2 = 1$, $\vartheta_{NS} + \vartheta_{SN} = \vartheta_S + \vartheta_N$ follow from the unitarity of $\hat{S}$. Possible scalar phases are omitted in Eq. (3), as they play no role in the final results.

We next concentrate on subgap energies. The anomalous amplitudes can be decomposed into singlet and triplet components, $f = (f_s + f_t\,\underline{\sigma_3})(i\underline{\sigma_2})$. Defining $f_\sigma = (f_s + \sigma f_t)/2$, we obtain on the top of the normal overlayer ($x = d$) $f_\sigma(\varepsilon) = -\mathrm{sgn}(\alpha_\sigma)t_\uparrow t_\downarrow/\sqrt{\alpha_\sigma^2 - (t_\uparrow t_\downarrow)^2}$ with $\alpha_\sigma = \sin(2\varepsilon d/v_{Fx} + \vartheta_{\sigma+}) + r_\uparrow r_\downarrow \sin(2\varepsilon d/v_{Fx} + \vartheta_{\sigma-})$. Here, $\vartheta_{\sigma\pm} = \frac{\sigma}{2}(\vartheta_N \pm \vartheta_S) \pm \arcsin(\varepsilon/\Delta)$, and ε has to be supplemented by an infinitesimally small positive imaginary part. The interface parameters and the Fermi velocity component in x-direction, $v_{Fx} = v_F\cos\psi$, depend on the impact angle ψ. The relevant energy scale in the problem is the ballistic Thouless energy, $\varepsilon_{Th} = v_F/2d$. The DOS is non-zero only for $|\alpha| > t_\uparrow t_\downarrow$, which for sufficiently large impact angle always is fulfilled. Clearly, the most interesting regime concerns $\varepsilon/\varepsilon_{Th} \sim |\vartheta_{\sigma\pm}| \sim t_\uparrow t_\downarrow$.

In the tunneling limit, for small excitation energies $\varepsilon/\varepsilon_{Th} \ll 1$ and small spin mixing angles $\vartheta_{\sigma\pm}$ we obtain $\alpha_\sigma = (4\varepsilon d/v_{Fx} + \sigma\vartheta_N)$. In this case, due to $\vartheta_{\sigma+} + \vartheta_{\sigma-} = \sigma\vartheta_N$, only the spin mixing angle for reflection at the normal side of the interface enters, and acts as an effective exchange field $b = \vartheta_N v_{Fx}/4d$ on the quasiparticles. Especially interesting is the case $\varepsilon = 0$, for which all proximity amplitudes are even in momentum. For $\varepsilon = 0$ we obtain $\alpha_\sigma = \sigma\vartheta_N$, and the pairing amplitudes are either purely (odd-frequency) triplet for $|\vartheta_N| > t_\uparrow t_\downarrow$,

$$f_s(0) = 0, \quad f_t(0) = -t_\uparrow t_\downarrow \cdot \mathrm{sgn}(\vartheta_N)/\sqrt{\vartheta_N^2 - (t_\uparrow t_\downarrow)^2} \quad (4)$$

or purely (even-frequency) singlet for $|\vartheta_N| < t_\uparrow t_\downarrow$,

$$f_s(0) = \mathrm{i}\cdot t_\uparrow t_\downarrow/\sqrt{(t_\uparrow t_\downarrow)^2 - \vartheta_N^2}, \quad f_t(0) = 0. \quad (5)$$

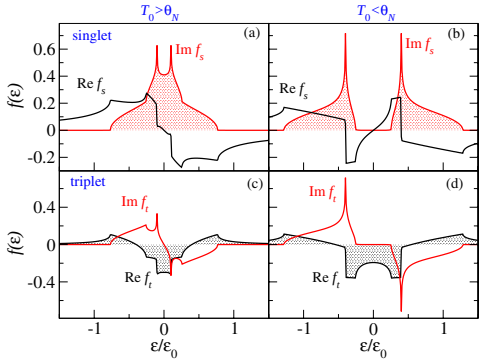

FIG. 3: (Color online) Momentum-averaged proximity amplitudes at the surface of the normal layer. Parameters: $d = v_F/\Delta$, $T_0 = 0.1$ (see text). (a) and (c): $\vartheta_N = \vartheta_S = 0.05 < T_0$; (b) and (d): $\vartheta_N = \vartheta_S = 0.15 > T_0$. Energy units are $\varepsilon_0 = T_0\,\varepsilon_{Th}$. Even frequency singlet components are shown in (a-b), odd frequency triplet components in (c-d).

Comparing with the results for the diffusive case, we find that G_ϕ/G_T corresponds to $-\vartheta_N/(t_\uparrow t_\downarrow)$.

In Fig. 3, we show results for the proximity amplitudes in the ballistic limit, and focus on positive values of ϑ_N without loss of generality. A systematic expansion of all terms in the tunneling probability shows that in the tunneling limit the spin dependence of the transmission probabilities can be neglected, and only that of the phase shifts needs to be kept. Thus, we assume $t_\uparrow = t_\downarrow = t$. We model the dependence on the impact angle ψ as $t(\mu) = (t_0)^{\frac{1}{\mu}}$, $\mu = \cos\psi$, and assume for simplicity spin mixing angles independent of μ. The tunneling probability for normal impact is $T_0 = t_0^2$. In the case $T_0 < \vartheta_N$ at small energies the odd frequency triplet amplitude dominates, and it is the only non-zero amplitude at $\varepsilon = 0$. On the other hand, for $T_0 > \vartheta_N$ both singlet and triplet amplitudes contribute. This is due to the fact that for large impact angles the transmission probability $t(\mu)^2$ drops below the value for the spin mixing angle ϑ_N.

We turn now to the DOS. The general expression, assuming the bulk solution in the superconductor, is $N(\varepsilon)/N_0 = \mathrm{Re}\sum_{\sigma=\pm1}\int_0^1 |\alpha_\sigma|/\sqrt{\alpha_\sigma^2 - (t_\uparrow t_\downarrow)^2}\,d\mu$. In the tunneling limit, this simplifies again, and provided that $|\vartheta_N| > t_\uparrow t_\downarrow$ for all impact angles, the DOS at the Fermi level is enhanced above its normal state value, $N(0)/N_0 = \int d\mu\ |\vartheta_N|/\sqrt{\vartheta_N^2 - (t_\uparrow t_\downarrow)^2}$. In Fig. 4, we show results for the DOS. In (a-b) we assume the dependence on the impact angle as above, whereas in (c-d) we allow tunnelling only in a narrow tunneling cone of 10 degrees. The DOS for the cases of dominating triplet amplitudes and dominating singlet amplitudes differ qualitatively. In the case of a tunneling cone this difference is most drastic, and a comparison with the results above

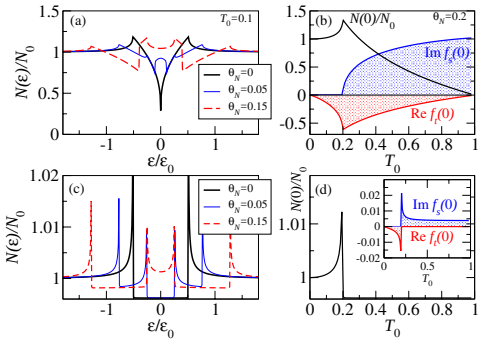

FIG. 4: (Color online) (a) DOS as function of energy at the top of the normal layer for fixed transmission probability $T_0 = 0.1$, and various values of $\vartheta_N = \vartheta_S$. Remaining parameters are as in Fig. 3. (b) DOS and proximity amplitudes at $\varepsilon = 0$ for $\vartheta_N = \vartheta_S = 0.2$ as function of T_0. In (c) and (d) we show the results corresponding to (a) and (b) when assuming an (abrupt) tunneling cone with opening angle of 10 degree.

shows that it is very similar to the diffusive case. In the right panels, where $\vartheta_N = \vartheta_S = 0.2$, we demonstrate that for $T_0 < 0.2$ only the odd frequency triplet amplitude is present at the chemical potential, while the singlet amplitude is zero. The corresponding zero-energy DOS is enhanced in this region, whereas it is reduced in the region when singlet correlations are present at $\varepsilon = 0$.

The simplest experimental manifestation of the odd-frequency component is a zero-energy peak in the DOS [17, 20, 21]. In S|F layers, where this phenomenon has been discussed, a clear peak at zero energy is often masked by the presence of singlet correlations f_s, which tend to suppress the DOS at low energy. This is not so in the system we consider, provided $T_0 < |\vartheta_N|$ in the ballistic limit, or equivalently, $G_T < |G_\phi|$ in the diffusive limit. This is ideal for an observation of the odd-frequency component, manifested as a zero-energy peak in the DOS.

The important factor, with regard to isolation of the odd-frequency correlations at zero energy is the interface. The even-frequency correlations vanish when the interface transmission T_0 is sufficiently low. The parameters ϑ_N, or equivalently, G_ϕ can be increased by increasing the magnetic polarization of the barrier separating the superconducting and normal layers. By fabricating several samples with progressively increasing strength of magnetic moment $\vec{\mu}$ of the barrier, one should be able to observe an abrupt change at the zero-energy DOS above a certain strength of $\vec{\mu}$. Alternatively, one could alter T_0 by varying the thickness of the insulating region.

In summary, we have investigated the proximity-effect in a S|N bilayer with spin-active interface. We find that both in the ballistic and diffusive limits, the even-frequency correlations may vanish at zero energy, while odd-frequency correlations persist. This result is independent of the specific values for the layer thicknesses and barrier resistances, indicating that it is a robust and general feature of spin-active interfaces. Our findings suggest a way of obtaining unambiguous experimental identification of superconducting odd-frequency correlations.

A. Cottet and D. Huertas-Hernando are thanked for helpful communications. J.L. and A.S. were supported by the Norwegian Research Council Grants No.158518/431 and No.158547/431 (NANOMAT), and No.167498/V30 (STORFORSK). T.Y. was supported by the JSPS.

[1] F. S. Bergeret *et al.*, Rev. Mod. Phys. **77**, 1321 (2005).
[2] A. I. Buzdin, Rev. Mod. Phys. **77**, 935 (2005).
[3] Y. Tanaka *et al.*, Phys. Rev. Lett. **99**, 037005 (2007); Y. Tanaka *et al.*, Phys. Rev. Lett. **98**, 037003 (2007).
[4] M. Eschrig *et al.*, J. Low Temp. Phys. **147** 457 (2007).
[5] T. Yokoyama *et al.*, Phys. Rev. B **78**, 012508 (2008).
[6] V. L. Berezinskii, JETP Lett. **20**, 287 (1974).
[7] A. Volkov *et al.*, Phys. Rev. Lett. **90**, 117006 (2003)
[8] J. Linder *et al.*, Phys. Rev. B **77**, 174514 (2008).
[9] M. Kupriyanov *et al.*, Zh. Exp. Teor. Fiz. **94**, 139 (1988); Yu. Nazarov, Superlatt. Microstruct. **25**, 1221 (1999).
[10] H. le Sueur *et al.*, Phys. Rev. Lett. **100**, 197002 (2008).
[11] T. Tokuyasu *et al.*, Phys. Rev. B **38**, 4504 (1988); A. Millis *et al.*, Phys. Rev. B **38**, 4504 (1988).
[12] A. Brataas *et al.*, Phys. Rev. Lett. **11**, 2481 (2000); A. Brataas *et al.*, Phys. Rep. **427**, 157 (2006).
[13] D. Huertas-Hernando *et al.*, Phys. Rev. Lett. **88**, 047003 (2002).
[14] M. Eschrig *et al.*, Phys. Rev. Lett. **90**, 137003 (2003); M. Eschrig and T. Löfwander, Nature Physics **4**, 138 (2008).
[15] A. Cottet *et al.*, Phys. Rev. B **72**, 180503 (2005).
[16] M. Eschrig, Phys. Rev. B **61**, 9061 (2000); M. Fogelström, Phys. Rev. B **62**, 11812 (2000); E. Zhao *et al.*, Phys. Rev. B **38**, 134510 (2004).
[17] Y. Asano *et al.*, Phys. Rev. Lett. **98**, 107002 (2007).
[18] J. W. Serene *et al.*, Phys. Rep. **101**, 221 (1983)
[19] K. Usadel, Phys. Rev. Lett. **25**, 507 (1970).
[20] T. Yokoyama *et al.*, Phys. Rev. B **75**, 134510 (2007).
[21] V. Braude *et al.*, Phys. Rev. Lett. **98**, 077003 (2007).
[22] R. Meservey *et al.*, Phys. Rep. **238**, 173 (1994).
[23] A. M. Clogston, Phys. Rev. Lett. **9**, 266 (1962); B. S. Chandrasekhar, Appl. Phys. Lett. **1**, 7 (1962).

Addendum: My contribution to the papers

In Papers III, IV, V, VI, VII, VIII, IX, XI, XII, XIII, XV, XVI, XVII, XX, XXII, and XXIV, I performed the majority of the analytical calculations, produced the numerical results, and contributed substantially to all parts of the text.

In Papers I, II, XIV, XVIII, XIX, and XXV, I did the main part of the analytical calculations and numerical work together with one of the co-authors, and contributed substantially to all parts of the text.

In Paper XXIII, I contributed to the numerical code and was involved in writing the paper.

In Paper X, I derived the analytical formula used to obtain the results and was involved in writing the paper.

In Paper XXI, I contributed to the analytical calculations and was involved in writing the paper.